# Crystal Engineering of Novel Solid Forms of Active Pharmaceutical Ingredients and their Physicochemical Properties

A Thesis
Submitted for the Degree of
DOCTOR OF PHILOSOPHY
By

Suryanarayana Allu

November
2020

*School of Chemistry, University of Hyderabad (IoE), Hyderabad-500 046, India*

प्रतिष्ठित संस्थान
INSTITUTION OF EMINENCE
राष्ट्रीय अपेक्षाएँ, वैश्विक मानक
National Needs, Global Standards

# Crystal Engineering of Novel Solid Forms of Active Pharmaceutical Ingredients and their Physicochemical Properties

A Thesis
Submitted for the Degree of
**DOCTOR OF PHILOSOPHY**

***By***

**Suryanarayana Allu**


**School of Chemistry**
**University of Hyderabad (IoE)**
**Hyderabad 500046**
**Telangana**
**India**

**November 2020**

# Dedication

***To,***

***My Family,***
***Teachers***
***&***
***Friends***

# DECLARATION

I, **Suryanarayana Allu** hereby declare that the matter embodied in the thesis entitled **"Crystal Engineering of Novel Solid Forms of Active Pharmaceutical Ingredients and their Physicochemical Properties"** is the result of investigation carried out by me under the supervision of **Prof. Ashwini Nangia**, School of Chemistry, University of Hyderabad, Hyderabad, India.

In keeping with the general practice of reporting scientific observations, due acknowledgements have been made on the basis of the findings of other investigators. Any omission, which might have occurred by oversight or error, is regretted. This research work is free from Plagiarism. I hereby agree that my thesis can be deposited in shodganga/INFLIBNET. A report on plagiarism statistics from the University Library is enclosed.

A. Suryanarayana

**Suryanarayana Allu**
(14CHPH15)

Prof. Ashwini Nangia
School of Chemistry
University of Hyderabad
Hyderabad-500 046, INDIA.

**Prof. Ashwini K. Nangia**
(Supervisor)

S.K.Das 16/11/2020

**Prof. Samar Kumar Das**
(Supervisor I/c)

Prof. Samar K. Das
School of Chemistry
University of Hyderabad
Hyderabad-500 046., INDIA.

University of Hyderabad

November, 2020

India's Institution of Eminence

NATIONAL NEEDS, GLOBAL STANDARDS

# CERTIFICATE

This is to certify that the thesis entitled **"Crystal Engineering of Novel Solid Forms of Active Pharmaceutical Ingredients and their Physicochemical Properties"** submitted by **Suryanarayana Allu** holding registration number **14CHPH15** in partial fulfilment of the requirements for award of Doctor of Philosophy in the School of Chemistry is a bonafide work carried out by him under my supervision and guidance.

This thesis is free from plagiarism and has not been submitted previously in part or in full to this or any other University or Institution for award of any degree or diploma.

**Parts of the thesis have been:**

**A. Published in following publication**

- Supramolecular Synthons in Bumetanide Cocrystals and Ternary Products. **Suryanarayana Allu,** Geetha Bolla, Srinu Tothadi, and Ashwini Nangia. *Cryst. Growth Design.* **2017,** 17, 4225-4236.
- Role of hydrogen bonding in cocrystals and coamorphous solids: indapamide as a case study.
  **Suryanarayana Allu,** Kuthuru Suresh, Geetha Bolla, M.K.Chaitanya Mannava and Ashwini Nangia. *CrystEngComm*, **2019**, 21, 2043-2048.
- Novel Pharmaceutical Cocrystals and Salts of Bumetanide.
  **Suryanarayana Allu,** Geetha Bolla, Srinu Tothadi, and Ashwini K. Nangia. *Cryst. Growth Design.* **2020**, 20, 793-803.

**B. Presented in the following conferences**

**1.** ChemFest-2017 **2.** IUCR-2017 **3.** Chemfest-2019 **4.** CRSI-2019

Further the student has passed the following courses towards fulfilment of course work requirement for Ph.D.

| | Course | Subject Title | Credits | Pass/Fail |
|---|---|---|---|---|
| 1. | CY-801 | Research Proposal | 3 | Pass |
| 2. | CY-805 | Instrumental Methods A | 3 | Pass |
| 3. | CY-502 | Advanced Organic Synthesis | 3 | Pass |
| 4. | CY-501 | Spectroscopic Methods for Structural Elucidation | 3 | Pass |

Ashwini Nangia 6/11/2020

**Prof. Ashwini K. Nangia**
Thesis Supervisor (on lien)

Prof. Ashwini Nangia
School of Chemistry
University of Hyderabad
Hyderabad-500 046, INDIA.

SK Das 16/11/2020

**Prof. Samar Kumar Das**
(Supervisor I/c)

Prof. Samar K. Das
School of Chemistry
University of Hyderabad
Hyderabad-500 046., INDIA.

**Dean**
School of Chemistry

Dean
School of Chemistry
University of Hyderabad
P.O. Central University
Gachibowli, Hyderabad-500 046.

# Acknowledgements

I express my deep sense of gratitude and profound thanks to my supervisor **Prof. Ashwini Nangia** for introducing me to the fascinating research field with highest degrees of freedom. His views on science and technology, optimistic way of approach and scientific administration are always admirable and inspiring. Throughout my Ph.D. tenure, he was always been approachable, helpful, and friendly. I will forever be grateful for being a part of his research family.

I specially thank my in-charge supervisor **Prof. Samar Kumar Das** for his support and encouragement. I take this opportunity to thank Prof. Anunay Samanta, Dean, School of Chemistry, and former Deans Prof. T. P. Radhakrishnan, Prof. M. Durga Prasad, Prof. M.V. Rajasekharan and all faculty members for providing the facilities needed for our research.

I take this opportunity to thank my doctoral committee members **Prof. A. K. Sahoo** and **Prof. P. Ramu Sridhar** for their constant encouragement, discussions and support during my Ph.D. period.

I sincerely thank all the non-teaching staff of School of Chemistry for their help and assistance on various occasions. I specially thank to Mr. Gupta, Mr. Dilip, Mr. Abraham, Mr. Shetty, Mr. Mallaya Shetty, Mr. Vijay Bhaskar, Mr. Naik, Late Mr. Aleem, Smt. Geeta, Smt. Rani, Smt. Radhika, Mr. David and Mr. Venkey anna, Mr. Durgesh, Mr. Mahinder, Mr. Satyanarayana, Mr. Turabuddin, Mr. Subramanyam, and Smt. Vijayalakshmi.

I am sincerely thankful to all my colleagues in School of Chemistry for fruitful scientific and social discussions and making my research life productive. I wish to thank CSIR for fellowship, DST-SERB, UOH-UPE and UGC for providing required instruments, chemicals and facilities.

I am hearty thankful to Dr. B. Geetha, Dr. K. Suresh, Dr. Sudheer, Dr. Sudalai, Dr. Maddileti, Dr. Anil, Mr. Chaitanya, Mrs. Swapna, Mr. Manish, Mr. Sharath for being my generous co-workers, guides and friends. A special thanks to my lab seniors Dr. Anthony, Dr. Jagadeesh Babu, Dr. Bipul Sarma, Dr. Ranjit Thakuria, Dr. Naba Kamal Nath, Dr. Palash Sanphui, Dr. Suryanarayan and Dr. Rajesh Goud. I am glad to have a friendly working environment with Vishwanath, Srikanth, Kranthi, Uday, Kiran, Swarupa, Divya, Dr. Daman, Dr. Abin, Dr. Sreenivasulu, Dr. Srinu Tothadi, Dr. Abhijit and D. Chaitanya. I really enjoyed being in work discussions with project students Gita, Joy, Uma, Prashant, Girishma, Evelin, Vatsa, Arka, Basanta, Pradeep and for maintaining an innovative and friendly atmosphere in the lab. I am thankful for my research collaborators Dr. Sunil, Dr. Naba K Natha,

I am thankful to my parents Shri. Allu Polinaidu and Smt. Roddamma and my Sister smt. Kondamma and shri. Mahesh (Bava) for everything. I am greatful for Kanakamma (Peddamma), Ramayya (Peddayya), Nanamma & Tathayya, Ammama, Appadu, Ramunaidu (Pedananna), Appalamma, Appalaswamy, Kanakamma, Chinnamma, Somulamma & Lakshmu, Ramanamma (Pinni, Pedananna,) Eswararao & Chanti annayya, Satyanarayana & Eswararao Annayya, Appalanaidu Tammudu, sraswathi & Bangarathalli

Akka. Appalanaidu & Nayak mavayya, Ganga, Appalanaidu (niece, nephew) one of my another family Brothers and Brother-in-law's Ramesh, Srinu, Suresh, Ganesh, Ashok, Naidu, Hari, Prasanth, Satyam and Satyam bava, Krishna(Army), Srinu(Zaheer), Chiru, Akku, Mahesh, Srinu, Krishna, Girish, Rambabu, Devudu, Apparao, Suresh. I would like to express my gratitude towards Satyanarayana yedla Bava and Sanyasirao bodavalla Bava, Amar Annayya for their continuous motivation.

I am lucky to have friendly colleagues Nagamaiah, Chandrahas, Prabhakar, Anil, Uma, Satish, Majji, Junaid, Sandeep, Jagjeet, Rambabu, Chandu anna, Ashok anna, Sudhir anna, Sunil Anna, Shivani, Naidu Bava, Suresh Anna(love guru), Narendra Anna, Murali Anna Allu Srinu Anna, Nagarjuna Anna, Narayana Anna, Vikranth Anna, Obiah Anna, Nandu Anna, Satish Anna, Naren Anna, Siva Anna, Shoukath, Mohan, Sugata, Ramakrishna, Uday Anna, Harish Anna, Prasad Anna, Srinu Anna, V.V.Rao, Anif, Sudipta, Ramesh, Surendra, Subho, Rangu, Suresh, Srujana akka, Sneha, Tasnim, Sabari, Divya, Anjana, Radhika. I am thankful for my juniors Ravindar, Vinay, Hemanth, Vamshi, Vinod, Sandeep, Hema, Olivea, Sneha, Sarada, Suman, Aleem, Sumanto, Somanath, Navaneetha, Ankit, Apurba, Saddam, Soutrick, Jayakrushna, Tanmaya, Mamina, Sameeta, Sipra, Tausif, Senthil, Arun, Pritam, Ashok, Bhasha, Shailendra, Umashish, Naresh, Laxman, and Venkateshulureddy, Mangababu, Ramunaidu, Santhosh, Rana.

I am thankful to my 10$^{th}$ batch mates' Mouli, Raju, Srinu, Sai Sivani, Manognya and my +2 friends Ravi, Ramana, Jagnadham, Varma, Venki, my Degree friends Devudu, Chinnamnaidu and M.sc friends Ramana, Dinesh, Sivaganesh, Govind, Satish. Bongu, Rangaswamy, Jaggu, NNV, Surya, Rupa, Vaneela, Ramalakshmi, Bavani, Nagesh, Kurminelli, Rambabu, Kankanala, Narendra, Sai siva (Premasai). I specially thank my football, cricket (14-eliminaters), badminton, kabaddi and running friends for their entertaining cooperation and encouragement.

Lastly this acknowledgement would be incomplete without expressing my gratitude to my family members, lab mates, friends and teachers who have been a constant source of inspiration and support throughout my Ph.D. tenure. I specially thank my sister Kondamma for love and care. Without her I wouldn't have been in Ph.D. I can't imagine my life without my parents, My mother taught me the value of education and father taught me the value of hard work, without them I would be nowhere and with their blessings, I am now here.

*Suryanarayana Allu*

University of Hyderabad
November, 2020.

# SYNOPSIS

This thesis entitled "**Crystal Engineering of Novel Solid Forms of Active Pharmaceutical Ingredients and their Physicochemical Properties"** is divided into 7 chapters. Chapter 1 provides an introduction to the topic and Chapter 7 gives an overview of all the results presented in Chapters 2 to 6.

## Chapter 1: General Introduction

This Chapter gives a basic background of Crystal engineering and the design of organic solids as a mainline area in chemical research. It relies on molecular building blocks that are assembled into organized structures with desired properties and functions. Among all the intermolecular interactions, hydrogen bonds are the most important non-covalent interactions which are strong and directional in nature, and play a pivotal role in organizing the molecules in the solid state. Polymorphism in organic crystals, their different types, solvates/ hydrates and their applications in the pharmaceutical industry are described. Cocrystals, their preparation, along with examples of pharmaceutical cocrystals/ salts are described. The use of cocrystals of a few drugs following the 'spring and parachute' model for the enhancement of the solubility is covered. Details are given about the ternary cocrystals which are more difficult to prepare and relatively less published due to many possible interactions that may result due to insolubility of the components and formation of lower order aggregates of two components instead of three. Polymorphism in ternary cocrystals is a new phenomenon due to its rarity and examples are presented in the thesis.

In summary, this chapter gives a brief description of crystal engineering principles and pharmaceutical solids forms. It acts as a prelude to the working chapters of this thesis which deal with identifying novel heterosynthons for solid form development and discovering various pharmaceutical solids with promising physicochemical properties along with an analysis of their physicochemical properties.

## Chapter 2: Novel Pharmaceutical Cocrystals, Salts and Ternary Products of Bumetanide

A novel design strategy for cocrystals of the diuretic sulfonamide drug bumetanide (BUM) with carboxamides is carried out based on reliable supramolecular synthons. Binary cocrystals of BUM with pyridine carboxamides, pyridones, cytosine and 5-fluorocytosine were obtained by solvent-assisted grinding followed by solution crystallization. All cocrystal structures exhibit hydrogen bonding of the coformer with the carboxylic acid group of BUM via heterosynthons which replace the acid homodimer in the drug crystal structure. Pyridones are inserted as N−H···O dimers which are in turn bonded to the acid group of BUM, while the pyridine amide coformers interact via the acid−amide

heterosynthon. Cocrystal polymorphs were obtained for bumetanide−isonicotinamide cocrystal structure with the sulfonamide−pyridine and sulfonamide−acid synthons. Careful crystal packing analysis of BUM structure and nine new binary adducts gave an idea for the design ternary cocrystals, and four new ternary crystalline products were successfully crystallized. New crystalline forms of bumetanide, namely, four cocrystals, two salts, and one salt-cocrystal were also crystallized. Urea and lactams such as valerolactam, caprolactam, and N-methylcaprolactam formed cocrystals with bumetanide, whereas 4-aminopyridine gave a salt. Piperazine afforded a salt hydrate, and 5-fluorocytosine gave a salt-cocrystal. The supramolecular synthons in bumetanide−lactam cocrystals are amide dimer between drug and coformer, and acid homo dimer between bumetanide molecules. In bumetanide salts, the acid proton is transferred from bumetanide to coformer amine, whereas in bumetanide salt-cocrystal proton transfer and free acid were observed in the crystal structure. Furthermore, solubility, dissolution, and diffusion membrane permeability experiments were performed on all solid forms. The piperazine salt shows high dissolution and permeability crossover when compared to other binary forms of bumetanide.

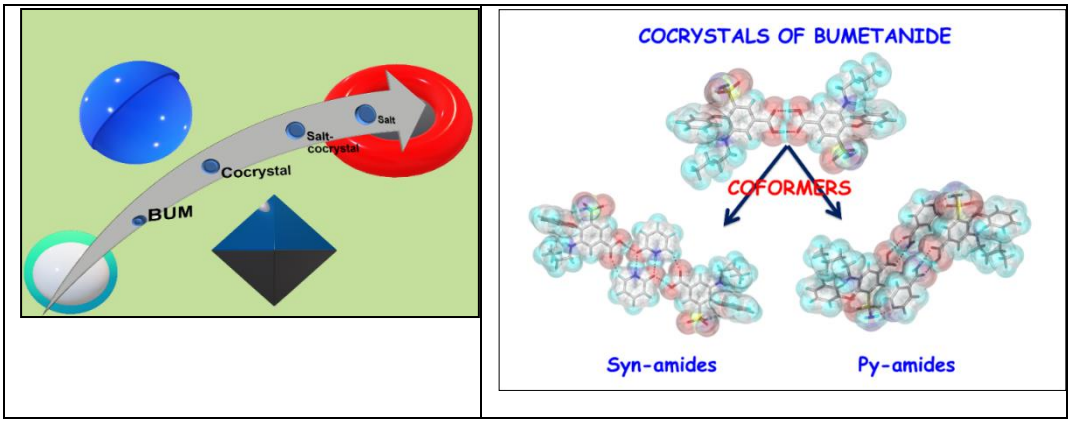


**Figure 1:** Novel crystalline forms of Bumetanide such as salt, salt-cocrystal and cocrystal, were prepared to improve the solubility and permeability of the drug. BUM with pyridines, pyridine amides and cytosine are designed to provide cocrystal structures with pyrodine dimer, acid−amide, and extended synthons of acid bonded to pyridone. The sulfonamide group is bonded as dimer or catemer chain in cocrystal structures.

## Chapter 3: Role of Hydrogen Bonding in Cocrystal and Coamorphous Solids: Indapamide as a Case Study

The relationship of supramolecular synthons with the formation of cocrystal or coamorphous forms is tested using Indapamide (IDP), a sulfonamide diuretic drug utilized in the treatment of hypertension. Cocrystals and coamorphus forms of IDP have been identified and characterized by X-ray powder diffraction (XRD), differential scanning

calorimetry (DSC) and FT-IR. The apparent solubility, dissolution and permeability studies of coamorphous IDP samples were performed in aqueous media. A systematic gradation in supramolecular synthons resulting in a cocrystal or coamorphous product of IDP is observed as the hydrogen bonds between the drug and the coformer become weaker. The stronger sulfonamide-pyridine ($SO_2NH_2\cdots Py$) and sulfonamide-carboxamide ($SO_2NH_2\cdots CONRH$) hetero synthons with rigid/ aromatic coformers drive cocrystal products while the weaker sulfonamide-amine ($SO_2NH_2\cdots NR_2H$) synthon with flexible molecules gave coamorphous products of IDP. This guidance supplements recent observations from our group on synthon strength with molecular likeness/ dissimilarity to give cocrystal, solid solution or eutectic products. Secondly, the higher aqueous solubility and better diffusion membrane permeability of IDP-ARG shows that amino acids can be used to enhance not only powder dissolution but also diffusion kinetics. Surprisingly, IDP-PIP coamorphous system was stable for up to 3 months but other piperazine derivatives of IDP were unstable and converted to the crystalline form after 24 h under the accelerated ICH conditions (40 °C, 75% RH). These findings suggest an approach to develop novel coamorphous forms and amorphous solid dispersions guided by crystal engineering for improved solid-state pharmaceuticals.

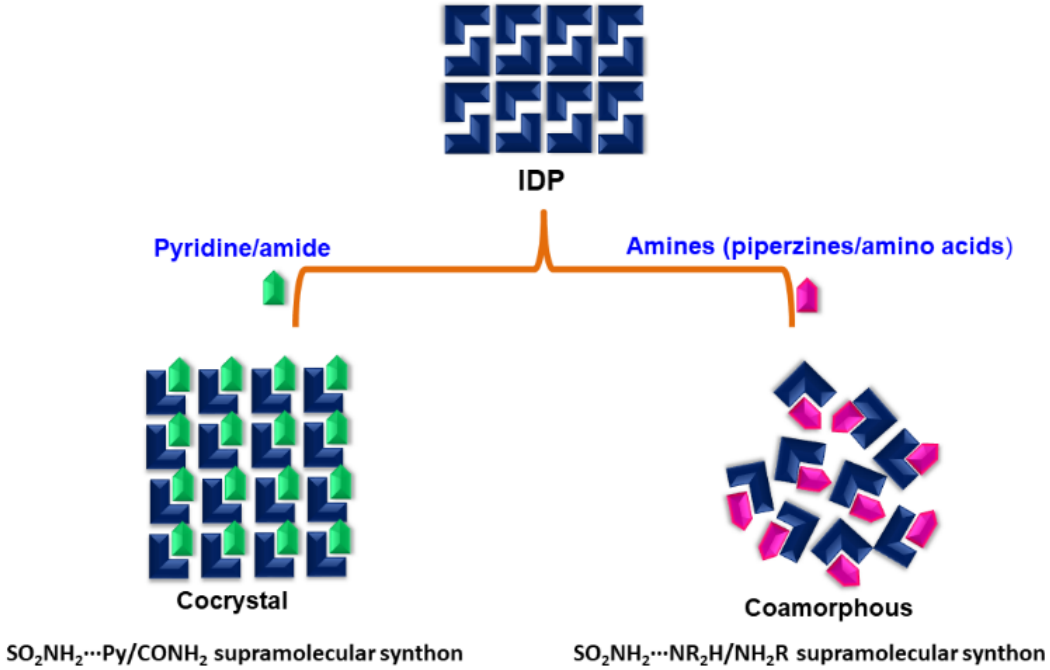


**Figure 2:** The sulfonamide-pyridine ($SO_2NH_2\cdots Py$) and sulfonamide-carboxamide ($SO_2NH_2\cdots CONH_2$) supramolecular synthons drive cocrystal formation and sulfonamide-amine ($SO_2NH_2\cdots NR_2H$ or $SO_2NH_2\cdots NRH_2$) supramolecular synthon give coamorphous adducts with amines.

## Chapter 4: Salts and Cocrystal of Etodolac: Advantage of Solubility, Dissolution and Permeability

This work deals with the salts and cocrystal screening of an anti-inflammatory drug Etodolac (ETD), which has poor aqueous solubility and high permeability. A series of salts and cocrystals of ETD were prepared to establish a relation for solubility and dissolution with respect to nature of the coformer. In case of cocrystals only one adduct ETD•INT was successfully obtained. Solubility and dissolution and permeability experiments were done for the salts in pH 7.0 phosphate buffer solution. The obtained equilibrium solubility order was $ETD^-$•$isoPA^+$ > $ETD^-$•$nHA^+$ > $ETD^-$•$cycloHA^+$ > $2(ETD)^-$•$PPZ^{2+}$ > $ETD^-$•$phEA^+$ > ETD, and IDR order was $ETD^-$•$isoPA^+$ > $ETD^-$•$nHA^+$ > $2(ETD)^-$•$PPZ^{2+}$ > ETD > $ETD^-$•$cycloHA^+$ > $ETD^-$•$phEA^+$. Analysis with respect to pH of saturated solubility media did not support any of these orders. Similarly, lipophilicity of counter ions was also not established in any direct relation with respect to the solubility and IDR. PXRD analysis showed solid phase stability of all salts under solubility and dissolution conditions. Yet another correlation with respect to melting point of salts was done but it did not show a regular trend. Analysis of intermolecular interactions showed that crystal lattice of all salts were stabilized by a network of strong N–H···O hydrogen bonds but patterns of hydrogen bonding were different in each of the salts. $ETD^-$•$isoPA^+$ showed highest solubility and dissolution rate due to lower lipophilicity of counter ion and high affinity towards hydration (since $2(ETD)^-$•$PPZ^{2+}$ is a 2:1 salt, it is difficult to compare its solubility directly with 1:1 salts of monoamines). Permeability and flux studies of ETD salts suggested that tight ion-pairs were intact during the membrane permeation process and thus directed the rate of permeability. Molecular mobility and dissolution rate were the key factors to determine the rate of permeability in the same series of salts. Consequently, $ETD^-$•$isoPA^+$ showed highest cumulative permeability and flux. Overall, short chain (low lipophilic) amines are preferred over long chain (high lipophilic) amines to improve the solubility, dissolution and permeability of new chemical entities or existing drugs like Etodolac.

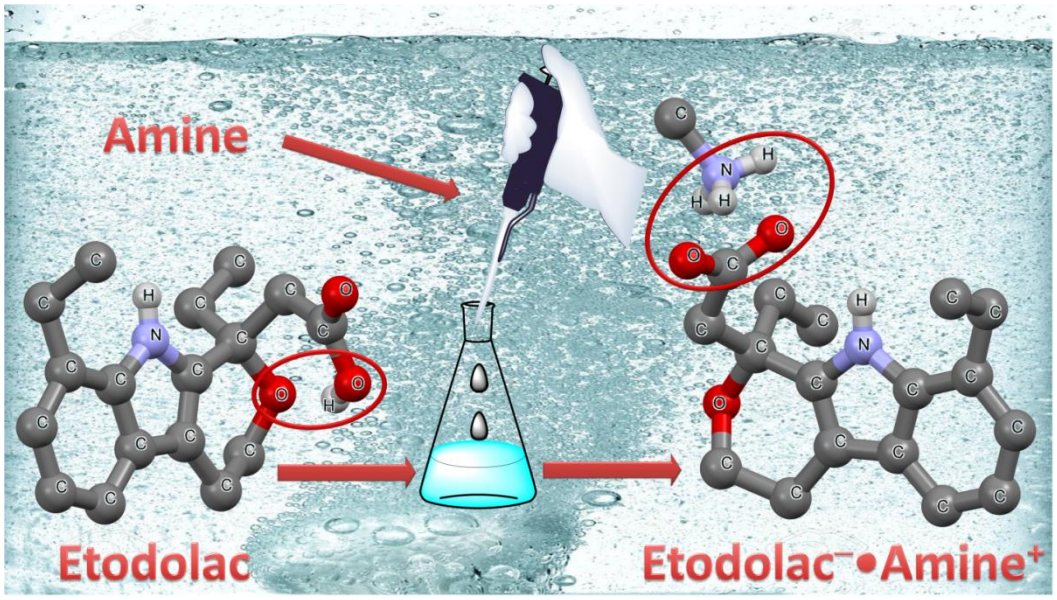


**Figure 3:** Etodolac drug with amines to improve the solubility, dissolution and other physical properties of new chemical entities or existing drugs.

## Chapter 5: Enhancing the Permeability of Acefylline in Ternary Salt, Cocrystals and Polymorphs

Acefylline (ACF), a stimulant xanthane derivative drug, in combination with piperazine, is used in the treatment of bronchial asthma. However, its poor rate of permeability limits the development of ACF drug in pharmaceutical formulation. In this chapter, ACF binary and ternary cocrystals/salt-cocrystals/polymorphs are designed and synthesized using solvent assisted grinding with various coformers. The crystal structures of the binary and ternary systems are studied by employing single crystal X-ray diffraction. One of the binary structures is studied using powder X-ray diffraction. Two polymorphic forms of the three component system ACF-GA-INA were crystallized as a rare example. The crystal structures show the role of carboxylate-pyridinium and imidazole-acid heterosynthons in the assembly of binary and ternary systems. The intermolecular interactions between ACF and various coformers are further corroborated from the Hirshfeld surface analysis, 2D fingerprint plots and energy analysis. The permeability of ACF increases in binary and ternary systems, which is rationalized by the lowering of melting point. ACF ternary systems exhibit higher drug permeability as a route to improve bioavailability and development of ACF oral formulation.

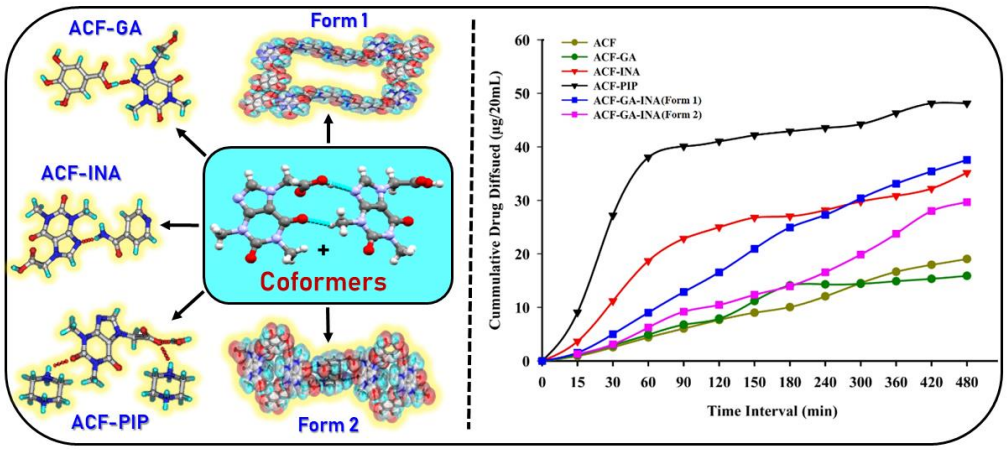


**Figure 4:** Enhancing the permeability rate of Acefylline by designing ternary salt cocrystals/polymorphs

## Chapter 6: Synergistic Interactions in Tinidazole Cocrystals with Acid-hydroxyl Synthon and their Dissolution and Permeability

Tinidazole (TNZ) is a 5-nitroimidazole derivative used as an antiamoebic, antiprotozoal, antibacterial, antiparastic and also used to treat vaginal trichomoniasis including giardiasis. TNZ is BCS class II drug with low solubility and high permeability. Nine novel solid forms (cocrystals) of tinidazole (TNZ) were synthesized with both aliphatic acids like oxalic acid (OA), citric acid (CA) and aromatic acids like 2,6-dihydroxy benzoic acid (2,6-DHBA), 4-Hydroxy benzoic acid (PHBA), 4-amino benzoic acid (PABA), Ferulic acid (FA), p-coumaric acid (PCA), and vanilic acid (VA). The acid-imidazole and acid-acid supramolecular synthons are observed in TNZ-OA, TNZ-CA, TNZ-2,6-DHBA cocrystals. FA, PCA, VA, PHBA, PABA coformers form different synthons with tinidazole, such as phenol-imidazole, acid-acid dimer, amine-carbonyl and nitroimidazole dimer synthons in crystal structures. Preference of acid-imidazole and/or hydroxy-imidazole was studied computationally and validated via experimental cocrystal synthesis. Solubility, dissolution and permeability experiments were performed on TNZ and new solid forms show high dissolution rates: TNZ-2,6DHBA, TNZ-FA, TNZ-OA, TNZ-CA, and TNZ-PCA. All products were characterized by PXRD, SC-XRD, DSC and IR. Similarities and differences in the crystal packing and thermal behavior of crystalline materials are also presented.

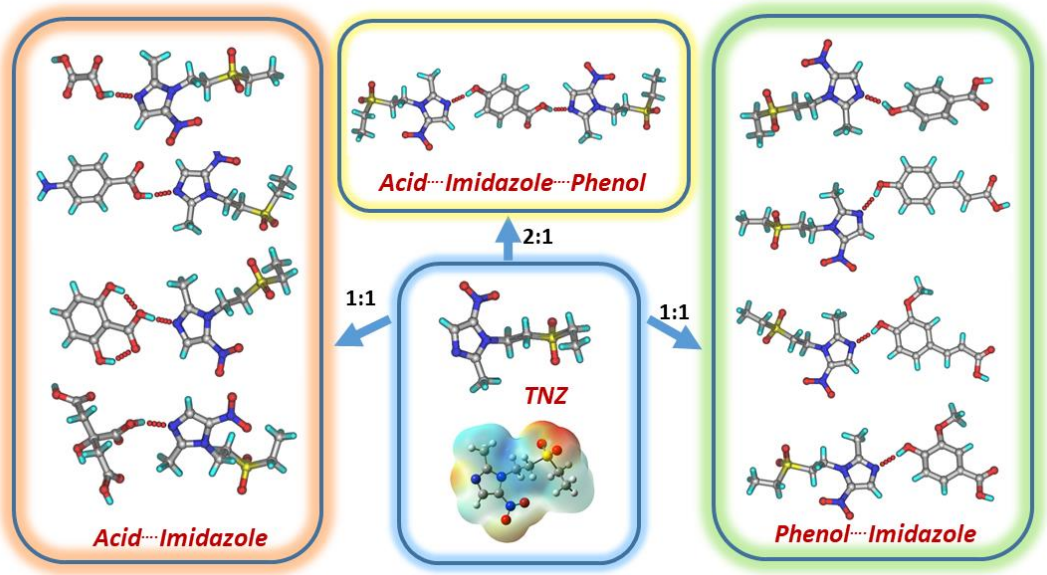


**Figure 5:** Different supramolecular synthons observed in TNZ cocrystals.

## Chapter 7: Conclusions and Future Prospects

From the above five working chapters 2 to 6 the following summary and conclusions can be drawn. Crystal engineering principles and hydrogen bonding rules were applied to a few pharmaceutical drugs to improve the physicochemical properties such as solubility and dissolution rate and increase melting point and stability. Polymorphism is important in both pharmaceutical and materials science. In recent years, polymorphism has gained attention in the pharmaceutical industry to avoid late stage discovery setback of new polymorphic forms and patent litigations. In this thesis, studies are described on various solid forms such as salts, cocrystals, polymorphs and coamorphous compounds. In chapter 2, bumetanide cocrystals, salts and ternary products were prepared which have potential pharmaceutical applications. In chapter 3, the role of hydrogen bonding in cocrystals and coamorphous solids of IDP was investigated. The results showed that hydrogen bonding is considerably stronger in the cocrystals compared to coamorphous forms. Chapter 4 deals with improving pharmacological properties of ETD through various salts of ETD with amines containing different chain lengths. The salts showed higher solubility, dissolution rate and permeability along with phase stability. A designed ternary cocrystal of acefylline with coformers is discussed in chapter 5. The ternary cosryatsl ACF-INA-GA (1:1:1) exhibits dimorphism with higher solubility, dissolution rate and permeability than ACF. The remaining ternary complexes were formed in non-stoichiometric ratios. In chapter 6, cocrystals of TNZ with different coformers showed better physicochemical properties. The acid-imidazole and/or hydroxy-imidazole synthons in this cocrystal were studied computationally and validated by experimental cocrystal synthesis. These studies improve our understanding and knowledge about crystal engineering of novel organic solid forms of active pharmaceutical

cocrystals, polymorphs, slats and coamorphous forms to improve physicochemical properties and pharmacological activity and their potential use in novel pharmaceutical formulations.

# CONTENTS


Declaration……. i

Certificate ……..... iii

Acknowledgements……..... v-vi

Synopsis ……..... vii-xiv

Contents …… xv-xvii

## Chapter 1

**Introduction to Crystal Engineering of Novel solid forms of Active Pharmaceutical Ingredients** **1-42**

1.1 Introduction to supramolecular chemistry …… 2
1.2 Crystal Engineering …….. 3
1.3 Introduction to Pharmaceutical Drugs ……..…… 6
1.4 Non-covalent interactions …...……...……... 8
1.5 Classification of pharmaceutical solids …… 10
1.6 Polymorphism ……..... 11
1.6.1 Classification of Polymorphs …… 12
1.6.2 Ostwald's Law of Stages …….. 15
1.6.3 Solvates and Hydrate-Pseudopolymorphism ……..…….. 17
1.7 Pharmaceutical salts …….. 18
1.8 Cocrystals ……..... 19
1.8.1 Supramolecular synthon …… 21
1.8.2 Ternary Cocrystals …… 22
1.8.3 Applications of cocrystals …… 23
1.9 Amorphous solids ……..... 26
1.9.1 Coamorphous solids ……..……..... 27
1.10 References ……..... 28

## Chapter 2

**Novel Pharmaceutical Cocrystals, Salts and Ternary Products of Bumetanide** **43-100**

2.1 Introduction ……... 43
2.2 Results and Discussion…….. 45
2.2.1 Crystal Structure Description …..…… 46
2.2.2 Conformational Analysis……... 66
2.2.3 Powder X-ray Diffraction ……..…… 68
2.2.4 Thermal Analysis……..…….. 71
2.2.5 Infrared Spectroscopy ……...…… 72
2.2.6 Solution NMR ……...……..... 76
2.2.7 Solubility and Dissolution Studies.....…… 81
2.2.8 Diffusion Measurements ……..…….. 85
2.3 Conclusions ……... 87
2.4 Experimental Section……. 88
2.5 References.....……. 95

## Chapter 3

**Role of Hydrogen Bonding in Cocrystal and Coamorphous Solids: Indapamide as a Case Study** **101-143**

3.1 Introduction…… 102
3.2 Results and Discussion…….. 104
3.2.1 Crystal Structure Description …… 105
3.2.2 Conformational Analysis ……..……. 111
3.2.3 Powder X-ray Diffraction ……..…… 112
3.2.4 Thermal Analysis ……..…… 115
3.2.5 Infrared Spectroscopy ……... 118
3.2.6 Solution NMR ……..…… 121
3..2.7 Solubility and Dissolution Stability studies ……..……... 129
3.2.8 Diffusion Measurements ……. 133
3.3 Conclusions ……. 102
3.4 Experimental Section …….. 135
3.5 References …….. 139

## Chapter 4

**Salts and Cocrystal of Etodolac: Advantage of Solubility, Dissolution and Permeability** **144-177**

4.1 Introduction…… 145
4.2 Results and Discussion…….. 147
4.2.1 Crystal Structure Description..……. 148
4.2.2 Powder X-ray Diffraction ……..……. 157
4.2.3 Thermal Analysis……..…….. 158
4.2.4 Infrared Spectroscopy ……... 160
4.2.5 Solubility and Dissolution Studies ……..…….. 161
4.2.6 Diffusion and Flux Study..... 165
4.3 Conclusions..... 167
4.4 Experimental Section..... 168
4.5 References…….. 172

## Chapter 5

**Enhancing the Permeability of Acefylline by in Ternary Salt, Cocrystals and Polymorphs** **178-230**

5.1 Introduction…… 179
5.2 Results and Discussion …..... 180
5.2.1 Crystal Structure Description....…… 184
5.2.2 Hirshfeld Surface Analysis …..…… 196
5.2.3 Structure solution from powder diffraction data …… 206
5.2.4 Powder X-ray Diffraction …..……. 207
5.2.5 Thermal Analysis ……..... 208
5.2.6 Solution NMR ……...…… 210
5.2.7 Permeability and Solubility Studies …… 214
5.3 Conclusions ……..... 216
5.4 Experimental Section ……..……..... 217
5.5 References …….. 223

## Chapter 6

**Synergistic Interactions in Tinidazole Cocrystals with Acid-hydroxyl Synthon: Dissolution and Permeability** **231-276**

6.1 Introduction…… 232
6.2 Results and Discussion.....…….. 233
6.2.1 Crystal Structure Description...……. 234
6.2.2 Molecular electrostatic potential calculations...…… 246
6.2.3 Conformational Analysis ……. 252
6.2.4 Powder X-ray Diffraction ……..…… 254
6.2.5 Thermal Analysis ……..……. 255
6.2.6 Infrared Spectroscopy ……... 256
6.2.7 FE-SEM Analysis ……. 258
6.2.8 Solubility and Dissolution Studies …… 259
6.3 Conclusions ……... 264
6.4 Experimental Section …… 264
6.5 References ……. 269

## Chapter 7

**Conclusions and Future Prospects** **277-282**

7.1 Conclusions…… 277
7.2 Future Prospects……. 281
About the Author…….. 283
List of Publications……... 284
Participation in Symposia, Workshops & Conferences…… 285

# *CHAPTER ONE*

## Introduction to Crystal Engineering of Novel solid forms of Active Pharmaceutical Ingredients

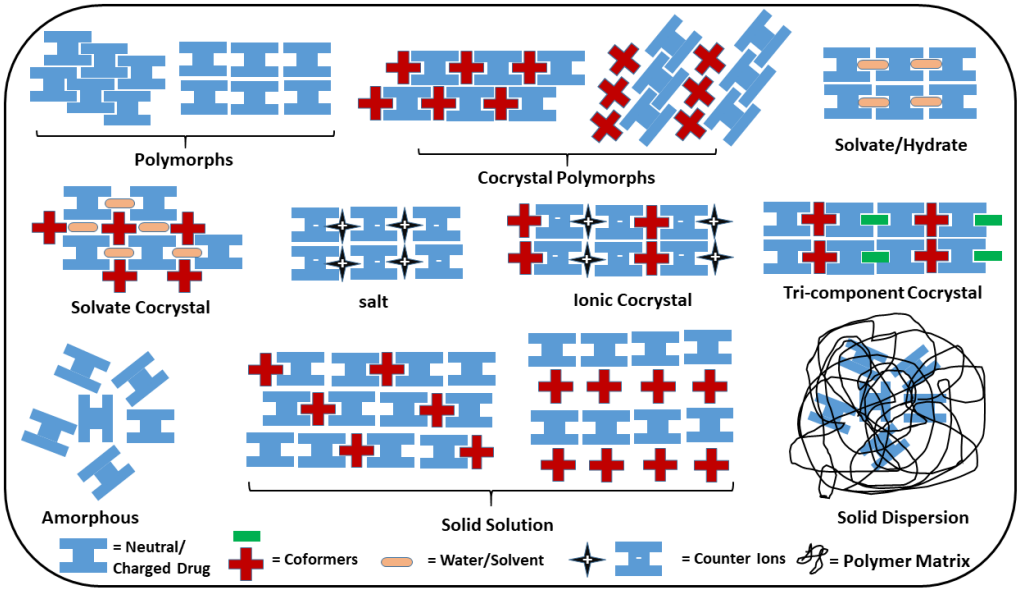


***Schematic representation of the possible different solid forms (a) Polymorphs (b) Cocrystal Polymorphs (c) Solvate/Hydrate (d) Solvate Cocrystal (e) Salt (f) Ionic Cocrystal (g) Tri-component Cocrystal (h) Amorphous (i) Solid Solution (j) Solid Dispersion.***

## 1.1 Introduction to supramolecular chemistry

Supramolecular chemistry[1] is revolutionary to the field of chemistry. The pioneering work of Charles Pedersen, Jean-Marie Lehn and Donald Cram in the 1960s was an inspiring impetus to chemistry[2], and in particular to organic chemistry, which was about 200 years old at that time. The field of supramolecular chemistry is among one of the most interesting and promising ones in chemistry. Although relatively young, it has advanced rapidly over the years and has reached a high level of sophistication and maturity. The terms of supramolecular chemistry as an emerging field were introduced in 1978 by Jean-Marie Lehn as a development and generalization of earlier works[3-4] *"As there is a field of molecular chemistry based on covalent bond, there is a field of molecular assemblies and of intermolecular bonds"* reformulated later as "*Supramolecular chemistry may be defined as "chemistry beyond the molecule*". This successful attempt to organize old and novel chemistries represents the moment when supramolecular chemistry was clearly established and gave rise to a new language, new concepts, and applications[5-7].

Supramolecular chemistry takes its origin in organic chemistry, which itself derives from studying the chemistry of living systems. The synthetic power of organic chemistry made possible to synthesize useful natural products and to prepare complex artificial pharmaceutical molecules. This branch of chemistry started to develop from mid1960's and honored with Noble prize in chemistry in 1987 to three pioneers in this area namely Pedersen, Lehn and Cram[2]. According to Jean Marie Lehn, "Supramolecular chemistry, the designed chemistry of the intermolecular bond, is rapidly expanding at the frontiers of molecular science with physical and biological phenomena." Similarly, Emil Fischer's Lock-and-Key concept for enzyme-substrate interactions,[8-9] coordination chemistry principles from Alfred Werner[10] and Paul Ehrlich's molecular receptors[11] encouraged and guided to establish principles of supramolecular chemistry. Numerous number of articles and books were published on the principles of supramolecular chemistry[12-14, 4]. For better understanding, one should have knowledge on molecular chemistry as well as noncovalent molecular interactions on self-assembly to tune the structure, properties and performance of products (Figure 1.1). Lehn quoted that*," Molecular chemistry, the chemistry of the covalent bond, is concerned with uncovering and mastering the rules that govern the structures, properties and transformations of molecular species".* The

design and understanding of such noncovalent intermolecular interactions in the solid state is referred to as "Crystal Engineering[12]."

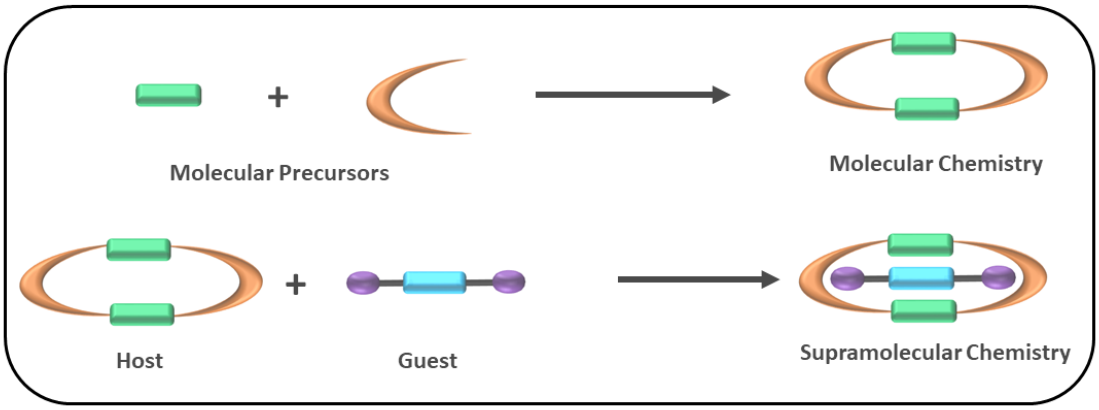


**Figure 1.1:** Comparison between the scope of molecular and supramolecular chemistry (Lehn)

## 1.2 Crystal Engineering

The physical and chemical properties of Molecular crystals are different from other categories of crystalline substances, which are closely related to the internal periodic arrangement of molecules. Crystal engineering has given rise to the understanding of intermolecular interactions in the molecular solids and to apply them in designing solid-state assemblies with tailor-made properties[15-16]. The main objective of crystal engineering is to tune the physiochemical properties of crystalline solids at molecular level. It uses chemistry along with crystallography to understand molecular solids[17]. In 1955, Pepinsky[17] introduced the term "Crystal Engineering" but it was conceptualized and elaborated by Gerhard Schmidt in connection with photodimerization reactions in crystalline cinnamic acids[18-19](Figure 1.2). Crystal Engineering is defined as "*the understanding of intermolecular interactions in the context of crystal packing and the utilization of such understanding in the design of new solids with desired physical and chemical properties*". In 1921, the evolution of crystal engineering began by Bragg's[20]. In his observation, he noted that the unit cell parameters of two axial lengths were nearly same whilst third was 8.66 Å in naphthalene and 11.66 Å in anthracene. Subsequently Robertson, who is the student of W. H. Bragg made significant contributions on a large number of polynuclear aromatic hydrocarbons based on the molecular thickness and molecular area. Similarly, Bernal proposed molecular structures phenanthrene related aromatic hydrocarbons from crystal unit cell parameters[21-24]. Schmidt and his coworkers

realized the importance of X-ray crystallography and foundation of the new subject, "*organic solid-state chemistry"* was laid. Initially, he studied the solution state (2+2) photo addition reaction in *trans*-cinnamic acid and its derivatives and there was no progress which made him work on different state i.e., solid state and an excellent control on initiation and progress observed throughout the reaction, the obtained products are comprehensible and significant[18-19, 25].

In later years, chemical crystallographers made tremendous effort at the designing of reactive solids. Scientists, Mendel Cohen, Meir Lahav and Leslie Leiserowitz successfully designed topochemical 2+2 reactions and group headed by John M. Thomas developed cyclic ketones, namely the 2-benzyl-5- benzylidenecyclopentanones, which showed an interdependence of crystal structure and solid state reactivity[25-26]. Later in the period of 1970s to 1980s, the importance of intermolecular interaction has increased tremendously, in the same period A. I. Kitaigorodskii invoked a question "molecules to crystals" and addressed that packing of molecular solids was largely governed by considerations of size and shape, the so-called principle of close packing[27-28]. In 1986, Desiraju and J. A. R. P. Sarma tried to explain the Schmidt's observations on the chloroaromatic compounds on the basis of Cl···Cl short interaction, now it is called halogen bond. A new era of modern crystal engineering started with the monograph by Desiraju entitled as *"Crystal Engineering: The Design of Organic Solids"* later in 1995 further he introduced the term supramolecular synthon to design new multicomponent molecular crystals[29-30].

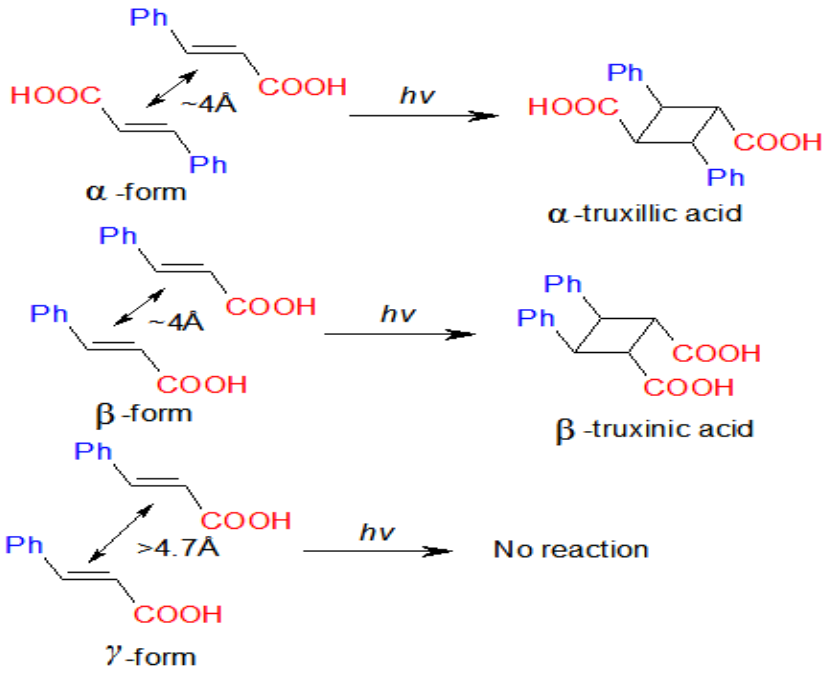


**Figure 1.2:** Photo irradiation of α, β forms of trans-cinnamic acid

**Table 1.1:** The Timeline of Crystal Engineering

| Year | Scientist | Event |
|---|---|---|
| 1828 | F. Wohler | Idea of molecule by synthesis of Urea from ammonium cyanate |
| 1873 | van der Waals | Existence of intermolecular forces |
| 1894 | Emil Fisher | "lock and key" model for enzyme-substrate interactions |
| 1920's | L. Pauling | Systematization of interionic distances |
| 1921 | W. H. Bragg | Crystal structure correlations of naphthalene and anthracene |
| 1935 | J. D. Bernal | Forerunner of crystallographic databases |
| 1948 | H. M. Powell | Network structure of β-hydroquinone |
| 1951 | J. M. Robertson | Crystal structure of polynuclear hydrocarbons |
| 1955 | R. Pepinsky | Coined the term 'Crystal engineering' |
| 1964 | G. M. J. Schmidt | Principles of photo dimerization in Cinnamic acids |
| 1967 | E.J. Corey | Defined the synthon |
| 1969 | Jean-Marie Lehn | Defined the term supramolecular chemistry |
| 1973 | A. I. | Described the close packing principle in Molecular crystal |

| | | |
|---|---|---|
| | Kitaigorodski | and molecule |
| 1977 | A. Ludi | Crystal structure determination of Prussian Blue |
| 1988 | O. Ermer | Crystal structure of interpenetrated organic compound adamantine-1,3,5,7-tetracarboxylic acid |
| 1989 | G. R. Desiraju | A general definition Crystal Engineering |
| 1990 | R. Robson | Coordination polymers chemistry introduced. |
| 1990 | M. C. Etter | Hydrogen bond rules |
| 1991 | J. D. Dunitz | Used the term *supramolecule par excellence* |
| 1995 | G. R. Desiraju | Concept of '*Supramolecular Synthon'* introduced. |

## 1.3 Introduction to Pharmaceutical Drugs

A drug (Active Pharmaceutical Ingredient) is a chemical substance that is used for diagnosis, prevention, treatment/cure of disease by exploring physiological systems or pathological states in the form of a medicine[31-34]. Drugs can initiate the pharmacological action only when they are absorbed and distributed all over, including sites of action, through the systemic circulation[35]. Thus drug absorption is an important key step where the fraction of administered dose that gets absorbed. Depends on the choice of appropriate route, various drugs can be administered. Thus the route of administration has been broadly divided into two types. One of them is local action (topical, deeper tissue, arterial supply) and other was systematic routes (oral, sublingual, rectal, cutaneous, inhalation, nasal, parenteral) [36-38]. The oral route is the most assessable, acceptable and affordable route of administration. The absorption through the oral route can be effected by physicochemical properties like water solubility, physical/chemical stability, permeability which influences bioavailability of a drug. The drug was sold out in solid form due to its ease of manufacture, storage and convenience to patients which are in the form of tablet, capsule, or lyophilized powder forms[39-41].

The Biopharmaceutics Classification System (BCS) was introduced by Amidon[42] on the interpretation of the kinetics and dynamics of the drug, which were divided into four Classes based on solubility and permeability (Figure 1.3). BCS is a regulatory mechanism through which drug companies can obtain a waiver of clinical bioequivalence called bio waiver. According to the 2000 US-FDA BCS Guidance, compounds that are classified as Class I (highly soluble, highly permeable) are eligible for BCS bio waivers. For such compounds, the rate and extent of drug absorption is

unlikely to be affected by drug dissolution and/or GI tract and permeability across the cell membrane[43]. About 40% of drugs (mainly BCS II and IV dugs) and emerging new chemical entities (NCEs) under research and development exhibit poor aqueous solubility. Such drug candidates and nutraceutical molecules tend to be eliminated from the gastrointestinal tract before they get completely dissolved and absorbed into the blood circulation. This results in low bioavailability and less potency. In case of low solubility, drug augmentation would be required. However drug augmentation may lead to adverse/toxic effects on human body. Thus, novel forms without doing any chemical modification of the drug for an optimal pharmaceutical solid formulation greatly reduces the risk, time and cost in drug development[44-48]. The polymorphs are the conventional practice in the solid space later followed by ionic salts, non-organized atoms leads to amorphous, binding solvate or hydrate in the crystal lattice, cocrystal, eutectic, solid solution/alloy and coamorphous solid blended with excipients (polymeric matrix) etc. Broadly, these solid forms demonstrates superior physicochemical properties, for instance the good flowability leads to better solubility with greater dissolution rate that result in bioavailability, as a final point to govern the drug efficiency. Thus the study of solid state chemistry of drugs has fundamental importance in the optimization of a drug solid form in pharmaceutics. This process is decisive for better patient's compliance through oral administration. Understanding the nature of solid forms in terms of their molecular packing, stability, and physicochemical properties will avoid complications in drug development

Simply the classification of BCS categories in terms of solubility and permeability:

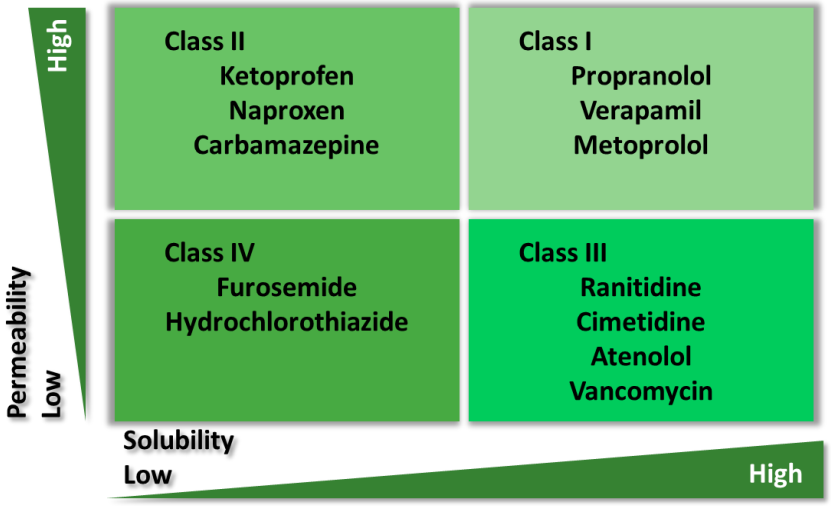

**Figure 1.3:** Biopharmaceutics Classification System of drugs (adapted form adsorption systems website)

## 1.4 Non-covalent interactions

Jeremy M. Berg stated that "*Readily reversible, non-covalent molecular interactions are key steps in the dance of life. Such weak, non-covalent forces play essential roles in a faithful replication of DNA, the folding of proteins into intricate three-dimensional forms, the specific recognition of substrates by enzymes, and the detection of molecular signals".* The well-known covalent bond is formed by the sharing of electrons. Covalent bond is strong and have high bond energies whereas, non-covalent interactions are weak and reversible in nature, plays a crucial role and reveals the structure and functions of many biological functions. Over the last few decades, researchers are consciously working on non-covalent interactions for the synthesis of materials, molecular recognition and molecular machines etc. Classification of non-covalent interactions is shown below (Figure 1.4).

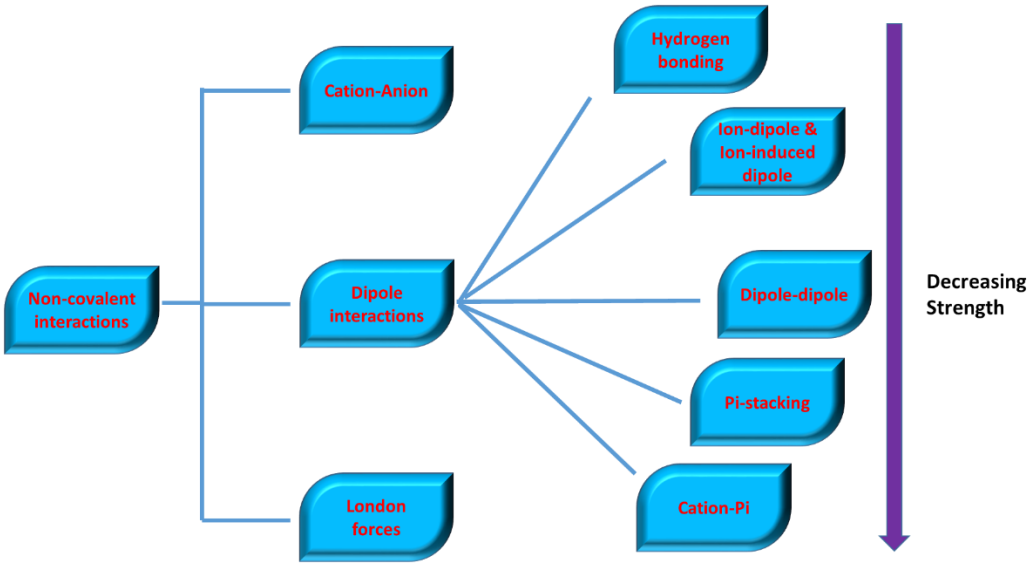


**Figure 1.4:** Classification of non-covalent interactions.

### Hydrogen bond

The hydrogen bond is *an "attractive interaction between a hydrogen atom from a molecule or a molecular fragment X–H in which X is more electronegative than H, and an atom or a group of atoms in the same or a different molecule, in which there is evidence of bond formation".*

Hydrogen bond is one of the non-covalent interactions and plays a crucial role in supramolecular chemistry, crystal engineering, materials science and biological sciences[49]. The hydrogen bond phenomenon was first introduced by Nernst in 1891. George A. Jeffrey and Wolfram Saenger felt that "*The discovery of the hydrogen bond could have won someone the Nobel Prize, but it didn't"*, shows of the thinking about hydrogen bonding[50-57] at that time. In 1935-36 Bernal and Huggins proposed the term "Hydrogen bond". The classic hydrogen bond can be represented as X-H···Y–Z, here the three dots represents the bond. And the hydrogen bond donor is represented by X–H. The Y denotes as an acceptor it can be an atom or an anion, or Y is bonded to Z depicts as Y-Z (fragment or a molecule). In some cases, X and Y both looks same. In particular, X and Y are the same when X–H and Y–H distances are identical as well give rise to symmetric hydrogen bonds. In any case, the acceptor will be an electron rich region such that there is no limited to a lone pair of Y /π bonded pair of Y–Z. Hydrogen bonds are electrostatic in nature and plays pivotal role in stabilizing the molecular aggregates. Neutron diffraction, NMR, IR and other spectroscopic techniques can be used to investigate the hydrogen bonding (Figure 1.5).

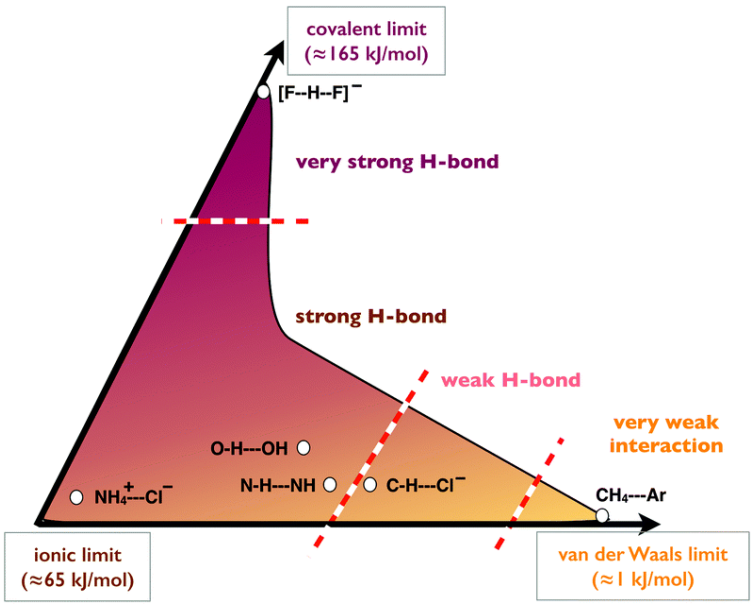


**Figure 1.5:** Hydrogen Bridge with different interactions

❖ Ion dipole & ion induced dipole: In ion-dipole interaction, one pole of a dipole is attracted to an oppositely charged ion. Whereas in ion-induced dipole interaction

an ion approaches a molecule without dipole and causes a change in the distribution of charges to induce a dipole.

- ❖ Dipole-Dipole Interactions: When bond dipoles are attracted to opposite charges: the positive end of one dipole is attracted to the negative end of the second dipole.
- ❖ Cation-Pi: When a cation is electrostatically attracted to a pi electron cloud.

## 1.5 Classification of pharmaceutical solids

Generally, solids can be classified into either crystalline or amorphous depending on the lattice structure, rigidity of the solid. The pharmaceutical solid may exists in a single or multicomponent system, either as crystalline or amorphous state. Polymorphs are the different crystalline arrangements of the same chemical substance and those with multicomponent (two or more neutral chemical species) in a single crystalline solid referred to co-crystal. Ionic co-crystals are salts forms interacting with organic compound in the crystal lattice. The supramolecular family of multicomponent solids therefore includes salts, hydrates, solvates, cocrystals, eutectics, solid solutions, alloys, etc. all are assessed as pharmaceutical forms (Figure 1.6-1.7). In co-crystal and eutectic solids, the stoichiometry is fixed whereas in alloy multiple components are present. Polymorphism is possible in multicomponent crystalline solids such as salts, cocrystals, solvates etc. In coamorphous solids, the stoichiometric ratios of two or more solids are held together through weak, but discrete interactions in an aperiodic arrangement; the individual components are crystalline but the resulted adducts are X-ray diffraction amorphous (broad halo peak).

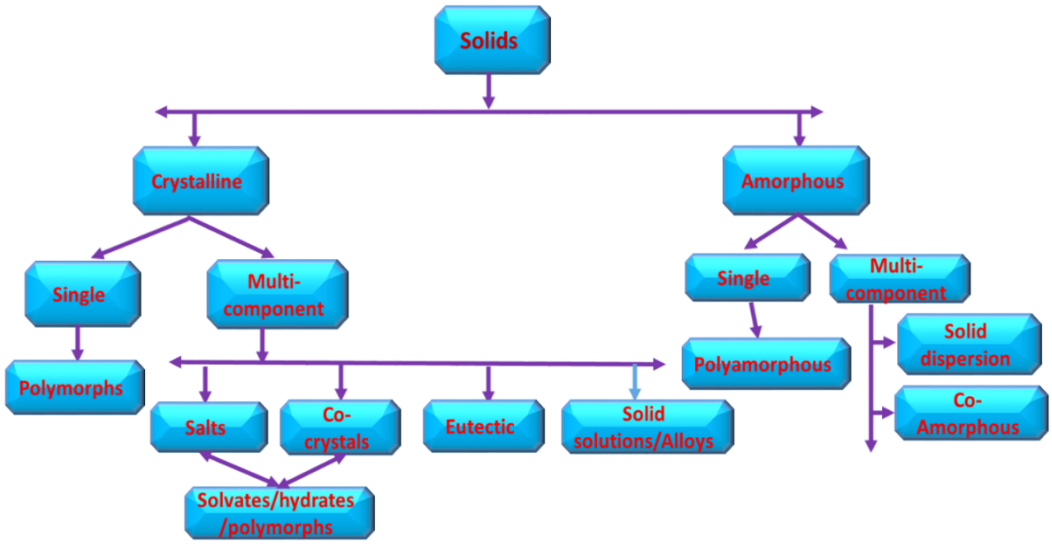


**Figure 1.6:** Classification of Pharmaceutical solids.

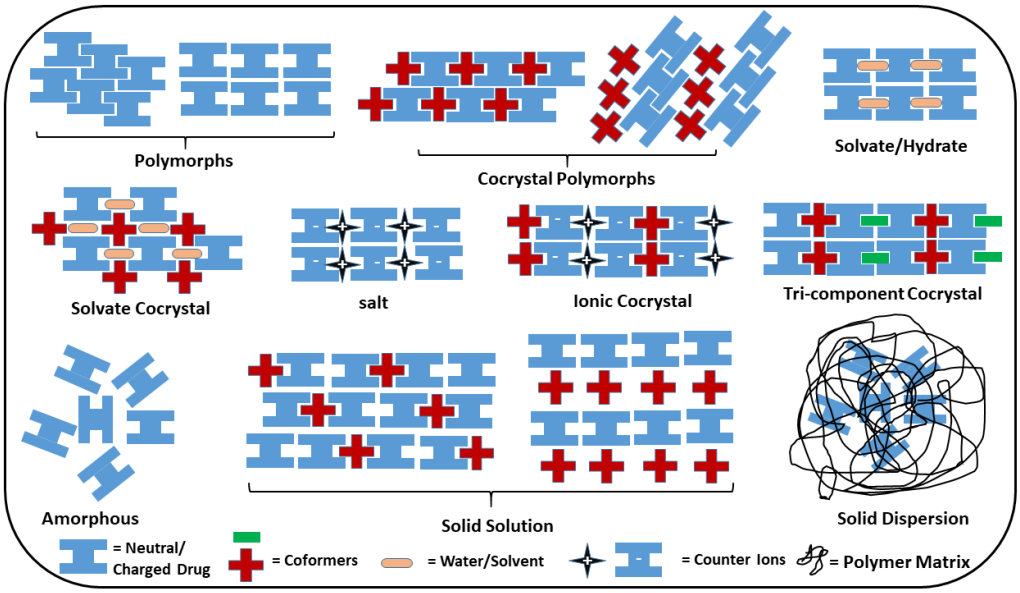


**Figure 1.7:** Different types of the various pharmaceutical solid forms (a) Polymorphs (b) Cocrystal Polymorphs (c) Solvate/Hydrate (d) Solvate Cocrystal (e) Salt (f) Ionic Cocrystal (g) Tri-component Cocrystal (h) Amorphous (i) Solid Solution (j) Solid Dispersion.

## 1.6 Polymorphism

The word "*Polymorphism*" originally comes from the Greek (*poly* = many, *morph* = form). Even though in the early nineteenth century, the concept of existence of different crystal forms came into existence, the widely accepted definition for polymorphism was given by McCrone[58-59]. He stated that "*a polymorph is a solid crystalline phase of a given compound resulting from the possibility of at least two different arrangements of the molecules of that compound in the solid state*". Another scientist, Burger simplified it as "*if these (solids composed of only one component) can exist in different crystal lattices, then we speak of polymorphism*". In modern chemistry, a crystal is described as a 'supermolecule par excellence' by Dunitz[60]. In his view polymorphic modifications are 'superisomers' and polymorphism is a kind of 'superisomerism'. In materials science, polymorphism is the ability of a solid material to exist in more than one form or crystal structure. It can be found in any crystalline material including polymers, minerals, and metals, and is related to allotropy, which refers to chemical elements. It is relevant to the fields of pharmaceuticals, agrochemicals, pigments, dyestuffs, foods, and explosives[61-64].

In 1822, Mitscherlich, documented the word polymorphism in the extent of crystallography[65]. He discovered the different crystal forms of arsenates and phosphates. Berzelius[66] mentioned polymorphism as an allotrope that exists in different forms for the same crystal structure. If there is structural diversity in the molecular compounds called as polymorphism whereas if there is structural diversity of elements called as allotropes[67-68]. The invention of polarizing microscope by Amici in the year 1844 is certainely witnessed the development of chemical crystallography in polymorphism[69]. Mallard defined the difference in packing arrangement for the minute crystallites result in different crystal forms[70]. The change in phase as irreversible monotropic and reversible enantiotropic in the polymorphism was initially characterized by Lehman in 1891[71]. In 1897, Ostwald[72] carried huge development in polymorphism, and found that for a particular solvent, metastable polymorphic means unstable forms have an increased solubility than the chemically stable forms and later it became the well-known "Rule of Steps" on relative polymorph's stability. In the early twentieth century many experimental and theoretical models were introduced such as to see variation of crystallites on hot stage microscopy (Lehman, 1891), solubility measurement, heat capacity and transition point determination, the Clapeyron equation and Gibbs Phase Rule are to determine thermodynamic relations to test the early observations and experimental outcomes. Identification and characterization of materials became easy with the help of polarizing microscope. Later Bloom and Buerger stated the change in the fundamental property and polymorphism importance. Later on McCrone worked on the pharmaceutical importance of polymorphism[73-78, 58].

## 1.6.1 Classification of Polymorphs

With reference to literature, polymorphs synonymously are so-called as 'forms', or their 'modifications'/ 'phases' and denoted by numerals (Arabic: 1,2,3,4 etc. and Roman numbers: I, II, III, IV etc.) or with an alphabets (Greek: α, β, γ,δ etc. and an English: A, B,C,D etc.). Polymorphs can be broadly classified into three types[79] i) Packing polymorphism ii) Conformational polymorphism and iii) Synthon polymorphism (Figure 1.8). Conformational polymorphism is the variance in molecular structure lead to dissimilar crystal structures of the same molecule. e.g. dimorphs of oligothiophene derivative[80] and N-acetyl cysteine[81](Figure 1.9). Synthon polymorphism is the non-covalent interactions or supramolecular synthons which are different in different crystal structures of the same molecule. e.g. Eparlestat (EPR) polymorphs[82]. Packing

polymorphism is the arrangement of molecules varies in crystal structures. By default all the polymorphs can be classified under packing polymorphism because all the polymorphs differ in their packing. Although these diverse classifications are subjective since overlapping is possible among them and coexist more than one in a specified system. For e.g. synthon conformations and synthon polymorphs of furosemide the diuretic drug [83] and anti-diabetic aldose reductase enzyme inhibitor eparlestat. Eparlestat is also an example for color polymorphism[82-85]. Figure 1.10 and 1.11)

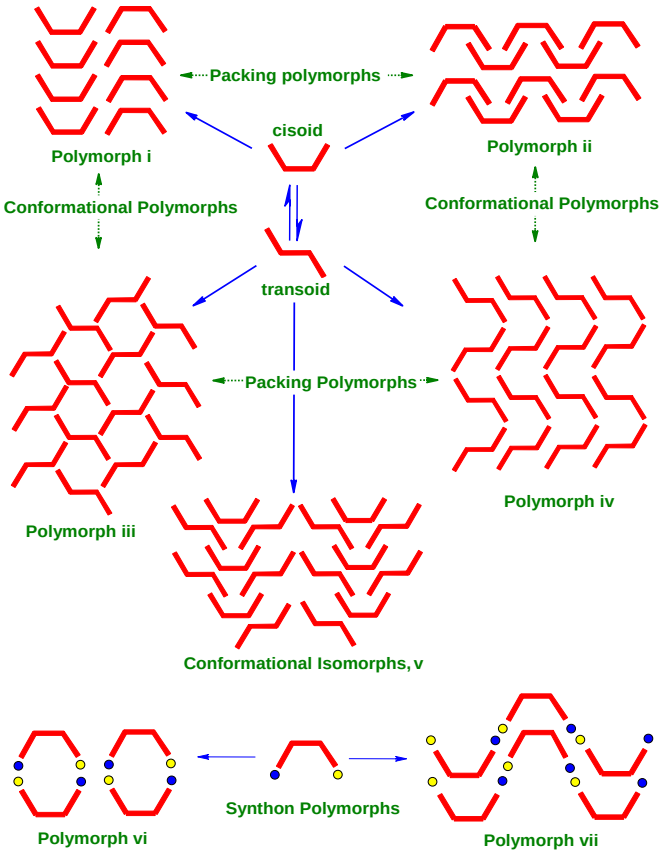


**Figure 1.8:** Schematic representation of different types of polymorphs (Adapted from Reference 79).

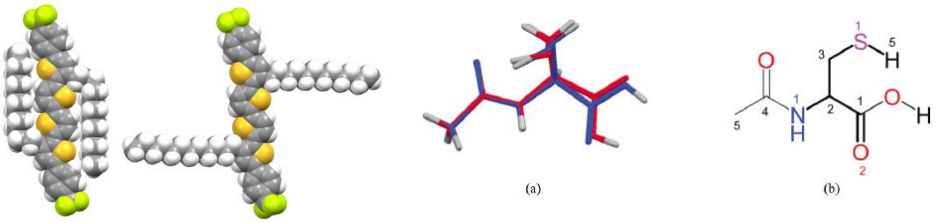

(a) (b)

**Figure 1.9** (a) Oligothiophene derivative of conformational polymorphism (Adapted from ref. 80) (b) Overlay of molecular conformations (red form I and blue form II) and main conformational difference are highlighted in bold single bonds (Adapted from ref. 81).

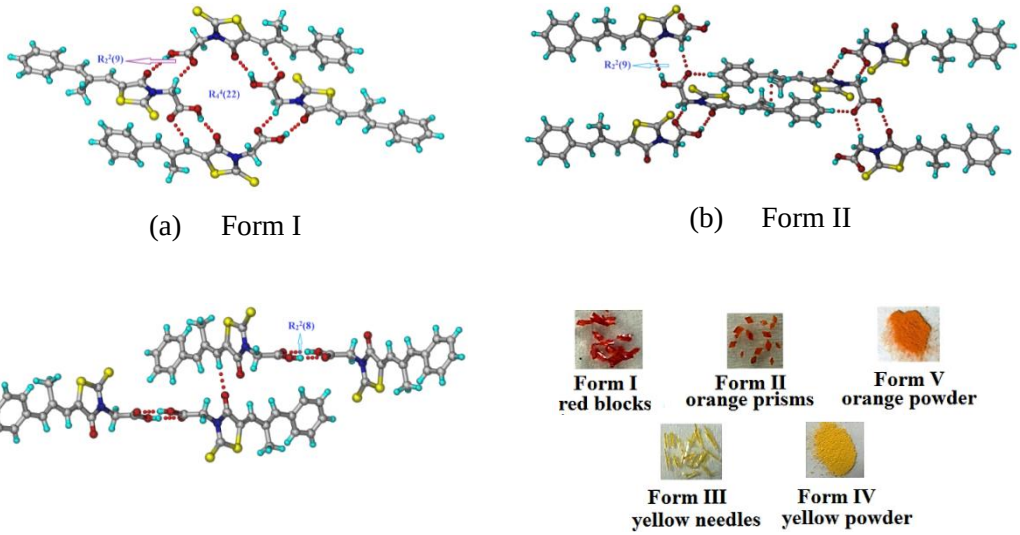


(a) Form I (b) Form II

(c) Form III (d) Color polymorphism

**Figure 1.10** **(a)** EPR molecules $R_2^2(9)$ dimeric and $R_4^4(22)$ tetrameric assembly of via O–H···O and C–H···O hydrogen bonds (b) EPR together with π stacking and C–H···O interactions through $R_2^2(9)$ dimeric motif in Form II (c) form III crystal structure contains acid-acid dimer homosynthon ring motif between molecules connected through C–H···O interactions (d) photographs of different colored EPR polymorphs and The archetype color polymorphism in ROY (red, orange, yellow colors) was ascribed to conformational differences between polymorphs(adapted from ref. 82).

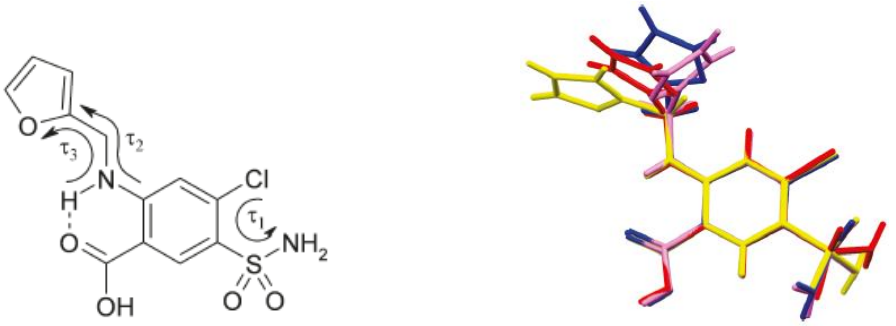


**(a)**

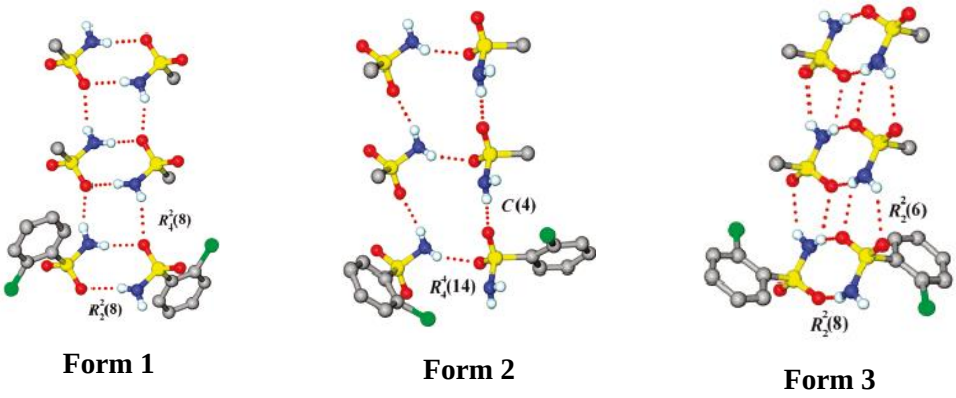


**(b)**

**Figure 1.11** (a) Conformational polymorphism in Furosemide. The three torsion parameters in Furosemide: τ1=C-C-S-N, τ2=C-N-C-C, τ3=N-C-C-O. The anthranilic acid moiety is conformationally locked by intramolecular hydrogen bond but conformational flexibility in the furan and sulfonamide moieties resulted in four conformers (red, blue, pink and yellow) manifested in three polymorphs. (b) Synthon polymorphism in Furosemide. $R_2^2(8)$ N−H···O dimer and $R_4^2(8)$ motif in form 1, $C(4)$ catemer and $R_4^4(14)$ tetramer motif in form 2, $R_2^2(8)$ N−H···O motif and $R_2^2(6)$ rings in skewed dimer of form 3 (Adapted from ref. 83).

## 1.6.2 Ostwald's Law of Stages

In general crystallization won't happen without nucleation, nucleation is a kinetically controlled process. After nucleation, ions/molecules aggregates into small clusters later able to convert as crystallites and crystals. According to classical nucleation theory, the rate of nucleation depends on the frequency factor, temperature, interfacial tension and

supersaturation. After immediate nucleation metastable polymorph crystallizes first further transforms into stable one. Several methods of crystallization were known apart from conventional crystallization in various solvents including sublimation, laser induced nucleation, rotavaporization. Recently new polymorphs can be obtained by cocrystallization techniques. The minute, a polymorph obtained with desired properties, it must be avoid potential stable polymorph transformations with respective to the time. This can see since 'free energy' surface are at different levels and therefore inter-conversions in the polymorphs are quite noticeable that alter the properties of bulk drug material finally it give rise to effectiveness. Ever since, it is essential to understand their properties to optimize the parameters for a desired polymorph formulation.

Polymorphs are formed from crystallization due to thermodynamic and kinetic factors. In accordance with Ostwald rule, which stated that when an energy reaches low and attains equilibrium state which is followed from its initial high-energy state with minimal variations in free energy that involves different stages with in their different intermediate forms. The metastable form with lowest energy barrier crystallizes first latter it transform to subsequent form with low energy barrier and continues until the thermodynamic stable form was crystallized. The activation of free energy leads to nucleation which is time dependent is the main parameter for transformation from metastable to the stable form in between there will be intermediate forms during the process development. The other side, the difference in energy between the polymorphs lies within a 5 kcal $mol^{-1}$ frame, quite a number of polymorphs crystallizes concurrently if their nucleation rates are identical called the '*concomitant polymorphism*' which are 'near-energetic' in general (Figure 1.12).

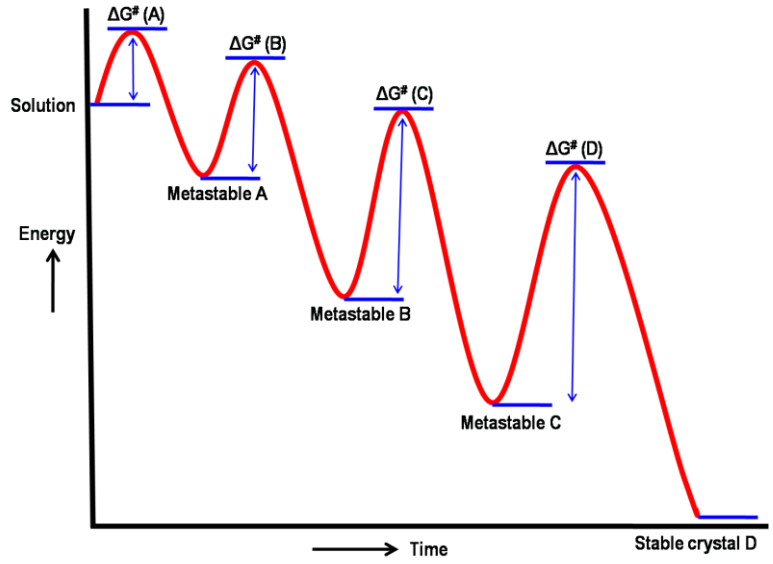


**Figure 1.12:** Ostwald's rule of stages of transformation showing transition energy states of polymorphs during crystallization time. (Adapted from Ref. 72)

Polymorphic transformations can be thermodynamically reversible or irreversible resulting as monotropic and enantiotropic systems[86-87]. The regardless of temperature, the single form is more stable called monotropic whereas the relative stability of the two polymorph inverts at their respective temperatures are enantiotropic. In this aspect, if the free energy curves of two polymorphs cross below its melting point i.e lower melting polymorph said to be enantiotropic and if the free energy curves lies below the lower melting polymorph, they are said to be monotropic [88-90].

## 1.6.3 Solvates and Hydrate-Pseudopolymorphism

The definition of Pseudopolymorphism is stated as "*Compound which obtained in crystalline forms that differ in the nature or stoichiometry included solvent molecules*" resulting solid forms known as pseudopolymorphs which is synonyms for pseudopolymorphism[91] are considered in terms like hydrate, solvate and solvatomorphs. Different stoichiometries of same solvent can form solvates with molecular solid and resulting the incorporation of solvent molecules into the lattices of crystals[92]. Particularly, water molecule even though having small size, it acts as both donor and acceptor hydrogen bond and forms new crystal structures unlike other solvents by connecting drug molecules. It is found to be one third of active APIs can form crystalline hydrates. Often different stoichiometric ratios of the same solvent can be incorporated into crystalline solids for example, norfloxacin an antibiotic drug consist hydrated form

in 1.25 and 1.125 stoichiometric ratios in different crystal structures[93]. Also in the crystal lattices sometimes different solvents can be incorporated for example, nitrofurantoin (antibacterial drug) forms has solvates with water, dimethyl sulfoxide (DMSO), dimethylformamide (DMF), methanol etc. Sometimes solvated polymorphs was observed in nitrofurantoin monohydrate polymorphs I and II (Figure 1.13)[94]. Thus the phenomenon offers tuning of the properties of compounds which are different from original materials. Properties like stability under different conditions, shelf life, etc. deciding factor for solvated or unsolvated forms of a drug. Numerous drug molecules are currently marketed as solvates/hydrates, for example, Indinavir sulfate is marketed as its ethanol solvate and Paroxetine hydrochloride and Prantlukast are marketed as their hemihydrates respectively. Essentially, hydrate/solvate formation can have diverse applications in pharmaceutics.

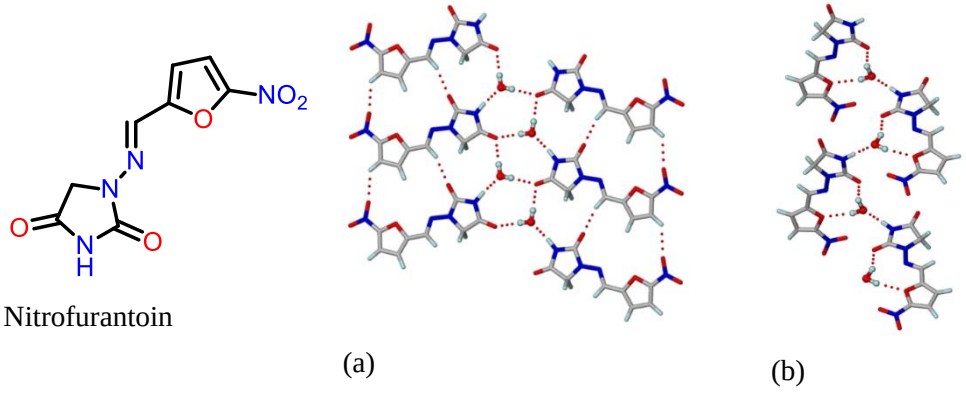


Nitrofurantoin

(a) (b)

**Figure 1.13:** Pseudopolymorphs of Nitrofurantoin monohydrate. (a) In form I, tapes of translation related nitrofurantoin molecules are connected by water molecules through O–H···O and N– H···O hydrogen bonds. (b) In form II, discrete nitrofurantoin molecules form a zigzag tape through water molecules (Adapted from Ref. 94).

## 1.7 Pharmaceutical salts

Salt formation is the most common and effective method for improving the physicochemical properties of drug molecules[95-97]. To predict salt formation between organic acids and bases, the concept of "Rule of three" was beneficial. To test this hypothesis, Nangia and coworkers formed molecules containing salts and cocrystals between several acid and pyridine containing molecules and summerized that the "carboxylic acid–pyridine O–H···N interaction will be neutral when $\Delta pK_a < 0$ and it will have an intermediate Hydrogen bond character, O–H···N and/or $N^+$–H···$O^-$, when the

transition range $0 < \Delta pK_a < 3.75$. The interaction will be ionic $N^+–H\cdots O^-$ when $\Delta pK_a > 3.75$" [98].

Salt formation has diverse implications in pharmaceutical industry[99-102]. Salt formation bestowed the solubility and thermal stability to drug molecules. For example, antiulcer drug Ranitidine , which is having poor solubility and low melting point can be overcome by forming hydrochloride salt of the drug showing prominent solubility and melting point. The plethora of counterions provides ample options for developing the optimal solid formulation for maximal therapeutic efficiency[103-108] (Figure 1.14).

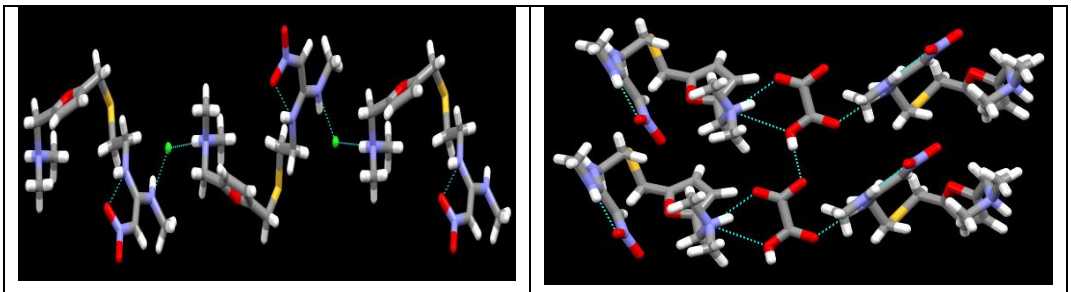

(a) (b)

**Figure 1.14:** Ranitidine salts. (a) Ranitidine hydrochloride salts (b) Ranitidine oxalate salts (Ref. 108).

## 1.8 Cocrystals

FDA defined Cocrystal as *"Solids that are crystalline materials composed of two or more molecules in the same crystal lattice".*

"*Cocrystal*[12, 109-111] *formation from supramolecular synthons is to be considered as forming from discrete neutral molecular species that are solids at ambient temperatures, and where the cocrystal is a structurally homogeneous crystalline material that contains the building blocks in a definite stoichiometric amounts*". Stated by renowned scientist Aakeroy. Later on, scientists defined cocrystal as "*Cocrystals are the solids that are crystalline single phase materials composed of two or more different molecular and/or ionic compounds generally in a stoichiometric ratio which are neither solvates nor simple salts*". In other way, cocrystals[112-116] can be defined as "a stoichiometric multi-component system where the individual components are held together by heteromeric interactions like hydrogen bonds and are solids at room temperature". Even though the alteration of physiochemical properties were reported in early 1946, the complete benefits of cocrystal was reported in early 2000 by Krantz. He reported that the stoichiometric (1:1) cocrystal containing the sodium salt of theophylline and glycine

increased the water solubility of the Active Pharmaceutical Ingredient (API). Different methods[117] were employed to synthesize the cocrystals in which the solids are mixed together and later solution crystallization, sublimation, solid state grinding, liquid assisted grinding, bulk slurry crystallization, reaction crystallization, spray drying etc (Figure 1.15). Recently novel techniques like inkjet printing and crystallization at solvent-solvent interface were used to form cocrystals[118-119]. The physicochemical properties of a cocrystal can be greatly influenced by conformers ultimately affecting the parent drug[120-127]. With few exceptions, it was observed that a high melting coformer always produces a high melting cocrystal and a high soluble coformer confers higher solubility to a cocrystal.

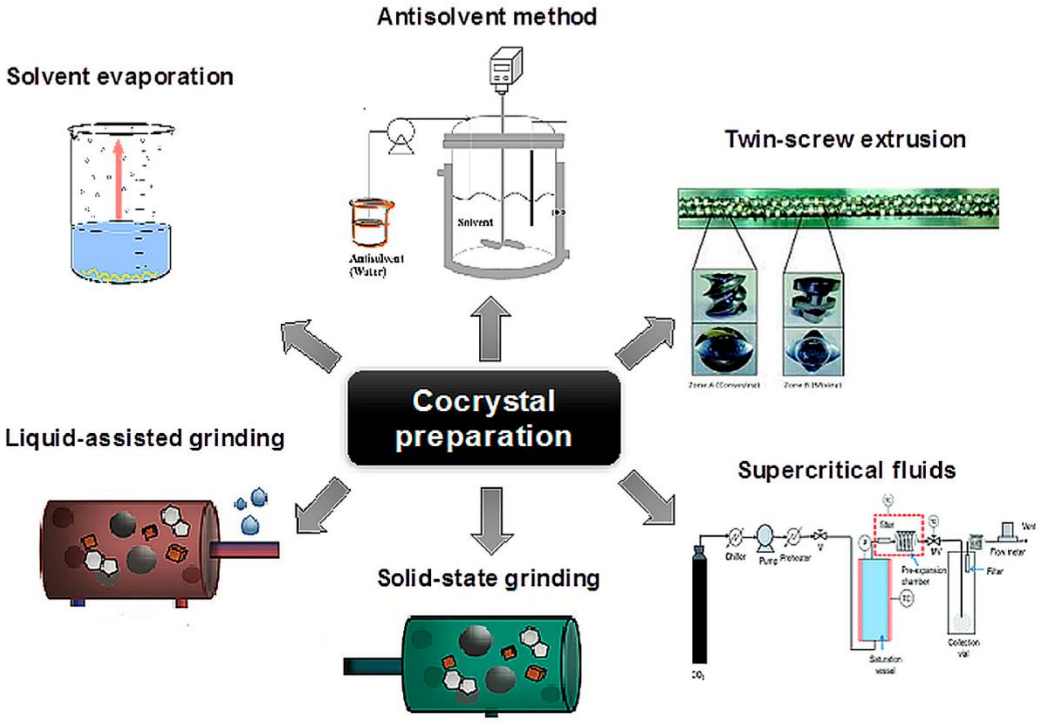


**Figure 1.15**: Schematic presentation of methods applied in cocrystal formation. (Adapted from Reference 117)

Recently, Nangia[128] et al. proposed a model explaining the role of coformer for improving the cocrystals solubility on adoption of 'spring and parachute' a model for amorphous forms. It means a cocrystal contains a high soluble coformer drags the low soluble component that resulting faster dissolution[129-130]. This phenomenon occurs via a higher soluble coformer into the solution media that results in the detachment of cocrystal, thereby leaving the low soluble component in an amorphous/randomized state,

resulting an increase in the free energy of the system leading to enhanced solubility/dissolution of the low soluble component[131-136](Figure 1.16).

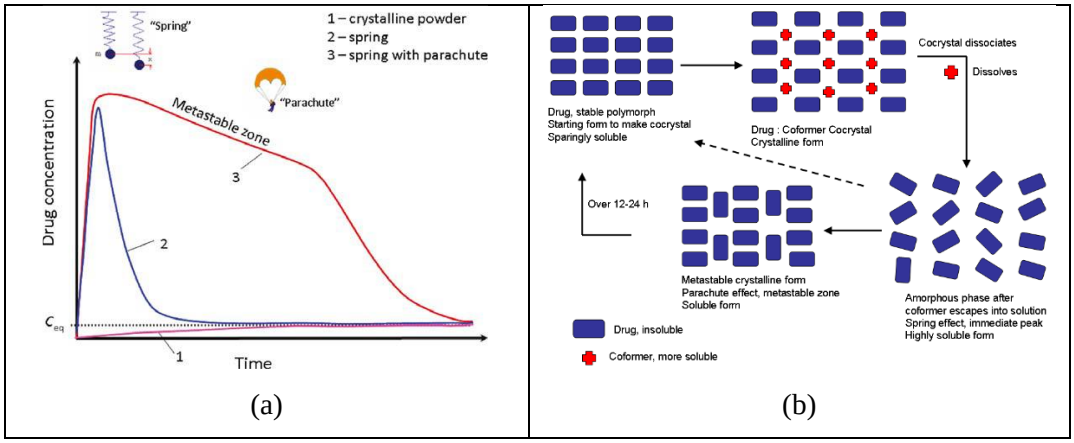


**Figure 1.16:** (a) The spring and parachute concept to achieve high apparent solubility for insoluble drugs. (1) The crystalline (stable) form has low solubility. (2) A short-lived metastable species (i.e., amorphous phase) shows peak solubility but quickly drops (within minutes to an hour) to the low solubility of the crystalline form. (3) Highly soluble drug forms manage to remain for a long enough time (usually hours) in the metastable zone. (b) Possible mechanisms of pharmaceutical cocrystals solubility enhancement of a drug in dissolution medium.

## 1.8.1 Supramolecular synthon

The analysis of cocrystals structures shows that hydrogen bonds are the predominant form of interaction between cocrystal components and the patterns of hydrogen bonds occurred in cocrystal called supramolecular synthons. In 1967, the term “synthon” was introduced by E. J. Corey , while Desiraju mainly used the term “supramolecular synthons” meant that “structural units in the supramolecule which can be formed or assembled by known or possible intra-/intermolecular interactions” when describing a series of cocrystals[29,137-138]. The assembly of the cocrystal was regulated by introducing supramolecular synthons to a specific group of crystals. Bis et.al. Conducted numerous experiments on homo and hetero synthons and found that supramolecular heterosynthons were preferred over supramolecular homosynthons[139-142](Figure 1.17).

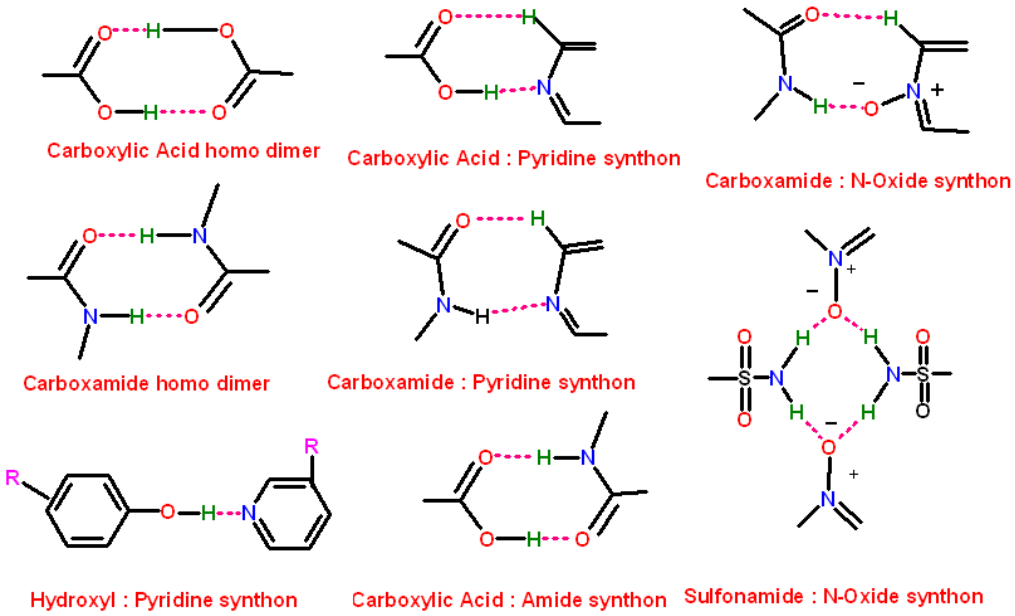


**Figure 1.17:** supramolecular homo/heterosynthons reported from the literature.

## 1.8.2 Ternary Cocrystals

Numerous strategies were successfully employed for the preparation of binary cocrystals as explained in earlier sections. Formation of ternary cocrystals with 1:1:1 is found to be extremely difficult and the exmples of such ternary cocrystals are very few. The first ternary cocrystal containing three component in 1:1:1 ratio was reported by Aakeroy[143-144] (2001). Their design is based upon two simple principles: 1) Hydrogen bonds often form in a hierarchical fashion (best donor to best acceptor, second best donor to second-best acceptor, etc.) and 2) a small number of specific intermolecular interactions can provide a large part of the stabilization energy of molecular crystals. Desiraju et al. employed a novel concept to design ternary cocrystals by its morphology such as shape and size mimics the strategy concept with 2 and 5-methyl resorcinol: 4,4'-bipyridine and a likewise shape and size anthracene, pyrene, phenazine, 2,2'-bithiophene as a third compound[145-152] (Figure 1. 18b). ternary cocrystals with supramolecular synthon Phloroglucinol-tetramethylpyrazine-pyrene(PGL-TMP-PYR); phloroglucinol-tetramethylpyrazine-1,2-bis(4-pyridyl)ethane(PGL-TMP-DPE)[153-157](Figure 1.18c).while this people used simple organic molecule for the preparation of ternary cocrystals, use of API s in the formation ternary adducts whole new setup challenges as its required these complexes to show better pharmaceutical properties. Atipamula[158] et al used this strategies to prepare a stable ternary cocrystal using anti-tuberculosis Isoniazid the only

other study of ternary cocrystals using API was carried out by Geetha et al[159]. With this knowledge, we succeeded in preparing ternary cocrystals of Acefylline: pyridine carboxamide, piperazine and carboxylic acids as a third component (discussed in chapter fifth).

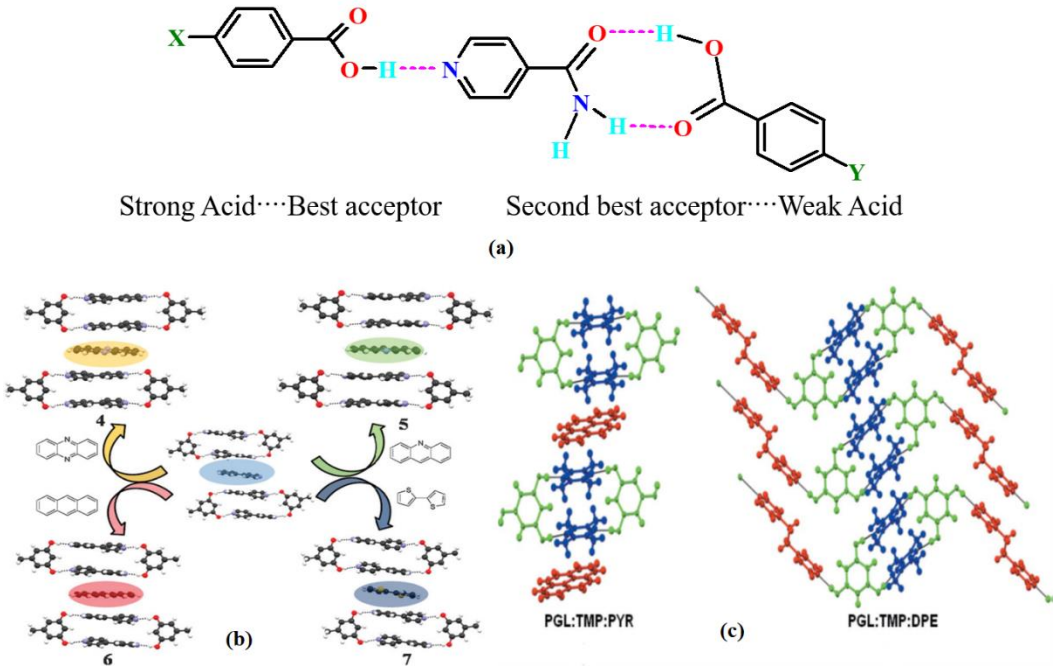


**Figure 1.18:** (a) Proposed design for the construction of a ternary cocrystals with variation of donor, acceptor ability (adapted from ref. 143). (b) Shape and size with geometrical replacing of the ‘‘free’’ 4, 4’-bipyridine molecule in orcinol: 4, 4’-bipyridine binary cocrystal structure by suitable guests (anthracene, pyrene, phenazine, 2, 2’-bithiophene) to give ternary cocrystals (adapted from ref. 145). (c) 2:2:1 stoichiometric ternary cocrystals with supramolecular synthon Phloroglucinol-tetramethylpyrazine-pyrene; phloroglucinol-tetramethylpyrazine-1,2-bis(4-pyridyl)ethane (adapted from ref. 153).

## 1.8.3 Applications of cocrystals

Cocrystals are the sub-class of multi-component systems consists of two or more solid components held together by non-covalent interactions in stoichiometric ratios. In 1844, the first reported cocrystal[160] while working on quinine by Wohler. He mixed the colorless quinine solutions and yellow colored hydroquinone resulting a crystalline substance was obtained called as green hydroquinone. Later, Ling and Baker published numerous cocrystals by using halogenated quinines and quinhydrone[161]. The first crystal

structure of a monoclinic quinhydrone crystal was reported in the year 1958 with quinone, hydroquinone molecules forms with zig-zag alternative chains by hydrogen bonds[162] O–H···O (Figure 1.19).

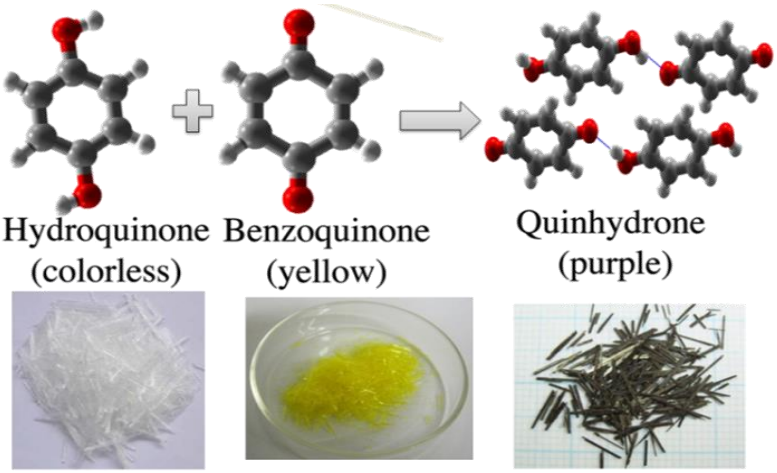


**Figure 1.19:** Reaction and packing structure of quinhydrone cocrystals and formation was indicated by colour change.

Cocrystals have various applications (Figure 1.20) in both in materials and pharmaceuticals fields. In pharmaceuticals, cocrystal methodology optimizes the physicochemical properties of drugs such as solubility, stability, hydration control, mechanical properties, melting and pharmacokinetic properties such as bioavailability/permeability without altering the chemical composition and pharmaceutical activity.

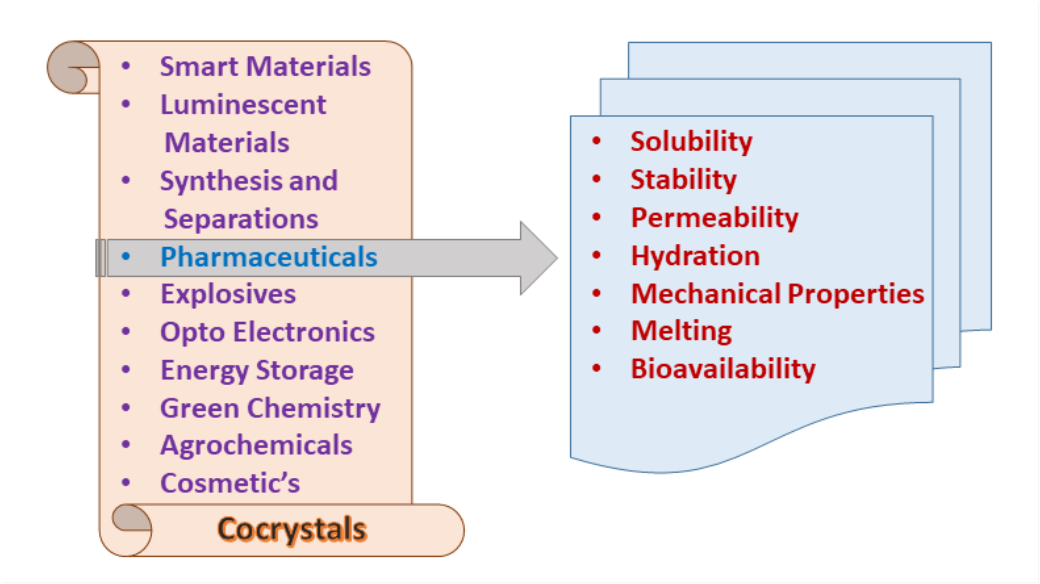

**Figure 1.20:** Cocrystal applications in various scientific areas.

**Table 1.2:** Literature survey of the cocrystal with multiple applications.

| Enhanced property | Cocrystal (in medicine and materials chemistry | References |
|---|---|---|
| Mechanical property | Voriconazole Cocrystals;<br>Lamotrigine cocrystals;<br>Paracetamol Cocrystals;<br>Piroxicam–Saccharin. | *Mol. Pharmaceutics*, 2015, **12**, 889;<br>*Cryst. Growth Des.* 2015, **15**, 5816;<br>*Adv. Mater*, 2009, **21**, 3905;<br>*Cryst. Growth Des.* 2014, **14**, 3864. |
| chemical stability | Temozolomide cocrystals;<br>Tranilast cocrystals;<br>Nitrofurantoin cocrystals.<br>Indapamide cocrystals and coamorphus products case study (**discussed in chapter Three).** | *Chem. Asian J.*, 2012, **7**, 2274;<br>*Cryst. Growth Des.*, 2013, **13**, 3546;<br>*CrystEngComm*, 2011, **13**, 759. |
| Hydration stability | Etirocoxib cocrystals;<br>Niclosamide cocrystals;<br>Theophylline-oxalicacid cocrystal;<br>Quercetin cocrystals; | *CrystEngComm*, 2016, **18**, 2825;<br>*Cryst. Growth Des.*, 2012, **12**, 4588;<br>*Int. J. Pharm.*, 2006, **320**, 114;<br>*Mol. Pharmaceutics*, 2011, **8**, 1867. |
| Solubility and Dissolution rate | Fluoxetinehydrochloride–Succinic acid;<br>Piroxicam–Saccharin;<br>Itraconazole-L-malic acid cocrystal.<br>Etodolac salts and cocrystals **(discussed in chapter Four).** | *J. Am. Chem. Soc.* 2004, **126**, 13335;<br>*J. Pharm. Sci.* 2005, **94**, 93;<br>*J. Am. Chem. Soc*., 2003, **125**, 8456. |
| Bioavailability | Sildenafil–Dicarboxylic Acids;<br>Apixaban-oxalic acid cocrystal;<br>Telmisartan cocrystals. | *Mol. Pharmaceutics*, 2013, 10, 4687;<br>*Cryst. Growth Des.*, 2016, **16**, 2923;<br>*CrystEngComm*, 2014, **16**, 8375. |
| Permeability | Hydrochlorothiazide cocrystals;<br>Theophylline cocrystals;<br>Acyclovir cocrystals;<br>Acefylline salt-cocrystal polymorphs **(discussed in chapter Five).** | *Mol. Pharmaceutics*, 2015, **12**,1615;<br>*Cryst. Growth Des.*, 2015, **15**, 5593;<br>*CrystEngComm*, 2013, **15**, 6457. |
| Thermal stability | Hexamethylene bisacetamide Cocrystals;<br>Propolol-isonicotinamide cocrystal;<br>3-Iodo-2-propynyl-N-butylcarbamate (IPBC, Preservative) cocrystals;<br>Adefovir dipivoxil corystals. | *J. Am. Chem. Soc.* 2009, 131, 17048;<br>*Cryst. Growth Des*. 2014, 14, 2422;<br>*Mol. Pharmaceutics*, 2013, **10**, 1760;<br>*Int. J. Pharm.*, 2012, **438**, 327. |
| Dying | Pyridine-2,4-dione based based | *CrystEngComm*, 2015, **17**, 2083; |

| | | |
|---|---|---|
| applications | heterocyclic dye;<br>Colour-tuned fluorescein cocrystals. | *CrystEngComm*, 2013, **15**, 6289. |
| Conductivity improvement | Phenazine:deuterated chloranillic acid;<br>Phenazine- chloranillic acid;<br>Anilic acid-phenazine. | *J. Am. Chem. Soc.* 2005, **127**, 5010.<br>*J. Phys. Condens. Matter* 2007, **19**, 226203.<br>*J. Mater. Chem.* 2009, **19**, 4421. |
| High energy materials | diacetonediperoxide, triacetonetriperoxide Cocrystals;<br>Cocrystals of CL-20;<br>2,4,6-Trinitrotoluene Cocrystal.. | *Angew. Chem. Int. Ed.* 2013, 52, 6468;<br>*CrystEngComm*, 2012, 14, 3742;<br>*Cryst. Growth Des.*, 2010, 10, 5341. |

## 1.9 Amorphous solids

In amorphous solids long range order in the lattice space characteristic of a crystal was missed[163-167]. It has a prominent place in pharmaceuticals due to their ability to improve solubility and dissolution rate APIs which was extent to excess thermodynamic functions of amorphous phases. Amorphous compounds do not show a regular diffraction pattern compared to crystalline solids. The techniques in general used are spray and freeze drying, melt quenching, milling, wet granulation and recently manual grinding[165] was significant to produce amorphous salts. It can be characterized by thermal techniques with glass transition temperature ($T_g$). It is the temperature at which a glassy material (super cooled liquid) is converted to rubbery phase retaining some properties of the liquid[166]. Surprisingly, amorphous forms are also exhibit polymorphism[168-169] which is termed as 'polyamorphism'. For reference, polyamorphism in $H_2O$ is broadly studied, but the interpretation data was tough task since the diffraction pattern does not show any Bragg lines. In another example, the evolution of acetaminophen polyamorphous phases I and II forms corresponding polymorphs I and II in different solvent systems was also studied by radial distribution functions derived from the pair distribution function (PDF). On one hand the excess thermodynamic functions of amorphous phases confer solubility/dissolution advantage of the poorly soluble APIs. Therefore drugs Itraconazole, Lopinavir, Cefuroxime axetil, Quinapril hydrochloride etc., are marketed either as purely amorphous phases or in combination with other solid forms. But on the other hand, the higher entropy and enthalpy can be disadvantageous since they make the amorphous solid forms highly unstable[170]. More than a few excipients for instance methyl cellulose, polyvinyl pyrrolidone (PVP), polyethylene glycol (PEG) and alginic acid have been utilized for the amorphous stable forms.

## 1.9.1 Coamorphous solids

Recently Norman Chieng, in 2009 introduced the concept of "coamorphous" system and the formulation of binary amorphous mixture of ranitidine hydrochloride and γ-indomethacin in different stoichiometric (1:1, 1:2, and 2:1) ratios[171-172]. After that Thomas Rades and his co-workers started to explore the coamorphous system as a formulation[173-174]. Coamorphous system has thus gained considerable interest in the pharmaceutical field because of their potential to improve the solubility and dissolution rate of poorly soluble drugs. In the past decade, instead of using macromolecules such as polymers, mixing specific low molecular weight co-formers with APIs at the molecular level has been developed as an alternative approach to stabilize the amorphous form and enhance the dissolution profiles of poorly water-soluble drugs. This coamorphous system is characterized as a single phase amorphous solid system composed of binary or multi-components[175-178].

For example Zhang[179] et.al has reported the enhanced stability and solubility of Lurasidone hydrochloride (LH) with saccharin in a 1:1 equimolar ratio. They calculated the LH-SAC coamorphous solid material stored at 25 °C/60% RH, is stable up to 60 days and it has more stability compare to pure LH amorphous which exhibited only 7 days stability at same conditions (Figure 1.21). Laitinen[180] et.al reported the drug-drug coamorphous of glipizide (GPZ) and simvastatin (SVP) in different stoichiometric ratios (1:1, 2:1 and 1:2). Cryo-milled 1:1 and 1:2 of the SVP-GPZ showed two months phase stability at 25 °C/65% RH (Figure 1.25b). In chapter 3 we highlit the Indapamide-Piperzine and amino acid derivatives of coamophous solids case study solubility and permiability enhancement.

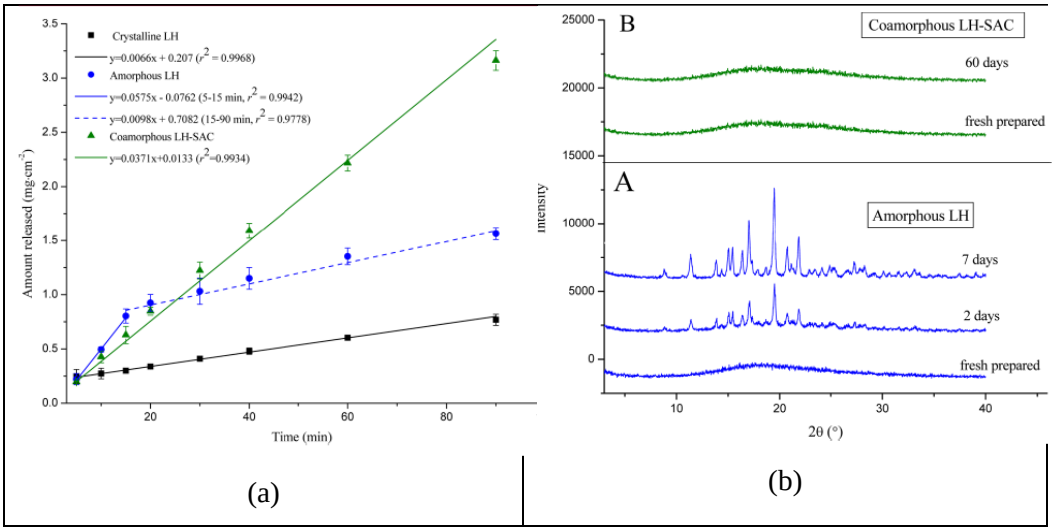


**Figure1.21:** (a)Intrinsic dissolution rate profiles crystalline LH, amorphous LH, and coamorphous LH-SAC in 0.2M phosphate buffer solution (3.8, n=6). (b) PXRD pattterns for amorphous LH (A), coamorphous LH-SAC (B) stored at 25 °C/60% RH over a specified period.

**Table 1.3:** List of FDA approved amorphous drugs and solid dispersions available in the market[181]

| S. No | Drug | FDA Approval |
|---|---|---|
| 1 | Zafirlukast | 1999 |
| 2 | Quinapril hydrochloride | 1991 |
| 3 | Cefuroximeacetyl | 1994 |
| 4 | Rosuvastatincalcium | 2003 |
| 5 | Nelfinavirmesylate | 1996 |
| 6 | Etravirine | 2008 |
| 7 | Fenofibrate | 1993 |
| 8 | Griseofulvin | 1959 |
| 9 | Itraconazole | 2001 |
| 10 | Ivacaftor | 2012 |
| 11 | Lopinavir/Ritanovir | 2000 |
| 12 | Nabilone | 1985 |
| 13 | Tacrolimus | 2000 |
| 14 | Troglitazone | 1999 |
| 15 | Verapamil | 1982 |
| 16 | Verumafenib | 2017 |

## 1.10 References

1. Lehn, J. M. Supramolecular chemistry: receptors, catalysts, and carriers. *Science* **1985**, 227, 849-856

2. Cram, D. J.; Lehn, J. M.; Pederson, C. J. The Nobel Prize in Chemistry **1987**. Available online at: https://www.nobelprize.org/nobel_prizes/chemistry/laureates/1987/ (accessed September 23, 2017).
3. Lehn, J. M. 1978. Cryptates: inclusion complexes of macropolycyclic receptor molecules. *Pure Appl. Chem.* **1978**, 50, 871-892.
4. Lehn, J. M. *Supramolecular Chemistry*, Publisher: Wiley VCH **1995**.
5. Davis, A. V.; Yeh, R. M.; Raymond, K. N. Supramolecular assembly dynamics. *PNAS*. **2002**, 99, 4793-4796.
6. G. R. Desiraju, *Nature*, **2001**, 412, 397-400.
7. Pederson, C. J. Cyclic polyethers and their complexes with metal salts. *J. Am. Chem. Soc.* **1967**, 89, 2495–2496
8. Fischer, E. Influence of the configuration on the effect of the enzymes. *Ber. Dtsch. Chem Ges*. **1894**, 27, 2985-2993.
9. Fisher, H. E. The Nobel Prize in Chemistry **1902**. Available online at: https://www.nobelprize.org/nobel_prizes/chemistry/laureates/1902/
10. Werner, A. Contribution to the constitution of inorganic compounds. *Z. Anorg. Chem*. **1893**, 3, 267-330.
11. Ehrlich, P. Studies on Immunity, *John Wiley & Sons, Inc.* New York **1906**.
12. Desiraju, G. R. Crystal Engineering. The Design of Organic Solids; Elsevier: Amsterdam, **1989**.
13. James, T. D. Specialty grand challenges in supramolecular chemistry. *Frontiers in Chemistry* **2017**, 5, 83.
14. Desiraju, G. R.; Vittal, J. J.; and Ramanan, A. *Crystal Engineering. A Textbook*, World Scientific Publishing, Singapore, **2011**.
15. Nangia, A. K.; Desiraju, G. R. Crystal Engineering. An Outlook for the Future. *Angew. Chem. Int. Ed.* **2019**, 58, 4100 – 4107.
16. Desiraju, G. R. Crystal Engineering: From Molecule to Crystal. *J. Am. Chem. Soc*. **2013**, 135, 9952−9967.
17. Pepinsky, R. *Phys. Rev.* **1955**, *100*, 971
18. Cohen, M. D.; Ludmer, Z.; Thomas, J. M.; Williams. The role of structural imperfections in the photodimerization of 9-cyanoanthracene. *Proceedings of the Royal Society of London. A. Mathematical and Physical Sciences* **1971**, 324, 459-468.

19. Cohen, M. D.; Schmidt, G. M. J.; and Sonntag. F. I. Topochemistry. Part II. The photochemistry of *trans*-cinnamic acids. *J. Chem. Soc*. **1964**, 2000-2013.
20. Bragg, W. H. The structure of organic crystals. *Proc. Phys. Soc.* **1921**, 34, 33.
21. Robertson, J. M.; White, J. G. The crystal structure of coronene: a quantitative X-ray investigation. *J. Chem. Soc.* **1945**, 607-617.
22. Robertson, J. M.; White, J. G. The crystal structure of pyrene. A quantitative X-ray investigation. *J. Chem. Soc.* **1947**, 358-368.
23. Robertson, J. M. The measurement of bond lengths in conjugated molecules of carbon centres. *Proc. R. Soc.* **1951**, A207, 101-110.
24. Bernal, J. D.; Crowfoot, D. The structure of some hydrocarbons related to the sterols. *J. Chem. Soc.* **1935**, 93.
25. Schmidt, G. M. *J*. Photo dimerization in the solid state. *Pure Appl. Chem*. **1971**, *27*, 647-678.
26. Thomas, J. M. Philos. *Trans. R. Soc. London, Ser. A* **1974**, 277, 251.Yan, D.; Delori, A.; Lloyd, G. O.; Friščić, T.; Day, G. M.; Jones, W.; Duan, X. A Cocrystal Strategy to Tune the Luminescent Properties of Stilbene Type Organic Solid State Materials *Angew. Chem. Int. Ed.* **2011**, 50, 12483-12486.
27. Kitaigorodskii, A. I. *Molecular Crystals and Molecules*, Academic Press: New York, **1973**.
28. Pertsin, A. J. Kitaigorodskii, A. I. *The Atom-Atom Potential Method*, Springer-Verlag, **1987**.
29. Desiraju, G. R. Supramolecular Synthons in Crystal Engineering—A New Organic Synthesis Angew. Chem., Int. Ed. Engl. **1995**, 34, 2311-2327.
30. Sarma, J. A. R. P.; Desiraju, G. R. *Acc. Chem. Res*. **1986**, *19*, 222.
31. Drug definition US-FDA Drug approval process. *Pharmacists Pharma Journal* **2010**.
32. US Federal Food, Drug, and Cosmetic Act, SEC. 210. (g) (1) (B). Accessed 30 September **2019**.
33. Hardman, J.G.; Limbird, L. E.; Gilman, A. G. *The Pharmacological Basis of Therapeutics 10th Edition*.
34. Definition and classification of Drug or Pharmaceutical Regulatory aspects of drug approval Accessed 30 December **2013**.
35. Richard, F.; Luigi, C.; Michelle, C. *Lippencott's Illustrated Reviews: Pharmacology* 4th Edition. Lippencott Williams & Wilkins. **2009**.

36. Byrn, S. R.; Pfeiffer, R. R.; Stowell, J. G. *Solid-State Chemistry of Drugs*. SSCI, West Lafayette, IN, **1999**.
37. Monkhouse, D. C. Stability aspects of preformulation and formulation of solid pharmaceuticals. *Drug Dev. & Indus. Pharm*. **1984**, 10, 1373-1412.
38. Zhang, G. G.; Law, D.; Schmitt, E. A.; Qiu, Y. Phase transformation considerations during process development and manufacture of solid oral dosage forms. *Adv. Drug Deliv. Rev*. **2004**, 56, 371-390.
39. Mullard, A. 2018 FDA drug approvals. *Nature Reviews Drug Discovery* **2019**, 18, 85-89.
40. Sanphui, P.; Mishra, M. K.; Ramamurty, U.; Desiraju, G. R. Tuning mechanical properties of pharmaceutical crystals with multicomponent crystals: voriconazole as a case study. *Mol. Pharm.* **2015**, 12, 889-897.
41. Qiu, Y.; Chen, Y.; Zhang, G. G. Z. *Developing Solid Oral Dosage Forms. Pharmaceutical Theory and Practice*. Academic Press, New York, **2009**.
42. Amidon, G. L.; Lennernäs, H.; Shah V. P.; Crison, J. R. *A Theoretical Basis for a Biopharmaceutic Drug Classification: The Correlation of In Vitro Drug Product Dissolution and In Vivo Bioavailability. Pharm. Res.* **1995**, 12, 413-420.
43. Dahan, A.; Miller, J. M.; Amidon, G. L. Prediction of solubility and permeability class membership: provisional BCS classification of the world's top oral drugs. *AAPS Journal* **2009**, 11, 740-746.
44. Kasim, N. A.; Whitehouse, M.; Ramachandran, C.; Bermejo, M.; Lennernäs, H.; Hussain, A. S.; Junginger, H. E.; Stavchansky, S. A.; Midha, K. K.; Shah, V. P. Amidon, G. L. Molecular properties of WHO essential drugs and provisional biopharmaceutical classification. *Mol. Pharm.* **2004**, 1, 85-96.
45. Hendriksen, B. A.; Felix, M. V. S.; Bolger, M. B. The composite solubility versus pH profile and its role in intestinal absorption prediction. *AAPS Pharm Sci*. **2003**, 5, 35-49.
46. Charalabidis, A.; Sfouni, M.; Bergström, C.; Macheras, P. The Biopharmaceutics Classification System (BCS) and the Biopharmaceutics Drug Disposition Classification System (BDDCS): Beyond guidelines. *International Journal of Pharmaceutics* **2019**, 566, 264–281.

47. Krikorian, S.; Pories, S.; Tataronis, G.; Caughey, T.; Chervinsky, K.; Lotz, M.; Shen, A. H.; Weissmann, L. Adherence to oral chemotherapy: Challenges and opportunities. *J. Oncol. Pharm. Practice* **2018**, 1078155218800384.
48. Liewer, S.; Huddleston, A. N. Oral targeted therapies: managing drug interactions, enhancing adherence and optimizing medication safety in lymphoma patients. *Expert Rev. Anticancer Ther*. **2015**, *15*, 453-464.
49. Steiner, T. The hydrogen bond in the solid state. *Angew. Chem. Int. Ed*. **2002**, 41, 48-76.
50. Desiraju, G. R. The C-H…O hydrogen bond in crystals: what is it? *Acc. Chem. Res.* **1991**, 24, 290-296.
51. Jeffrey, G. A.; Saenger, W. *Hydrogen Bonding in Biological Structures*. Springer-Verlag, Berlin, **1991**.
52. Werner, A. *Leibig's Annalen der Chemie*, **1902**, 322, 261-97.
53. Pauling, L. *The Nature of Chemical Bond*, Cornell University Press, Ithaca, New York, **1939**.
54. Arunan, E.; Desiraju, G. R.; Klein, R. A.; Sadlej, J.; Scheiner, S.; Alkorta, I.; Clary, D. C.; Crabtree, R. H.; Dannenberg, J. J.; Hobza, P.; Kjaergaard, H. G.; Legon, A. C.; Mennucci, B.; Nesbitt. D. J. Definition of the hydrogen bond (IUPAC Recommendations 2011) *Pure Appl. Chem*. **2011**, 83, 1619-1636.
55. Pauling, L. *The Nature of Chemical Bond*, Cornell University Press, Ithaca, New York, **1939**.
56. Arunan, E.; Desiraju, G. R.; Klein, R. A.; Sadlej, J.; Scheiner, S.; Alkorta, I.; Clary, D. C.; Crabtree, R. H.; Dannenberg, J. J.; Hobza, P.; Kjaergaard, H. G.; Legon, A. C.; Mennucci, B.; Nesbitt, D. J. *Pure Appl. Chem*. **2011**, 83, 1619-1636.
57. Scheiner, S. *Hydrogen bonding: a theoretical perspective*. Oxford University Press on Demand. **1997**.
58. Haleblian, J.; McCrone, W. Pharmaceutical applications of polymorphism. *J. Pharm. Sci*. **1969**, 58, 911-929.
59. Bernstein, J. *Polymorphism in Molecular Crystals*. Clarendon, Oxford, U. K. **2002**.
60. Dunitz, J. D.; and Bernstein, J. Disappearing Polymorphs. *Acc. Chem. Res.***1995**, 28, 193-200.
61. J. Berzelius, *Jahresbericht*, **1844**, 23, 44.

62. Brittain, H. G. *Polymorphism in Pharmaceutical Solids*. Informa Healthcare USA Inc. New York, **2009**.
63. Hilfiker, R. *Polymorphism in the Pharmaceutical Industry*, Wiley-VCH, Weinheim, Germany, **2006**.
64. Bernstein, J. Polymorphism- a perspective. *Crystal Growth & Design* **2011**, 11, 632-650.
65. Mitscherlich, E. Über die Körper, welche in zwei verschiedenen krystallisieren Formen, *Abhl. Akad. Berlin*, **1822**, 43-48.
66. Berzelius, J. Ueber die Verbindungen des Phosphors mit Schwefel. Eur. J. Org. Chem. **1843**, 46, 129-154.
67. F. Wöhler, J. Liebig, *Annal. Pharm.*, **1832**, 3, 249
68. Wöhler, F. Ueber die Constitution der Cyanursäure. Eur. J. Org. Chem. **1847**, 62, 241-253.
69. Amici, G. B.; Série, T. Note sur un appareil de polarization. *Ann. Chim. Phys. Ser.* **1844**, 12, 114-120.
70. Mallard, E. Anomalies optiques. Annual Mines Mem (VII Ser), **1876**, 10, 60.
71. Lehmann, O. *Die Krystallanalyse oder die chemische Analyse durch Beobachtung der Krystallbildung mit Hülfe des Mikroskps*, Wilhelm Engelmann, Liepzig, **1891**.
72. Ostwald, W. Studies on the formation and transformation of solid bodies. *Journal of Physical Chemistry* **1897**, 22, 289-330.
73. Brittain, H. G. Polymorphism in pharmaceutical solids in Drugs and Pharmaceutical Sciences, **2009**, 192, 2nd Edn, Informa Healthcare USA. Inc., New York.
74. Hilfiker, R. (Ed.). Polymorphism: in the pharmaceutical industry. John Wiley & Sons, **2006**.
75. Thun, J.; Seyfarth, L.; Butterhof, C.; Senker, J.; Dinnebier, R. E.; Breu, J. Wöhler and Liebig Revisited: 176 Years of Polymorphism in Benzamide-and the Story Still Continues! *Crystal Growth & Design* **2009**, 9, 2435-2441.
76. Raza, K.; Kumar, P.; Ratan, S.; Malik, R.; Arora, S. Polymorphism: The Phenomenon Affecting the Performance of Drugs. *SOJ Pharm. Sci*. **2014**, 1, 10.

77. Gentili, D.; Gazzano M.; Melucci M.; Jones D.; Cavallini M.; Polymorphism as an additional functionality of materials for technological applications at surfaces and interfaces. *Chemical Society Reviews* **2019**, 48, 2502-2517.

78. López-Mejías, V.; Kampf, J. W.; Matzger, A. J. Nonamorphism in flufenamic acid and a new record for a polymorphic compound with solved structures. *Journal of the American Chemical Society* **2012**, 134, 9872-9875.

79. Nangia, A. Conformational polymorphism in organic crystals. *Accounts of Chemical Research* **2008**, 41, 595-604.

80. Cruz-cabeza, A. J.; and Bernstein, J. Conformational Polymorphism. *Chem. Rev.* **2014**, 114, 2170-2191.

81. Kumar, S. S.; and Nangia, A. A new conformational polymorph of N-acetyl-Lcysteine. The role of S–H…O and C–H…O interactions *CrystEngComm***, 2013**, 15, 6498-6505.

82. Swapna, B.; Suresh K.; and Nangia, A. Color polymorphs of aldose reductase inhibitor epalrestat: configurational, conformational and synthon differences *Chem. Commun.*, **2016**, 52, 4037-4040

83. Babu, N, J.; Cherukuvada, S.; Thakuria, R.; Nangia, A. Conformational and synthon polymorphism in furosemide (Lasix). *Crystal Growth & Design* **2010**, 10, 1979-1989.

84. Braun, D, E.; Gelbrich, T.; Kahlenberg, V.; Laus, G.; Wieser, J.; Griesser, U. J. Packing polymorphism of a conformationally flexible molecule (aprepitant). *New Journal of Chemistry* **2008**, 32, 1677-1685.

85. Porter.; Iii, W. W.; Elie, S. C.; Matzger, A. J. Polymorphism in carbamazepine cocrystals. *Crystal Growth & Design* **2008**, 8, 14-16.

86. Bernstein, J.; Davey, R. J.; and Henck, J. -O. New polymorph of armodafinil and its stability studies. *Angew. Chem., Int. Ed.*, **1999**, 38, 3440-3461

87. Cherukuvada, S.; Thakuria, R.; and Nangia, A. Pyrazinamide Polymorphs: Relative Stability and Vibrational Spectroscopy. *Cryst. Growth Des.*, **2010**, 10, 3931-3941.

88. Braga, D.; Grepioni, F. Making crystals from crystals: a green route to crystal engineering and polymorphism. *Chem. Commun.* **2005**, 3635-3645.

89. Rodrıguez-Spong, B.; Price, C. P.; Jayasankar, A.; Matzger, A. J.; Rodrı´guez-Hornedo, N. General principles of pharmaceutical solid polymorphism: a supramolecular perspective. *Adv. Drug Deliv. Rev.* **2004**, 56, 241-274.

90. Price, C. P.; Grzesiak, A. L.; Matzger, A. J. Crystalline polymorph selection and discovery with polymer heteronuclei. *Journal of the American Chemical Society* **2005,** 127, 5512-5517.

91. Nangia, A.; Desiraju, G. R. Pseudopolymorphism: occurrences of hydrogen bonding organic solvents in molecular crystals. *Chemical Communications* **1999**, 7, 605-606.

92. Byrn, S. R.; Pfeiffer, R. R.; Stephenson, G.; Grant, D. J. W.; Gleason, W. B. Solid-State Pharmaceutical Chemistry. *Chem. Mater*. **1994**, 6, 1148-1158.

93. Roy, S.; Goud, N. R.; Babu, N. J.; Iqbal, J.; Kruthiventi, A. K.; Nangia, A. Crystal Structures of Norfloxacin Hydrates. *Cryst. Growth. Des*. **2008**, 8, 4343-4346.

94. Caira, M. R.; Pienaar, E. W.; and Lötter, A. P. Polymorphism and Pseudopolymorphism of the antibacterial nitrofurantoin. *Mol. Cryst. Liq. Cryst*., **1996**, 279, 241.

95. Gould, P. L. Salt selection for basic drugs. *International Journal of Pharmaceutics* **1986**, 33, 201-217.

96. Paulekuhn, G. S.; Dressman, J. B.; Saal, C. Trends in active pharmaceutical ingredient salt selection based on analysis of the orange book database. *Journal of Medicinal Chemistry* **2007**, 50, 6665-6672.

97. Childs, S. L.; Stahly, G. P.; Park, A. The salt- cocrystal continuum: the influence of crystal structure on ionization state. *Molecular Pharmaceutics* **2007**, 4, 323-338.

98. Sarma, B.; Nath, N. K.; Bhogala, B. R.; Nangia, A. Synthon competition and cooperation in molecular salts of hydroxybenzoic acids and aminopyridines. *Crystal Growth & Design* **2009**, 9, 1546-1557.

99. Cruz-Cabeza, A. J. Acid-base crystalline complexes and the pKa rule. *CrystEngComm.* **2012**, 14, 6362-6365.

100. Black, S. N.; Collier, E. A.; Davey, R. J.; Roberts, R. J. Structure, solubility, screening, and synthesis of molecular salts. *Journal of Pharmaceutical Sciences* **2007**, 96, 1053-1068.

101. Serajuddin, A. T. Salt formation to improve drug solubility. *Advanced Drug Delivery Reviews* **2007**, 59, 603-616.

102. Stahl, P. H.; Wermuth, C. G. Handbook of pharmaceutical salts: properties, selection and use. *Chem. Int.* **2002**, 24, 1-7.

103. Gupta, D.; Bhatia, D.; Dave, V.; Sutariya, V.; Varghese, G. S. Salts of therapeutic agents: chemical, physicochemical, and biological considerations. *Molecules* **2018**, 23, 1719.
104. Rubino, J. T. Solubilities and solid state properties of the sodium salts of drugs. *Journal of Pharmaceutical Sciences* **1989**, 78, 485-489.
105. Thomas, E.; Rubino, J. Solubility, melting point and salting-out relationships in a group of secondary amine hydrochloride salts. *International Journal of Pharmaceutics* **1996**, 130, 179-185.
106. Chowhan, Z. T. pH-solubility profiles of organic carboxylic acids and their salts. *Journal of Pharmaceutical Sciences* **1978**, 67, 1257-1260.
107. Forbes, R. T.; York, P.; Davidson, J. R. Dissolution kinetics and solubilities of p-aminosalicylic acid and its salts. *International Journal of Pharmaceutics* **1995**, 126, 199-208.
108. Kojic-Prodic, B.; and Ruzic-Toros, Z. Ranitidine Hydrogen Oxalate. *Acta Cryst.* **1982**. B38, 1837-1840.
109. Friscic, T.; Trask, A. V.; Jones, W.; Motherwell, W. D. S. Screening for Inclusion Compounds and Systematic Construction of Three-Component Solids by Liquid-Assisted Grinding. *Angew. Chem. Int. Ed*. **2006**, 45, 7546 –7550
110. Jones, W.; Motherwell, W. S.; Trask, A. V. Pharmaceutical cocrystals: an emerging approach to physical property enhancement. *MRS Bulletin* **2006**, 3, 875-879.
111. Desiraju, G. R. Crystal Engineering: From Molecule to Crystal. *J. Am. Chem. Soc*. **2013**, 135, 9952−9967
112. Aakeröy, C. B.; Forbes, S.; Desper, J. Using cocrystals to systematically modulate aqueous solubility and melting behavior of an anticancer drug. *Journal of the American Chemical Society* **2009**, 131, 17048-17049.
113. Bolla, G.; and Nangia, A. Pharmaceutical cocrystals: walking the talk. *Chem. Commun*, **2016**, 52, 8342-8360
114. Yousef, M. A.; Vangala, V. R. Pharmaceutical Co-crystals: Molecules, Crystals, Formulations, Medicines. *Cryst. Growth Des.* **2019,** 19, 7420-7438.
115. Whitesides, G. M. Reinventing chemistry. *Angewandte Chemie International Edition* **2015**, 54, 3196-3209.

116. Gadade, D. D.; Pekamwar, S. S. Pharmaceutical cocrystals: regulatory and strategic aspects, design and development. *Advanced Pharmaceutical Bulletin* **2016**, 6, 479.

117. Karagianni, A.; Malamatari, M.; and Kachrimanis, K. Pharmaceutical Cocrystals: New Solid Phase Modification Approaches for the Formulation of APIs. *Pharmaceutics* **2018**, 10, 18

118. Bond, A. D. What is a co-crystal? *CrystEngComm***, 2007**,9**,** 833-834

119. Karimi-jafari, M.; Padrela, L.; Walker, G. M.; and Croker, D. M. Creating Cocrystals: A Review of Pharmaceutical Cocrystal Preparation Routes and Applications. Cryst. Growth Des. **2018**, 18, 6370−6387

120. Schultheiss, N.; and Newman, A. Pharmaceutical Cocrystals and Their Physicochemical Properties. *Cryst. Growth Des.* **2009**, 9, 2950-2967.

121. Mullins, J. D.; Macek, T. J. Some pharmaceutical properties of novobiocin. *J. Am. Pharm. Assoc.* **1960**, 49, 245-248.

122. Stahly, G. P. Diversity in Single- and Multiple-Component Crystals. The Search for and Prevalence of Polymorphs and Cocrystals. *Cryst. Growth Des.* **2007**, 7, 1007–1026

123. Stahly, G. P. A Survey of Cocrystals Reported Prior to 2000. *Cryst. Growth Des.* **2009**, 9, 4212–4229

124. Alhalaweh, A.; Roy, L.; Rodríguez-Hornedo, N.; Velaga, S. P. pH-Dependent Solubility of Indomethacin−Saccharin and Carbamazepine−Saccharin Cocrystals in Aqueous Media. *Mol. Pharmaceutics* **2012**, *9*, 2605-2612.

125. Shan, N.; Zaworotko, M. J.; The role of cocrystals in pharmaceutical science. *Drug Discovery Today* **2008**, 13, 440-446.

126. Smith, A. J.; Kavuru, P.; Wojtas, L.; Zaworotko, M. J.; and Shytle, R. D. Cocrystals of Quercetin with Improved Solubility and Oral Bioavailability. *Mol. Pharmaceutics* **2011**, 8, 1867–1876

127. Duggirala, N. K.; Perry, M. L.; Almarsson, O.; and Zaworotko, M. J. Pharmaceutical cocrystals: along the path to improved medicines. *Chem. Commun*., **2016**, 52, 640-655

128. Babu, N. J.; Nangia, A. Solubility advantage of amorphous drugs and pharmaceutical cocrystals. *Crystal Growth & Design* **2011**, 11, 2662-2679.

129. Sanphui, P.; Devi, V. K.; Clara, D.; Malviya, N.; Ganguly, S.; Desiraju, G. R. Cocrystals of Hydrochlorothiazide: Solubility and Diffusion/Permeability

Enhancements through Drug−Coformer Interactions. *Mol. Pharmaceutics* **2015**, 12, 1615−1622

130. Banik, M.; Gopi, S. P.; Ganguly, S.; Desiraju, G. R. Cocrystal and Salt Forms of Furosemide: Solubility and Diffusion Variations. *Cryst. Growth Des*. **2016**, 16, 5418−5428
131. Schultheiss, N.; and Newman, A. Pharmaceutical Cocrystals and Their Physicochemical Properties. *Cryst. Growth Des.* **2009**, 9, 2950-2967.
132. Food and Drug Administration. Regulatory Classification of Pharmaceutical Co-Crystals, Guidance for Industry. **2013**.
133. Aakery, C. B.; Salmon, D. J. Building co-crystals with molecular sense and supramolecular sensibility. **2005.**
134. Chen, Y.; Li, L.; Yao, J.; Ma, Y. Y.; Chen, J. M.; Lu, T. B. Improving the Solubility and Bioavailability of Apixaban via Apixaban−Oxalic Acid Cocrystal. *Cryst. Growth Des.* **2016**, 16, 2923−2930
135. Dai, X. L.; Voronin, A. P.; Gao, W.; Perlovich, G. L.; Lu, T.; Chen, J. Intermolecular interactions and permeability of 5-fluorouracil cocrystals with a series of isomeric hydroxybenzoic acids: a combined theoretical and experimental study. *CrystEngComm*, **2019**, 21, 5095–5105
136. Yan, Y.; Chen, J. M.; and Lu, T.B. Simultaneously enhancing the solubility and permeability of acyclovir by crystal engineering approach. CrystEngComm, **2013**, 15, 6457–6460
137. Sreekanth, B. R.; Vishweshwar, P.; Vyas, K. Supramolecular synthon polymorphism in 2: 1 co-crystal of 4-hydroxybenzoic acid and 2, 3, 5, 6-tetramethylpyrazine. *Chemical Communications* **2007**, 23, 2375-2377.
138. Sarma, B.; Nath, N. K.; Bhogala, B. R.; Nangia, A. Synthon competition and cooperation in molecular salts of hydroxybenzoic acids and aminopyridines. *Crystal Growth & Design* **2009**, 9, 1546-1557.
139. Nangia, A.; Desiraju, G. R. Supramolecular synthons and pattern recognition. *In Design of Organic Solids* **1998**, 57-95.
140. Saikia, B.; Bora, P.; Khatioda, R.; Sarma, B. Hydrogen bond synthons in the interplay of solubility and membrane permeability/diffusion in variable stoichiometry drug cocrystals. *Crystal Growth & Design* **2015**, 15, 5593-5603.

141. Etter, M. C. A new role for hydrogen-bond acceptors in influencing packing patterns of carboxylic acids and amides. *J. Am. Chem. Soc.* **1982,** *104*, 1095–1096.

142. Etter, M. C.; Macdonald, J. C.; and Bernstein, J. Graph-set analysis of hydrogen-bond patterns in organic crystals. *Acta Crystallogr., Sect. B.* **1990**, *46*, 256–262.

143. Aakeroy, C. B.; Beatty, A.M.; Helfrich, B. A. Total Synthesis Supramolecular Style: Design and Hydrogen-Bond-Directed Assembly of Ternary Supermolecules. *Angew. Chem. Int. Ed.* **2001**, 40, 3240-3242

144. Aakeroy, C. B.; Desper, J.; Smith, M. M. Constructing, deconstructing, and reconstructing ternary supermolecules. *Chem. Commun*., **2007**, 3936–3938

145. Tothadi, S.; Mukherjee, A.; Desiraju, G. R. Shape and size mimicry in the design of ternary molecular solids: towards a robust strategy for crystal engineering. *Chem. Commun.*, **2011**, **47**, 12080–12082

146. Bhogala, B. R.; Basavoju, S.; Nangia, A. Three-Component Carboxylic Acid−Bipyridine Lattice Inclusion Host. Supramolecular Synthesis of Ternary Cocrystals. *Crystal Growth & Design* **2005**, 5, 1683-1686

147. Tothadi, S.; Desiraju, G. R. Designing ternary cocrystals with hydrogen bonds and halogen bonds. *Chem. Commun.*, **2013**, 49, 7791−7793

148. Bolla, G.; Nangia, A. Multicomponent ternary cocrystals of the sulfonamide group with pyridine-amides and lactams. *Chem. Commun.*, **2015**, 51, 15578—15581

149. Saha, B. K.; Nangia, A.; Jaskolski, M. Crystal engineering with hydrogen bonds and halogen bonds. *CrystEngComm*, **2005**, 7, 355–358

150. Paul, M.; Chakraborty, S.; Desiraju, G. R. Six-Component Molecular Solids: ABC[D1−(x+y)ExFy]2. *J. Am. Chem. Soc.* **2018**, 140, 2309−2315

151. Dubey, R.; Desiraju, G. R. Combinatorial selection of molecular conformations and supramolecular synthons in quercetin cocrystal landscapes: a route to ternary solids. *IUCrJ* **2015**. 2, 402–408

152. Dabros, M.; Emery, P. R.; Thalladi, V. R. A Supramolecular Approach to Organic Alloys: Cocrystals and Three and Four-Component Solid Solutions of 1,4 Diazabicyclo[2.2.2]octane and 4-X-Phenols (X=Cl, CH3, Br). *Angew. Chem*. **2007**, 119, 4210 –4213

153. Dubey, R.; Mir, N. A.; Desiraju, G. R. Quaternary cocrystals: combinatorial synthetic strategies based on long-range synthon Aufbau modules (LSAM). *IUCrJ* **2016**. 3, 102–107

154. Mir, N. A.; Dubey, R.; Desiraju, G. R. Four- and five-component molecular solids: crystal engineering strategies based on structural inequivalence. *IUCrJ* **2016**. 3, 96–101

155. Mir, N. A.; Dubey, R.; Tothadi, S.; Desiraju, G. R. Combinatorial crystal synthesis of ternary solids based on 2-methylresorcinol. *CrystEngComm*, **2015**, 17, 7866–7869

156. Dubey, R.; Pavan, M. S.; Guru Row, T. N.; Desiraju, G. R. Crystal landscape in the orcinol:4,4'-bipyridine system: synthon modularity, polymorphism and transferability of multipole charge density parameters. *IUCrJ* **2014**. 1, 8–18

157. Dubey, R.; Desiraju, G. R. Combinatorial Crystal Synthesis: Structural Landscape of Phloroglucinol: 1, 2-bis(4-pyridyl)ethylene and Phloroglucinol:Phenazine. *Angew. Chem. Int. Ed.* **2014**, 53, 13178 –13182

158. Aitipamula, S.; Wong, A. B. H.; Chow, P. S.; Tan, R. B. H. Novel solid forms of the anti-tuberculosis drug, Isoniazid: ternary and polymorphic cocrystals. *CrystEngComm*, **2013**, 15, 5877–5887

159. Bolla, G.; Nangia, A.; Binary and ternary cocrystals of sulfa drug acetazolamide with pyridine carboxamides and cyclic amides. *IUCrJ* **2016**. 3, 152–160

160. Wohler, F. *Annalen*, **1844**, 51, 145.

161. Ling, A. R.; and Baker, J. L. Derivatives of quinhydrone. J. Chem. Soc., **1893**, 63, 1314

162. Roche, F. H.; Basel (Switzerland), CH 187826, **1937**

163. Hilden L R.; Morris K R.; Physics of amorphous solids. *Journal of Pharmaceutical Sciences* **2004**, 93, 3-12.

164. Zallen, R. The physics of amorphous solids. *John Wiley & Sons.* **1983**.

165. Thakuria, R.; Nangia, A. Highly soluble olanzapinium maleate crystalline salts. *CrystEngComm.* **2011**, 13, 1759-1764.

166. Yu L. Amorphous pharmaceutical solids: preparation, characterization and stabilization. *Advanced drug delivery reviews* **2001**, 48, 27-42.

167. Willart, J. F.; Descamps, M. Solid state amorphization of pharmaceuticals. *Molecular Pharmaceutics* **2008**, 5, 905-920.

168. Poole, P. H.; Grande, T.; Angell, C. A.; McMillan, P. F. Polymorphic phase transitions in liquids and glasses. *Science* **1997**, 275, 322-323.

169. Kieffer, J. Structural transitions and glass formation. *The Journal of Physical Chemistry B.* **1999**, 103, 4153-4158.

170. Duggirala, N. K.; Li, J.; Kumar, N. K.; Gopinath, T.; Suryanarayanan, R. A supramolecular synthon approach to design amorphous solid dispersions with exceptional physical stability. *Chemical Communications* **2019**, 55, 5551-5554.

171. Chieng, N.; Aaltonen, J.; Saville, D.; Rades, T. Physical characterization and stability of amorphous indomethacin and ranitidine hydrochloride binary systems prepared by mechanical activation. *European Journal of Pharmaceutics and Biopharmaceutics* **2009**, 71, 47-54.

172. Laitinen, R.; Löbmann, K.; Strachan, C. J.; Grohganz, H.; Rades, T. Emerging trends in the stabilization of amorphous drugs. *International Journal of Pharmaceutics* **2013**, 453, 65-79.

173. Laitinen, R.; Priemel, P. A.; Surwase, S.; Graeser, K.; Strachan, C. J.; Grohganz, H.; Rades T. Theoretical considerations in developing amorphous solid dispersions. *In Amorphous Solid Dispersions* **2014**, 35-90.

174. Löbmann K.; Laitinen, R.; Grohganz, H.; Gordon, K. C.; Strachan, C.; Rades, T. Coamorphous drug systems: enhanced physical stability and dissolution rate of indomethacin and naproxen. *Molecular Pharmaceutics* **2011**, 8, 1919-1928.

175. Chiou, W. L.; Riegelman, S.; Pharmaceutical applications of solid dispersion systems. *Journal of Pharmaceutical Sciences* **1971**, 60, 1281-1302.

176. Löbmann, K.; Jensen, K. T.; Laitinen, R.; Rades, T.; Strachan, C. J.; Grohganz, H. Stabilized amorphous solid dispersions with small molecule excipients. *In Amorphous Solid Dispersions* **2014**, 613-636.

177. Shi, Q.; Moinuddin, S. M.; Cai, T. Advances in coamorphus drug delivery systems. *Acta pharmaceutica sinica B* **2019**, 9, 19-35.

178. Suresh, K.; Mannava, M. C.; Nangia, A. A novel curcumin-artemisinin coamorphous solid: Physical properties and pharmacokinetic profile. *RSC Advances* **2014**, 4, 58357-58361.

179. Qian, S.; Heng, W.; Wei, Y.; Zhang, J.; Gao, Y. Coamorphous lurasidone hydrochloride-saccharin with charge-assisted hydrogen bonding interaction shows improved physical stability and enhanced dissolution with pH-

independent solubility behavior. *Crystal Growth & Design* **2015**, 15, 2920-2928.

180. Löbmann, K.; Strachan, C.; Grohganz, H.; Rades, T.; Korhonen, O.; Laitinen, R. Co-amorphous simvastatin and glipizide combinations show improved physical stability without evidence of intermolecular interactions. *European Journal of Pharmaceutics and Biopharmaceutics* **2012**, 81, 159-169.

181. Couillaud, B. M.; Espeau, P.; Mignet, N.; Corvis, Y. State of the art of pharmaceutical solid forms: from crystal property issues to nanocrystals formulation. *ChemMedChem.* **2019**, 14, 8-23.

## *CHAPTER TWO*

# Novel Pharmaceutical Cocrystals, Salts and Ternary Products of Bumetanide

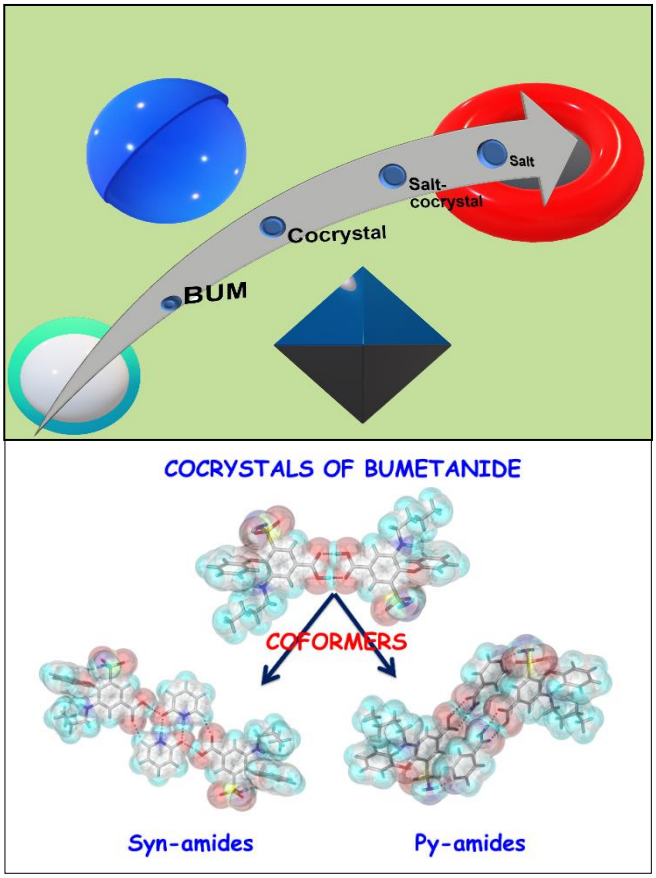


***Bumetanide (BUM) is a potent diuretic drug in BCS class II with low solubility. BUM molecule has multiple functional groups to form salts, cocrystals and ternary products. In general, salts, cocrystals are preferred to improve the physiochemical properties of drugs such as solubility, dissolution rate and permeability. Herein we report novel solid forms of bumetanide binary cocrystals/salts and ternary products.***

## 2.1 Introduction

Cocrystals of active pharmaceutical ingredients (APIs) are important to fine tune physicochemical properties such as solubility, dissolution, bioavailability and stability.[1-2] The design of cocrystals requires an understanding of hydrogen bonding functional groups and supramolecular synthons[3] between the drug and the conformer molecules.[4-5] Synthons are sub-classified as homosynthons and heterosynthons, i.e. those between like and unlike functional groups, respectively.[6-7] We have reported sulfonamide cocrystals with lactams, syn-amides and pyridine-carboxamides to produce binary and ternary cocrystals.[8-11] The novel supramolecular synthons of the sulfonamide group identified in our study were successfully applied towards a ternary pharmaceutical cocrystal of acetazolamide drug.[9] This study deals with another sulfonamide drug bumetanide, which is in the same class as the well-known furosemide (lasix), piretanide, azosemide, and torsemide.[12-13]

Bumetanide (3-n-butylamino-4-phenoxy-5-sulfamoyl-benzoic acid, abbreviated as BUM) is a sulfamoyl category diuretic drug[14] which is 40 times more effective than the well-known known furosemide (common name Lasix).[15] BUM is a potent diuretic drug used in the treatment of congestive heart failure, hepatic, renal diseases as well as to cure mild or moderate hypertension. Its principal site of action is the thick ascending limb of the henle loop, where it exerts its diuretic and natriuretic effect and it produces a rapid marked diuresis, thus increasing urinary excretion of sodium, chloride, and other electrolytes which persist for several hours. However, low water solubility limits its use. BUM molecule has multiple hydrogen bonding functional groups of $SO_2NH_2$, COOH, phenoxy, and aliphatic secondary amine NH. Hence it can form salts and cocrystals. In general, salts and cocrystals are preferred to improve the physiochemical properties of the drugs such as solubility, bioavailability dissolution rate, and stability.[2,16-20] As a general rule, complete proton transfer from the acid to the base occurs in salts whereas in cocrystal the proton remains on the acid site; and in salt-cocrystal the proton is shared in-between the acid and the base, or in case of multiple acidic/ basic sites, one proton is free and the other is shared.[21-22] Among the functional groups COOH, $CONH_2$, pyridine, and OH, the sulfonamide group is chemically different due to conformational flexibility, two O acceptors and 2 NH donors, and it is able to form the more stable homo dimer.[23-26] Sulfa drugs are limited by their physicochemical properties of low solubility and hence the design of soluble cocrystals and salts is essential.

Herein we report new binary crystal phases of cocrystals/salts and ternary products of BUM by exploiting the supramolecular synthon design approach.[27] Sodium and potassium salt hydrates and cocrystal polymorphs of BUM-4-aminobenzoic acid have been reported.[28-29] Most of the coformers, used for the synthesis of cocrystals/salts/hydrates are listed in US-FDA list as GRAS (Generally Regarded As Safe) category molecules and these are used in marketed drugs. Due to their potential applications in the pharmaceutical industry, we selected those molecules which will exhibit enhancement in solubility and dissolution rate. From the molecular structure of BUM, there are two strong hydrogen bond bonding groups (acid and sulfonamide) and hence complementary hydrogen bonding groups in coformers were selected. In addition, based on a survey of the Cambridge Structural Database (CSD)[30-33], These coformers form a larger number of cocrystals/ salts/ hydrates with functionalized molecules. Solvent-assisted grinding method is preferred to make binary complexes compared to neat grinding because reactivity is accelerated.[34-35] The liquid acts as lubricant and together with mechanical force form initial cocrystal nucleus. Cocrystals of BUM with selected coformers such as pyridines (labeled as AB1) e.g. 2-hydroxy pyridone (2HP), 6-methyl-2-pyridone (MeHP), 3-methoxypyridone (OMeHP), with pyridine caboxamides (labeled as AB2), e.g. isonicotinamide (INA), picolinamide (PAM) and nicotinamide (NAM) crystallized. The cocrystal of BUM with nicotinamide (NAM) could not afford single crystals and aromatic acids, such as 2-picolinic acid (PCA), 4-aminosalicylic acid (PASA), vanillic acid (VLA) were used as the third component labeled C such as lactams include caprolactam (CPR), N-methyl caprolactam (NMeCPR), valerolactam (VLM), urea; and amines include piperazine (PIP) Cytosine (CYT) and 5-flouro-cytosine (5FCYT) were used as the fourth component labeled D. All the products were characterized by PXRD, IR and DSC.

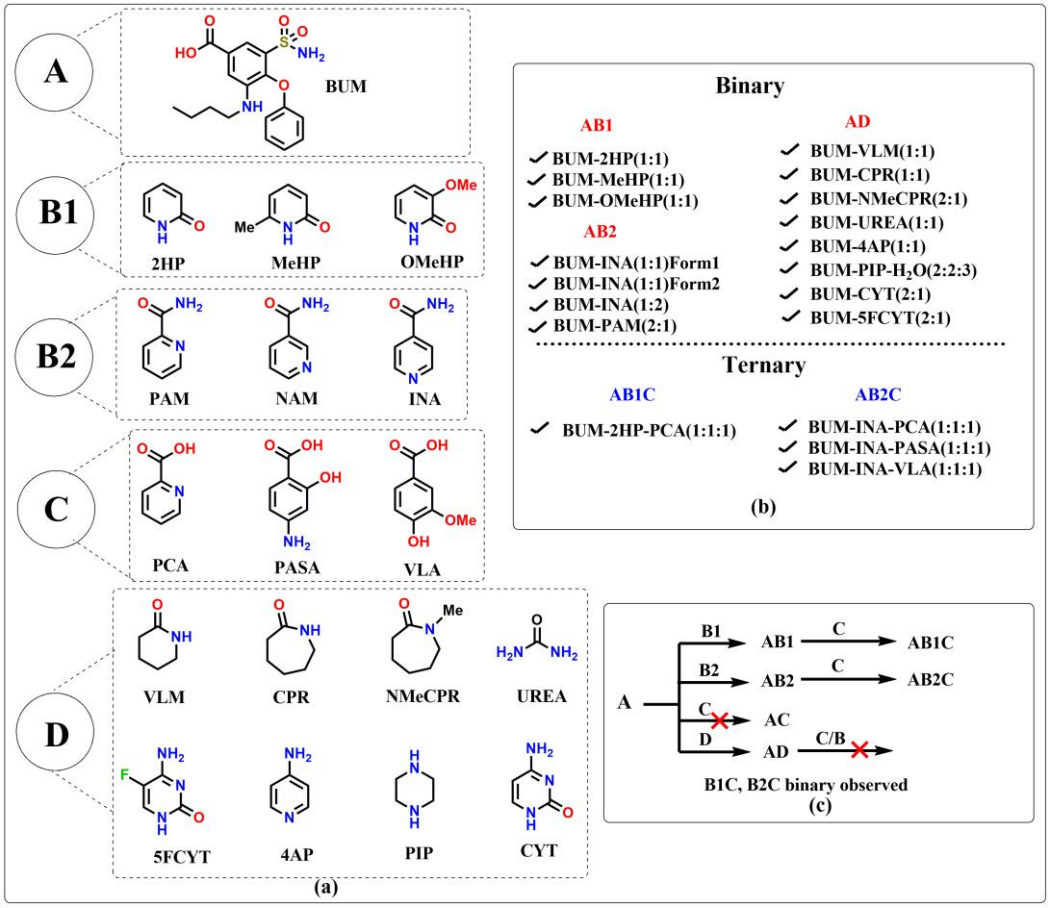


**Figure 2.1:** (a) Chemical structures of BUM, **A**; coformers syn−amides, **B1**; pyridine carboxamides, **B2**; carboxylic acids, **C** and lactams, amines, **D**. (b) and (c) Binary and ternary adducts obtained in this study.

## 2.2 Results and Discussion

BUM crystallizes in the monoclinic (space group $P2_1/c$) with one molecule of bumetanide in the asymmetric unit. Its crystal structure (Figure 1a) shows the acid-acid dimer $R_2^2(8)$ motif and sulfonamide catemer chain (C4) synthon.[36-37] Supramolecular synthons are shown in Scheme 2. The single crystal structure of BUM has molecules connected via the carboxylic acid dimer homosynthon and N−H···O hydrogen bonds. These intermolecular interactions together with our experience with similar molecules such as furosemide,[15] acetazolamide,[11] and p-sulfonamide benzoic acid[10] suggested that coformers such as pyridones (2HP, MeHP, OMeHP), pyridine carboxamides (INA, PAM and NAM) and acids, lactams will result in binary and possibly ternary cocrystals.

The solubility, dissolution and permeability of cocrystals were performed to compare their physicochemical behavior with the reference drug BUM. There is moderate improvement in the physicochemical properties of the binary adducts. Additionally, we crystallized four ternary crystalline pharmaceutical materials (AB1C and AB2C) along with sulfonamide−amide binary adducts (AB1, AB2, AD). All coformers used in this study are GRAS (generally regarded as safe) compounds defined by the US-FDA.[38] Single crystals were grown from different solvents and X-ray diffraction data was solved to obtain crystal structures which are classified as cocrystal, salt, and salt-cocrystal. BUM afforded eleven binary cocrystals BUM-2HP, BUM-MeHP, BUM-OMeHP, BUM-INA (three forms), BUM-PAM, BUM−VLM, BUM−CPR, BUM−NMeCPR, BUM−UREA, two salt-cocrystal adduct BUM−CYT, BUM−5FCYT, two salts BUM−4AP, BUM−PIPH and four ternary cocrystal products BUM–INA–PCA (1:1:1), BUM–INA–VLA (1:1:1), BUM–INA–PASA (1:1:1) BUM–2HP–PCA (1:1:1). These products were characterized by IR, DSC, and PXRD.

## 2.2.1 Crystal Structure Description

**Bumetanide (BUM, A):**

Bumetanide crystallizes in the monoclinic space group $P2_1/c$ ($Z' = 1$) with molecules connected through the acid−acid homosynthon (O4−H4A···O5, 1.76 Å, 177°) via the $R_2^2(8)$ ring motif.[37,39] Such dimeric units are connected by a chain of N−H···O hydrogen bonds (N2−H2A···O1, 2.37 Å, 140°) from the sulfonamide group (Figure 2.2a). The molecular crystal packing is further stabilized by weak C−H···O hydrogen bonds (Figure 2.2b).

The discussion on bumetanide cocrystals is categorized into three sections based on the coformer: (a) BUM−pyridones (AB1), (b) BUM−pyridine carboxamides (AB2), (c) BUM-lactams, amines (AD) (d) BUM ternary systems (AB1C and AB2C). The labels A, B, C, D are those given in Figure 2.1. Crystallographic parameters and hydrogen bond distances are listed in Table 2.1- 2.3

**Binary cocrystals of BUM−Pyridones (AB1):**

Pharmaceutically safe coformers, e.g. 2HP, MeHP, OMeHP, were cocrystallized with BUM as detailed in the experimental section to harvest good quality single crystals for X-ray diffraction. 2HP and MeHP are connected through N–H···O catemer chain in their native crystal structures. Interestingly, the coformer disrupts the acid dimer synthon of

BUM to result in four point synthon of acid–pyridone O–H···N and N–H···O bonds of pyridine dimer in $R_3^2(9)R_2^2(8)R_3^2(9)$ motif (Figure 2.2c). Similar kind of H bonded rings can also be seen in acemetacin drug which contains the COOH functional group.[40] The sulfonamide group participates in a catemer chain, similar to that in BUM structure. The 2D mixed stack packing of BUM−2HP is displayed in Figure 2.2d.

BUM−MeHP crystallizes in space group *C*2/*c* with one BUM and one MeHP molecule in the asymmetric unit. Similar to BUM−2HP, the molecular packing in BUM−MeHP is stabilized by N−H···O and O−H···O hydrogen bonds, but now via pyridine dimers connected to the COOH donor in a $R_2^2(8)R_2^2(8)R_2^2(8)$ motif. The sulfonamide catemer chains extend along the *b*-axis (Figure 2.2e). The individual layer packing in BUM−MeHP is shown in Figure 2.2f.

In the structure of BUM−OMeHP ($P2_1/n$), BUM molecules are connected through sulfonamide dimer homosynthon with $R_3^2(9)R_1^2(5)R_2^2(8)R_1^2(5)R_3^2(9)$ graph set motif (Figure 2.2g), which mimics the synthon in BUM−2HP structure. The main difference between this structure and previous ones is that the sulfonamide groups extend via dimer synthon whereas in BUM−2HP and BUM−MeHP structures catemer chains are present. The 2D segregated packing of BUM−OMeHP is shown in Figure 2.2h.

$BUM^-$−BUM−$CYTH^+$ (1:1:1) cocrystal salt crystallized in *P*-1 space group with two BUM and one CYT molecules/ ions in the asymmetric unit. In this structure compete proton transfer from the acid group of BUM to the pyridine acceptor of CYT is observed. The two BUM molecules (neutral + anion) are bonded via the acid dimer homosynthon as well carboxylate−cytosinium heterosynthon. There are five different ring motifs in the crystal structure (labeled 1 through 5 (Figure 2.2i). CYT molecules form pyridine dimer type synthon of $R_2^2(8)$ motif (N5−H5A···O5, 1.99 Å, 166°). The $R_3^2(8)$ bridged sulfonamide···carboxylate (N2−H2A···O9, 2.05Å, 153°), sulfonamide···CYT carbonyl (N2−H2B···O5, 2.30Å, 138°) and $CYTH^+\cdots CO_2^-$ (N4−H4A···O9, 1.95Å, 176°) are present in the synthon rich structural motifs. The amino-pyridine···carboxylate $R_2^2(8)$ motif (N4−H4A···O9 1.95 Å, 176°; N3−H3A···O10 1.84Å, 168°) and sulfonamide···amine catemer chain (N3−H3B···O1, 2.16 Å, 142°) and sulfonamide···carboxylate carbonyl dimer ring motif $R_2^2(16)$ (N1−H1B···O10 2.13 Å, 155°) are present in the network of hydrogen bonds. The acid dimers extend the packing in 2D (O8−H8A···O7, 1.86Å, 176°) of the salt-cocrystal structure (Figure 2.2j).

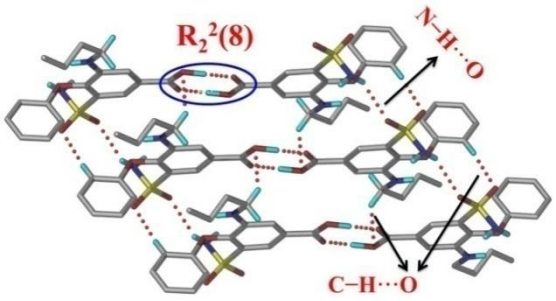
$R_2^2(8)$
N–H···O
C–H···O

**(a)**

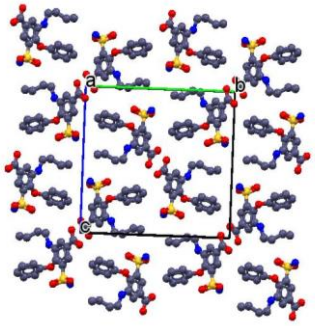
a
b
c

**(b)**

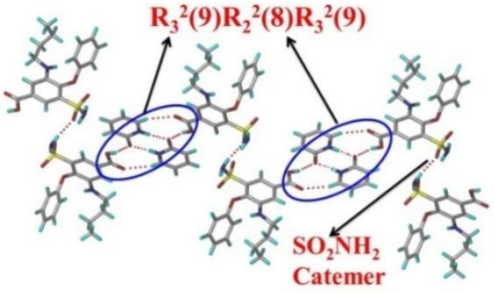
$R_3^2(9)R_2^2(8)R_3^2(9)$
$SO_2NH_2$
Catemer

**(c)**

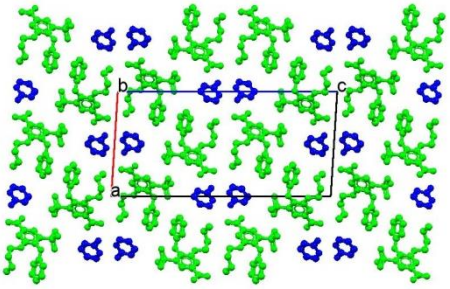
b
c
a

**(d)**

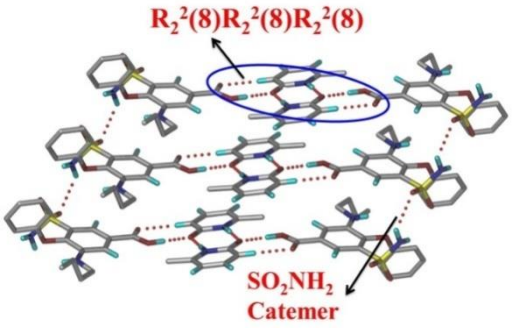
$R_2^2(8)R_2^2(8)R_2^2(8)$
$SO_2NH_2$
Catemer

**(e)**

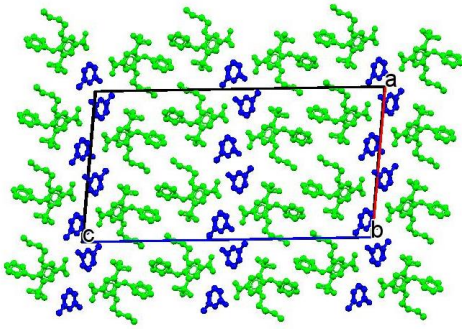
a
c
b

**(f)**

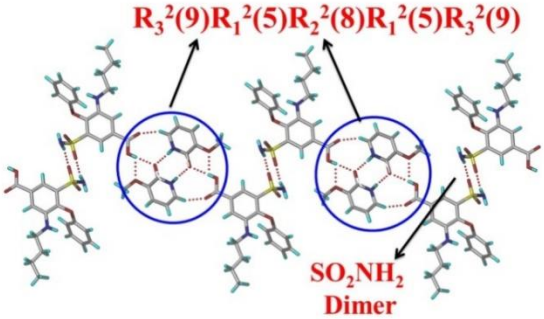
$R_3^2(9)R_1^2(5)R_2^2(8)R_1^2(5)R_3^2(9)$
$SO_2NH_2$
Dimer

**(g)**

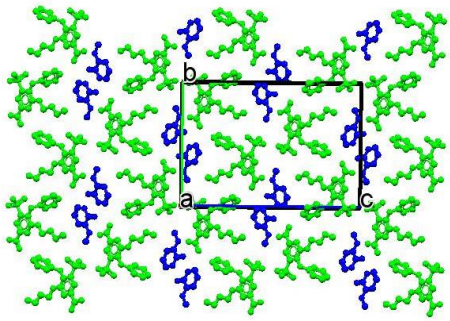
b
a
c

**(h)**

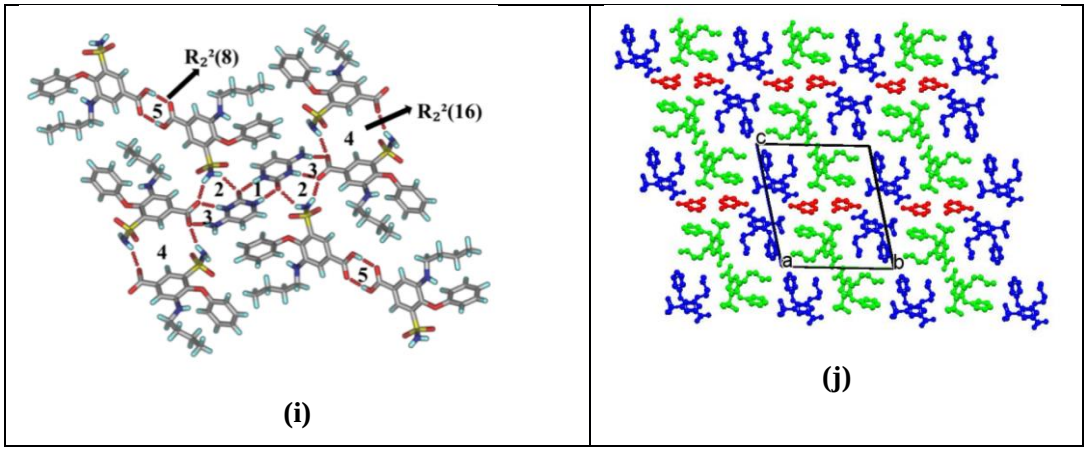


**Figure 2.2:** (a) BUM molecules are connected through carboxylic acid dimer synthon in $R_2^2(8)$ ring motif. (b) Sulfonamides catemers are connected by N−H···O hydrogen bonds in the structure of BUM. (c) BUM–2HP (1:1) cocrystal structure contains amide dimer synthon $R_2^2(8)$ rings connected with carbocylic acid together with sulfonamide catemer chains. (d) 2D packing of BUM–2HP. (e) BUM–MeHP (1:1) structure is shown with amide dimer synthon ring $R_2^2(8)$ ring. (f) 2D tape sulfonamide catemer chain in BUM–MeHP. (g) BUM–OMeHP (1:1) structure shows molecules connected through amide dimer synthon $R_2^2(8)$ ring connected with acid and sulfonamide dimer ring of $R_2^2(8)$ motif. (h) 2D packing in the BUM–OMeHP. (i) BUM–CYT (2:1) cocrystal-salt structure with molecules connected via amide dimer synthon ring and sulfonamide bridged $R_3^2(8)$ ring motif and carboxylate···amino-pyridinium ring motif. (j) BUM−CYT salt-cocrystal 2D molecular packing.

**Binary cocrystals BUM−Pyridine carboxamides (AB2):**

Isomers of pyridine carboxamide coformers, such as INA, NAM, PAM were used for cocrystallization with multi-functional BUM drug. Single crystals of BUM−INA and BUM−PAM were obtained, but diffraction quality crystals of BUM−NAM could not be obtained from any of the crystallization experiments. BUM−INA resulted in two polymorphic cocrystals (Form I, II) and a cocrystal with 1:2 stoichiometry.

BUM−INA crystallized in the monoclinic space group $P2_1/c$ (Form I) via the robust acid···amide heterosynthon $R_2^2(8)$ ring (O3−H3A···O6, 1.86 Å, 175°; N4−H4B···O2 2.20 Å, 157°; Figure 2.3a). The dimeric pair extends through acid···sulfonamide ($COOH\cdots SO_2NH_2$: N2−H2A···O4, 2.22Å, 165°) and amide···sulfonamide ($CONH_2\cdots SO_2NH_2$: N4−H4A···O4, 2.21Å, 163°) synthons. The other side of BUM

molecule interacts with INA through N2−H2B···N3 (2.08Å, 165°) hydrogen bond and the 2D packing is shown in Figure 2.3b.

Crystals of BUM−INA Form II were obtained concomitantly with Form I during crystallization in EtOAc–$CH_3CN$ in orthorhombic space group *Pbca*. BUM and INA molecules associate via acid···amide heterosynthon (O4−H4C···O6, 1.79 Å, 175°; N4−H4B···O5 2.06 Å, 168°) with $R_2^2(8)$ motif. Similar to Form I, the molecular packing extends through N−H···O and N−H···N hydrogen bonds on either side of acid-amide heterosynthon (Figure 2.3c). The difference between Form I and II is the orientation of alkyl chain and distance between alkyl chain and the phenyl ring, e.g. in Form II the C11 and C14 distance is 3.852(8) Å whereas the corresponding distance in Form I is 4.020(7) Å. Sulfonamide···pyridine N2−H2A···N3 (2.12Å, 166°) hydrogen bond further strengthens the crystal packing (Figure 2.3d).

The cocrystal of BUM−INA crystallizes in the monoclinic space group $P2_1/c$ with one BUM and two INA molecules in the asymmetric unit. BUM and INA molecules associate with four ring motifs, amide homosynthon $R_2^2(8)$ ring (N4−H4B···O7, 1.93 Å, 175°; N6−H6B···O62.13Å, 173°). The second ring motif is two-dimensional hydrogen bonding of primary amides extended in a ladder type network of $R_4^2(8)$ ring (three point synthon) (Figure 2.3e). The third motif is $R_6^6(26)$ ring motif (amide···acid, N6−H6A···O5, 2.09Å, 161° and acid···pyridine synthon, O4−H4C···N31.77Å, 179°). The fourth $R_2^2(15)$ ring motif is formed with amide···acid (N6−H6A···O5, 2.09Å, 161°) and sulfonamide···pyridine synthon (N2−H2B···N52.15Å, 165°), and the 2D packing is displayed in Figure 2.3f.

BUM−PAM (2:1) crystallizes in the triclinic space group *P*1. BUM and PAM are associated *via* acid···amide hetero synthon with $R_2^2(8)$ motif (O9−H9C···O11, 1.53Å, 166° and N6−H6A···O10, 2.18 Å, 160°) (Figure 2.3g, h). Another motif is formed between acid carbonyl···acid hydroxyl $R_2^2(6)$ ring (O4−H4C···O10, 1.84 Å, 177°) and acid carbonyl···amide N−H hydrogen (N6−H6A···O5, 2.45 Å, 110°). An additional $R_2^2(8)$ ring motif is obtained with sulfonamide homodimer (N2−H2B···O7, 2.26 Å, 155°; N4−H4A···O1, 2.16 Å, 166°). In the structure of BUM−PAM, the 2D tape extends via weak C−H···N hydrogen bond (C39−H39···N2, 2.72 Å, 154.94°; Figure 2.3h).

The ΔpKa rule [$\Delta pK_a$ = $pK_a$ (conjugate acid of base) − $pK_a$ (acid)], is a simple guide to know primarily the ionization state of an acid−base complex. The product is a neutral

cocrystal ($\Delta pK_a < 3$) or an ionic salt ($\Delta pK_a > 3$). A more practical cut-off for organic salts is $\Delta pK_a < 0$ for cocrystal, $\Delta pK_a > 3$ for salts, and the range $0 < \Delta pK_a < 3$ being an in-between zone where multiple proton states could be observed.[41] It is observed that careful analysis cytosine crystal structures, it forms salts in 77% cases and 23% are neutral compounds. The nitrogen which is located between amine and carbonyl groups is prone to be more basic and it accepts a proton from other donors.

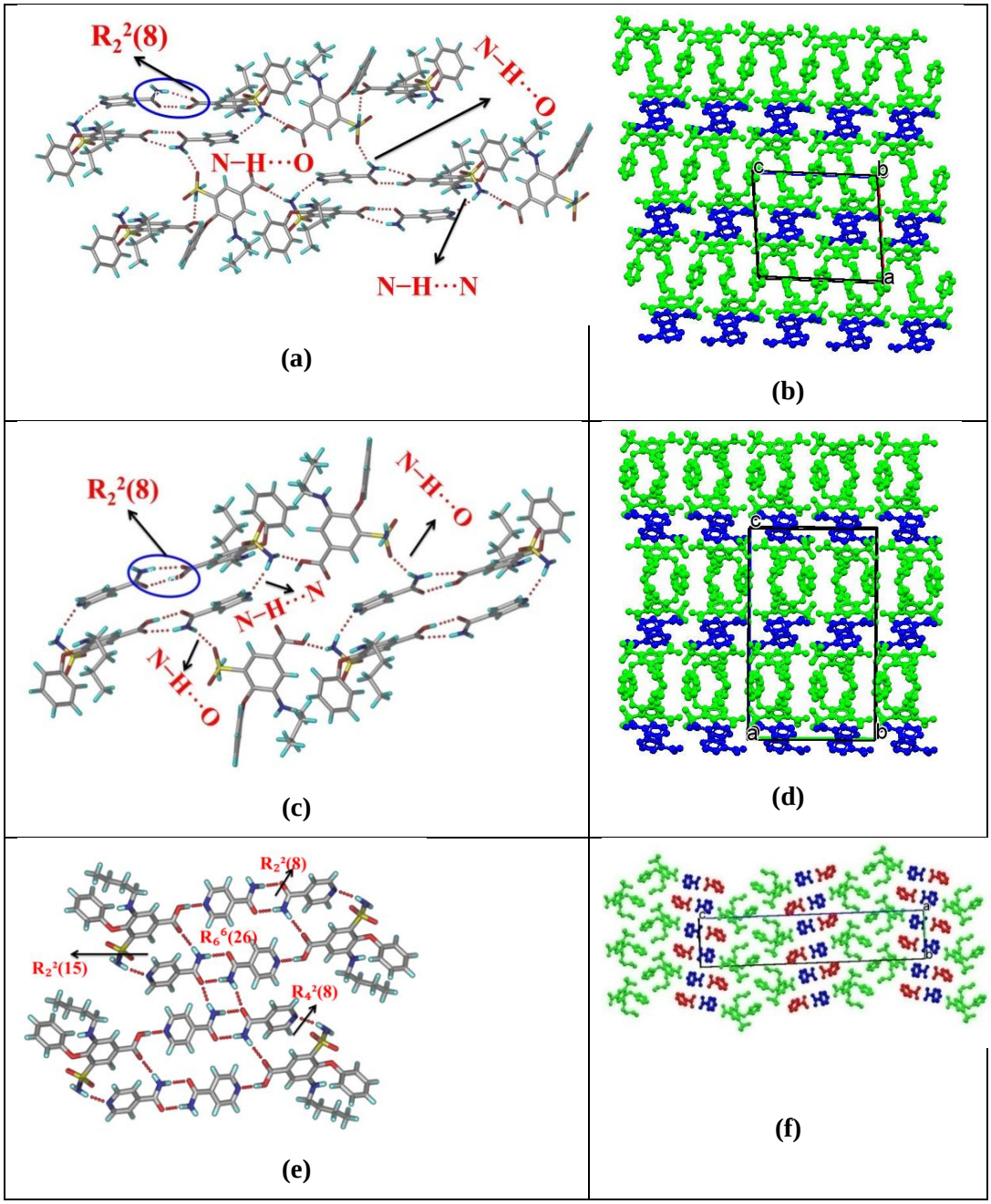

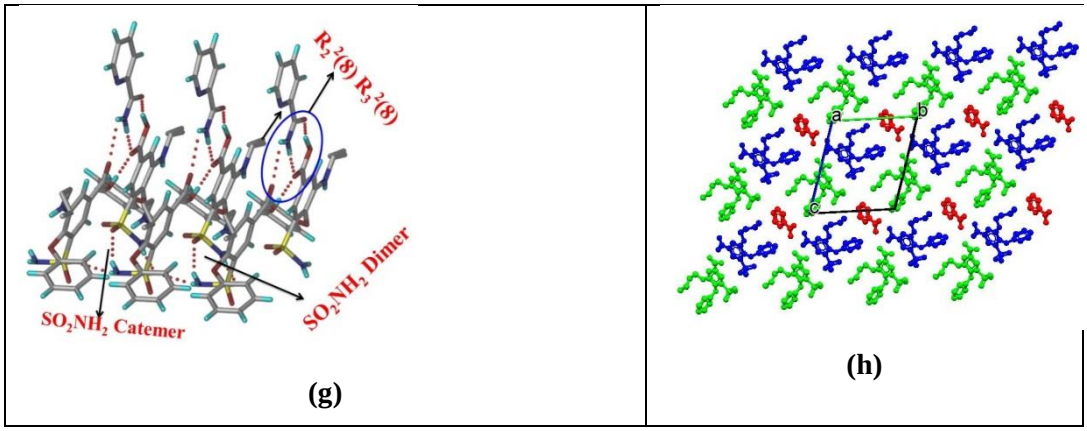


**Figure 2.3:** (a) BUM–INA Form I (1:1) cocrystal: The molecules are connected through acid···amide dimer heterosynthon in $R_2^2(8)$ ring motif along with sulfonamide···pyridine synthon. (b) BUM–INA Form I (1:1) cocrystal 2D packing. (c) BUM–INA Form II (1:1) cocrystal: The molecules are connected through acid···amide dimer heterosynthon similar to Form I and sulfonamide···pyridine synthon. (d) BUM–INA Form II (1:1) cocrystal 2D packing. (e) BUM–INA (1:2): The molecules are connected through amide···amide homodimer, sulfonamide···pyridine, acid···pyridine synthons followed by four ring motifs. (f) Molecular packing in BUM–INA (1:2) cocrystal. (g) BUM–PAM (2:1) cocrystal: The molecules are connected through acid···amide dimer synthon hydrogen bonded with another acid of BUM molecule. (h) BUM−PAM (2:1) cocrystal extend in a 2D tape via weak C−H···N hydrogen bonds between carboxamide C−H and sulfonamide nitrogen.

**Binary cocrystals BUM−lactams (AD):**

BUM−VLM (1:1) crystallized in the monoclinic crystal system, $P2_1/c$ with one molecule of each component in the asymmetric unit. The molecules are associated through BUM sulfonamide dimer and VLM heterosynthon (Figure 2.4b). BUM and VLM molecules are bonded via lactam dimer N−H···O (N3−H3B···O6, 2.14 Å, 173°) hydrogen bond to $SO_2NH_2$ synthon (N2−H2B···O6, 2.138 Å, 170°; lactam-$SO_2NH_2$. In contrast to pyridine coformers,[10-11,27] cocrystallization experiment do not affect the acid-acid homodimer of BUM (Figure 2.4a) and the $R_2^2(8)$ ring motif (O3−H3A···O4, 1.81 Å, 168°) is observed. BUM−CPR crystallized in the monoclinic system $P2_1/c$ and is similar to BUM−VLM homolog. CPR molecules associated through syn-amide $R_2^2(8)$ ring motif (N3−H3A···O6, 1.96 Å, 172°) are bonded with BUM sulfonamide and sulfonamide···synamide heterosynthon of N−H···O hydrogen bond (N2−H2B···O6, 2.02 Å, 176°). BUM retains the acid-acid homodimer $R_2^2(8)$ (O4−H4A···O5, 1.77 Å, 175°)

(Figure 2.4c). BUM−NMeCPR (2:1) crystallized in triclinic *P*-1 space group (two BUM and one NMeCPR in asymmetric unit). The acid···acid homodimer $R_2^2(8)$ of BUM (O4−H4C···O10, 1.80 Å, 169° and O9−H9C···O5, 1.80 Å, 168°) is present and interacts with NMeCPR through catemer chain (Figure 2.4d). BUM−UREA (1:1) crystallized in the monoclinic system $P2_1/c$ with BUM and urea bonded through N−H···O hydrogen bonds of sulfonamide···amide dimer $R_2^2(8)$ ring motif (N2−H2B···O6, N4−H4C···O1), BUM acid extends to form N−H···O, O−H···O synthons (N4−H4B···O5, O4−H4A···O6; Figure 2.4e). The structures of BUM, BUM−VLM, BUM−CPR, and BUM−NMeCPR contain the same sulfonamide-lactam synthon.

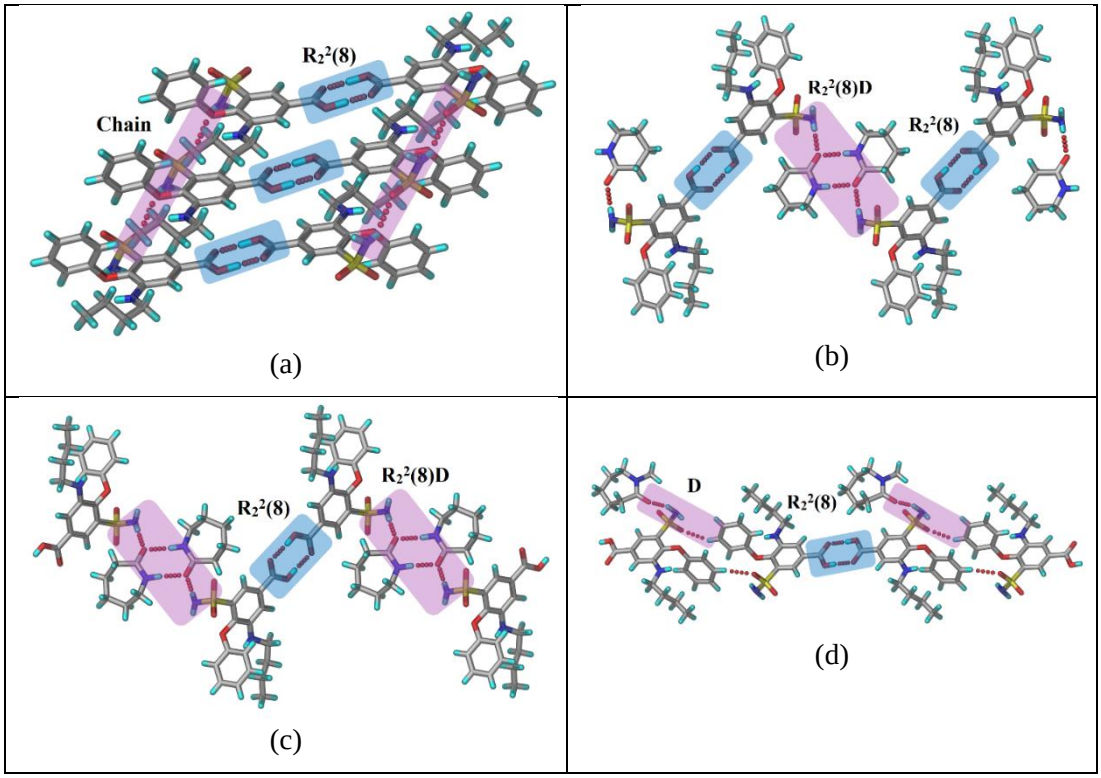

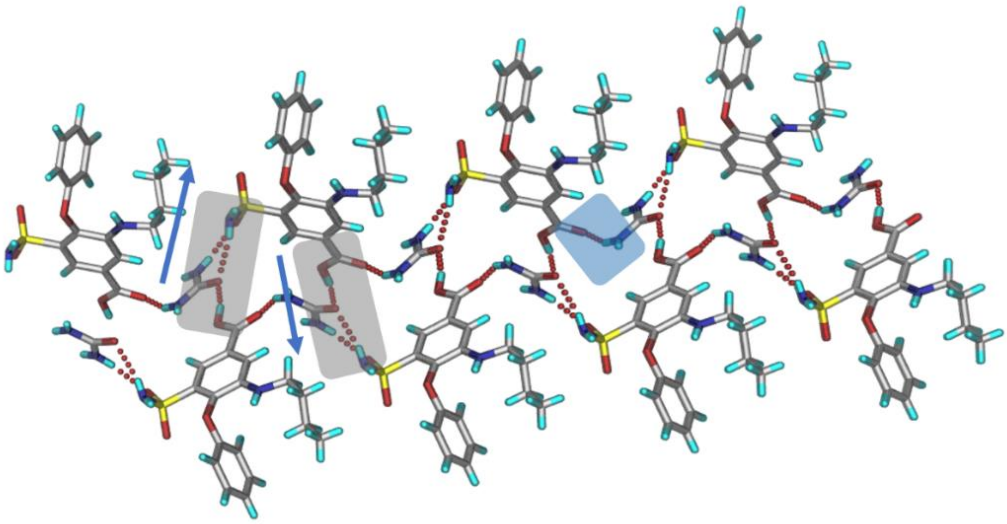

(e)

**Figure 2.4:** (a) BUM molecules are connected through acid···acid dimer synthon via $R_2^2(8)$ ring motif and sulfonamide catemer is connected by N–H···O hydrogen bond. (b) In BUM –VLM (1:1) cocrystal, VLM molecules are connected through amide···amide dimer synthon with $R_2^2(8)$ motif. BUM molecule is connected through acid-acid dimer of $R_2^2(8)$ motif. The difference arises in cocrystals due to the hydrogen bonding functional groups present in coformers. (c) In BUM–CPR (1:1) cocrystal, CPR (lactam) molecules are connected through amide dimer by $R_2^2(8)$ motif and BUM is connected to acid···acid dimer with $R_2^2(8)$ motif. (d) BUM–NMeCPR (2:1) cocrystal molecules are connected through acid dimer synthon ring motif $R_2^2(8)$, sulfonamide catemer chain hydrogen bond with lactam carbonyl oxygen. (e) BUM–UREA (1:1) cocrystal molecules are connected through sulfonamide···amide dimer synthon ring motif $R_2^2(8)$.

**Binary Salts/salt-cocrystals BUM amine (AD):**

BUM–5FCYT (2:1) salt cocrystal with composition ($BUM^-$−BUM−$5FCYTH^+$ (1:1:1) crystallized in *P*-1 space group with one $BUM^-$, one neutral BUM and one $CYTH^+$ molecule/ion in the asymmetric unit (Figure 2.5b). BUM–5FCYT (2:1) salt cocrystal is isostructural with BUM–CYT (2:1) salt cocrystal (Figure 2.5a).[27] Xpac analysis[42] was performed to estimate the disimilarity index of BUM–5FCYT and BUM–CYT to give a value of 1.4, which confirms the 3D isostructural supramolecular construct of both cocrystals (Figure 2.5c). The acid group of bumetanide transfers its proton to the pyridine of 5FCYT. The second BUM forms acid- dimer homosynthon. There are five

different ring motifs in the crystal structure (Figure 2.5b) with 5FCYT molecules making pyridine dimer synthon of $R_2^2(8)$ motif (N5−H5A···O5, 1.99 Å, 166°). The $R_3^2(8)$ bridged sulfonamide···carboxylate (N2−H2A···O9, 2.05Å, 153°), sulfonamide···CYT carbonyl (N2−H2B···O5, 2.30Å, 138°) and $CYTH^{+}\cdots CO_2^{-}$ (N4−H4A···O9, 1.95Å, 176°) synthons are present. The amino-pyridine···carboxylate $R_2^2(8)$ (N4−H4A···O9 1.95 Å, 176°; N3−H3A···O10 1.84Å, 168°) and sulfonamide···amine catemer chain (N3−H3B···O1, 2.16 Å, 142°) and sulfonamide···carboxylate carbonyl dimer ring motif $R_2^2(16)$ (N1−H1B···O10 2.13 Å, 155°) sustain the network of hydrogen bonds. Acid dimers extend the packing (O8−H8A···O7, 1.86Å, 176°) of the salt-cocrystal structure. BUM−PIP−$H_2O$ (2:2:3) salt hydrate crystallized in the triclinic space group *P*-1 with two BUM, two PIP and three $H_2O$ molecules in the asymmetric unit. The carboxylic acid proton of BUM is transferred to piperazine basic nitrogen as salt, BUM and PIP are bonded through N−H···O hydrogen bond of carboxylate···piperazinium tetrameric ring motif $R_2^2(18)$ (N5−H5A···O5, N5−H5B···O4). BUM–4AP (1:1) salt molecules are connected through sulfonamide···carboxylate dimer synthon ring motif $R_2^2(16)$. BUM–PIP salt hydrate molecules are connected through carboxylate···piperazinium tetrameric ring motif $R_2^2(18)$ (Figure 2.5d). BUM–4AP (1:1) salt crystallized in the monoclinic space group $P2_1/c$. BUM acid proton is transferred to 4-amino pyridine basic nitrogen as a salt, BUM and 4AP are bonded through N−H···O hydrogen bond of sulfonamide···carboxylate dimer $R_2^2(16)$ ring motif (N2−H2B···O4). BUM acid with 4AP amine extend via N−H···O synthon (Figure 2.5e, 2.5f). The functional groups attached to the drug as well as coformer shape and size of molecule, and complementary hydrogen bonds are important parameters to make novel crystal forms for similar molecules. This last point has been dealt with using CSD analysis.[31-33]

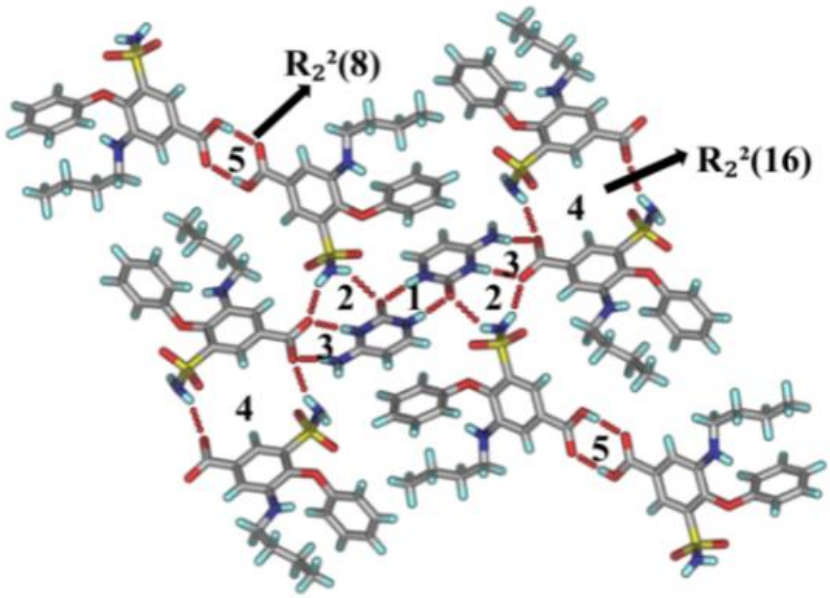
$R_2^2(8)$
$R_2^2(16)$
5
4
3
2
1
2
3
4
5

**(a)**

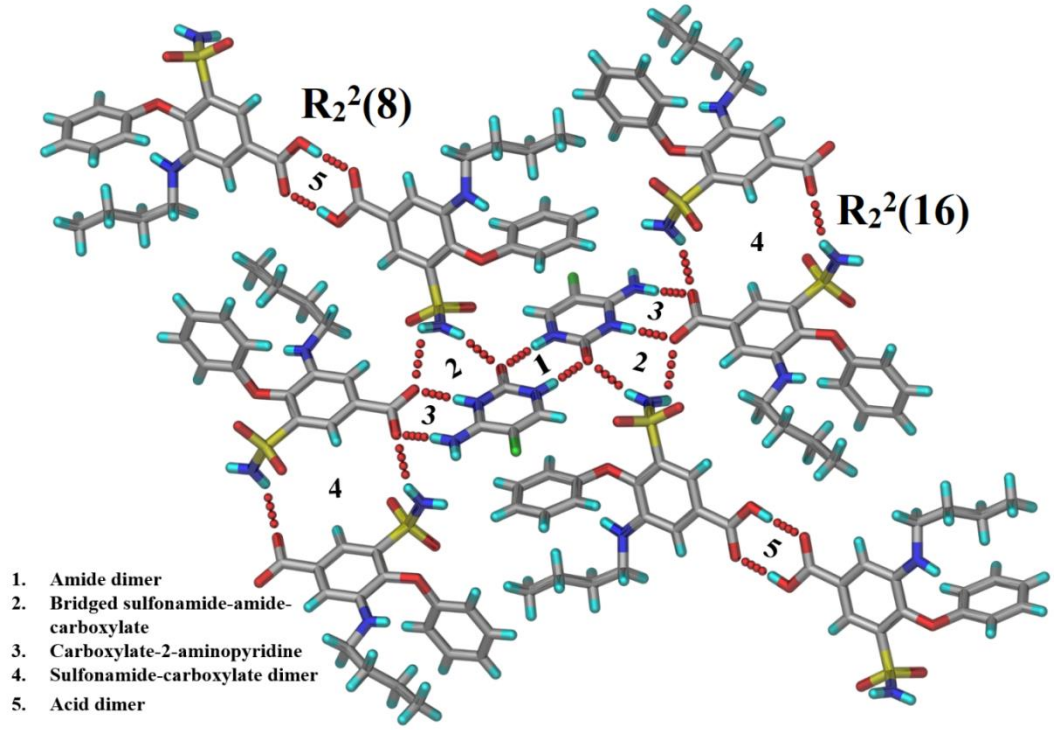
$R_2^2(8)$
$R_2^2(16)$
5
4
3
2
1
2
3
4
5
1. Amide dimer
2. Bridged sulfonamide-amide-carboxylate
3. Carboxylate-2-aminopyridine
4. Sulfonamide-carboxylate dimer
5. Acid dimer

(b)

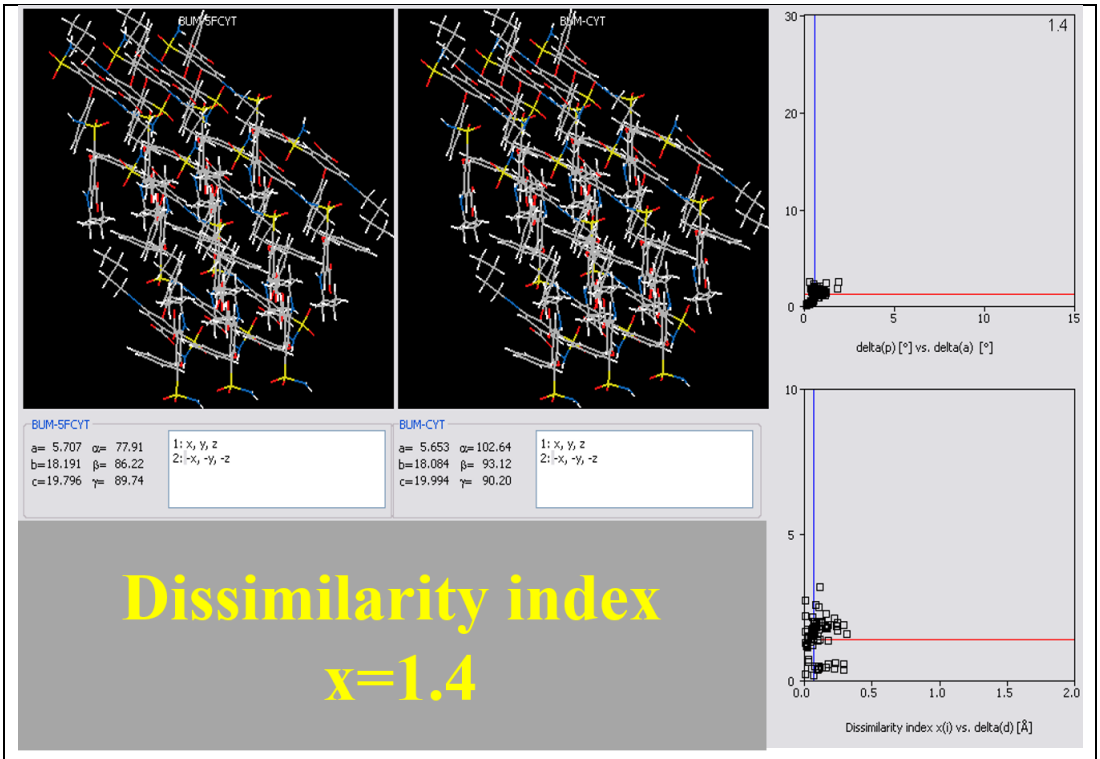
BUM-5FCYT
BUM-CYT
1.4
delta(p) [°] vs. delta(a) [°]
BUM-5FCYT
a= 5.707 α= 77.91
b=18.191 β= 86.22
c=19.796 γ= 89.74
1: x, y, z
2: -x, -y, -z
BUM-CYT
a= 5.653 α=102.64
b=18.084 β= 93.12
c=19.994 γ= 90.20
1: x, y, z
2: -x, -y, -z
Dissimilarity index
x=1.4
Dissimilarity index x(i) vs. delta(d) [Å]

**(c)**

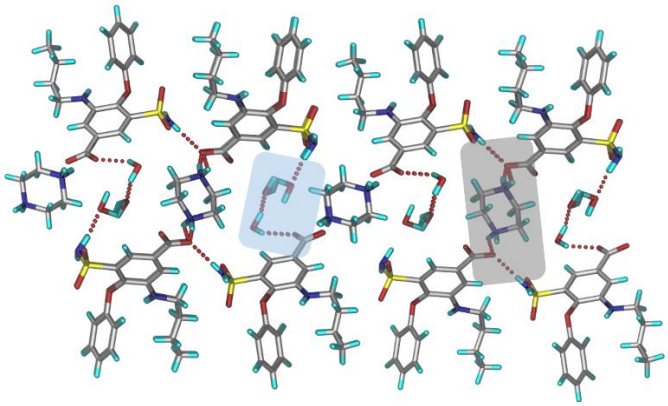

**(d)**

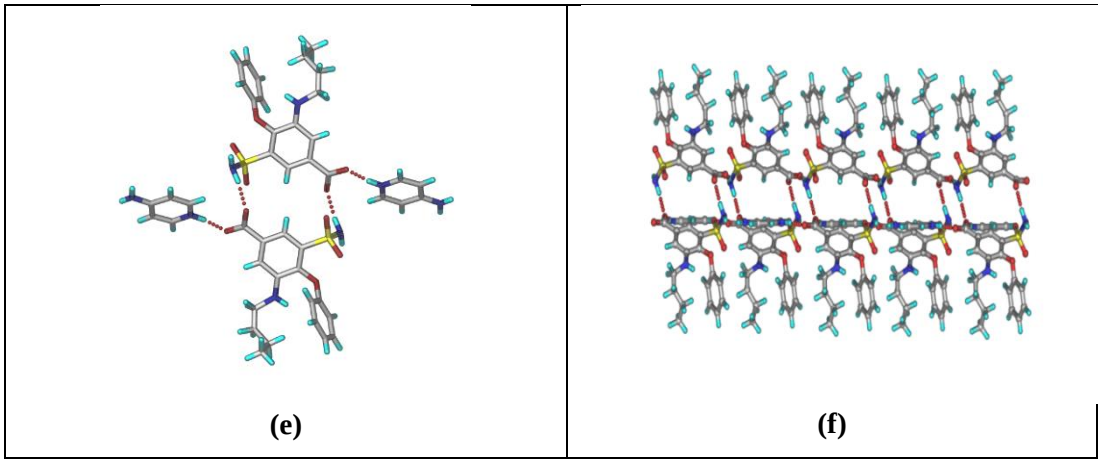

**(e)** **(f)**

**Figure 2.5:** (a) BUM–CYT (2:1) cocrystal-salt structure adopted from reference 15. (b) BUM–5FCYT (2:1) cocrystal-salt structure with molecules connected via amide dimer synthon ring and sulfonamide bridged $R_3^2(8)$ ring motif and carboxylate···amino-pyridinium ring motif. (c) BUM–CYT and BUM–5FCYT Xpac analysis resulted in dissimilarity index 1.4 and confirms the 3D isostrucal supramolecular constructs in crystal lattice. (d) BUM−PIP−$H_2O$ (2:2:3) salt hydrate BUM and PIP are bonded through N−H···O hydrogen bond of carboxylate···piperazinium tetrameric ring motif $R_2^2(18)$. (e) and (f) BUM–4AP (1:1) salt molecules are connected through sulfonamide···carboxylate dimer synthon ring motif $R_2^2(16)$.

**Table 2.1:** Crystallographic parameters of bumetanide cocrystals and salts.

| | **BUM** | **BUM–INA Form I (1:1)** | **BUM–INA Form II (1:1)** | **BUM–INA (1:2)** | **BUM–PAM (2:1)** |
|---|---|---|---|---|---|
| **Empirical Formula** | $C_{17}H_{20}N_2O_5S$ | $C_{17}H_{20}N_2O_5S$, $C_6H_6N_2O$ | $C_{17}H_{20}N_2O_5S$, $C_6H_6N_2O$ | $C_{17}H_{20}N_2O_5S$, $2(C_6H_6N_2O)$ | $2(C_{17}H_{20}N_2O_5S)$, $C_6H_6N_2O$ |
| **Formula weight** | 364.41 | 486.54 | 486.54 | 608.67 | 850.95 |
| **Crystal System** | Monoclinic | Monoclinic | Orthorhombic | Monoclinic | Triclinic |
| **Space Group** | $P2_1/c$ | $P2_1/c$ | $Pbca$ | $P2_1/c$ | $P1$ |
| **T (K)** | 298(2) | 298(2) | 298(2) | 298(2) | 298(2) |
| ***a* (Å)** | 5.3952(13) | 13.461(2) | 11.1739(5) | 5.5352(4) | 5.4926(3) |
| ***b* (Å)** | 18.206(4) | 11.1251(18) | 15.9284(6) | 10.7253(9) | 13.6479(12) |
| ***c* (Å)** | 18.119(4) | 15.944(3) | 26.5728(11) | 49.103(3) | 15.1627(11) |
| ***α* (°)** | 90 | 90 | 90 | 90 | 104.660(7) |
| ***β* (°)** | 98.222(4) | 95.375(3) | 90 | 91.220(2) | 98.660(6) |
| ***γ* (°)** | 90 | 90 | 90 | 90 | 101.399(6) |

| | | | | | |
|---|---|---|---|---|---|
| ***V*** **(Å$^3$)** | 1761.4(7) | 2377.2(7) | 4729.5(3) | 2914.4(4) | 1053.55(13) |
| ***D*$_{calc}$ (g cm$^{-3}$)** | 1.374 | 1.359 | 1.367 | 1.387 | 1.341 |
| **Z** | 4 | 4 | 8 | 4 | 1 |
| ***F*(000)** | 768 | 1024 | 2048 | 1280 | 448 |
| **Δρ$_{max}$, Δρ$_{min}$ (e Å$^{-3}$)** | 0.32, -0.20 | 1.07, -0.60 | 1.36, -0.52 | 0.31, -0.39 | 0.32, -0.30 |
| **h range** | -6 → 6 | -16 → 16 | -14 → 14 | -6 → 6 | -4 → 6 |
| **k range** | -22 → 22 | -13 → 13 | -18 → 20 | -12 → 13 | -16 → 15 |
| **l range** | -22 → 22 | -19 → 19 | -34 → 34 | -61 → 60 | -18 → 17 |
| **measured reflections** | 18781 | 24607 | 55359 | 22878 | 6921 |
| **independent reflections** | 3658 | 4827 | 5467 | 5815 | 4487 |
| **Reflections with I> 2σ(I)** | 2670 | 4278 | 4198 | 3405 | 3702 |
| **R$_{int}$** | 0.044 | 0.029 | 0.066 | 0.118 | 0.036 |
| ***R*$_1$*[I* >2σ(*I*)]** | 0.0481 | 0.0545 | 0.0652 | 0.061 | 0.0590 |
| ***w*R$_2$ (all)** | 0.1266 | 0.1657 | 0.1769 | 0.1270 | 0.1700 |
| **Goodness of fit** | 1.025 | 1.041 | 1.074 | 1.020 | 1.067 |
| **X-ray diffractometer** | BRUKER APEX | BRUKER APEX | BRUKER APEX | BRUKER APEX | OXFORD CCD |

| | **BUM–CYT(2:1)** | **BUM–2HP (1:1)** | **BUM–MeHP (1:1)** | **BUM–OMeHP (1:1)** | **BUM–5FCYT (2:1)** |
|---|---|---|---|---|---|
| **Empirical Formula** | $C_{17}H_{20}N_2O_5S$, $C_{17}H_{20}N_2O_5S$, $C_4H_6N_3O$ | $C_{17}H_{20}N_2O_5S$, $C_5H_5NO$ | $C_{17}H_{20}N_2O_5S$, $C_6H_7NO$ | $C_{17}H_{20}N_2O_5S$, $C_6H_7NO_2$ | $C_{17}H_{19}N_2O_5S$, $C_{17}H_{20}N_2O_5S$, $C_4H_5FN_3O$ |
| **Formula Weight** | 839.93 | 459.51 | 473.54 | 489.54 | 857.92 |
| **Crystal system** | Triclinic | Monoclinic | Monoclinic | Monoclinic | Triclinic |
| **Space group** | *P*-1 | *P*2$_1$/*n* | *C*2/*c* | *P*2$_1$/*n* | P-1 |
| **T (K)** | 298(2) | 298(2) | 298(2) | 298(2) | 298(2) |
| **a (Å)** | 5.6531(10) | 14.0882(8) | 22.1109(17) | 5.2967(3) | 5.7073 (7) |
| **b (Å)** | 18.084(3) | 5.3214(3) | 5.0482(3) | 17.7044(10) | 18.191 (2) |
| **c (Å)** | 19.994(4) | 29.5649(1) | 42.255(3) | 25.5680(15) | 19.796 (3) |

| | | | | | |
|---|---|---|---|---|---|
| **α (°)** | 102.641(3) | 90 | 90 | 90 | 77.907 (7) |
| **β (°)** | 93.116(4) | 93.591(5) | 95.892(3) | 91.307(2) | 86.220 (7) |
| **γ (°)** | 90.204(4) | 90 | 90 | 90 | 89.743 (7) |
| **V (Å3)** | 1991.3(6) | 2212.1(2) | 4691.6 (6) | 2397.0(2) | 2005.2 (4) |
| **Dcalc (gcm–3)** | 1.401 | 1.380 | 1.341 | 1.357 | 1.421 |
| **Z** | 2 | 4 | 8 | 4 | 2 |
| **F(000)** | 884 | 968 | 2000 | 1032 | 900 |
| **Δρmax, Δρmin (e Å−3)** | 0.44, -0.25 | 0.28, -0.40 | 0.26, -0.31 | 0.97, -0.45 | 0.46, -0.44 |
| **h range** | -6 → 6 | -17 → 15 | -29 → 27 | -6 → 6 | -7 → 7 |
| **k range** | -21 → 21 | -4 → 6 | -6 → 6 | -21 → 21 | -23 → 23 |
| **l range** | -23 → 23 | -34 → 36 | -55 → 55 | -31 → 31 | -25 → 25 |
| **measured reflections** | 19392 | 8087 | 28546 | 42870 | 44620 |
| **independent reflections** | 7012 | 4269 | 5604 | 4563 | 8871 |
| **Reflections with I> 2σ(I)** | 3444 | 2724 | 3372 | 3710 | 4289 |
| **$R_{int}$** | 0.097 | 0.050 | 0.076 | 0.046 | 0.183 |
| **$R_1$[I >2σ(I)]** | 0.0691 | 0.0571 | 0.0568 | 0.0572 | 0.078 |
| **wR2 (all)** | 0.1609 | 0.1525 | 0.1267 | 0.1558 | 0.201 |
| **Goodness-of-fit** | 0.925 | 0.983 | 1.055 | 1.038 | 1.08 |
| **X–ray Diffractometer** | BRUKER APEX | OXFORD CCD | BRUKER APEX | BRUKER APEX | Bruker APEX-II CCD |

| | **BUM–VLM (1:1)** | **BUM–CPR (1:1)** | **BUM–NMeCPR (2:1)** | **BUM–UREA (1:1)** | **BUM–4AP (1:1)** | **BUM–PIP–H2O (2:2:3)** |
|---|---|---|---|---|---|---|
| **Empirical Formula** | $C_{17}H_{20}N_2O_5S$, $C_5H_9NO$ | $C_{17}H_{20}N_2O_5S$, $C_6H_{11}NO$ | $C_{34}H_{40}N_4O_{10}S$, $C_7H_{13}NO$ | $C_{17}H_{20}N_2O_5S$, $C_1H_4N2O$ | $C_{17}H_{20}N_2O_5S$, $C_5H_6N_2$ | $C_{34}H_{40}N_4O_{10}S$, $C_4H_{10}N_2$, $H_6O_3$ |
| **Formula weight** | 463.54 | 477.57 | 856.00 | 424.47 | 458.53 | 869.00 |
| **Crystal System,** | Monoclinic | Monoclinic | Triclinic | Monoclinic | Monoclinic | Triclinic |
| **Space Group** | $P2_1/c$ | $P2_1/c$ | $P$-1 | $P2_1/c$ | $P2_1/c$ | $P$-1 |
| **T (K)** | 298(2) | 298(2) | 298(2) | 298(2) | 298(2) | 298(2) |
| **a (Å)** | 5.5259 (1) | 5.6576 (3) | 10.2441 (7) | 5.5390 (1) | 14.5281 (9) | 5.5221 (3) |
| **b (Å)** | 13.9225 (4) | 14.4387 (8) | 11.9621 (11) | 35.7753 (9) | 11.0313 (7) | 18.2884 (9) |
| **c (Å)** | 30.7622 (10) | 29.6895 (18) | 19.4819 (18) | 10.4272 (3) | 15.0788 (9) | 22.0551 (12) |
| **α (°)** | 90 | 90 | 73.234 (8) | 90 | 90 | 80.311 (3) |

| | | | | | | |
|---|---|---|---|---|---|---|
| **β (°)** | 91.963 (3) | 92.469 (5) | 84.081 (7) | 92.846 (1) | 110.913 (3) | 86.949 (4) |
| **γ (°)** | 90 | 90 | 69.235 (7) | 90 | 90 | 87.992 (3) |
| **V (Å3)** | 2365.28(11) | 2423.0 (2) | 2137.4 (3) | 2063.70 (9) | 2257.4 (2) | 2191.7 (2) |
| **Dcalc (g cm–3)** | 1.302 | 1.309 | 1.330 | 1.366 | 1.349 | 1.317 |
| **Z** | 4 | 4 | 2 | 4 | 4 | 2 |
| **F (000)** | 984 | 1016 | 908 | 896 | 968 | 924 |
| **Δρmax, Δρmin (e Å−3)** | 0.54, -0.55 | 0.51, -0.45 | 0.91, -0.31 | 0.53, -0.30 | 0.51, -0.55 | 0.62, -0.41 |
| **h range** | -4 → 6 | -6 → 5 | -12 → 6 | -6 → 6 | -18 → 18 | -6 → 6 |
| **k range** | -16 → 14 | -17 → 17 | -14 → 14 | -42 → 42 | -13 → 13 | -22 → 22 |
| **l range** | -36 → 37 | -36 → 34 | -23 → 23 | -12 → 12 | -18 → 18 | -27 → 27 |
| **measured reflections** | 9535 | 9447 | 17800 | 23510 | 29069 | 40597 |
| **independent reflections** | 4463 | 4622 | 8140 | 3678 | 4661 | 8803 |
| **Rint** | 0.024 | 0.045 | 0.057 | 0.050 | 0.045 | 0.096 |
| **R1 [I >2σ(I)]** | 0.091 | 0.069 | 0.092 | 0.053 | 0.056 | 0.094 |
| **wR2 (all)** | 0.243 | 0.190 | 0.300 | 0.147 | 0.164 | 0.262 |
| **Goodness-of-fit** | 1.12 | 1.07 | 1.01 | 1.15 | 1.08 | 1.05 |
| **X-ray Diffractometer** | Xcalibur, Eos, Gemini | Xcalibur, Eos, Gemini | Xcalibur, Eos, Gemini | Bruker APEX-II CCD | Bruker APEX-II CCD | Bruker APEX-II CCD |

**Ternary Crystal Structure Description (ABC):**

Four ternary cocrystal products obtained in this study are BUM–INA–PCA (1:1:1), BUM–INA–VLA (1:1:1), BUM–INA–PASA (1:1:1) BUM–2HP–PCA (1:1:1) out of which the two ternary systems BUM-INA-PCA (1:1:1) and BUM-2HP-PCA (1:1:1) were solved by Structure Determination by Powder Diffractometry (SDPD). These two ternary cocrystals were found to have monoclinic crystal system with two different space groups namely $P2_1/c$, $C2/c$ and 4, 8 as Z (Table 2.2).

**Table 2.2:** Crystallographic parameters of bumetanide Ternary cocrystals from SDPD.

| | **BUM–INA–PCA (1:1:1)** | **BUM-2HP-PCA (1:1:1)** |
|---|---|---|

| | | |
|---|---|---|
| | 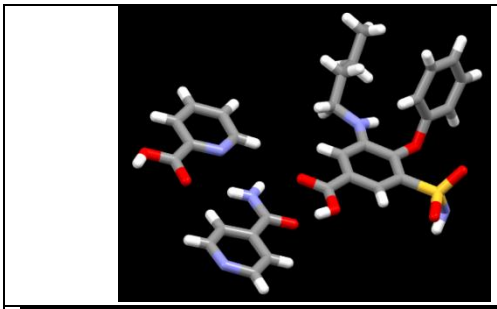 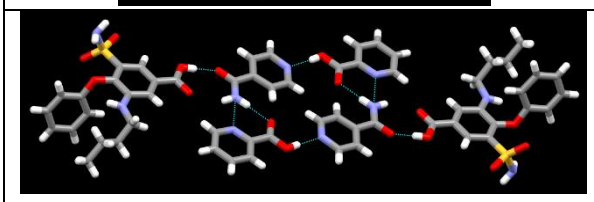 | 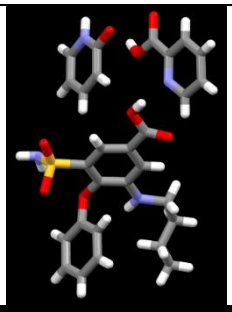 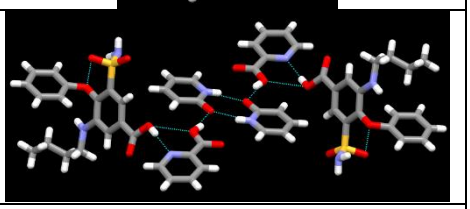 |
| **Empirical Formula** | $C_{17}H_{20}N_2O_5S \cdot C_6H_6N_2O \cdot C_6H_5NO_2$ | $C_{17}H_{20}N_2O_5S \cdot C_5H_5NO \cdot C_6H_5NO_2$ |
| **Formula Weight** | 609.65 | 582.62 |
| **Crystal system** | Monoclinic | Monoclinic |
| **Space group** | $P2_1/c$ | $C2/c$ |
| **T (K)** | 298 | 298 |
| **a (Å)** | 27.3556 (19) | 59.486 (2) |
| **b (Å)** | 5.3055 (7) | 5.3361 (7) |
| **c (Å)** | 20.7341 (17) | 18.0820 (18) |
| **α (°)** | 90 | 90 |
| **β (°)** | 94.689 (16) | 101.084 (14) |
| **γ (°)** | 90 | 90 |
| **V (Å3)** | 2999.2 (5) | 5632.6 (9) |
| **Dcalc (gcm–3)** | 1.350 | 1.374 |
| **Z** | 4 | 8 |
| **F (000)** | 1280 | 2448 |
| **2θmin-2θmax Δ2θ (o)** | 3.00 – 75.00, 0.01 | 2.00 – 75.00, 0.01 |
| **no. params/restraints** | 169/138 | 161/135 |
| **$R_p$, $R_{wp}$, $R_{exp}$** | 0.019, 0.026, 0.017 | 0.034, 0.044, 0.031 |
| **R1 [I >2σ(I)]** | 1.9 | 3.39 |

**Table 2.3:** Hydrogen bonds in BUM Cocrystals and salts.

| D−H···A | D···A (Å) | H···A (Å) | D−H···A (°) | symmetry code |
|---|---|---|---|---|
| **BUM** | | | | |
| N1−H1A···O3 | 2.7500(7) | 2.39 | 108 | Intramolecular |
| N2−H2A···O1 | 3.0096(7) | 2.37 | 140 | −1+x,y,z |
| O4−H4A···O5 | 2.6276(6) | 1.76 | 177 | 3−x,1−y,1−z |
| C6−H6···O1 | 2.8348(7) | 2.44 | 106 | Intramolecular |
| C17−H17···O2 | 3.4679(8) | 2.54 | 174 | −1+x,y,z |
| **BUM-2HP(1:1)** | | | | |
| N1−H1A···O3 | 2.7449(2) | 2.45 | 101 | Intramolecular |
| N2−H2A···O3 | 2.9933(2) | 2.44 | 128 | Intramolecular |
| N2−H2B···O2 | 2.9889(2) | 2.08 | 166 | −1/2−x,1/2+y,1/2−z |
| N3−H3A···O6 | 2.8117(2) | 1.90 | 175 | 1−x,2−y,−z |
| O4−H4A···O6 | 2.5952(1) | 1.73 | 165 | −1+x,−1+y,z |
| C17−H17···O1 | 3.4733(2) | 2.60 | 157 | x,1+y,z |
| C19−H19···O5 | 3.3421(2) | 2.52 | 147 | −x,1−y,−z |
| **BUM-MeHP(1:1)** | | | | |
| N1−H1A···O3 | 2.7618(2) | 2.43 | 106 | Intramolecular |
| N2−H2A···O3 | 2.9575(2) | 2.43 | 118 | Intramolecular |
| N2−H2B···O2 | 3.0486(2) | 2.49 | 123 | x,−1+y,z |
| N3−H3A···O6 | 2.8581(2) | 2.01 | 174 | −x,1−y,−z |
| O4−H4A···O6 | 2.5682(2) | 1.67 | 160 | 1/2−x,3/2−y,−z |
| C19−H19···O5 | 3.3148(3) | 2.46 | 154 | 1/2−x,3/2−y,−z |
| C20−H20···O5 | 3.2701(3) | 2.49 | 141 | x,−1+y,z |
| **BUM-OMeHP(1:1)** | | | | |
| N1−H1A···O3 | 2.7457(2) | 2.34 | 108 | Intramolecular |
| N2−H2A···O3 | 2.9830(2) | 2.45 | 121 | Intramolecular |
| N2−H2B···O1 | 3.0033(2) | 2.17 | 167 | 1−x,1−y,1−z |
| N3−H3A···O6 | 2.8434(2) | 2.00 | 176 | 1−x,1−y,−z |
| O4−H4A···O6 | 2.7095(2) | 1.95 | 177 | −1/2+x,1/2−y,1/2+z |
| O4−H4A···O7 | 2.8080(2) | 2.46 | 109 | −1/2+x,1/2−y,1/2+z |
| C22−H22···O5 | 3.2260(2) | 2.39 | 150 | 1/2−x,1/2+y,1/2−z |
| **BUM-CYT(2:1)** | | | | |
| N1−H1A···O1 | 3.2446(6) | 2.60 | 138 | −1+x,y,z |
| N1−H1B···O10 | 2.9063(5) | 2.13 | 155 | 2−x,−y,1−z |
| N2−H2A···O9 | 2.8255(5) | 2.05 | 153 | 2−x,1−y,1−z |
| N2−H2B···O5 | 2.9655(5) | 2.30 | 138 | 1−x,1−y,1−z |
| N3−H3A···O10 | 2.6841(5) | 1.84 | 168 | −1+x,y,z |
| N3−H3B···O1 | 2.8854(5) | 2.16 | 142 | 2−x,−y,1−z |
| N4−H4A···O9 | 2.8100(5) | 1.95 | 176 | −1+x,y,z |
| N5−H5···O5 | 2.8326(5) | 1.99 | 166 | 1−x,1−y,1−z |
| N6−H6A···O6 | 2.7797(5) | 2.37 | 112 | Intramolecular |
| N7−H7A···O11 | 2.7429(5) | 2.35 | 112 | Intramolecular |
| O8−H8A···O7 | 2.6094(5) | 1.86 | 176 | 3−x,1−y,−z |
| C13−H13···O2 | 3.5194(6) | 2.59 | 178 | −1+x,y,z |
| C30−H30···O4 | 3.4932(6) | 2.57 | 174 | −1+x,y,z |

| | | | | |
|---|---|---|---|---|
| **BUM–INA (1:1) Form I** | | | | |
| N1−H1A···O1 | 2.7418(5) | 2.39 | 107 | Intramolecular |
| N2−H2A···O3 | 3.0502(6) | 2.23 | 164 | x,1/2−y,−1/2+z |
| N2−H2B···N3 | 2.9820(6) | 2.08 | 165 | Intramolecular |
| O3−H3A···O6 | 2.5669(5) | 1.86 | 175 | 1−x,−y,1−z |
| N4−H4A···O4 | 3.0309(6) | 2.21 | 163 | 1−x,1/2+y,1/2−z |
| N4−H4B···O2 | 2.9776(6) | 2.20 | 156 | 1−x,−y,1−z |
| C14−H14···O5 | 3.2619(6) | 2.42 | 151 | −x,−y,−z |
| **BUM–INA (1:1) Form II** | | | | |
| N1−H1A···O3 | 2.7534(1) | 2.41 | 106 | Intramolecular |
| N2−H2A···N3 | 2.9893(1) | 2.12 | 166 | −1/2+x,1/2−y,−z |
| N2−H2B···O4 | 3.0821(1) | 2.40 | 158 | 1/2−x,−1/2+y,z |
| N4−H4A···O1 | 3.0411(1) | 2.29 | 165 | 1+x,y,z |
| N4−H4B···O5 | 2.9633(1) | 2.06 | 168 | 1/2−x,−1/2+y,z |
| O4 −H4C···O6 | 2.5600(1) | 1.79 | 175 | 1/2−x,1/2+y,z |
| C16−H16···O2 | 3.2016(1) | 2.56 | 125 | 1/2+x,y,1/2−z |
| **BUM–INA (1:2)** | | | | |
| N1−H1A···O3 | 2.7734(2) | 2.37 | 108 | Intramolecular |
| N2−H2A···O1 | 3.1505(3) | 2.55 | 132 | −1+x,y,z |
| N2−H2B···N5 | 2.9991(3) | 2.16 | 165 | 1+x,−1+y,z |
| N4−H4A···O7 | 2.9456(2) | 2.18 | 156 | 1+x,y,z |
| N4−H4B···O7 | 2.9037(2) | 1.93 | 175 | 2−x,1−y,−z |
| O4−H4C···N3 | 2.6837(2) | 1.77 | 179 | 1+x,y,z |
| N6−H6A···O5 | 2.9319(2) | 2.09 | 160 | −1+x,1+y,z |
| N6−H6B···O6 | 2.9931(3) | 2.13 | 173 | 2−x,1−y,−z |
| C13−H13···O2 | 3.4584(3) | 2.51 | 173 | −1+x,y,z |
| **BUM–PAM (2:1)** | | | | |
| N2−H2A···O1 | 3.0989(3) | 2.45 | 133 | 1+x,y,z |
| N2−H2A···O3 | 3.1553(3) | 2.60 | 123 | Intramolecular |
| N2−H2B···O7 | 3.0299(3) | 2.26 | 155 | −1+x,1+y,z |
| N3−H3A···O8 | 2.7673(2) | 2.51 | 100 | Intramolecular |
| O4−H4C···O10 | 2.6544(2) | 1.84 | 177 | −2+x,1+y,z |
| N4−H4A···O1 | 3.0036(3) | 2.16 | 166 | 1+x,−1+y,z |
| N4−H4B···O8 | 2.9915(3) | 2.54 | 114 | Intramolecular |
| N6−H6A···O5 | 2.8600(3) | 2.45 | 110 | 1+x,y,z |
| N6−H6A···O10 | 3.0058(3) | 2.18 | 160 | −1+x,1+y,z |
| N6−H6B···N5 | 2.6336(2) | 2.26 | 106 | Intramolecular |
| O9−H9C···O11 | 2.5456(2) | 1.53 | 166 | 1+x,−1+y,z |
| C30−H30···O6 | 3.3476(3) | 2.47 | 158 | −1+x,y,z |
| **BUM–UREA (1:1)** | | | | |
| N1−H1A···O3 | 2.767(4) | 2.44 | 109 | Intramolecular |
| N2−H2A···O1 | 3.145(4) | 2.49 | 137 | 1+x,y,z |
| N2−H2B···O6 | 2.984(4) | 2.18 | 167 | x,y,1+z |
| N3−H3A···O5 | 3.073(4) | 2.33 | 151 | Intramolecular |
| N3−H3B···O4 | 2.985(4) | 2.42 | 129 | 1+x,1/2-y,-1/2+z |
| O4−H4A···O6 | 2.568(3) | 1.67 | 163 | -1+x,1/2-y,1/2+z |
| O4−H4A···N3 | 2.985(4) | 2.62 | 104 | -1+x,1/2-y,1/2+z |
| N4−H4B···O5 | 2.975(4) | 2.26 | 151 | Intramolecular |

| | | | | |
|---|---|---|---|---|
| N4−H4C···O1 | 2.986(4) | 2.13 | 167 | x,y,-1+z |
| C6−H6···O1 | 2.858(4) | 2.47 | 105 | Intramolecular |
| **BUM–CPR (1:1)** | | | | |
| N1−H1A···O3 | 2.793(5) | 2.47 | 108 | Intramolecular |
| N2−H2B···O6 | 2.879(6) | 2.02 | 176 | 1-x,1-y,-z |
| N3−H3A···O6 | 2.915(5) | 1.96 | 172 | 2-x,2-y,-z |
| O4−H4A···O5 | 2.618(4) | 1.77 | 175 | 2-x,1-y,-z |
| C11−H11B···O2 | 3.298(7) | 2.36 | 166 | -x,1/2+y,1/2-z |
| C19−H19A···O1 | 3.340(5) | 2.55 | 139 | x,1+y,z |
| **BUM–NMeCPR (2:1)** | | | | |
| N2−H2A···O7 | 3.038(8) | 2.32 | 130 | -x,1-y,1-z |
| N2−H2B···O3 | 2.946(8) | 2.41 | 123 | Intramolecular |
| N2−H2B···O6 | 3.333(8) | 2.59 | 148 | -x,1-y,1-z |
| N4−H4A···O11 | 2.847(8) | 1.83 | 160 | x,-1+y,1+z |
| N4−H4B···O1 | 3.081(7) | 2.52 | 123 | 1-x,1-y,1-z |
| O4−H4C···O10 | 2.611(6) | 1.80 | 169 | 1+x,1+y,-1+z |
| O9−H9C···O5 | 2.610(7) | 1.80 | 168 | -1+x,-1+y,1+z |
| C16−H16···O6 | 3.358(9) | 2.54 | 146 | x,1+y,z |
| C30−H30···O2 | 3.359(9) | 2.47 | 160 | 1-x,1-y,1-z |
| **BUM–VLM (1:1)** | | | | |
| N1−H1A···O3 | 2.768(5) | 2.45 | 102 | Intramolecular |
| N2−H2A···O2 | 3.108(6) | 2.37 | 135 | -1+x,y,z |
| N2−H2B···O6 | 2.900(7) | 2.14 | 171 | 1-x,1-y,-z |
| N3−H3A···O6 | 2.922(7) | 2.07 | 175 | 1-x,2-y,-z |
| O4−H4A···O5 | 2.618(5) | 1.81 | 168 | 3-x,1-y,-z |
| C11−H11A···O1 | 3.338(10) | 2.41 | 162 | 1-x,1/2+y,1/2-z |
| C22−H22A···O2 | 3.435(7) | 2.50 | 161 | -1+x,1+y,z |
| **BUM–4AP (1:1)** | | | | |
| N1−H1A···O3 | 2.744(3) | 2.40 | 108 | Intramolecular |
| N2−H2A···O5 | 3.007(3) | 2.14 | 169 | x,1/2-y,1/2+z |
| N2−H2B···O4 | 2.870(3) | 1.93 | 168 | 2-x,1-y,1-z |
| N3−H3A···O5 | 2.668(3) | 1.77 | 172 | 1-x,1-y,-z |
| N4−H4A···O4 | 2.842(4) | 1.91 | 167 | 1-x,-1/2+y,1/2-z |
| N4−H4B···O1 | 3.307(4) | 2.58 | 162 | 1-x,1-y,1-z |
| C8−H8B···O2 | 3.273(5) | 2.47 | 141 | x,1/2-y,-1/2+z |
| C14−H14···O2 | 3.404(4) | 2.53 | 157 | 1-x,1-y,1-z |
| **BUM–PIP–$H_2O$ (2:2:3)** | | | | |
| N2−H2A···O1 | 3.182(6) | 2.59 | 132 | 1+x,y,z |
| N2−H2B···O9 | 2.837(7) | 2.04 | 177 | -x,-y,1-z |
| N4−H4A···O11 | 2.890(11) | 1.84 | 167 | Intramolecular |
| N4−H4B···O7 | 3.150(6) | 2.47 | 139 | 1+x,y,z |
| N5−H5A···O4 | 2.756(5) | 1.87 | 172 | 1+x,y,z |
| N5−H5A···O5 | 3.154(5) | 2.50 | 130 | 1+x,y,z |
| N5−H5B···O5 | 2.701(5) | 1.82 | 173 | Intramolecular |
| N6−H6A···O9 | 2.748(6) | 1.85 | 165 | Intramolecular |
| N6−H6B···O10 | 2.674(6) | 1.80 | 157 | 1+x,y,z |
| O12−H12D···O13 | 2.761(11) | 2.21 | 117 | -1+x,y,z |
| O13−H13D···O12 | 2.761(11) | 1.77 | 165 | 1+x,y,z |

| | | | | |
|---|---|---|---|---|
| C30−H30···O6 | 3.477(7) | 2.56 | 171 | 1+x,y,z |
| C36−H36A···O7 | 3.236(5) | 2.56 | 127 | -x,-y,1-z |
| C38−H38B···O1 | 3.299(7) | 2.54 | 136 | -x,1-y,1-z |
| **BUM-5FCYT (2:1)** | | | | |
| N2−H2A···O11 | 2.944(5) | 2.14 | 155 | 1+x,y,z |
| N4−H4B···O9 | 2.928(5) | 2.21 | 142 | 1-x,-y,1-z |
| N5−H5A···O10 | 2.761(4) | 1.90 | 178 | -1+x,y,z |
| O5−H5B···O4 | 2.612(5) | 1.80 | 172 | -x,1-y,-z |
| N6−H6···O11 | 2.809(5) | 1.96 | 170 | -x,1-y,1-z |
| N7−H7A···O9 | 2.652(4) | 1.80 | 173 | -1+x,y,z |
| N7−H7B···O6 | 2.888(5) | 2.14 | 146 | 1-x,-y,1-z |
| C14−H14···F1 | 3.348(6) | 2.48 | 156 | 2-x,1-y,1-z |
| C30−H30···O7 | 3.523(7) | 2.59 | 177 | -1+x,y,z |
| C38−H38···O2 | 3.112(5) | 2.31 | 144 | 1-x,1-y,1-z |

## 2.2.2 Conformational Analysis

**Conformation:** Even as supramolecular synthons repeat in different structures, the molecular conformation of BUM is different. For structures with BUM syn-amide and lactam synthons, the conformations are different, e.g. in BUM–CPR (type 1) and BUM–VLM, BUM–NMeCPR (type 2) (Figure 2.6). In addition, the syn amide in BUM–2HP, BUM–OMeHP has type 1 category whereas in BUM–MeHP it is type 2. These observations suggest that though the hydrogen bonding heterosynthon is the same, the flexible molecules change conformations and adjust to the final 3D crystal packing.[26,43] The torsion angles are shown in Table 2.4

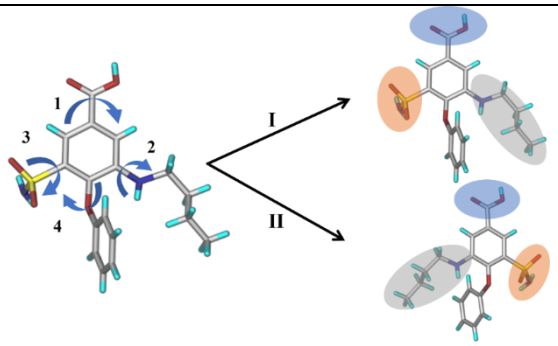


(a)

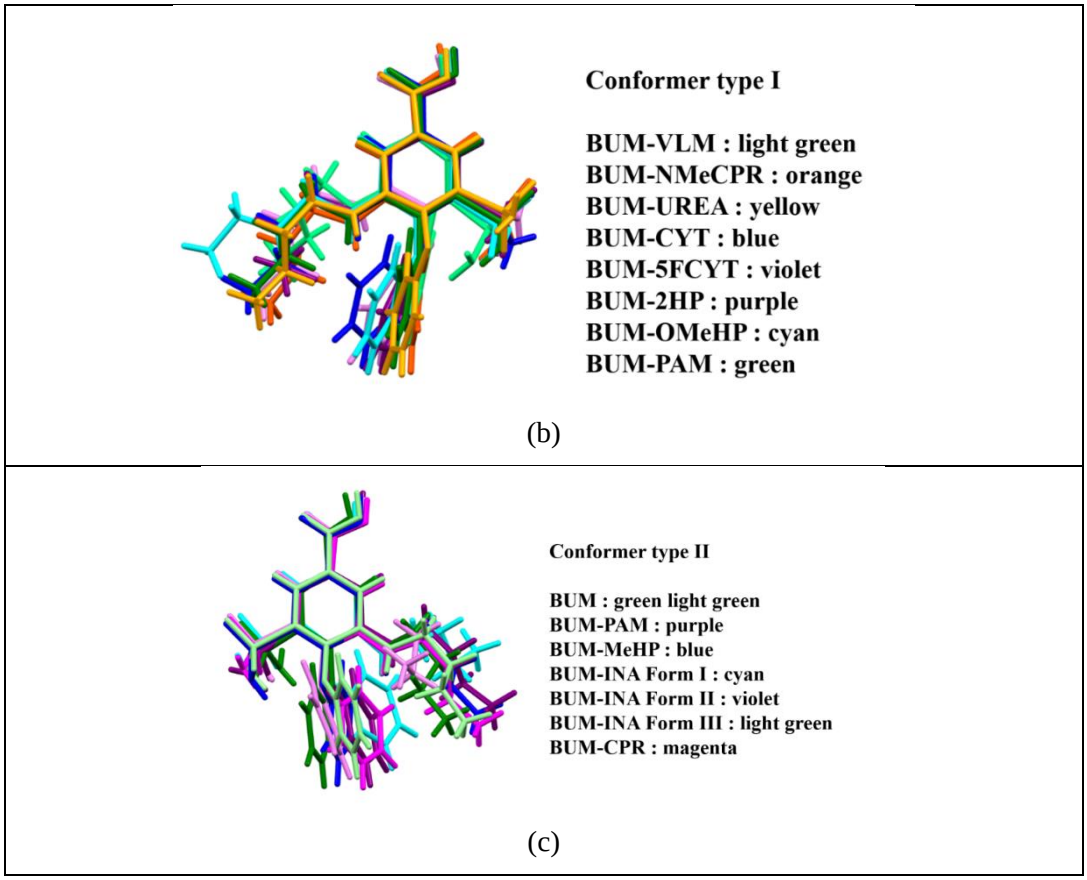


**Figure 2.6:** (a) Classification of BUM conformers. (b), (c) Conformation comparison of BUM conformation in different new crystal structures.

**Table 2.4:** Torsion angles of the BUM in different adducts.

| | **Torsion 1 OCCC** | **Torsion 2 CCNC** | **Torsion 3 SCCC** | **Torsion 4 CCOC** |
|---|---|---|---|---|
| **Conformer type 1** | | | | |
| BUM–VLM | -4.88 | -162.41 | -178.08 | 10.64 |
| BUM–NMeCPR | -5.09 | -172.38 | 178.59 | -5.75 |
| BUM–UREA | 4.67 | -170.66 | -179.57 | 9.96 |
| BUM–CYT | -3.41 | -160.03 | 179.48 | 17.08 |
| BUM–5FCYT | 4.61 | 160.11 | -179.64 | -17.44 |
| BUM–2HP | -2.81 | 167.65 | 178.81 | -14.81 |
| BUM–OMeHP | 2.37 | 176.79 | 177.63 | -16.68 |
| BUM–PAM | 2.10 | 168.01 | 178.08 | -8.65 |
| **Conformer type 2** | | | | |
| BUM | -4.08 | -167.32 | 178.69 | 2.71 |
| BUM–PAM | 4.38 | 174.61 | -176.72 | -15.05 |
| BUM–MeHP | 8.04 | 179.21 | -178.86 | -2.37 |
| BUM–INA Form-1 | -6.27 | 165.12 | 177.42 | -25.84 |
| BUM–INA Form-2 | -16.91 | -158.99 | 178.36 | 13.99 |
| BUM–INA Form-3 | 7.17 | -164.07 | -177.81 | 28.17 |
| BUM–CPR | 3.59 | 161.50 | 179.56 | -12.92 |

**Supramolecular synthons present in Bumetanide cocrystals/salts**

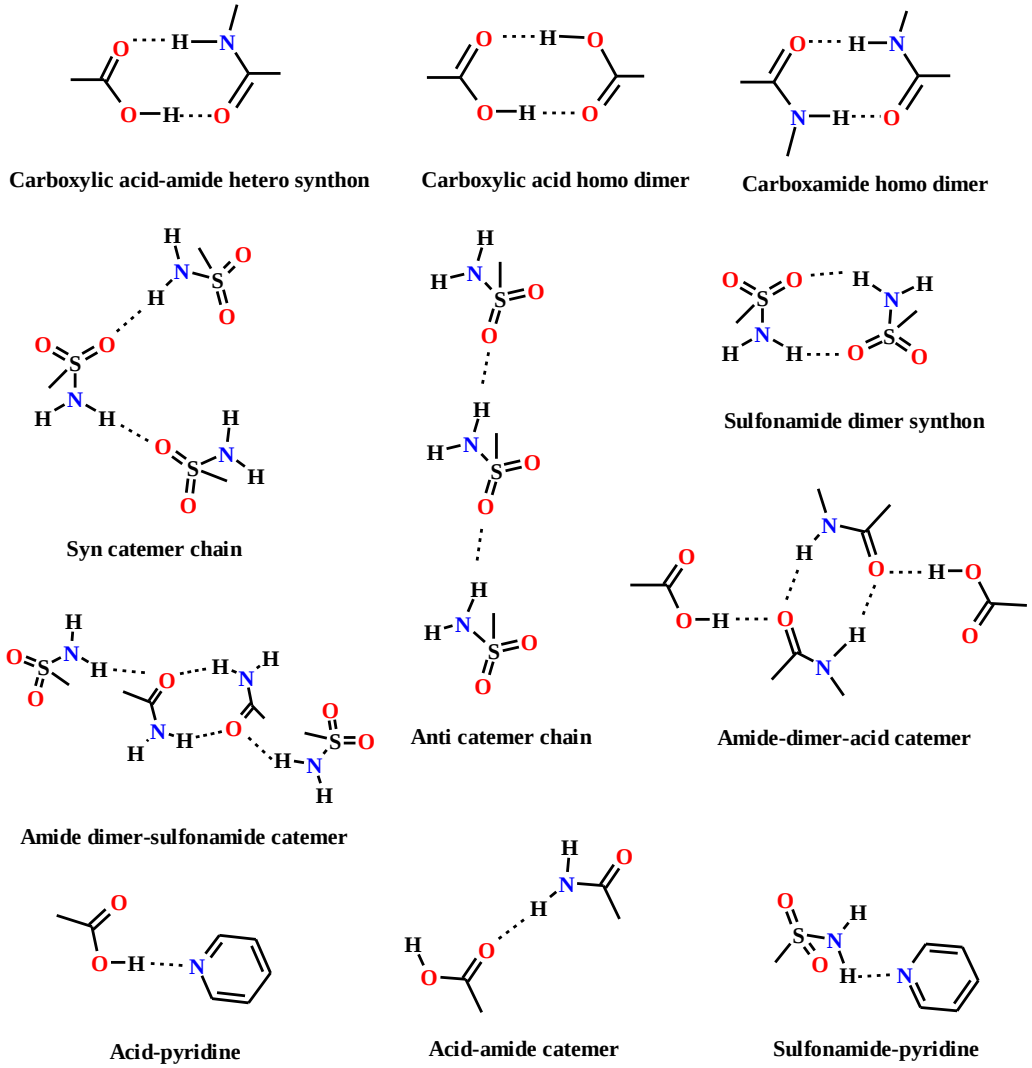


**Figure 2.7:** The observed supramolecular synthons in binary cocrystals of BUM.

## 2.2.3 Powder X-ray Diffraction

Novel solid forms identification and bulk phase purity using PXRD is a prime characterization technique for standard practice in pharmaceutics through their unique diffraction lines. Herein, Bumetanide (BUM) multicomponent solid forms (cocrystal/salts) prepared in this work confirm the exhibit unique diffraction pattern show excellent match of the experimental PXRD with the calculated pattern from the X-ray crystal structure (Figure 2.9). On the other hand, bumetanide ternary solid forms

determined through their unique diffraction patterns which are different from that of the starting components demonstrating new solid forms (Figure 2.8).

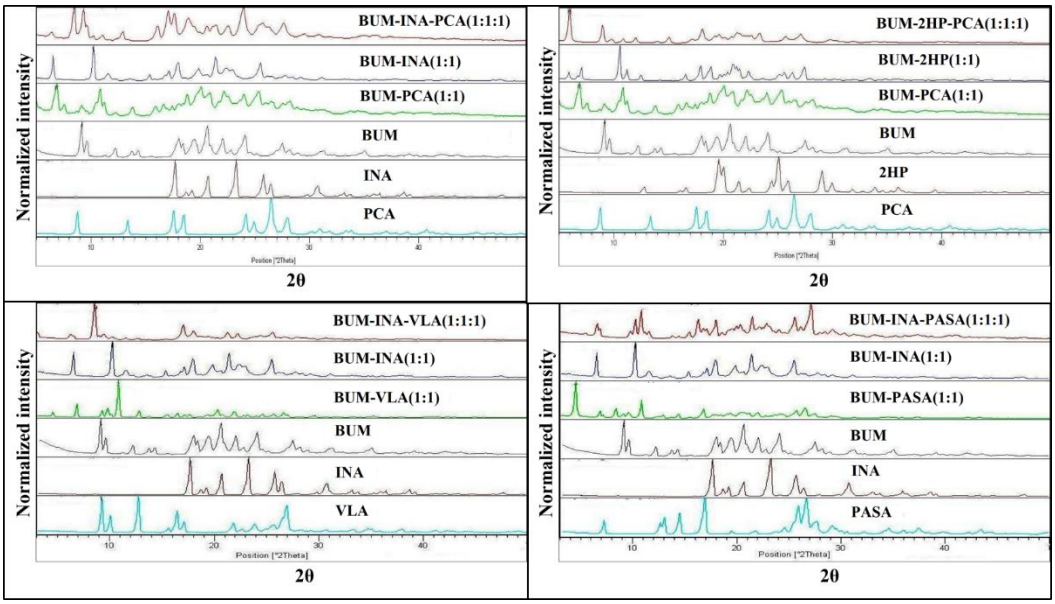


**Figure 2.8:** PXRD patterns of three component crystalline materials. Starting materials and binary combinations are compared with three-component crystalline material.

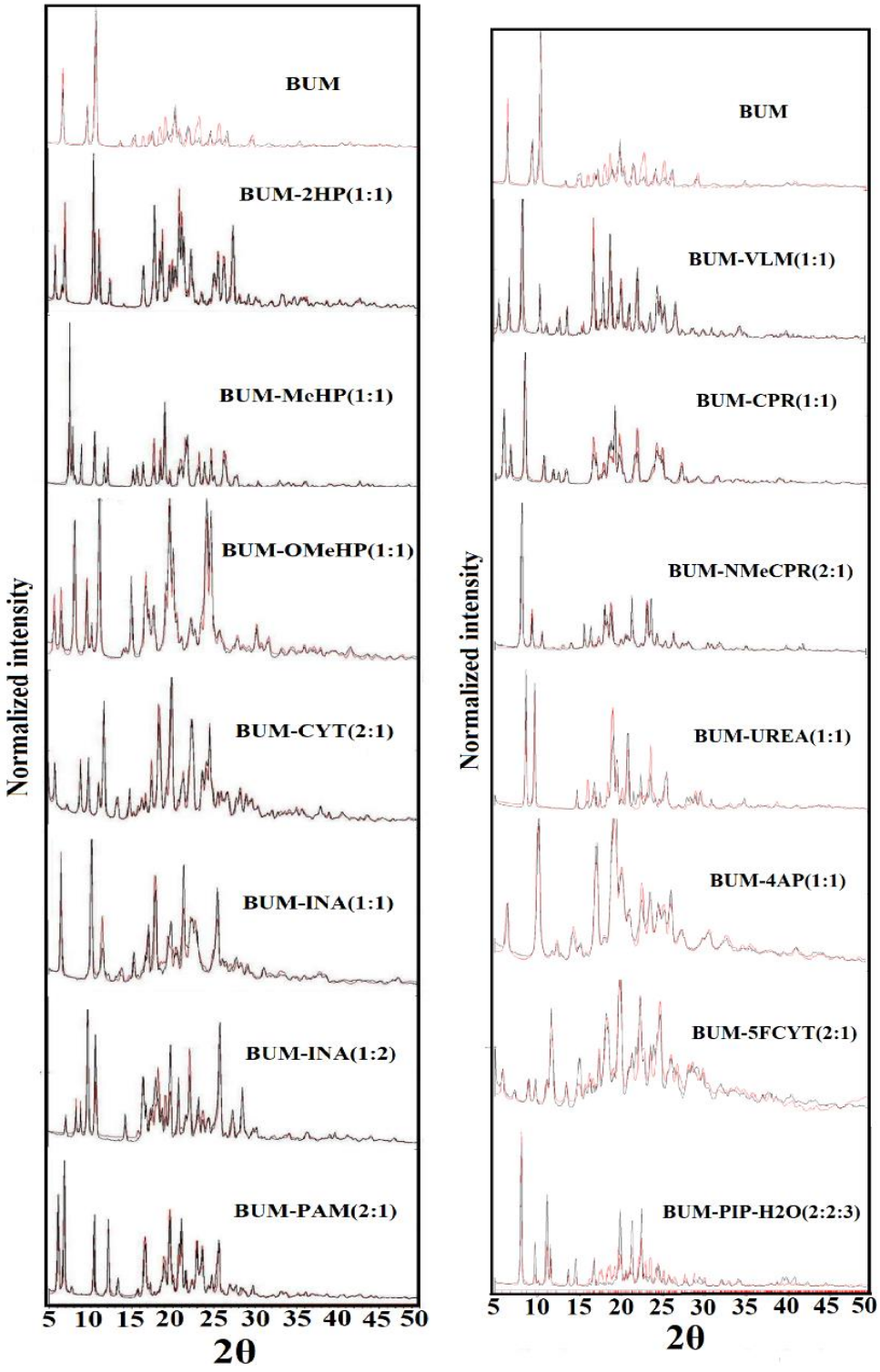


**Figure 2.9:** Overlay of experimental PXRD patterns (black) of novel crystal forms of BUM on the calculated lines (red) from the X-ray crystal structure.

## 2.2.4 Thermal Analysis

Thermal behavior of Bumetanide (BUM) binary and ternary solid forms was tested using differential scanning calorimetry (DSC). Differential Scanning Calorimetry (DSC) is a reliable technique to know solid form purity for a polymorph, cocrystal, and salt, solvate, eutectic or amorphous. The DSC heating curves and melting temperatures of bumetanide binary cocrystals/salts represented in Figure 2.10-2.11. The BUM exhibits a sharp melting endotherm at 239 °C and does not shows the any phase changes/transformation on heating before melting. BUM binary cocrystals like lactams shows low melting point range 125-150 °C, Pyridine carboxamides shows 140-170 °C, syn amides shows 160-190 °C and Salts shows higher melting point range 220-240 °C. On the other hand, DSC of bumetanide ternary cocrystals shows melting point range at 140-160 °C without any phase transformation presented in Figure 2.12-2.13

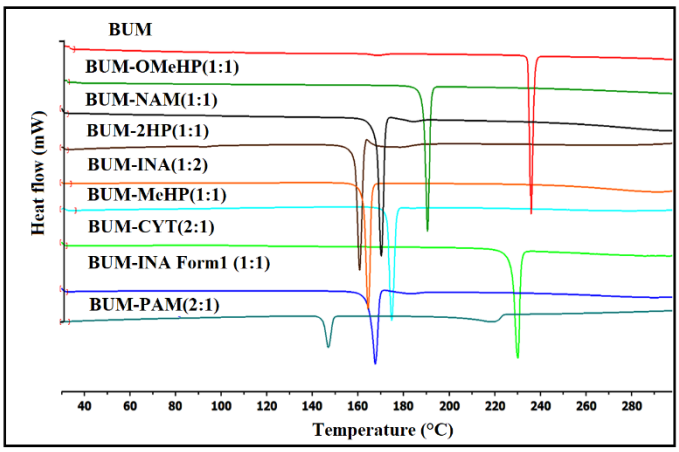


**Figure 2.10:** DSC thermograms of BUM salts/cocrystals.

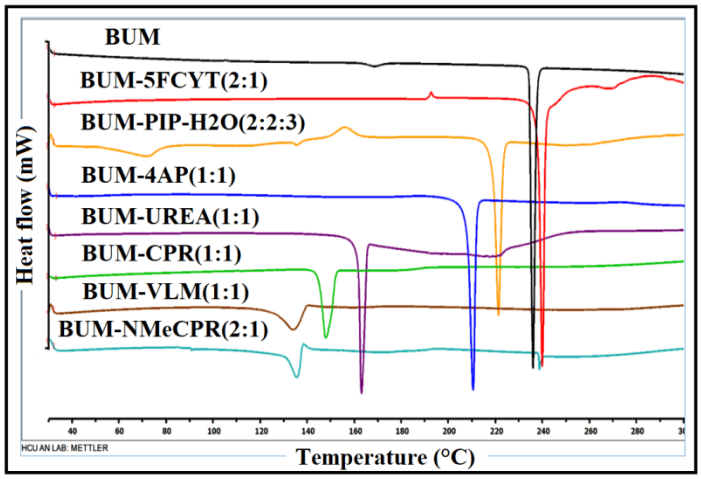

**Figure 2.11:** DSC thermograms of BUM salts/cocrystals.

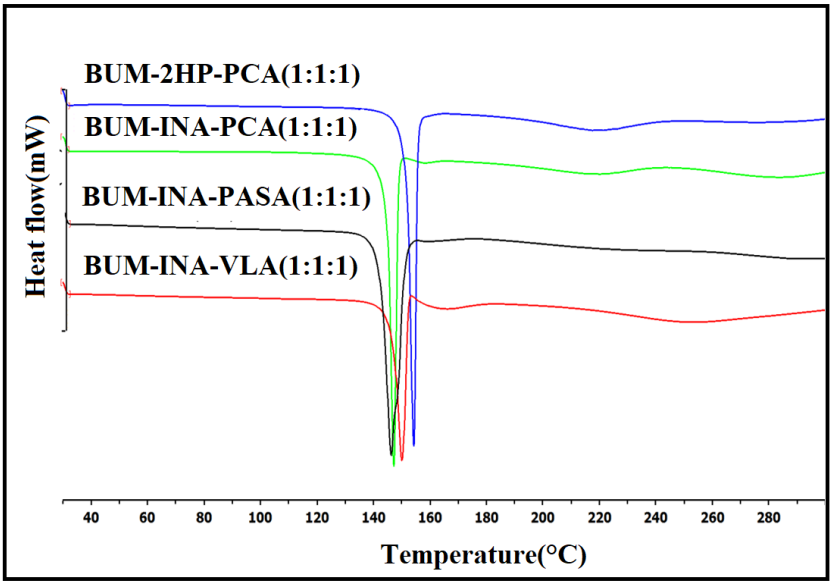


**Figure 2.12:** DSC thermograms of BUM salts/cocrystals.

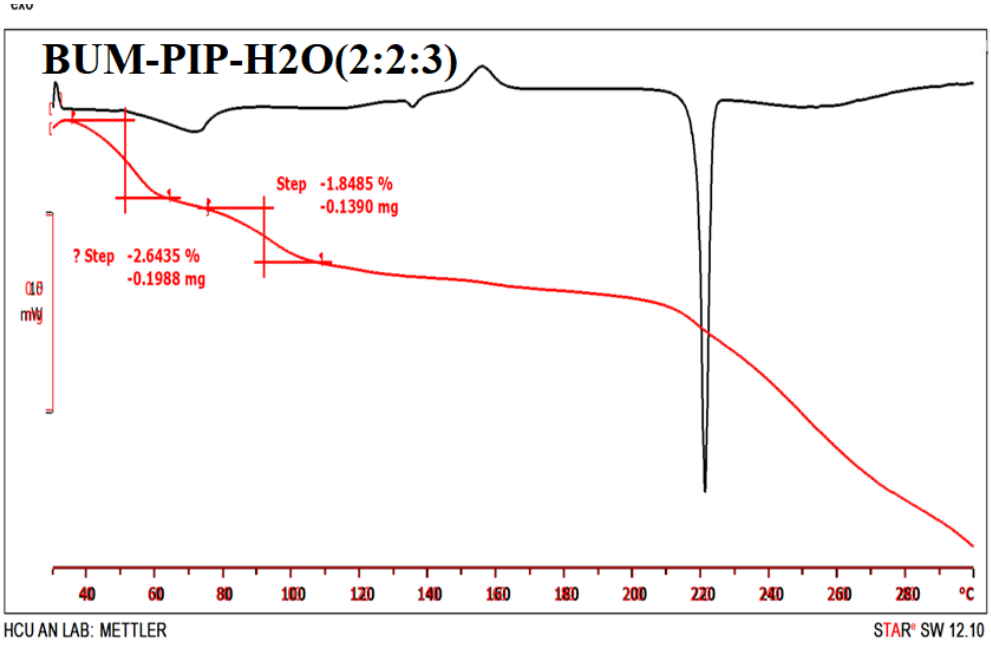


**Figure 2.13:** DSC and TGA thermograms of BUM salts/cocrystals.

## 2.2.5 Infrared Spectroscopy

Infrared spectroscopy shows useful information about vibrational modes of multicomponent solid forms their changes in the presence of hydrogen bonding of

different functional groups. The FT-IR spectrum of bumetanide (BUM) shows a Carboxylic acid carbonyl and hydroxyl (O-H) stretch at 1695cm$^{-1}$, 3401cm$^{-1}$ as well as sulfonamide (N-H) stretch at 3292 cm$^{-1}$. The carboxylic acid stretching frequency was blue shifted in all cocrystals, salts and ternary products crystalline phases. Sulfonamide (N-H) stretch in all the cocrystal and salts are shifted to blue shift but in BUM-MeHP shows red shift at 3312cm$^{-1}$ as well as two ternary systems BUM-INA-PCA and BUM-INA-PASA stretch at 3319, 3315 cm$^{-1}$ . The carboxylic acid, sulfonamide and lactams, amides functional groups (C=O / OH / NH) exhibit different stretching frequency are presented in Table 2.5 and Figure 2.14.

**Table 2.5:** Selected functional group stretching frequency in FT-IR spectra of BUM cocrystals.

| | **C=O (carboxylic acid/amide) (cm$^{-1}$)** | **Acid/Hydroxyl −OH/Amide NH (cm$^{-1}$)** | **NH in $SO_2NH_2$ (cm$^{-1}$)** |
|---|---|---|---|
| **BUM** | 1695 | 3401 | 3292 |
| **BUM−2HP (1:1)** | 1697 | 3337 | 3262 |
| **BUM−MeHP (1:1)** | 1706 | 3405 | 3312 |
| **BUM−OMeHP (1:1)** | 1707 | 3381 | 3273 |
| **BUM-CYT(2:1)** | 1693 | 3364 | 3199 |
| **BUM−INA (1:1)** | 1711 | 3313 | 3204 |
| **BUM−INA (1:2)** | 1685 | 3374 | 3170 |
| **BUM−NAM (1:1)** | 1672 | 3378 | 3270 |
| **BUM−PAM (2:1)** | 1723 | 3361 | 3292 |
| **BUM−2HP−PCA (1:1:1)** | 1689 | 3370 | 3212 |
| **BUM−INA−PCA(1:1:1)** | 1698 | 3361 | 3319 |
| **BUM−INA−PASA (1:1:1)** | 1711 | 3384 | 3315 |
| **BUM−INA−VLA (1:1:1)** | 1677 | 3344 | 3260 |
| **BUM−VLM (1:1)** | 1687 | 3359 | 3194 |
| **BUM−CPR (1:1)** | 1689 | 3377 | 3210 |
| **BUM−NMeCPR (2:1)** | 1688 | 3375 | 3311 |
| **BUM−UREA (1:1)** | 1672 | 3365 | 3179 |
| **BUM-5FCYT(2:1)** | 1692 | 3384 | 3204 |
| **BUM−4AP (1:1)** | 1665 | 3337 | 3187 |
| **BUM−PIP−$H_2O$ (2:2:3)** | 1629 | 3375 | 3293 |

| | | | |
|---|---|---|---|
| **VLM** | 1632 | 3273 | ––– |
| **CPR** | 1636 | 3429 | ––– |
| **NMeCPR** | 1627 | ––– | ––– |
| **UREA** | 1683 | 3442,3346 | ––– |
| **5FCYT** | 1685 | 3372 | ––– |
| **4AP** | 1687 | 3436 | ––– |
| **PIP** | 1689 | 3454 | ––– |
| **INA** | 1677 | 3371 | ––– |
| **NAM** | 1698 | 3366 | ––– |
| **PAM** | 1677 | 3278 | ––– |
| **CYT** | 1661 | 3381 | ––– |
| **2HP** | 1673 | 3266 | ––– |
| **MeHP** | 1670 | 3268 | ––– |
| **OMeHP** | 1655 | 3448 | ––– |
| **PCA** | 1719 | 3112 | ––– |
| **PASA** | 1664 | 3495,3387 | ––– |
| **VLA** | 1681 | 3483 | ––– |

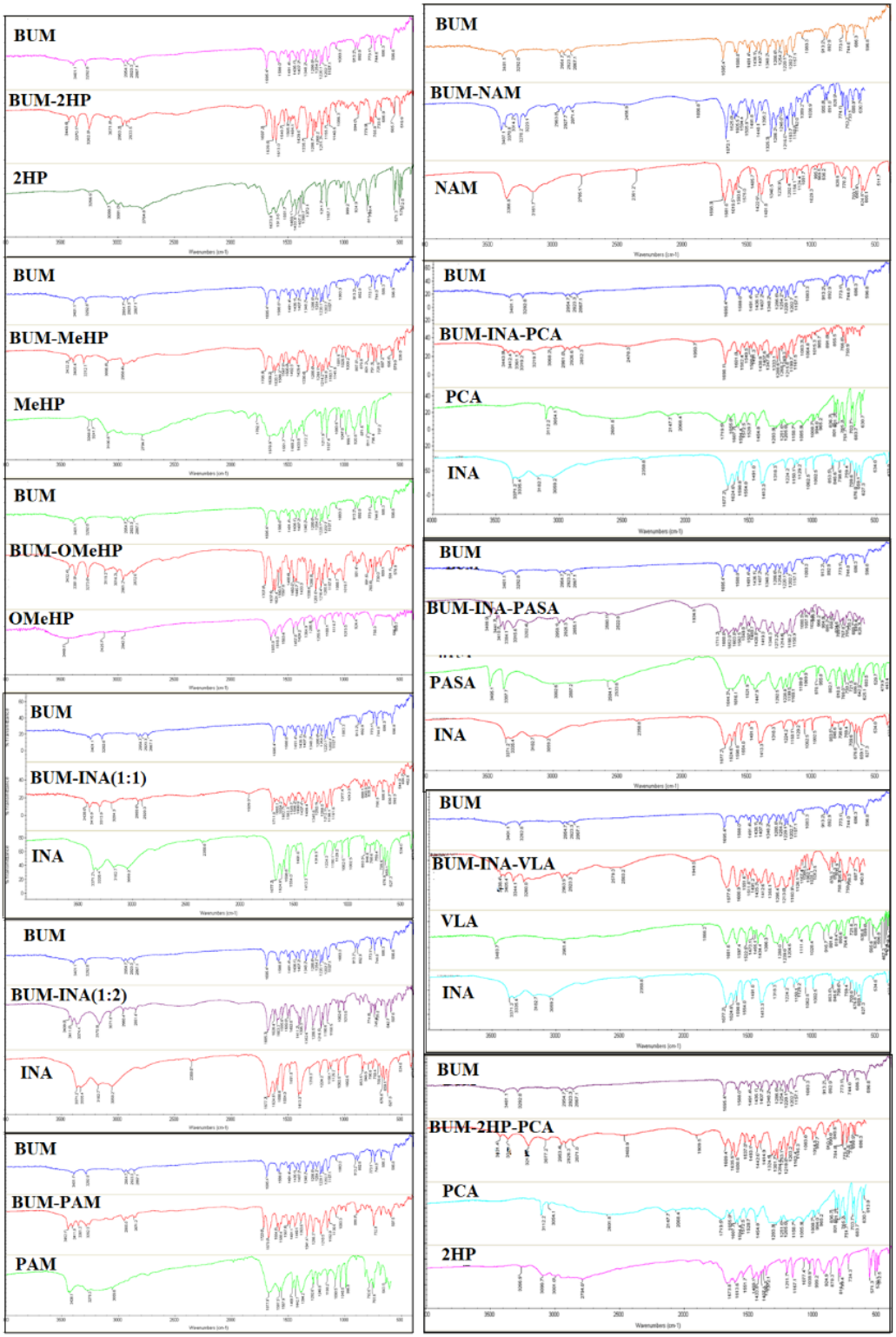
BUM
BUM-2HP
2HP
BUM
BUM-MeHP
MeHP
BUM
BUM-OMeHP
OMeHP
BUM
BUM-INA(1:1)
INA
BUM
BUM-INA(1:2)
INA
BUM
BUM-PAM
PAM
BUM
BUM-NAM
NAM
BUM
BUM-INA-PCA
PCA
INA
BUM
BUM-INA-PASA
PASA
INA
BUM
BUM-INA-VLA
VLA
INA
BUM
BUM-2HP-PCA
PCA
2HP

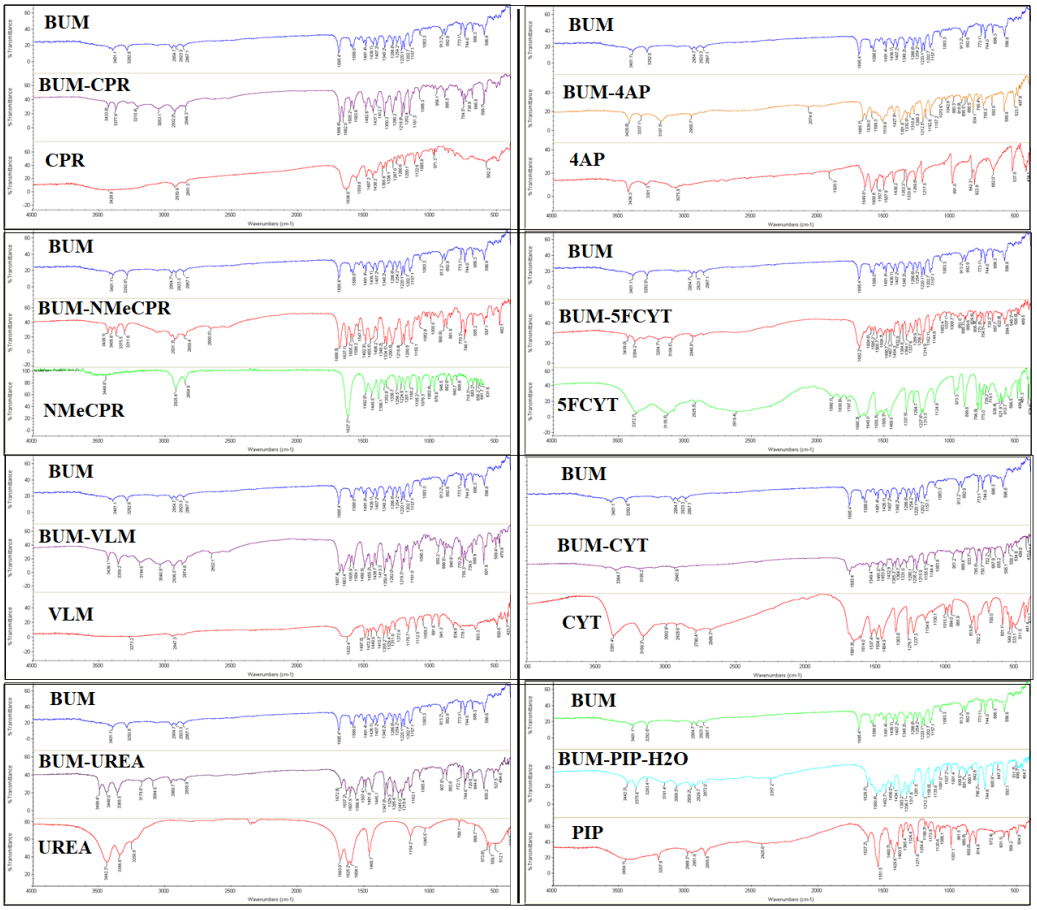


**Figure 2.14:** IR comparison of BUM novel solid forms with its starting materials.

## 2.2.6 Solution NMR

In order to find out the exact composition in the ternary crystalline materials, NMR experiments were performed of the single components as well as ternary crystalline materialsinDMSO-D6 solvent (solvent peak at 2.50(5) ppm). In NMR spectra, the different colour dots correspond to different protons of the component molecule. Here, three different molecules are highlighted which is indication of three different molecules in the crystalline product. In NMR spectra, well separated and distinct protons of the molecules are taken into account. The area under curve is an indication of number of protons attached to that molecule in the product. In all cases the ratio present in the reaction product is the same as that used for crystallization. The stoichiometry of the ternary system is established by 1H NMR integration.

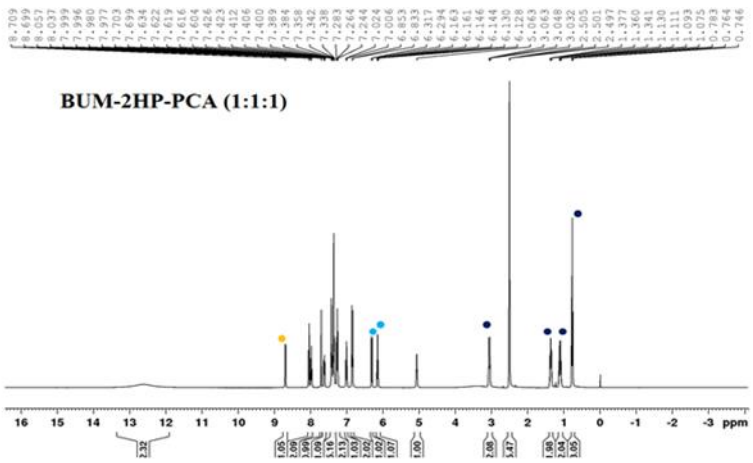


**Figure 2.15:** 1H-NMR of BUM-2HP-PCA: yellow, light blue and deep blue correspond to 2HP, PCA and BUM.

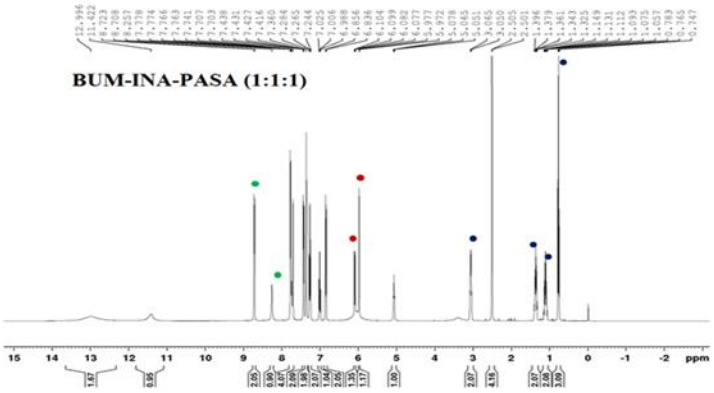


**Figure 2.16:** 1H NMR of BUM-INA-PASA: green, red and dark blue correspond to INA, PASA and BUM.

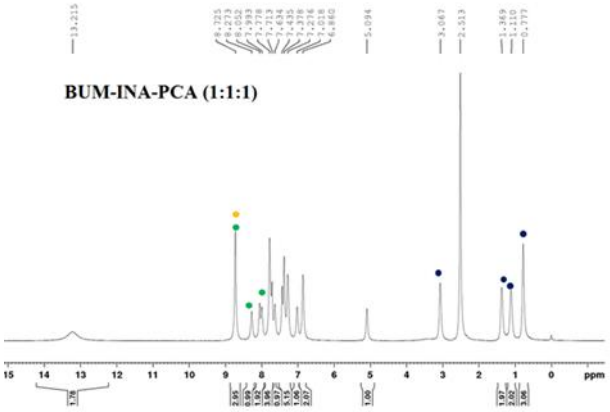


**Figure 2.17:** 1H-NMR of BUM-INA-PCA: yellow, green and dark blue correspond to PCA, INA and BUM.

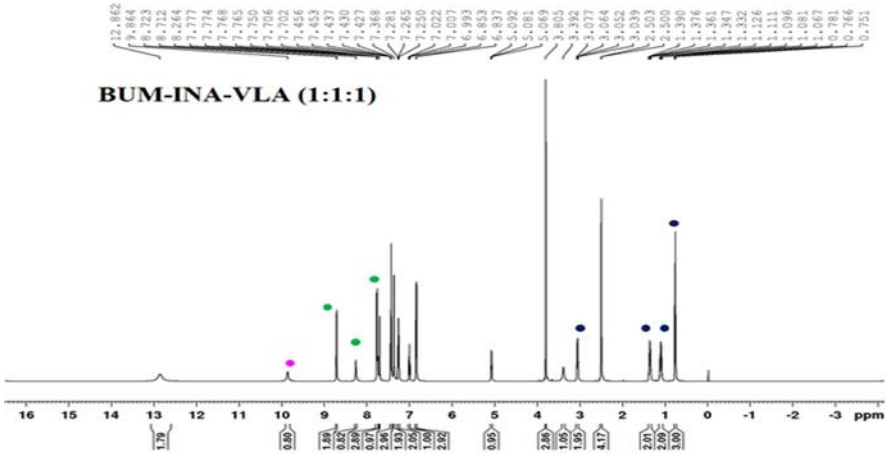


**Figure 2.18:** 1H-NMR of BUM-INA-VLA: pink, green and dark blue correspond to VAL, INA and BUM.

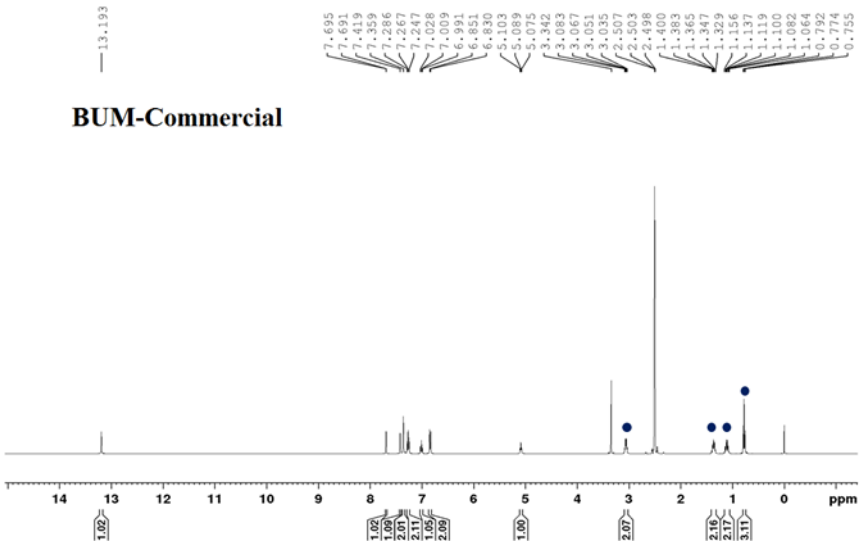


**Figure 2.19:** 1H-NMR of BUM: dark blue corresponds to alkyl group in BUM. The remaining protons are functional groups hydrogen atoms.

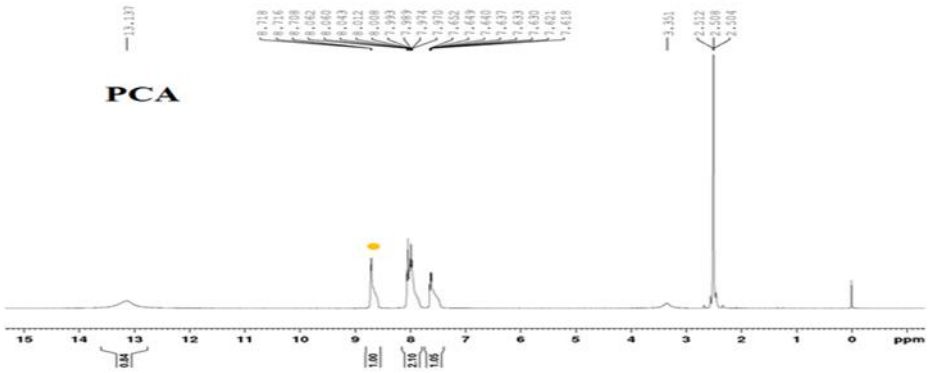


**Figure 2.20:** 1H-NMR of PCA: protons used to calculate integration are color coded.

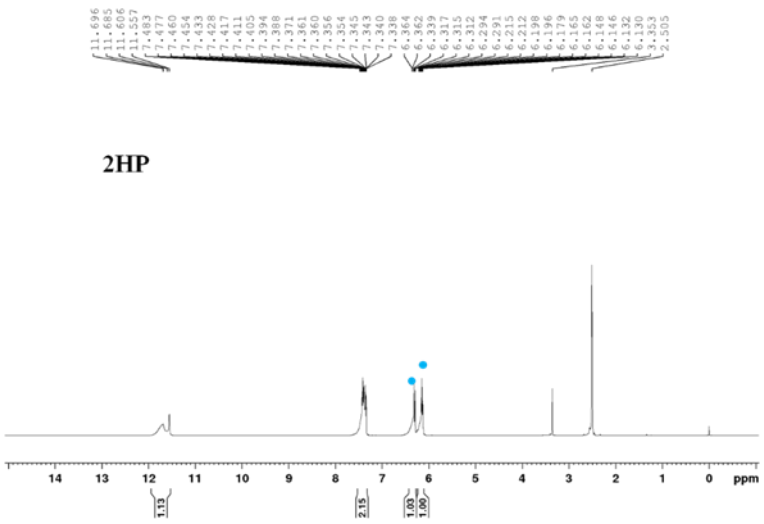


**Figure 2.21:** 1H-NMR of 2HP: protons used to calculate integration are color coded.

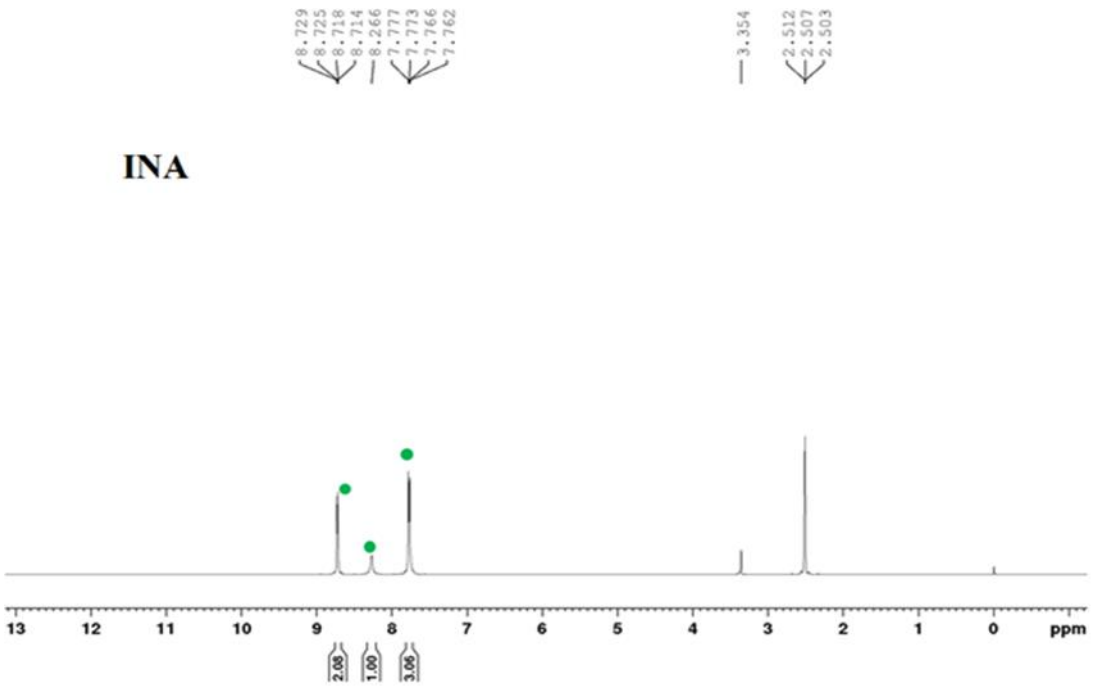


**Figure 2.22:** 1H-NMR of INA: protons used to calculate integration are color coded.

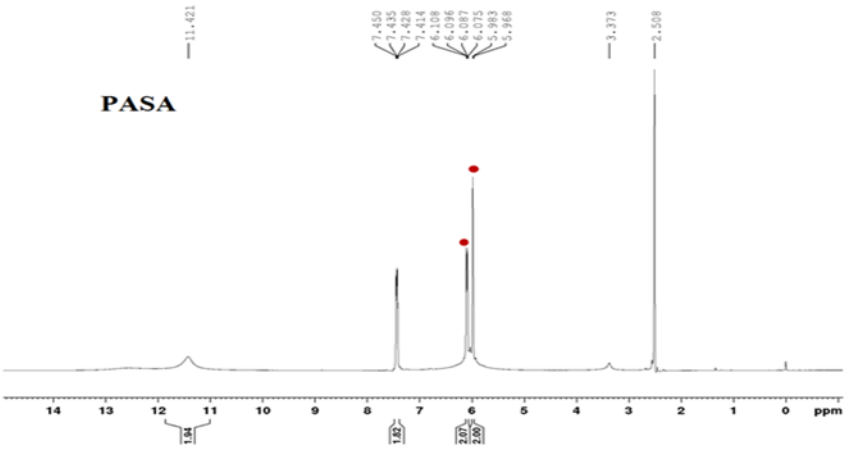


**Figure 2.23:** 1H-NMR of PASA: protons used to calculate integration are color coded.

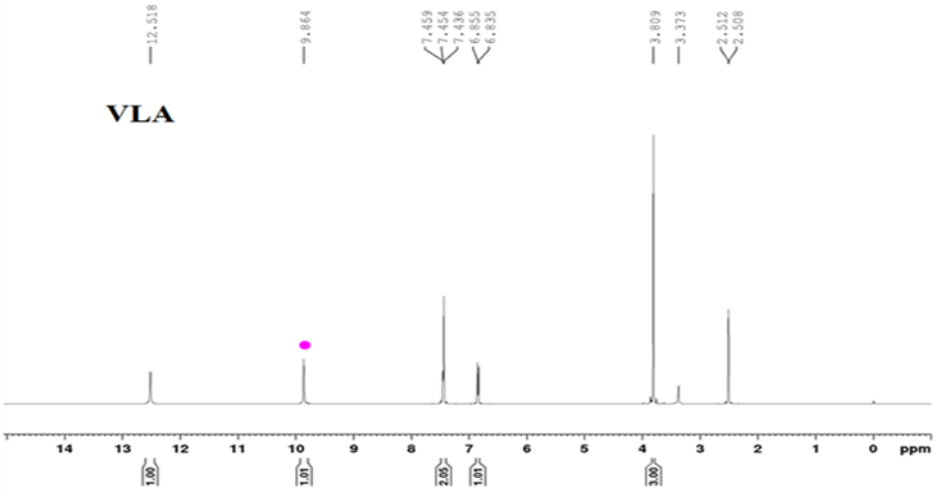


**Figure 2.24:** 1H-NMR of VLA: protons used to calculate integration are color coded.

## 2.2.7 Solubility and Dissolution Studies

Solubility and dissolution experiments is the key parameter of new solid forms(cocrystals, salts, polymorphs) to achieve the bioavilability of the API. Solubility studies of bumetanide solid forms (with GRAS coformers) were conducted in phosphate buffer (pH 7). Salt hydrate (BUM–PIP–$H_2O$) and salt cocrystals (BUM–CYT and BUM–5FCYT) show stability after 24 hours in equilibrium conditions. Cocrystals BUM–CPR (1:1) and BUM–UREA are unstable, and converted to BUM at the end of 24 h (Figure 2.26). These crystalline materials are completely dissociated into the corresponding

components to the physical mixture; no new phases were observed. Intrinsic dissolution rate (IDR) measurements were performed for all systems (including the less stable cocrystals) up to 8 h. BUM-CPR and BUM-UREA during the 8 h duration of IDR experiment (Figure 2.27). Salt hydrate, cocrystals and salts exhibit higher solubility compared to drug BUM (Figure 2.25, Table 2.6). Specifically, BUM–PIP salt exhibits 4.52 times higher dissolution rate compared to BUM. BUM-CYT and BUM-5FCYT salt cocrystals showed enhanced dissolution rates of 2.35, 2.00 times. The dissolution rate trend of salts > salt cocrystal > cocrystal correlates with the extent of ionic synthon. Compared to other coformers, piperazine is highly soluble in water and its salt has highest dissolution rate. Moreover, piperazine possesses high safety with $LD_{50}$ of 2050 mg/kg for rat and 600 mg/kg for mouse orally (acute toxicity) from a pharmaceutical viewpoint. The dissolution rate showed 4-fold faster dissolution of PIP salt hydrate and CYT salt-cocrystal showed 2-fold increase. This is a general phenomenon that high soluble partner molecule usually enhances higher solubility. Stability data by PXRD are presented in Figure 2.26-2.27.

**Table 2.6:** Solubility and intrinsic dissolution rate of BUM and new solid phases.

| Compound | Molar Extinction coefficient ($mM^{-1}$ $cm^{-1}$) | Equilibrium solubility after 24 h slurry (mg $mL^{-1}$) | Residue after 24 h slurry confirmed by PXRD | Intrinsic dissolution rate, IDR ($mg/cm^2$)/min ($x10^{-3}$) (x)[a] | Residual pellet after IDR (8 h) confirmed by PXRD |
|---|---|---|---|---|---|
| BUM | 3.5 | 2.19 | BUM (stable) | 0.42 | BUM (stable) |
| BUM–CPR | 3.6 | 3.78 | Unstable | 0.59 (x1.40) | BUM–CPR |
| BUM–UREA | 3.5 | 2.53 | Unstable | 0.55 (x1.30) | BUM–UREA |
| BUM–PIP–$H_2O$ | 3.6 | 3.69 | BUM–PIPH | 1.90 (x4.52) | BUM–PIPH |
| BUM–CYT | 3.5 | 1.92 | BUM–CYT | 0.99 (x2.35) | BUM–CYT |
| BUM–5FCYT | 3.6 | 2.01 | BUM–5FCYT | 0.84 (x2.00) | BUM–5FCYT |

[a] times increase compared to reference drug BUM

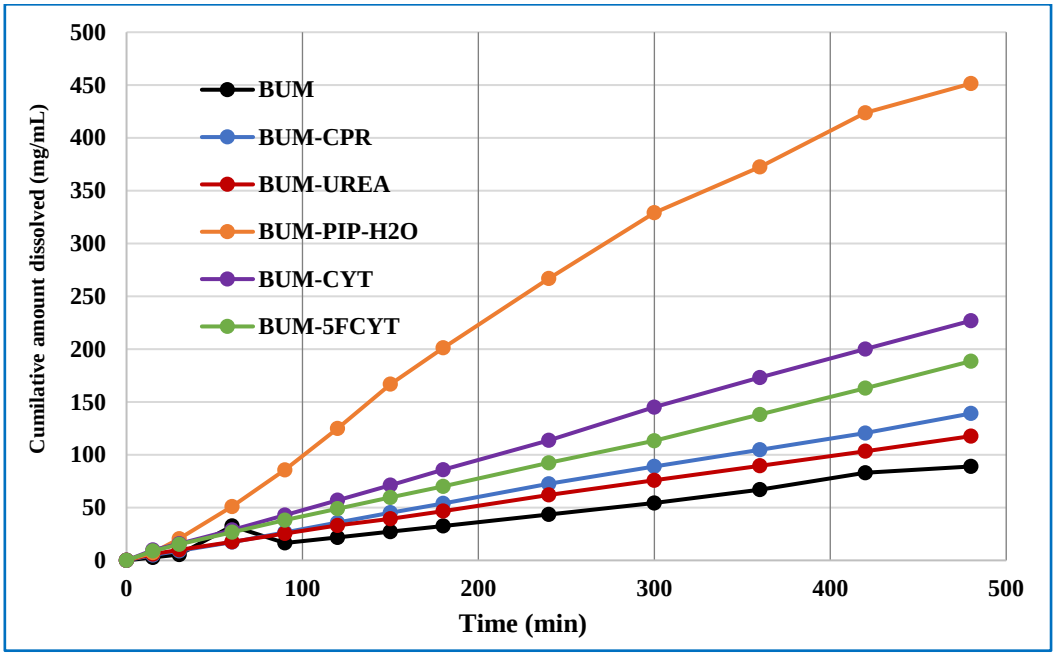


(a)

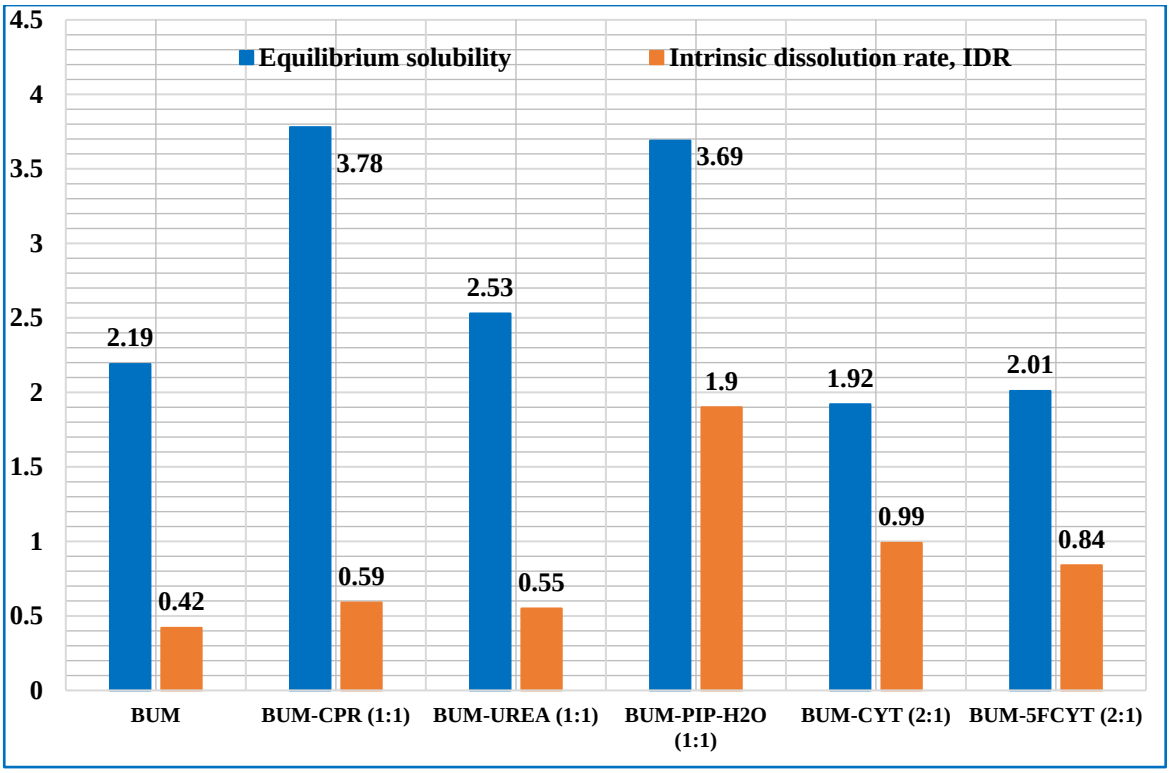


(b)

**Figure 2.25:** (a) Intrinsic dissolution rates curves of BUM cocrystal and salts in phosphate buffer (pH 7). (b) Comparison of drug solubility and IDR of BUM adducts to

show the enhanced solubility of CPR and PIP adducts while others showed decrease in solubility. Even though the solubility decreased in some cases (Figure 2.25b), all cocrystals and salts showed enhancement in IDR during the 8 h study (Figure 2.25a).

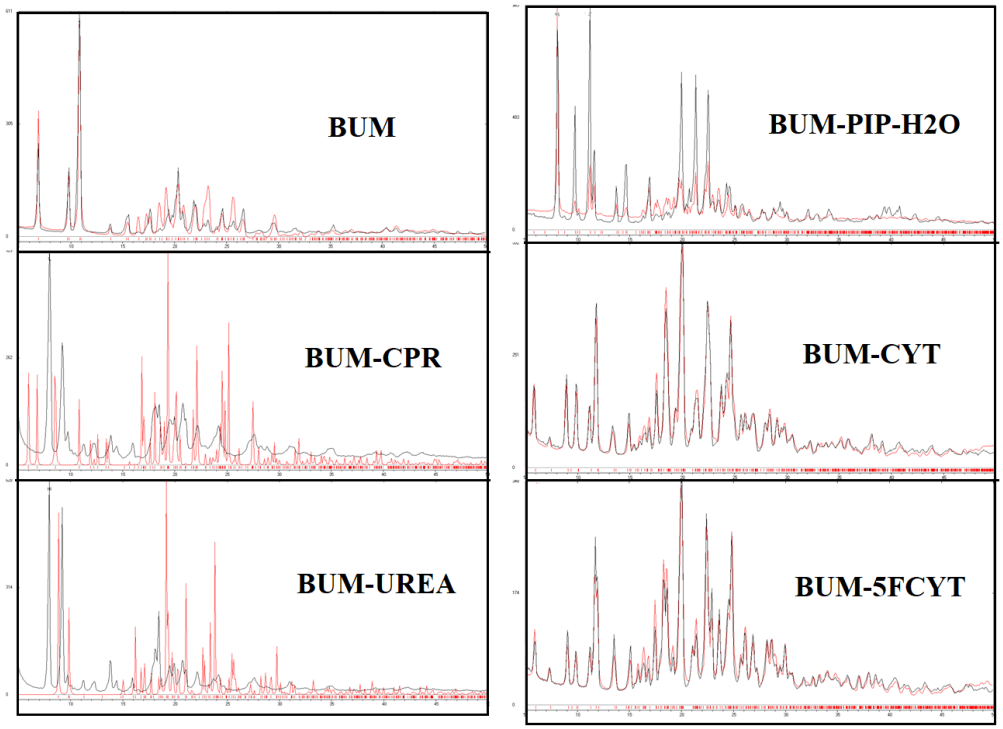


**Figure 2.26:** PXRD analysis to determine BUM cocrystal salt forms phase stability at 24 h (equilibrium solubility) in pH 7 buffer media.

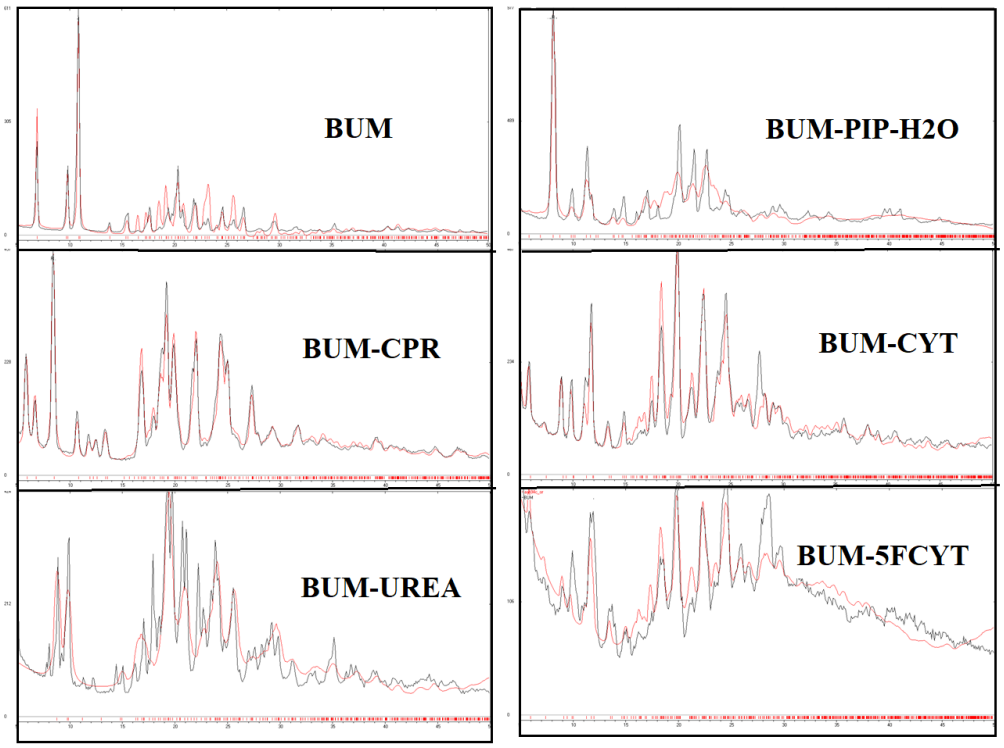


**Figure 2.27:** PXRD analysis to determine the BUM cocrystal salt forms phase stability at 8h (dissolution) in pH 7 buffer media.

## 2.2.8 Diffusion Measurements

Drug permeability on the crystalline adducts of BUM was performed using a diffusion cell membrane at pH 7 buffer at different time intervals (Figure 2.28). The cumulative amount of BUM diffusing through the membrane increases slowly over 8 h whereas the flux increases rapidly in the first hour and reaches a steady state after 2 h. The plot of cumulative drug diffused and flux against time indicate that BUM−PIP exhibits superior diffusion rate compared to other cocrystals. The diffusion rate of cocrystals BUM−CPR, BUM−CYT, BUM−5FCYT and BUM−UREA showed a marginal increase of two-fold in diffusion rate compared to the parent drug. This trend supports the recent reports wherein cocrystals exhibit rate improvement in permeability of a few drugs such as theophylline,[44] hydrochlorothiazide,[45-46] and 5-fluorouracil.[47] The present study shows that cocrystals and salts provide 2-4-fold increase in diffusion rate, even though CYT, 5FCYT and CPR cocrystals were not very effective in solubility enhancement.

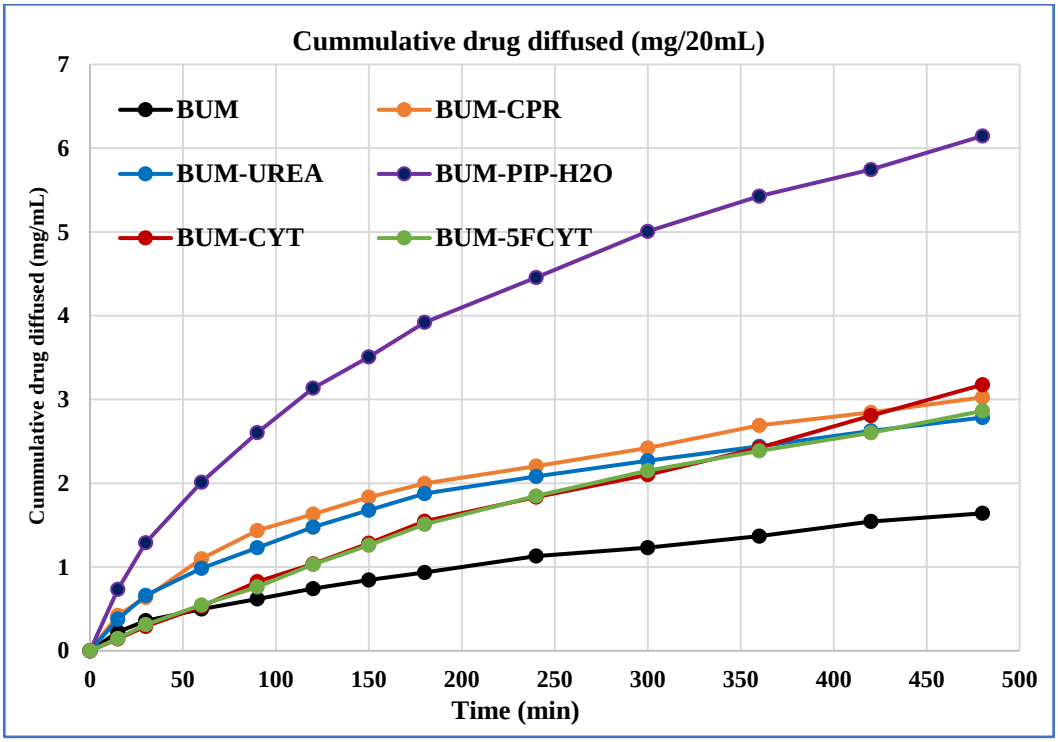
Cummulative drug diffused (mg/20mL)
BUM
BUM-CPR
BUM-UREA
BUM-PIP-H2O
BUM-CYT
BUM-5FCYT
Cummulative drug diffused (mg/mL)
Time (min)
0
1
2
3
4
5
6
7
0
50
100
150
200
250
300
350
400
450
500

(a)

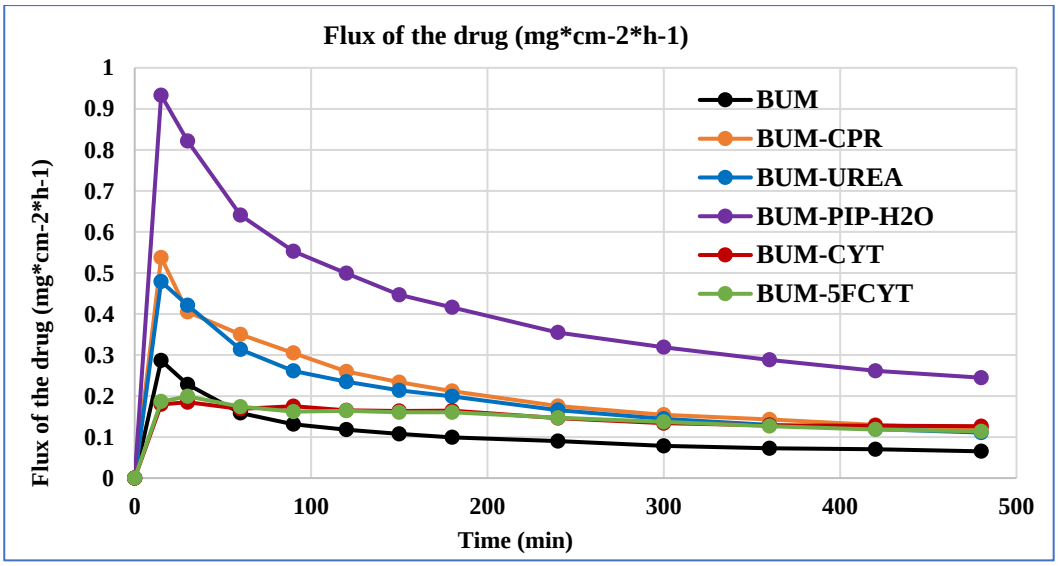
Flux of the drug (mg*cm-2*h-1)
BUM
BUM-CPR
BUM-UREA
BUM-PIP-H2O
BUM-CYT
BUM-5FCYT
Flux of the drug (mg*cm-2*h-1)
Time (min)
0
0.1
0.2
0.3
0.4
0.5
0.6
0.7
0.8
0.9
1
0
100
200
300
400
500

(b)

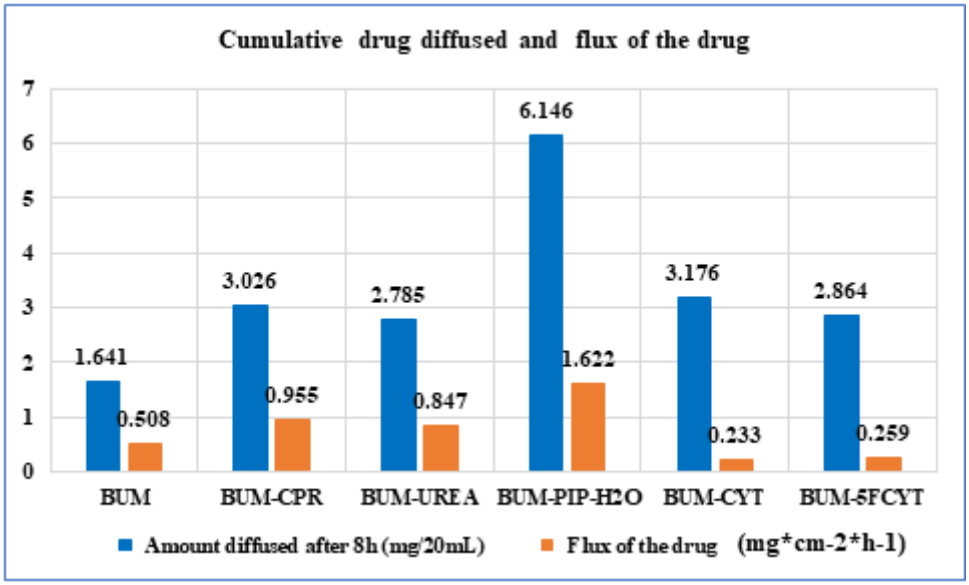


(c)

**Figure 2.28:** (a) Cumulative amount of the BUM, cocrystals and salt diffusion with time. (b) Flux of BUM cocrystals and salts with time. (c) Comparison of cumulative drug diffused and flux of the drug shows that the novel adducts exhibit improved permeability between 2 to 6 times compared to the reference drug BUM.

## 2.3 Conclusions

Supramolecular synthons of sulfonamide and carboxylic acid groups in bumetanide were systematically studied with pyridine carboxamide, pyridine, lactams, amines and aromatic carboxylic acid coformers. Carboxylic acid homosynthon in the crystal structure of bumetanide is replaced by pyridone amide dimer in HP cocrystals with the COOH donor bonded to it in a $R_3^2(9)$ ring motif. Bumetanide−isonicotinamide was crystallized as a dimorphic cocrystal system with acid–amide heterosynthon. Bumetanide−cytosine, 5-flourocytosines (amines) cocrystal salt contains both acid homosynthon and cytosine dimer along with carboxylate–amino-pyridinium synthon. Bumetanide with lactams obtained cocrystals containing syn-amide dimers followed by sulfonamide-catemer synthons. Among these cocrystal structures, few cocrystals were obtained ternary cocrystals as homogenous phases of three components, namely BUM–INA–PCA, BUM–INA–PASA, BUM–INA–VLA, and BUM–2HP–PCA. Dissolution studies of the crystal forms showed that BUM–PIP has the highest dissolution rate which is attributed to the coformer being highly soluble in water and this release in turn drags

the drug faster into solution. The cocrystals exhibit 2-fold improvement in solubility, while the increase for PIP salt is 4-fold compared to BUM. Permeability improved 5-fold with piperazine salt but only a marginal improvement with cocrystals. BUM-CPR cocrystal improved permeability and solubility nearly two-fold and this could be an alternative formulation for BUM.

## 2.4 Experimental Section

Active pharmaceutical ingredient bumetanide was purchased from Shanghai Xunxin Chemical Co., Ltd. China. Its purity is confirmed by NMR and DSC. All The coformers used in this study were purchased from Sigma-Aldrich, Hyderabad, India. All chemicals are of analytical or chromatographic grade was used in the experiments. Typical synthesis of cocrystals/salts is explained. Solvent assisted grinding experiments were performed using EtOAc solvent (0.3-0.5 mL was added) to the physical mixture and ground for 5-8 min, and the same procedure was repeated 2-3 times to ensure the system is completely homogeneous. The ground crystalline mixture was dissolved EtOAc and suitable solvent (solvent mixtures) and allowed for crystallization.

**BUM single crystals:** Bumetanide single crystals could not obtain directly from the corresponding powder by crystallization. Instead, cocrystallization experiments of BUM-PAM in EtOAc–$CH_3NO_2$ (1:1 v/v) gave BUM single crystals. In order to obtain the stable from of BUM, 150 mg of BUM was taken in 10 mL EtOAc. The mixture was kept on a stirrer for 24 h to make a slurry. The bulk phase purity was checked by PXRD and compared with the calculated PXRD line pattern. The powder material was kept for crystallization in EtOAc and $CH_3NO_2$ (5 mL) and suitable single crystals are obtained for SC-XRD. M.p. 235-239 °C.

**BUM−2HP (1:1):** BUM (100 mg, 0.274 mmol) and 2HP (26 mg, 0.274 mmol) were ground in a mortar and pestle for 20-25 min after adding 4-5 drops of EtOAc. The ground material was kept for crystallization from solvent mixture EtOAc and $CH_3CN$ (5 mL) as well as the pure solvents in 10 mL test tubes at room temperature. Colorless good quality single crystals were observed by slow evaporation. M.p. 157-163 °C.

**BUM−MeHP (1:1):** BUM (100 mg, 0.274 mmol) and MeHP (30 mg, 0.274 mmol) were ground in a mortar and pestle for 20-25 min after adding 4-5 drops of EtOAc. The ground material was kept for crystallization from EtOAc and $CH_3CN$ (5 mL) solvent mixture as well as the individual solvents in 10 mL test tubes at room temperature.

Colorless good quality single crystals were observed after slow evaporation. M.p. 172-177 °C.

**BUM−OMeHP (1:1):** BUM (100 mg, 0.274 mmol) and OMeHP (34 mg, 0.274 mmol) were ground in a mortar and pestle for 20-25 min after adding 4-5 drops of EtOAc. The ground material was kept for crystallization from EtOAc and $CH_3CN$ (5 mL) solvent mixture as well as the individual solvents in 10 mL test tubes at room temperature. Colorless good quality single crystals were observed by slow evaporation. M.p. 186-191 °C.

**BUM−INA (1:1):** BUM (100mg, 0.274 mmol) and INA (33.51mg, 0.274 mmol) were ground in a mortar and pestle for 20−25 min in stoichiometric ratio by adding catalytic amount (4−5 drops) of EtOAc solvent. The ground material was kept for crystallization from solvent mixture of EtOAc and $CH_3CN$ (1:1 v/v) 5ml in a 25ml conical flask at room temperature. Both Form I and Form II were obtained concomitantly. The same experimental procedure was repeated several times but only BUM−INA (1:1) Form I was obtained. Form II could not be crystallized in bulk amount for measurement of physical, thermal and diffraction parameters. Form I M.p. 162-167 ° C

**BUM−INA (1:2):** BUM (100 mg, 0.274 mmol) and INA (672 mg, 0.548 mmol) were ground in a mortar and pestle for 20-25 min after adding 4-5 drops of EtOAc. The ground material was kept for crystallization from of EtOAc and $CH_3CN$ (1:1 v/v, 5 mL) mixture in a 25 mL conical flask at room temperature. Colorless good quality single crystals were observed by slow evaporation. M.p. 160-165 °C.

**BUM−PAM (1:0.5):** BUM (100 mg, 0.274 mmol) and PAM (17 mg, 0.137 mmol) were ground in a mortar and pestle for 20-25 min after adding 4-5 drops of EtOAc. The ground material was kept for crystallization from solvent EtOAc and $CH_3CN$ (1:1 v/v) mixture (5 mL) in a 25 mL conical flask at room temperature. Colorless good quality single crystals were observed after slow evaporation. M.p. 145-150 °C.

**BUM−NAM (1:1):** BUM (100 mg, 0.274 mmol) and NAM (33 mg, 0.274 mmol) were ground in a mortar and pestle for 20-25 min after adding 4-5 drops of EtOAc. The ground material was kept for crystallization from solvent EtOAc and $CH_3CN$ (1:1 v/v) mixture (5 mL) in a 25 mL conical flask at room temperature. Diffraction quality single crystals could not be obtained by slow evaporation and different cooling rates. M.p. 168-173 ° C.

**BUM-CYT (2:1):** BUM (100 mg, 0.274 mmol) and CYT (15 mg, 0.137 mmol) were ground in a mortar and pestle for 20-25 min by adding 4-5 drops of EtOAc. The ground material was kept for crystallization from solvent mixture of EtOAc and $CH_3OH$ (1:1 v/v) in a 25 mL conical flask at room temperature. Colorless good quality single crystals were observed after slow evaporation. M.p. 225-230 °C.

**BUM−VLM (1:1):** BUM (100 mg, 0.274 mmol) and VLM (27 mg, 0.274 mmol) were ground in a mortar and pestle for 20-25 min in stoichiometric 1:1 ratio by adding catalytic amount (four to five drops) of EtOAc solvent. The ground material was kept for crystallization from solvent mixture EtOAc and $CH_3CN$ (5 mL) as well as individual solvents in 10 mL test tubes at room temperature. Colorless good quality single crystals were observed by slow evaporation. M.p. 133-135 °C

**BUM−CPR (1:1):** BUM (100 mg, 0.274 mmol) and CPR (31 mg, 0.274 mmol) were ground in a mortar and pestle for 20-25 min in 1:1 stoichiometric ratio by adding catalytic amount (four to five drops) of EtOAc solvent. The ground material was kept for crystallization from solvent mixture EtOAc and $CH_3CN$ (5 mL) as well as individual solvents in 10 mL test tubes at room temperature. Colorless good quality single crystals were observed by slow evaporation. M.p. 147-152 °C

**BUM−NMeCPR (1:0.5):** BUM (100 mg, 0.274 mmol) and NMeCPR (35 mg, 0.274 mmol) were ground in a mortar and pestle for 20-25 min in stoichiometric 1:1 ratio by adding catalytic amount (four to five drops) of EtOAc solvent. The ground material was kept for crystallization from solvent mixture EtOAc and $CH_3CN$ (5 mL) as well as individual solvents in 10 mL test tubes at room temperature. Good quality single crystals were observed by slow evaporation and structure determination by single crystal X-ray diffraction confirmed the ratio as 1:0.5 of BUM and NMeCPR. The experiment was reproduced by taking BUM (100 mg, 0.274 mmol) and NMeCPR (17 mg, 0.137 mmol) with identical results. M.p. 135-137 °C

**BUM−UREA (1:1):** BUM (100 mg, 0.274 mmol) and Urea (16.48 mg, 0.274 mmol) were ground in a mortar and pestle for 20-25 min in 1:1 stoichiometric ratio by adding catalytic amount (four to five drops) of EtOAc solvent. The ground material was kept for crystallization from solvent mixture EtOAc and $CH_3OH$ (5 mL) as well as individual solvents in 10 mL test tubes at room temperature. Good quality single crystals were observed by slow evaporation. M.p. 162-165 °C

**BUM−4-AP (1:1):** BUM (100 mg, 0.274 mmol) and 4-aminopyridine (26 mg, 0.274 mmol) were ground in a mortar and pestle for 20-25 min in stoichiometric ratio by adding catalytic amount (four to five drops) of EtOAc solvent. The ground material was kept for crystallization from solvent mixture EtOAc and $CH_3OH$ (5 mL) as well as individual solvents in 10 mL test tubes at room temperature. Good quality single crystals were observed by slow evaporation. M.p. 209-211 °C

**BUM−PIP-$H_2O$ (2:2:3):** BUM (100 mg, 0.274 mmol) and Piperazine (24 mg, 0.274 mmol) were ground in a mortar and pestle for 20-25 min in stoichiometric ratio by adding catalytic amount (four to five drops) of EtOAc solvent. The ground material was kept for crystallization from solvent mixture EtOAc and $CH_3OH$ (5 mL) as well as individual solvents in 10 mL test tubes at room temperature and confirmed as 2:2:3 ratio of a salt hydrate. Later experiments were repeated in the same ratio for bulk material preparation and powder purity conformed by PXRD. Colorless good quality single crystals were observed by slow evaporation and confirmed by single crystal structure of the hydrate. M.p. 220-223 °C

**BUM−5FCYT (2:1):** BUM (100 mg, 0.274 mmol) and 5-fluorocytosine (18 mg, 0.137 mmol) were ground in a mortar and pestle for 20-25 min in stoichiometric ratio by adding catalytic amount (four to five drops) of EtOAc solvent. The ground material was kept for crystallization from solvent mixture EtOAc and $CH_3OH$ (5 mL) as well as individual solvents in 10 mL test tubes at room temperature. Single crystals were observed by slow evaporation. M.p. 238-241 °C

**BUM−INA−PCA (1:1:1):** BUM (100 mg, 0.274 mmol) and INA (34 mg, 0.274 mmol) and PCA (34 mg, 0.274 mmol) were ground in a mortar and pestle for 20-25 min after adding 4-5 drops of EtOAc. The ground material was kept for crystallization from different solvents. However, no single crystals could be obtained from different solvents and so the product was characterized by PXRD, DSC, and IR. M.p. 144-148 °C.

**BUM−INA−PASA (1:1:1):** BUM (100 mg, 0.274 mmol) and INA (33 mg, 0.274 mmol), PASA (42 mg, 0.274 mmol) were ground in a mortar and pestle for 20-25 min in stoichiometric ratio after adding 4-5 drops of EtOAc solvent. The ground material was kept for crystallization from different solvents, but no single crystals were obtained, and so the product was characterized by PXRD, DSC, IR. M.p. 142-150 °C.

**BUM−INA−VLA (1:1:1):** BUM (100 mg, 0.274 mmol) and INA (33 mg, 0.274 mmol), VLA (46 mg, 0.274 mmol) were ground in a mortar and pestle for 20-25 min after adding 4-5 drops of EtOAc. The ground material was kept for crystallization from different solvents. However, no single crystals were obtained, and so the product was characterized by PXRD, DSC, IR. M.p. 145-149 °C.

**BUM−2HP−PCA (1:1:1):** BUM (100 mg, 0.274 mmol), 2HP (26 mg, 0.274 mmol), PCA (34 mg, 0.274 mmol) were ground in a mortar and pestle for 20-25 min after adding 4-5 drops of EtOAc. The ground material was kept for crystallization from different solvents, but no grow single crystals could be obtained, and so the product was characterized by PXRD, DSC, IR. M.p. 151-156°C.

**X–ray Crystallography**

X-ray reflections for all the BUM solid forms were collected on Bruker SMART-APEX CCD diffractometer equipped with a graphite monochromator and Mo-Kα fine-focus sealed tube (λ=0.71073 Å). Data reduction was performed using Bruker SAINT Software.[48] Intensities were corrected for absorption using SADABS,[49] and the structure was solved and refined using SHELX-97.[50] X-ray reflections for BUM−VLM, BUM−CPR, BUM−NMeCPR, BUM-PAM and BUM-2HP cocrystals were collected at 298 K on Oxford Xcalibur Gemini Eos CCD diffractometer using (Cu-Kα radiation source, λ=1.54184 Å) Mo-Kα radiation (λ = 0.7107 Å). Data reduction was performed using CrysAlisPro (version 1.171.33.55)[51] and OLEX2-1.0[52] was used to solve and refine the structures. All non-hydrogen atoms were refined as anisotropic. Hydrogen atoms on heteroatoms were located from difference electron density maps and all C−H hydrogens were fixed geometrically. Hydrogen bond geometries were determined in Platon.[53-54] X-Seed[55] and Mercury was used to prepare packing diagrams. Crystallographic cif files are available at www.ccdc.cam.ac.uk/data_request/cif (CCDC Nos. 1543072-1543080 and 1950679-1950685).

**Powder X-ray Diffraction**

Powder X-ray diffraction of all the samples were recorded on Bruker D8 Advance diffractometer (Bruker-AXS, Karlsruhe, Germany) using Cu-Kα X-radiation (λ = 1.5406 Å) at 40 kV and 30 mA power. X-ray diffraction patterns were collected over the 2θ range 5-50° at a scan rate of 1°/min. Powder Cell 2.4[56] was used for Profile fitting refinement of experimental PXRD and calculated lines from the X-ray crystal structure.

**Structure determination from powder data**

The crystal structure of ternary cocrystals were determined with the use of SDPD methods.[57-58] The X-ray powder diffraction data in a 3 – 75° 2θ range were collected using a Huber G670 Guinier camera (Cu $K_{\alpha 1}$ radiation, λ = 1.54059 Å) equipped with an imaging-plate detector. The powder pattern was indexed in a monoclinic unit cell, and the crystal structures were solved with the use of simulated annealing technique and refined with the program MRIA following the known procedures described by us earlier.[59] powder X-ray diffraction data of ternary systems were recorded at ambient temperature (25 ºC) on a Bruker D8 Advance diffractometer operating in the transmission mode and using $CuK_{\alpha 1}$ radiation (λ=1.5406 Å). The indexing of powder pattern of ternary systems carried out using the program NTREOR indicates monoclinic unit cell. The full pattern decomposition was performed with EXPO 2004 following the Le Bail algorithm and using a split type pseudo-Voigt peak profile function. The structures were solved by global optimization of structural models in direct-space based on a Monte Carlo search using the simulated annealing technique (in parallel tempering mode), as implemented in the program FOX. The initial molecular geometry input in FOX was determined by the MOPAC 2009 program. The atomic coordinates obtained from FOX was used as the starting model for the Rietveld refinement using the program GSAS program package with an EXPGUI interface.[60] The lattice parameters, background coefficients and profile parameters were refined initially followed by the refinement of positional coordinates of all non-hydrogen atoms with soft constraints on bond lengths and bond angles, and planar restraints on the phenyl moieties. Hydrogen atoms were placed in the calculated positions with a common $B_{iso}$ value of 0.06 $Å^2$. In the final stage of refinement, preferred orientation correction was applied using the generalized spherical harmonic model, and the order of spherical harmonics necessary to describe the preferred orientation 16 (texture index=1.1988).

**Vibrational Spectroscopy**

Thermo-Nicolet 6700 Fourier transform infrared spectrophotometer (Thermo Scientific, Waltham, Massachusetts) was used to record IR spectra. IR spectra were recorded on samples dispersed in KBr pellets. Data was analyzed using the Omnic software (Thermo Scientific, Waltham, Massachusetts).

**Solution NMR spectroscopy**

Solution $^{1}H$ NMR spectra of Bumetanide and ternary crystalline materials were recorded on a Bruker Ultra shield 400 spectrometer (Bruker BioSpin, Karlsruhe, Germany). The stoichiometry of ternary systems was established by proton NMR integration.

**Thermal Analysis**

DSC experiments were performed on a Mettler Toledo DSC 822e module and TGA on a Mettler Toledo TGA/SDTA 851e module. Samples were placed in sealed aluminum sample pans for DSC and vented aluminum pans for TGA experiments. A typical sample size is 4-6 mg for DSC and 6-10 mg for TGA. The temperature range was 30-300 °C at 5°C $min^{-1}$ and 10°C $min^{-1}$ for DSC, TGA. Samples were purged with a stream of dry $N_2$ flowing at 80−90 mL $min^{-1}$.

**Dissolution and Solubility Measurements**

The solubility of BUM solid forms was measured by prepared pH-7.4 buffer medium at ambient conditions. First, the absorbance of a known concentration of the salt/salt hydrate/cocrystal was measured at the given $\lambda_{max}$ 328 nm in pH-7.4 buffer on Thermo Scientific Evolution 300 UV-vis spectrometer (Thermo Scientific, Waltham, MA). These absorbance values were plotted against several known concentrations to prepare the concentration vs. intensity calibration curve. From the slope of the calibration curves, molar extinction coefficients for all the BUM solid forms were calculated. Intrinsic dissolution rate (IDR) measurements were carried out on a USP certified Electrolab TDT-08 L Dissolution Tester (Electrolab, Mumbai, MH, India). Dissolution experiments were performed for 480 min in pH 7 buffer at 37 °C. Prior to IDR estimation, standard curves for all the compounds were obtained spectrophotometrically at their respective $\lambda_{max}$. The slope of the plot from the standard curve gave the molar extinction coefficient (ε) by applying the Beer−Lambert's law, which was used to determine the IDR values. For IDR measurements, 400 mg of the solid material of each solid form was taken in the intrinsic attachment and compressed to a 0.5 $cm^2$ pellet using a hydraulic press at a pressure of 2.5 ton/$inch^2$about 4 min. The pellet was compressed to provide a flat surface on one side and the other side was sealed. Then the pellet was dipped into 500 mL of pH 7 buffer water medium at 37 °C with the paddle rotating at 100 rpm. At a specific time, interval, 5 mL of the dissolution medium was withdrawn and replaced by an equal volume of fresh medium to maintain a constant volume. Samples were filtered through 0.2 μm nylon filter and assayed for drug content spectrophotometrically as mention above at $\lambda_{max}$. There was no interference with BUM $\lambda_{max}$ (328 nm) in UV-vis as

salt/cocrystal formers $\lambda_{max}$ at 210−280 nm. The amount of drug dissolved in each time intervals was calculated using the calibration curve.

**Permeability and diffusion study**

The diffusion studies were performed using a diffusion apparatus (Model EMFDC-06, Orchid Scientific, Maharashtra, India) on BUM cocrystals and salts through a dialysis membrane-135 (dialysis membrane-135, average flat width 33.12 mm, average diameter 23.8 mm, capacity approximately 4.45 mL/cm) obtained from HiMedia, India. The treated dialysis membrane was placed in diffusion cells with an effective surface area of 3.14 $cm^2$. Suspensions of the BUM adducts were prepared and placed on the dialysis membrane in donor compartment. The temperature of diffusion medium maintained at 37 °C ± 1 °C throughout the experiment and stirred at 600 rpm and diffuse through the membrane toward the receptor compartment containing 20 mL of phosphate-buffered solution (PBS, pH = 7). The release of the compounds at predetermined intervals were withdrawn (0.5 mL for each intervals) and replaced by equal volume and concentration measured in UV-vis spectrophotometer as such as solubility experiments.

## 2.5 References

1. Schultheiss, N.; Newman, A. Pharmaceutical Cocrystals and Their Physicochemical Properties *Cryst. Growth Des.* **2009**, *9*, 2950–2967.
2. Bolla, G.; and Nangia, A. Pharmaceutical cocrystals: walking the talk. *Chem. Commun*, **2016**, *52*, 8342-8360.
3. Desiraju, G. R. Supramolecular Synthons in Crystal Engineering—A New Organic Synthesis *Angew. Chem., Int. Ed. Engl*. **1995**, *34*, 2311-2327.
4. Aakeroy, C. B.; Fasulo, M.; Schultheiss, N.; Desper, J.; Moore, C. Structural Competition between Hydrogen Bonds and Halogen Bonds *J. Am. Chem. Soc.* **2007**, *129*, 13772−13773.
5. Childs, S. L.; Chyall, L. J.; Dunlap, J. T.; Smolenskaya, V. N.; Stahly, B. C.; Stahly, G. P. Crystal Engineering Approach To Forming Cocrystals of Amine Hydrochlorides with Organic Acids. Molecular Complexes of Fluoxetine Hydrochloride with Benzoic, Succinic, and Fumaric Acids. *J. Am. Chem. Soc.* **2004**, *126*, 13335–13342.
6. Bis, J. A.; Zaworotko, M. J. The 2-Aminopyridinium-carboxylate Supramolecular Heterosynthon: A Robust Motif for Generation of Multiple-Component Crystals. *Cryst. Growth Des.* **2005**, *5*, 1169–1179.

7. Bis, J. A.; Mclaughlin, O. L.; Vishweshwar, P.; Zaworotko, M. J. Supramolecular Heterocatemers and Their Role in Cocrystal Design. *Cryst. Growth Des.* **2006**, *6*, 2648–2650.
8. Bolla, G.; Mittapalli, S.; Nangia, A. Celecoxib cocrystal polymorphs with cyclic amides: synthons of a sulfonamide drug with carboxamide coformers *CrystEngComm,* **2014**, *16*, 24–27.
9. Bolla, G.; Mittapalli, S.; Nangia, A. Modularity and three-dimensional isostructurality of novel synthons in sulfonamide–lactam cocrystals. *IUCrJ* **2015**, *2*, 389–401.
10. Bolla, G.; Nangia, A. Multicomponent ternary cocrystals of the sulfonamide group with pyridine-amides and lactams. *Chem. Commun.*, **2015**, *51*, 15578—15581.
11. Bolla, G.; Nangia, A.; Binary and ternary cocrystals of sulfa drug acetazolamide with pyridine carboxamides and cyclic amides. *IUCrJ* **2016**. *3*, 152–160.
12. Ward, A.; Heel, R. C. Bumetanide. A review of its pharmacodynamic and pharmacokinetic properties and therapeutic use. *Drugs* **1984**, *28*, 426–464.
13. Nielsen, H. W.; Bechgaard, E.; Twile, B.; Didriksen. E.; Almtorp, G. T. Intranasal administration of different liquid formulations of bumetanide to rabbits. *Pharm. Dev. Technol*. **2001**, *6*, 145–149.
14. Asbury, M. J.; Gatenby, P. B. B.; O'Sullivan, S.; Bourke, E. Bumetanide: Potent New "Loop" Diuretic. *Br. Med. J*. **1972**, *1*, 211− 213.
15. Goud, N. R.; Gangavaram, S.; Suresh, K.; Pal, S.; Manjunatha, S.G.; Nambiar, S.; Nangia, A. Novel furosemide cocrystals and selection of high solubility drug forms. *J Pharm. Sci.* **2012**, *101*, 664–680.
16. Bolla, G.; Nangia, A. Pharmaceutical cocrystals: walking the talk. *Chem. Commun.*, **2016**, ***52***, 8342−8360.
17. Karimi-Jafari, M.; Padrela, L.; Walker, G. M.; Croker, D. M. Creating Cocrystals: A Review of Pharmaceutical Cocrystal Preparation Routes and Applications. *Cryst. Growth Des.*, **2018**, *18*, 6370–6387.
18. Duggirala, N. K.; Perry, M. L.; Almarsson, O.; Zaworotko, M. J. Pharmaceutical cocrystals: along the path to improved medicines. *Chem. Commun.* **2016**, *52*, 640−655.
19. Steed, J. W. The role of co-crystals in pharmaceutical design. *Trends in Pharm. Sci.* **2013,** *34*, 185−193.

20. Kavanagh. O. N.; Croker. D. M.; Walker. G. M.; Zaworotko, M. J. Pharmaceutical cocrystals: from serendipity to design to application. *Drug Disc. Today* **2019**, *24*, 796−804.
21. Childs, S. L.; Stahly, G. P.; A. Park. The Salt−Cocrystal Continuum: The Influence of Crystal Structure on Ionization State. *Mol. Pharm*aceutics **2007**, *4*, 323–338.
22. Sanphui, P.; Bolla,G.; Nangia,A. High Solubility Piperazine Salts of the Nonsteroidal Anti-Inflammatory Drug (NSAID) Meclofenamic Acid. *Cryst. Growth Des.* **2012**, *12*, 2023–2036.
23. Babu, N. J.; Reddy, L. S.; Nangia, A. Amide−*N*-Oxide Heterosynthon and Amide Dimer Homosynthon in Cocrystals of Carboxamide Drugs and Pyridine *N*-Oxides. *Mol. Pharmaceutics* **2007**, *4*, 417–434
24. Goud, N. R.; Babu, N. J.; Nangia, A.Sulfonamide−Pyridine-N-oxide Cocrystals. *Cryst. Growth Des.* **2011**, *11*, 1930–1939.
25. Babu, N. J.; Cherukuvada, S.; Thakuria, R.; Nangia, A. Conformational and Synthon Polymorphism in Furosemide (Lasix). *Cryst. Growth Des.* **2010**, *10*, 1979–1989.
26. Cruz-Cabeza, A. J.; Bernstein, J. Conformational Polymorphism. *Chem. Rev.* **2014**, *114*, 2170–2191.
27. Allu, S.; Bolla, G.; Tothadi, S.; Nangia, A. Supramolecular Synthons in Bumetanide Cocrystals and Ternary Products. *Cryst. Growth Des.* **2017**, *17*, 4225–4236.
28. Ong, W.; Cheung, E. Y.; Schultz, K. A.; Smith, C.; Bourassa, J.; Hickey, M. B. Sodium and potassium salts of bumetanide trihydrate: Impact of counterion on structure, aqueous solubility and dehydration kinetics. *CrystEngComm*, **2012**, ***14***, 2428–2434.
29. Bruni, G.; Maietta, M.; Berbenni, V.; Mustarelli, P.; Ferrara, C.; Freccero, M.; Grande, V.; Maggi, L.; Milanese, C.; Girella, A.; Marini, A. Mechanochemical Synthesis of Bumetanide–4-Aminobenzoic Acid Molecular Cocrystals: A Facile and Green Approach to Drug Optimization. *J. Phys. Chem. B* **2014**, *118*, 9180–9190.
30. The Cambridge Structural Database version 5.40 November **2018** (update 3 Aug 2019). ConQuest 2.03; Cambridge Crystallographic Data Centre: Cambridge, U.K.

31. Fabian, L. Cambridge Structural Database Analysis of Molecular Complementarity in Cocrystals. *Cryst. Growth Des.* **2009**, *9*, 1436-1443
32. Allen, F. H. The Cambridge Structural Database: a quarter of a million crystal structures and rising. *Acta Cryst.* **2002**. *B58*, 380-388
33. Allen, F. H.; and Motherwell, W. D. S. Applications of the Cambridge Structural Database in organic chemistry and crystal chemistry. *Acta Cryst.* **2002**. *B58*, 407-422.
34. Friscic, T.; Jones, W. Recent Advances in Understanding the Mechanism of Cocrystal Formation via Grinding. *Cryst. Growth Des.* **2009**, *9*, 1621–1637.
35. Friscic, T.; Fabian, L.; Burley, J. C.; Jones, W.; Motherwell, W. D. S. Exploring cocrystal–cocrystal reactivity *via* liquid-assisted grinding: the assembling of racemic and dismantling of enantiomeric cocrystals. *Chem. Commun.* **2006**, 5009−5011.
36. Etter, M. C. A new role for hydrogen-bond acceptors in influencing packing patterns of carboxylic acids and amides. *J. Am. Chem. Soc.* **1982,** *104*, 1095–1096.
37. Etter, M. C.; Macdonald, J. C.; Bernstein, J. Graph-set analysis of hydrogen-bond patterns in organic crystals. *Acta Crystallogr., Sect. B.* **1990**, *46*, 256–262.
38. https://www.fda.gov/food/food-ingredients-packaging/generally-recognized-safe-gras, accessed 12/05/2019.
39. Etter, M. C.; Frankenbach, G. M. Hydrogen-bond directed cocrystallization as a tool for designing acentric organic solids. *Chem. Mater.* **1989**, *1*, 10–12.
40. Sanphui, P.; Bolla, G.; Nangia, A.; Chernyshev, V. Acemetacin cocrystals and salts: structure solution from powder X-ray data and form selection of the piperazine salt. *IUCrJ* **2014**. 1, 136–150.
41. Sarma, B.; Nath, N. K.; Bhogala, B. R.; Nangia, A Synthon Competition and Cooperation in Molecular Salts of Hydroxybenzoic Acids and Aminopyridines. *Cryst. Growth Des.* **2009**, *9*. 1546–1557.
42. Gelbrich, T.; Threlfall, T. L.; Hursthouse, M. B. XPac dissimilarity parameters as quantitative descriptors of isostructurality: the case of fourteen 4,59-substituted benzenesulfonamido-2-pyridines obtained by substituent interchange involving CF3/I/Br/Cl/F/Me/H. *CrystEngComm*, **2012**, *14*, 5454–5464.
43. Nangia, A. Conformational polymorphism in organic crystals. *Acc. Chem. Res.* **2008,** *41*, 595−604

44. Banik, M.; Gopi, S. P.; Ganguly, S.; Desiraju, G. R. Hydrogen Bond Synthons in the Interplay of Solubility and Membrane Permeability/Diffusion in Variable Stoichiometry Drug Cocrystals. *Cryst. Growth Des.* **2016**, 16, 5418−5428.

45. Sanphui, P.; Devi, V. K.; Clara, D.; Malviya, N.; Ganguly, S.; Desiraju, G. R. Cocrystals of Hydrochlorothiazide: Solubility and Diffusion/Permeability Enhancements through Drug−Coformer Interactions. *Mol. Pharmaceutics* **2015**, *12*, 1615−1622.

46. Wang, J. R.; Ye, C.; Mei, X. Structural and physicochemical aspects of hydrochlorothiazide co-crystals. *CrystEngComm,* **2014**, *16*, 6996–7003.

47. Dai, X.; Li, S.; Chen, J.; Lu, T. Improving the Membrane Permeability of 5-Fluorouracil via Cocrystallization. *Cryst. Growth Des*. **2016**, *16*, 4430−4438.

48. SAINT-Plus, Ver. 6.45; Bruker AXS: Madison, WI, **2003**.

49. Sheldrick, G. M. *SADABS, Program for Empirical Absorption Correction of Area Detector Data*; University of Göttingen: Göttingen, Germany, **1997**.

50. Sheldrick, G. M. *SHELX-97, Program for the Solution and Refinement of Crystal Structures*; University of Göttingen: Göttingen, Germany, **1997**.

51. *CrysAlis CCD and CrysAlis RED*, versions 1.171.33.55; Oxford Diffraction: Oxford, **2008.**

*52.* Dolomanov O. V.; Blake A. J; Champness N. R.; Schroder, M. "OLEX: new software for visualization and analysis of extended crystal structures". *J. Appl. Cryst***. 2003**, *36*, 1283–1284.

*53.* Spek, A. L. PLATON: A Multipurpose Crystallographic Tool; Utrecht University: Utrecht, The Netherlands, ***2002***.

*54.* PLATON, A Multipurpose Crystallographic Tool; Spek, A. L., Ed.;Utrecht University: Utrecht, The Netherlands, ***2002***. *Spek, A. L. J. Appl. Crystallogr.***2003**, *36*, 7−13.

55. Barbour, L. J.X-Seed, Graphical Interface to SHELX-97 and POV-Ray; University of Missouri–Columbia: Columbus, MO, **1999**.

56. Powder Cell, a program for structure visualization, powder pattern calculation and profile fitting. http://www.ccp14.ac.uk/tutorial/powdcell/.

57. Harris, K. D. M.; Tremayne, M.; Kariuki, B. M. Contemporary Advances in the Use of Powder X-Ray Diffraction for Structure Determination. *Angew. Chem. Int. Ed*. **2001**, *40*, 1626–1651.

58. Harris, K. D. M.; and Cheung, E. Y. How to determine structures when single crystals cannot be grown: opportunities for structure determination of molecular materials using powder diffraction data. *Chem. Soc. Rev*., **2004**, *33*, 526–538.

59. Sanphui, P.; Bolla, G.; Nangia, A.; Chernyshev, V. Acemetacin cocrystals and salts: structure solution from powder X-ray data and form selection of the piperazine salt. *IUCrJ* **2014**. 1, 136–150.

60. Larson, A. C.; Von Dreele, R. B. General Structure Analysis System (GSAS). 2000, Los Alamos National laboratory Report, LAUR 86-748.

## *CHAPTER THREE*

# Role of Hydrogen Bonding in Cocrystal and Coamorphous Solids: Indapamide as a Case Study

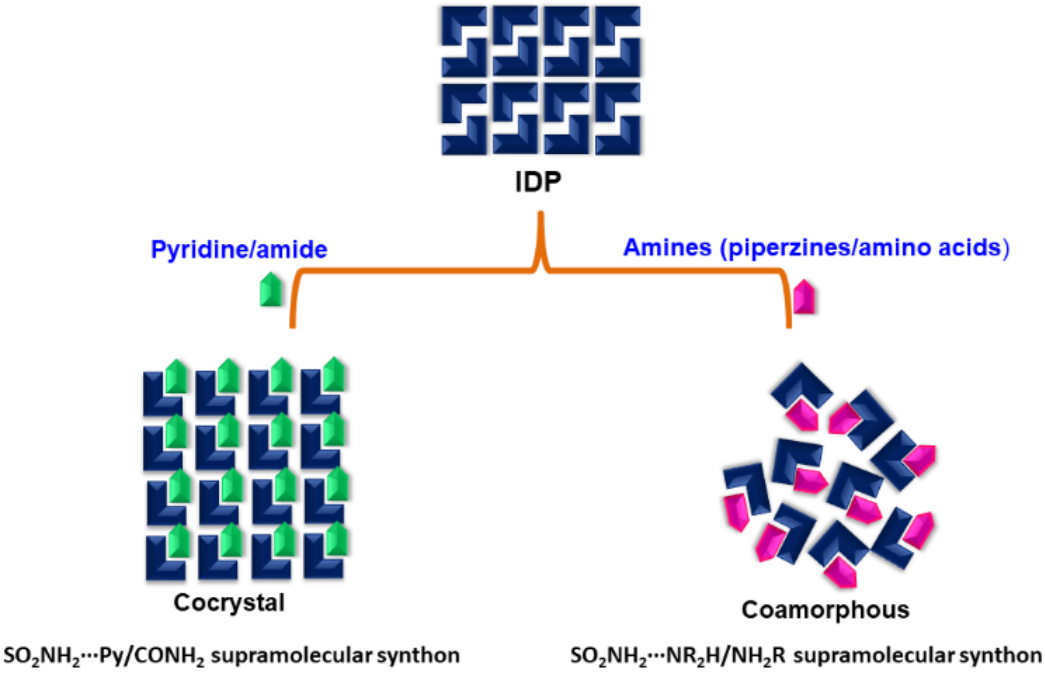


***Indapamide (IDP) is a BCS class II drug with low solubility and a potent diuretic which is mainly used as a treatment for hypertension. The stronger sulfonamide-pyridine ($SO_2NH_2$···N-Py) and sulfonamide-carboxamide ($SO_2NH_2$···O=C-NRH) hydrogen bonding directs the formation of cocrystals while the weaker sulfonamide-amine ($SO_2NH_2$···$NR_2H$) hydrogen bond results in coamorphous products. IDP-PIP and IDP-ARG coamorphous solids exhibit remarkable stability under accelerated conditions.***

## 3.1 Introduction

The molecular packing in crystal structures controls the physicochemical properties, i.e. solubility and dissolution, physical and chemical stability, and photochemical reactivity.[1-3] Crystal engineering[4] deals with *the understanding of intermolecular interactions in the context of crystal packing and the utilization of such understanding in the design of new solids with desired physical and chemical properties*. Multiple strategies have been reported for pharmaceuticals to alter their pharmacokinetic behavior.[5-7] The inverse of crystal engineering, i.e. identifying features that prevent crystallization and lead to quasi-crystalline or amorphous products (those lacking in long-range periodicity and ordered arrangement of the constituent molecules)[8] is far less investigated.[9-12] Cherukuvada and Nangia[12] recently postulated that in multicomponent systems, "very strong adhesive interactions give a cocrystal product irrespective of size/shape/symmetry factors. When the cohesive interactions are strong but auxiliary interactions are weak to nil, then the result is a solid solution (shape similarity) or a eutectic (mismatched shape)." If a eutectic microstructure is considered as 'a conglomerate of solid solutions'[12] then extending the limits of weak interactions between the bimolecular components gives rise to coamorphous products. Investigations on structure-property relations have directed the synthesis of molecular amorphous materials.[13,14] In general, molecules with rigid structure, non-planner shape, and lack of hydrogen bonding functional groups exhibit packing or organization difficulties in the crystal structure leading to amorphous and glassy states.[15] Depending on the rigidity and close packing difficulty as well as the hydrogen bonding groups, one may obtain an amorphous form (e.g. salicyl-salicylic acid).[16] Drug molecules and active pharmaceutical ingredients (APIs) consist of hydrogen bonding functionalities such as COOH, $CONH_2$, OH, $NH_2$, $SONH_2$,and are generally flexible which promote crystallization directed by supramolecular synthons.[17] Thus a majority of the APIs exist in crystalline form. However, amorphous forms of APIs are desirable because they exhibit higher solubility due to high free energy and these have been produced by various methods such as melt-quench cooling/hot melt extrusion, lyophilization and spray drying.[18,19] Amorphous formulations signify a promising approach to overcome the limited bioavailability and poor solubility of crystalline drugs. However, there is an inherent risk that amorphous forms will crystallize during the shelf-life and storage of the drug, thereby limiting the

benefits of such high free energy forms. Solid dispersions consist of high glass transition ($T_g$) polymeric excipients[20,21] which increase the $T_g$ and inhibit crystallization of amorphous drugs. Other methods such as polymer heteronucleation are also used to extend crystal nucleation in aqueous medium.[22] However, these formulations can still have stability issues under accelerated ICH conditions (International Conference on Harmonization). Multi-component systems such as cocrystals have gained wide coverage to modify the mechanical and physicochemical properties of APIs.[23-27] More recently coamorphous drugs have been developed to overcome the solubility challenges for oral delivery. A *coamorphous phase is a multicomponent single phase amorphous solid system which lacks periodic arrangement in the lattice and is associated by weak and discrete intermolecular interactions between the components.*[28] Coamorphous systems have been reported to have improved drug stability along with the excellent solubility and bioavailability.[29,30] Some of the reported coamorphous systems were obtained serendipitously or by trial and error.[31,32]

Indapamide (chloro-4-N-(methyl-2-indolinyl- 1-)sulfamyl-3-benzamide namely Indapamide (IDP) is a sulfonamide diuretic drug utilized in the treatment of hypertension. It's mechanism of drug action remains similar and having a slightly different chemical structure than thiazides (e.g., hydrochlorothiazide). Apart from the diuretic action IDP exerts also spasmolytic effects on blood vessels, consequently reducing the blood pressure and increases the urine volume by increasing the renal excretion of sodium, chlorine, potassium and magnesium ions. During the past decade improvement of solubility of poorly water-soluble medicines has become one of the most important aspects of pharmaceutical research. It should be noted that an amorphous form can also improve process ability of drugs. Herein we report new binary crystal phases of cocrystals and amorphous products of IDP by exploiting the supramolecular synthon design approach The cocrystal of IDP with selected pyridine derivatives such as 4,4'-bipyridine (DPI), 2,2'-bipyridine (BIP), trans-1,2-Bis(4-pyridyl) ethylene (DPE), phenazine (PHE), 6-methyl-2-pyridone (MeHP) and amorphous products with selected piperazine derivatives and amino acids such as piperazine (PIP), N-Methyl piperazine (MPIP), N-ethyl piperazine (EPIP), N-Boc-piperazine (BPIP) and arginine (ARG), lysine (LYS). Cocrystals and coamorphus forms of IDP have been identified and characterized by X-ray powder diffraction (XRD), differential scanning calorimetry (DSC) and FT-IR were used. Finally, the apparent solubility dissolution and permeability

studies of coamorphous IDP samples were performed in aqueous media. We present in this report a systematic gradation in supramolecular synthons to result in a cocrystal or coamorphous product of indapamide as the hydrogen bonds between the drug and the coformer become weaker.

## 3.2 Results and Discussion

Indapamide (IDP) is a classic diuretic drug used to treat hypertension and decompensated heart failure. It exists as non-stoichiometric 0.35 hydrate.[33] there is no report on multicomponent crystal forms of indapamide. In background of our interest with polymorphs and cocrystals of sulfonamide drugs such as Lasix[34] as well as heterosynthons of the sulfonamide functional group,[35] we conducted a solid form screen of indapamide with amide, pyridine and amine coformers. The stronger sulfonamide-pyridine (SO2NH$_2$···Py) and sulfonamide-carboxamide ($SO_2NH_2$···CONRH, Figure 3.2a and 3.2b) synthons resulted in cocrystals while the weaker sulfonamide-amine ($SO_2NH_2$···$NR_2H$) hydrogen bonding (Figure 3.2c) gave coamorphous products (Figure 3.1).

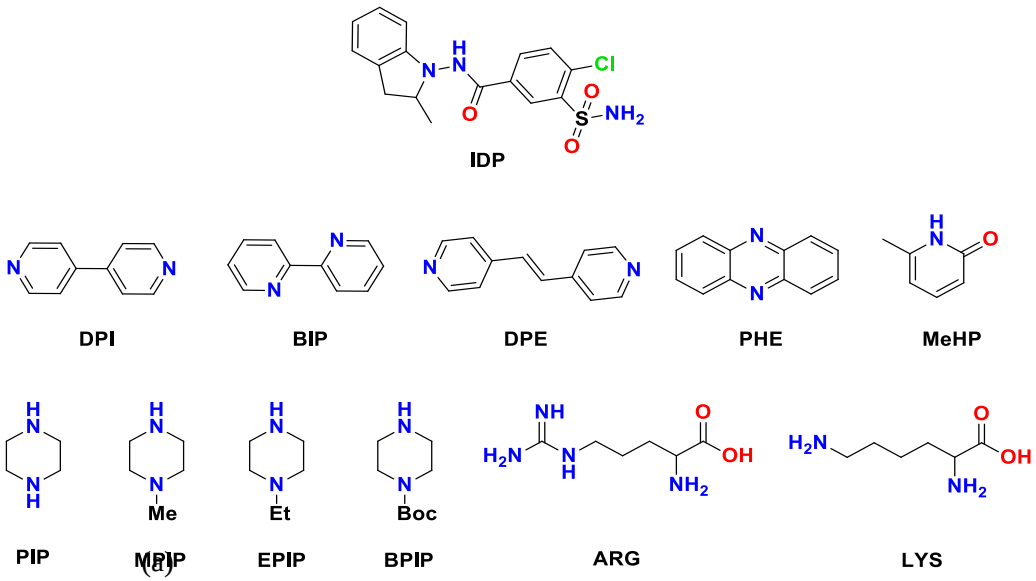


(a)

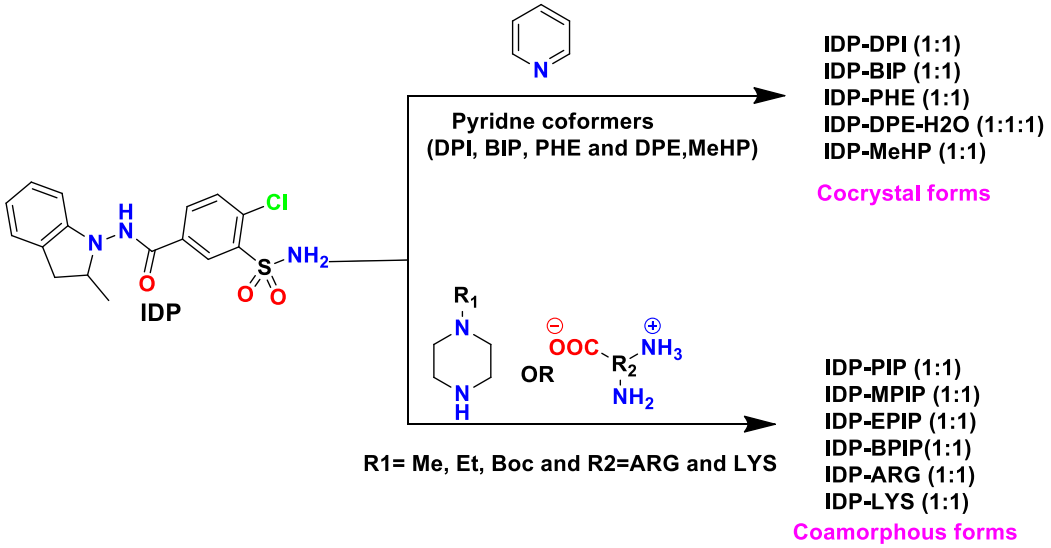


(b)

**Figure 3.1: (a)** Chemical structures of IDP and coformers **(b)** Cocrystal and coamorphous products of IDP with pyridine and amine coformers

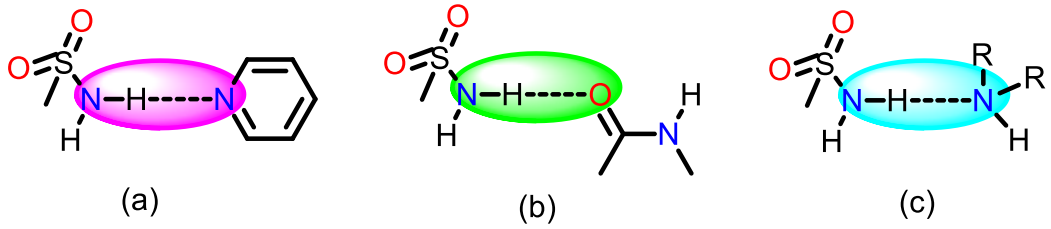


**Figure 3.2:** (a) Sulfonamide···pyridine (N–H···N) and (b) sulfonamide···amide (N–H···O) heterosynthon in cocrystal structures. (c) Sulfonamide···amine (N–H···N) hydrogen bond in coamorphous forms.

## 3.2.1 Crystal Structure Description

**IDP-DPI (1:1) Cocrystal:** Crystallization of IDP and DPI in a 1:1 ratio from EtOH and $CHCl_3$ mixture this is crystallized in the monoclinic space group $P2_1/n$ with Z=4. The asymmetric unit contains one IDP molecule and one DPI molecule crystallized in the crystal lattice these molecules linked through the primary $NH_{sulfonamide}$ and $N_{pyridine}$ N–H···N (N3–H3A···N4 2.19 Å, 151°) synthon followed by $R_4^4(22)$ ring motif (Figure 3.3a) and Indapamide molecule itself N–H···O (N2–H2A···O3 2.00 Å, 161°) hydrogen bond through 1-D chain with bipyridine (Figure 3.3b).

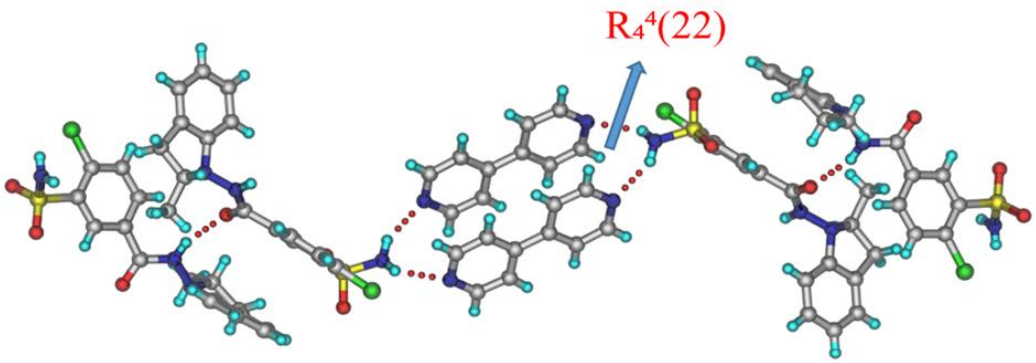


**(a)**

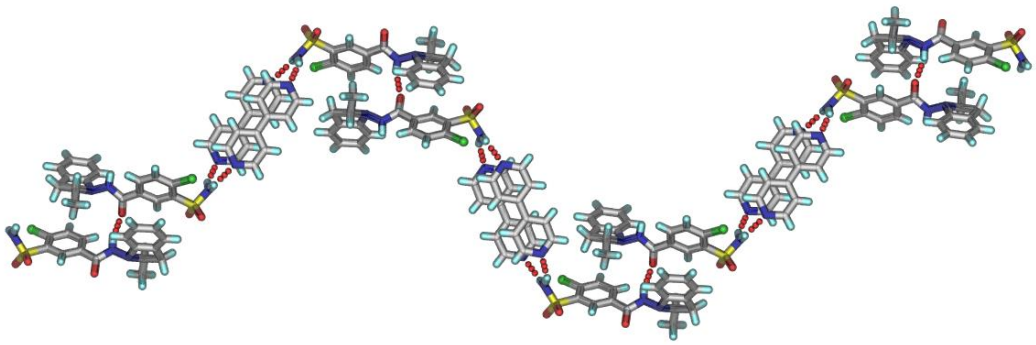

**(b)**

**Figure 3.3:** (a) IDP molecules are connected through Primary sulfonamide with 4,4'-bipyridine(DIP) $R_4^4(22)$ ring motif. (b) 1-D chain of IDP molecules in IDP-DPI.

**IDP- BIP (1:1) Cocrystal:** crystallization of IDP and BIP in a 1:1 ratio from EtOH and EtOAc mixture this is crystallized in the monoclinic space group $P2_1/c$ with Z=4. the asymmetric unit consists of a molecule of IDP and a molecule of BIP in this crystal lattice major hydrogen bonding interactions involved the primary $NH_{sulfonamide}$ and $N_{pyridine}$ N−H···N (N3−H3A···N4 2.09 Å, 158°) synthon followed by $R_4^4(14)$ ring motif (Figure 3.4) and Indapamide molecule itself forms N−H···O (N2−H2A···O3 1.98 Å, 172°) hydrogen bond.

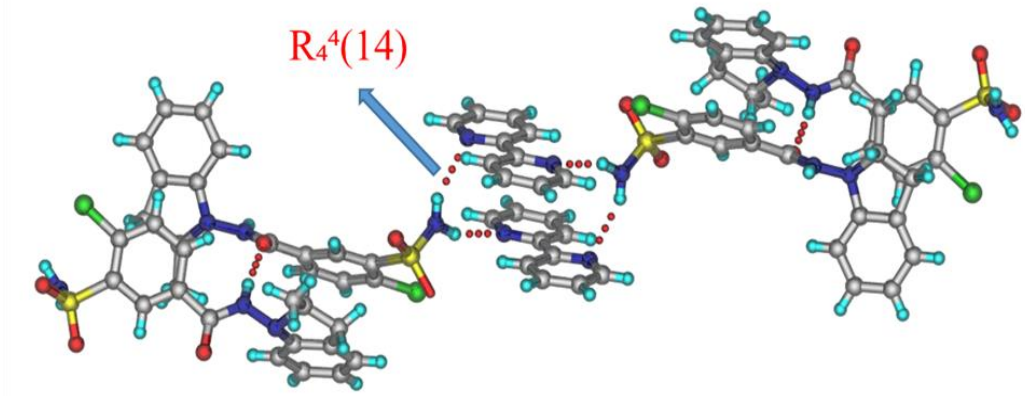


**Figure 3.4:** IDP molecules are connected through Primary sulfonamide with 2,2'-bipyridine(BIP) forms $R_4^4(14)$ ring motif.

**IDP- DPE-$H_2O$ (1:1:1)) Cocrystal Hydrate:** crystallaiztion of IDP and DPE in a 1:1 ratio from EtOH and EtOAc mixture this is crystallized in the Triclinic space group *P*-1with Z=4. The asymmetric unit consists of two IDP, two DPE and two water molecules in the single crystal structure. two IDP molecules and DPE molecules are packed in a sandwich fashion, one sandwich unit interact with another via N−H···N (N3−H3A···N9 2.09 Å, 172°) synthon followed by $R_6^6(34)$ ring motif and interestingly water molecule play important role in building the H-bonding network through N−H···O, O−H···O (N3−H3B···O7 2.02 Å, 165°; O8−H8A···O2 2.25 Å, 173°) hydrogen bond three distinctive H-bonding interactions are associated with each water molecule. One water molecule is bridged with two IDP and one DPE molecules (Figure 3.5).

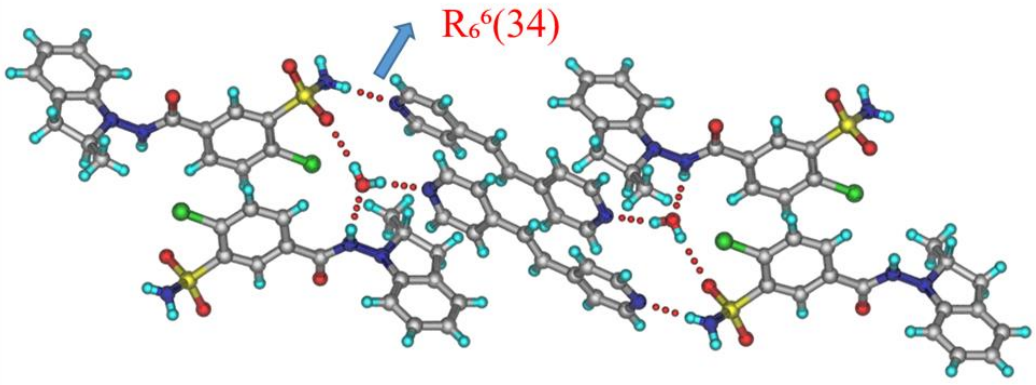


**Figure 3.5:** IDP molecules are connected through Primary sulfonamide with trans-1,2-Bis(4-pyridyl) ethylene(DPE) $R_4^4(14)$ ring motif.

**IDP- PHE (1:1) Cocrystal:** Crystallaiztion of IDP and PHE in a 1:1 ratio from EtOH and EtOAc mixture this is crystallized in the monoclinic space group $P2_1/c$ with Z=4.the asymmetric unit consists of one molecule of IDP and one molecule PHE, in the crystal packing of cocrystal showing major H-bonding interaction is N−H···N and N−H···O (N3−H3A···N5 2.17 Å, 162°; N1−H1A···O1 2.03 Å, 165°) synthon (Figure 3.6).

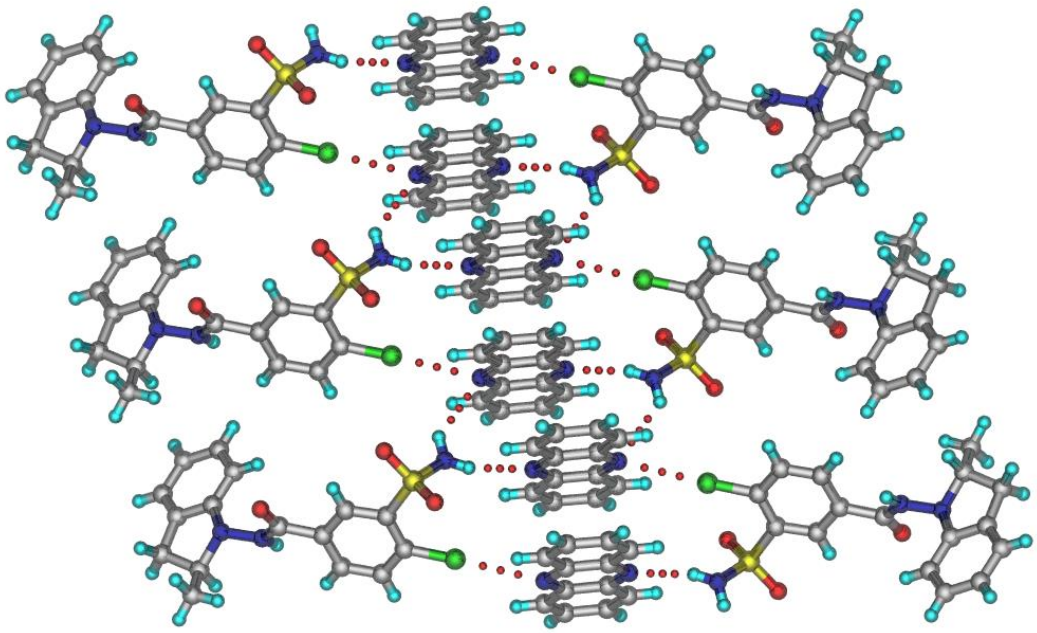

**Figure 3.6:** IDP molecules are connected through Primary sulfonamide with phenazine(PHE) shows N−H···N and N−H···O hydrogen bond.

**IDP-MeHP (1:1) Cocrystal:** crystallaiztion of IDP and MeHP in a 1:1 ratio from EtOH and EtOAc mixture this is crystallized in the monoclinic space group $P2_1/c$ with Z=4. There are one IDP molecule and one methyl pyridone molecule in the asymmetric unit, in the crystal packing shows pyridone N−H···O (N4−H4A···O4 1.95 Å, 173° homodimer $R_2^2(8)$ ring motif followed through pyridone oxygen of MeHP participates in N−H···O (N3−H3A···O4 2.14 Å, 169°; N3−H3B···O4 2.11 Å, 164°) H-bonding with two primary sulfonamide functional groups leads to form tetrameric $R_4^2(8)$ ring motif (Figure 3.7). Crystallographic parameters and hydrogen bond distances are listed in Table 3.1- 3.2.

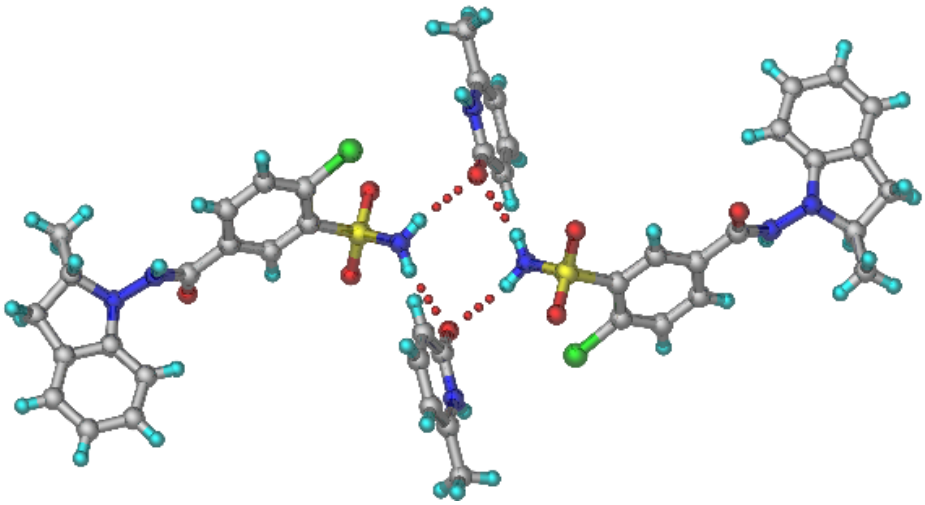

**(a)**

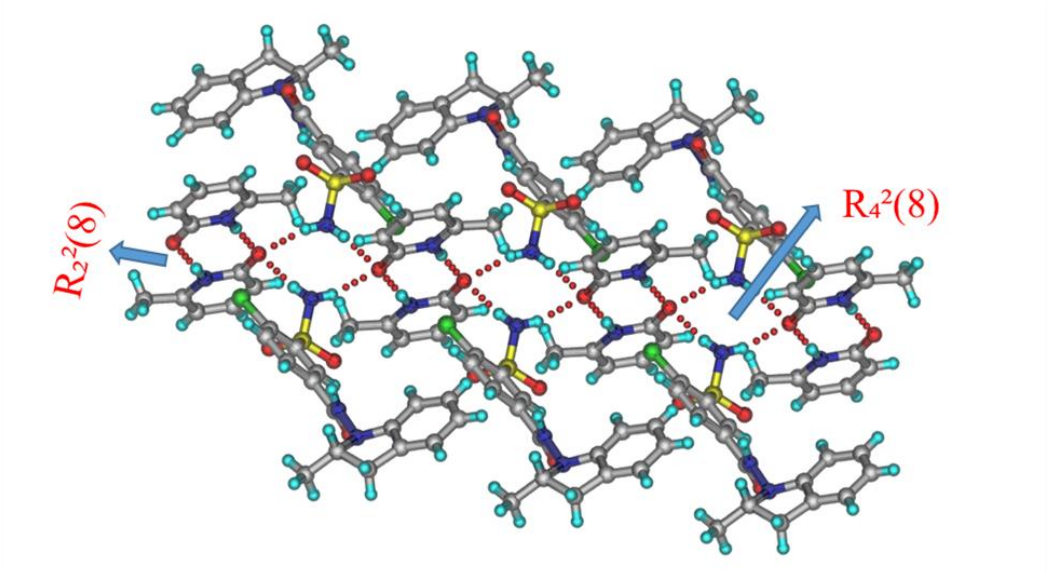


**(b)**

**Figure 3.7:** (a) IDP molecules are connected through Primary sulfonamide with methyl pyridone (MeHP) $R_4^4(14)$ tetramer ring motif.(b) MeHP molecules are shows homodimer $R_2^2(8)$ ring motif followed by inversion center through primary sulfonamide $R_4^4(14)$ tetramer ring motif.

**Table 3.1:** Crystallographic parameters of Indapamide cocrystals.

| | **IDP-DPI (1:1)** | **IDP-BIP (1:1)** | **IDP-DPE-H2O (1:1:1)** | **IDP-PHE (1:1)** | **IDP-MeHP (1:1)** |
|---|---|---|---|---|---|

| **Empirical Formula** | $C_{16}H_{16}ClN_3O_3S \cdot C_{10}H_8N_2$ | $C_{16}H_{16}ClN_3O_3S \cdot C_{10}H_8N_2$ | $C_{16}H_{16}ClN_3O_3S \cdot C_{12}H_{10}N_2 \cdot H_2O$ | $C_{16}H_{16}ClN_3O_3S \cdot C_{12}H_8N_2$ | $C_{16}H_{16}ClN_3O_3S \cdot C_6H_7NO$ |
|---|---|---|---|---|---|
| **Formula weight** | 522.01 | 522.01 | 566.06 | 546.03 | 474.95 |
| **Crystal System** | Monoclinic | Monoclinic | Triclinic | Monoclinic | Monoclinic |
| **Space Group** | $P2_1/n$ | $P2_1/c$ | $P$-1 | $P2_1/c$ | $P2_1/c$ |
| **T (K)** | 298(2) | 298(2) | 298(2) | 298(2) | 298(2) |
| ***a* (Å)** | 7.2851 (14) | 7.3151 (2) | 12.2238 (2) | 7.1759 (3) | 7.765 (7) |
| ***b* (Å)** | 9.0281 (17) | 8.9370 (3) | 14.8267 (3) | 9.4074 (4) | 8.741 (8) |
| ***c* (Å)** | 38.510 (7) | 38.9526 (12) | 16.2328 (3) | 39.0523 (17) | 34.52 (3) |
| ***α* (°)** | 90 | 90 | 93.228 (1) | 90 | 90 |
| ***β* (°)** | 95.230 (3) | 93.702 (2) | 107.264 (1) | 93.389 (2) | 93.96 (4) |
| ***γ* (°)** | 90 | 90 | 90.122 (1) | 90 | 101.399(6) |
| ***V* (Å$^3$)** | 2522.3 (8) | 2541.21 (14) | 2804.46 (9) | 2631.68 (19) | 90 |
| $D_{calc}$**(g cm$^{-3}$)** | 1.375 | 1.364 | 1.341 | 1.378 | 1.349 |
| **Z** | 4 | 4 | 4 | 4 | 4 |
| ***F*(000)** | 1088 | 1088 | 1184 | 1136 | 992 |
| **$\Delta\rho_{max}$, $\Delta\rho_{min}$ (e Å$^{-3}$)** | 0.26, -0.23 | 0.23, -0.29 | 0.79, -0.39 | 0.30, -0.47 | 0.45, -0.52 |
| **h range** | -8 → 8 | -8 → 8 | -16 → 16 | -9 → 9 | -9 → 9 |
| **k range** | -10 → 10 | -10 → 10 | -19 → 19 | -12 → 12 | -10 → 10 |
| **l range** | -45 → 45 | -47 → 47 | -21 → 21 | -50 → 52 | -43 → 43 |
| **measured reflections** | 23382 | 47789 | 76699 | 25417 | 32668 |
| **independent reflections** | 4477 | 4804 | 14012 | 6467 | 4763 |
| **$R_{int}$** | 0.030 | 0.160 | 0.060 | 0.027 | 0.045 |
| ***R*$_1$ [*I* >2σ(*I*)]** | 0.042 | 0.080 | 0.072 | 0.053 | 0.061 |
| ***w*R$_2$ (all)** | 0.111 | 0.154 | 0.179 | 0.128 | 0.144 |
| **Goodness of fit** | 1.09 | 1.09 | 1.10 | 1.14 | 1.10 |
| **X-ray diffractometer** | BRUKER SMART | BRUKER APEX | BRUKER APEX | BRUKER APEX | BRUKER APEX |
| CCDC No. | 1849062 | 1849065 | 1849066 | 1849063 | 1849064 |

**Table 3.2:** Hydrogen-bonds geometry in IDP cocrystals (neutron-normalized).

| D−H···A | D···A (Å) | H···A (Å) | D−H···A (°) | symmetry code |
|---|---|---|---|---|
| **IDP-DPI(1:1)** | | | | |
| N2−H2A···O3 | 2.815(2) | 2.00 | 161 | 3/2-x,-1/2+y,1/2-z |
| N3−H3A···N4 | 2.973(3) | 2.19 | 151 | 3/2-x,-3/2+y,1/2-z |
| N3−H3B···N5 | 3.037(3) | 2.33 | 149 | 1/2+x,1/2-y,1/2+z |
| C13−H13···O3 | 3.322(4) | 2.46 | 155 | 5/2-x,-1/2+y,1/2-z |
| C23−H23···O1 | 3.405(3) | 2.51 | 162 | -1/2+x,3/2-y,-1/2+z |
| **IDP-BIP (1:1)** | | | | |
| N2−H2A···O3 | 2.798(4) | 1.98 | 172 | 1-x,-1/2+y,1/2-z |
| N3−H3A···N4 | 2.973(6) | 2.09 | 158 | 1-x,1-y,-z |
| N3−H3B···N5 | 3.120(6) | 2.36 | 147 | x,-1+y,z |
| **IDP-DPE-H2O (1:1:1)** | | | | |
| C13−H13···O3 | 3.384(6) | 2.49 | 160 | 2-x,-1/2+y,1/2-z |
| N2−H2A···O8 | 2.9938 | 2.16 | 163 | 1-x,1-y,1-z |
| N3−H3A···N9 | 2.8658 | 2.09 | 172 | x,y,-1+z |
| N3−H3B···O7 | 2.8835 | 2.02 | 165 | 1-x,1-y,-z |
| N5−H5A···O3 | 2.9989 | 2.24 | 162 | 1-x,1-y,-z |
| N6−H6A···N8 | 2.9957 | 2.23 | 161 | Intramolecular |
| O7−H7A···N7 | 2.8854 | 2.08 | 165 | 1-x,1-y,1-z |
| O7−H7B···O6 | 2.8203 | 2.06 | 168 | -1+x,y,z |
| O8−H8A···O2 | 2.9876 | 2.25 | 173 | x,y,1+z |
| O8−H8B···N10 | 2.8355 | 2.08 | 165 | 1-x,-y,1-z |
| C6−H6···O8 | 3.4078 | 2.50 | 167 | 1-x,1-y,1-z |
| C39−H39···O1 | 3.3674 | 2.50 | 155 | 1-x,1-y,-z |
| C46−H46···O5 | 3.5189 | 2.60 | 172 | 2-x,-y,1-z |
| C51−H51···O5 | 3.3837 | 2.54 | 151 | 2-x,-y,1-z |
| **IDP-PHE (1:1)** | | | | |
| N1−H1A···O1 | 2.864(2) | 2.03 | 165 | 1-x,-1/2+y,1/2-z |
| N3−H3A···N5 | 2.969(3) | 2.17 | 162 | 1-x,1-y,-z |
| N3−H3B···N4 | 3.166(3) | 2.54 | 132 | x,-1+y,z |
| C13−H13···O1 | 3.394(3) | 2.55 | 151 | 2-x,-1/2+y,1/2-z |
| C20−H20···O3 | 3.174(3) | 2.44 | 136 | Intramolecular |
| **IDP-MeHP(1:1)** | | | | |
| N2−H2A···O3 | 2.825(4) | 1.99 | 152 | 1-x,-1/2+y,1/2-z |
| N3−H3A···O4 | 2.973(4) | 2.14 | 169 | 1-x,1-y,-z |
| N3−H3B···O4 | 2.904(4) | 2.11 | 164 | x,-1+y,z |
| N4−H4A···O4 | 2.814(4) | 1.95 | 173 | -x,2-y,-z |
| C20−H20···O1 | 3.365(5) | 2.52 | 151 | -1+x,y,z |
| C22−H22A···O1 | 3.484(5) | 2.59 | 155 | -1+x,y,z |

## 3.2.2 Conformational Analysis

**Conformation:** IDP molecule of multicomponent cocrystals with their molecular conformation and torsion angles are reported in this study. The cocrystal of IDP-DPE-$H_2O$ shows two different IDP molecules in asymmetric unit in that both IDP molecules have different torsion angles and different confirmations. The IDP molecule shows mainly difference in phenyl ring and sulfonamide group conformational orientation. cocrystal structures with IDP sulfonamide-pyridine (N-H···N), sulfonamide-amide (N-H···O) as well as IDP with hydrate show N-H···O strong synthons, these observations suggest that though the hydrogen bonding the flexible molecules change conformations and adjust to the final 3D crystal packing. The torsion angles are shown in Figure 3.8.

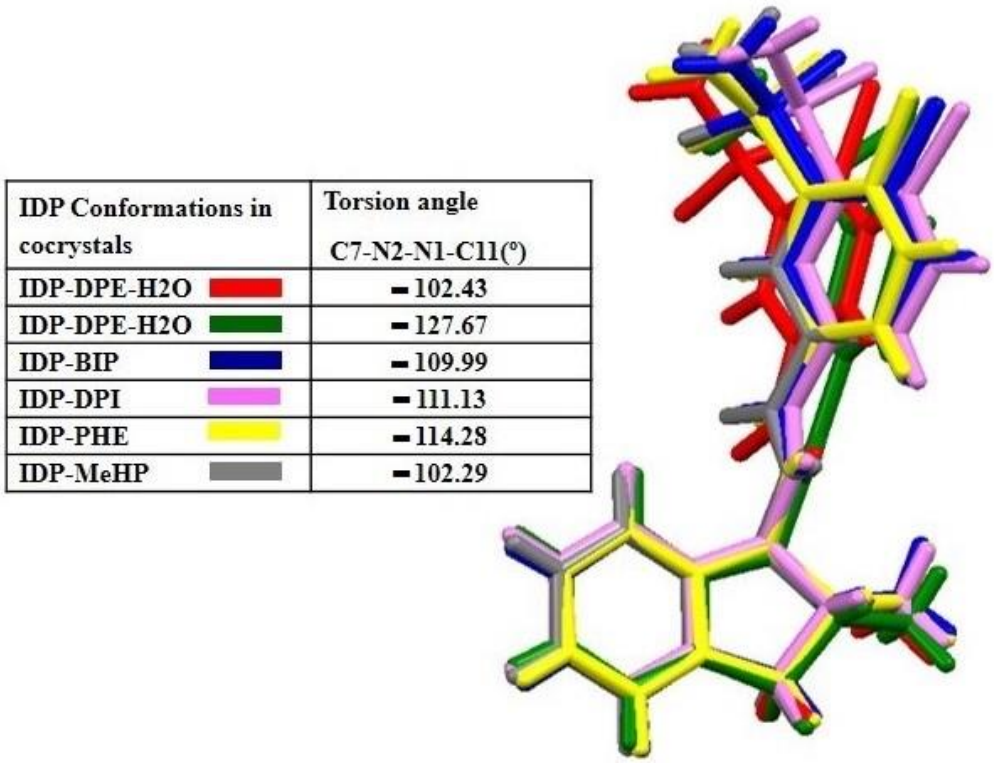

| IDP Conformations in cocrystals | Torsion angle C7-N2-N1-C11(°) |
|---|---|
| IDP-DPE-H2O | -102.43 |
| IDP-DPE-H2O | -127.67 |
| IDP-BIP | -109.99 |
| IDP-DPI | -111.13 |
| IDP-PHE | -114.28 |
| IDP-MeHP | -102.29 |

**Figure 3.8:** Overlay diagram of conformations in Indapamide (IDP).

## 3.2.3 Powder X-ray Diffraction

Cocrystals can be easily distinguished by their unique powder X-ray diffraction. It is a liable characterization technique to monitor homogeneity of phase purity of the new solid forms during rotoevaporazation and grinding experiments. Our aim was to make IDP cocrystals and coamorphous products with COOH, $CONH_2$, Pyridine, $NH_2$, and OH

functional group coformers but in selectively with pyridine coformers gave cocrystals through Co-grinding technique and other case with amine based coformers gave coamorphous through rotevaporation or cogrinding technique. PXRD is the good charcterzation technique to differentiate Cocrystals and coamorphous products. To confirm the IDP cocrystals shows unique diffraction crystalline pattern with respect to the starting materials. Overlay of IDP cocrystals shows excellent match of the experimental powder pattern with single crystalline calculated powder pattern (Figure 3.10). The amorphous nature was observed in powder X-ray diffraction (Figure 3.9) as a broad halo pattern (humph) and the absence of discrete diffraction lines (featureless PXRD).

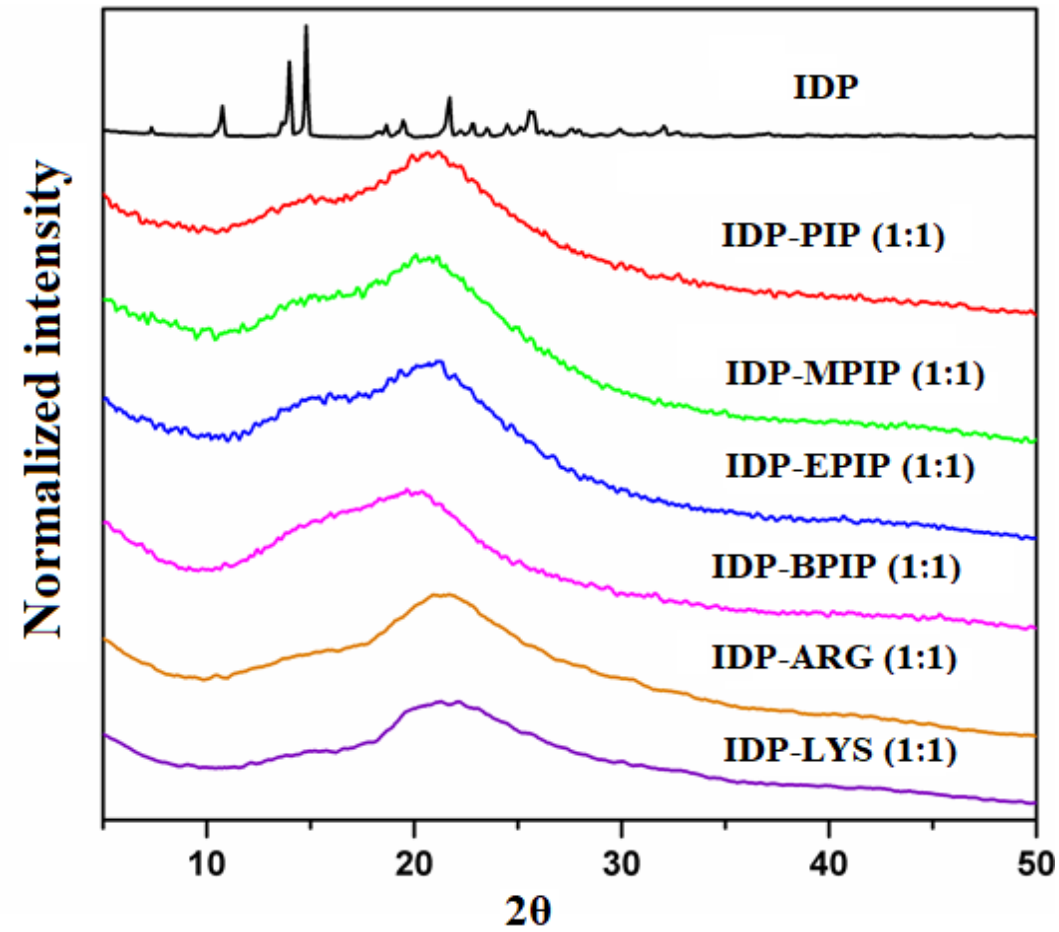


**Figure 3.9:** Powder XRD of coamorphous forms (1:1 stoichiometry) and drug IDP.

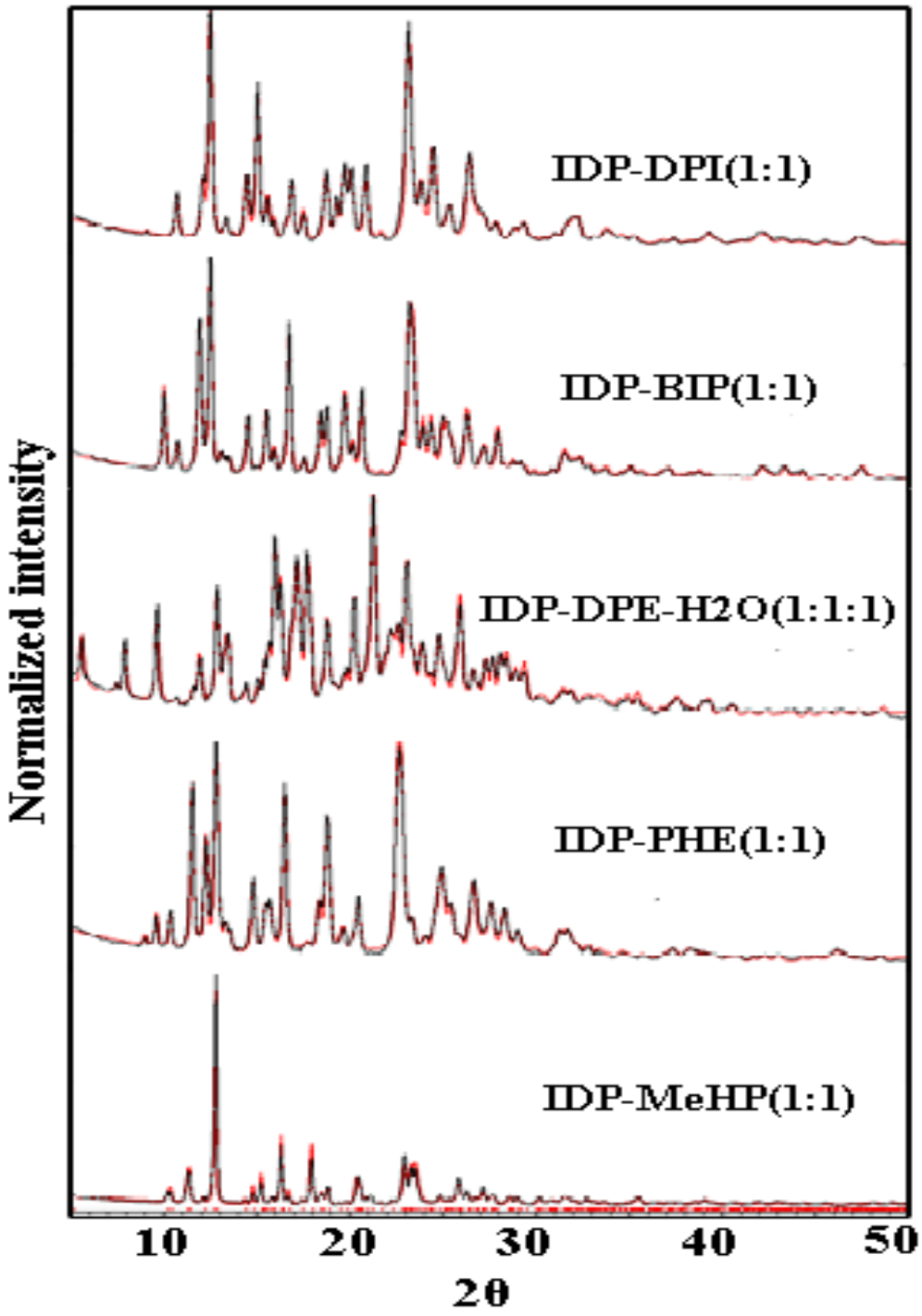


**Figure 3.10:** Overlay of experimental PXRD (black) of IDP cocrystals match with the calculated lines from the crystal structure (red).

## 3.2.4 Thermal Analysis

Thermal analysis of cocrystals and coamorphous products were performed with differential scanning calorimetry (DSC). The DSC heating curves IDP shows single endotherm at 171°C and IDP cocrystals shows sharp melting endotherms in that IDP-PHE, IDP-DPI shows higher melting point 207 °C, 203 °C and IDP-DPE-$H_2O$ shows lower melting endotherm at 95 °C (Figure 3.11, Table 3.3). In other case coamorphous solids does not have sharp melting endotherms but glass transition temperature (Tg) followed crystallzation/decomposition in IDP coamorphus with PIP, MPIP, EPIP, BPIP, ARG and LYS at 106 °C, 90 °C, 100 °C, 85 °C, 150 °C and 160 °C (Figure 3.12). These coamorphous solids were analyzed by hotstage microscopy for studying by visual examination the thermal transitions and transformations (Figure 3.13).

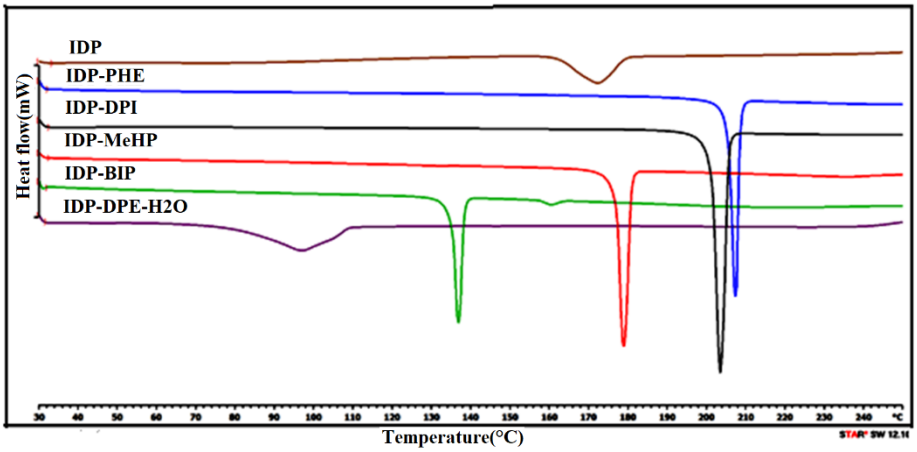


**Figure 3.11:** DSC thermograms of IDP cocrystals.

**Table 3.3:** Melting point of IDP, coformers and cocrystals.

| Drug/ coformer | Melting point (°C) | cocrystal | Melting point of cocrystal (°C) |
|---|---|---|---|
| IDP | 168-174 | - | - |
| DPI | 112-114 | IDP-DPI | 200-205 |
| BIP | 70-73 | IDP-BIP | 134-138 |
| DPE | 148-152 | IDP-DPE-$H_2O$ | 90-97 |
| PHE | 174-177 | IDP-PHE | 205-209 |
| MeHP | 157-159 | IDP-MeHP | 176-180 |

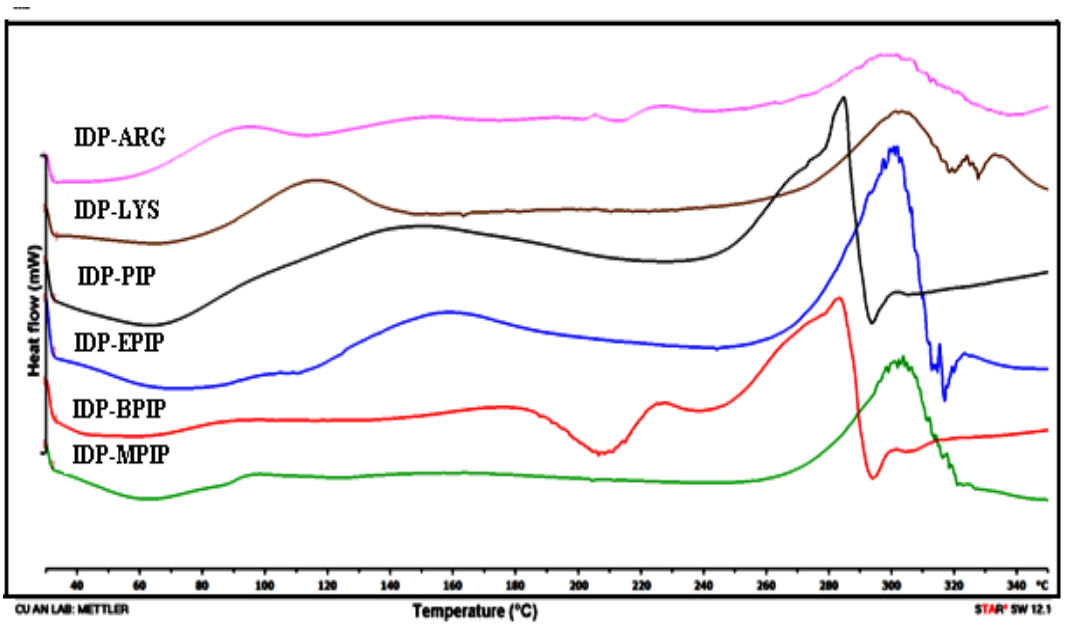


**Figure 3.12:** DSC thermograms of Indapamide coamorphus solids.

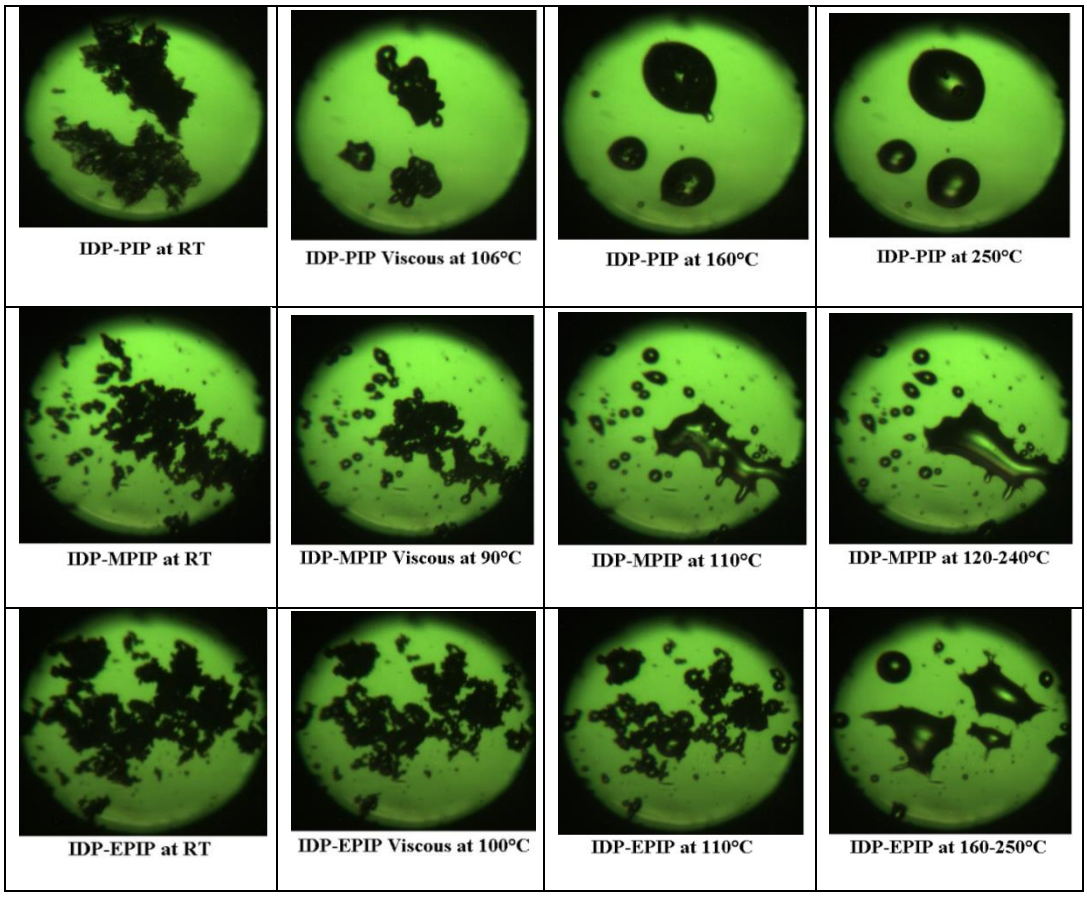

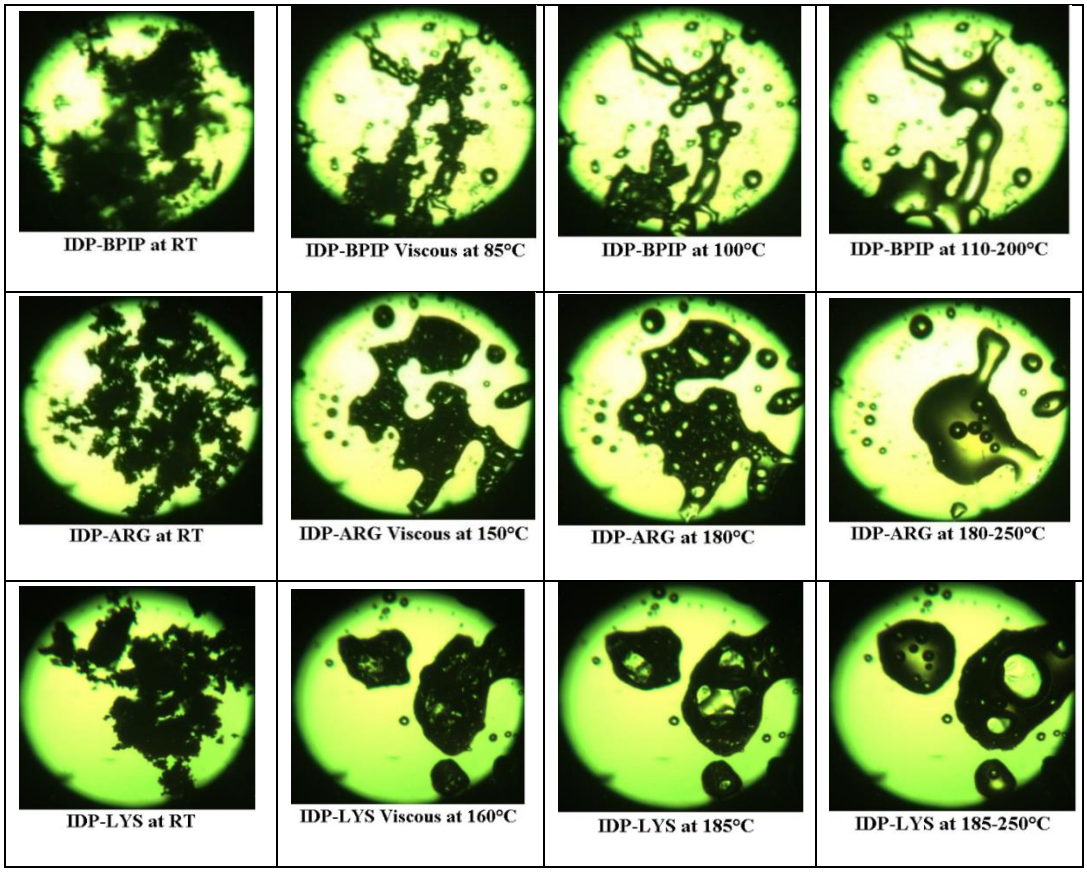


**Figure 3.13:** Hot stage microscope analaysis of amorphous materials.

## 3.2.5 Infrared Spectroscopy

Further information on the intermolecular interactions in cocrystal structures as well as for coamorphous forms was determined by FT-IR spectroscopy. The secondary amide carbonyl (C=O) stretching frequency of IDP peak is at 1659 $cm^{-1}$ and sulfonamide $NH_2$sym and asym stretching bands at 3507 and3432 $cm^{-1}$as well as amide sym and asym stretching bands NH at 3310 and 3226 $cm^{-1}$. All these functional groups showed significant changes in their vibrational patterns on cocrystal formation (Figure 3.14 and overlay Figure 3.15 and Table 3.4).Specifically, the $SONH_2$ group NH sym and asym stretch peaks are buried in the envelope of hydrogen bonding groups but are red shifted in the cocrystals due to hydrogen bond of the sulfonamide group with the coformer ($SONH_2$···Py/CONRH (N–H···N/O). The NH group stretching band is buried and red shifted compared to the parent components and these changes are similar in the cocrystals and the amorphous forms (Figure 3.14 and overlay Figure 3.15, and Table 3.4). This indicates that the $SO_2NH_2$ group is engaged in hydrogen bonding with piperazine and amino acid coformers through sulfonamide ···amine N–H···N bond

(Figure 3.2c). The carbonyl group (C=O) and the fingerprint region stretching bands of cocrystals/coamorphous forms were shifted in frequency when compared to the starting materials IDP and the conformer, indicating intermolecular hydrogen bonding.

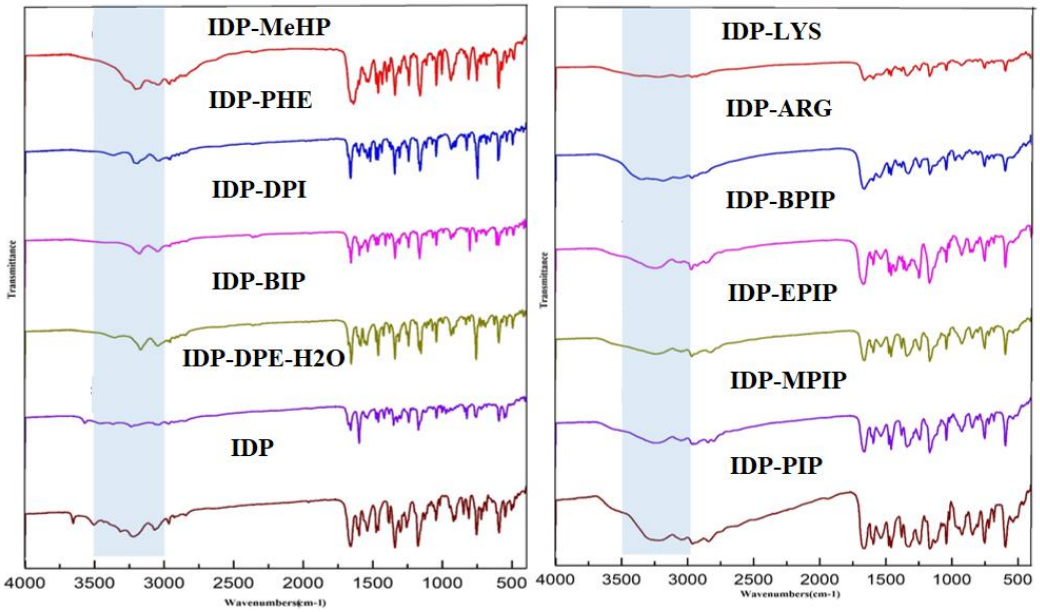


**Figure 3.14:** Selected functional group stretching frequency in FT-IR spectra of IDP cocrystals and coamorphus compounds.

**Table 3.4:** Selected functional group stretching frequency in FT-IR spectra of IDP cocrystals and coamorphous products.

| | **C=O (amide) ($cm^{-1}$)** | **SO2 (indapamide) ($cm^{-1}$)** | **NH($cm^{-1}$) sulfonamide** | **NH($cm^{-1}$) amide** |
|---|---|---|---|---|
| **IDP** | 1659 | 1175 | 3507, 3432 (asym and sym) | 3226 |
| **IDP−DPI (1:1)** | 1655 | 1162 | --- | 3177 |
| **IDP−BIP (1:1)** | 1654 | 1163 | 3361 | 3169 |
| **IDP−DPE−H2O (1:1:1)** | 1659 | 1172 | 3458, 3369 | 3235 |
| **IDP−PHE (1:1)** | 1660 | 1160 | 3363 | 3192 |
| **IDP−MeHP (1:1)** | 1657 | 1159 | 3281 | 3203 |
| **IDP-PIP(1:1)** | 1664 | 1166 | 3224 (3454 for PIP) | 3224 |
| **IDP-MPIP(1:1)** | 1665 | 1167 | 3245 (3425 for MPIP) | 3245 |
| **IDP-EPIP(1:1)** | 1663 | 1167 | 3235 (3427 for EPIP) | 3235 |
| **IDP-BPIP(1:1)** | 1669 | 1168 | 3252(3324 for | 3252 |

| | | | | |
|---|---|---|---|---|
| | | | BPIP) | |
| **IDP-ARG(1:1)** | 1664 | 1167 | 3352 (3358, 3299 for ARG) | 3182 |
| **IDP-LYS(1:1)** | 1659 | 1168 | 3375 (3342 for LYS) | 3218 |

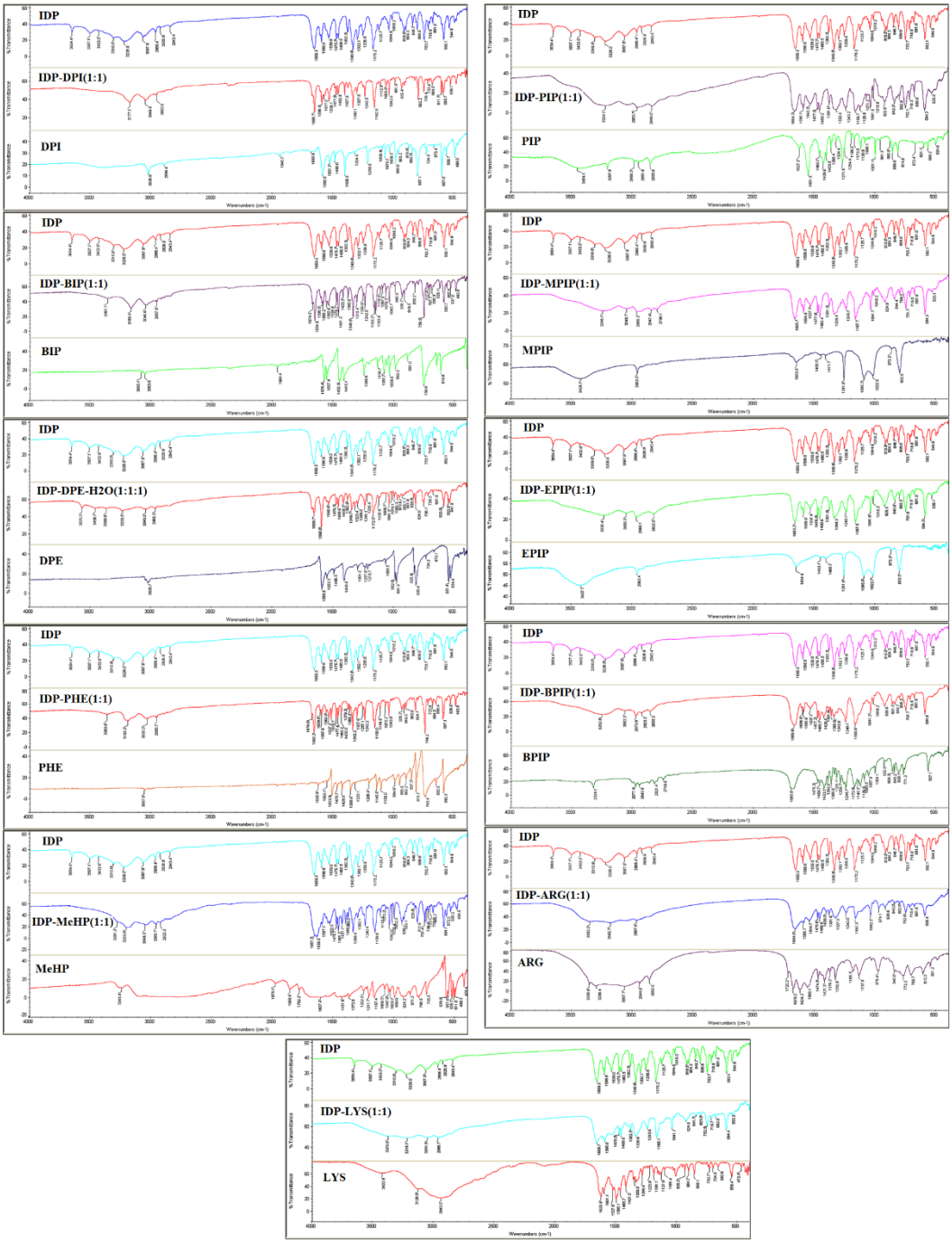


**Figure 3.15:** IR comparison of IDP novel solid forms with its starting materials.

## 3.2.6 Solution NMR

Solution NMR spectra were recorded on Bruker Avance 500 MHzspectrometer (Bruker-Biospin, Karlsruhe, Germany) and Bruker Avance 400 MHzspectrometer (Bruker-Biospin, Karlsruhe, Germany) Solution NMR spectra of IDP(API), IDP-LYS (1:1) recorded on Bruker Avance 400 MHz spectrometer (Bruker-Biospin, Karlsruhe,

Germany).DMSO-D6 solvent (solvent peak at 2.50(5) ppm). In NMR spectra, well separated and distinct protons of the molecules are taken into account. The area under curve is an indication of number of protons attached to that molecule in the product. In all cases the ratio present in the reaction product is the same as that used for crystallization. The stoichiometry of the amorphous system is established by 1H NMR integration.

**1H NMR spectra**

Solution NMR spectra were recorded on Bruker Avance 500 MHzspectrometer (Bruker-Biospin, Karlsruhe, Germany) and IDP(API), IDP-LYS (1:1) recorded on Bruker Avance 400 MHz spectrometer (Bruker-Biospin, Karlsruhe, Germany).

**IDP** (DMSO-$d_6$,δ, ppm, Figure S1a): 10.52 (s, 1H); 8.5 (s, 1H); 8.11 (dd, J=6.4Hz, 8.4Hz 1H); 7.81-7.72 (m, 3H); 7.11 (d, 6.8Hz, 1H); 7.04 (t, J=7.6Hz, 1H); 6.76 (t, J=7.4Hz, 1H); 6.50 (d, J=7.6Hz, 1H); 3.97 (s, 1H); 3.20-3.14 (m, 1H); 2.62-2.5 (m, 1H); 1.31 (d, J=6.4Hz, 3H).

**IDP-PIP (1:1**) (DMSO-$d_6$, δ, ppm, Figure S1b): 10.56 (brs, 1H); 8.51 (s, 1H); 8.51 (s, 1H); 8.11 (d, J=8.5Hz, 1H); 7.81 (d, J=8.0Hz, 1H); 7.11 (d, J=7.5Hz, 1H); 7.04 (t, J=7.5Hz, 1H); 6.77 (t, J=7.5Hz, 1H); 6.50 (d, J=7.5Hz, 1H); 4.64 (s, 4H); 3.97 (s, 1H); 3.17 (dd, J= 15.0Hz,8.0Hz, 1H);2.61-2.59 (m, 7H); 2.50(s, 2H); 1.31 (d, J=6.0Hz, 3H).

**IDP-MPIP (1:1**) (DMSO-$d_6$, δ, ppm, Figure S1c): 10.59 (s, 1H); 8.53 (s, 1H); 8.13 (d, J=8.5Hz, 1H); 7.81 (d, J=8.0Hz, 1H); 6.77 (t, J=7.5Hz, 1H); 6.51 (d, J=8.0Hz, 1H); 3.17 (dd, J=15.5Hz,8.0Hz, 1H); 2.66-2.65 (m, 3H); 2.61-2.56 (m, 1H); 2.19 (brs, 3H); 2.10-2.09 (m, 2H); 1.31 ( d, J=6.0Hz, 3H)

**IDP-EPIP (1:1**) (DMSO-$d_6$, δ, ppm, Figure S1d): 10.58 (brs, 1H); 8.52 (d, J=2.0Hz,1H); 8.13 (dd, J=8.0Hz, 2.0Hz, 1H); 7.81 (d,J=8.0Hz,1H); 7.11 (d,J=7.0Hz,1H); 7.05 (t,J=7.5Hz 1H); 6.77 (t, J=7.5Hz, 1H); 6.50 (d, J=8.0Hz, 1H); 4.51 (brs 6H); 3.98 (s, 1H); 3.17 (dd,J=15.5Hz,8.0Hz, 1H); 2.67 (t, J=4.5Hz, 3H); 2.59 (dd, J=15.5Hz,11.0Hz, 1H); 2.27-2.22 (m, 5H); 1.31 (d, J=6.5Hz, 3H); 0.96 (t, J=7.5Hz, 2H).

**IDP-BPIP (1:1)** (DMSO-$d_6$, δ, ppm, Figure S1e): 10.55 (s,1H); 8.50 (s, 1H); 8.11 (d, J=8.0Hz, 1H); 7.81 (d, J=8.0Hz, 1H); 7.11 (d,J=7.0Hz, 1H); 7.04 (t, J=7.5Hz, 1H); 6.77 (t, J=7.5Hz, 1H); 6.50 (d, J=7.5Hz, 1H); 3.97 (brs, 1H); 3.33 (s, 3H); 3.21-3.15 (m, 5H); 2.61-2.59 (m, 5H); 1.39 (s, 9H); 1.31-1.30 (m, 3H)

**IDP-ARG (1:1)** (MeOH-$d_4$,δ, ppm, Figure S1f): 8.62 (d, J=2Hz, 1H); 8.07 (dd, J=6,8.5Hz, 1H); 7.75 (d, J=8Hz, 1H); 7.14-7.08 (m, 2H); 6.85(t, J=7.5Hz, 1H); 6.62 (d,

J=7.5Hz, 1H); 3.87 (s,1H); 3.33-3.32 (m, 4H); 3.22-3.17 (m, 2H); 2.73-2.68 (m, 2H); 1.73-1.62 (m, 2H); 1.42 (d, J=6Hz, 3H)

**IDP-LYS (1:1)** (MeOH-$d_4$,δ, ppm, Figure S1g): 8.54 (d, J=2.4Hz, 1H); 8.09 (dd, J=6.4Hz, 8.4Hz, 1H); 7.82 (d, J=8.4Hz, 1H); 7.19-7.11 (m, 2H); 6.89 (t, 7.6Hz, 1H); 6.63 (d, J=7.6Hz, 1H); 3.85 (brs, 1H); 3.62-3.55 (m, 1H); 3.33-3.31 (m, 4H); 3.23-3.17 (m, 1H); 2.98 (t, J=7.6Hz, 1H); 2.75-2.67 (m, 1H); 1.90-1.83 (m, 2H); 1.76-1.68 (m, 2H); 1.55-1.33 (m, 6H)

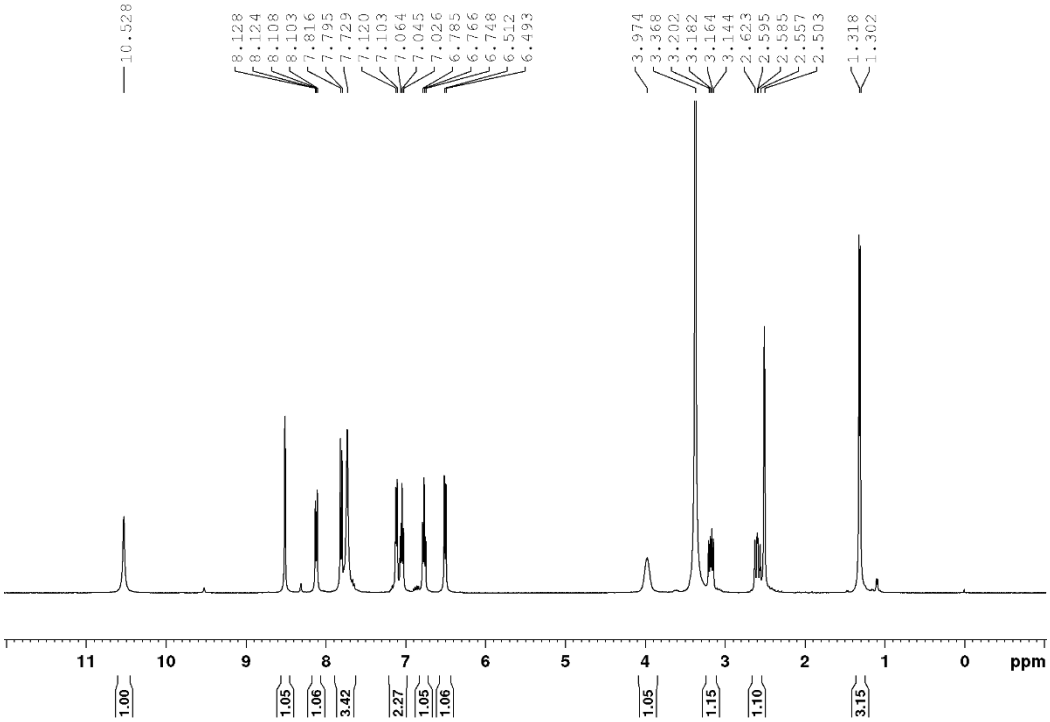


**Figure 3.16:** 1H NMR spectrum of IDP.

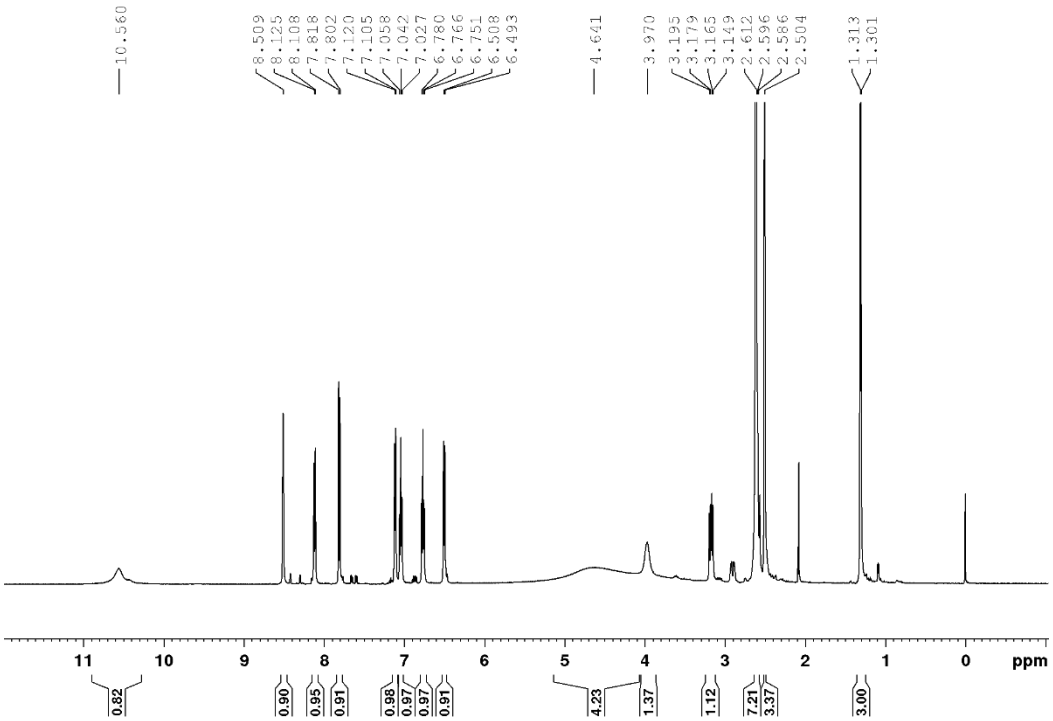


**Figure 3.17:** 1H NMR Spectrum of IDP-PIP.

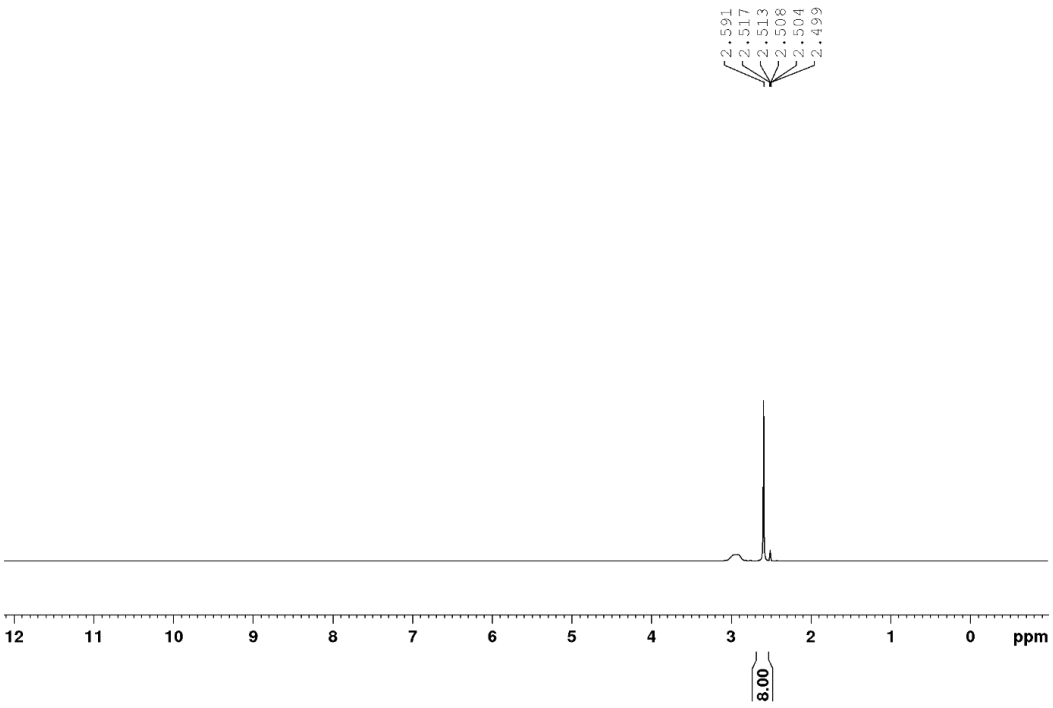


**Figure 3.18:** 1H NMR spectrum of PIP.

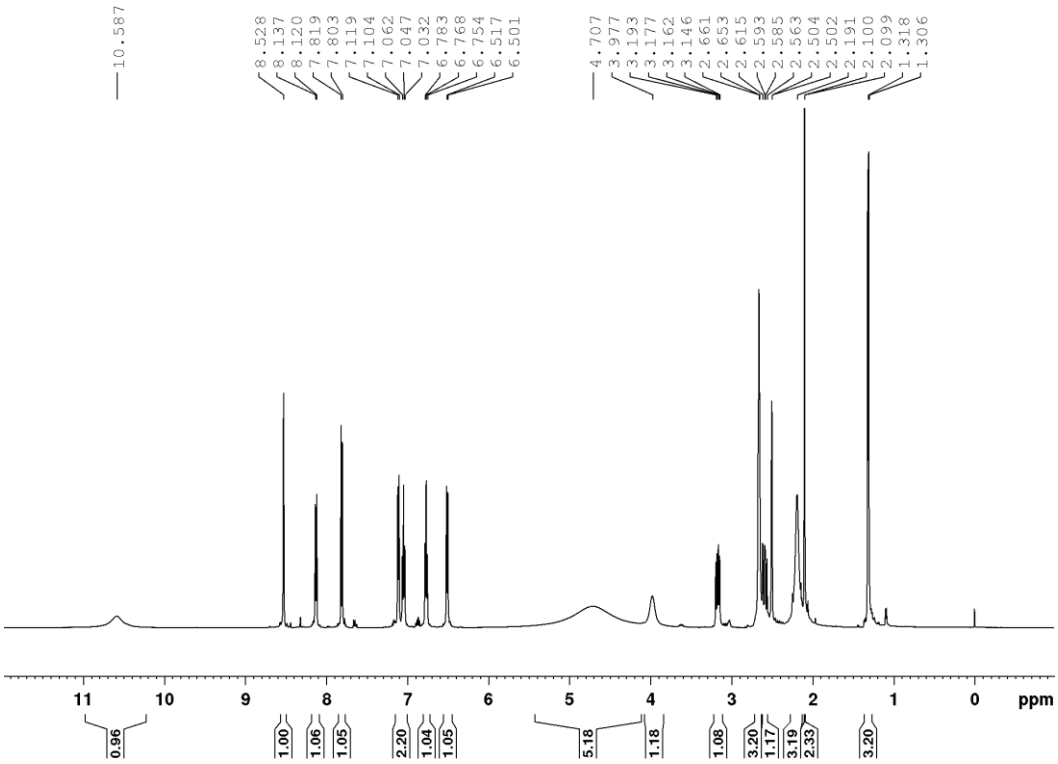


**Figure 3.19:** 1H NMR spectrum of IDP-MPIP.

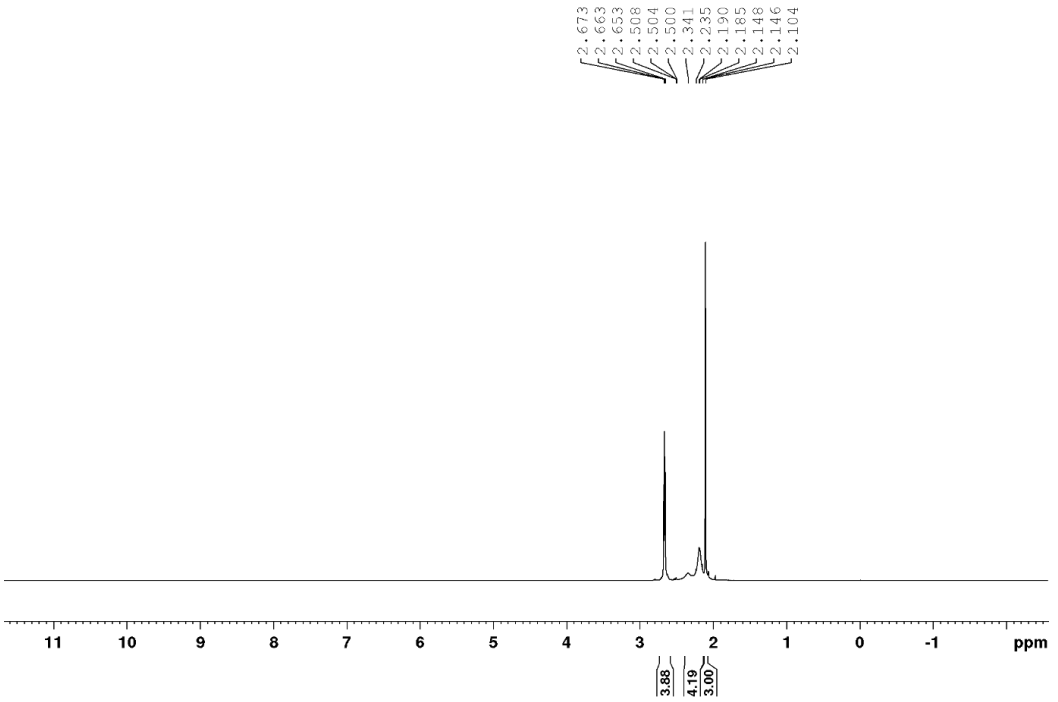


**Figure 3.20:** 1H NMR spectrum of MPIP.

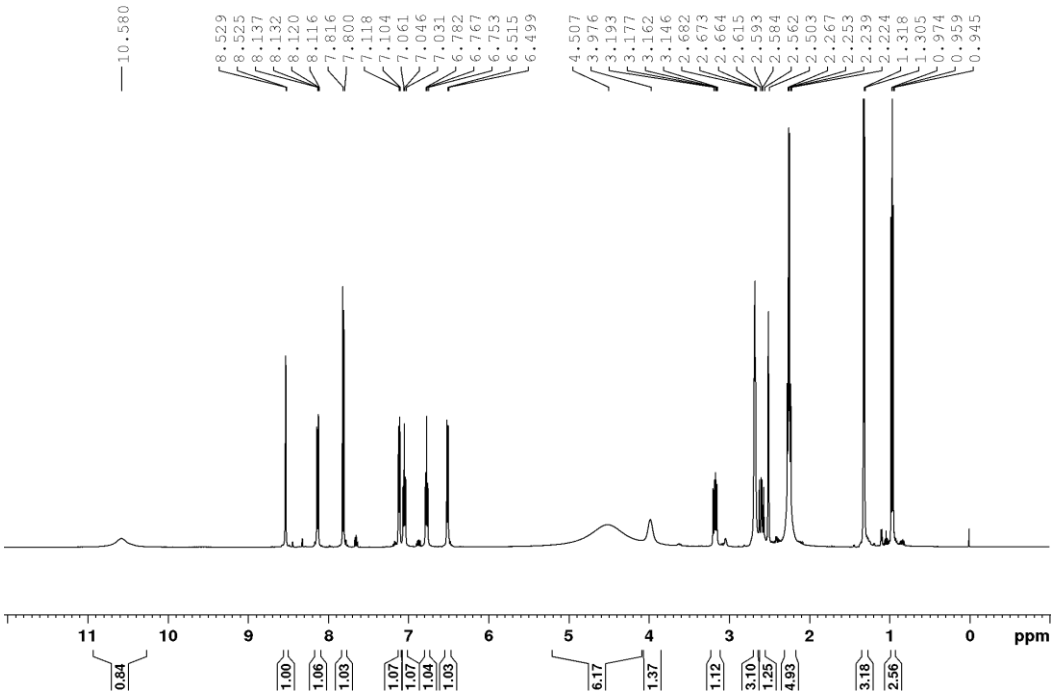


**Figure 3.21:** 1H NMR spectrum of IDP-EPIP.

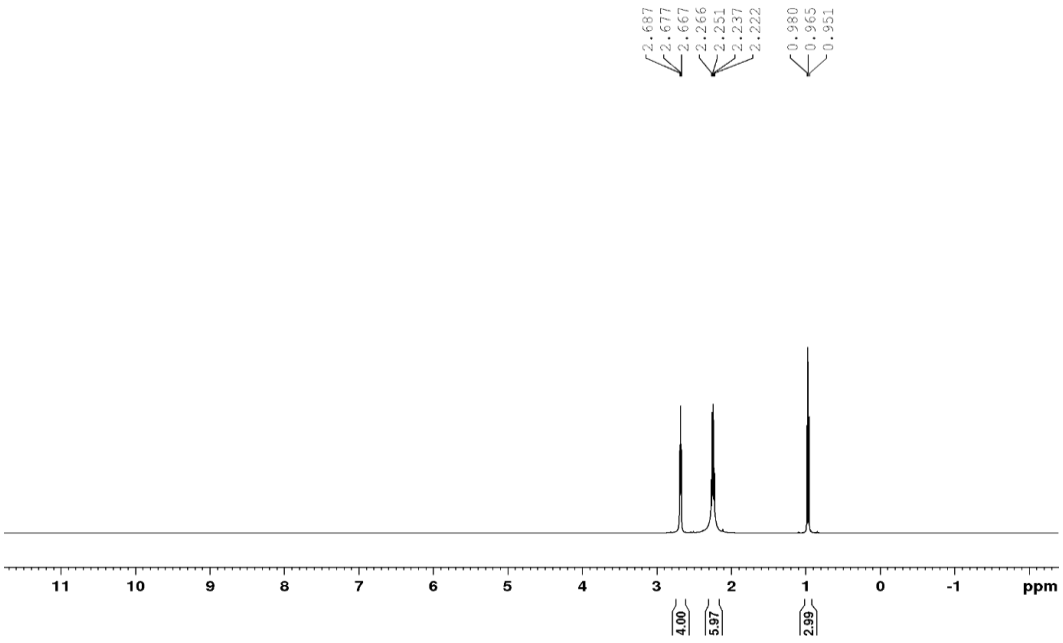


**Figure 3.22:** 1H NMR spectrum of EPIP.

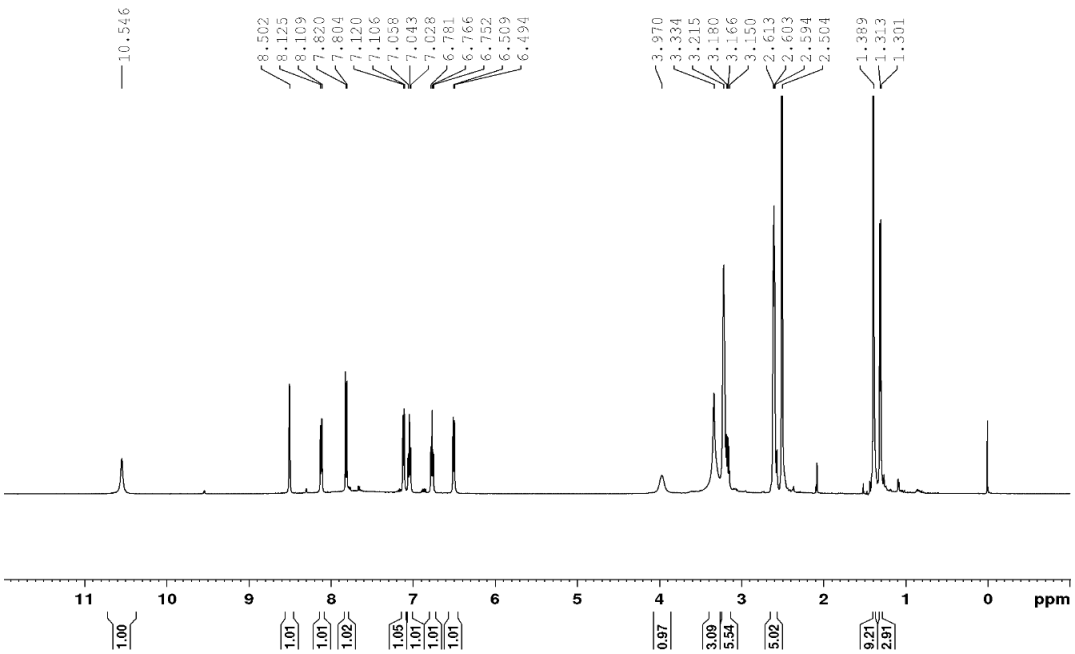


**Figure 3.23:** 1H NMR spectrum of IDP-BPIP.

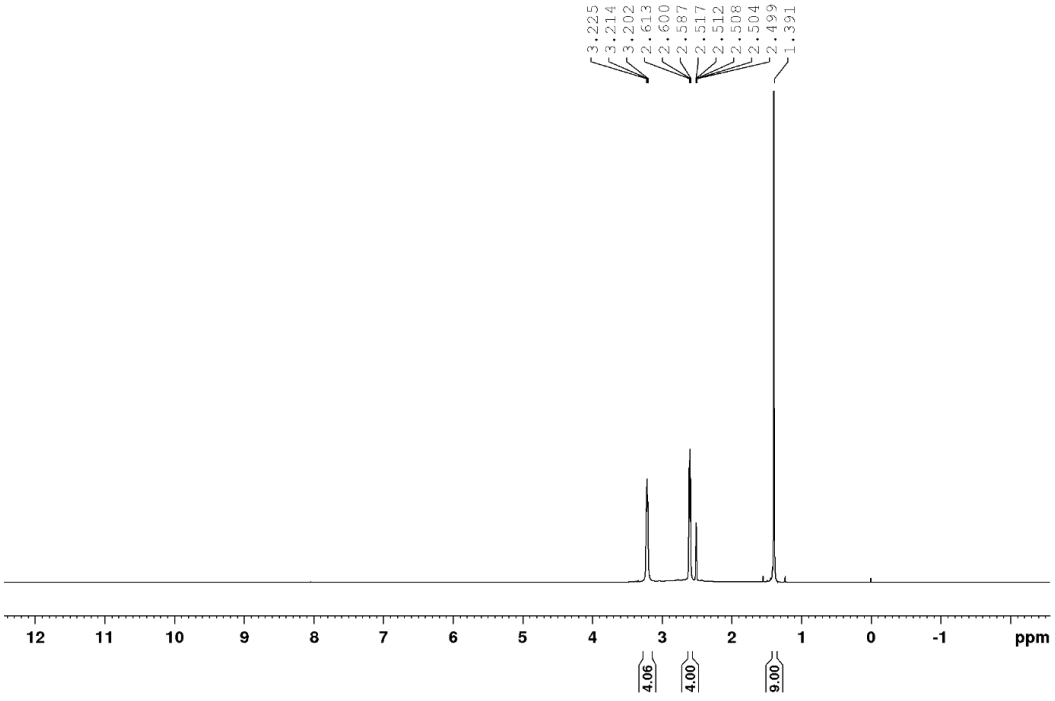


**Figure 3.24:** 1H NMR spectrum of BPIP.

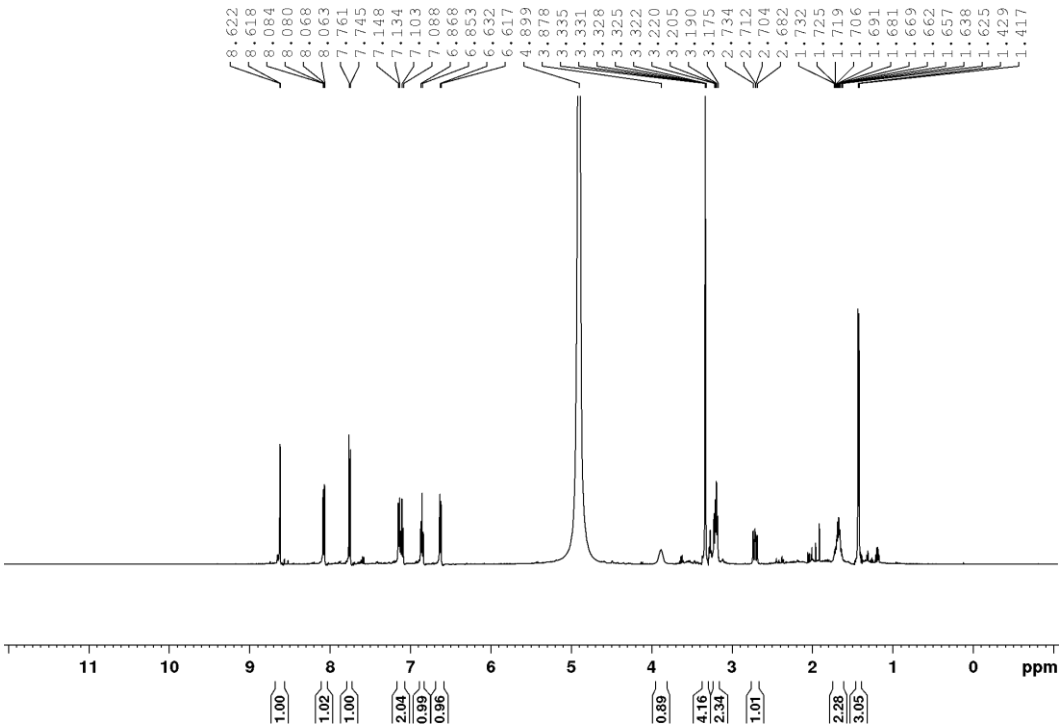


**Figure 3.25:** 1H NMR spectrum of IDP-ARG.

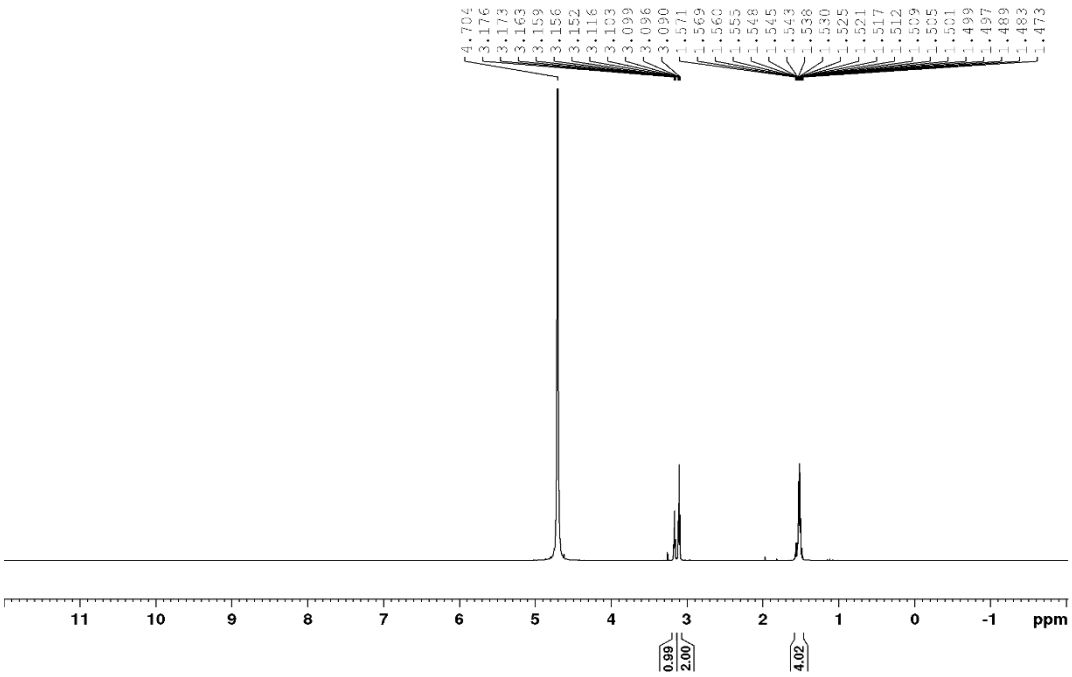


**Figure 3.26:** 1H NMR spectrum of ARG.

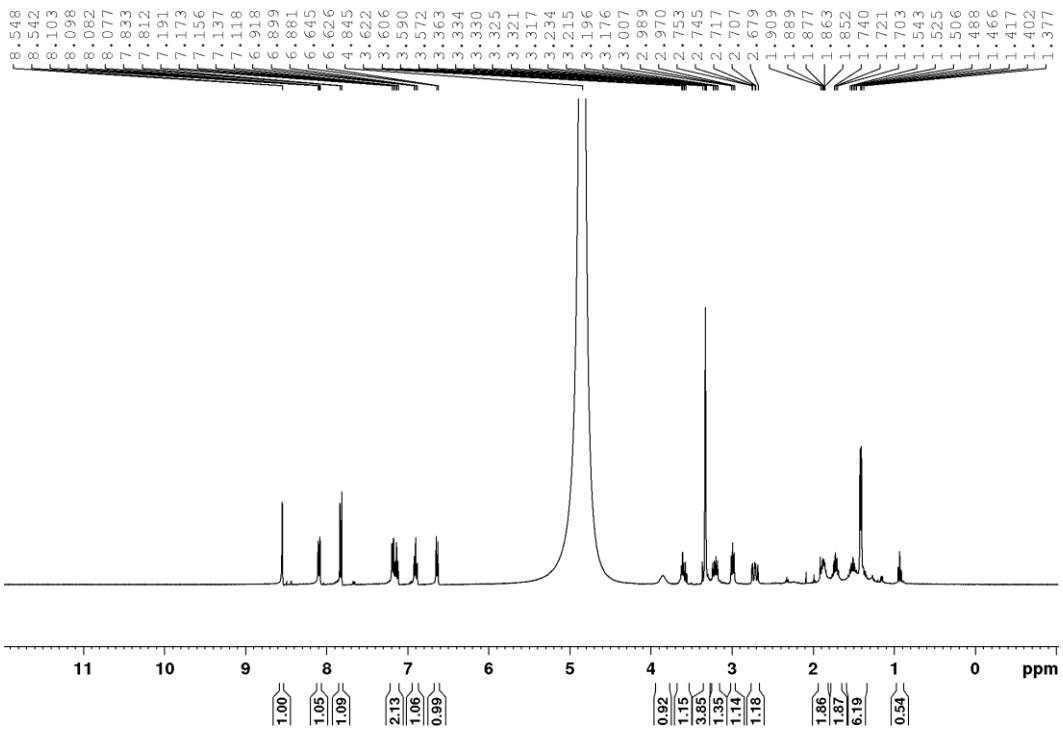


**Figure 3.27:** 1H NMR spectrum of IDP-LYS.

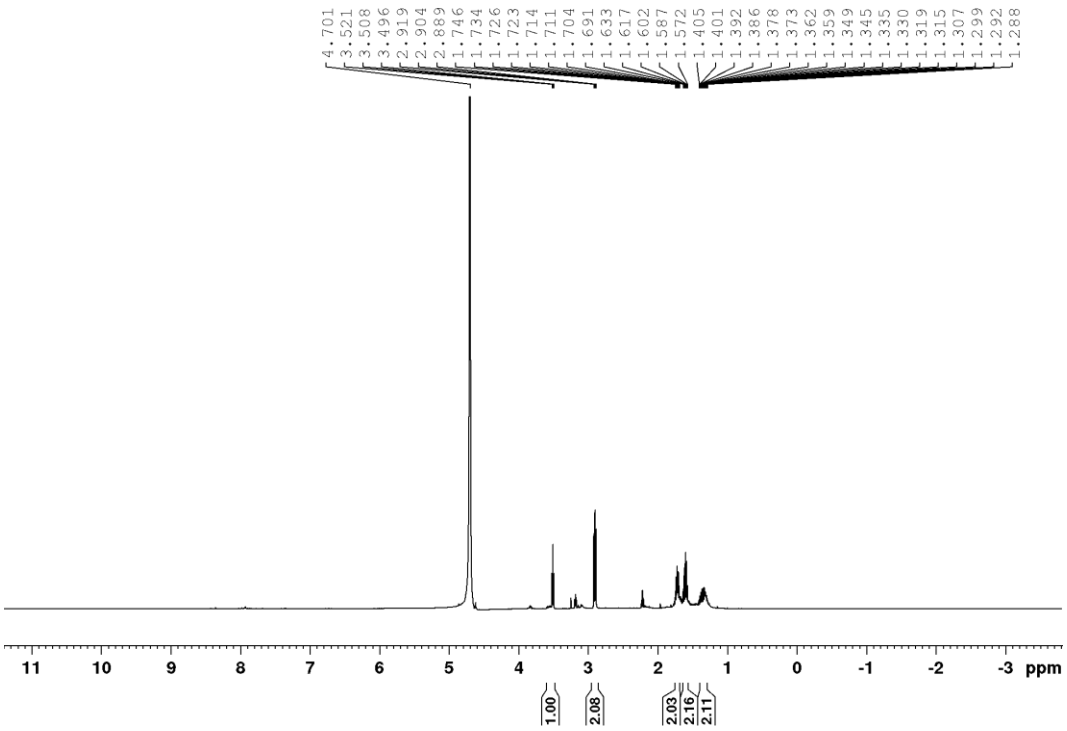


**Figure 3.28:** 1H NMR spectrum of LYS.

## 3.2.7 Solubility and Dissolution Stability studies

The cocrystals contain a specific heterosynthon for the hydrogen bonding functional groups. The coamorphous forms exist through interactions in the structure of high thermodynamic function and free energy. The coamorphous systems are thermodynamically less stable than the cocrystals. Crystallization from solution resulted in coamorphous form along with the crystalline components whereas the cocrystals gave the product crystals. The cocrystals of IDP with rigid / aromatic coformers and stronger N–H···O and N–H···N-Py are crystalline whereas the crystal structures with flexible molecules and weaker N–H···N-amine hydrogen bond with piperazine and amino acid coformers afforded amorphous products.

Cocrystals obtained in this study are non GRAS (generally regarded as safe by the US-FDA) coformers in view of this particularly Solubility and stability studies on coamorphous forms with GRAS coformers (PIP, MPIP, EPIP, BPIP, ARG, LYS) were conducted at accelerated ICH conditions (40 °C, 75% RH) and powder dissolution in phosphate buffer (pH7). IDP-PIP system was stable for up to 3 months (Figure 3.29) but subsequently converted to a crystalline form by PXRD analysis. In contrast, other piperazine derivatives of IDP were unstable and converted to the crystalline physical mixture after 24h under the test conditions (Figure 3.30). IDP-ARG was stable for more than a month whereas IDP-LYS became crystalline within 24 h (Figure 3.31). Powder dissolution studies of coamorphous products showed faster dissolution rate compares to IDP crystalline form (Figure 3.32). IDP-ARG and IDP-LYS coamorphous exhibited highest dissolution rate curves compared to the other solids and other amine based piperazine derivatives shows low soluble compared to amino acid derivatives. These amino acids highly soluble in water than the other solids. This is the general phenomenon in that the highly soluble partner molecule usually enhances the higher dissolution rate.

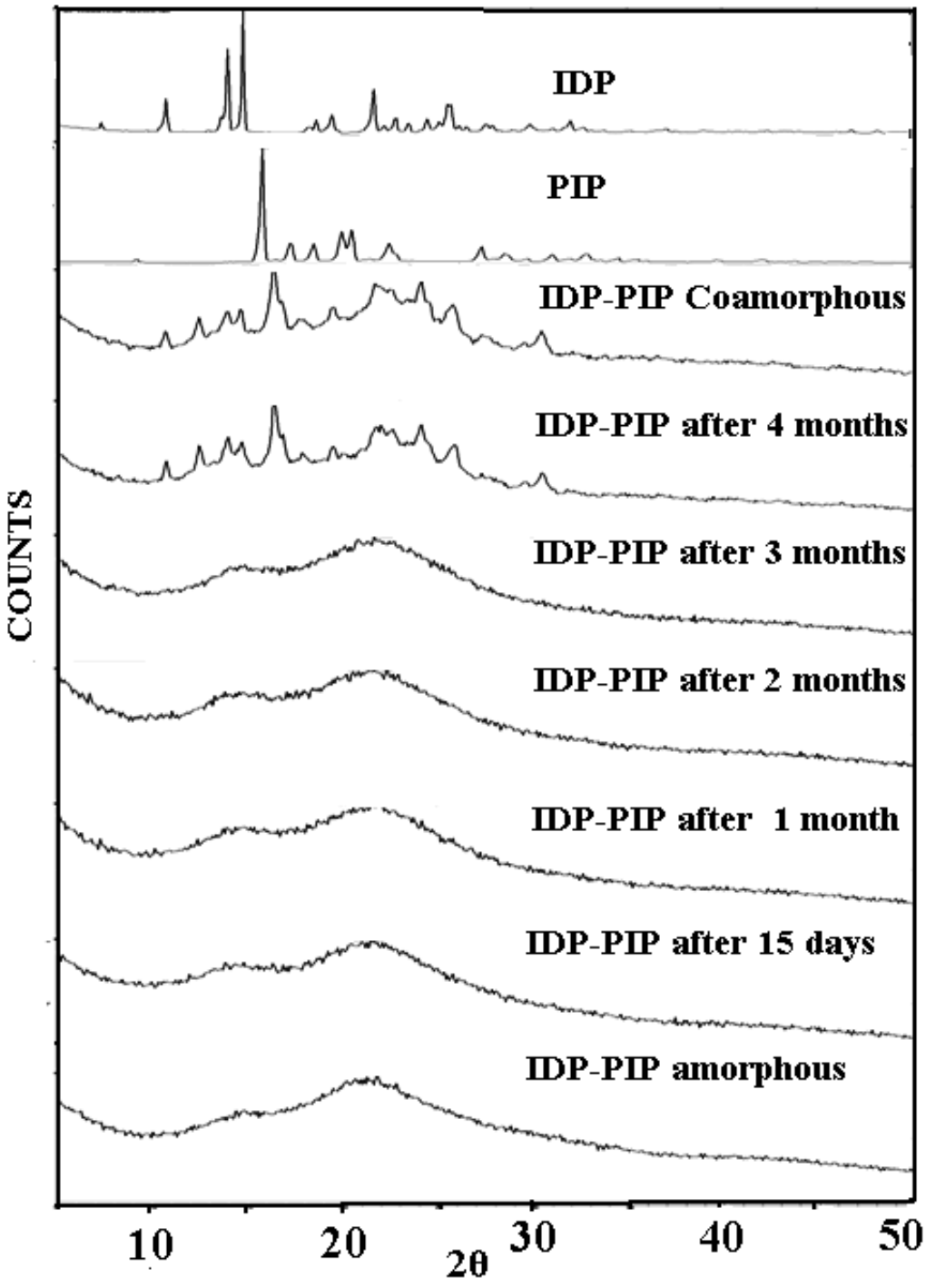


**Figure 3.29:** Stability study at 40 °C and 75% RH of IDP-PIP shows that is stable up to 3 months. After that it transforms to the crystalline phase.

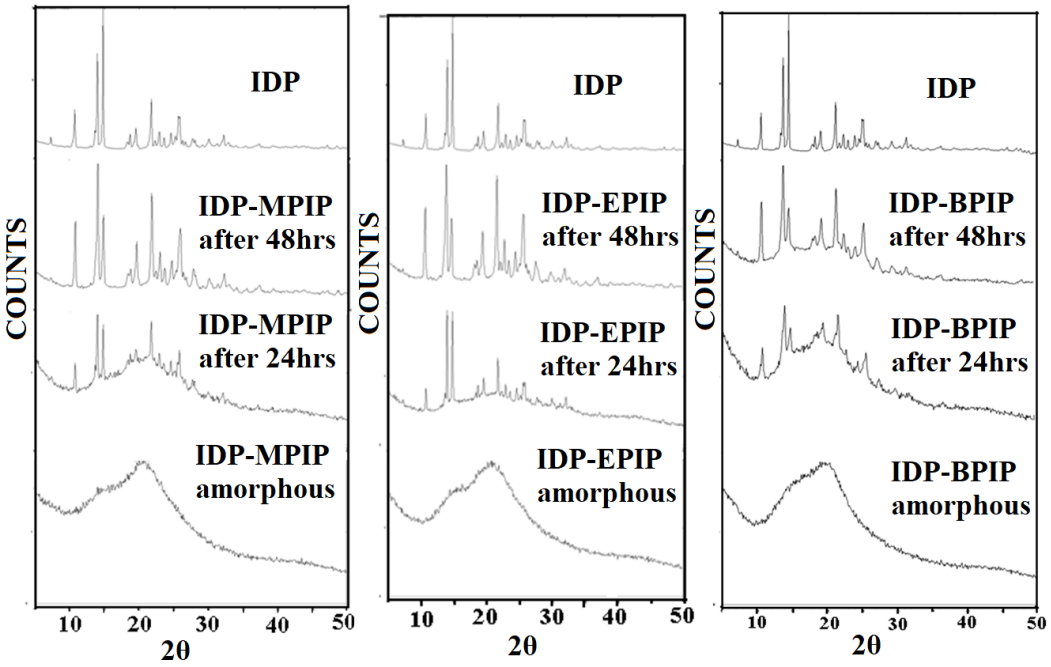


**Figure 3.30:** Stability study at 40 °C and 75% RH of IDP-MPIP, IDP-EPIP and IDP-BPIP amorphous forms at ambient conditions shows that after 2 days it transforms to crystalline IDP.

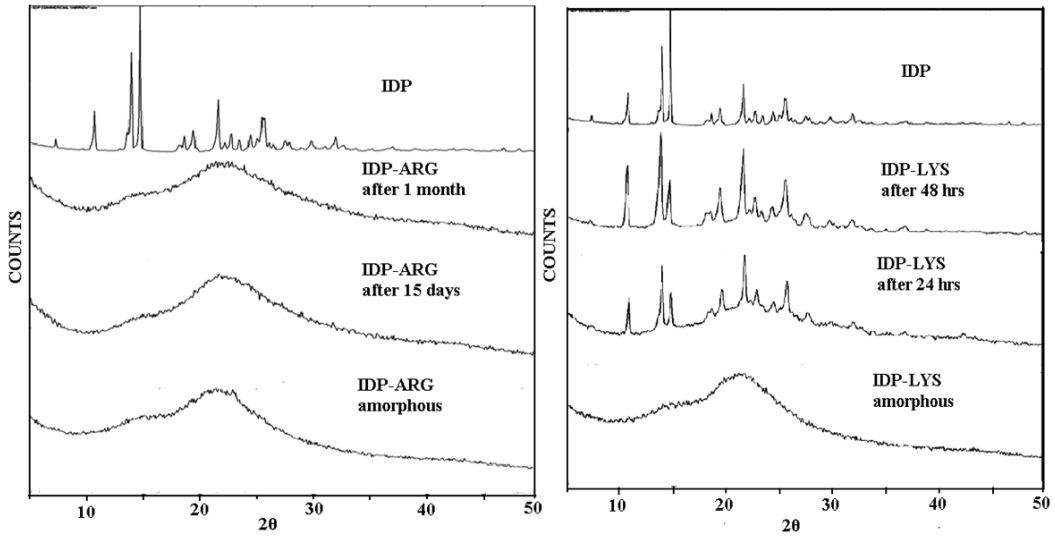


**Figure 3.31:** Stability study at 40 °C and 75% RH of IDP-ARG amorphous form at ambient conditions shows that for up to one month it stable and there is transformation to the crystalline phase and Stability of IDP-LYS amorphous form at ambient conditions shows that after 2 days it transforms to crystalline IDP.

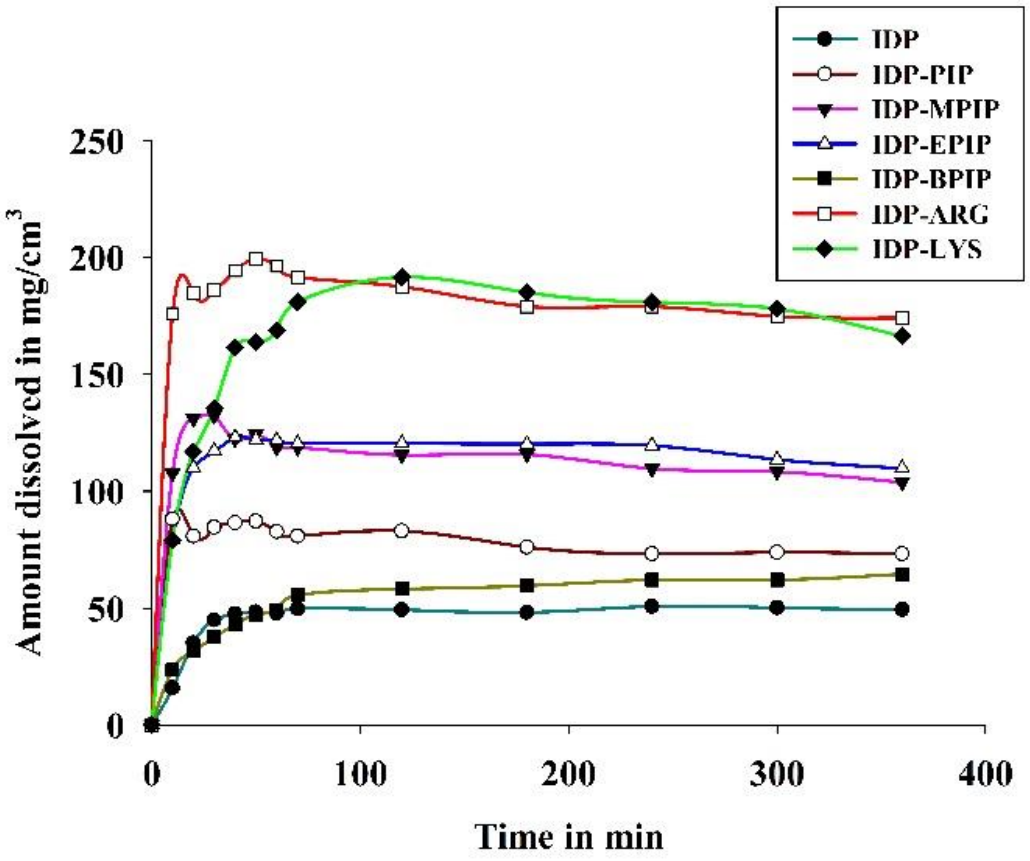


**Figure 3.32:** Powder dissolution rate of IDP and coamorphous forms over 6h.

## 3.2.8 Diffusion Measurements

The diffusion kinetics and the flux rate of IDP crystalline and coamorphous forms (Figure 3.33 and Figure 3.34) were faster than IDP crystalline. IDP-ARG is superior to the other solid forms followed by IDP-LYS and IDP-PIP. This is caused by changes in flux rate. Based on the solubility data we expected the diffusion and flux rate of coamorphous solids to be faster than that of pure IDP. In IDP-ARG and IDP-LYS the high solubility resulted in faster diffusion across the semi-permeable membrane. In summary IDP-PIP, IDP-LYS and IDP-ARG are the best 3 amorphous forms of indapamide with high drug solubility and high membrane permeability (BCS class I category of high solubility and permeability).

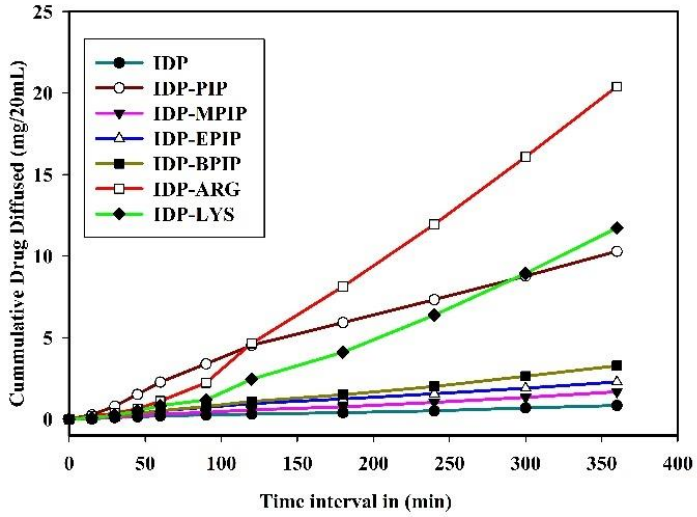


**Figure 3.33:** Diffusion curves of the IDP and coamorphous through dialysis membranein PBS solution (pH7.4)

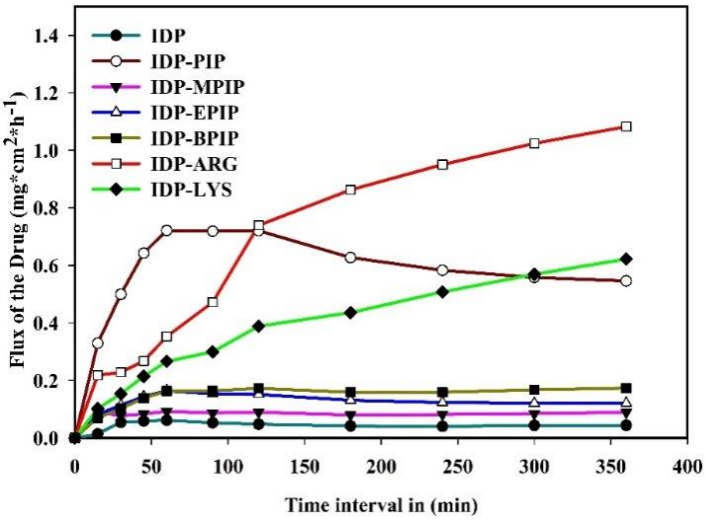


**Figure 3.34:** Flux of the IDP and coamorphous through dialysis membrane in PBS solution (pH 7). The slight drop in flux for IDP-PIP after 2 h is due to partial crystallization and precipitation.

## 3.3 Conclusions

In summary, this study relates supramolecular synthons with the formation of cocrystal or coamorphous forms. The stronger sulfonamide-pyridine ($SO_2NH_2\cdots Py$) and

sulfonamide-carboxamide ($SO_2NH_2\cdots CONRH$) hetero synthons with rigid/ aromatic coformers drive cocrystal products while the weaker sulfonamide-amine ($SO_2NH_2\cdots NR_2H$) synthon with flexible molecules gave coamorphous products with IDP. These guidance supplement our recent observations on synthon strength with molecular likeness/ dissimilarity to give cocrystal, solid solution or eutectic products.[12] Secondly, the higher aqueous solubility and better diffusion membrane permeability of IDP-ARG shows that amino acids can be used to enhance not only powder dissolution but also diffusion kinetics. Reports on improving solubility and permeability via cocrystal form selection are relatively few in the literature.[36] The change in the crystalline to coamorphous state of the API with suitable coformers has proven to be a simple and efficient methodology for improving drug bioavailability. The physical form stability of IDP-PIP coamorphous system is surprising but there are other examples in the recent literature.[37,38] These findings suggest an approach to develop novel coamorphous forms and amorphous solid dispersions guided by crystal engineering for improved solid-state pharmaceuticals.

## 3.4 Experimental Section

Indapamide was purchased from Yarrow Chem Products (Mumbai, India). Purity of the compound was confirmed by NMR PXRD and DSC. The coformers used in this study were purchased from Sigma-Aldrich, Hyderabad, India. All chemicals are analytical and solvents are chromatographic grade.

**Preparation of Cocrystals and Coamorphous:**

**IDP−DPI (1:1):** IDP (100 mg, 0.273 mmol) and DPI (42.69 mg, 0.273 mmol) were ground in a mortar and pestle for 20-25 min after adding 4-5 drops of EtOH. The ground material was kept for crystallization from solvent mixture EtOH and $CH_3CN$ (5 mL) as well as the pure solvents in 10 mL conical at room temperature. Colorless good quality single crystals were observed by slow evaporation. M.p. 200-205 °C.

**IDP−BIP (1:1):** IDP (100 mg, 0.273 mmol) and BIP (42.69 mg, 0.273 mmol) were ground in a mortar and pestle for 20-25 min after adding 4-5 drops of EtOH. The ground material was kept for crystallization from EtOH and THF (5 mL) solvent mixture in 10 mL conical at room temperature. Colorless good quality single crystals were observed after slow evaporation. M.p. 134-138 °C.

**IDP−DPE-HYD (1:1:1):** IDP (100 mg, 0.273 mmol) and DPE (49.81 mg, 0.273 mmol) were ground in a mortar and pestle for 20-25 min after adding 4-5 drops of EtOH. The ground material was kept for crystallization from EtOH and $CH_3CN$ (5 mL) solvent mixture in 10 mL conical at room temperature. Colorless good quality single crystals were observed by slow evaporation. M.p. 90-97°C.

**IDP−PHE (1:1):** IDP (100 mg, 0.273 mmol) and PHE (49.26 mg, 0.273 mmol) were ground in a mortar and pestle for 20−25 min in stoichiometric ratio by adding catalytic amount (4−5 drops) of EtOH solvent. The ground material was kept for crystallization from solvent mixture of EtOH and THF (1:1 v/v) 5 mL in a 25 mL conical flask at room temperature. Pale yellow green color good quality single crystals were observed by slow evaporation. M.p. 205-209 °C

**IDP−MeHP (1:1):** IDP (100 mg, 0.273 mmol) and MeHP (29.87 mg, 0.273 mmol) were ground in a mortar and pestle for 20-25 min after adding 4-5 drops of EtOAc. The ground material was kept for crystallization from of EtOH and EtOAc (1:1 v/v, 5 mL) mixture in a 25 mL conical flask at room temperature. Colorless good quality single crystals were observed by slow evaporation. M.p. 176-180 °C.

**IDP−PIP (1:0.5):** IDP (100 mg, 0.273 mmol) and PIP (23.54 mg, 0.273 mmol) were ground in a mortar and pestle for 20-25 min after adding 4-5 drops of CH3CN then it formed rubbery amorphous phase. Another method is Rotavaporization by dissolving the two components in a solvent and then fast evaporation under high vacuum. The product was characterized by PXRD, DSC, IR and NMR.

**IDP−MPIP (1:1):** IDP (100 mg, 0.273 mmol) and MPIP (27.37 mg or 30.31µl, 0.273 mmol) were ground in a mortar and pestle for 20-25 min after adding 4-5 drops of CH3CN then it formed rubbery amorphous phase. Another method is Rotavaporization by dissolving the two components in a solvent and then fast evaporation under high vacuum. The product was characterized by PXRD, DSC, IR and NMR.

**IDP−EPIP (1:1):** IDP (100 mg, 0.273 mmol) and EPIP (31.21 mg or 34.72µl, 0.273 mmol) were ground in a mortar and pestle for 20-25 min by adding 4-5 drops of CH3CN then it formed rubbery amorphous phase, Another method is Rotavaporization by dissolving the two components in a solvent and then fast evaporation under high vacuum. The product was characterized by PXRD, DSC, IR and NMR.

**IDP−BPIP (1:1):** IDP (100 mg, 0.274 mmol) and BPIP (50.91 mg, 0.273 mmol) were ground in a mortar and pestle for 20-25 min after adding 4-5 drops of CH3CN then it formed rubbery amorphous phase. Another method is Rotavaporization by dissolving the two components in a solvent and then fast evaporation under high vacuum. The product was characterized by PXRD, DSC, IR and NMR.

**IDP−ARG (1:1):** IDP (100 mg, 0.273 mmol) and ARG (47.61 mg, 0.273 mmol) were ground in a mortar and pestle for 20-25 min in stoichiometric ratio after adding 4-5 drops of EtOH then it formed rubbery amorphous phase. Another method is Rotavaporization by dissolving the two components in a solvent and then fast evaporation under high vacuum. The product was characterized by PXRD, DSC, IR and NMR.

**IDP−LYS (1:1):** IDP (100 mg, 0.273 mmol) and LYS (39.96 mg, 0.273 mmol) were ground in a mortar and pestle for 20-25 min after adding 4-5 drops of EtOH then it formed rubbery amorphous phase. Another method is Rotavaporization by dissolving the two components in a solvent and then fast evaporation under high vacuum, The product was characterized by PXRD, DSC, IR and NMR.

**X-ray crystallography**

Bruker D8 QUEST, CCD diffractometer. Mo-Kα (λ = 0.71073 Å) radiation was used to collect X-ray reflections on all crystals. Bruker D8 Quest diffractometer equipped with a graphite monochromator and Mo−Kα fine-focus sealed tube (λ = 0.71073 Å) Data reduction was performed using Bruker SAINT Software.[39] Intensities for absorption were corrected with SADABS,[40] and the structure was solved and refined using SHELX-97.[41] All non-hydrogen atoms were refined as anisotropic. Hydrogen atoms on heteroatoms were located from difference electron density maps and all C−H hydrogens were fixed geometrically with HFIX command in SHELX-TL program of Bruker-AXS.[42] Hydrogen bond geometries were determined in Platon.[43-44] X-Seed[45-46] and Mercury was used to prepare packing diagrams. Crystallographic cif files are available at www.ccdc.cam.ac.uk/data.( ccdc no. 1849062-1849066).

**Powder X-ray diffraction**

Powder X-ray diffraction (PXRD) was recorded on Bruker D8 Advance diffractometer (Bruker-AXS, Karlsruhe, Germany) using Cu-Kα X-radiation (λ = 1.5406 Å) at 40 kV and 30 mA power. Diffraction patterns were collected over the 2θ range 5–50° at scan

rate of 5°/min. Powder Cell 2.4[47] was used for Profile fitting refinement of experimental PXRD and calculated lines from the X-ray crystal structure.

**Vibrational spectroscopy**

Thermo-Nicolet 6700 Fourier transform infrared spectrophotometer (Thermo Scientific, Waltham, Massachusetts) was used to record IR spectra. IR spectra were recorded on samples dispersed in KBr pellets. Data was analyzed using the Omnic software (Thermo Scientific, Waltham, Massachusetts).

**Thermal analysis**

Differential scanning calorimetry (DSC) was performed on Mettler-Toledo DSC 822e module. Compounds were placed in sealed pin-pricked aluminum pans for DSC experiments. The characteristic sample size is 3-5 mg for DSC. The temperature range for the heating curves was 30-350°C, and the sample was heated at a rate of 10 °C/ min. Samples were purged in a stream of dry nitrogen flowing at 80 mL/min.

**Hot stage Microscopy (HSM)**

HSM was performed on a Wagner & Munz, Polytherm A Hot Stage and Heiztisch microscope. A Moticam 1000 (1.3 MP) camera supported by software Motic Image Plus 2.0 ML was used to record images and videos.

**Solution NMR spectroscopy**

Solution NMR spectra were recorded on Bruker Avance 500 MHzspectrometer (Bruker-Biospin, Karlsruhe, Germany) and IDP(API), IDP-LYS (1:1) recorded on Bruker Avance 400 MHz spectrometer (Bruker-Biospin, Karlsruhe, Germany).

**Stability under ICH Conditions**

IDP-PIP coamorphous systems were found to be stable for up to 4 months ambient conditions of 40 °C and 75% RH exposure to humidity. Remaining coamorphous systems under 40 °C and 75% RH exposure to humidity after two days it will convert to crystalline form of IDP.

**Solubility measurements**

Powder Dissolution (PD) study was carried out on USP-certified Electrolab TDT-08L dissolution tester (Mumbai, India). The solubility curves of IDP coamorphous solids were measured using the Higuchi and Connor method[48] in pH7 phosphate buffer medium

at 30 °C. Standard curves for all the compounds were obtained spectrophotometrically at their respective $\lambda_{max.}$ The powder dissolution studies of IDP and coamorphous solids was done using IDP 200 mg, IDP-PIP 247 mg, IDP-MPIP 254 mg, IDP–EPIP 262 mg, IDP–BPIP 302 mg IDP–LYS 280 mg and IDP–ARG 295 mg which was directly poured into 500 mL of pH 7 phosphate buffer dissolution medium. The paddle rotation was fixed at 100 rpm and dissolution experiments were continued up to 6h at 37 ºC. At regular intervals, 5 mL of the dissolution medium was withdrawn and replaced by an equal volume of fresh medium to maintain a constant volume and the concentration of the aliquots was determined with proper dilutions from the predetermined standard curves of the respective compounds.

**Diffusion studies**

Diffusion studies were conducted using a glass Franz-type diffusion cell (Model JFDC-07, Orchid Scientific, Maharashtra, India) with a 20 mL volume. The membrane used was a dialysis membrane-135 [dialysis membrane-135, average flat width 33.12 mm, average diameter 23.8 mm, capacity 4.45 mL/cm] obtained from HiMedia, India. The dialysis membrane was placed between the two compartments and held by a stainless steel clamp with an effective mass transfer area of 3.14 $cm^2$. The receptor compartment was filled with PBS solution, and air bubbles were removed. Afterwards, the donor compartment was loaded with pure crystalline API and its coamorphous in equimolar ratio powders and 2 mL of PBS were added. The temperature of diffusion medium was thermostatically maintained at 37±1 °C throughout the experiment and the IDP and its coamorphous was then allowed to stir at 600 rpm and diffuse through the membrane towards the receptor compartment. Aliquots of 1 mL were withdrawn from the receptor compartment at predetermined time periods (15, 30, 45, 60, 90, 120, 150, 180, 240, 270, 300, 360 min) and fresh PBS was added to replenish volume. The determination of IDP diffused was performed by UV spectroscopy (Thermo Scientific EVOLUTION 300 UV-VIS). The cumulative concentration of drug which diffuses into the receptor compartment at each interval was determined taking into consideration the replacement of aliquots with PBS and the dilution derived from the addition of PBS buffer.

## 3.5 References

1. Biradha, K.; and Santra, R. Crystal engineering of topochemical solid state reactions. *Chem. Soc. Rev.*, **2013**, 42, 950–967.

2. Champness, N.; Steed, J. W.; Dastidar, P.; Gale, P.; Ghosh, P. Mukhopadhyay, P.: Vittal, J. J.: Saha, S.; Alessandro, D. M. D.; Ma, S.; Lloyd, G. A.; Clegg, J.; El-Kaderi, H. M.; and Maji, T. K. *Materials. Royal Society of Chemistry*, 2017.
3. Steed, K. M.; and Steed, J. W. Packing Problems: High Z′ Crystal Structures and Their Relationship to Cocrystals, Inclusion Compounds, and Polymorphism. *Chem. Rev.*, **2015**, 115,2895–2933.
4. Desiraju, G. R. *Crystal Engineering: The Design of Organic Solids*, Elsevier, **1989.**
5. Saha, S.; and Desiraju, G. R. Crystal Engineering of Hand-Twisted Helical Crystals. *J. Am. Chem. Soc.*, **2017**, 139, 1975–1983.
6. Blagden, N.; Matas, M. D.; Gavan, P. T.; and York, P. Crystal engineering of active pharmaceutical ingredients to improve solubility and dissolution rates. *Adv. Drug Delivery Rev.*,**2017**, 59, 617–630.
7. Bolla, G.; Nangia, A. Pharmaceutical cocrystals: walking the talk. *Chem. Commun.*, **2016**, *52*, 8342−8360.
8. Roy, R. classification of non-crystalline solids. *J. Non-Crystalline Solids*,**1970**, 3, 33–40.
9. Moorthy, J. N.; Venkatakrishnan, P.; Natarajan, P.; Huang, D.-F.; and Chow, T. J. De Novo Design for Functional Amorphous Materials: Synthesis and Thermal and Light-Emitting Properties of Twisted Anthracene-Functionalized Bimesitylenes. *J. Am. Chem. Soc.*, **2008**, 130, 17320–17333.
10. Roy, R.; Deb, J.; Jana, S. S.; and Dastidar, P. Exploiting Supramolecular Synthons in Designing Gelators Derived from Multiple Drugs. *Chem. Eur. J.*, **2014**, 20, 15320-15324.
11. Dean, P. M.; Turanjanin, J.; Yoshizawa-Fujita, M.; MacFarlane, D. R.; and Scott, J. L. Exploring an Anti-Crystal Engineering Approach to the Preparation of Pharmaceutically Active Ionic Liquids. *Cryst. Growth Des.*, **2009**, 9, 1137–1145.
12. Cherukuvada, S.; and Nangia, A. Eutectics as improved pharmaceutical materials: design, properties and characterization. *Chem. Commun.*, **2014**, 50, 906-923.
13. Hu, Z.-Q.; Wang, A.-M.; Zhang, H.-F. Amorphous Materials. *Modern Inorganic Synthetic Chemistry (Second Ed.)*, **2017**, 641–667.

14. Thakral, S.; Terban, M. W.; Thakral, N. K.; Suryanarayanan, R. Recent advances in the characterization of amorphous pharmaceuticals by X-ray diffractometry. *Adv. Drug Delivery Rev.*, **2016**, 100, 183–193.
15. Zhou, C.; Cui, Q.; McDowell, C.; Seifrid, M.; Chen, X.; Bredas, J-L.; Wang, M.; Huang, F.; and Bazan, G. C. Topological Transformation Reduces Resistance to Crystallization. *Angew. Chem. Int. Ed.*, **2017**, 56, 9318 –9321.
16. Habgood, M.; Lancaster, R. W.; Gateshki, M.; Kenwright, A. M. The Amorphous Form of Salicylsalicylic Acid: Experimental Characterization and Computational Predictability. *Cryst. Growth Des.*, **2013**, 13, 1771–1779.
17. Desiraju, G. R. Supramolecular Synthons in Crystal Engineering—A New Organic Synthesis. *Angew. Chem., Int. Ed. Engl.*, **1995**, 34, 2311-2327.
18. Yu, L. Amorphous pharmaceutical solids: preparation, characterization and stabilization. *Adv. Drug Delivery Rev.*,**2001,** *4*8, 27-42.
19. Healy, A. M.; Worku, Z. A.; Kumar, D.; Madi, A. M. Pharmaceutical solvates, hydrates and amorphous forms: A special emphasis on cocrystals. *Adv. Drug Delivery Rev.*, **2017**, 117, 25–46.
20. Serajuddin, A. T, M. Solid Dispersion of Poorly Water-Soluble Drugs: Early Promises, Subsequent Problems, and Recent Breakthroughs. *J. Pharm. Sci.*, **1999**, 88, 1058–1066.
21. Mitra, A.; Zhu, W.; and Kesisoglou, F. Physiologically Based Absorption Modeling for Amorphous Solid Dispersion Formulations. *Mol. Pharmaceutics*, **2016**, 13, 3206–3215.
22. Frank, D. D.; and Matzger, A. J.; Influence of Chemical Functionality on the Rate of Polymer-Induced Heteronucleation. *Cryst. Growth Des.*, **2017**, 17, 4056-4059.
23. Khandavilli, U. B. R.; Bhogala, B. R.; Maguire, A. R.; and Lawrence, S. E. Symmetry assisted tuning of bending and brittle multi-component forms of probenecid. *Chem. Commun.*, **2017**, 53, 3381–3384.
24. Duggirala, N. K.; Perry, M. L.; Almarsson, Ö.; and Zaworotko, M. J. Pharmaceutical cocrystals: along the path to improved medicines. *Chem. Commun.*, **2016**, 52, 640–655.
25. Berry, D. J.; Steed, J. W. Pharmaceutical cocrystals, salts and multicomponent systems; intermolecular interactions and property based design. *Adv. Drug Delivery Rev.*, **2017,** 117, 3–24.

26. Suresh, K.; Mannava, M. K. C.; and Nangia, A. Cocrystals and alloys of nitazoxanide: enhanced pharmacokinetics. *Chem. Commun.*, **2016**, 52, 4223–4226.
27. Suresh, K.; Mannava, M. K. C.; and Nangia, A. A novel curcumin–artemisinin coamorphous solid: physical properties and pharmacokinetic profile. *RSC Adv.*, **2014**, 4, 58357–58361.
28. Dengale, S. J.; Grohganz, H.; Rades, T.; and Löbmann, K. Recent advances in co-amorphous drug formulations. *Adv. Drug Delivery Rev.*, **2016**, 100, 116–125.
29. Newman, A.; Reutzel-Edens, S. M.; and Zografi, G. Coamorphous Active Pharmaceutical IngredienteSmall Molecule Mixtures: Considerations in the Choice of Coformers for Enhancing Dissolution and Oral Bioavailability. *J. Pharm. Sci.*, **2018**, 107, 5–17.
30. Ueda, H.; Muranushi, N.; Sakuma, S.; Ida, Y.; Endoh, T.; Kadota, K.; and Tozuka, Y. A Strategy for Co-former Selection to Design Stable Co-amorphous Formations Based on Physicochemical Properties of Non-steroidal Inflammatory Drugs. *Pharm. Res.*, **2016**, 33, 1018–1029.
31. Laitinen, R.; Löbmann, K.; Grohganz, H.; Strachan, C.; and Rades, T. Amino Acids as Co-amorphous Excipients for Simvastatin and Glibenclamide: Physical Properties and Stability. *Mol. Pharmaceutics*, **2014**, 11, 2381–2389.
32. Kasten, G.; Grohganz, H.; Rades, T.; and Löbmann, K. Development of a screening method for co-amorphous formulations of drugs and amino acids. *Eur. J. Pharm. Sci.*, **2016**, 95, 28–35.
33. Smrkolj, M.; and Meden, A. Crystal structure of indapamide determined from powered diffraction data. *Pharmazie*, **2006**, 12, 999–1004.
34. Babu, N. J.; Cherukuvada, S.; Thakuria, R.; and Nangia, A. Conformational and Synthon Polymorphism in Furosemide (Lasix). *Cryst. Growth Des.*,**2010**, 10, 1979–1989.
35. Bolla, G.; Nangia, A.; Binary and ternary cocrystals of sulfa drug acetazolamide with pyridine carboxamides and cyclic amides. *IUCrJ*, **2016**. 3, 152–160
36. Sanphui, P.; Devi, V. K.; Clara, D.; Malviya, N.; Ganguly, S.; Desiraju, G. R. Cocrystals of Hydrochlorothiazide: Solubility and Diffusion/Permeability

Enhancements through Drug−Coformer Interactions. *Mol. Pharmaceutics,* **2015**, 12, 1615−1622.

37. Lehmkemper, K.; Kyerematen, S. O.; Heinzerling, O.; Degenhardt, M.; and Sadowski, G. Long-term physical stability of PVP- and PVPVA-amorphous solid dispersions. *Mol. Pharmaceutics,* **2017**, 14, 157−171.
38. Theil, F.; Anantharaman, S.; Kyerematen, S. O.; Lishaut, H. V.; Dreiskuhne, S. H.; Rosenberg, J.; Magerlein, M.; and Woehrle, G. H. Frozen in Time: Kinetically Stabilized Amorphous Solid Dispersions of Nifedipine Stable after a Quarter Century of Storage. *Mol. Pharmaceutics.,* **2017**, 14, 183−192
39. SAINT-Plus, Ver. 6.45; Bruker AXS: Madison, WI, **2003**.
40. Sheldrick, G. M. *SADABS, Program for Empirical Absorption Correction of Area Detector Data*; University of Göttingen: Göttingen, Germany, **1997**.
41. Sheldrick, G. M. *SHELX-97, Program for the Solution and Refinement of Crystal Structures*; University of Göttingen: Göttingen, Germany, **1997**.
42. Bruker SMART, Version 5.625, SHELXTL, Version 6.12. Bruker AXS Inc., Madison, Wisconsin, USA, **2000**.
43. Spek, A. L. PLATON: A Multipurpose Crystallographic Tool; Utrecht University: Utrecht, The Netherlands, ***2002***.
44. PLATON, A Multipurpose Crystallographic Tool; Spek, A. L., Ed.;Utrecht University: Utrecht, The Netherlands, **2002**. Spek, A. L. *J. Appl. Crystallogr*., **2003**, 36, 7−13.
45. Barbour, L. J.X-Seed, Graphical Interface to SHELX-97 and POV-Ray; University of Missouri–Columbia: Columbus, MO, **1999**.
46. Barbour, L. J.X-Seed-A Software Tool for Supramolecular Crystallography. *Supramol. Chem*., **2001**, 1, 189-191.
47. Powder Cell, a program for structure visualization, powder pattern calculation and profile fitting. http://www.ccp14.ac.uk/tutorial/powdcell/.
48. Higuchi, T.; Connors, K. A. Phase-solubility techniques. *Adv. Anal. Chem. Instrum.,* **1965**, 4, 117-212.

## *CHAPTER FOUR*

# Salts and Cocrystal of Etodolac: Advantage of Solubility, Dissolution and Permeability

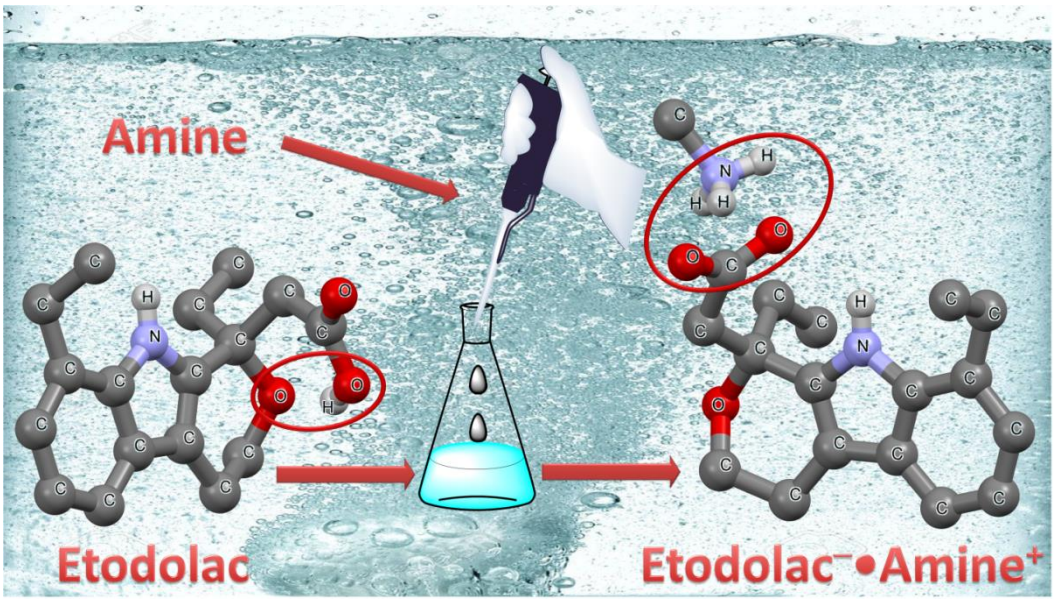


***Etodolac (ETD) is a BCS Class II nonsteroidal anti-inflammatory drug used for the treatment of rheumatoid arthritis. The present study deals with the screening of stable salts of an ETD by using GRAS coformers, due to low solubility and high permeability. All salts and cocrystal were characterized through SXRD and DSC analysis. Among five salts, isopropylamine salt of Etodolac showed highest solubility ≈20 times faster intrinsic dissolution rate than Etodolac in pH 7.0 phosphate buffer.***

## 4.1 Introduction

Among several routes for drug administration, oral pills are the most preferred and commonly employed due to ease of administration, high patient compliance, and affordable costs.[1-3] Oral formulations have flexible and multiple design routes, fewer sterility constraints and longer shelf life compared to suspensions and gels.[4] Over 40% of approved drugs and almost 90% of molecules in development pipeline are poorly soluble or practically insoluble in aqueous media.[5,6] Crystal engineering can guide in improving the solubility and stability of drugs through solid form screen of new chemical entities (NCE) and active pharmaceutical ingredients (API) by tweaking the structures of salts, cocrystals and polymorphs.[7-12] Screening of active pharmaceutical ingredients (APIs) for polymorphs, salts and cocrystals has becomes an integral part of pharmaceutical development post the discovery phase.[13-15] Recent studies show that new drug discovery must partner with pharmaceutical development to achieve therapeutic benchmarks and market economy,[16,17] whereas solid form modification of existing drugs is a low hanging fruit.[18,19] The limited quantity of API available in early stages of R&D compels the scientist to make strategic decisions with the limited structural data and supply of material.[20-22] It is crucial to select the best possible formulation with available outcomes, so that one can solve the challenge of drug attrition due to poor pharmacokinetics (low solubility), toxicity (higher dosage), and limited efficacy (low bioavailability).[23,24] Such formulations under several restrictions generate the opportunity to do further modification (i.e. salts, cocrystals and polymorphs) for existing drugs which may be open for generic competition.[25] Almost 50% of the therapeutic drugs are administered in the form of salts which indicate that salt forms of APIs have considerable effect on the quality, safety, and performance of drugs.[26] Sodium cation is the most commonly used counter ion for acidic APIs especially the carboxylic acid functional group.[26,27] However, intake of sodium ion is restricted in treatment of hypertension and diabetes which limits the therapeutic benefits of such salts.[28] This limitation encourages the discovery of substitute counter ions without any adverse safety implications and potential toxicity. The solid-state properties of saline drugs are generally controlled by the nature of the counter ion but scantiness of literature on such work makes it difficult to establish a clear correlation.[29-32]

This work deals with the salts and cocrystal screening of the anti-inflammatory drug Etodolac (**ETD**), which is a member of the pyranocarboxylic acid group of nonsteroidal anti-inflammatory drugs (NSAIDs).[33] **ETD** was approved for medical use in 1985 and then

by the US-FDA in January 1991. A limitation of Etodolac (brand name Lodine)[34] is high dosage and multiple administrations, making it difficult for patient compliance and convenience. For example, the prescribed dose is 300 mg orally 2 to 3 times a day, or 400 mg twice daily, or 500 mg twice. A typical 400 mg tablet / caplet is shown in Figure 4.1. Researchers have tried to improve the solubility of BCS Class II drug **ETD** through solid dispersions, self-emulsifying systems, and inclusion complexes with cyclodextrins.[35-37] There are a few reports on solubility improvement of salts and cocrystals of **ETD**.[38,39] Surprisingly, the Cambridge Structural Database (CSD)[40] analysis shows only one structure of **ETD** (Refcode: DONSOO)[41] and does not contain its salt or cocrystal structure (data was retrieved on 12-01-2020, CSD version 5.40). Crystal structure analysis of salts and cocrystals provides insight into understanding the supramolecular interactions in the crystal lattice and thereby in rationally tuning the physicochemical properties of APIs (crystal engineering).[10,11]


**Figure 4.1:** Typical Etodolac tablet of 400 mg is 18 x 8 mm in size. Image extracted from Ref 34.

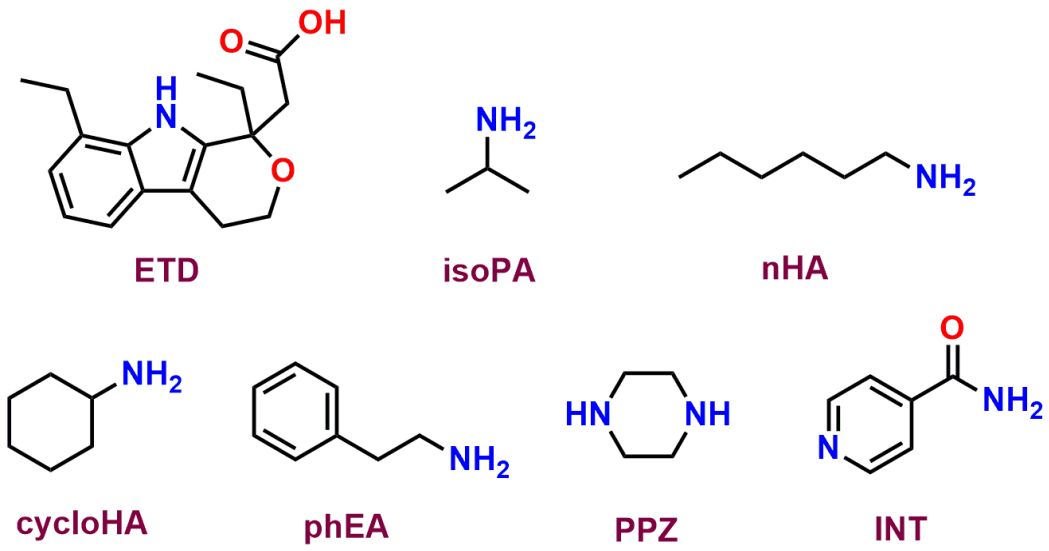


**Figure 4.2:** Chemical Structure of Etodolac and Coformers

## 4.2 Results and Discussion

The supramolecular synthons analysis of **ETD** showed a carboxyl group that could form either salt or cocrystals using heterosynthons. pKa analysis shows that **ETD** will form salts cocrystals or salts (rule of 3)[42-44] with aliphatic amines and cocrystals with amides or pyridines synthons (Table 4.1).[45] Cocrystal preparation was done through mechanical grinding followed by crystallization in a range of protic and aprotic solvents. It was observed in our experiments that either one of the components crystallized out or formed a sticky mass. Isonicotinamide (**INT**) CCF afforded **ETD•INT** cocrystal in acetonitrile solvent. In case of amines and pyridine CCFs screening, single crystal X-ray quality crystals were grown for the salts **ETD$^{-}$•isoPA$^{+}$**, **ETD$^{-}$•nHA$^{+}$**, **ETD$^{-}$•cycloHA$^{+}$**, **ETD$^{-}$•phEA$^{+}$**, and **2(ETD)$^{-}$•PPZ$^{2+}$** in acetonitrile-methanol mixture (2:1) of solvents at room temperature by slow evaporation of the solvents.

**Table 4.1:** pKa values of ETD and coformers.[45]

| Compounds Name | pKa in water | ΔpKa between ETD and Coformer |
|---|---|---|
| Etodolac | 4.73 | ---- |
| Isopropyl amine | 10.43 | 5.70 |
| n-Hexyl amine | 10.21 | 5.48 |
| cyclo-Hexyl amine | 10.45 | 5.72 |
| Phenethylamine | 9.79 | 5.06 |
| Piperazine | 9.56, 5.18 | 4.83, 0.45 |
| Isonicotinamide | basic 3.45, acidic 13.71 | -1.28 |

## 4.2.1 Crystal Structure Description

The salts and cocrystal preparation of ETD were attempted with a wide range of generally recognized as safe (GRAS) coformers. The salts of ETD were easily prepared with the aliphatic amines (i.e.1°, 2°, and 3°–amines) because of sufficiently high p*K*a values of amines.[45] Most of the ETD salts of amines were hygroscopic in nature and did not produce any stable crystal under our laboratory environment. The reported ETD salts of primary amines (i.e. isoPA, nHA, cycloHA and phEA) and PIP were stable under ambient conditions and no hydrate/solvate was observed either during crystallization or storage. All ETD salts were formed due to the transfer of a proton from carboxylic group of ETD to the nitrogen atoms of amine groups. Therefore, each salt of mono amine has an ammonium cation and a carboxylate anion. In the crystal packing of salts, ammonium cations and ETD anions were stabilized by forming the supramolecular chains followed by their cross linking through N–H···O interactions. In the supramolecular array, ammonium cations and ETD anions were arranged in alternate fashion. However, each salt have their specific higher graph sets which are shown in Figure 4.3-4.9.[46] Crystallographic parameters and hydrogen bonding parameters are summarized in Table 4.2-4.3.

**ETD:** The purchased ETD from the market was crystallized without further purification and crystals obtained from acetonitrile solvent were cube shape. Single crystal X-ray diffraction showed orthorhombic crystal system with the space group *Pbca*. The crystal packing analysis showed that carboxyl group of ETD formed an intramolecular hydrogen bonding through O2–H2···O3 contacts that can be represented by $S_1^1(6)$ graph-set (Figure 4.3, Table 4.3).[46] The crystal packing was stabilized by strong hydrogen bonds N1–H1···O1 that were identified as unitary graph-set $C_1^1(7)$ and a weak interaction C2–H2B···O1 (Figure 4.3, Table 4.3).

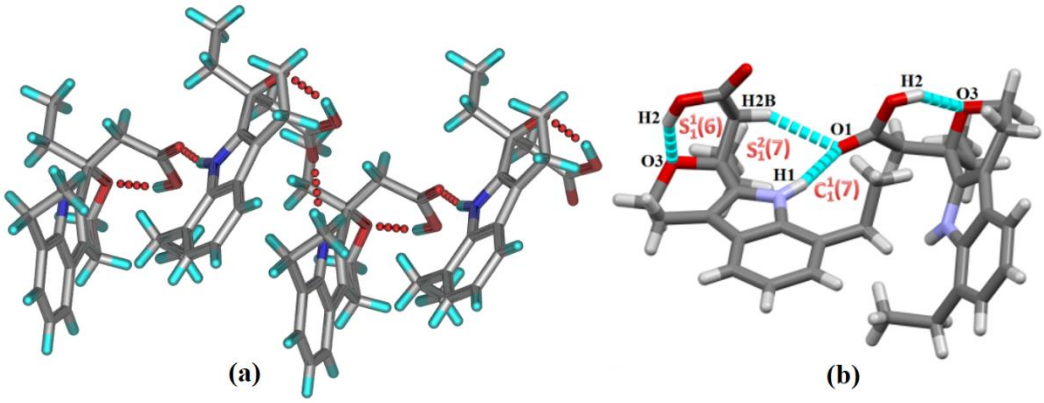


**Figure 4.3:** (a) ETD molecules are connected through O-H···O and N-H···O synthon followed by 1-D chain motif (b) supramolecular interactions in the crystal structure of ETD molecules graph set notation.

**ETD$^-$-isoPA$^+$ (2:2) Salt:** crystallization of ETD and isoPA in a 2:2 ratio from $CH_3CN$ and MeOH mixture this is crystallized in the monoclinic space group $P2_1/c$ with Z=8. The asymmetric unit consists of a two molecules of ETD and two molecules of isoPA. Although, intramolecular hydrogen bonding between an oxygen atom of carboxylate and hydrogen atom of pyrrole N-H of ETD was observed in every salt, which was represented by $S_1^1(7)$ graph-set. The supramolecular arrangement in the crystal structure of ETD$^-$-isoPA$^+$ showed an $R_4^3(12)$ graph-set, which was formed among two isoPA$^+$ and two ETD$^-$ (Figure 4.4, Table 4.3). Notwithstanding the alternate positions of the ions in $R_4^3(12)$ graph-set, one side interaction showed the bifurcated N–H···O interactions on carboxylate oxygen (i.e. H3A···O6 and H4B···O6), however, other side, one ammonium cation interacted with carboxylate oxygen and other ammonium cation interacted with the oxygen atom of pyran ring of the same ETD.

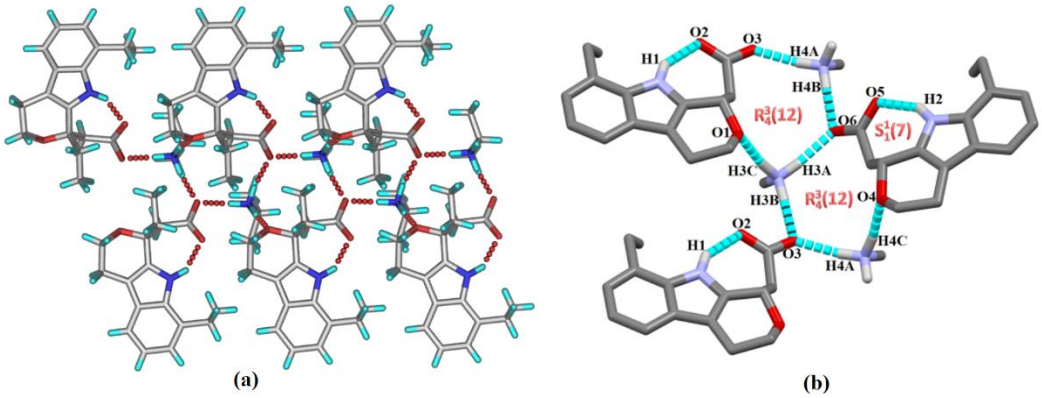

**Figure 4.4:** (a) Two ETD molecules are connected through N-H···O synthon with two isoPA molecules forms $R_4^3(12)$ ring motif (b) supramolecular interactions in the crystal structure of ETD-isoPA molecules graph set notation.

**ETD$^-$-nHA$^+$ (2:2) Salt:** ETD-nHA salt were crystallized in the monoclinic space group $P2_1/c$ with Z=8 and ETD acidic proton transfer to the n-Hexylamine (nHA). In the crystal structure of ETD$^-$-nHA$^+$ (Figure 4.5), the nHA$^+$ and ETD$^-$ are arranged in an alternate fashion with symmetrical and unsymmetrical supramolecular interactions that are represented as $R_4^2(8)$ and $R_4^3(10)$ graph sets. Interestingly, the asymmetric unit cell of ETD$^-$-nHA$^+$ had two ETD$^-$ and two nHA$^+$, where one nHA$^+$ showed *anti*-conformation on all C-C bonds but other nHA$^+$ showed *gauche*-conformation for one of the C-C bonds. Unlike ETD$^-$-isoPA$^+$, the two ETD$^-$ molecules in ETD$^-$-nHA$^+$ showed different orientation of carboxylate group. Figure 4.5, clearly showed that carboxyl group in one of the ETD$^-$ formed intramolecular hydrogen bond with hydrogen atom of the pyrrole N-H which is denoted as by $S_1^1(7)$ graph-set, however, in other ETD$^-$ carboxyl group was away from the pyrrole N-H (*N.B.* both pyrrole N-H are forming bifurcated hydrogen bond at the same oxygen atom O3 of a carboxylate group). Additionally, ETD$^-$-nHA$^+$ shows $R_1^2(6)$, $R_3^2(7)$ and $R_3^3(13)$ graph sets, which further stabilizes the crystal packing.

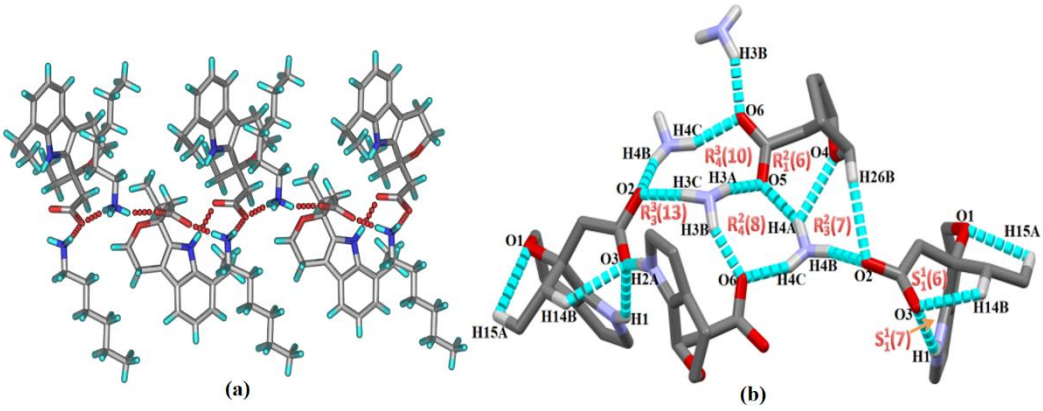


**Figure 4.5:** (a) Two ETD molecules are connected through N-H···O hydrogen bond interaction with two nHA molecules (b) supramolecular synthons in the crystal structure of ETD$^-$-nHA$^+$ molecule.

**ETD$^-$-cycloHA$^+$ (2:2) Salt:** The salt was obtained in acetonitrile and methanol equimolar ratio crystallized in the triclinic space group *P-1* with Z=4. Intramolecular hydrogen bonding between an oxygen atom of carboxylate and hydrogen atom of pyrrole N-H of

ETD was observed in this salt, which is represented by $S_1^1(7)$ graph-set. The higher level supramolecular aggregations in ETD$^-$-cycloHA$^+$ were constructed by alternate positioning of ETD$^-$ and cycloHA$^+$ that are represented by $R_4^4(12)$ and $R_4^2(8)$ graph sets (Figure 4.6).

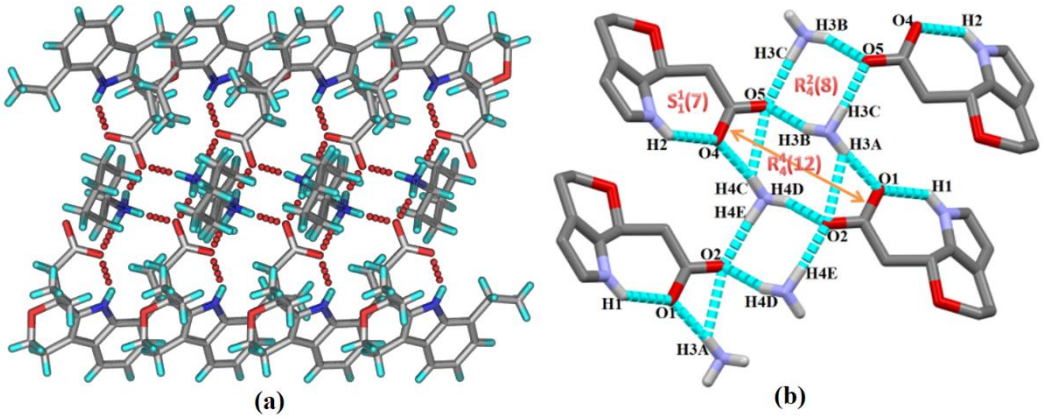


**Figure 4.6:** (a) Two ETD molecules are connected through N-H···O hydrogen bond interaction with two cycloHA molecules (b) supramolecular synthons in the crystal structure of ETD$^-$-cycloHA$^+$ molecule.

**ETD$^-$-phEA$^+$ (2:2) Salt:** The salt was prepared by taking ETD and PhEA in 1:1 stoichiometric ratios and the resulting material was kept for crystallization in methanol and acetonitrile solvent after 3-4 days, good quality diffraction crystals were obtained. The crystal structure asymmetric unit contains two molecules of ETD and two molecules of phEA, crystallized in the monoclinic space group *C2/C* with Z=16. Unlike other ETD salts of 1°-amines, ETD$^-$•phEA$^+$ showed that one of the two independent $-NH_3^+$ group of phEA$^+$ in asymmetric unit cell formed three N–H···O hydrogen bonds, however another formed only two N–H···O hydrogen bonds and remaining one was directed towards interfacial C═C centroid of pyran ring and pyrrole ring of ETD which showed a strong C–H···π interaction with D···A = 3.31 Å, H···A = 2.40 Å and ∠D─H···A = 174° (Figure 4.7, Table 4.3).

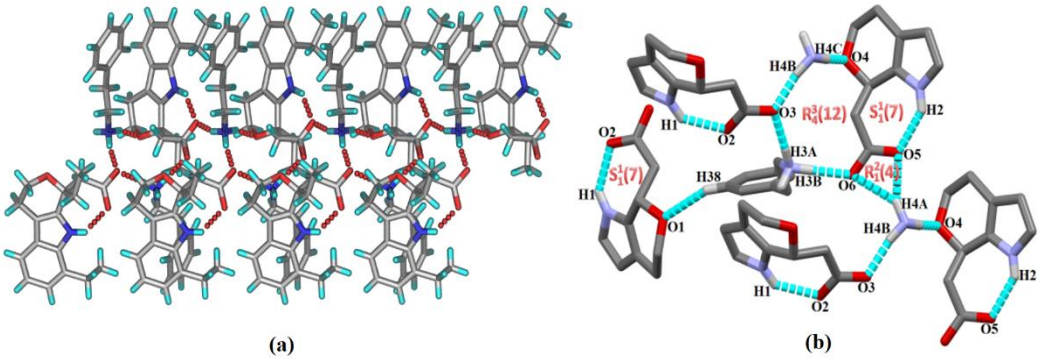


**Figure 4.7:** (a) Two ETD molecules are connected through N-H···O hydrogen bond interaction with two phEA molecules (b) supramolecular synthons in the crystal structure of $ETD^{-}$-$phEA^{+}$ molecule.

**$ETD^{-}$-$PPZ^{+}$ (2:1) Salt:** The Salt was obtained by taking ETD and PPZ in 1:0.5 stoichiometric ratios and the resulting product was crystallized in methanol and acetonitrile solvent equimolar mixture after 3-5 days, good quality single crystals were formed that was represented as $2(ETD)^{-}\bullet PPZ^{2+}$. The salt structure was refined and solved in triclinic space group *P-1* with Z=2. The supramolecular analysis showed that both nitrogen atoms of PPZ were protonated and formed N–H···O hydrogen bonding with four neighboring oxygen atoms of carboxylate groups in the ETD. In the crystal lattice, $PPZ^{2+}$ was in chair conformation where 1,4-equotorial hydrogen atoms formed N–H···O hydrogen bonding with in-plane oxygen atoms of $ETD^{+}$, however, 1,4-axial hydrogen atoms cross-linked the vertical layers (Figure 4.8). The supramolecular aggregate which stabilized the crystal three dimensional net was presented by $R_4^4(18)$ graph-set.

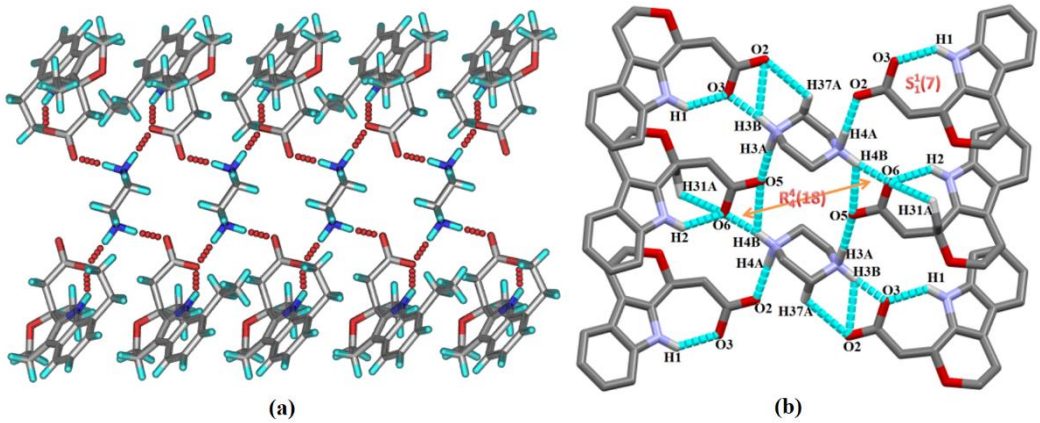

**Figure 4.8:** (a) Two ETD molecules are connected through N-H···O hydrogen bond interaction with one PPZ molecule (b) supramolecular synthons in the crystal structure of $ETD^{-}$-$PPZ^{+}$ molecule.

**ETD-INT (1:1) Cocrystal:** Attempts to grow the X-ray quality single crystals of ETD with various amide and pyridines GRAS coformers in several solvents were unsuccessful in our laboratory conditions, except ETD•INT which was grown in acetonitrile solvent and characterized through single crystal X-ray diffraction data. The crystal structure was refined and solved in monoclinic space group *P21/C* with Z=4. To our great delight, INT unveiled both amide and pyridine synthon interactions with ETD in the solid form of ETD•INT as shown in Figure 4.9. Supramolecular aggregation of ETD and INT in the cocrystal lattice showed a higher level graph set $R_4^4(22)$ which was constructed with N2–H2B···O2 and O3–H3···N3 hydrogen bonding. Here N2–H2B···O2 hydrogen bonding was between amide N–H and acid C═O, however, O3–H3···N3 was acid-pyridine hydrogen bonding. Contrary to amine salts of ETD, ETD•INT did not show $S_1^1(7)$ graph-set. However, pyrrole N-H formed strong hydrogen bonding with carbonyl oxygen of INT and one of the hydrogen atoms of the INT was hydrogen bonded with the lone pair of carboxyl oxygen atom of C-O-H group of same ETD. This supramolecular interaction formed a ring of $R_2^2(11)$ graph set.

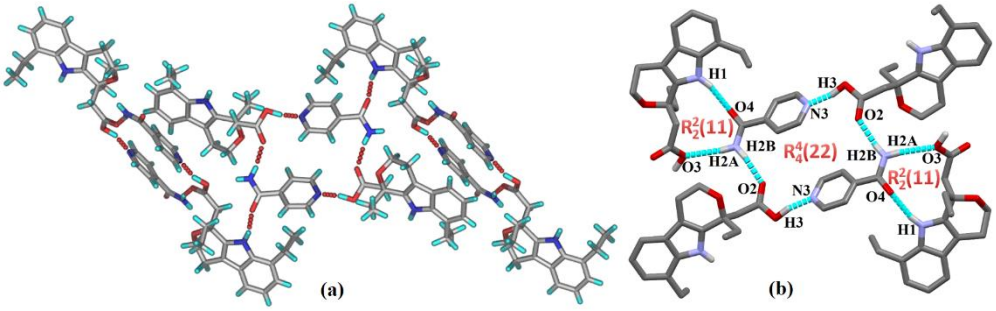


**Figure 4.9:** (a) One ETD molecules are connected through N-H···O and O-H···N hydrogen bond interaction with INT molecules (b) supramolecular synthons in the crystal structure of ETD-INT molecule.

**Table 4.2:** Crystallographic parameters of Etodolac Salts and cocrystals.

| | **ETD** | **$ETD^{-}$-isoP$A^{+}$** | **$ETD^{-}$-nH$A^{+}$** | **$ETD^{-}$-cycloH$A^{+}$** |
|---|---|---|---|---|
| **Empirical Formula** | $C_{17}H_{21}NO_3$ | $C_{17}H_{20}NO_3 \cdot C_3H_{10}N$ | $C_{17}H_{20}NO_3 \cdot C_6H_{16}N$ | $C_{17}H_{20}NO_3 \cdot C_6H_{14}N$ |

| **Formula weight** | 287.35 | 346.46 | 388.54 | 386.52 |
|---|---|---|---|---|
| **Crystal System** | Orthorhombic | Monoclinic | Monoclinic | Triclinic |
| **Space Group** | *Pbca* | *$P2_1/c$* | *Cc* | *P-1* |
| **T (K)** | 100 | 100 | 100 | 100 |
| ***a* (Å)** | 8.5463 (2) | 20.1252 (8) | 16.6401 (11) | 11.2693 (3) |
| ***b* (Å)** | 18.5894 (5) | 7.9084 (3) | 27.1785 (11) | 13.1319 (4) |
| ***c* (Å)** | 18.9481 (5) | 24.4255 (11) | 10.5425 (5) | 15.9168 (5) |
| ***α* (°)** | 90 | 90 | 90 | 91.890 (1) |
| ***β* (°)** | 90 | 94.264 (2) | 101.074 (2) | 106.570 (1) |
| ***γ* (°)** | 90 | 90 | 90 | 106.399 (1) |
| ***V* (Å$^3$)** | 3010.30 (13) | 3876.8 (3) | 4679.1 (4) | 2149.26 (11) |
| ***$D_{calc}$* (g cm$^{-3}$)** | 1.268 | 1.187 | 1.103 | 1.195 |
| ***μ (mm−1)*** | 0.09 | 0.08 | 0.07 | 0.08 |
| **Z** | 8 | 8 | 8 | 4 |
| ***F*(000)** | 1232 | 1504 | 1696 | 840 |
| **$\Delta\rho_{max}$, $\Delta\rho_{min}$ (e Å$^{-3}$)** | 0.53, −0.25 | 0.48, −0.38 | 0.52, −0.31 | 0.50, −0.43 |
| **h range** | -13 → 13 | -29 → 29 | -23 → 23 | -17 → 16 |
| **k range** | -28 → 28 | -11 → 9 | -38 → 38 | -20 → 20 |
| **l range** | -26 → 29 | -35 → 35 | -11 → 15 | -24 → 24 |
| **measured reflections** | 102447 | 128567 | 28463 | 147412 |
| **independent reflections** | 5756 | 12934 | 10707 | 17162 |
| **Reflections with I> 2σ(I)** | 5256 | 10355 | 4668 | 10787 |
| **$R_{int}$** | 0.039 | 0.076 | 0.144 | 0.074 |
| ***$R_1$*[*I* >2σ(*I*)]** | 0.038 | 0.076 | 0.088 | 0.052 |
| ***w*$R_2$ (all)** | 0.105 | 0.210 | 0.242 | 0.172 |
| **Goodness of fit** | 1.07 | 1.20 | 1.01 | 1.03 |
| **X-ray diffractometer** | BRUKER APEX | BRUKER APEX | BRUKER APEX | BRUKER APEX |

| | **$ETD^-$-$phEA^+$** | **$2(ETD)^-$-$PPZ^{2+}$** | **ETD-INT** |
|---|---|---|---|
| **Empirical Formula** | $C_{17}H_{20}NO_3 \cdot C_8H_{12}N$ | $2(C_{17}H_{20}NO_3) \cdot C_4H_{12}N_2$ | $C_{17}H_{21}NO_3 \cdot C_6H_6N_2O$ |
| **Formula weight** | 408.52 | 660.83 | 409.47 |

| **Crystal System** | Monoclinic | Triclinic | Monoclinic |
|---|---|---|---|
| **Space Group** | *C2/c* | *P-1* | $P2_1/c$ |
| **T (K)** | 100 | 100 | 100 |
| ***a* (Å)** | 54.319 (8) | 10.8896 (7) | 8.9580 (7) |
| ***b* (Å)** | 7.7714 (11) | 11.3187 (6) | 11.8073 (11) |
| ***c* (Å)** | 21.372 (3) | 14.9446 (9) | 19.8402 (18) |
| ***α* (°)** | 90 | 99.854 (2) | 90 |
| ***β* (°)** | 101.532 (4) | 97.357 (2) | 90.114 (3) |
| ***γ* (°)** | 90 | 102.548 (2) | 90 |
| ***V* (Å$^3$)** | 8840 (2) | 1745.15 (18) | 2098.5 (3) |
| **$D_{calc}$ (g cm$^{-3}$)** | 1.228 | 1.258 | 1.296 |
| ***μ (mm−1)*** | 0.08 | 0.09 | 0.09 |
| **Z** | 16 | 2 | 4 |
| ***F*(000)** | 3520 | 712 | 872 |
| **$\Delta\rho_{max}$, $\Delta\rho_{min}$ (e Å$^{-3}$)** | 0.23, −0.24 | 0.41, −0.37 | 0.36, −0.38 |
| **h range** | -53 → 53 | -17 → 17 | -13 → 13 |
| **k range** | -7 → 7 | -17 → 17 | -17 → 17 |
| **l range** | -21 → 21 | -23 → 23 | -30 → 26 |
| **measured reflections** | 43151 | 102299 | 26374 |
| **independent reflections** | 4440 | 13930 | 7711 |
| **Reflections with I> 2σ(I)** | 3628 | 8291 | 3936 |
| **$R_{int}$** | 0.084 | 0.077 | 0.125 |
| **$R_1[I > 2\sigma(I)]$** | 0.052 | 0.056 | 0.068 |
| **$wR_2$ (all)** | 0.124 | 0.180 | 0.178 |
| **Goodness of fit** | 1.12 | 1.03 | 1.00 |
| **X-ray diffractometer** | BRUKER APEX | BRUKER APEX | BRUKER APEX |

**Table 4.3:** Hydrogen bonding parameters in Salts and Cocrystals of Etodolac

| **D−H···A** | **H···A (Å)** | **D···A (Å)** | **D−H···A (deg)** | **symmetry code** |
|---|---|---|---|---|
| **ETD** | | | | |
| N1–H1···O1 | 1.99 | 2.8455(1) | 164 | 1/2+x,y,1/2-z |
| O2–H2···O3 | 1.77 | 2.6086(1) | 151 | Intramolecular |
| C2–H2B···O1 | 2.43 | 3.3426(1) | 153 | 1/2+x,y,1/2-z |
| **$ETD^-$-$isoPA^+$** | | | | |

| | | | | |
|---|---|---|---|---|
| N1–H1···O2 | 1.97 | 2.7789(1) | 149 | Intramolecular |
| N2–H2···O5 | 1.90 | 2.7340(1) | 148 | Intramolecular |
| N3–H3A···O6 | 1.85 | 2.7774(1) | 172 | x,1/2-y,1/2+z |
| N3–H3B···O3 | 1.76 | 2.7262(1) | 175 | x,3/2-y,1/2+z |
| N3–H3C···O1 | 1.80 | 2.8143(1) | 169 | x,1/2-y,1/2+z |
| N4–H4A···O3 | 1.86 | 2.7812(1) | 168 | 1-x,1-y,-z |
| N4–H4B···O5 | 2.56 | 3.2048(1) | 126 | 1-x,1-y,-z |
| N4–H4B···O6 | 1.81 | 2.7471(1) | 169 | 1-x,1-y,-z |
| N4–H4C···O4 | 1.93 | 2.8854(1) | 169 | 1-x,-y,-z |
| **$ETD^{-}$-$nHA^{+}$** | | | | |
| N1–H1···O3 | 2.23 | 2.8917(2) | 131 | Intramolecular |
| N2–H2A···O3 | 2.04 | 2.9090(2) | 168 | 1/2+x,1/2-y,-1/2+z |
| N3–H3A···O5 | 1.90 | 2.7917(2) | 168 | 1/2+x,-1/2+y,z |
| N3–H3B···O6 | 1.85 | 2.7044(2) | 155 | 1/2+x,1/2-y,1/2+z |
| N3–H3C···O2 | 1.81 | 2.7129(2) | 169 | 1+x,y,z |
| N4–H4A···O4 | 2.36 | 3.0059(2) | 128 | -1/2+x,1/2-y,-1/2+z |
| N4–H4A···O5 | 1.95 | 2.7349(2) | 143 | -1/2+x,1/2-y,-1/2+z |
| N4–H4B···O2 | 1.87 | 2.7546(2) | 163 | x,y,z |
| N4–H4C···O6 | 1.94 | 2.8083(2) | 159 | -1/2+x,-1/2+y,z |
| C14–H14B···O3 | 2.44 | 3.0700(2) | 121 | Intramolecular |
| C15–H15A···O1 | 2.51 | 2.8439(2) | 100 | Intramolecular |
| C26–H26B···O2 | 2.55 | 3.4403(2) | 149 | 1/2+x,1/2-y,1/2+z |
| C29–H29B···O2 | 2.49 | 3.4682(2) | 168 | 1/2+x,1/2-y,-1/2+z |
| C33–H33A···O3 | 2.59 | 3.5020(2) | 154 | 1/2+x,1/2-y,-1/2+z |
| **$ETD^{-}$-$cycloHA^{+}$** | | | | |
| N1–H1···O1 | 2.09 | 2.8001(1) | 137 | Intramolecular |
| N2–H2···O4 | 2.10 | 2.8140(1) | 137 | Intramolecular |
| N3–H3A···O1 | 1.88 | 2.7883(1) | 175 | 1-x,1-y,1-z |
| N3–H3A···O2 | 2.51 | 3.1312(1) | 126 | 1-x,1-y,1-z |
| N3–H3B···O5 | 1.95 | 2.8304(1) | 162 | x,-1+y,z |
| N3–H3C···O5 | 1.82 | 2.7236(1) | 170 | 2-x,1-y,1-z |
| N4–H4C···O4 | 1.88 | 2.7857(1) | 171 | 1-x,1-y,1-z |
| N4–H4C···O5 | 2.47 | 3.1343(1) | 130 | 1-x,1-y,1-z |
| N4–H4D···O2 | 1.93 | 2.8139(1) | 164 | x,-1+y,z |
| N4–H4E···O2 | 1.81 | 2.7137(1) | 172 | 1-x,1-y,1-z |
| C4–H4A···O1 | 2.58 | 3.1530(1) | 118 | Intramolecular |
| C31–H31A···O4 | 2.59 | 3.1689(1) | 119 | Intramolecular |
| **$ETD^{-}$-$phEA^{+}$** | | | | |
| N1–H1···O2 | 2.04 | 2.7335(4) | 135 | Intramolecular |
| N2–H2···O5 | 2.02 | 2.7541(4) | 141 | Intramolecular |
| N3–H3A···O3 | 1.79 | 2.6926(4) | 172 | x,-1+y,z |
| N3–H3B···O6 | 1.81 | 2.7236(4) | 177 | x,y,z |
| N4–H4A···O5 | 2.03 | 2.8535(4) | 150 | x,-1+y,z |
| N4–H4A···O6 | 2.33 | 3.0858(5) | 140 | x,-1+y,z |
| N4–H4B···O3 | 1.82 | 2.7221(4) | 169 | x,-1+y,z |
| N4–H4C···O4 | 2.02 | 2.8916(4) | 161 | x,y,z |
| C37–H37···O6 | 2.59 | 3.5251(5) | 169 | x,1-y,1/2+z |

| | | | | |
|---|---|---|---|---|
| C38–H38···O1 | 2.49 | 3.3417(5) | 149 | x,1-y,1/2+z |
| **2(ETD)$^{-}$-PPZ$^{2+}$** | | | | |
| N1–H1···O3 | 2.00 | 2.7760(2) | 138 | Intramolecular |
| N2–H2···O6 | 2.07 | 2.8114(2) | 138 | Intramolecular |
| N3–H3A···O5 | 1.75 | 2.6710(2) | 169 | x,y,z |
| N3–H3B···O2 | 2.56 | 3.2117(2) | 124 | x,y,z |
| N3–H3B···O3 | 1.67 | 2.6459(2) | 175 | x,y,z |
| N4–H4A···O2 | 1.76 | 2.7008(2) | 167 | -x,-y,1-z |
| N4–H4B···O5 | 2.47 | 3.1239(2) | 124 | -x,1-y,1-z |
| N4–H4B···O6 | 1.69 | 2.6643(2) | 172 | -x,1-y,1-z |
| C31–H31A···O6 | 2.52 | 3.0539(2) | 113 | Intramolecular |
| C37–H37A···O2 | 2.58 | 3.1700(2) | 118 | x,y,z |
| **ETD-INT** | | | | |
| N1–H1···O4 | 1.99 | 2.8333(3) | 165 | 1-x,-1/2+y,1/2-z |
| N2–H2A···O3 | 2.36 | 3.2152(3) | 173 | 1-x,1/2+y,1/2-z |
| N2–H2B···O2 | 1.97 | 2.8187(3) | 167 | x,y,z |
| O3–H3···N3 | 1.61 | 2.5934(2) | 160 | 1-x,-y,1-z |
| C3–H3A···O1 | 2.36 | 3.2188(3) | 153 | x,1/2-y,-1/2+z |
| C15–H15C···O1 | 2.58 | 2.9345(3) | 102 | Intramolecular |

## 4.2.2 Powder X-ray Diffraction

Active pharmaceutical solid forms identification and bulk phase purity using PXRD is a liable characterization technique for standard practice in pharmaceutics through their unique diffraction lines. Herein, etodolac slat, cocrystal solid forms determined through their unique diffraction patterns (peak positions and intensities which are different from that of the starting components demonstrating new solid forms (Figure 4.10a). On the other hand, etodolac (ETD) multicomponent solid forms (cocrystal/salts) prepared in this work exhibit unique diffraction pattern overlay show excellent match of the experimental PXRD with the calculated pattern from the X-ray crystal structure (Figure 4.10b).

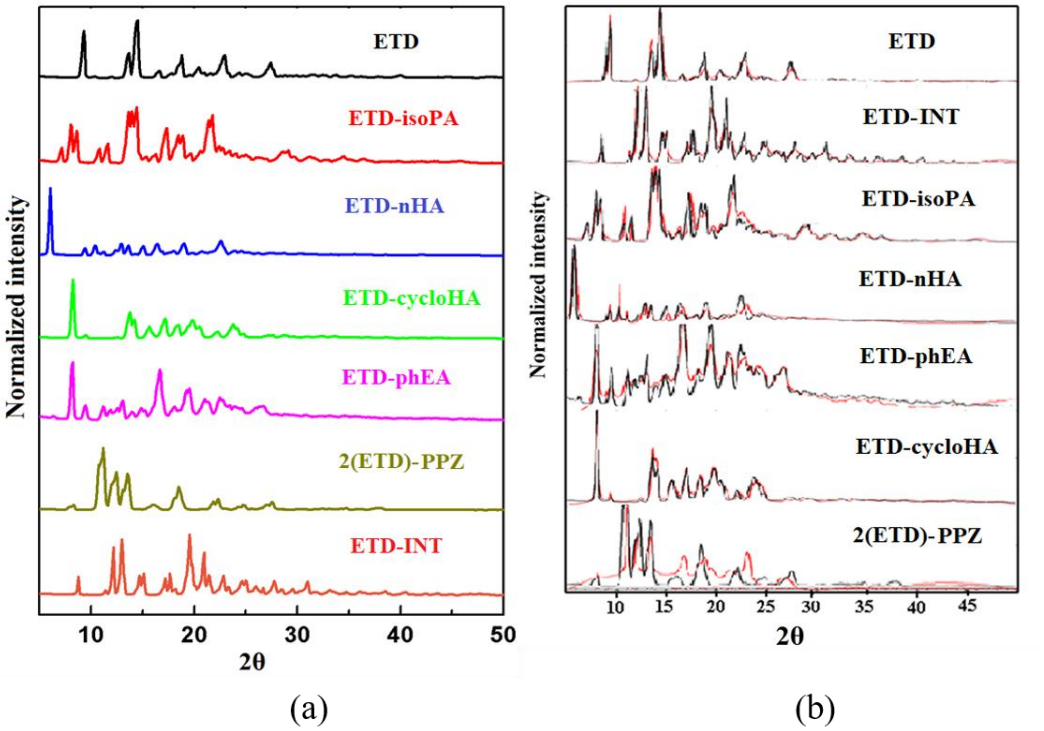


**Figure 4.10: (a)** PXRD pattern of etodolac salts, cocrystals and ETD. (b) Overlay of experimental PXRD (black) of ETD salts, cocrystal match with the calculated lines from the crystal structure (red).

## 4.2.3 Thermal Analysis

DSC thermograms of **ETD**, **ETD$^{-}$•nHA$^{+}$** and **2(ETD)$^{-}$•PPZ$^{2+}$** (Figure 4.11 Table 4.4) showed a sharp melting endotherm at 150 °C, 139 °C and 208 °C, respectively, indicating thermal stability. The melting endotherms are broad and unsymmetrical with onset, peak and endset values at 141 °C, 152 °C, and 157 °C, for **ETD$^{-}$•isoPA$^{+}$**, and 186 °C, 194 °C, and 197 °C, for **ETD$^{-}$•cycloHA$^{+}$**, suggesting that these solids melt with decomposition. The DSC thermogram of **ETD$^{-}$•phEA$^{+}$** showed a small endotherm at 152 °C followed by a sharp melting endotherm at 160 °C. Since crystallographic analysis did not show any solvation or hydration of **ETD$^{-}$•phEA$^{+}$**, the endotherm at 152 °C could be due to a solid-solid phase transition. To establish a relation between two solid forms a fresh sample of **ETD$^{-}$•phEA$^{+}$** was heated up to 155 °C followed by cooling down to 30 °C. There were no crystallization exotherm observed during cooling cycle. However, second heating did not show the solid-solid transition endotherm at 152 °C but only melting endotherm at 160 °C was observed (Figure 4.12). This shows a monotropic relation between the two solid forms.[47] A low enthalpy of transition ($\Delta H \approx 16$ J/g) as well as overlapping of transition

and melting endotherms indicate that the metastable and stable forms are structurally similar except probably conformational adjustment. For **ETD•INT** the onset and endset peaks are at 165 °C, 167 °C, and 169 °C (Figure 4.11, Table 4.4).

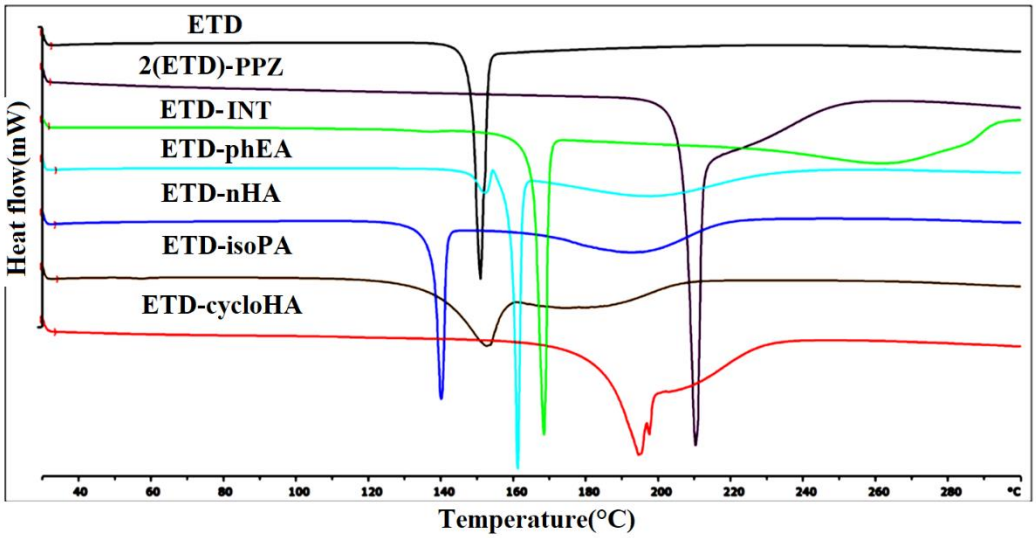


**Figure 4.11:** DSC endotherms of **ETD** cocrystal salts.

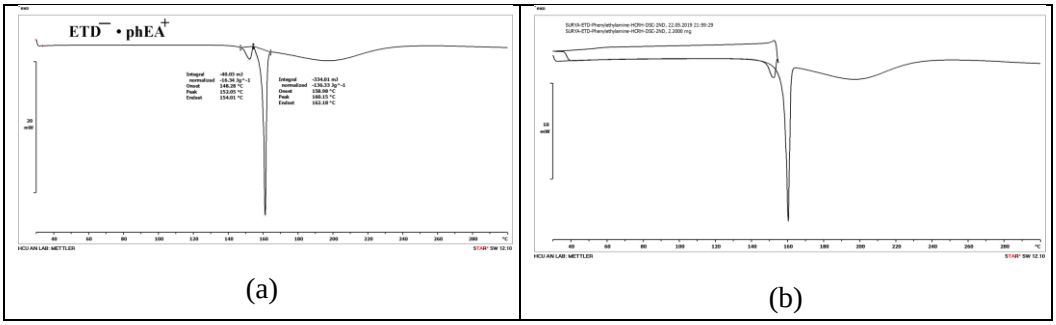


(a) (b)

**Figure 4.12: (a)** DSC thermogram of **ETD⁻•phEA⁺**. (b) DSC thermogram of **ETD⁻•phEA⁺** for two heating cycles at the heating rate of 10 °C $min^{-1}$. First heating was done up to 155 °C followed by cooling down to 30 °C and subsequently second heating was done up to 300 °C.

**Table 4.4:** Melting point of ETD, salts and cocrystals.

| **Drug/Salts/ Cocrystals** | **Melting point of cocrystal/salt (°C)** |
|---|---|
| ETD | 150 ± 2 |
| $ETD^{-}$•$isoPA^{+}$ | 152 ± 2 |
| $ETD^{-}$•$nHA^{+}$ | 139 ± 2 |
| $ETD^{-}$•$cycloHA^{+}$ | 194 ± 2 |
| $ETD^{-}$•$phEA^{+}$ | 160 ± 2 |
| $2(ETD)^{-}$•$PPZ^{2+}$ | 208± 2 |
| ETD-INA | 170 ± 2 |

## 4.2.4 Infrared Spectroscopy

IR spectroscopy is a good technique to analyze inter/intramolecular hydrogen bonding interactions and purpose of this study was to verify whether salt/cocrystal formed between the new solid forms. Etodolac free acid (COOH) stretching frequency is present at 1740 $cm^{-1}$ and carboxylate ions ($COO^-$) in salts around at 1650-1620 $cm^{-1}$. In other case ETD-INT cocrystal shows (blue shift) carbonyl stretching frequency at 1710-1673. The acid OH/amine NH groups of ETD shows stretching frequency at 3339 cm-1 but the cocrystals/salts show red shift in (ETD-INT, $ETD^-•nHA^+$, $ETD^-•cycloHA^+$, $2(ETD)^-•PPZ^{2+}$ 3408, 3373, 3360, 3344 $cm^{-1}$ two systems shows blue shift in $ETD^-•isoPA^+$, $ETD^-•phEA^+$ at 3129, 3181 $cm^{-1}$ (Figure 4.13, Table 4.5).

**Table 4.5:** Selected functional group stretching frequency in FT-IR spectra of ETD cocrystals and salts.

| | **C=O($cm^{-1}$) acid** | **OH/NH($cm^{-1}$)** | **NH($cm^{-1}$) of Coformer** |
|---|---|---|---|
| **ETD** | 1740 | 3339 | ------- |
| **ETD−INT (1:1)** | 1710,1673 | 3408 | 3360 |
| **$ETD^-•isoPA^+$ (1:1)** | 1638 | 3129 | 3055 |
| **$ETD^-•nHA^+$ (1:1)** | 1633 | 3373 | 3055 |
| **$ETD^-•cycloHA^+$ (1:1)** | 1620 | 3360 | 3272,3352 |
| **$ETD^-•phEA^+$ (1:1)** | 1638 | 3181 | 3290,3362 |
| **$2(ETD)^-•PPZ^{2+}$ (2:1)** | 1648 | 3344 | 3270 |

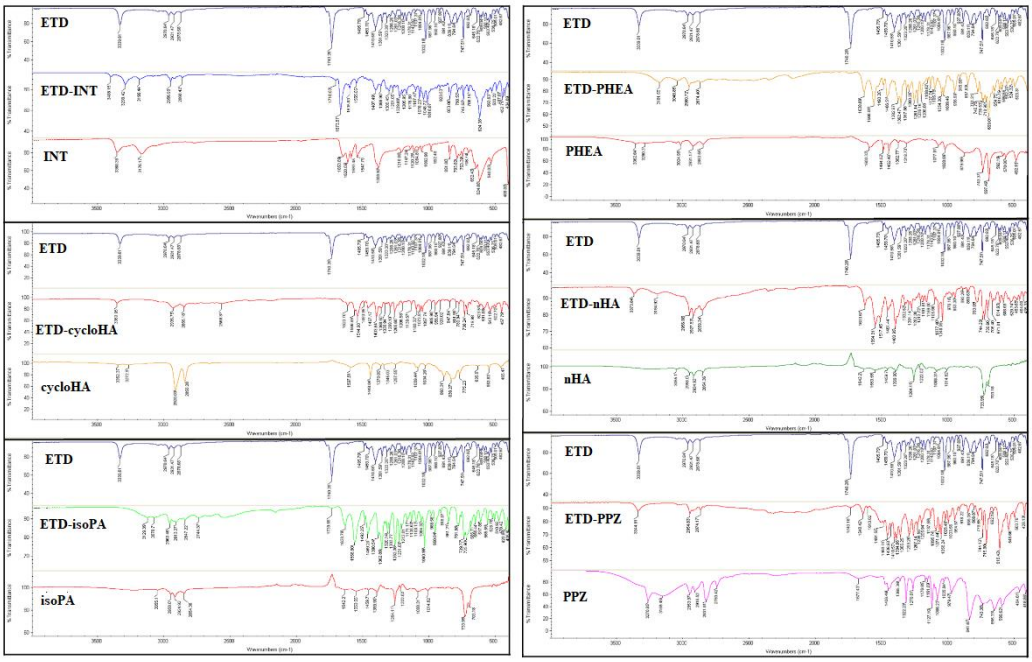


**Figure 4.13:** IR comparison of ETD cocrystals/salts with its starting materials.

## 4.2.5 Solubility and Dissolution Studies

The selection of salt of drugs for the formulation development should normally be non-hygroscopic so that it does not form a hydrate during prolonged storage. Even though amines tend to be hygroscopic, the acid-amine salts are non-hygroscopic and stable under humid conditions.[38] The **ETD** salts of amines prepared in this study are stable under ambient conditions, as confirmed by PXRD and DSC over time intervals. The aqueous equilibrium solubility of **ETD**, **ETD$^{-}$•isoPA$^{+}$**, **ETD$^{-}$•nHA$^{+}$**, **ETD$^{-}$•cycloHA$^{+}$**, **ETD$^{-}$•phEA$^{+}$**, and **2(ETD)$^{-}$•PPZ$^{2+}$** salts was checked in pH 7.0 phosphate buffer solution by stirring for 24 h at ambient temperature (Table 4.6). The solubility of **ETD$^{-}$•isoPA$^{+}$** was highest among all five salts which is ≈50 times higher than **ETD** free acid. **ETD$^{-}$•phEA$^{+}$** salt showed the lowest equilibrium solubility among the salts, even lower than **ETD** free acid which is surprising. A study solubility trend in a series of amine salts of carboxylic acid drugs (including **ETD** salts) showed that as the chain length of the homologous alkylamine increases, the lipophilicity (log P value) of the counter ion also increases and thus aqueous solubility reduces.[48] However, apart from lipophilicity other factors such as the enthalpy of fusion, hydration and crystal lattice energy along with the crystal packing properties (the characteristics of the hydrogen bond network) play a substantial role in determining the solubility of a salt.[31] In the reported salts, solubility of

**ETD⁻•isoPA⁺** is ≈27 times higher than **ETD⁻•nHA⁺** (log P = 0.391 for isopropylamine and 2.1 for n-hexylamine). In case of n-hexylamine and cyclohexylamine, the lipophilic area of n-hexylamine (log P = 2.1) is greater than that of cyclohexylamine (log P = 1.5) and consequently **ETD⁻•cycloHA⁺** ought to show higher equilibrium solubility than the **ETD⁻•nHA⁺**, if lipophilicity plays a major role in determining solubility. However, equilibrium solubility of **ETD⁻•nHA⁺** was observed higher than **ETD⁻•cycloHA⁺**, which suggests that mere lipophilicity is not controlling the solubility but also other crystal lattice parameters contribute to variation in solubility. In case of cyclohexylamine and 2-phenylethylamine (log P = 1.41), lipophilic nature is virtually indistinguishable. However, solubility of **ETD⁻•cycloHA⁺** is higher than **ETD⁻•phEA⁺**, therefore, influence of the lattice free energy and hydrogen bond environment on the solubility is supposed to be much significant than lipophilicity (Table 4.6). Unlike monoamines piperazine formed a 2:1 salt with **ETD**. The observed solubility of **2(ETD)⁻•PPZ²⁺** is lower than that of aliphatic amines but slightly higher than that of **ETD⁻•phEA⁺**. The pH of the solubility medium influences the solubility of drug salts. pH of each solubility medium was measured at the end of the solubility experiment.[32] The solubility order is **ETD⁻•isoPA⁺** > **ETD⁻•nHA⁺** > **ETD⁻•cycloHA⁺** > **2(ETD)⁻•PPZ²⁺** > **ETD⁻•phEA⁺** > **ETD**. The pH measured for equilibrium solubility media follows the order **ETD⁻•isoPA⁺** > **ETD⁻•nHA⁺** ≃ **ETD⁻•cycloHA⁺** ≃ **ETD⁻•phEA⁺** > **2(ETD)⁻•PPZ²⁺** > **ETD**. From the order of solubility and pH of saturated solubility media, one can say that solubility of **ETD⁻•isoPA⁺** is the highest because of the highest pH (7.25 ± 0.05) of saturation solubility medium and solubility of **2(ETD)⁻•PPZ²⁺** is comparatively lower because of the lowest pH (6.85 ± 0.05) of the medium. In between these two pH range, three other salts (i.e. **ETD⁻•nHA⁺**, **ETD⁻•cycloHA⁺** and **ETD⁻•phEA⁺**) showed pH 7.05 ± 0.05 of saturated solubility medium but the equilibrium solubility is different for each salt. Therefore, mere consideration of the pH of the saturated solubility medium is also not sufficient to infer the solubility order of different organic salts. Another generalized trend in the literature is: the order of solubility of organic salts is reverse to the order of their melting point, due to reduced energy required to break the crystal lattice.[49] The amine salts of **ETD** in the present study did not show such a relationship between the melting point of the salt and its solubility value (Table 4.6).

Quantitative kinetic solubility information obtained from intrinsic dissolution rate (IDR) and dissolution rate measurements are used to determine the extent of regulatory concern

about the different solid forms of the same drug.[50] The reason is that both IDR and the dissolution rate give the direct information about rate of drug release from the crystal lattice to the solution. The intrinsic dissolution profile of **ETD** and its amine salts were recorded over 3 hours in phosphate buffer at pH 7.0 (Figure 4.14). Intrinsic dissolution rate profile of **ETD$^{-}$•isoPA$^{+}$** salt was very high in comparison to the other salts and attained peak concentration within 1 hour. The order of observed IDR was **ETD$^{-}$•isoPA$^{+}$** > **ETD$^{-}$•nHA$^{+}$** > **2(ETD)$^{-}$•PPZ$^{2+}$** > **ETD** > **ETD$^{-}$•cycloHA$^{+}$** > **ETD$^{-}$•phEA$^{+}$**. The IDR experiment showed that **ETD$^{-}$•isoPA$^{+}$**, **ETD$^{-}$•nHA$^{+}$**, **2(ETD)$^{-}$•PPZ$^{2+}$** has higher dissolution rate than the **ETD**. Even though fast dissolving salts are of paramount interest for drug formulation, they must be stable under the solubility and dissolution media conditions. Simulated PXRD patterns for each salt were compared with the PXRD pattern of the solid residues left at the end of the dissolution and solubility experiments (Figure 4.15-4.16). Thus all the salts are stable enough under the solubility and dissolution media conditions.

**Table 4.6:** Physicochemical properties, equilibrium solubility and IDR of **ETD** and its amine salts in pH 7.0 buffer solution. Digits in the bracket represent the X-fold of IDR with respect to **ETD** free acid.

| **Name of compounds** | **pH of saturated solubility media after 24 h** | **Equilibrium solubility after 24 h slurry (mg mL$^{-1}$ )** | **Intrinsic dissolution rate (mg/min/cm$^2$) x10$^{-3}$** |
|---|---|---|---|
| ETD | 6.60 ± 0.05 | 5.40 | 0.466 |
| ETD$^{-}$•isoPA$^{+}$ | 7.25 ± 0.05 | 267.50 | 9.613 (20.62X) |
| ETD$^{-}$•nHA$^{+}$ | 7.05 ± 0.05 | 9.82 | 1.084 (2.326X) |
| ETD$^{-}$•cycloHA$^{+}$ | 7.05 ± 0.05 | 7.84 | 0.380 (0.815X) |
| ETD$^{-}$•phEA$^{+}$ | 7.05 ± 0.05 | 5.30 | 0.293 (0.628X) |
| 2(ETD)$^{-}$•PPZ$^{2+}$ | 6.85 ± 0.05 | 6.33 | 0.685 (1.46X) |

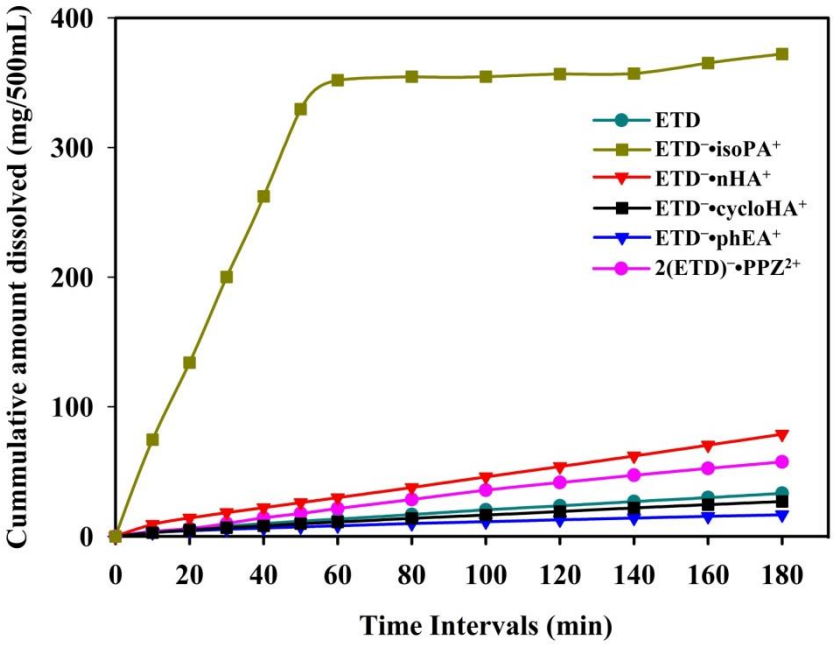


**Figure 4.14:** Intrinsic dissolution profile of **ETD** and its amine salts measured over a time period of 3 hours and at pH 7.0 in phosphate buffer.

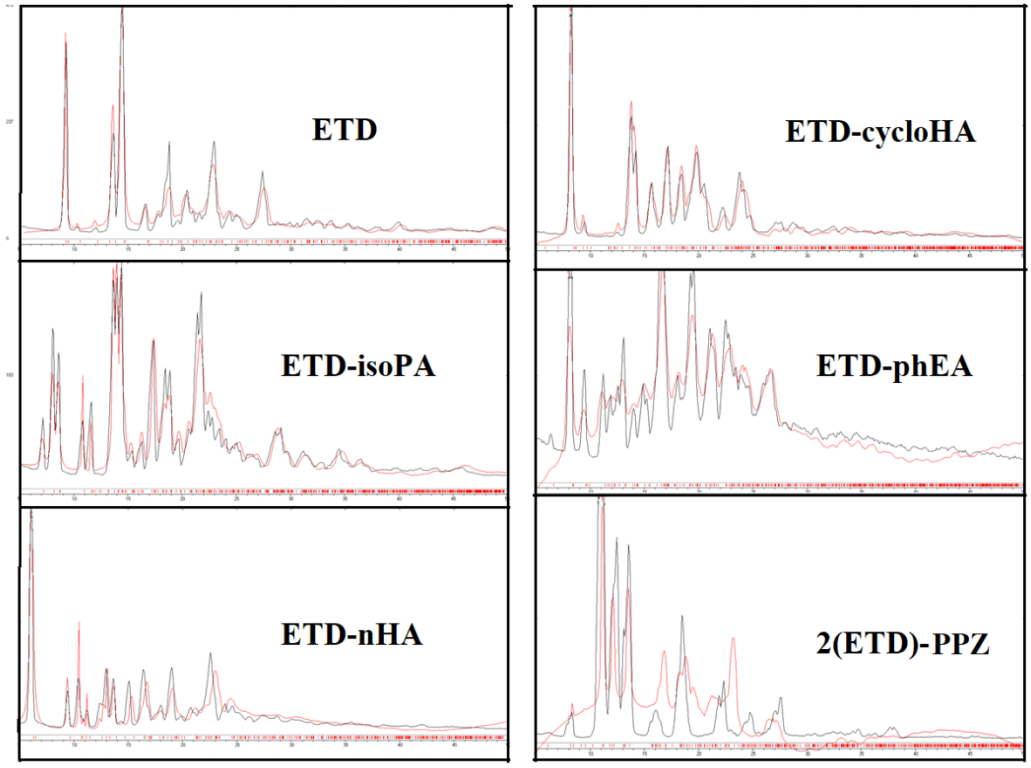

**Figure 4.15:** Overlay of PXRD patterns of **ETD** left at the end of equilibrium solubility experiment (black) in pH 7.0 buffer medium with calculated XRD pattern of **ETD** (red). Peak fittings indicate that **ETD** solid form was stable at pH 7.0 buffer.

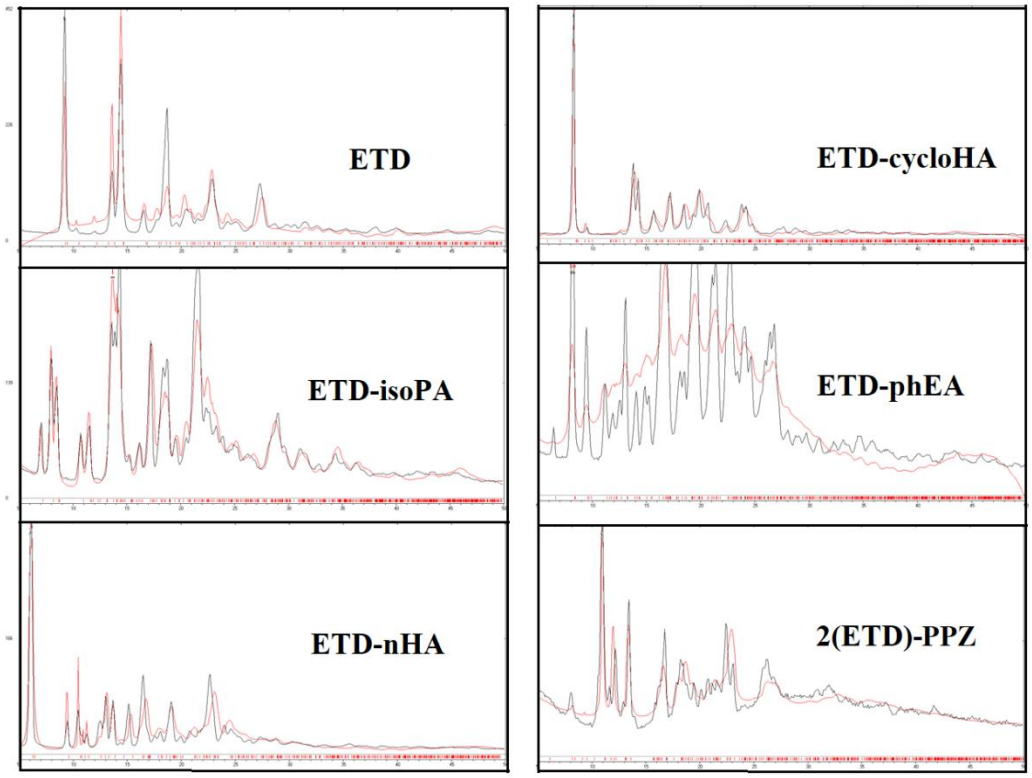


**Figure 4.16:** Overlay of PXRD patterns of **ETD** left at the end of dissolution experiment (black) in pH 7.0 buffer medium with calculated XRD pattern of **ETD** (red). Peak fittings indicate that **ETD** solid form was stable under dissolution media at pH 7.0 buffer.

## 4.2.6 Diffusion and Flux Study

Measuring membrane permeability is a major determinant of pharmacokinetic behavior of a drug, specifically for its absorption, distribution and excretion. In vitro diffusion analysis of **ETD** and its salts was done through a dialysis membrane which gives an idea of relative permeation behavior of different solids of the same series of salts. In general, diffusion of any solute across artificial/ biological membrane shows a lag time, that is necessary to diffuses across, and the drug is released into the receptor fluid/ cytosol to attain steady state of diffusion. During the lag period, diffusion is rapid and thus flux shows an exponential growth which drops off when the diffusion reaches the steady state. The diffusion of **ETD** and its salts was measured in phosphate buffer pH 7.0 medium over a

time period of 3 h. There were no significant changes in pH of the receptor compartment during the experiment except a little deviation in a few cases (Table 4.6). The equilibrium solubility and PXRD analysis shows the stability of salts under the buffer conditions which indicated the tight ion pairing of each salts in the solution. Further, the tightness of ion pair is governed by the pKa difference between the acid and base of ion pair, which is sufficient enough between the **ETD** and amines (ΔpKa ranges from 5 to 6).[51] It is believed that **ETD** and amine ion pairs cross the permeable membrane without disproportionation and ion exchange. Figure 4.17a represents the cumulative drug diffused vs. time graph which shows that the cumulative drug diffused across the permeable membrane is the highest for **ETD$^{-}$•isoPA$^{+}$**. In case of hexyl amines, **ETD$^{-}$•nHA$^{+}$** showed faster diffusion than the **ETD$^{-}$•cycloHA$^{+}$**, however the latter showed almost similar pattern to that of **2(ETD)$^{-}$•PPZ$^{2+}$** but faster than **ETD$^{-}$•phEA$^{+}$**. The neutral species **ETD** showed the slowest diffusion compared to ionic species. If we compare order of cumulative drug diffused and IDR in case of primary amine salts, both showed the order as **ETD$^{-}$•isoPA$^{+}$** > **ETD$^{-}$•nHA$^{+}$** > **ETD$^{-}$•cycloHA$^{+}$** > **ETD$^{-}$•phEA$^{+}$**. According to the lipophilicity order of amine cations, the order of lipophilicity of tight ion pairs should be **ETD$^{-}$•nHA$^{+}$** > **ETD$^{-}$•cycloHA$^{+}$** > **ETD$^{-}$•phEA$^{+}$** > **ETD$^{-}$•isoPA$^{+}$**. Exceptionally, the fastest diffusion/flux of **ETD$^{-}$•isoPA$^{+}$** among all solids could be due to the high concentration gradient across the membrane because of high IDR. There are some studies which suggest that in vitro permeability increases with increasing lipophilicity (log D) of drugs but for the same log D if molecular mass decreases, the permeability will further increases. In the case of primary amine salts **ETD$^{-}$•isoPA$^{+}$** has the lowest molecular mass that allows it to move faster than other ion-pairs. Figure 4.17b shows that the permeability flux of **ETD** salts reaches the maximum value within 10 minutes except for **ETD$^{-}$•isoPA$^{+}$**. Even though the peak concentration for **ETD$^{-}$•isoPA$^{+}$** was reached at a later time point of ~1 h, yet it showed the highest flux at all the time points among the salts studied. In this series of **ETD** salts, molecular mobility and dissolution rate both play a significant role in determining the rate of permeability and maximum can be achieved by decreasing the molecular mass and increasing the dissolution rate.

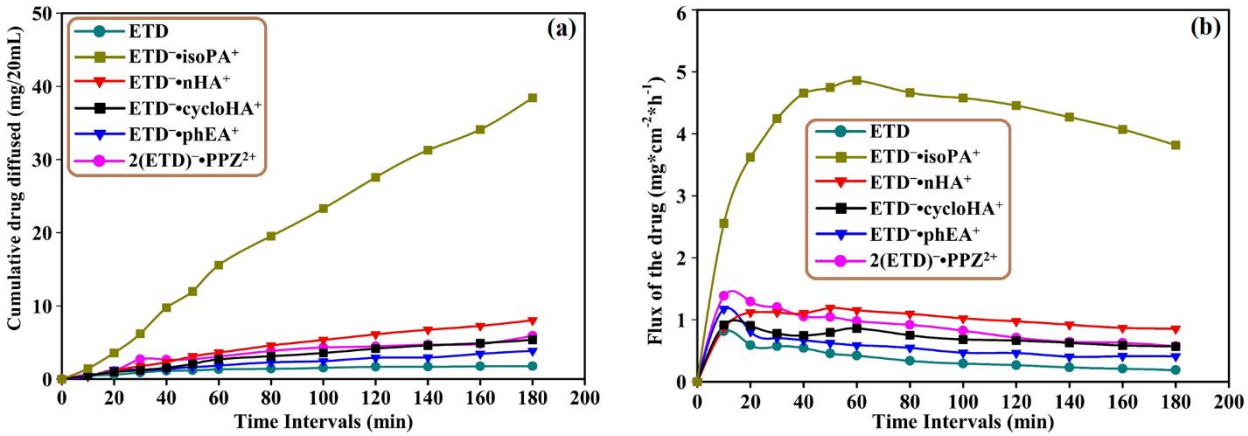


**Figure 4.17:** (a) Represents the cumulative amount of **ETD** and its salts diffused across the dialysis membrane at different intervals, and (b) represents the flux of **ETD** and its salts across the dialysis membrane at different intervals. Measurements were done over a time period of 3 hours at pH 7.0 phosphate buffer.

## 4.3 Conclusions

This study deals with a series of salts and cocrystals of **ETD** to establish a relation of solubility and dissolution with respect to the nature of coformers. Since intermolecular interactions in the crystal structure have a significant role in controlling the mechanical and physical properties of the solid forms, only those salts and cocrystals were selected which are fully characterized by X-ray crystallography. Among the cocrystals, only **ETD•INT** was successfully solved by X-ray diffraction in our hands, which is helpful in analyzing supramolecular synthons between **ETD** and pyridine/amide coformers.[51] Therefore, solubility, dissolution and permeability experiments were done for the salts in pH 7.0 phosphate buffer solution. The obtained equilibrium solubility order is **ETD⁻•isoPA⁺ > ETD⁻•nHA⁺ > ETD⁻•cycloHA⁺ > 2(ETD)⁻•PPZ²⁺ > ETD⁻•phEA⁺ > ETD**, and IDR order is **ETD⁻•isoPA⁺ > ETD⁻•nHA⁺ > 2(ETD)⁻•PPZ²⁺ > ETD > ETD⁻•cycloHA⁺ > ETD⁻•phEA⁺**. Our simple analysis with respect to pH of saturated solubility media did not supported any of these orders. Similarly, lipophilicity of counter ions was also not established with respect to any direct relation with the solubility and IDR of the coformers. PXRD analysis showed solid phase stability of all salts under solubility and dissolution conditions. Therefore, another correlation with respect to melting point of salts was done but it was difficult to derive a correlation. The analysis of intermolecular interactions showed that crystal structures of all salts are stabilized by a network of strong N–H···O hydrogen bonds, even though the pattern of hydrogen bonds is different in each

salt structure. Another crystallographic parameter is crystal density which is directly related to the tightness of molecular packing, consequently it determines the lattice energy in a homologous series of the crystals. However, solubility is determined by the energy difference of hydration/ solvation and lattice energy. Interestingly, the crystal density in **ETD** salts followed the inverse order of lipophilicity in counter ions. In the studied salts **ETD$^{-}$•isoPA$^{+}$** showed the highest solubility and dissolution rate perhaps due to lower lipophilicity of counter ions and high affinity towards hydration (since **2(ETD)$^{-}$•PPZ$^{2+}$** is a 2:1 salt, it is difficult to compare its solubility with 1:1 salts of monoamines). Permeability and flux studies of **ETD** salts suggest that tight ion-pairs are intact during the membrane permeation process and discriminate the rate of permeability.[52] Molecular mobility and dissolution rate were the key factors to determine the rate of permeability in same series of salts. Consequently, **ETD$^{-}$•isoPA$^{+}$** showed highest cumulative permeability and flux. To summarize, short chain (low lipophilic) amines are preferred over long chain (high lipophilic) amines to improve the solubility, dissolution and permeability of Etodolac. These learning points are of general utility for other BCS class IV drugs.

## 4.4 Experimental Section

**ETD** was purchased from Swapan Roop Drugs & Pharmaceuticals (Aurangabad, Maharashtra, India). Coformers and solvents were purchased either from Sigma Aldrich or TCI Chemicals, and used without further purifications. All salts and cocrystals were prepared from neutral **ETD**.Subsequently, the received neutral **ETD** was attempted to crystallize in a range of solvents and finally single crystal X-ray quality crystal was grown in the nitromethane. Crystallization was done at room temperature through slow solvent evaporation technique.

**Preparation of Salts and cocrystlas**

**ETD** with all solid cocrystal formers (CCFs) were attempted by solvent drop grinding method[53] (e.g. piperazine = **PPZ** and isonicotinamide = **INT**), however salts of liquid CCFs (e.g. isopropylamine = **isoPA**, n-hexylamine **= nHA**, cyclohexylamine **= cycloHA** and 2-phenylethylamine = **phEA**) were prepared by adding them into a solution of **ETD** (Figure 4.2). More specifically, salts of amines were prepared by dissolving the **ETD** (1.0 g, 3.48 mmol) in acetonitrile (30 mL) followed by addition of amines (1.2 equivalents, 4.18 mmol).

**ETD-isoPA (1:1):** In a 50 mL conical flask, saturated solution of **ETD** (1000 mg, 3.48 mmol) was prepared by dissolving in acetonitrile (30 mL). In the stirring solution of **ETD**, isopropylamine (341.89 µL, 247 mg, 4.18 mmol) was added and stirring was continued for 10 min. The flask was kept at room temperature to evaporate the solvents. From the bulk material ~30 mg of salt was dissolved in acetonitrile (3 mL) and kept at room temperature for slow evaporation to afford single crystals after 3-5 days.

**ETD-nHA (1:1):** In a 50 mL conical flask, saturated solution of **ETD** (1000 mg, 3.48 mmol) was prepared by dissolving in acetonitrile (30 mL). In the stirring solution of **ETD**, n-hexylamine (548.79 µL, 420 mg, 4.18 mmol) was added and stirring was continued for 10 min. The flask was kept at room temperature to evaporate the solvents. From the bulk material ~30 mg of salt was dissolved in acetonitrile (3 mL) and kept at room temperature for slow evaporation to afford single crystals after 3-5 days.

**ETD-cycloHA (1:1):** In a 50 mL conical flask, saturated solution of **ETD** (1000 mg, 3.48 mmol) was prepared by dissolving in acetonitrile (30 mL). In the stirring solution of **ETD**, cyclohexylamine (478.78 µL, 414 mg, 4.18 mmol) was added and stirring was continued for 10 min. The flask was kept at room temperature to evaporate the solvents. From the bulk material ~30 mg of salt was dissolved in acetonitrile (3 mL) and kept at room temperature for slow evaporation to afford single crystals after 3-5 days.

**ETD-phEA (1:1):** In a 50 mL conical flask, saturated solution of **ETD** (1000 mg, 3.48 mmol) was prepared by dissolving in acetonitrile (30 mL). In the stirring solution of **ETD**, phenyl ethylamine (526.03 µL, 507 mg, 4.18 mmol) was added and stirring was continued for 10 min. The flask was kept at room temperature to evaporate the solvents. From the bulk material ~30 mg of salt was dissolved in acetonitrile followed by adding a few drops of methanol (3 mL) and kept at room temperature for slow evaporation to afford single crystals after 3-5 days.

**ETD-PPZ (2:1):** In an Agate Mortar, **ETD** (1000 mg, 3.48 mmol) and piperazine (150 mg, 1.74 mmol) were taken and ground with the help of pestle by adding a few drop of methanol solvent for 10 min. The formation of a new complex was confirmed by PXRD. Subsequently, blends were dissolved in ~30-35 mL acetonitrile at ~80 °C and kept at ambient condition for slow evaporation of the solvent. Single crystal X-ray quality crystals were obtained within a week.

**ETD-INT (1:1):** In an Agate Mortar, **ETD** (1000 mg, 3.48 mmol) and isonicotinamide (425 mg, 3.48 mmol) were taken and ground with the help of pestle by adding a few drop of methanol solvent for 10 min. The formation of a new complex was confirmed by PXRD. Subsequently, blends were dissolved in ~30-35 mL acetonitrile at ~80 °C and kept at ambient condition for slow evaporation of the solvent. Single crystal X-ray quality crystals were obtained within a week.

**X-ray crystallography**

Single crystal X-ray diffraction data were collected on a Bruker SMART APEX II single crystal X-ray CCD diffractometer having graphite monochromatized (Mo-Kα, λ = 0.71073 Å) radiation at low temperature (100 K).[54] The X-ray generator was operated at 50 kV and 30 mA. Data reduction was performed using APEX-II Software. Intensities were corrected for absorption using SADABS,[54] and the structure was solved and refined using SHELX97.[55] All non-hydrogen atoms were refined anisotropically, and hydrogen atoms were geometrically fixed with thermal parameters equivalent to 1.2 times that of the atom to which they are bonded, except those which are involved in strong hydrogen bonding. Molecular diagrams for all compounds were prepared using ORTEP, and the packing diagrams were generated using Mercury version 3.10.[56] PLATON was used for the analysis of bond lengths, bond angles, and other geometrical parameters.[57] Crystallographic parameters of synthesized salts and cocrystals are summarized in Table 4.2.

**Powder X-ray diffraction**

Powder X-ray diffraction data was recorded on a Bruker D8 Advance diffractometer (Bruker-AXS, Karlsruhe, Germany) using Cu-Kα X-radiation (λ = 1.5406 Å) at 40 kV and 30 mA power. X-ray diffraction patterns were collected over the 2θ range 5-50° at a scan rate of 3.9°/min. Powder Cell 2.4 (Federal Institute of Materials Research and Testing, Berlin, Germany) was used for profile fitting of experimental PXRD and calculated lines from the X-ray crystal structure.[58]

**Vibrational spectroscopy**

FT-IR spectroscopy was carried out using Thermo-Nicolet 6700 FT-IR-NIR spectrometer with NXR FT-Raman module (Thermo Scientific, Waltham, MA) with the samples dispersed in KBr pellets and Omnic software (Thermo Scientific, Waltham, MA) was utilized to analyse the data.

**Thermal analysis**

Differential Scanning Calorimetry (DSC) analysis was performed on a Mettler Toledo DSC 822e module. The sample size for the data collection was ranging from 2 to 5 mg. Each sample was placed in a pin-pricked aluminum pan and kept in the furnace under a stream of dry nitrogen flowing at 80 mL $min^{-1}$. The heating rate was maintained at 10 °C $min^{-1}$ throughout the experiment and temperature range was fixed from 30 °C to 300 °C.

**Solubility and Dissolution Experiments**

The solubility of **ETD** solid forms was measured in aqueous solution of pH 7.0 phosphate buffer under ambient conditions. To measure the molar extinction coefficients, the absorbance of several known concentrations of each salt was recorded at $\lambda_{max}$ = 276 nm in pH 7.0 phosphate buffer on Thermo Scientific Evolution 300 UV-vis spectrometer (Thermo Scientific, Waltham, MA). Subsequently, concentration vs. intensity calibration curve was plotted for each sample. From the slope of the calibration curve, molar extinction coefficient for **ETD** solid forms was calculated. Intrinsic dissolution rate (IDR) measurements were carried out on a USP certified Electrolab TDT-08 L Dissolution Tester (Electrolab, Mumbai, MH, India). Dissolution experiments were performed for 180 minutes in pH 7.0 phosphate buffer at 37 °C. Prior to IDR estimation, standard curves for all the compounds were obtained spectrophotometrically at their respective $\lambda_{max}$. The slope of the plots from the standard curve gave the molar extinction coefficient (ε) by applying the Beer−Lambert's law, which was used to determine the IDR values. For IDR measurements, 400 mg of the solid material of each solid form was compressed between the smooth surfaces by applying 2.5 ton/$inch^2$ pressure for 4 minutes in a circular area of 0.5 $cm^2$. The pellet was compressed to provide a flat surface on one side and the other side was sealed. Then the pellets were dipped separately into 500 mL of pH 7.0 phosphate buffer solution at 37 °C so that only one surface was exposed to the solution and rotating disk was set at a rate of 100 rpm. A 5 mL of each dissolution media were collected at 10 minutes for first hour and then at time intervals of 20 minutes up to 180 minutes and replaced each time with the same amount of fresh pH 7.0 phosphate buffer to maintain a constant volume. The amount of drug dissolved in each fraction was calculated by using the calibration curves and stability of undissolved residues were checked after air dry by

recording PXRD data followed by comparison with simulated PXRD patterns from single crystal data.

**Diffusion and Flux Measurements**

Diffusion experiments of **ETD** salts were carried out on a diffusion apparatus (model EMFDC-06, Orchid Scientific, Maharashtra, India) with dialysis membrane-135 (average flat width 33.12 mm, average diameter 23.8 mm, capacity approximately 4.45 mL/cm) that was purchased from Hi-Media, India. Prior to experiments, trace impurities from dialysis membrane were removed by treating with 2% NaHCO3 (to remove sulfides), followed by 10 mM of EDTA (to remove traces of heavy metal) and subsequently treated with deionized water (to remove glycerin), where each treatment was done at 80 °C for 30 min. Purified dialysis membranes were placed in different diffusion cells by mounting in clips with an effective surface area 3.14 $cm^2$. Afterwards, suspension of **ETD** and its salts was placed on the dialysis membrane in donor compartment and temperature of diffusion medium was maintained at 37±1 °C throughout the experiment. The solution was allowed to stir at 600 rpm and diffuse through the membrane towards the receptor compartment containing 20 mL of phosphate-buffer solution (PBS, pH = 7). The release of the drug/salt was determined by using the calibration curves as in the solubility experiments at different time intervals (10, 20, 30, 40, 50, 60, 80, 100, 120, 140, 160 and 180 min). The volume withdrawn at each time interval was 0.5 mL that was refilled by phosphate-buffered solution (PBS, pH = 7). The flux (*J*) of drugs across the membrane was calculated by the formula $J = Q/(A \times t)$ where Q is the quantity of the solute traversing the membrane in time t and A is the area of exposed membrane for diffusion.

## 4.5 References

1. Liewer, S.; Huddleston, A. N. Oral targeted therapies: managing drug interactions, enhancing adherence and optimizing medication safety in lymphoma patients. *Expert Rev. Anticancer Ther.* **2015**, *15*, 453-464.
2. Krikorian, S.; Pories, S.; Tataronis, G.; Caughey, T.; Chervinsky, K.; Lotz, M.; Shen, A. H.; Weissmann, L. Adherence to oral chemotherapy: Challenges and opportunities. *J. Oncol. Pharm. Practice* **2018**, 1078155218800384.
3. Kini, V.; Ho, P. M. Interventions to improve medication adherence: a review. *Jama* **2018**, *320*, 2461-2473.
4. Krishnaiah, Y. S. Pharmaceutical technologies for enhancing oral bioavailability of poorly soluble drugs. *J. Bioequiv. Availab.* **2010**, *2*, 28-36.

5. Kalepu, S.; Nekkanti, V. Insoluble drug delivery strategies: Review of recent advances and business prospects. *Acta Pharm. Sin. B* **2015**, *5*, 442–453.
6. Draft guidance for industry: Waiver of In Vivo Bioavailability and Bioequivalence Studies for Immediate-Release Solid Oral Dosage Forms Based on a Biopharmaceutics Classification System. December 2017 Biopharmaceutics; http://www.fda.gov/Drugs/GuidanceComplianceRegulatoryInformation/Guidances/default.htm. Accessed August 10, 2019.
7. Censi, R.; Di Martino, P. Polymorph impact on the bioavailability and stability of poorly soluble drugs. *Molecules* **2015**, *20*, 18759-18776.
8. Karagianni, A.; Malamatari, M.; Kachrimanis, K. Pharmaceutical cocrystals: new solid phase modification approaches for the formulation of APIs. *Pharmaceutics* **2018**, *10*, 18.
9. Sathisaran, I.; Dalvi, S. Engineering cocrystals of poorly water-soluble drugs to enhance dissolution in aqueous medium. *Pharmaceutics* **2018**, *10*, 108.
10. Nangia, A. K.; Desiraju, G. R. Crystal Engineering: An Outlook for the Future. *Angew. Chem. Int. Ed.* **2019**, *58*, 4100-4107.
11. Bolla, G.; Nangia, A. Pharmaceutical cocrystals: walking the talk. *Chem. Comm.* **2016**, *52*, 8342-8360.
12. Gunnam, A., Nangia, A. K. High Solubility Salts of Multiple Sclerosis Drug Teriflunomide. *Cryst. Growth Des.* **2019**, *19*, 5407-5417.
13. Ross, S. A.; Lamprou, D. A.; Douroumis, D. Engineering and manufacturing of pharmaceutical co-crystals: a review of solvent-free manufacturing technologies. *Chem. Comm.* **2016**, *52*, 8772-8786.
14. Malamatari, M.; Ross, S. A.; Douroumis, D.; Velaga, S. P. Experimental cocrystal screening and solution based scale-up cocrystallization methods. *Adv. Drug Deliv. Rev.* **2017**, *117*, 162-177.
15. Duggirala, N. K.; Perry, M. L.; Almarsson, Ö.; Zaworotko, M. J. Pharmaceutical cocrystals: along the path to improved medicines. *Chem. Comm.* **2016**, *52*, 640-655.
16. Schuhmacher, A.; Gassmann, O.; Hinder, M. Changing R&D models in research-based pharmaceutical companies. *J. Transl. Med.* **2016**, *14*, 105.
17. Kraljevic, S.; Stambrook, P. J.; Pavelic, K. Accelerating drug discovery. *EMBO Reports* **2004**, *5*, 837-842.

18. Lee, C. Y.; Chen, X.; Romanelli, R. J.; Segal, J. B. Forces influencing generic drug development in the United States: a narrative review. *J. Pharm. Policy Pract. BioMed. Central* **2016**, *9*, 26.
19. Shargel, L.; Kanfer, I. Generic drug product development: solid oral dosage forms. *CRC Press* **2013**.
20. Newman, A. Specialized solid form screening techniques. *Org. Process Res. Dev.* **2012**, *17*, 457-471.
21. Aaltonen, J.; Allesø, M.; Mirza, S.; Koradia, V.; Gordon, K. C.; Rantanen, J. Solid form screening–a review. *Eur. J. Pharm. Biopharm.* **2009**, *71*, 23-37.
22. Palucki, M.; Higgins, J. D.; Kwong, E.; Templeton, A. C. Strategies at the interface of drug discovery and development: early optimization of the solid state phase and preclinical toxicology formulation for potential drug candidates. *J. Med. Chem.* **2010**, *53*, 5897-5905.
23. Fridgeirsdottir, G. A.; Harris, R.; Fischer, P. M.; Roberts, C. J. Support tools in formulation development for poorly soluble drugs. *J. Pharm. Sci.* **2016**, *105*, 2260-2269.
24. Aungst, B. J. Optimizing oral bioavailability in drug discovery: an overview of design and testing strategies and formulation options. *J. Pharm. Sci.* **2017**, *106*, 921-929.
25. Newman, A.; Wenslow, R. Solid form changes during drug development: good, bad, and ugly case studies. *AAPS Open* **2016**, *2*, 2.
26. Paulekuhn, G. S.; Dressman, J. B.; Saal, C. Trends in active pharmaceutical ingredient salt selection based on analysis of the orange book database. *J. Med. Chem.* **2007**, *50*, 6665-6672.
27. Stahl PH, Wermuth G. Handbook of pharmaceutical salts: properties, selection, and use. *Wiley-VCH, Zurich* **2002**.
28. De Boer, I. H.; Bangalore, S.; Benetos, A.; Davis, A. M.; Michos, E. D.; Muntner, P.; Rossing, P; Zoungas, S.; Bakris, G. Diabetes and hypertension: a position statement by the American Diabetes Association. *Diabetes Care* **2017**, *40*, 1273-1284.
29. Gupta, D.; Bhatia, D.; Dave, V.; Sutariya, V.; Varghese Gupta, S. Salts of therapeutic agents: chemical, physicochemical, and biological considerations. *Molecules* **2018**, *23*, 1719.

30. S. de Moraes, L.; Edwards, D.; Florence, A. J.; Johnston, A.; Johnston, B. F.; Morrison, C. A.; Kennedy, A. R. Aqueous solubility of organic salts. Investigating trends in a systematic series of 51 crystalline salt forms of methylephedrine. *Cryst. Growth Des.* **2017**, *17*, 3277-3286.
31. Williams, H. D.; Trevaskis, N. L.; Charman, S. A.; Shanker, R. M.; Charman, W. N.; Pouton, C. W.; Porter, C. J. Strategies to address low drug solubility in discovery and development. *Pharmacol. Rev.* **2013**, *65*, 315-499.
32. Serajuddin, A. T. Salt formation to improve drug solubility. *Adv. Drug Deliv. Rev.* **2007**, *59*, 603-616.
33. Humber, L. G. Etodolac: The chemistry, pharmacology, metabolic disposition, and clinical profile of a novel anti-inflammatory pyranocarboxylic acid. *Med. Res. Rev.* **1987**, *7*, 1-28.
34. https://www.drugs.com/etodolac.html. Accessed February 22, 2020.
35. Özkan, Y.; Doğanay, N.; Dikmen, N.; Işımer, A. Enhanced release of solid dispersions of etodolac in polyethylene glycol. *Farmaco* **2000**, *55*, 433-438.
36. Barakat, N. S. Enhanced oral bioavailability of etodolac by self-emulsifying systems: in-vitro and in-vivo evaluation. *J. Pharm. Pharmacol.* **2010**, *62*, 173-180.
37. Sherje, A. P.; Kulkarni, V.; Murahari, M.; Nayak, U. Y.; Bhat, P.; Suvarna, V.; Dravyakar, B. Inclusion complexation of etodolac with hydroxypropyl-beta-cyclodextrin and auxiliary agents: Formulation characterization and molecular modeling studies. *Mol. Pharmaceutics* **2017**, *14*, 1231-1242.
38. David, S. E.; Timmins, P.; Conway, B. R. Impact of the counterion on the solubility and physicochemical properties of salts of carboxylic acid drugs. *Drug Dev. Ind. Pharm* **2012**, *38*, 93-103.
39. Gadade, D. D.; Pekamwar, S. S.; Lahoti, S. R.; Patni, S. D.; Sarode, M. C. Cocrystallization of Etodolac: Prediction of Cocrystallization, Synthesis, Solid State Characterization And In Vitro Drug Release. *Marmara Pharm. J.* **2016**, *21*, 78-88.
40. Groom, C. R.; Bruno, I. J.; Lightfoot, M. P. Ward, S. C. The Cambridge structural database. *Acta Cryst.* **2016,** *B72*, 171-179.
41. Humber, L. G.; Demerson, C. A.; Swaminathan, P. 1, 8-Diethyl-1, 3, 4, 9-tetrahydropyrano [3, 4-b] indole-1-acetic acid: a potent anti-inflammatory drug.

Conformation and absolute configuration of its active enantiomer. *J. Med. Chem.* **1986**, *29*, 871-874.

42. Bhogala, B. R.; Basavoju, S.; Nangia, A. Tape and layer structures in cocrystals of some di- and tricarboxylic acids with 4,4′-bipyridines and isonicotinamide. From binary to ternary cocrystals *CrystEngComm*, **2005,** *7*, 551-562.
43. Childs, S. L.; Stahly, G. P.; Park, A. The salt−cocrystal continuum: the influence of crystal structure on ionization state. *Mol. Pharmaceutics* **2007**, *4*, 3, 323-338.
44. Cruz-Cabeza, A. J. Acid–base crystalline complexes and the pKa rule. *CrystEngComm*, **2012**, 14, 6362-6365.
45. https://docs.chemaxon.com/display/docs/pKa+Plugin. Accessed June 30, 2019.
46. Bernstein, J.; Davis, R. E.; Shimoni, L.; Chang, N. L. Patterns in hydrogen bonding: functionality and graph set analysis in crystals. *Angew. Chem. Int. Ed.* **1995**, *34*, 1555-1573.
47. Threlfall, T. L. Turning DSC charts of polymorphs into phase diagrams: a tutorial paper. *Org. Process Res. Dev*. **2009**, *13*, 1224-1230.
48. Arnott, J. A.; Planey, S. L. The influence of lipophilicity in drug discovery and design. *Expert Opin. Drug. Discov.* **2012**, *7*, 863-875.
49. Aulton, M. E.; Taylor, K. M. Aulton's Pharmaceutics: The Design and Manufacture of Medicines, *Elsevier, Philadelphia* **2013**.
50. Issa, M. G.; Ferraz, H. G. Intrinsic dissolution as a tool for evaluating drug solubility in accordance with the Biopharmaceutics Classification System. *Dissolution Technol.* **2011**, *18*, 6-11.
51. Yousef, M. A.; Vangala, V. R. Pharmaceutical Co-crystals: Molecules, Crystals, Formulations, Medicines. *Cryst. Growth Des.* **2019,** 19, 7420-7438.
52. Miller, J. M.; Dahan, A.; Gupta, D.; Varghese, S.; Amidon, G. L. Enabling the intestinal absorption of highly polar antiviral agents: ion-pair facilitated membrane permeation of zanamivir heptyl ester and guanidino oseltamivir. *Mol. Pharmaceutics* **2010**, *7*, 1223-1234.
53. Trask, A. V.; Haynes, D. A.; Motherwell, W. D. S.; Jones, W. Screening for crystalline salts via mechanochemistry. *Chem. Commun.* **2006,** 51-53.
54. Bruker. APEX3, SAINT and SADABS. Bruker AXS Inc., 2016, Madison, Wisconsin, USA.
55. Sheldrick, G. M. Crystal Structure Refinement with SHELXL. *Acta Crystallogr., Sect. C*: *Struct. Chem.* **2015**, *71*, 3−8.

56. Farrugia, L. J. WinGX and ORTEP for Windows: an update. *J. Appl. Crystallogr.* **2012**, *45*, 849–854.
57. Spek, A. L. Structure Validation in Chemical Crystallography. *Acta Cryst.* **2009**, *D65*, 148–155.
58. Powder Cell, A Program for Structure Visualization, Powder Pattern Calculation and Profile Fitting. http://www.ccp14.ac.uk/tutorial/powdcell/. Accessed July 16, 2019.

## *CHAPTER FIVE*

# Enhancing the Permeability of Acefylline by in Ternary Salt, Cocrystals and Polymorphs

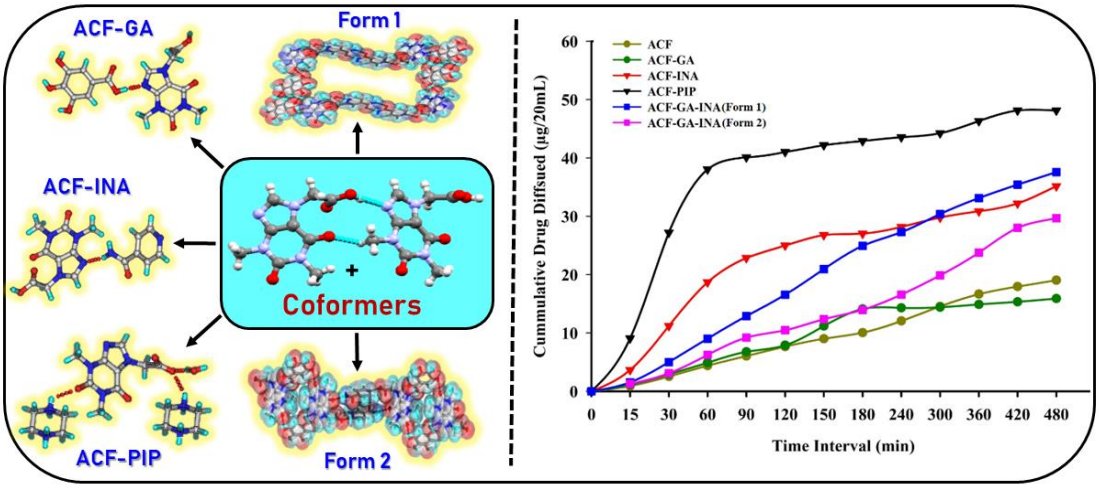


***Acefylline (ACF) is a BCS Class IV xanthine stimulant used in combination with piperazine in the treatment of bronchial asthma. However, its low solubility and poor rate of permeability limits the development of ACF drug in pharmaceutical formulation. In this chapter, ACF binary and ternary cocrystals/salt-cocrystals/polymorphs are designed and synthesized using solvent-assisted grinding with various coformers.***

## 5.1 Introduction

Multicomponent molecular solids such as cocrystals, salts and solid solutions exhibit novel and superior functionality compared to their individual components.[1-7] Among the various molecular cocrystals and polymorphs, binary cocrystals are the most studied over the past two decades.[8-11] The design and crystallization of stoichiometric ternary cocrystals and higher order molecular solids still remains a challenge, owing to difficulties in assembling larger number of molecular components in the crystal lattice.[12-15] Ternary cocrystals are crystalline structures consisting of three neutral molecular solids in a fixed stoichiometry.[16-18] Optimization of intermolecular interactions, such as hydrogen bonding, halogen bonding, shape fit and close packing contribute to the formation of binary and ternary cocrystals; at higher order molecular crystals, the self-assembly problem becomes increasingly challenging.[19-22] Molecular mimicry or exchange of molecules having similar interactions and size/ shape is one strategy to progress from ternary to hexanary and even 7/8 component crystals/ solid solutions.[23-24]

Ternary cocrystals have been synthesized by various groups using multiple approaches. Aakeroy et al.[13] synthesized hydrogen-bond directed ternary supermolecule assembly with the predominant hydrogen bond between the strongest acid donor and pyridine acceptor, and at the second level between acid and amide (2001). A similar strategy was applied to molecules containing pyridyl and benzimidazolyl moieties (2005).[12] Furthermore, the ternary cocrystals were synthesized by an initial creation of dimer through charge transfer interaction followed by hydrogen bonding between the dimer and a third component (Seaton et. al. 2013).[25] Desiraju and coworkers[21] formulated a different approach in obtaining the ternary cocrystals by combining the intermolecular interactions (chemical) and the size and shape (geometrical) of the molecules (2011). These authors also synthesized ternary cocrystals by employing the selection of hydrogen bonds and halogen bonds (2013).[19-22,26-30] Based on the literature survey, and to the best of our knowledge, the majority of reports on ternary cocrystals are of model compounds. There are very few reports of drug-molecules-based ternary cocrystals (2013, 2016).[31-32] Recently, Nangia and coworkers[32-33] selected a bifunctional sulfa drug (acetazolamide) to synthesize ternary cocrystals with pyridine amide and lactam coformers (2015, 2016). Aitipamula et. al.[31] designed ternary cocrystals of anti-tuberculosis drug isoniazid in combination with nicotinamide plus fumaric / succinic acids coformers (2013). (years of publication are given in parentheses to indicate progression of this topic over the past 2 decades)

High aqueous solubility and high membrane permeability of APIs (active pharmaceutical ingredients) are essential for the development of high bioavailability drugs in the pharmaceutical industry.[34-36] However, low solubility and permeability of APIs limits full efficacy of several drugs in development stages.[37-38] According the Biopharmaceutics Classification System (BCS) drug molecules are classified based on high/ low solubility and permeability in four quadrants.[39] The solubility of APIs have been improved using crystal engineering by designing salts, cocystals and salt-cocrystals as well as through solid dispersion and membrane permeability to improve oral bioavailability via surfactants, liposomes, and microencapsulation as well as nanoparticle based methods.[40-45] The permeability of APIs can be improved by structural modification using cofomers/ excipients of high lipophilicity.[46-49]

Acefylline (ACF) is a one such API having poor aqueous solubility (1 mg/mL) and relatively low membrane permeability (log P 0.8-1.1) in BCS class IV category.[50-51] ACF consists of one hydrogen bond donating and four hydrogen bond accepting sites, which can participate in hydrogen bonding with molecules such as aromatic carboxylic acids, amides and piperazine to form 1:1 binary cocrystals (shown in Figure 5.3 for acefylline acid). A recent survey of the Cambridge Crystallographic Database showed that there are no reports on salts/ cocrystals of ACF except a single crystal of ACF (Refcode CEJRAL).[52-54] we report in this study designed ternary salts-cocrystals of ACF with coformers shown in Figure 5.1. The permeability and solubility of the ternary salts-cocrystals of ACF showed improvement in physicochemical properties of the drug.

## 5.2 Results and Discussion

Ternary salt-cocrystal adducts of ACF (theophylline acetic acid, labeled A) were synthesized by selecting different function group coformers labeled as B (basic functional group), C (3,5-di/3,4,5-tri hydroxy-benzoic acid), D (amide functional group), and E (4-hydroxy-benzoic acid) (Figure 5.1), which can form either O–H···N or O–H···O hydrogen bonds with ACF carboxylic acid and imidazole groups. The presence of different functional groups in ACF which can give rise to multiple pairing combinations of hydrogen bonding open the possibility to make ternary systems but also pose a challenge to predict the actual synthons that will form. To derive the synthon information, different binary cocrystals of ACF (A) with coformers B to E were crystallized (Experimental section) by solvent-drop and liquid assisted grinding in a mortar-pestle[5] and the powder

material was recrystallized (Experimental Section for details) to obtain diffraction quality single crystals.

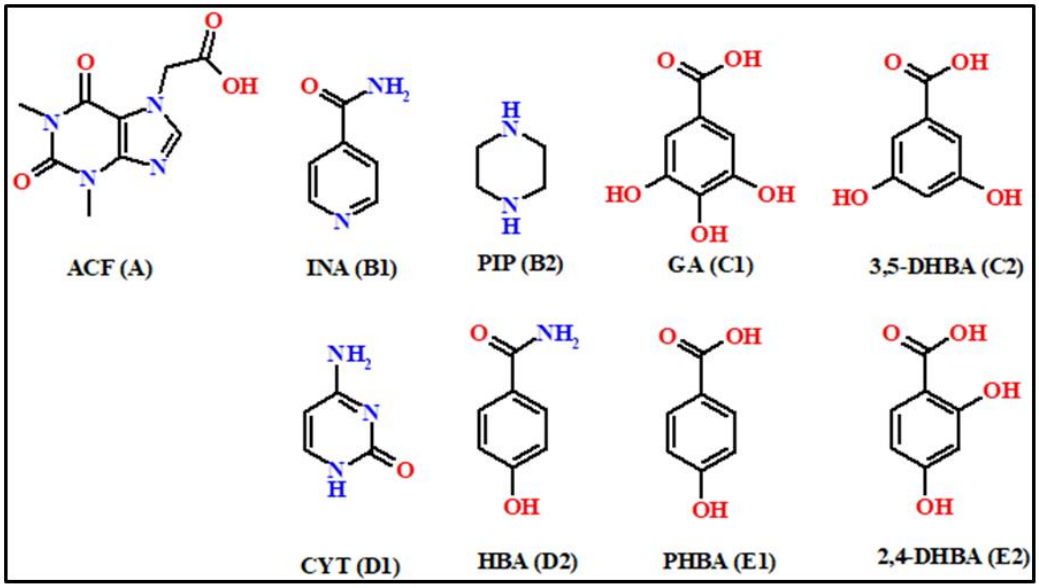


**Figure 5.1:** Chemical Structures of ACF and Coformers in Different Functional Group Categories to Assemble Binary and Ternary Salt-Cocrystals.

ACF formed 1:1 binary cocrystals with the six coformers (INA, PHBA, 2,4-DHBA, 3,5-DHBA, GA, HBA) and salts with the more basic coformers CYT (1:1) and PIP (1:0.5). pKa values are listed in (Table 5.1).[55] The crystal structures were confirmed by single crystal X-ray diffraction (Figure 5.3-5.4, and Table 5.2, Crystallographic parameters). Single crystals of ACF-INA could not be obtained but its structure was determined by powder X-ray diffraction file (structure determination from powder data, Table 5.9).[56-58] The crystal structures were solved in monoclinic $P2_1/n$ or $P2_1/c$ space group with one molecule of ACF and the coformer in the asymmetric unit, except ACF-INA which crystallized in *P*-1 space group with one ACF and two INA molecules in the asymmetric unit. Crystal structure of ACF (Figure 5.3) was redetermined and matches with the reported crystal structure (Refcode CEJRAL).[59]

**Table 5.1:** $pK_a$ values[a] of API and coformers used in this study.

| **API/Coformer** | **$pK_a$** | **ΔpKa** | **Cocrystal/Salt** |
|---|---|---|---|
| ACF | 3.262 | -- | -- |
| INA | 3.455 | 0.193 | 1:1 cocrystal/salt |
| PIP | 9.559 | 6.297 | 1:1 salt |
| GA | 3.942 | 0.68 | 1:1 cocrystal |
| 35DHBA | 3.614 | 0.352 | 1:1 cocrystal |
| PHBA | 4.380 | 1.118 | 1:1 cocrystal |
| 24DHBA | 3.100 | 0.162 | 1:1 cocrystal |
| CYT | 2.346 | 0.916 | 1:1 salt |

[a] $pK_a$ calculations were carried out in ChemAxon calculator.

Ternary salt-cocrystals were synthesized upon mixing combinations of cofomers (Figure 5.1) by solvent-drop or liquid assisted grinding followed by recrystallization. Addition of B coformers (B1, B2) to ACF resulted in binary cocrystals and then addition of C coformers (C1, C2) gave ternary cocrystals (A-B-C); the addition of C first and then B gave identical products. Attempts to crystallize ternary salt-cocrystals by initial addition of D and E to ACF were not successful. The product binary and ternary systems are shown in Figure 5.2.

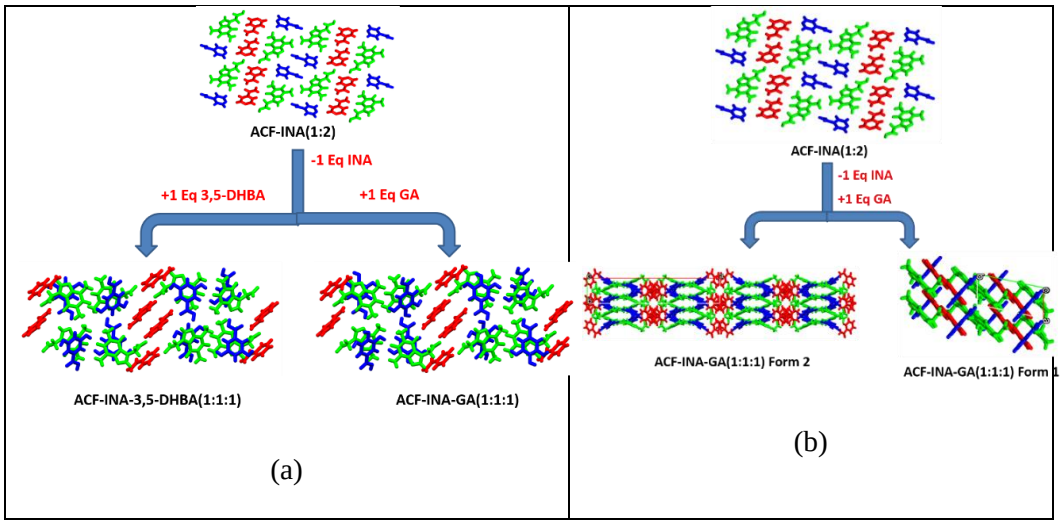

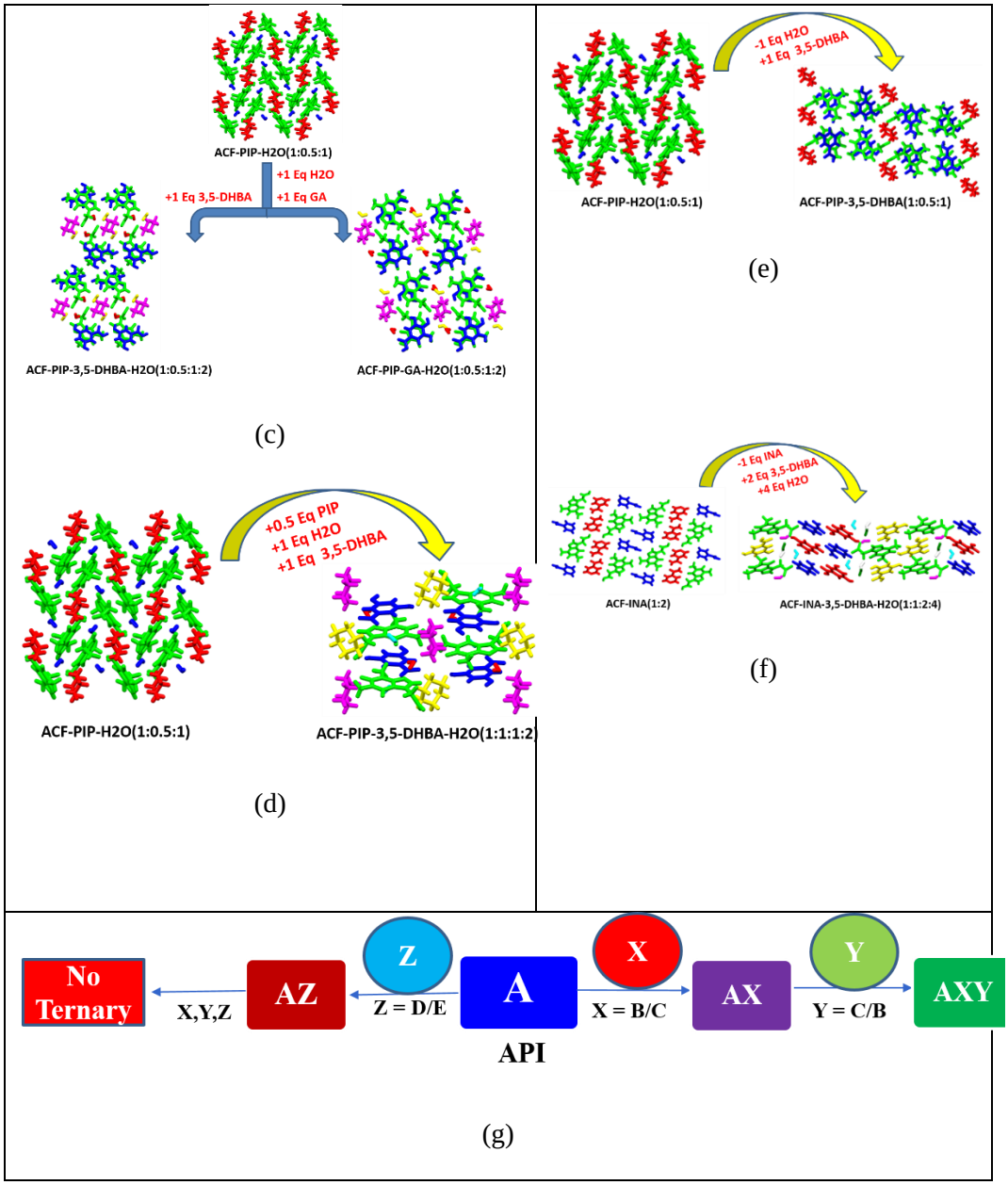


**Figure 5.2:** (a) Packing arrangement in binary cocrystal ACF-INA (1:2) and the related ternary ACF-INA-GA (1:1:1) and ACF-INA-3,5DHBA (1:1:1) salt-cocrystal to show the isostructural replacement of one equivalent of INA by a second coformer. (b) ACF-INA (1:2) binary cocrystal and one equivalent of INA is replaced by GA to form ACF-INA-GA (1:1:1) polymorphs 1 and form 2 with different crystal structures. (c) Binary salt hydrate ACF-PIP-$H_2O$ (1:0.5:1) to give ternary hydrates ACF-PIP-GA-$H_2O$ and ACF-PIP-3,5-DHBA-$H_2O$ (both of 1:0.5:1:2 stoichiometry). (d) ACF-PIP-$H_2O$ binary salt-hydrate with half molecule of PIP and one equivalent of 3,5-DHBA-$H_2O$ to form ACF-PIP-3,5-DHBA (1:1:1:2). (e) In binary salt-hydrate ACF-PIP-$H_2O$ (1:0.5:1) one equivalent

of $H_2O$ is replaced by 3,5-DHBA to form ACF-PIP-3,5-DHBA (1:0.5:1). (f) Binary cocrystal ACF-INA (1:2) shows one equivalent of INA is replaced by two 3,5-DHBA and four water molecules to form ACF-INA-3,5-DHBA-$H_2O$ (1:1:2:4). (g) Schematic representation of binary and ternary salt cocrystal polymorphs synthesized in this study. A is ACF and B to E are different coformers.

## 5.2.1 Crystal Structure Description

**Crystal structure description of binary and ternary components**

The crystal structures of binary cocrystals are discussed first, followed by ternary salt-cocrystals. Hydrogen bonding synthons are crucial role to play for individual molecules to binary systems and ternary systems. All the crystallographic parameters are summarized in Table 5.2.

**Crystal structures of binary cocrystals**

**ACF (A):** Acefylline crystallized in the monoclinic space group $P2_1/n$ one molecule in asymmetric unit. The crystal structure of contains acid-imidazaole O−H···N synthon (1.92 Å, 165°) and weak interaction C−H···O (2.56 Å, 100°) followed by ring motif (Figure 5.3a).

**ACF-INA (AB1):** the cocrystal structure takes the space group *P*-1, with one molecule of ACF and two molecules of INA in the asymmetric unit. The crystal structure packing contains N2B−H2B1···O1B amide homodimers (2.00 Å, 174°) $R_2^2(8)$ motif of INA with O2−H2···N1B and N2A−H2A1···N2 hydrogen bonds (1.77 Å,174°;2.26 Å,165°) to ACF (Figure 5.3b).

**ACF-PIP hydrate (AB2):** the ground material of ACF and PIP in a 1:0.5 ratio salt crystallized in $P2_1/c$ space group with one molecule of hydrate in the asymmetric unit. In the crystal structure, the ACF acid proton is transferred to the PIP by making N5−H5A···O1 hydrogen bond (2.16 Å, 145°) (Figure 5.3c).

**ACF-GA-MeoH (AC1):** the crystal structure takes the space group $P2_1/n$, with one molecule each of ACF, GA and MeoH in the asymmetric unit. Here methanol played major role for bridging MeoH O10−H10A···O3 synthon (1.82 Å, 163°) to ACF and GA followed by O5−H5A···N2 and O7−H7D···O4 synthon (1.80 Å, 173°; 1.87 Å, 170°) $R_8^8$ (43) ring motif to ACF (Figure 5.3d).

**ACF-3,5-DHBA (AC2):** the crystal structure of ACF and 3,5-DHBA crystallizes in the $P2_1/n$ space group, with one molecule each in asymmetric unit. ACF crystal structure contains acid and imidazole O−H···N synthon. This synthon ACF acid replaced by 3,5-DHBA in that crystal packing contains O6−H6A···N2 and O2−H2A···O5 synthons (1.72 Å, 165°; 1.68 Å, 163°) followed by $R_4^4(22)$ ring motif (Figure 5.3e).

**ACF-CYT (AD1):** the crystal structure of ACF and CYT crystallizes in the $P2_1/c$ space group, with one molecule each in asymmetric unit. In the crystal structure the ACF acid proton transfer to the CYT by making N7−H7A···O2 and N6−H6A···O1 synthon (1.77 Å, 171°;1.96 Å;170°) followed by heterodimers $R_2^2(8)$ ring motif (Figure 5.3f).

**ACF-HBA (AD2):** the crystal structure takes the space group $P2_1/n$, with 1:1 ratio of ACF and HBA in the asymmetric unit. The crystal packing contains N5−H5A···O5 amide homodimers (2.00 Å, 173°) in the $R_2^2(8)$ motif of HBA with O6−H6A···O3 and O2−H2A···N2 hydrogen bonds(1.91 Å, 169°; 1.94 Å, 146°) through inversion center of ACF (Figure 5.3g).

**ACF-PHBA (AE1):** the cocrystal structure takes the space group $P2_1/n$, with one molecule each of ACF and PHBA in the asymmetric unit. The crystal structure packing contains O5−H5A···O6 acid homodimers (1.70 Å, 167°) in the $R_2^2(8)$ motif of PHBA with O7−H7A···O3 and O2−H2A···N2 hydrogen bonds(1.83 Å, 174°; 1.91 Å, 152°) to ACF (Figure 5.3h).

**ACF-2,4-DHBA (AE2):** the ground material crystallizes in the $P2_1/n$ space group, with one molecule each of ACF and 2,4-DHBA in the asymmetric unit. The crystal structure contains O6−H6A···O5 acid homodimers (1.72 Å, 175°) in the $R_2^2(8)$ ring motif of 2,4-DHBA with O8−H8A···O3 and O2−H2A···N2 hydrogen bonds(1.92 Å,170°; 1.92 Å,152° to ACF. (Figure 5.3i) ACF-PHBA (AE1) and ACF-2,4-DHBA (AE2) both are binary isostructural (Figure 5.4) cocrystals, which were differentiated by using XPac, structural unit-cell similarity index equation.

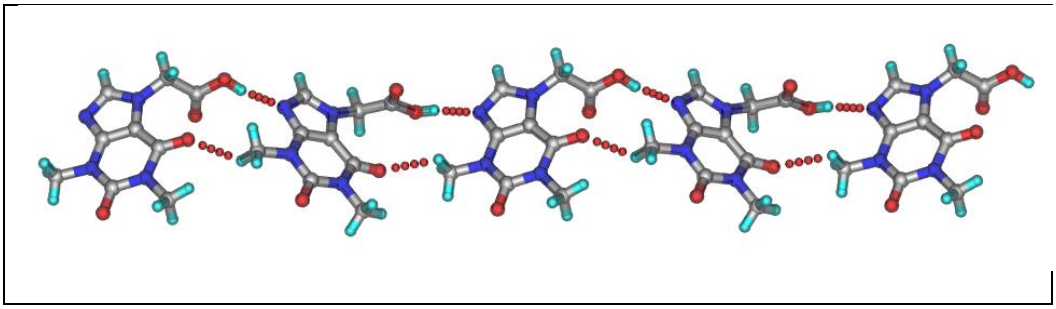

(a)ACF

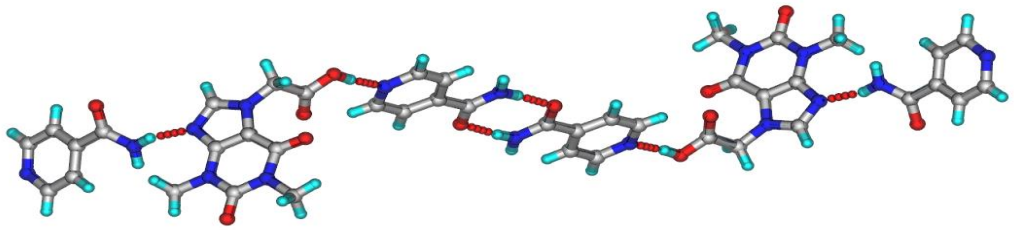

(b) ACF-INA(1:2)

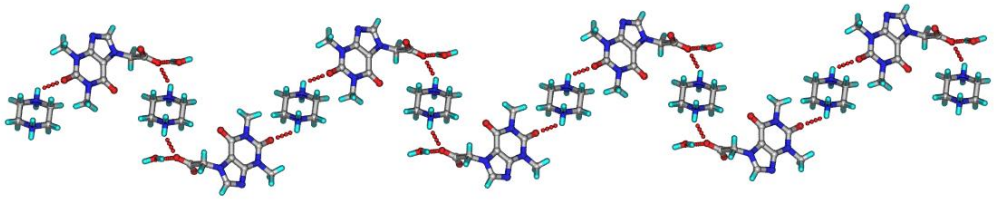

(c) ACF-PIP-H2O(1:05:1)

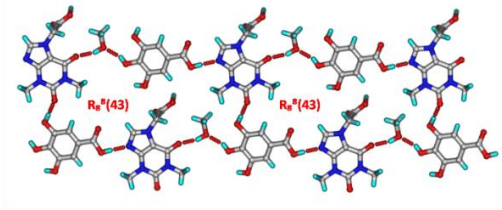


(d) ACF-GA-MeOH(1:1:1)

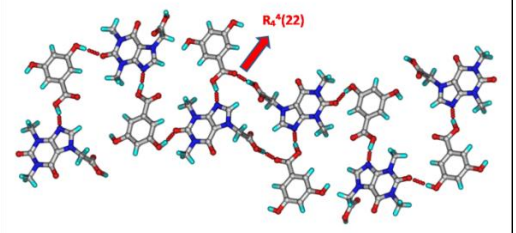


(e) ACF-3,5-DHBA(1:1)

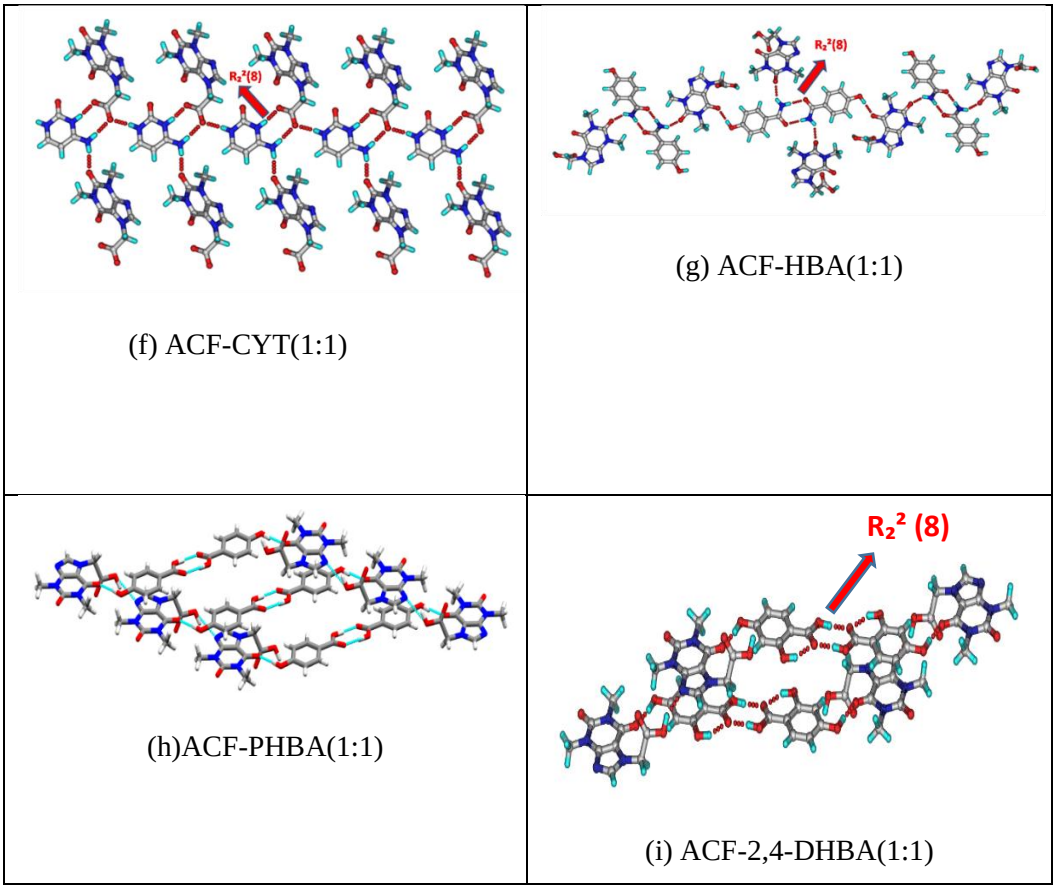


**Figure 5.3:** Supra molecular synthons and molecular packing in Binary cocrystal/salts of ACF with INA, PIP, GA, 3,5-DHBA, CYT, HBA, PHBA, 2,4-DHBA

**Structural similarity in the binary cocrystals**

The binary cocrystals of ACF-24DHBA and ACF-PHBA adopt the monoclinic space group $P2_1/n$ with very similar unit cell parameters (Table 5.2), and they are three dimensional isostructural (Figure 5.4) the isostructurality of ACF-24DHBA and ACF-PHBA was quantified by the XPac method

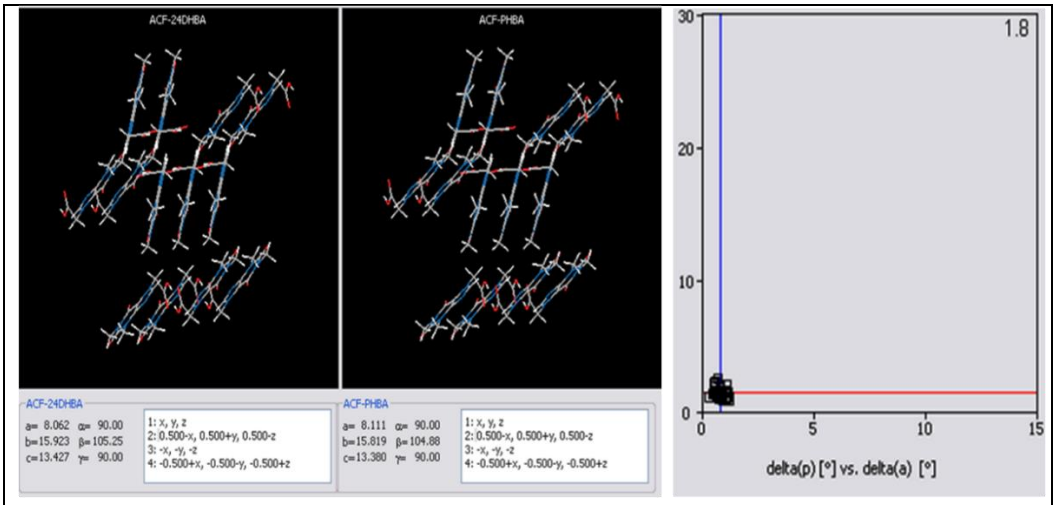


**Figure 5.4:** (a) Two-dimensional supramolecular construct of ACF-24DHBA and ACF-PHBA cocrystals, indicated by XPac Analysis 12 molecules are identically arranged in the supramolecular construct.(b) The inter-planar angular deviation (δp, x-axis) versus angular deviation(δa, y-axis) plot (in °) indicates a dissimilarity index of 1.8,which means that the two cocrystals form the same two-dimensional supramolecular construct.

**Crystal structures of ternary slat-cocrystals**

Four ternary cocrystals with 1:1:1 stoichiometry were obtained upon mixing A with B and C coformers. Furthermore, the variation in the stoichiometry of the cofomers B and C compared to A resulted in different crystal forms. Interestingly, the different combinations of B and C with A led to the formation of multiple ternary systems such cocrystals, salt-cocrystals and polymorphs. The new crystalline phases obtained after grinding (A:B:C) was confirmed by powder X-ray diffraction (PXRD), DSC (Figure 5.14 and Figure 5.15-5.16) and later the microcrystalline powder was recrystallized with suitable solvents for single crystals of eight ternary salt-cocrystals for X-ray diffraction.

When two groups hydrogen bonding donor-acceptor groups are in competition in a multi-functional system, the best-donor bonds to the best-acceptor and the second best-donor to the next best-acceptor.[60-61]In our interaction scheme, ACF COOH donor bonds with the strongest base INA pyridyl N or PIP NH and then GA or DHBA donor bond to ACF heterocycle N or INA amide acceptor to results in the ternary supramolecular complex of equimolar ratio (Figure 5.5). The pKa values of these functional groups are given in Table 5.1.[51]

Addition of a second conformer GA/DHBA to the binary ACF-INA/PIP results in addition of a third molecule in the growing crystal complex rather than a replacement, implying that strong hydrogen bonding or enthalpy is driving the supramolecular assembly build up. ACF being ditopic in nature having two bonding sites, one strong acidic donor and a weak basic acceptor, the molecule has the ability to build the ternary drug cocrystal using the hydrogen bond hierarchy principle[60-61]with two different coformers (Figure 5.1). The hydrogen bonding synthons of the eight different ternary salt-cocrystals are pictorially represented in Figure 5.5.

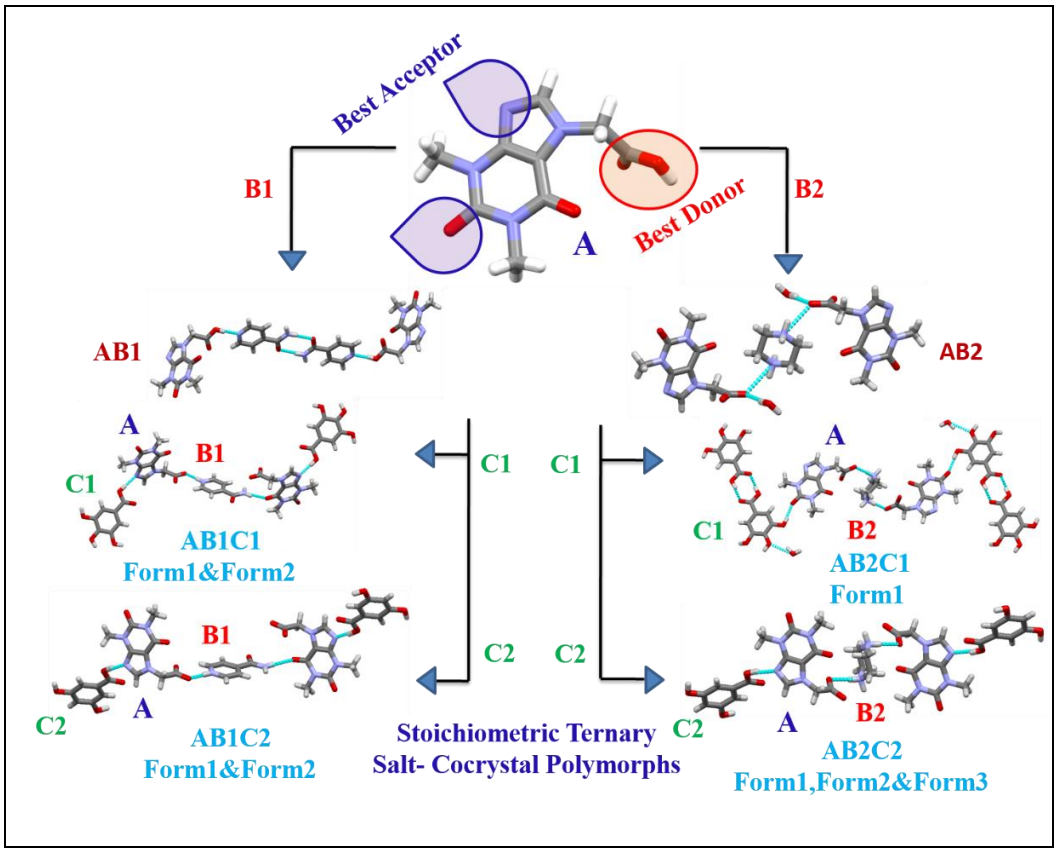


**Figure 5.5:** Eight ternary salt-cocrystals and their hydrogen bond synthons.

**ACF-INA-GA Form I (1:1:1):** The crystal structure takes the space group *P*-1, with one molecule of ACF, INA and GA in the asymmetric unit. The cocrystal salt structure contains N6−H6A···O5 amide homodimers(2.02 Å, 170°)$R_2^2(8)$ ring motif of INA followed by acefylline (ACF) acid proton transfer to nitrogen acceptor of isonicotinamide (INA) the same ACF molecule other side O10−H10A···O4 and O6−H6C···N2 (1.94 Å,174°;1.80 Å,175°)synthon with GA followed by O8−H8A···O7 (1.81 Å, 170°)$R_2^2(14)$ dimer ring motif (Figure 5.6a).

**ACF-INA-GA Form II (1:1:1):** The crystal structure takes the space group *C2/c*, with one molecule of ACF, INA and GA in the asymmetric unit. The cocrystal salt structure contains acefylline(ACF) acid proton transfer to the nitrogen acceptor of isonicotinamide (INA), the same INA molecule N6−H6A···O3 and N5−H5A···O2 (2.06 Å,166°;1.69 Å,178°) synthon to ACF carbonyl through $R_4^4(30)$ inversion center ring motif and other side ACF and GA molecules shows O6−H6C···N2, O10−H10A···O4 (1.83 Å,178°;1.76 Å,173°) synthon followed by $R_4^4(26)$ ring motif (Figure 5.6b).

**ACF-INA-35DHBA (1:1:1):** The crystal structure takes the space group *C2/c*, with one molecule of ACF, INA and 3,5-DHBA in the asymmetric unit. The cocrystal salt structure contains acefylline (ACF) acid proton transfer to the nitrogen acceptor of isonicotinamide (INA), the same INA molecule N−H···O synthon to ACF carbonyl through $R_4^4(30)$ ring motif and other side ACF and 3,5-DHBA molecules shows O−H···N, O−H···O synthon followed by $R_4^4(26)$ ring motif (Figure 5.6c). This crystal structure unit cell parameters, hydrogen bond packing and synthons similar to the ACF-INA-GA (form 2), because of this two crystal structure are isostructural (Figure 5.7).

**ACF-INA-35DHBA-$H_2O$ (1:1:2:4):** The crystal structure takes the space group *P-1*, with one molecule of ACF, INA, 3,5-DHBA and four hydrate molecules in the asymmetric unit. The salt cocrystal structure contains O7−H7A···O5, N6−H6A···O6 (1.88 Å, 170°; 2.09 Å, 164°) acid-amide hetero dimers$R_2^2$ (8) ring motif followed by ACF acid proton transfer to pyridine acceptor of INA. Here one hydrate molecule is bridge between two 3,5-DHBA molecules and two hydrate molecules bridged between ACF, 3,5-DHBA (Figure 5.6d).

**ACF-PIP-GA-$H_2O$ (1:0.5:1:2):** The crystal structure takes the space group *P-1*, with one molecule of ACF, GA, half molecule PIP and two molecules of hydrate in the asymmetric unit. The crystal structure contains ACF acid proton transfer to basic PIP to form N5−H5A···O2 (1.92 Å, 155°) synthon and O6−H6A···O5 (1.76 Å, 171°) synthon acid homodimer of GA with hydrate molecule bridged between GA, PIP to form ring motif (Figure 5.6e).

**ACF-PIP-3,5-DHBA (1:0.5:1):** The crystal structure takes the space group *C2/C*, with one molecule of ACF, 3,5-DHBA and half molecule of PIP in the asymmetric unit. The salt cocrystal contains ACF acid proton transfer to the basic nitrogen of PIP forms

N5−H5A···O1 (1.88 Å, 166°) synthon followed by the same PIP another N5−H5B···O5 (2.10 Å, 133°) synthon with 3,5-DHBA to forms two type of ring motifs (Figure 5.6f).

**ACF-PIP-3,5-DHBA-$H_2O$ (1:0.5:1:2):** The crystal structure takes the space group *P-1*, with one molecule of ACF, 3,5-DHBA, half molecule PIP and two molecules of hydrate in the asymmetric unit. The crystal structure contains ACF acid proton transfer to the basic PIP to form N5−H5B···O2, O10−H10A···O3 (1.85 Å, 158°; 1.90 Å, 161°) synthon with hydrate to form pentagonal ring motifs and other side ACF, 3,5-DHBA form $R_4^4(26)$ ring motif (Figure 5.6g).

**ACF-PIP-3,5-DHBA-$H_2O$ (1:1:1:2):** The crystal structure takes the space group $P2_1/n$, with one molecule of ACF, PIP, 35DBA and two molecules of hydrate in the asymmetric unit. The crystal structure shows two PIP, hydrate and one ACF, 3,5-DHBA molecules form tetramer ring motifs via N−H···O hydrogen bonds. Here one PIP accept proton from ACF and another PIP accept proton from 3,5-DHBA to form tetramer ring motif with bridged hydrate. (Figure 5.6h) ACF forms hydrogen bond N5−H5A···O2, N6−H6A···O2 (1.75 Å, 178°; 2.20 Å, 140°) synthon and 3,5-DHBA forms N5−H6B···O5 (1.71 Å, 175°) synthon.

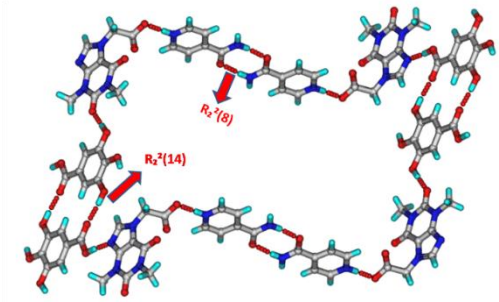


(a) ACF-GA-INA Form 1 (1:1:1)

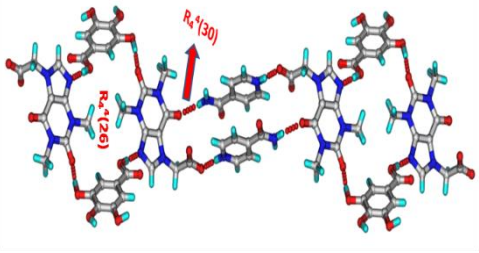


(b) ACF-GA-INA Form 2 (1:1:1)

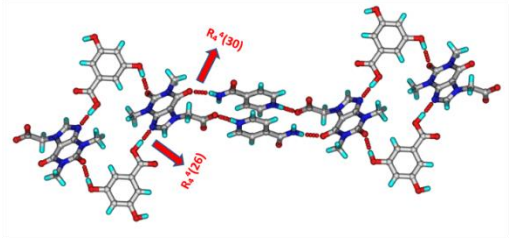


(c) ACF-3,5-DHBA-INA (1:1:1)

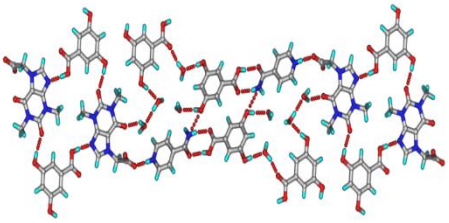

(d) ACF-3,5-DHBA-INA-H2O (1:2:1:4)

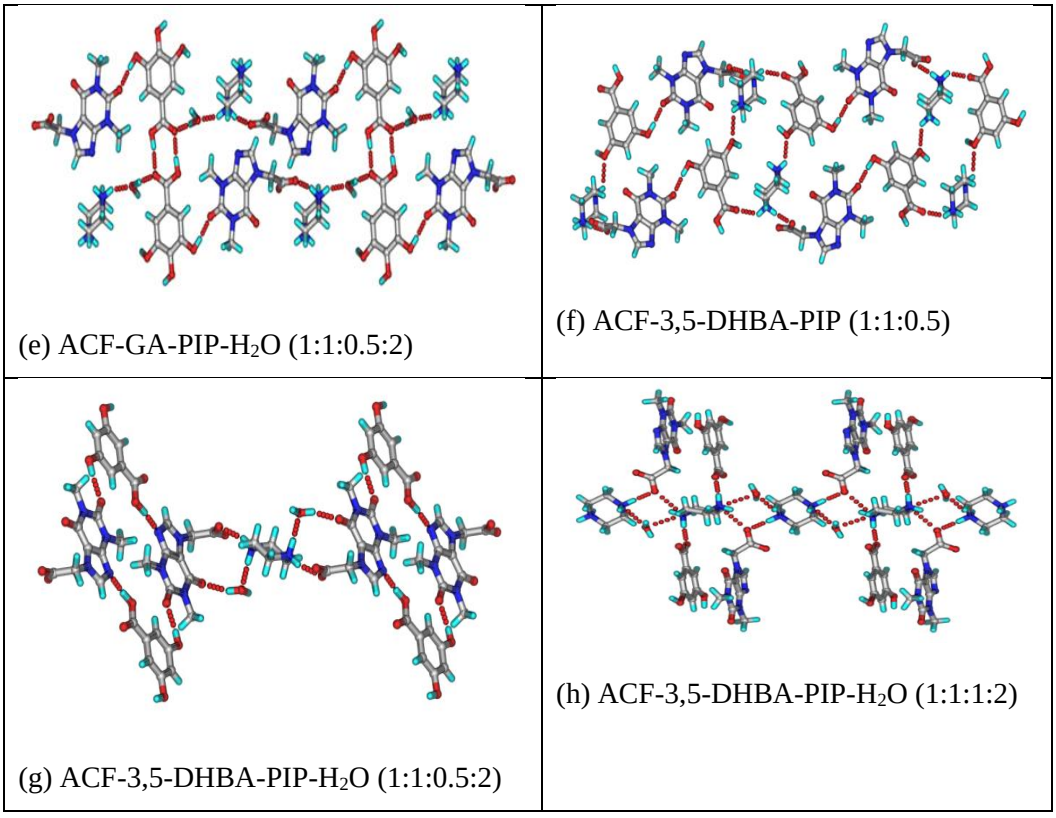


**Figure 5.6:** Crystal structures of ternary systems (a-h).

**Structural similarity in the ternary cocrystals**

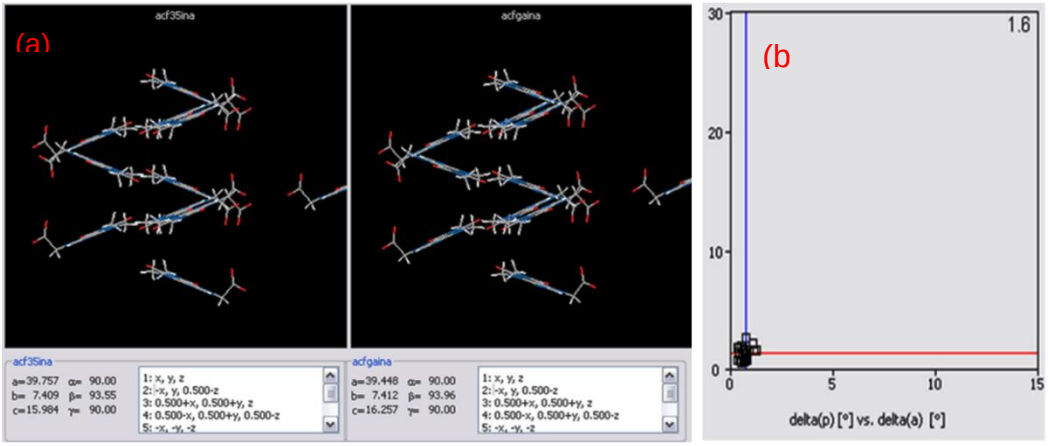


**Figure 5.7:** (a) Two-dimensional supramolecular construct of ACF-INA-GA (AB1C1) and ACF-INA-3,5-DHBA (AB1C2) salt-cocrystals by XPac analysis. (b) The interplanar angular deviation (δp, x-axis) against angular deviation (δa, y-axis) plot (in °).

Among the binary cocrystals in this study, ACF-PHBA (AE1) and ACF-2,4-DHBA (AE2) are isostructural in monoclinic space group $P2_1/n$ space group by XPac analysis (Figure 5.4).[62-64] The low dissimilarity index value of 1.8 (Figure 5.4) calculated by plotting the

interplanar angular deviation indicates that the two cocrystals form similar two-dimensional supramolecular construct. In ternary systems, isostructurality was noted for Form 2 of ACF-INA-GA with ACF-INA-3,5-DHBA in monoclinic space group $P2_1/n$. The unit cell parameter (Figure 5.7a) from XPac is the same. The three dimensional isostructural images of these ternary salt cocrystals (Figure 5.7a) have a dissimilarity index value of 1.6 (Figure 5.7b), lower than the dissimilarity index between the binary systems.

**Table 5.2:** Crystallographic parameters of Acefylline binary and ternary salt-cocrystals polymorphs.

| | **ACF-PHBA (1:1)** | **ACF-HBA (1:1)** | **ACF-PIP-$H_2O$ (1:05:1)** | **ACF-CYT (1:2)** | **ACF-GA-MeOH (1:1:1)** |
|---|---|---|---|---|---|
| **Empirical Formula** | $C_9H_{10}N_4O_4$, $C_7H_6O_3$ | $C_9H_{10}N_4O_4$, $C_7H_7NO_2$ | $C_9H_9N_4O_4$, 0.5($C_4H_{12}N_2$), $H_2O$ | $C_9H_9N_4O_4$, $C_4H_6N_3O$ | $C_9H_{10}N_4O_4$, $C_7H_6O_5$, $CH_4O$ |
| **Formula weight** | 376.33 | 375.35 | 299.30 | 349.32 | 440.37 |
| **Crystal System** | Monoclinic | Monoclinic | Monoclinic | Monoclinic | Monoclinic |
| **Space Group** | $P\ 2_1/n$ | $P\ 2_1/n$ | $P\ 2_1/c$ | $P2_1/c$ | $P\ 2_1/n$ |
| **T (K)** | 298(2) | 298(2) | 298(2) | 298(2) | 298(2) |
| ***a* (Å)** | 8.1114 (8) | 8.1658(7) | 11.0566 (9) | 12.6543 (12) | 11.8840 (12) |
| ***b* (Å)** | 15.8195 (16) | 15.7929 (13) | 11.0384 (9) | 14.2521 (14) | 13.1369 (14) |
| ***c* (Å)** | 13.3800 (14) | 13.3713 (12) | 10.7539 (9) | 8.5191 (8) | 12.4973 (13) |
| ***α* (°)** | 90 | 90 | 90 | 90 | 90 |
| ***β* (°)** | 104.884 (5) | 106.321 (3) | 95.393 (4) | 94.735 (5) | 94.939 (5) |
| ***γ* (°)** | 90 | 90 | 90 | 90 | 90 |
| ***V* (Å$^3$)** | 1659.3(3) | 1654.9 (2) | 1306.67 (19) | 1531.2 (3) | 1943.8 (4) |
| **$D_{calc}$ (g cm$^{-3}$)** | 1.506 | 1.507 | 1.521 | 1.515 | 1.505 |
| **Z** | 4 | 4 | 4 | 4 | 4 |
| ***F*(000)** | 784 | 784 | 632 | 728 | 920 |
| **$\Delta\rho_{max}$, $\Delta\rho_{min}$ (e Å$^{-3}$)** | 0.19, −0.22 | 0.36, − 0.25 | 0.23, −0.26 | 0.22, − 0.36 | 0.26, −0.22 |
| **h range** | -9 → 9 | -9 → 9 | -13 → 13 | -15 → 15 | -14 → 14 |
| **k range** | -18 → 18 | -18 → 18 | -13 → 13 | -16 → 17 | -15 → 15 |
| **l range** | -15 → 15 | -15 → 15 | -12 → 12 | -10 → 10 | -14 → 14 |
| **measured reflections** | 24992 | 20656 | 12294 | 24641 | 21500 |
| **independent reflections** | 2936 | 2934 | 2307 | 2738 | 3445 |

| | | | | | |
|---|---|---|---|---|---|
| **Reflections with I> 2σ(I)** | 2043 | 2549 | 2013 | 2028 | 2789 |
| **$R_{int}$** | 0.077 | 0.023 | 0.021 | 0.137 | 0.033 |
| **$R_1[I > 2\sigma(I)]$** | 0.049 | 0.041 | 0.042 | 0.052 | 0.043 |
| **$wR_2$ (all)** | 0.142 | 0.128 | 0.115 | 0.130 | 0.117 |
| **Goodness of fit** | 1.11 | 1.10 | 1.08 | 1.05 | 1.07 |
| **X-ray diffractometer** | BRUKER APEX | BRUKER APEX | BRUKER APEX | BRUKER APEX | BRUKER APEX |

| | **ACF-2,4DHBA (1:1)** | **ACF-3,5-DHBA (1:1)** | **ACF-3,5-DHBA-PIP-$H_2O$ (1:1:1:2)** | **ACF-3,5-DHBA-INA-H2O (1:2:1:4)** | **ACF-3,5-DHBA-INA (1:1:1)** |
|---|---|---|---|---|---|
| **Empirical Formula** | $C_9H_{10}N_4O_4$, $C_7H_6O_4$ | $C_9H_{10}N_4O_4$, $C_7H_6O_4$ | $C_9H_9N_4O_4$, $C_7H_5O_4$, $C_4H_{12}N_2$, $2(H_2O)$ | $C_9H_9N_4O_4$, $2(C_7H_6O_4)$, $C_6H_7N_2O$, $4(H_2O)$ | $C_9H_9N_4O_4$, $C_7H_6O_4$, $C_6H_7N_2O$ |
| **Formula Weight** | 392.33 | 392.33 | 514.50 | 740.64 | 514.45 |
| **Crystal system** | Monoclinic | Monoclinic | Monoclinic | Triclinic | Monoclinic |
| **Space group** | *P* $2_1/n$ | *P* $2_1/n$ | $P2_1/n$ | *P*-1 | *C*2/*c* |
| **T (K)** | 298(2) | 298(2) | 298(2) | 298(2) | 298(2) |
| **a (Å)** | 8.0623 (13) | 9.3016 (9) | 10.8804 (10) | 7.4385 (8) | 39.716 (3) |
| **b (Å)** | 15.923 (3) | 16.3751 (16) | 18.8687 (16) | 8.2775 (9) | 7.4150 (6) |
| **c (Å)** | 13.427 (2) | 11.1494 (11) | 11.6853 (10) | 28.182 (3) | 16.0031 (13) |
| **α (°)** | 90 | 90 | 90 | 93.339 (6) | 90 |
| **β (°)** | 105.245 (9) | 97.455 (5) | 102.960 (3) | 97.355 (6) | 93.845 (6) |
| **γ (°)** | 90 | 90 | 90 | 103.420 (6) | 90 |
| **V (Å3)** | 1663.1 (5) | 1683.9 (3) | 2337.9 (4) | 1667.0 (3) | 4702.2 (6) |
| **Dcalc (gcm–3)** | 1.567 | 1.548 | 1.462 | 1.476 | 1.453 |
| **Z** | 4 | 4 | 4 | 2 | 8 |
| **F(000)** | 816 | 816 | 1088 | 776 | 2144 |
| **Δρmax, Δρmin (e Å−3)** | 0.26, − 0.25 | 0.23, −0.24 | 0.49, −0.32 | 0.46, −0.25 | 0.33, −0.29 |
| **h range** | -9 → 9 | -11 → 11 | -14 → 14 | -8 → 8 | -46 → 46 |
| **k range** | -19 → 18 | -19 → 19 | -24 → 24 | -9 → 9 | -8 → 8 |
| **l range** | -16 → 15 | -13 → 13 | -14 → 15 | -33 → 33 | -19 → 19 |

| | | | | | |
|---|---|---|---|---|---|
| **measured reflections** | 21163 | 19725 | 56538 | 23756 | 37466 |
| **independent reflections** | 2966 | 2994 | 5312 | 5931 | 4124 |
| **Reflections with I> 2σ(I)** | 2047 | 2312 | 4797 | 3925 | 2104 |
| **$R_{int}$** | 0.080 | 0.044 | 0.026 | 0.051 | 0.250 |
| **$R_1$[I >2σ(I)]** | 0.048 | 0.039 | 0.049 | 0.056 | 0.091 |
| **wR2 (all)** | 0.111 | 0.106 | 0.131 | 0.137 | 0.217 |
| **Goodness-of-fit** | 1.04 | 1.02 | 1.07 | 1.04 | 1.05 |
| **X–ray Diffractometer** | BRUKER APEX | BRUKER APEX | BRUKER APEX | BRUKER APEX | BRUKER APEX |

| | **ACF-GA-INA Form I (1:1:1)** | **ACF-GA-INA Form II (1:1:1)** | **ACF-GA-PIP-$H_2O$ (1:1:0.5:2)** | **ACF-35-DHBA-PIP (1:1:0.5)** | **ACF-3,5-DHBA-PIP-H2O (1:1:0.5:2)** |
|---|---|---|---|---|---|
| **Empirical Formula** | $C_9H_9N_4O_4$, $C_7H_6O_5$, $C_6H_7N_2O$ | $C_9H_9N_4O_4$, $C_7H_6O_5$, $C_6H_7N_2O$ | $C_9H_9N_4O_4$, $C_7H_6O_5$, 0.5($C_4H_{12}N_2$), 2($H_2O$) | $C_9H_9N_4O_4$, $C_7H_6O_4$, 0.5($C_4H_{12}N_2$), | $C_9H_9N_4O_4$, $C_7H_6O_4$, 0.5($C_4H_{12}N_2$), 2($H_2O$) |
| **Formula Weight** | 530.46 | 530.46 | 487.43 | 435.40 | 471.43 |
| **Crystal system** | Triclinic | Monoclinic | Triclinic | Monoclinic | Triclinic |
| **Space group** | *P*-1 | *C*2/*c* | *P*-1 | *C*2/*c* | *P*-1 |
| **T (K)** | 298(2) | 298(2) | 100(2) | 298(2) | 298(2) |
| **a (Å)** | 5.0112 (2) | 39.4480 (14) | 6.9324 (4) | 33.531 (2) | 7.6567 (3) |
| **b (Å)** | 11.0262 (6) | 7.4122 (3) | 10.6301 (7) | 7.2809 (5) | 8.5609 (3) |
| **c (Å)** | 21.2481 (10) | 16.2574 (6) | 15.346 (1) | 15.7588 (11) | 17.0364 (6) |
| **α (°)** | 94.999 (3) | 90 | 72.127 (2) | 90 | 95.375 (2) |
| **β (°)** | 96.473 (3) | 93.959 (4) | 79.409 (2) | 100.953 (3) | 93.973 (2) |
| **γ (°)** | 101.247 (3) | 90 | 74.348 (2) | 90 | 107.274 (2) |
| **V (Å3)** | 1136.97 (9) | 4742.3 (3) | 1030.08 (11) | 3777.2 (5) | 1056.10 (7) |
| **Dcalc (gcm–3)** | 1.549 | 1.486 | 1.572 | 1.531 | 1.482 |
| **Z** | 2 | 8 | 2 | 8 | 2 |
| **F(000)** | 552 | 2208 | 512 | 1824 | 496 |
| **Δρmax, Δρmin (e Å−3)** | 0.25, − −0.28 | 0.23, −0.30 | 0.29, −0.27 | 0.23, −0.21 | 0.37, −0.31 |
| **h range** | -5 → 5 | -46 → 46 | -8 → 8 | -40 → 39 | -9 → 9 |
| **k range** | -13 → 13 | -8 → 8 | -12 → 12 | -8 → 8 | -10 → 10 |

| **l range** | -25 → 25 | -19 → 19 | -18 → 18 | -18 → 18 | -20 → 20 |
|---|---|---|---|---|---|
| **measured reflections** | 16995 | 39450 | 32685 | 15580 | 18371 |
| **independent reflections** | 4017 | 4261 | 3584 | 3367 | 3762 |
| **Reflections with I> 2σ(I)** | 2947 | 2685 | 3449 | 2722 | 3222 |
| **$R_{int}$** | 0.042 | 0.116 | 0.028 | 0.029 | 0.021 |
| **$R_1$[I >2σ(I)]** | 0.042 | 0.057 | 0.035 | 0.038 | 0.039 |
| **wR2 (all)** | 0.123 | 0.130 | 0.089 | 0.104 | 0.126 |
| **Goodness-of-fit** | 1.11 | 1.03 | 1.03 | 1.06 | 1.09 |
| **X–ray Diffractometer** | BRUKER APEX | BRUKER APEX | BRUKER APEX | BRUKER APEX | BRUKER APEX |

## 5.2.2 Hirshfeld Surface Analysis

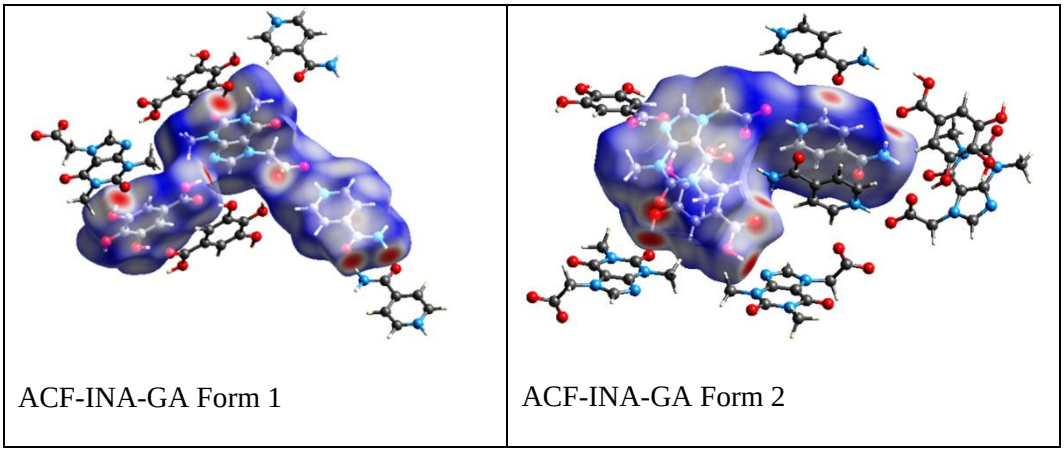

ACF-INA-GA Form 1 ACF-INA-GA Form 2

**Figure 5.8:** Hirshfeld surface comparison of ACF-INA-GA ternary salt-cocrystal polymorphs.

The intermolecular interactions between ACF and coformers were analyzed in Hirshfeld surfaces and 2D fingerprint plots in CrystalExplorer 3.1 (Figure 5.8-5.10)[65-71] for the polymorphic pair ACF-INA-GA. The dark red regimes in Figure 5.8-5.10 apparently correspond to the close contact interactions as a result of the intermolecular interactions such as N-H---O and O-H---O, moreover, the light red and other visible regimes on the surfaces are due to the C-H---O and H-H interactions, respectively.[65-66] 2D fingerprint plots of Figure 5.9 and Table 5.3 depict the intermolecular interactions contribution percentage polymorphs of ternary salt-cocrystal. The Hirshfeld surfaces indicate the percentage of O-H (37.4 % in Form 1 and 37.1 % in Form 2) and N-H (5.2 % in Form 1

and 5.3 % in Form 2), and a higher contribution of C-H (14.5% in Form 1 and 8.4% in Form 2) and C-O (7 % in Form 1 and 3.9 % in Form 2).

| | All | O-H | N-H | C-H | C-O |
|---|---|---|---|---|---|
| ACF | 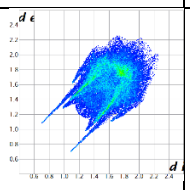 | 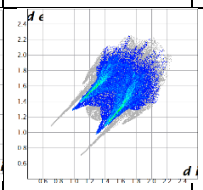 | 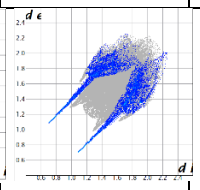 | 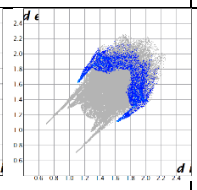 | 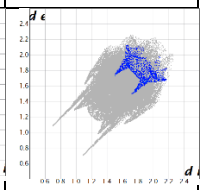 |
| ACF-INA | 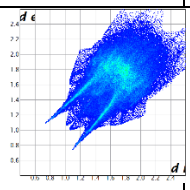 | 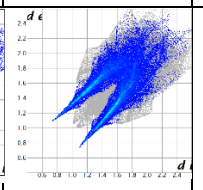 | 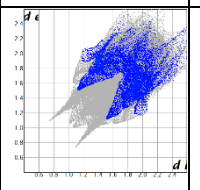 | 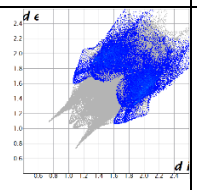 | 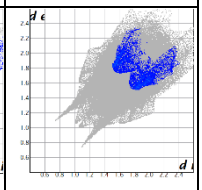 |
| ACF-GA | 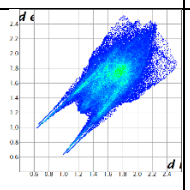 | 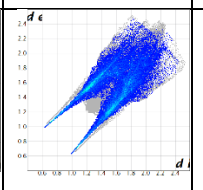 | 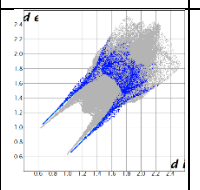 | 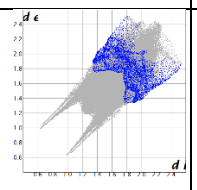 | 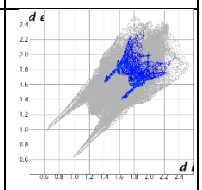 |
| ACF-PIP | 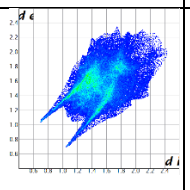 | 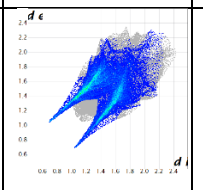 | 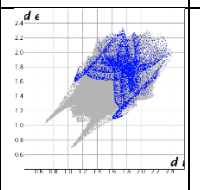 | 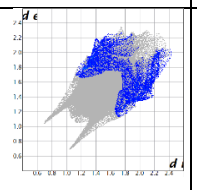 | 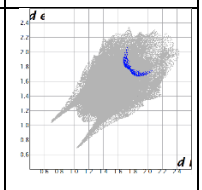 |
| ACF-GA-INA Form-1 | 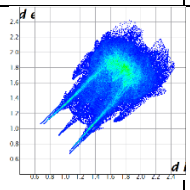 | 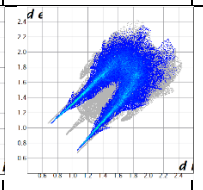 | 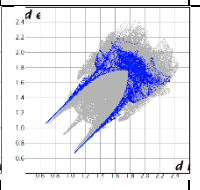 | 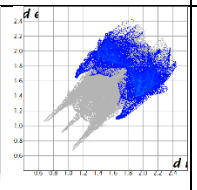 | 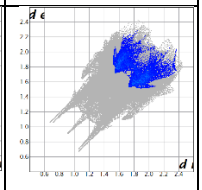 |
| ACF-GA-INA Form-2 | 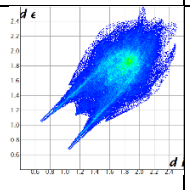 | 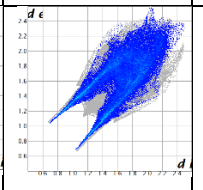 | 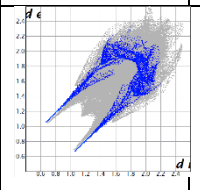 | 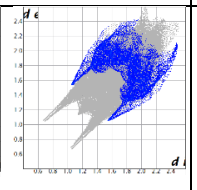 | 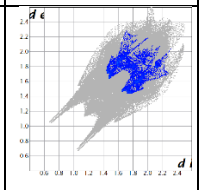 |

**Figure 5.9:** 2D Fingerprint plots for different intermolecular interactions in acefylline binary and ternary salt-cocrystals.

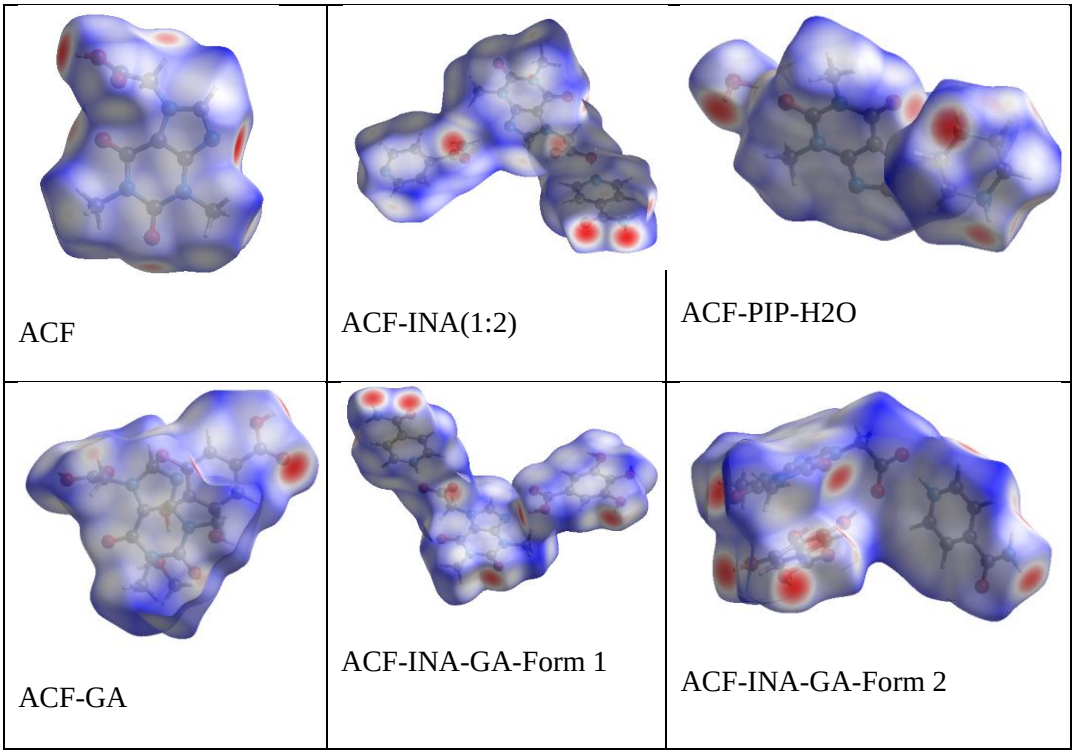


**Figure 5.10:** Hirshfeld surfaces for the acefylline binary and ternary salt-cocrystals.

**Table 5.3:** Percentage contributions to the Hirshfeld surface area for the various close intermolecular Contacts for molecules in Acefylline(ACF) and binary-ternary salt-cocrystals polymorphs. Percentages are given below table only for the major atom-type/atom-type contacts.

| **Compounds** | **%O-H** | **%N-H** | **%C-H** | **%C-O** |
|---|---|---|---|---|
| ACF | 40.1 | 11.3 | 7.7 | 2.1 |
| ACF-INA | 29.6 | 8.9 | 16.1 | 4.3 |
| ACF-GA-MeOH | 39.1 | 4.9 | 3.9 | 4.1 |
| ACF-PIP-H2O | 42.8 | 5.1 | 6.5 | 0.3 |
| ACF-GA-INA Form1 | 37.4 | 5.2 | 14.5 | 7 |
| ACF-GA-INA Form2 | 37 | 5.3 | 8.4 | 3.9 |

The hydrogen bonds are quantified in energetic terms by estimating the electrostatic and dispersion contribution in the crystal structures (Figure 5.11-5.13 and Table 5.4-5.7) using CrystalExplorer.[67-72] The energy frameworks corresponding to the electrostatic, dispersion and total energies of two ternary polymorphs of ACF-INA-GA (Figure 5.11 and Table 5.6-5.7) exhibits a higher contribution of dispersion term (46.7 kJ/mol) to the total energy while in Form 2 the electrostatic term (63.1 kJ/mol) plays an higher role (Figure 5.11 and

Table 5.6-5.7). Gaussian 9 calculations of crystal lattice stabilization energy have value of –21 kcal/mol and –25 kcal/mol for Form 1 and 2, respectively (Table 5.8).

| | | | |
|---|---|---|---|
| Form 1 | 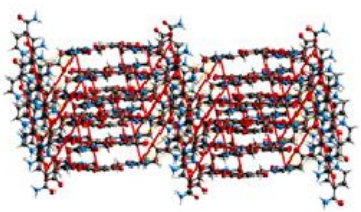 | 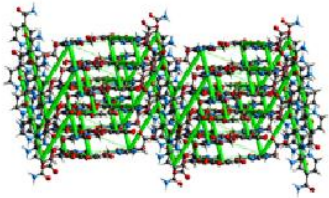 | 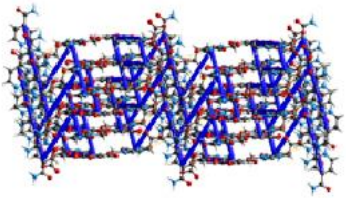 |
| Form 2 | 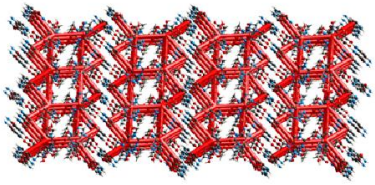 | 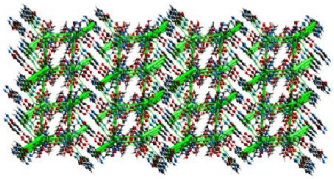 | 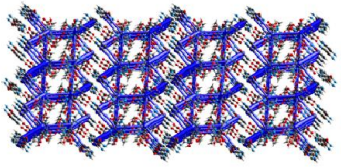 |
| | Electrostatic term | Dispersion term | Total interaction energy |

**Figure 5.11:** Crystal lattice energy contribution from electrostatic (red), dispersion (green) and total interaction energy (blue) components in Form 1 and Form 2. The energy scale factor is 25 and the energy threshold is 5 kJ/mol.

| | | |
|---|---|---|
| 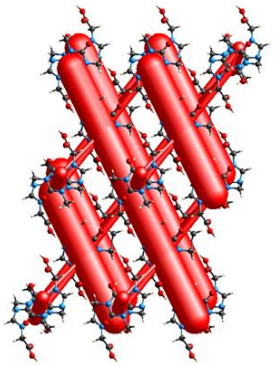 | 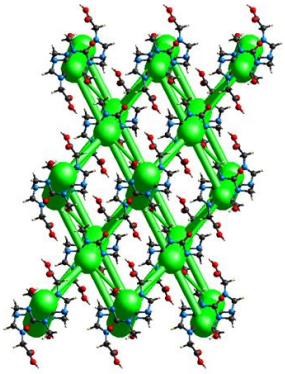 | 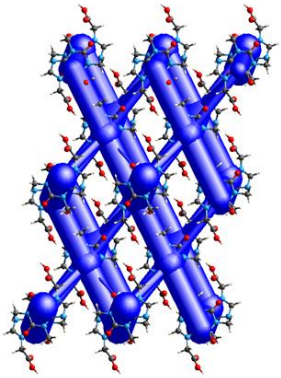 |
| Electrostatic term | Dispersion term | Total Energy |

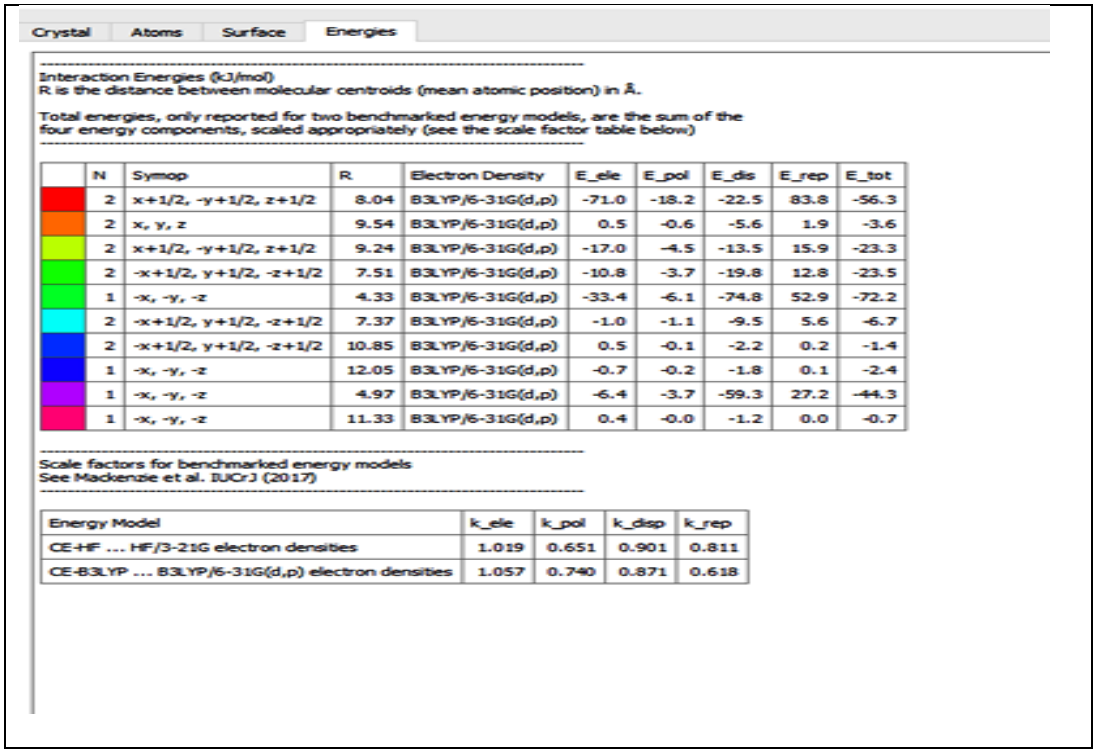

Crystal | Atoms | Surface | Energies

Interaction Energies (kJ/mol)
R is the distance between molecular centroids (mean atomic position) in Å.

Total energies, only reported for two benchmarked energy models, are the sum of the four energy components, scaled appropriately (see the scale factor table below)

| | N | Symop | R | Electron Density | E_ele | E_pol | E_dis | E_rep | E_tot |
|---|---|---|---|---|---|---|---|---|---|
| | 2 | x+1/2, -y+1/2, z+1/2 | 8.04 | B3LYP/6-31G(d,p) | -71.0 | -18.2 | -22.5 | 83.8 | -56.3 |
| | 2 | x, y, z | 9.54 | B3LYP/6-31G(d,p) | 0.5 | -0.6 | -5.6 | 1.9 | -3.6 |
| | 2 | x+1/2, -y+1/2, z+1/2 | 9.24 | B3LYP/6-31G(d,p) | -17.0 | -4.5 | -13.5 | 15.9 | -23.3 |
| | 2 | -x+1/2, y+1/2, -z+1/2 | 7.51 | B3LYP/6-31G(d,p) | -10.8 | -3.7 | -19.8 | 12.8 | -23.5 |
| | 1 | -x, -y, -z | 4.33 | B3LYP/6-31G(d,p) | -33.4 | -6.1 | -74.8 | 52.9 | -72.2 |
| | 2 | -x+1/2, y+1/2, -z+1/2 | 7.37 | B3LYP/6-31G(d,p) | -1.0 | -1.1 | -9.5 | 5.6 | -6.7 |
| | 2 | -x+1/2, y+1/2, -z+1/2 | 10.85 | B3LYP/6-31G(d,p) | 0.5 | -0.1 | -2.2 | 0.2 | -1.4 |
| | 1 | -x, -y, -z | 12.05 | B3LYP/6-31G(d,p) | -0.7 | -0.2 | -1.8 | 0.1 | -2.4 |
| | 1 | -x, -y, -z | 4.97 | B3LYP/6-31G(d,p) | -6.4 | -3.7 | -59.3 | 27.2 | -44.3 |
| | 1 | -x, -y, -z | 11.33 | B3LYP/6-31G(d,p) | 0.4 | -0.0 | -1.2 | 0.0 | -0.7 |

Scale factors for benchmarked energy models
See Mackenzie et al. IUCrJ (2017)

| Energy Model | k_ele | k_pol | k_disp | k_rep |
|---|---|---|---|---|
| CE-HF ... HF/3-21G electron densities | 1.019 | 0.651 | 0.901 | 0.811 |
| CE-B3LYP ... B3LYP/6-31G(d,p) electron densities | 1.057 | 0.740 | 0.871 | 0.618 |

**Figure 5.12:** Energy frameworks of ACF

**Energy framework of Isostructural binary cocrystals**

| | Elecrostatic term | Dispersion term | Total Energy |
|---|---|---|---|
| ACF-PHBA | 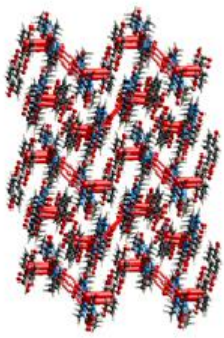 | 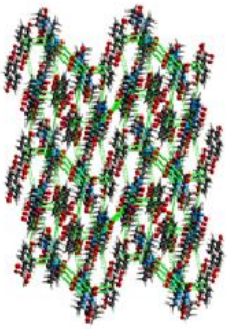 | 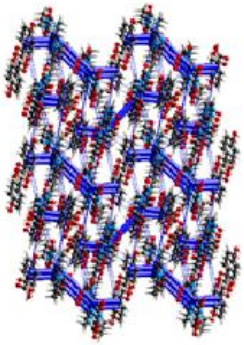 |

| | | | |
|---|---|---|---|
| ACF-24DHBA | 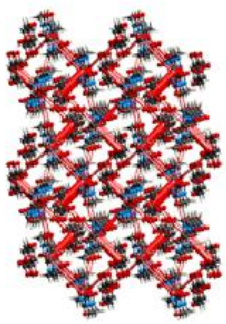 | 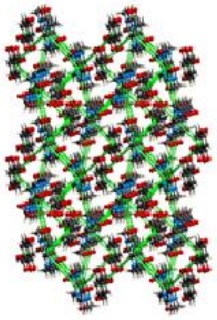 | 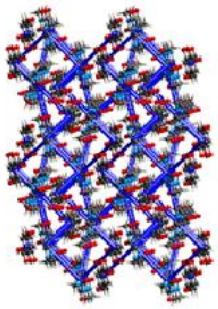 |

**Figure 5.13:** ACF-PHBA and ACF-24DHBA energy frameworks along A-axis

**Table 5.4: ACF-PHBA crystal structure and unique interaction energies (kj/mol)**

| | N | Symop | R | Electron Density | E_ele | E_pol | E_dis | E_rep | E_tot |
|---|---|---|---|---|---|---|---|---|---|
| | 1 | -x, -y, -z | 10.29 | B3LYP/6-31G(d,p) | -1.0 | -0.9 | -4.9 | 0.7 | -5.5 |
| | 2 | x, y, z | 8.11 | B3LYP/6-31G(d,p) | -60.7 | -14.4 | -19.2 | 67.7 | -49.7 |
| | 2 | -x+1/2, y+1/2, -z+1/2 | 9.78 | B3LYP/6-31G(d,p) | -4.0 | -0.3 | -7.7 | 6.6 | -7.1 |
| | 1 | - | 7.24 | B3LYP/6-31G(d,p) | 0.0 | nan | 0.0 | 0.0 | nan |
| | 2 | -x+1/2, y+1/2, -z+1/2 | 8.55 | B3LYP/6-31G(d,p) | 0.0 | 0.0 | 0.0 | 0.0 | 0.0 |
| | 1 | - | 7.89 | B3LYP/6-31G(d,p) | -4.0 | -0.3 | -7.7 | 6.6 | -7.1 |
| | 1 | -x, -y, -z | 6.74 | B3LYP/6-31G(d,p) | -22.2 | -4.7 | -25.0 | 19.3 | -36.7 |
| | 1 | - | 4.50 | B3LYP/6-31G(d,p) | -0.7 | -0.1 | -2.8 | 0.2 | -3.1 |
| | 2 | x+1/2, -y+1/2, z+1/2 | 7.51 | B3LYP/6-31G(d,p) | -1.4 | -0.8 | -4.9 | 1.9 | -5.2 |
| | 1 | - | 3.84 | B3LYP/6-31G(d,p) | -60.7 | -14.4 | -19.2 | 67.7 | -49.7 |
| | 1 | - | 8.31 | B3LYP/6-31G(d,p) | -0.3 | -0.0 | -0.1 | 0.0 | -0.4 |
| | 1 | - | 8.35 | B3LYP/6-31G(d,p) | -4.0 | -0.3 | -7.7 | 6.6 | -7.1 |
| | 2 | x+1/2, -y+1/2, z+1/2 | 9.18 | B3LYP/6-31G(d,p) | -0.7 | -0.1 | -2.8 | 0.2 | -3.1 |
| | 1 | - | 8.73 | B3LYP/6-31G(d,p) | -0.2 | -0.0 | -0.1 | 0.0 | -0.3 |

**Table 5.5: ACF-2,4DHBA crystal structure unique interaction energies (kj/mol)**

| | N | Symop | R | Electron Density | E_ele | E_pol | E_dis | E_rep | E_tot |
|---|---|---|---|---|---|---|---|---|---|
| | 2 | x, y, z | 8.06 | B3LYP/6-31G(d,p) | -60.0 | -14.2 | -19.5 | 68.2 | -48.8 |
| | 1 | - | 8.87 | B3LYP/6-31G(d,p) | 0.0 | nan | 0.0 | 0.0 | nan |
| | 1 | - | 3.78 | B3LYP/6-31G(d,p) | -0.7 | -0.1 | -2.8 | 0.3 | -3.1 |
| | 2 | -x+1/2, y+1/2, -z+1/2 | 8.60 | B3LYP/6-31G(d,p) | -10.3 | -3.1 | -12.5 | 6.6 | -20.1 |
| | 2 | x+1/2, -y+1/2, z+1/2 | 9.24 | B3LYP/6-31G(d,p) | -0.7 | -0.1 | -2.8 | 0.3 | -3.1 |
| | 2 | x+1/2, -y+1/2, z+1/2 | 7.55 | B3LYP/6-31G(d,p) | -1.2 | -0.6 | -4.4 | 1.2 | -4.9 |
| | 1 | - | 7.78 | B3LYP/6-31G(d,p) | 0.2 | -0.0 | -0.1 | 0.0 | 0.1 |
| | 1 | - | 8.34 | B3LYP/6-31G(d,p) | -10.3 | -3.1 | -12.5 | 6.6 | -20.1 |
| | 1 | - | 4.73 | B3LYP/6-31G(d,p) | -60.0 | -14.2 | -19.5 | 68.2 | -48.8 |
| | 1 | - | 7.17 | B3LYP/6-31G(d,p) | -0.2 | -0.0 | -0.1 | 0.0 | -0.3 |
| | 1 | - | 8.48 | B3LYP/6-31G(d,p) | 0.9 | -0.1 | -1.0 | 0.0 | 0.0 |
| | 2 | -x+1/2, y+1/2, -z+1/2 | 9.83 | B3LYP/6-31G(d,p) | -3.8 | -0.3 | -7.5 | 6.0 | -7.0 |
| | 1 | -x, -y, -z | 6.63 | B3LYP/6-31G(d,p) | -22.0 | -4.6 | -26.1 | 19.4 | -37.4 |
| | 1 | -x, -y, -z | 10.16 | B3LYP/6-31G(d,p) | -1.3 | -1.1 | -5.5 | 1.1 | -6.3 |

**Table 5.6: ACF-INA-GA (1:1:1) Form 1_p-1 crystal structure and unique interaction energies (kj/mol)**

Crystal | Atoms | Surface | Energies

---

Interaction Energies (kJ/mol)
R is the distance between molecular centroids (mean atomic position) in Å.

Total energies, only reported for two benchmarked energy models, are the sum of the four energy components, scaled appropriately (see the scale factor table below)

---

| | N | Symop | R | Electron Density | E_ele | E_pol | E_dis | E_rep | E_tot |
|---|---|---|---|---|---|---|---|---|---|
| | 2 | x, y, z | 5.01 | B3LYP/6-31G(d,p) | -17.2 | -7.8 | -46.7 | 33.3 | -44.1 |
| | 1 | - | 6.06 | B3LYP/6-31G(d,p) | 0.0 | nan | 0.0 | 0.0 | nan |
| | 1 | - | 8.35 | B3LYP/6-31G(d,p) | 1.4 | -0.2 | -1.9 | 0.1 | -0.3 |
| | 1 | - | 9.12 | B3LYP/6-31G(d,p) | 0.7 | -0.1 | -0.3 | 0.0 | 0.4 |
| | 1 | - | 7.82 | B3LYP/6-31G(d,p) | 0.0 | nan | 0.0 | 0.0 | nan |
| | 1 | -x, -y, -z | 10.83 | B3LYP/6-31G(d,p) | 0.0 | 0.0 | 0.0 | 0.0 | 0.0 |
| | 1 | - | 7.73 | B3LYP/6-31G(d,p) | -1.7 | -0.1 | -0.2 | 0.0 | -2.0 |
| | 1 | - | 6.71 | B3LYP/6-31G(d,p) | 0.6 | -0.2 | -0.8 | 0.0 | -0.1 |
| | 1 | - | 8.18 | B3LYP/6-31G(d,p) | -17.2 | -7.8 | -46.7 | 33.3 | -44.1 |
| | 1 | -x, -y, -z | 10.86 | B3LYP/6-31G(d,p) | 3.1 | -0.9 | -6.4 | 2.3 | -1.5 |
| | 1 | - | 8.26 | B3LYP/6-31G(d,p) | 0.7 | -0.1 | -0.3 | 0.0 | 0.4 |
| | 1 | - | 8.08 | B3LYP/6-31G(d,p) | 3.1 | -0.9 | -6.4 | 2.3 | -1.5 |
| | 1 | - | 6.46 | B3LYP/6-31G(d,p) | 0.6 | -0.2 | -0.8 | 0.0 | -0.1 |
| | 1 | - | 6.18 | B3LYP/6-31G(d,p) | 5.5 | -0.4 | -0.6 | 0.0 | 5.0 |
| | 1 | - | 7.94 | B3LYP/6-31G(d,p) | -17.2 | -7.8 | -46.7 | 33.3 | -44.1 |
| | 1 | - | 8.18 | B3LYP/6-31G(d,p) | 4.8 | -0.2 | -0.2 | 0.0 | 4.8 |

---

Scale factors for benchmarked energy models
See Mackenzie et al. IUCrJ (2017)

---

| Energy Model | k_ele | k_pol | k_disp | k_rep |
|---|---|---|---|---|
| CE-HF ... HF/3-21G electron densities | 1.019 | 0.651 | 0.901 | 0.811 |
| CE-B3LYP ... B3LYP/6-31G(d,p) electron densities | 1.057 | 0.740 | 0.871 | 0.618 |

**Table 5.7: ACF-INA-GA (1:1:1) Form 2_C2/c crystal structure and unique interaction energies (kj/mol)**

Crystal | Atoms | Surface | Energies

---

Interaction Energies (kJ/mol)
R is the distance between molecular centroids (mean atomic position) in Å.

Total energies, only reported for two benchmarked energy models, are the sum of the four energy components, scaled appropriately (see the scale factor table below)

---

| | N | Symop | R | Electron Density | E_ele | E_pol | E_dis | E_rep | E_tot |
|---|---|---|---|---|---|---|---|---|---|
| | 1 | - | 8.10 | B3LYP/6-31G(d,p) | -63.1 | -13.8 | -14.9 | 87.3 | -35.9 |
| | 2 | x, -y, z+1/2 | 9.69 | B3LYP/6-31G(d,p) | 1.1 | -0.1 | -1.4 | 0.0 | -0.2 |
| | 1 | -x+1/2, -y+1/2, -z | 10.87 | B3LYP/6-31G(d,p) | 3.2 | -0.7 | -5.2 | 1.3 | -0.9 |
| | 1 | - | 6.07 | B3LYP/6-31G(d,p) | 0.0 | nan | 0.0 | 0.0 | nan |
| | 1 | -x, y, -z+1/2 | 11.57 | B3LYP/6-31G(d,p) | 0.0 | -0.9 | 0.0 | 0.0 | -0.6 |
| | 1 | - | 3.69 | B3LYP/6-31G(d,p) | -67.4 | -17.9 | -61.5 | 101.0 | -75.8 |
| | 1 | - | 7.73 | B3LYP/6-31G(d,p) | -49.8 | -11.2 | -18.1 | 65.5 | -36.2 |
| | 1 | - | 8.50 | B3LYP/6-31G(d,p) | -6.9 | -1.9 | -7.3 | 6.5 | -11.0 |
| | 1 | - | 8.25 | B3LYP/6-31G(d,p) | 1.8 | -0.9 | -1.8 | 0.1 | -0.2 |
| | 1 | - | 7.08 | B3LYP/6-31G(d,p) | 1.1 | -0.1 | -1.4 | 0.0 | -0.2 |
| | 2 | x, -y, z+1/2 | 8.40 | B3LYP/6-31G(d,p) | -5.1 | -0.8 | -5.8 | 0.8 | -10.5 |
| | 2 | -x+1/2, y+1/2, -z+1/2 | 8.98 | B3LYP/6-31G(d,p) | -2.0 | -0.7 | -6.8 | 0.4 | -8.3 |
| | 1 | - | 7.03 | B3LYP/6-31G(d,p) | 0.8 | -0.5 | -2.4 | 0.0 | -1.6 |
| | 1 | - | 3.79 | B3LYP/6-31G(d,p) | -8.9 | -3.8 | -53.6 | 34.4 | -37.7 |
| | 1 | - | 8.98 | B3LYP/6-31G(d,p) | -0.9 | -0.1 | -0.1 | 0.0 | -1.1 |

---

Scale factors for benchmarked energy models
See Mackenzie et al. IUCrJ (2017)

---

| Energy Model | k_ele | k_pol | k_disp | k_rep |
|---|---|---|---|---|
| CE-HF ... HF/3-21G electron densities | 1.019 | 0.651 | 0.901 | 0.811 |
| CE-B3LYP ... B3LYP/6-31G(d,p) electron densities | 1.057 | 0.740 | 0.871 | 0.618 |

**Gaussian 09 Calculation of two polymorphs stabilization energy**

Two ternary Cocrystal polymorphs (isomers) structures were optimized by using DFT based B3LYP[73]/6-31G(d,p)[74] level of theory. The initial geometry parameters for the structural motifs were taken from crystal data. Single point energy calculations were done using B3LYP/6-31G(d,p) level of theory on the optimized geometries to calculate the stabilization energies. All the calculations were carried out with GAUSSIAN09[75] suite of programme.

Stabilization energy calculations:

The stabilization energies were calculated using the following formula

$E_{Stabilization} = E_{Ternary}(ABC) - E_A + E_B + E_C$

In the above equation, E ternary is the counterpoise corrected energy of cocrystal ($E_{ABC}$), $E_A$, $E_B$ and $E_C$ are the energies corresponding to single component molecules respectively.

ACF ($E_A$) = Energy HF= -868.9574841

INA ($E_B$) = Energy HF= -416.9983147

GA ($E_C$) = Energy HF= -646.4993657

D= $E_{A+}$ $E_{B+}$ $E_C$

= -868.9574841+ -416.9983147+ -646.4993657

= -1932.454

ACF-INA-GA (ABC) Form1 Energy HF= -1932.489

$Energy = E_{products} - E_{reactants}$

Form1 Energy (ABC) = -1932.489 +1932.454

= -0.035*627.51

= -21.96 Kcal/mol

ACF-INA-GA (ABC) Form2 Energy HF= -1932.495

Form2 Energy (ABC) = -1932.495 +1932.454

= -0.041*627.51

= -25.72 Kcal/mol

**Table 5.8:** Stabilization energy values for ternary salt-cocrystal polymorphs calculated in Gaussian 09 package.

| **Ternary salt-cocrystal polymorphs(Isomers) form1&form2** | **Stabilization energy (Kcal/mol) DFT-B3LYP/6-31g(d,p)** |
|---|---|
| 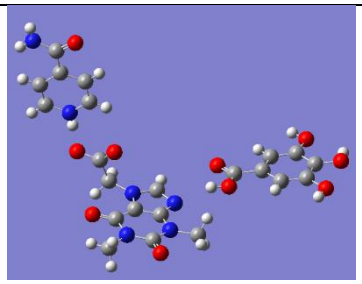 **Form 1** | **-21.96 Kcal/mol** |
| 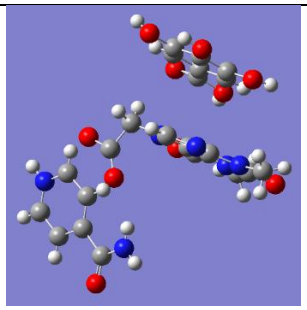 **Form 2** | **-25.72 Kcal/mol** |

## 5.2.3 Structure solution from powder diffraction data

The crystal structure of **ACF-INA** 1:2 cocrystal was determined with the use of SDPD methods.[56-58] The X-ray powder diffraction data in a 4 – 90° 2θ range were collected using a Huber G670 Guinier camera (Cu $K_{\alpha 1}$ radiation, λ = 1.54059 Å) equipped with an imaging-plate detector. The powder pattern was indexed in a triclinic unit cell, and the crystal structure was solved with the use of simulated annealing technique[6] and refined with the program MRIA[76] following the known procedures described by us earlier.[56-58] The crystal data, data collection and refinement parameters are given in Table 5.9. The diffraction profiles after the final bond-restrained Rietveld refinements are shown in Table 5.9. CCDC No. 2014730

**Table 5.9:** Crystallographic parameters and rietveld plot of ACF-INA (1:2) cocrystal.

| | ACF-INA (1:2) | Rietveld plot for **ACF-INA (**1:2) cocrystal |
|---|---|---|

| | |
|---|---|
| empirical formula | $C_9H_{10}N_4O_4$•2($C_6H_6N_2O$) |
| $M_r$ | 482.47 |
| crystal system | Triclinic |
| space group | *P-1* |
| *a*, Å | 11.1839(10) |
| *b*, Å | 20.5259(18) |
| *c*, Å | 5.0288(7) |
| $\alpha$, ° | 93.583(11) |
| $\beta$, ° | 100.418(14) |
| $\gamma$, ° | 95.469(12) |
| volume, $Å^3$ | 1126.5(2) |
| Z | 2 |
| $D_x$ (Mg $m^{-3}$) | 1.422 |
| μ, $\mu\mu^{-1}$ | 0.907 |
| $2\theta_{\mu\nu} - 2\theta_{\mu\alpha\xi}$ , Δ 2θ (°) | 4.00 – 90.00, 0.01 |
| no. params/restraints | 171/115 |
| $R_p$, $R_{wp}$, $R_{exp}$ | 0.0232, 0.0299, 0.0200 |

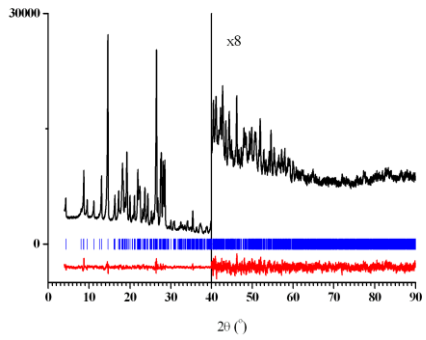


The Rietveld plot for ACF-INA 1:2 cocrystal showing the experimental (black) and difference (experimental minus calculated, red) curves after the final bond-restrained Rietveld refinement. The vertical blue bars denote calculated positions of the diffraction peaks.

## 5.2.4 Powder X-ray Diffraction

All the new solid phases of acefylline and coformers were analyzed by PXRD on a BrukerAXS D8 Diffractometer. The experimental powder diffraction pattern and simulated X-ray pattern from the single crystal structure were compared to confirm the bulk phase purity of binary and ternary slat cocrystals using powder cell.

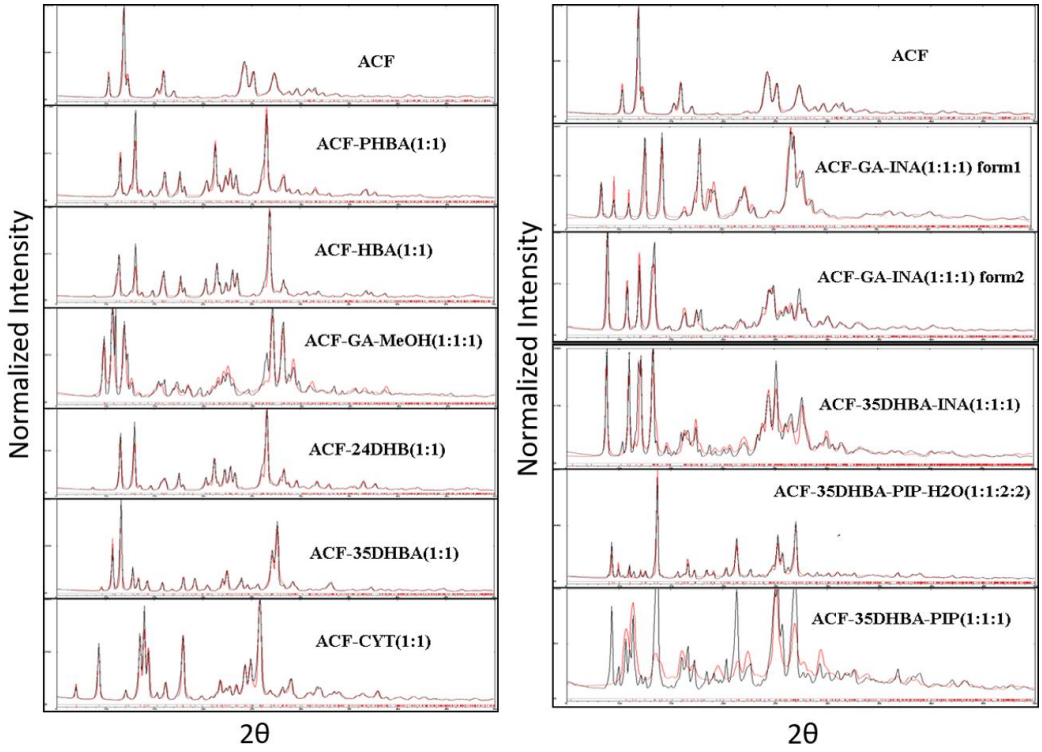


**Figure 5.14:** PXRD overlay of binary and teranry salts and cocrystals powder pattern (black) with calculated line pattern (red).

## 5.2.5 Thermal Analysis

The thermal behavior of acefylline and binary/ternary components were performed on a Mettler Toledo DSC 822e module samples were placed in vented aluminum sample pans for differential scanning calorimetry (DSC). A typical sample size 3-5mg for DSC the temperature range 30-300 °C at 5K/min for DSC samples were purged with a stream of dry N2 gas flowing at 80ml/min. the DSC thermal curves and melting temperatures represented in Figure 5.15-5.16 Table 5.10. The acefylline exhibits a single endotherm at 272°C and doesn't show any phase change. On the other hand all the binary and ternary components shows single endotherms different from that of starting materials indicates bulk phase purity and homogeneity.

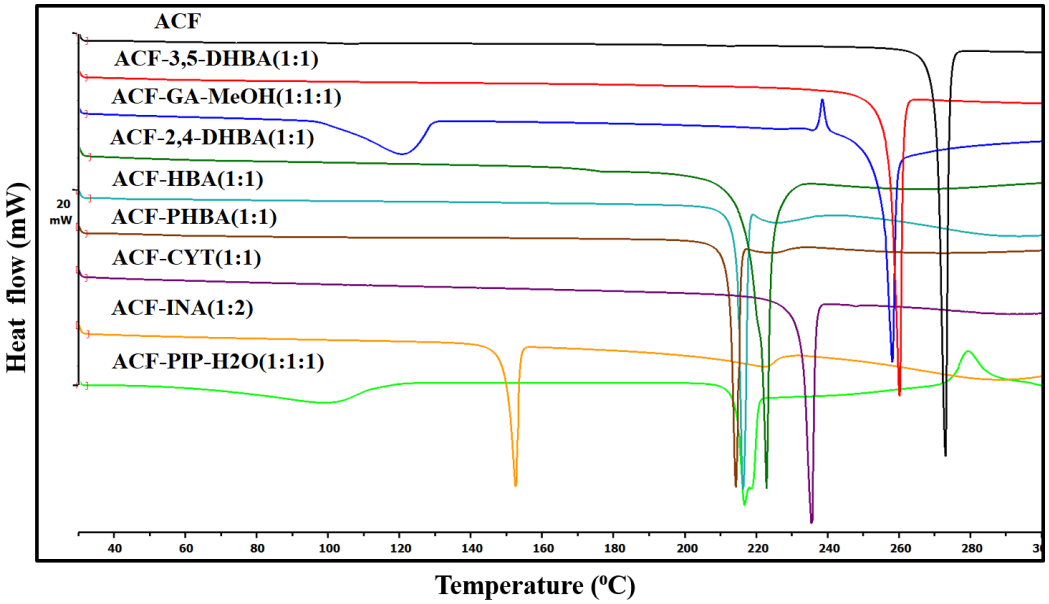


**Figure 5.15:** Comparison of melting point in binary salts and cocrystals observed in the present study with the corresponding single component systems.

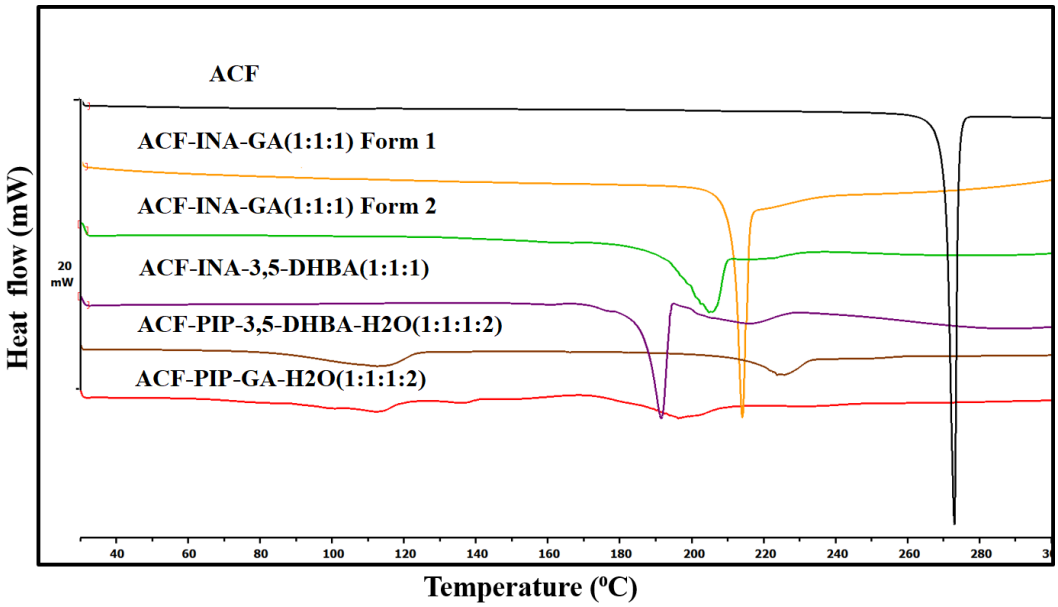


**Figure 5.16:** Comparison of melting point in ternary salt-cocrystal poymorphs observed in the present study with the corresponding single component systems.

**Table 5.10:** Melting points of ACF cocrystals and salts from DSC.

| API/Cocrystal/salt | Melting point ° C |
|---|---|
| ACF | 269-273 |
| ACF-INA(1:2) | 149-153 |
| ACF-PIP-H2O(1:1:1) | 218-220 |

| | |
|---|---|
| ACF-CYT(1:1) | 232-236 |
| ACF-HBA(1:1) | 214-218 |
| ACF-PHBA(1:1) | 211-215 |
| ACF-2,4-DHBA(1:1) | 219-223 |
| ACF-3,5-DHBA(1:1) | 256-260 |
| ACF-GA-MeOH(1:1:1) | 254-258 |
| ACF-INA-GA Form1(1:1:1) | 210-214 |
| ACF-INA-GA Form2(1:1:1) | 198-202 |
| ACF-INA-3,5-DHBA(1:1:1) | 188-192 |
| ACF-PIP-3,5-DHBA-H2O(1:1:1:2) | 218-222 |
| ACF-PIP-GA-H2O(1:1:1:2) | 196-201 |

## 5.2.6 Solution NMR

In order to find out the exact composition in the three/four component crystalline materials, NMR experiments were performed of the single components as well as ternary/quaternary crystalline materials in DMSO-D6 solvent (solvent peak at 2.50(5) ppm). In NMR spectra, the different colour dots correspond to different protons of the component molecule. Here, three/four different molecules are highlighted which is indication of three and four different molecules in the crystalline product of Form1 and Form2. In NMR spectra, well separated and distinct protons of the molecules are taken into account. The area under curve is an indication of number of protons attached to that molecule in the product. In all cases the ratio present in the reaction product is the same as that used for crystallization. The stoichiometry of the Form1 and Form2+HBA reaction mixture system is established by 1H NMR integration (Figure 5.17-5.22).

Solution NMR spectra were recorded on Bruker Avance 400 MHzspectrometer (Bruker-Biospin, Karlsruhe, Germany)

**ACF-GA-INA 1:1:1 (Form 1):** $^{1}$H NMR (400 MHz, DMSO-d6) $\delta$ 12.67–12.60 (m, 1.51 H), 9.26–8.94 (m, 2H), 8.73 (d, $J$ = 5.6 Hz , 2H), 8.27 (bs, 1H), 8.05 (s, 1H), 7.78 (d, $J$ = 5.6 Hz, 2H), 7.75 (s, 1H), 6.95 (s, 2H), 5.09 (s, 2H), 3.45 (s, 3H), 3.21 (s, 3H).

**ACF-GA-INA-HBA 1:1:1:1 (Form 2):** $^{1}$H NMR (400 MHz, DMSO-d6) $\delta$ 12.57 (bs, 1H), 9.97 (bs, 1H), 9.24–8.86 (m, 2H), 8.73 (d, $J$ = 4.8 Hz, 2H), 8.27 (bs, 1H), 8.05 (s, 1H), 7.81–7.73 (m, 6H), 7.10 (s, 1H), 6.95 (s, 2H), 6.78 (d, $J$ = 8.4 Hz, 2H), 5.09 (s, 2H), 3.45 (s, 3H), 3.22 (s, 3H).

**ACF:** $^{1}$H NMR (500 MHz, DMSO-d6) *$\delta$ 8.04* (s, 1H), 5.07 (s, 2H), 3.44 (s, 3H), 3.20 (s, 3H).

**INA:** $^{1}$H NMR (500 MHz, DMSO-d6) *δ 8.72* (dd, *J* = 9.5 & 1.5 Hz, 2H), 8.26 (s, 1H), 7.77 (dd, *J* = 9.25 & 1.75 Hz, 2H), 7.74 (s, 1H).

**HBA:** $^{1}$H NMR (500 MHz, DMSO-d6) *δ 9.99* (bs, 1H), 7.76 (dd, *J* = 6.75 & 1.75 Hz, 3H), 7.12 (bs, 1H), 6.83-6.77 (m, 2H).

**GA:** $^{1}$H NMR (500 MHz, DMSO-d6) *δ 12.24* (bs, 1H), 9.20 (s, 2H), 8.83 (bs, 1H), 6.93 (m, 2H).

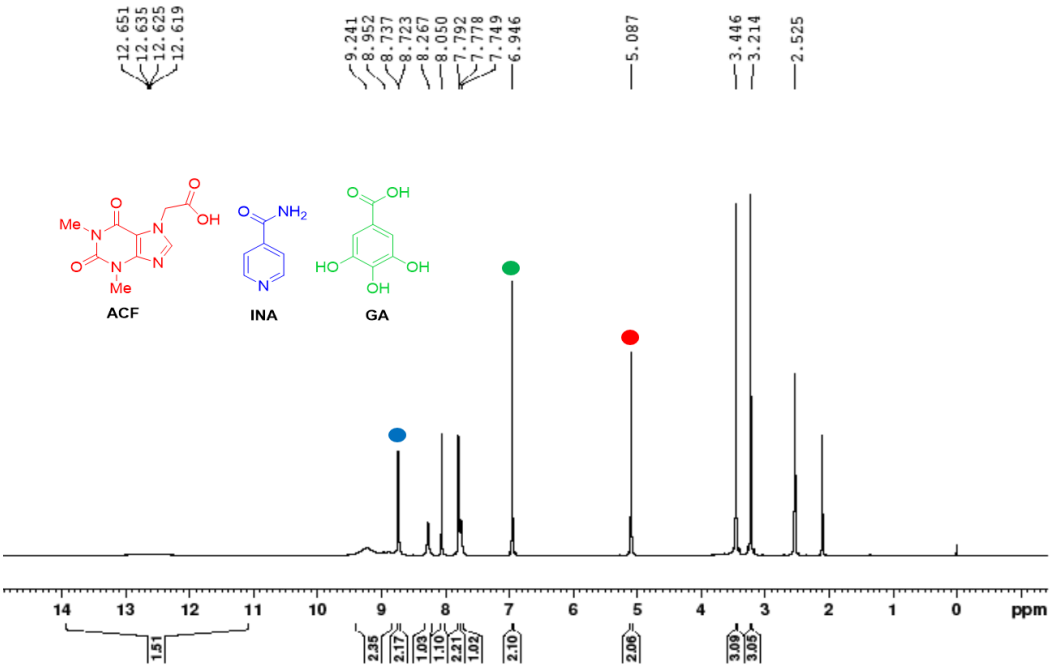


**Figure 5.17:** $^{1}$H NMR Spectra of ACF-INA-GA (1:1:1) (Form-1); ACF (Red), GA (Green), INA (Blue) color coded.

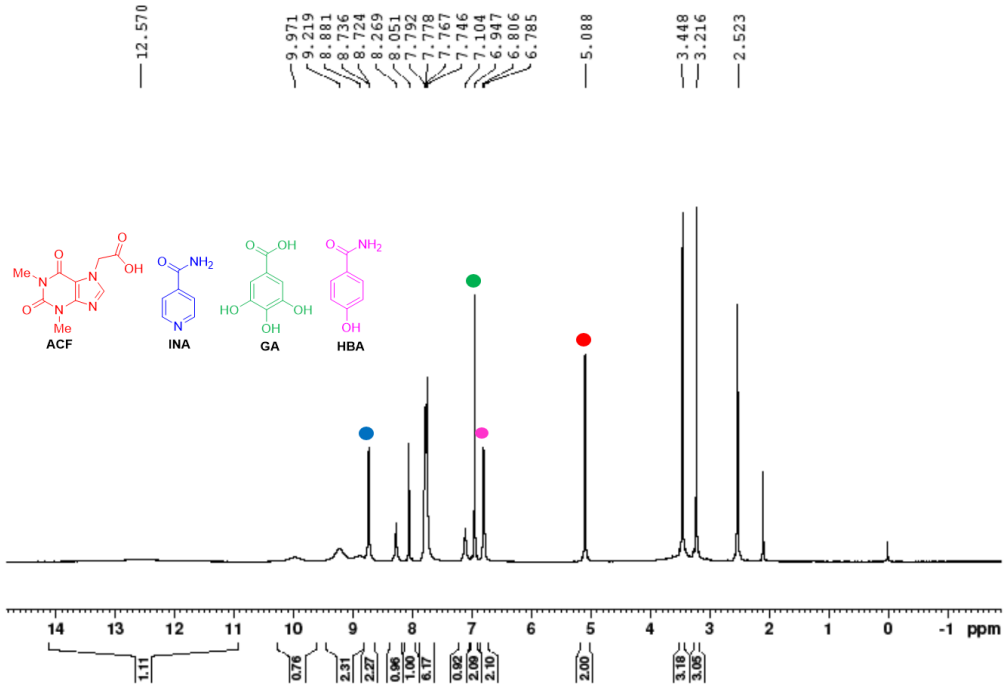


**Figure 5.18:** $^{1}$H NMR Spectra of ACF-INA-GA (1:1:1:1) (Form-2); ACF (Red), GA (Green), INA (Blue), HBA (Pink) color coded.

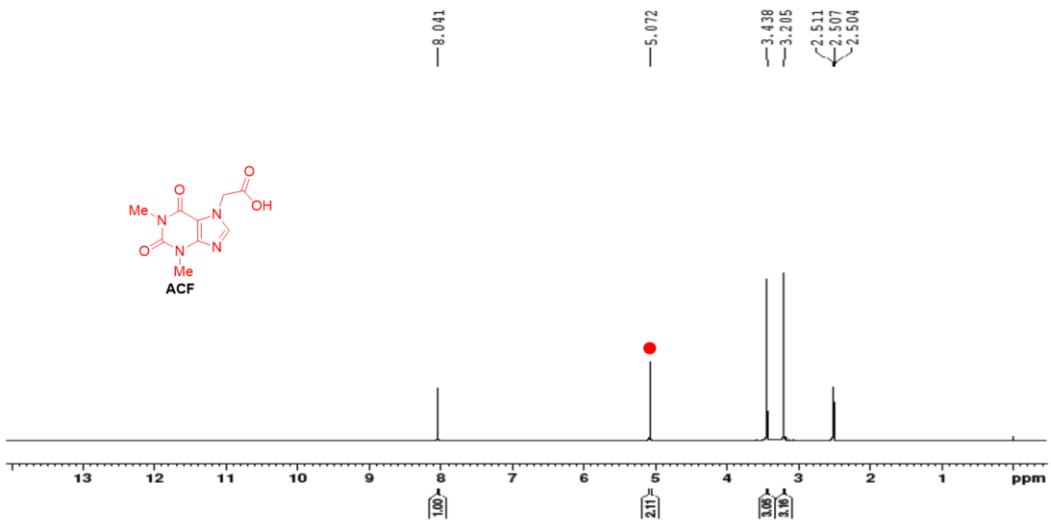


**Figure 5.19:** $^{1}$H NMR Spectra of ACF: protons used to calculate integration are color coded.

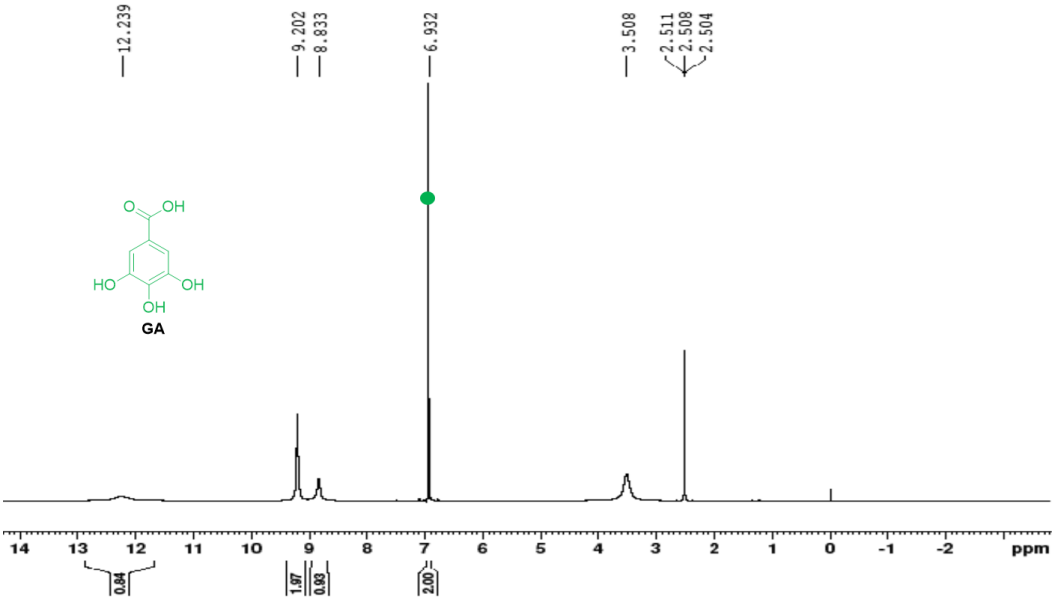


**Figure 5.20:** $^{1}$H NMR Spectra of GA: protons used to calculate integration are color coded.

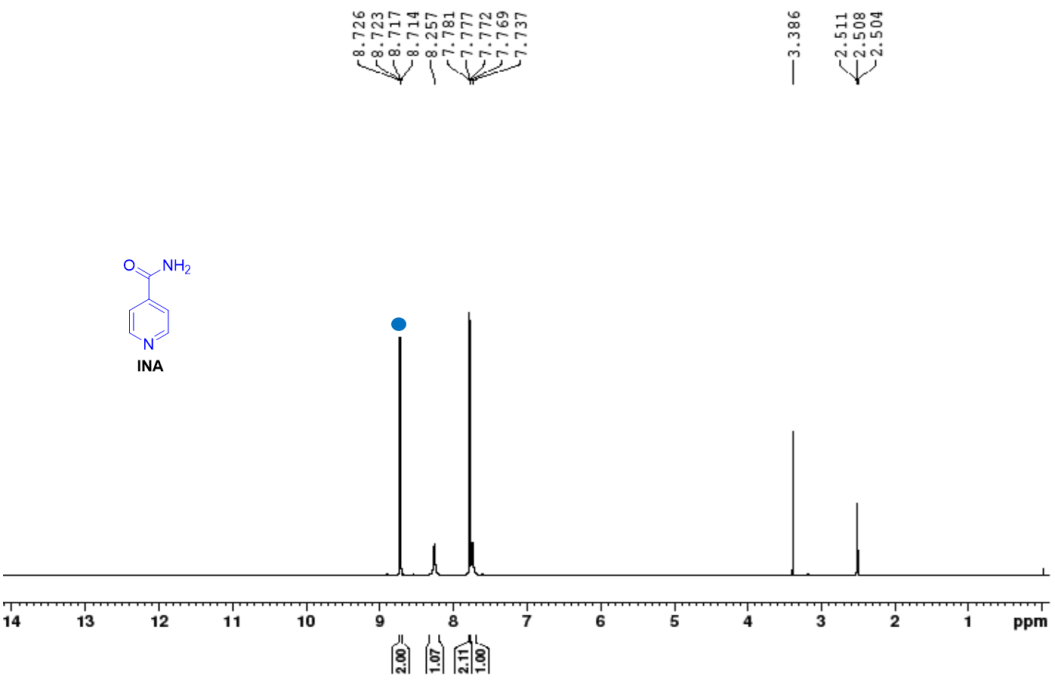


**Figure 5.21:** $^{1}$H NMR Spectra of INA: protons used to calculate integration are color coded.

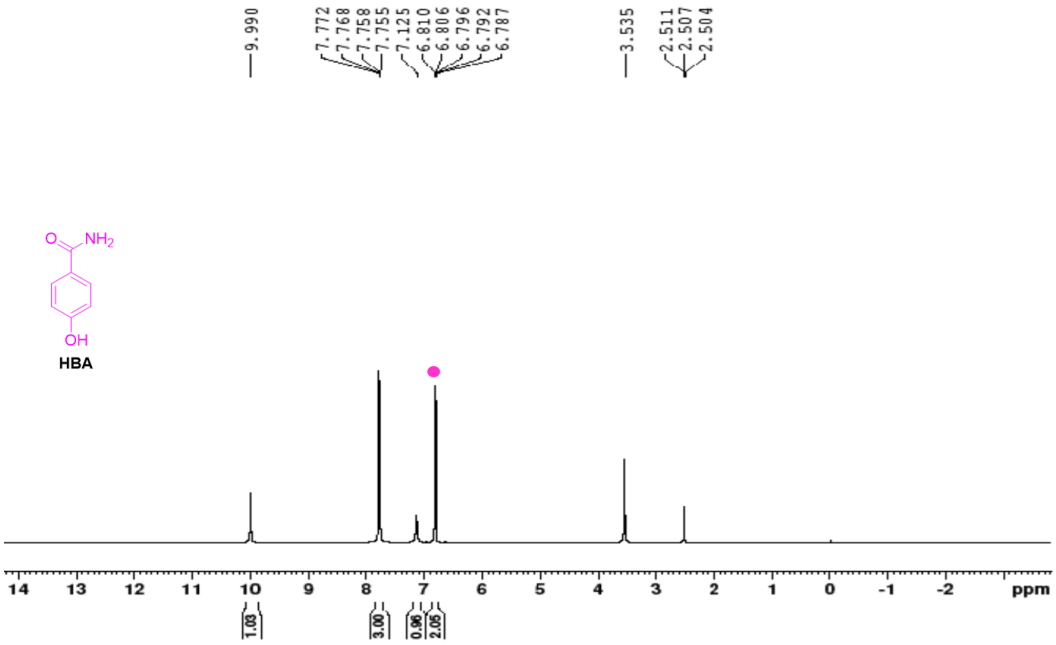


**Figure 5.22:** [1]H NMR Spectra of HBA: protons used to calculate integration are color coded.

## 5.2.7 Permeability and Solubility Studies

**Permeability and Solubility**

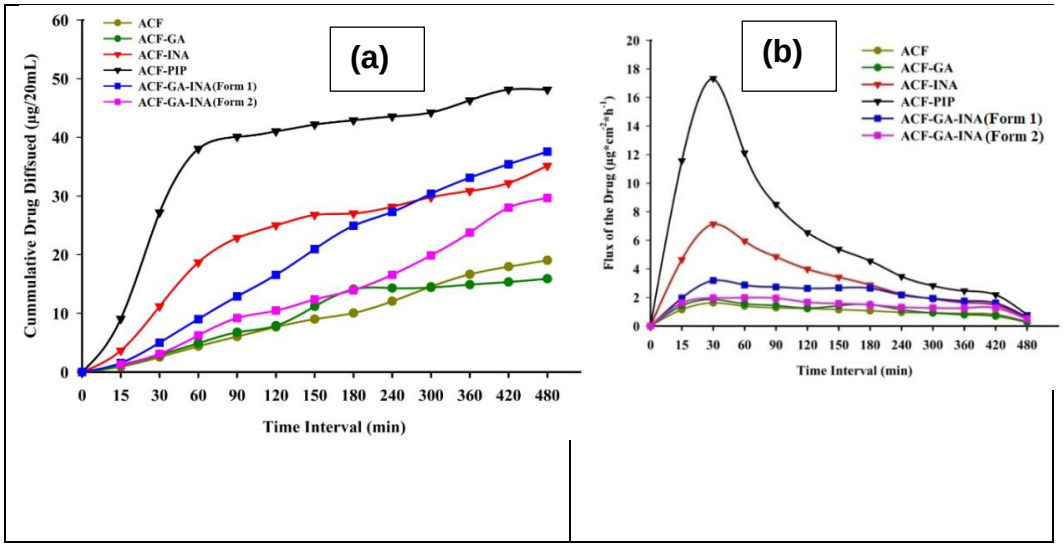

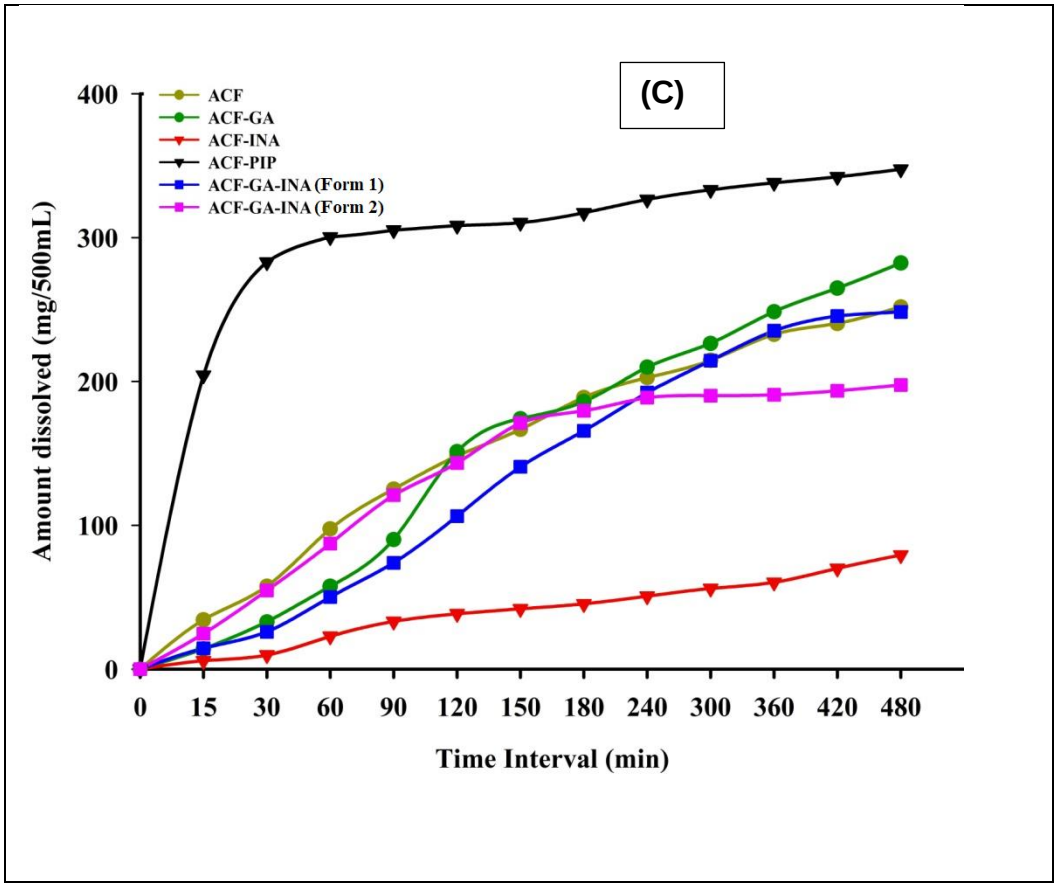


**Figure 5.23:** (a) Diffusion profile of the ACF and ternary salt-cocrystal polymorphs through a dialysis membrane in PBS solution (pH 7) represented as cumulative amount of salt/cocrystal diffused vs. time. (b) Flux of ACF and ternary salt-cocrystal polymorphs through a dialysis membrane in PBS solution (pH 7) to show the permeability of salt/cocrystal vs. time. (c) Dissolution rate of ACF and ternary salt-cocrystal polymorphs.

ACF can be categorized as a BCS class IV drug (Biopharmaceutics Classification System) owing to its low solubility and low permeability. [50-51] The permeability plots in Figure 5.23a and 5.23b show an increase in the flux of ACF for the binary and ternary systems. Diffusion behavior was studied using a Franz cell membrane in aqueous buffer (pH 7) measured at hourly intervals over 8 h. No discernable change in pH of the receptor solution compartment was observed after the diffusion experiment which means that the dissociation of the drug cocrystal had not happened. The increase in the degree of permeability is explained by the low melting point (Table 5.10) of the binary and ternary systems compared to ACF.[41,77] The highest permeability for ACF-PIP is due to the formation of ACF-PIP-salt-hydrate and its low melting point. The two ternary systems exhibited similar melting point (Table 5.10), nevertheless, the higher molecular weight of

ACF-GA-INA-HBA relative to ACF-GA-INA explains the higher permeability (flux) for ACF-GA-INA. The solubility curve for binary and ternary salt cocrystals in phosphate aqueous buffer (pH 7) for 8 h at 37 °C is shown in Figure 5.23c. There was not much increase in ACF solubility of binary and ternary systems, except ACF-PIP salt showing dissolution of 0.6 mg per mL in 30 min. The variation in the solubility of binary and ternary systems is due to salt formation. For example, increase in the solubility of ACF-GA-INA and ACF-GA-INA-HBA and ACF-PIP compared to ACF-INA and ACF is ascribed to proton transfer in salt-cocrystal. The highest solubility of ACF-PIP is because of the major contribution from ionic and hydrogen bonding interactions, especially O-H interactions, seen in the Hirshfeld surface analysis (Figure 5.8-5.10, Table 5.3). Furthermore, the highest solubility and permeability profiles of ACF-PIP salt attributed to its high aqueous solubility of PIP coformer.

## 5.3 Conclusions

Eight ternary salt-cocrystals and two polymorphs of acefylline are synthesized by design of multi-component cocrystal engineering using solvent-assisted grinding method. All salts and cocrystals were characterized by single-crystal X-ray diffraction analysis, powder X-ray diffraction analysis, and thermal stability by differential scanning calorimetry (DSC). Single crystal X-ray data show hydrogen bonding synthons such as imidazole-acid and carboxylate-pyridinium in ternary systems. The intermolecular interactions in ternary cocrystal polymorphs of ACF are further substantiated by Hirshfeld surface analysis, 2D fingerprint plots and energy frameworks. An increase in the permeability and solubility of ACF salt cocrystals/ polymorphs is observed in the binary and ternary systems, which is related to the lower melting point and ionic hydrogen bonding interactions. The improvement in the solubility and permeability of ACF in ternary systems may find application in fixed dose combination of drugs for solubility permeability enhancement. The ability to modulate both solubility and permeability of difficult to formulate drugs is demonstrated by crystal engineering.

## 5.4 Experimental Section

All the coformers were purchased from sigma-Aldrich, India. All chemicals are analytical and chromatographic grade. Acefylline purchased from TCI chemicals India pvt ltd, and its purity confirmed by NMR and DSC.

Solvent assisted grinding (SAG) experiments were executed using acetonitrile (ACN) solvent (0.4-0.6 mL was added) to the physical mixture and ground for 10-12 min, and the same method was repeated 2-3 times to confirm the system is entirely homogeneous. The ground crystalline mixture was dissolved in methanol (MeoH) and suitable solvent (solvent mixtures) and allowable for crystallization.

**ACF-INA (1:2)**

ACF (100 mg, 0.42 mmol) and INA (104 mg, 0.42 mmol) were ground well in a mortar and pestle for 25-30min by adding 5-6 drops acetonitrile (ACN). The ground material kept for crystallization in different solvent combinations did not afford single crystals and so the product was characterized by DSC and structure determination from powder X-ray diffraction study (SDPD) PXRD in the absence of diffraction quality single crystals.

**ACF-PIP hydrate (1:0.5:1)**

ACF (100 mg, 0.42 mmol) and PIP (18.08 mg, 0.42 mmol) were ground well in a mortar and pestle for 30 min by adding 5-6 drops acetonitrile (ACN). The ground material kept for crystallization in 5 mL of $CH_3NO_2$ and MeOH mixture (1:1 v/v) in 10mL test tubes at room temperature. Colorless good quality single crystals were observed by slow evaporation. The product crystallized as a monohydrate.

**ACF-CYT (1:1)**

ACF (100 mg, 0.42 mmol) and CYT (46.64 mg, 0.42 mmol) were ground well in a mortar and pestle for 30min by adding 5-6 drops acetonitrile (ACN). The ground material kept for crystallization in 5mL of $CH_3NO_2$ and MeOH mixture (1:1 v/v) in 10mL test tubes at room temperature. Colorless good quality single crystals were observed by slow evaporation.

**ACF-PHBA (1:1)**

ACF (100 mg, 0.42 mmol) and PHBA (57.98 mg, 0.42 mmol) were ground well in a mortar and pestle for 30min by adding 5-6 drops acetonitrile (ACN). The ground material kept for crystallization from a solvent mixture of $CH_3NO_2$ and MeOH (5 mL) as well as

individual solvents at room temperature in 10mL test tubes. Colorless good quality single crystals were observed by slow evaporation.

**ACF-HBA (1:1)**

ACF (100 mg, 0.42 mmol) and HBA (57.57 mg, 0.42 mmol) were ground well in a mortar and pestle for 30 min by adding 5-6 drops acetonitrile (ACN). The ground material kept for crystallization from a solvent mixture of $CH_3NO_2$ and MeOH (5mL) as well as individual solvents at room temperature in 10mL test tubes. Colorless good quality single crystals were observed by slow evaporation.

**ACF-24DHBA (1:1)**

ACF (100 mg, 0.42 mmol) and 24DHBA (64.70 mg, 0.42 mmol) were ground well in a mortar and pestle for 30min by adding 5-6 drops acetonitrile (ACN). The ground material kept for crystallization from a solvent mixture of $CH_3NO_2$ and MeOH (5mL) as well as individual solvents at room temperature in 10mL test tubes. Colorless good quality single crystals were observed by slow evaporation.

**ACF-35DHBA (1:1)**

ACF (100 mg, 0.42 mmol) and 35DHBA (64.70 mg, 0.42 mmol) were ground well in a mortar and pestle for 30min by adding 5-6 drops acetonitrile (ACN). The ground material kept for crystallization from a solvent mixture of $CH_3NO_2$ and MeOH (5mL) as well as individual solvents at room temperature in 10mL test tubes. Colorless good quality single crystals were observed by slow evaporation.

**ACF-GA-MeOH (1:1:1)**

ACF (100 mg, 0.42 mmol) and GA (71.42 mg, 0.42 mmol) were ground well in a mortar and pestle for 30min by adding 5-6 drops acetonitrile (ACN). The ground material kept for crystallization in 5mL of $CH_3NO_2$ and MeOH mixture (1:1 v/v) in 10mL test tubes at room temperature. Colorless good quality single crystals were observed by slow evaporation. The product crystallized as a methanol solvate.

**ACF-INA-GA (1:1:1) Form 1**

ACF (100 mg, 0.42 mmol) and INA (52 mg, 0.42 mmol) and GA (71.42 mg, 0.42 mmol) were ground well in a mortar and pestle for 30 min by adding 5-6 drops acetonitrile (ACN). The ground material kept for crystallization from a solvent mixture of $CH_3NO_2$ and MeOH (5mL) as well as individual solvents at room temperature in 10mL test tubes. Colorless

good quality single crystals were observed by slow evaporation. The product crystallized as a triclinic crystal system.

**ACF-INA-GA (1:1:1) Form 2**

ACF (100 mg, 0.42 mmol) and INA (52 mg, 0.42 mmol) and GA (71.42 mg, 0.42 mmol) HBA (57.57 mg, 0.42 mmol) were ground well in a mortar and pestle for 30min by adding 5-6 drops acetonitrile (ACN). The ground material kept for crystallization from a solvent mixture of $CH_3NO_2$ and MeOH (5mL) as well as individual solvents at room temperature in 10mL test tubes. Colorless good quality single crystals were observed by slow evaporation. The product crystallized as a ACF-INA-GA monoclinic crystal system (guest induced polymorph).

**ACF-INA-3,5-DHBA (1:1:1)**

ACF (100 mg, 0.42 mmol) and INA (52mg, 0.42 mmol) and 3,5-DHBA (64.70 mg, 0.42 mmol) were ground well in a mortar and pestle for 30min by adding 5-6 drops acetonitrile (ACN). The ground material kept for crystallization from a solvent mixture of $CH_3NO_2$ and MeOH (5 mL) as well as individual solvents at room temperature in 10mL test tubes. Colorless good quality single crystals were observed by slow evaporation.

**ACF-INA-3,5-DHBA-H2O (1:1:2:4)**

ACF (100 mg, 0.42 mmol) and INA (52 mg, 0.42 mmol) and 3,5-DHBA (129.40 mg, 0.42 mmol) were ground well in a mortar and pestle for 30min by adding 5-6 drops acetonitrile (ACN). The ground material kept for crystallization from a solvent mixture of $CH_3NO_2$ and MeOH (5 mL) as well as individual solvents at room temperature in 10mL test tubes. Colorless good quality single crystals were observed by slow evaporation. The product crystallized as a tetra hydrate.

**ACF-PIP-35DHBA (1:0.5:1)**

ACF (100 mg, 0.42 mmol) and PIP (18.08 mg, 0.42 mmol) and 3,5-DHBA (64.70 mg, 0.42 mmol) were ground well in a mortar and pestle for 30 min by adding 5-6 drops acetonitrile (ACN). The ground material kept for crystallization from a solvent mixture of $CH_3NO_2$ and MeOH (5mL) as well as individual solvents at room temperature in 10mL test tubes. Colorless good quality single crystals were observed by slow evaporation.

**ACF-PIP-3,5-DHBA-H2O (1:1:1:2)**

ACF (100 mg, 0.42 mmol) and PIP (36.16 mg, 0.42 mmol) and 3,5-DHBA (64.70 mg, 0.42 mmol) were ground well in a mortar and pestle for 30 min by adding 5-6 drops

acetonitrile (ACN). The ground material kept for crystallization from a solvent mixture of $CH_3NO_2$ and MeOH (5mL) as well as individual solvents at room temperature in 10mL test tubes. Colorless good quality single crystals were observed by slow evaporation. The product crystallized as a di-hydrate.

**ACF-PIP-3,5-DHBA-H2O (1:0.5:1:2)**

ACF (100 mg, 0.42 mmol) and PIP (18.08 mg, 0.42 mmol) and 3,5-DHBA (64.70mg, 0.42 mmol) were ground well in a mortar and pestle for 30 min by adding 5-6 drops acetonitrile (ACN). The ground material kept for crystallization from a solvent mixture of $CH_3NO_2$ and MeOH (5mL) as well as individual solvents at room temperature in 10mL test tubes. Colorless good quality single crystals were observed by slow evaporation. The product crystallized as a di-hydrate.

**ACF-PIP-GA-H2O (1:0.5:1:2)**

ACF (100 mg, 0.42 mmol) and PIP (18.08 mg, 0.42 mmol) and GA (71.42 mg, 0.42 mmol) were ground well in a mortar and pestle for 30 min by adding 5-6 drops acetonitrile (ACN). The ground material kept for crystallization from a solvent mixture of $CH_3NO_2$ and MeOH (5mL) as well as individual solvents at room temperature in 10mL test tubes. Colorless good quality single crystals were observed by slow evaporation. The product crystallized as a di-hydrate.

**X–ray Crystallography**

X-ray reflections for the all the binary and ternary solid forms were collected on Bruker SMART-APEX CCD diffractometer equipped with a graphite monochromator and Mo-Kα fine-focus sealed tube (λ=0.71073 Å) operated at 1500 W power (40 KV, 30 mA). The frames were integrated with the Bruker SAINT software[78] using a narrow-frame integration algorithm. Intensities were corrected for absorption effects using the multiscan method (SADABS)[79] and the structure was solved and refined using SHELX-97.[80-81] All non-hydrogen atoms were refined as anisotropic. Hydrogen atoms on heteroatoms were located from difference electron density maps and all C−H hydrogens were fixed geometrically. Hydrogen bond geometries were determined in Platon.[82-83] A check of the final crystallographic information file (CIF) with PLATON did not show any missed symmetry. X-Seed and Mercury was used to prepare the figures and packing diagrams.[84-85] Crystal structures are deposited as part of the Supporting Information and may be accessed at www.ccdc.cam.ac.uk/data_request/cif (CCDC Nos. 2014723-2014738).

**Powder X-ray Diffraction**

Powder X-ray diffraction of all the samples were recorded on Bruker D8 Advance diffractometer (Bruker-AXS, Karlsruhe, Germany) using Cu-Kα X-radiation (λ = 1.5406 Å) at 40 kV and 30 mA power. X-ray diffraction patterns were collected over the 2θ range 5-50° at a scan rate of 1º/min. Powder Cell 2.4[86] was used for Profile fitting refinement of experimental PXRD and calculated lines from the X-ray crystal structure.

**Thermal Analysis**

DSC experiments were performed on a Mettler Toledo DSC 822e module and TGA on a Mettler Toledo TGA/SDTA 851e module. Samples were placed in sealed aluminum sample pans for DSC and vented aluminum pans for TGA experiments. A typical sample size is 4-6 mg for DSC and 6-10 mg for TGA. The temperature range was 30-300 °C at 5°C $min^{-1}$ and 10°C $min^{-1}$ for DSC, TGA. Samples were purged with a stream of dry $N_2$ flowing at 80−90 mL $min^{-1}$.

**High Performance Liquid Chromatography (HPLC)**

HPLC was carried out on a Shimadzu LC-20AD liquid chromatography, Diode Array SPD-M20A detector, degasser DGU-20A3 with a RP HPLC column C18G (250 x 4.6 mm, 5 µm particle size), which was protected by a guard column of 33 mm × 4.6 mm. UV absorbance at 274 nm was used to quantify the drug. The calibration curve was obtained by TIZ (linearity $R^2$ > 0.999). The mobile phase consists of 0.05M orthophosphoric acid, acetonitrile sodium dihydrogen phosphate (85:15 v/v), which was filtered through 0.45 µm membrane filter, degassed by sonicator, and delivered at a rate of 1.0 mL/min at room temperature. The binary and ternary components of 20 µL was injected into HPLC with a run time of 10 min.

**Hirshfeld Surface Analysis**

The calculation of intermolecular energies, implemented in *Crystal Explorer*, [65-72] is automated for all unique molecular pairs in the first coordination sphere of a molecule. Monomer electron distributions were obtained with *Gaussian09* [73-75] at the B3LYP/6-31G (d,p)level, using experimental crystal geometries with bond lengths to H atoms normalised to standard neutron diffraction values.

Intermolecular electrostatic, polarization, dispersion and exchange-repulsion energy terms are calculated summed to obtain interaction energies for all unique molecular pairs for

which any atom is within 3.8 Å of a central molecule (This corresponds to the energy model labelled CE-B3LYP(Fit=D2).[73]

Energies between molecular pairs are represented as cylinders joining the centres of mass of the molecules, with the cylinder radius proportional to the magnitude of the interaction energy.

In the following tables of energies, the columns 'Coul.', 'Polariz.', 'Disp.' and 'Repul.'refer to *unscaled* components $E_{ele}$, $E_{pol}$, etc., while 'Total' represents the total energy,$E_{tot}$. 'Dist.' is the distance between centres of mass of pairs of molecules (Å), and 'Symop'gives the symmetry operation relationship between the two molecules. Interaction energies with magnitude less than a specified threshold can be ignored when constructing the energy frameworks. Model energies and energy frameworks have been incorporated in *Crystal Explorer* version 3.2, which is expected to be available at www.hirshfeldsurface.net.

**Dissolution and Solubility Measurements**

The solubility measurements of ACF and its salt-cocrystals were conducted in pH 7 buffer medium using Higuchi and Connor method.[87] The absorbance of the ACF was measured at given $\lambda_{max}$= 274 nm in purified buffer solution of pH 7 by HPLC analysis. The concentration *vs.* intensity calibration curve was plotted by using these absorbance values which were obtained from the known concentration of ACF. A molar extinction coefficient for ACF was calculated from the slope of the calibration curve. To measure the equilibrium solubility, excess amount of each sample (i.e. ACF and its salts/cocrystals) were added to 5 mL of purified buffer at pH 7 and stirred at 600 rpm using a magnetic stirrer at 37 °C to make the solution supersaturated. After 24 h, the suspension was filtered through a Whatman 0.45 µm syringe filter. The filtrate was used to calculate the equilibrium solubility from the area under curve (AUC) plotted against the standard curve. The undissolved residues were air dried and further characterized by PXRD. The intrinsic dissolution rate (IDR) of ACF and its salts/cocrystals were carried out on a USP certified Electrolab TDT-08L dissolution tester (Electrolab, Mumbai, MH, India). 400 mg sample (ACF and its salts/cocrystals) were compressed between the smooth surfaces by applying 2.5 ton/inch$^2$ pressure for 4 min in an area of 0.5 cm$^2$. The pellets inside the disk were dipped into 500 mL buffer solution of pH 7 at 37 °C so that only one surface is exposed to the solution and rotating disk was set at a rate of 150 rpm. 5 mL of the dissolution medium was collected at time intervals of 15 min, 30 min, 60 min, 90 min, 120 min, 150

min, 180 min, 240 min, 300 min, 360 min, 420 min, and 480 min, and replaced each time with the same amount of fresh pH 7 buffer. The IDR values of each compound (salt/cocrystal) were calculated from AUC plotted against time. The remaining residues were further analyzed by PXRD to check any possible conversion of the solid forms under the dissolution media.

**Permeability and diffusion study**

The diffusion studies were performed using a diffusion apparatus (Model EMFDC-06, Orchid Scientific, Maharashtra, India) on ACF cocrystals and salts through a dialysis membrane-135 (dialysis membrane-135, average flat width 33.12 mm, average diameter 23.8 mm, capacity approximately 4.45 mL/cm) obtained from HiMedia, India. The treated dialysis membrane was placed in diffusion cells with an effective surface area of 3.14 $cm^2$. Suspensions of the ACF adducts were prepared and placed on the dialysis membrane in donor compartment. The temperature of diffusion medium maintained at 37 °C ± 1 °C throughout the experiment and stirred at 600 rpm and diffuse through the membrane toward the receptor compartment containing 20 mL of phosphate-buffered solution (PBS, pH = 7). The release of the compounds at predetermined intervals were withdrawn (0.5 mL for each intervals) and replaced by equal volume and concentration measured in HPLC as such as solubility experiments.

## 5.5 References

1. Desiraju, G. R. Crystal Engineering. The Design of Organic Solids; Elsevier: Amsterdam, **1989**.
2. Desiraju, G. R. Supramolecular Synthons in Crystal Engineering—A New Organic Synthesis *Angew. Chem., Int. Ed. Engl.* **1995**, *34*, 2311-2327.
3. Bond, A. D. What is a co-crystal? *CrystEngComm***, 2007**, *9***,** 833-834
4. Thomas, S. P.; Sathishkumar, R.; Guru Row, T. N. Organic alloys of room temperature liquids thiophenol and selenophenol. *Chem. Commun.*, **2015**, *51*, 14255-14258
5. Friscic, T.; Trask, A. V.; Jones, W.; Motherwell, W. D. S. Screening for Inclusion Compounds and Systematic Construction of Three-Component Solids by Liquid-Assisted Grinding. *Angew. Chem. Int. Ed.* **2006**, *45*, 7546 –7550
6. Nangia, A. K.; Desiraju, G. R. Crystal Engineering. An Outlook for the Future. *Angew. Chem. Int. Ed.* **2019**, *58*, 4100 – 4107

7. Desiraju, G. R. Crystal Engineering: From Molecule to Crystal. *J. Am. Chem. Soc.* **2013**, *135*, 9952−9967
8. Bolla, G.; and Nangia, A. Pharmaceutical cocrystals: walking the talk. *Chem. Commun*, **2016**, *52*, 8342-8360
9. Yousef, M. A.; Vangala, V. R. Pharmaceutical Co-crystals: Molecules, Crystals, Formulations, Medicines. *Cryst. Growth Des.* **2019,** *19*, 7420-7438.
10. Bernstein, J. *Polymorphism in Molecular Crystals*; *Clarendon*: Oxford, **2002**.
11. Dunitz, J. D.; and Bernstein, J. Disappearing Polymorphs. *Acc. Chem. Res.***1995**, *28*, 193-200.
12. Aakeroy, C. B.; Desper, J.; Urbina, J. F. Supramolecular reagents: versatile tools for non-covalent synthesis. *Chem. Commun*., **2005**, 2820–2822
13. Aakeroy, C. B.; Beatty, A.M.; Helfrich, B. A. Total Synthesis Supramolecular Style: Design and Hydrogen-Bond-Directed Assembly of Ternary Supermolecules. *Angew. Chem. Int. Ed.* **2001**, *40*, 3240-3242
14. Aakeroy, C. B.; Desper, J.; Smith, M. M. Constructing, deconstructing, and reconstructing ternary supermolecules. *Chem. Commun*., **2007**, 3936–3938
15. Bhogala, B. R.; Basavoju, S.; Nangia, A. Three-Component Carboxylic Acid−Bipyridine Lattice Inclusion Host. Supramolecular Synthesis of Ternary Cocrystals. *Crystal Growth & Design* **2005**, *5*, 1683-1686
16. Dubey, R.; Desiraju, G. R. Combinatorial selection of molecular conformations and supramolecular synthons in quercetin cocrystal landscapes: a route to ternary solids. *IUCrJ* **2015**. *2*, 402–408
17. Topic, F.; Rissanen, K. Systematic Construction of Ternary Cocrystals by Orthogonal and Robust Hydrogen and Halogen Bonds. *J. Am. Chem. Soc*. **2016**, *138*, 6610−6616
18. Dabros, M.; Emery, P. R.; Thalladi, V. R. A Supramolecular Approach to Organic Alloys: Cocrystals and Three and Four-Component Solid Solutions of 1,4 Diazabicyclo[2.2.2]octane and 4-X-Phenols (X=Cl, CH3, Br). *Angew. Chem*. **2007**, *119*, 4210 –4213
19. Tothadi, S.; Desiraju, G. R. Designing ternary cocrystals with hydrogen bonds and halogen bonds. *Chem. Commun.*, **2013**, *49*, 7791−7793
20. Saha, B. K.; Nangia, A.; Jaskolski, M. Crystal engineering with hydrogen bonds and halogen bonds. *CrystEngComm*, **2005**, *7*, 355–358

21. Tothadi, S.; Mukherjee, A.; Desiraju, G. R. Shape and size mimicry in the design of ternary molecular solids: towards a robust strategy for crystal engineering. *Chem. Commun.*, **2011**, *47*, 12080–12082
22. Walsh, R. D. B.; Bradner, M. W.; Fleischman, S.; Morales, L. A.;Moulton, B.;Rodriguez-Hornedo, N.; Zaworotko, M. J. Crystal engineering of the composition of pharmaceutical phases. *Chem. Commun.*, **2003**, 186-187
23. Paul, M.; Chakraborty, S.; Desiraju, G. R. Six-Component Molecular Solids: ABC[D1−(x+y)ExFy]2. *J. Am. Chem. Soc.* **2018**, *140*, 2309−2315
24. Mir, N. A.; Dubey, R.; Desiraju, G. R. Strategy and Methodology in the Synthesis of Multicomponent Molecular Solids: The Quest for Higher Cocrystals. *Acc. Chem. Res.* **2019**, *52*, 2210-2220
25. Seaton, C, C.; Blagden, N.; Munshi, T.; and Scowen, I. J. Creation of Ternary Multicomponent Crystals by Exploitation of Charge-Transfer Interactions. *Chem. Eur. J.* **2013**, *19*, 10663-10671.
26. Dubey, R.; Desiraju, G. R. Combinatorial Crystal Synthesis: Structural Landscape of Phloroglucinol: 1, 2-bis(4-pyridyl)ethylene and Phloroglucinol:Phenazine. *Angew. Chem. Int. Ed.* **2014**, *53*, 13178 –13182
27. Mir, N. A.; Dubey, R.; Desiraju, G. R. Four- and five-component molecular solids: crystal engineering strategies based on structural inequivalence. *IUCrJ* **2016**. *3*, 96–101
28. Dubey, R.; Mir, N. A.; Desiraju, G. R. Quaternary cocrystals: combinatorial synthetic strategies based on long-range synthon Aufbau modules (LSAM). *IUCrJ* **2016**. *3*, 102–107
29. Mir, N. A.; Dubey, R.; Tothadi, S.; Desiraju, G. R. Combinatorial crystal synthesis of ternary solids based on 2-methylresorcinol. *CrystEngComm*, **2015**, *17*, 7866–7869
30. Dubey, R.; Pavan, M. S.; Guru Row, T. N.; Desiraju, G. R. Crystal landscape in the orcinol:4,4’-bipyridine system: synthon modularity, polymorphism and transferability of multipole charge density parameters. *IUCrJ* **2014**. *1*, 8–18
31. Aitipamula, S.; Wong, A. B. H.; Chow, P. S.; Tan, R. B. H. Novel solid forms of the anti-tuberculosis drug, Isoniazid: ternary and polymorphic cocrystals. *CrystEngComm*, **2013**, *15*, 5877–5887
32. Bolla, G.; Nangia, A.; Binary and ternary cocrystals of sulfa drug acetazolamide with pyridine carboxamides and cyclic amides. *IUCrJ* **2016**. *3*, 152–160

33. Bolla, G.; Nangia, A. Multicomponent ternary cocrystals of the sulfonamide group with pyridine-amides and lactams. *Chem. Commun.*, **2015**, *51*, 15578–15581
34. Fridgeirsdottir, G. A.; Harris, R.; Fischer, P. M.; Roberts, C. J. Support tools in formulation development for poorly soluble drugs. *J. Pharm. Sci.* **2016**, *105*, 2260-2269.
35. Lipinski, C. A.; Lombardo, F. B.; Dominy, W.; Feeney, P. J. Experimental and computational approaches to estimate solubility and permeability in drug discovery and development settings. *Adv. Drug Delivery Rev*. **1997**, *23*, 3−25.
36. Aungst, B. J. Optimizing oral bioavailability in drug discovery: an overview of design and testing strategies and formulation options. *J. Pharm. Sci.* **2017**, *106*, 921-929.
37. Williams, H. D.; Trevaskis, N. L.; Charman, S. A.; Shanker, R. M.; Charman, W. N.; Pouton, C. W.; Porter, C. J. Strategies to address low drug solubility in discovery and development. *Pharmacol. Rev.* **2013**, *65*, 315-499.
38. Schultheiss, N.; and Newman, A. Pharmaceutical Cocrystals and Their Physicochemical Properties. *Cryst. Growth Des.* **2009**, *9*, 2950-2967.
39. Amidon, G. L.; Lennernas, H.; Shah, V. P.; Crison, J. R. A theoretical basis for a biopharmaceutic drug classification: the correlation of in vitro drug product dissolution and in vivo bioavailability. *Pharm. Res.* **1995**, *12*, 413−420.
40. Babu, N, J.; Nangia, A. Solubility Advantage of Amorphous Drugs and Pharmaceutical Cocrystals. *Cryst. Growth Des.* **2011**, *11*, 2662–2679
41. Yan, Y.; Chen, J. M.; and Lu, T.B. Simultaneously enhancing the solubility and permeability of acyclovir by crystal engineering approach. *CrystEngComm*, **2013**, *15*, 6457–6460
42. Chen, Y.; Li, L.; Yao, J.; Ma, Y. Y.; Chen, J. M.; Lu, T. B. Improving the Solubility and Bioavailability of Apixaban via Apixaban−Oxalic Acid Cocrystal. *Cryst. Growth Des.* **2016**, *16*, 2923−2930
43. Dai, X. L.; Voronin, A. P.; Gao, W.; Perlovich, G. L.; Lu, T.; Chen, J. Intermolecular interactions and permeability of 5-fluorouracil cocrystals with a series of isomeric hydroxybenzoic acids: a combined theoretical and experimental study. *CrystEngComm*, **2019**, *21*, 5095–5105
44. Dai, X. L.; Li, S.; Chen, J. M.; Lu, T. B. Improving the Membrane Permeability of 5-Fluorouracil via Cocrystallization. *Cryst. Growth Des*. **2016**, *16*, 4430−4438

45. Suresh, K.; Mannava, M. K. C.; and Nangia, A. Cocrystals and alloys of nitazoxanide: enhanced pharmacokinetics. *Chem. Commun.*, **2016**, *52*, 4223-4226
46. Arnott, J. A.; Planey, S. L. The influence of lipophilicity in drug discovery and design. *Expert Opin. Drug Discov* **2012**, *7*, 863-875.
47. Sanphui, P.; Devi, V. K.; Clara, D.; Malviya, N.; Ganguly, S.; Desiraju, G. R. Cocrystals of Hydrochlorothiazide: Solubility and Diffusion/Permeability Enhancements through Drug−Coformer Interactions. *Mol. Pharmaceutics* **2015**, *12*, 1615−1622
48. Banik, M.; Gopi, S. P.; Ganguly, S.; Desiraju, G. R. Cocrystal and Salt Forms of Furosemide: Solubility and Diffusion Variations. *Cryst. Growth Des*. **2016**, *16*, 5418−5428
49. Rai, S.; Allu, S.; and Nangia, A. Salts and Cocrystal of Etodolac: Advantage of Solubility, Dissolution, and Permeability. *Cryst. Growth Des.* **2020**, *20*, 4512−4522.
50. https://www.targetmol.com/compound/Theophylline-7-acetic-acid
51. http://drugcentral.org/drugcard/49
52. Allen, F. H. The Cambridge Structural Database: a quarter of a million crystal structures and rising. *Acta Cryst.* **2002**. *B58*, 380-388
53. The Cambridge Structural Database version 5.40 November **2018** (update 3 Aug 2019). ConQuest 2.03; Cambridge Crystallographic Data Centre: Cambridge, U.K.
54. Fabian, L. Cambridge Structural Database Analysis of Molecular Complementarity in Cocrystals. *Cryst. Growth Des.* **2009**, *9*, 1436-1443
55. Cruz-Cabeza, A. J. Acid–base crystalline complexes and the pKa rule. *CrystEngComm*, **2012**, *14*, 6362-6365.
56. Harris, K. D. M.; Tremayne, M.; Kariuki, B. M. Contemporary Advances in the Use of Powder X-Ray Diffraction for Structure Determination. *Angew. Chem. Int. Ed*. **2001**, *40*, 1626–1651
57. Harris, K. D. M.; and Cheung, E. Y. How to determine structures when single crystals cannot be grown: opportunities for structure determination of molecular materials using powder diffraction data. *Chem. Soc. Rev.*, **2004**, *33*, 526–538.
58. Sanphui, P.; Bolla, G.; Nangia, A.; Chernyshev, V. Acemetacin cocrystals and salts: structure solution from powder X-ray data and form selection of the piperazine salt. *IUCrJ* **2014**. *1*, 136–150

59. Zhang, L. J.; Liu, M. C.; Ding, J. C.; Wu, H. Y. Crystal structure of theophylline-7-acetic acid, $C_9H_{10}N_4O_4$**.** Z. *Kristallogr. NCS* **2006**, *221*, 59-60

60. Etter, M. C. A new role for hydrogen-bond acceptors in influencing packing patterns of carboxylic acids and amides. *J. Am. Chem. Soc.* **1982,** *104*, 1095–1096.

61. Etter, M. C.; Macdonald, J. C.; and Bernstein, J. Graph-set analysis of hydrogen-bond patterns in organic crystals. *Acta Crystallogr., Sect. B.* **1990**, *46*, 256–262.

62. Gelbrich, T.; Threlfall, T. L.; Hursthouse, M. B. XPac dissimilarity parameters as quantitative descriptors of isostructurality: the case of fourteen 4,59-substituted benzenesulfonamido-2-pyridines obtained by substituent interchange involving CF3/I/Br/Cl/F/Me/H. *CrystEngComm*, **2012**, *14*, 5454–5464.

63. Nath, N. K.; Saha, B. K.; and Nangia, A. Isostructural polymorphs of triiodophloroglucinol and triiodoresorcinol. *New J. Chem*., **2008**, *32*, 1693–1701

64. Bolla, G.; Mittapalli, S.; Nangia, A. Modularity and three-dimensional isostructurality of novel synthons in sulfonamide–lactam cocrystals. *IUCrJ* **2015**. *2*, 389–401

65. Jayatilaka, D.; Spackman, M. A. Hirshfeld surface analysis. *CrystEngComm*, **2009**, *11*, 19-32

66. Spackman, M. A.; Mckinnon, J. J. Fingerprinting intermolecular interactions in molecular crystals. *CrystEngComm*, **2002**, *4(66)*, 378–392

67. Dey, D.; Thomas, S. P.; Spackman, M. A.; Chopra, D. 'Quasi-isostructural polymorphism' in molecular crystals: inputs from interaction hierarchy and energy frameworks. *Chem. Commun.,* **2016**, *52*, 2141-2144

68. Turner, M. J.; Thomas, S. P.; Shi, M. W.; Jayatilaka, D.; Spackman, M. A. Energy frameworks: insights into interaction anisotropy and the mechanical properties of molecular crystals. *Chem. Commun.,* **2015**, *51*, 3735-3738

69. Kitajgorodskij, A. I. The Principle of Close Packing and the Condition of Thermodynamic Stability of Organic Crystals. *Acta Cryst*. **1965**. *18*, 585-590

70. Mckinnon, J. J.; Spackman, M. A.; Mitchell, A. S. Novel tools for visualizing and exploring intermolecular interactions in molecular crystals. *Acta Cryst*. **2004**. *B60*, 627-668

71. Dunitz, J. D.; Gavezzotti, A. How molecules stick together in organic crystals: weak intermolecular interactions. *Chem. Soc. Rev*., **2009**, *38*, 2622–2633

72. Dey, D.; Bhandary, S.; Thomas, S. P.; Spackman, M. A.; Chopra, D. Energy frameworks and a topological analysis of the supramolecular features in in situ

cryocrystallized liquids: tuning the weak interaction landscape via fluorination. *Phys. Chem. Chem. Phys.*, **2016**, *18*, 31811-31820

73. Lee, C.; Yang, W.; Parr, R. G. *Phys. Rev. B* **1988**, *37*, 785.
74. Hehre, W. J.; Radom, L.; Schleyer, P. R.; Pople, J. A. *Ab initio molecular orbital theory*. Ed.; Wiley: New York, **1986**.
75. Frisch, M. J.; Trucks, G. W.; Schlegel, H. B.; Scuseria, G. E.; Robb, M. A.; Cheeseman, J. R.; Scalmani, G.; Barone, V.; Mennucci, B.; Petersson, G. A.; Nakatsuji, H.; Caricato, M.; Li, X.; Hratchian, H. P.; Izmaylov, A. F.; Bloino, J.; Zheng, G.; Sonnenberg, J. L.; Hada, M.; Ehara, M.; Toyota, K.; Fukuda, R.; Hasegawa, J.; Ishida, M.; Nakajima, T.; Honda, Y.; Kitao, O.; Nakai, H.; Vreven, T.; Montgomery, J. A.; Peralta, Jr., J. E.; Ogliaro, F.; Bearpark, M.; Heyd, J. J.; Brothers, E.; Kudin, K. N.; Staroverov, V. N.; Kobayashi, R.; Normand, J. ; Raghavachari, K.; Rendell, A.; Burant, J. C.; Iyengar, S. S.; Tomasi, J.; Cossi, M.; Rega, N.; Millam, J. M.; Klene, M.; Knox, J. E.; Cross, J. B.; Bakken, V.; Adamo, C.; Jaramillo, J.; Gomperts, R.; Stratmann, R. E.; Yazyev, O. ; Austin, A. J.; Cammi, R.; Pomelli, C.; Ochterski, J. W.; Martin, R. L.; Morokuma, K.; Zakrzewski, V. G.; Voth, G. A.; Salvador, P.; Dannenberg, J. J.; Dapprich, S.; Daniels, A. D. Farkas, J.; Foresman, B.; Ortiz, J. V.; Cioslowski, J.; Fox, D. J. *Gaussian 09*, Revision A.02; Gaussian, Inc.: Wallingford, CT, **2009**.
76. Zlokazov, V. B. & Chernyshev, V.V. *J. Appl. Crystallogr.* **1992**, *25*, 447-451.
77. Smith, A. J.; Kavuru, P.; Wojtas, L.; Zaworotko, M. J.; and Shytle, R. D. Cocrystals of Quercetin with Improved Solubility and Oral Bioavailability. *Mol. Pharmaceutics* **2011**, *8*, 1867–1876.
78. SAINT-Plus, Ver. 6.45; Bruker AXS: Madison, WI, **2003**.
79. Sheldrick, G. M. *SADABS, Program for Empirical Absorption Correction of Area Detector Data*; University of Göttingen: Göttingen, Germany, **1997**.
80. Sheldrick, G. M. *SHELX-97, Program for the Solution and Refinement of Crystal Structures*; University of Göttingen: Göttingen, Germany, **1997**.
81. Bruker SMART, Version 5.625, SHELXTL, Version 6.12. Bruker AXS Inc., Madison, Wisconsin, USA, **2000**.
82. Spek, A. L. PLATON: A Multipurpose Crystallographic Tool; Utrecht University: Utrecht, The Netherlands, ***2002***.

83. PLATON, A Multipurpose Crystallographic Tool; Spek, A. L., Ed.;Utrecht University: Utrecht, The Netherlands, **2002**. Spek, A. L. *J. Appl. Crystallogr.*, **2003**, *36*, 7−13.

84. Barbour, L. J.X-Seed, Graphical Interface to SHELX-97 and POV-Ray; University of Missouri–Columbia: Columbus, MO, **1999**.

85. Barbour, L. J.X-Seed-A Software Tool for Supramolecular Crystallography. *Supramol. Chem.*, **2001**, *1*, 189-191.

86. Powder Cell, a program for structure visualization, powder pattern calculation and profile fitting. http://www.ccp14.ac.uk/tutorial/powdcell/.

87. Higuchi, T.; Connors, K. A. Phase-solubility techniques. *Adv. Anal. Chem. Instrum.*, **1965**, *4*, 117-212.

# CHAPTER SIX

## Synergistic Interactions in Tinidazole Cocrystals with Acid-hydroxyl Synthon: Dissolution and Permeability

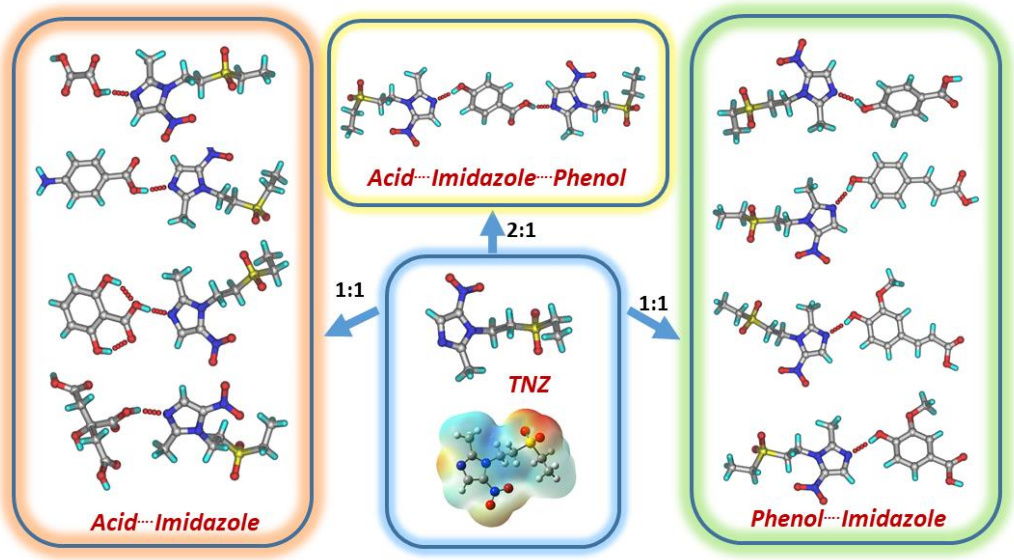


***Tinidazole (TNZ) is a 5-nitroimidazole derivative used as an antiamoebic, antiprotozoal, antibacterial, antiparasitic and also used to treat vaginal trichomoniasis including giardiasis. TNZ is a BCS class II drug with low solubility and high permeability. Nine novel solid forms (cocrystals) of tinidazole (TNZ) were synthesized with both aliphatic acids like oxalic acid (OA), citric acid (CA) and aromatic acids like 2,6-dihydroxy benzoic acid (2,6-DHBA), 4-Hydroxy benzoic acid (PHBA), 4-amino benzoic acid (PABA), ferulic acid (FA), p-coumaric acid (PCA), and vanillic acid (VA).***

## 6.1 Introduction

New solid forms of crystalline materials (pharmaceutical cocrystals and salts) have tremendous application in modifications of API's physicochemical properties without loss of its identity in the therapeutic activity. In addition, they also show advantages in energetic materials and nonlinear optics.[1-2] Crystal engineering is back bone to tailor the properties.[3-4] It is more about study and understanding of intermolecular interactions and supramolecular synthons.[5-6] Tinidazole (API) is a 5-nitroimidazole derivative used as an antiamoebic, antiprotozoal, antibacterial, antiparastic and also used to treat vaginal trichomoniasis including giardiasis.[7-12] It belongs to BCS II. The brand name is Tindmax® and the dosage form as tablet (250 mg, 500 mg) The IUPAC name of tinidazole is 1-(2 ethylsulfonylethyl)-2-methyl-5-nitroimidazole.[9] It belongs to family of nitroimadazole derivative antibiotic class which was developed in 1972. TNZ has been found to be equally or more effective than metronidazole in the treatment of trichomoniasis, giardiasis and amebiasis. It is also more important constituent of multidrug therapies for helicobacter pylori eradication regimes used to control ulcers. Tinidazole is a poor aqueous soluble drug pH 2: 8.01 mg/mL and pH 6: 7.44 mg/mL, at 37 °C)[13] and it is always challenging to crystallize new solid forms with improved physico-chemical properties.[14-19] Initially, tinidazole crystal structure was reported by S. G. Wood *et al.* in 1984 where molecules in the crystal structure are stabilized by C–H···O interactions.[8] Tinidazole contains sulfonyl group which can form sulfonyl dimers and imidazole can be used as strong hydrogen bond acceptor which could form hydrogen bonds with acids and/or hydroxy groups based on functional groups and structural fragments. Synthesis of cocrystals/salts of APIs isuseful in optimizing the physico-chemical properties, such as solubility,[20-26] permeability,[27-28] and bioavailability of API.[29-34] Recently, TNZ other solid forms such as nanofibers, microcrystals and solid dispersions were reported in addition some salts and cocrystals were analyzed to improve the solubility.[35-37]

Cocrystals[38-40] are crystalline single phase materials where two or more molecules present in the lattice with definite stoichiometry ratio which are neither simple salts[41-45] nor solvates.[46-47] Pharmaceutical cocrystals[48-49] contain at least one API and GRAS coformer. Modification of suitable solid dosage forms suitably alter solubility and dissolution rates in aqueous media. These factors will influence the rate of drug absorption and transport in the body. These modifications would provide more

opportunities to explore the properties of API by using a large range of FDA approved pharmaceutically accepted coformers.[50] Entresto[51] and escitalopram[52] oxalate are some of the new solid form recently marketed.

## 6.2 Results and Discussion

Recently, cocrystals/salts of imidazole-acid and imidazole-hydroxy synthons[53-60] are known in the literature, but, these synthons are not completely explored. However, these cocrystals are basis for choosing appropriated coformer for new cocrystals synthesis. The pKa value of tinidazole is 3.095, signifying its weak basic character. In addition, pKa rule determines the formation of cocrystal or salts depend on ΔpKa of API and coformer. The pKa difference of two component system is less than 0, it forms cocrystal, if pKa difference of two component system is greater than >3, it forms salts and in another scenario, pKa difference fall in between 0 and 3, it is difficult to predict whether it is salt or cocrystal or salt cocrystal continuum.[61-63] To explore more about imidazole-acid and imidazole-hydroxy synthons, first new solid forms of tinidazole (TNZ) were synthesized with selective coformers like aliphatic acids oxalic acid (OA), citric acid (CA) and aromatic acids like 2,6-dihydroxybenzoic acid (2,6-DHBA), 4-hydroxybenzoic acid (PHBA), 4-aminobenzoic acid(PABA), Ferulic acid (FA), p-coumaric acid (PCA), vanillic acid (VA). Later on, we also studied the solubility, permeability of new solid forms. All crystalline materials were completely characterized by PXRD, SXRD, IR and DSC.

**Table 6.1:** pKa Values of API and Coformers Used in This Study

| API&Coformers | pKa | Cocrystals | ΔpKa |
|---|---|---|---|
| TNZ | 3.095 | | |
| OA | 4.110 | TNZ-OA | 1.01 |
| CA | 4.675 | TNZ-CA | 1.58 |
| 2,6-DHBA | 1.514 | TNZ-2,6-DHBA | 1.58 |
| FA | 3.767 | TNZ-FA | 0.67 |
| PCA | 4.002 | TNZ-PCA | 0.90 |
| VA | 4.155 | TNZ-VA | 1.06 |
| PHBA | 4.380 | TNZ-PHBA | 1.28 |
| PABA | 4.770 | TNZ-PABA | 1.67 |

pKa calculations were carried out in ChemAxon calculator (Marvin 5.10.1; ChemAxon)

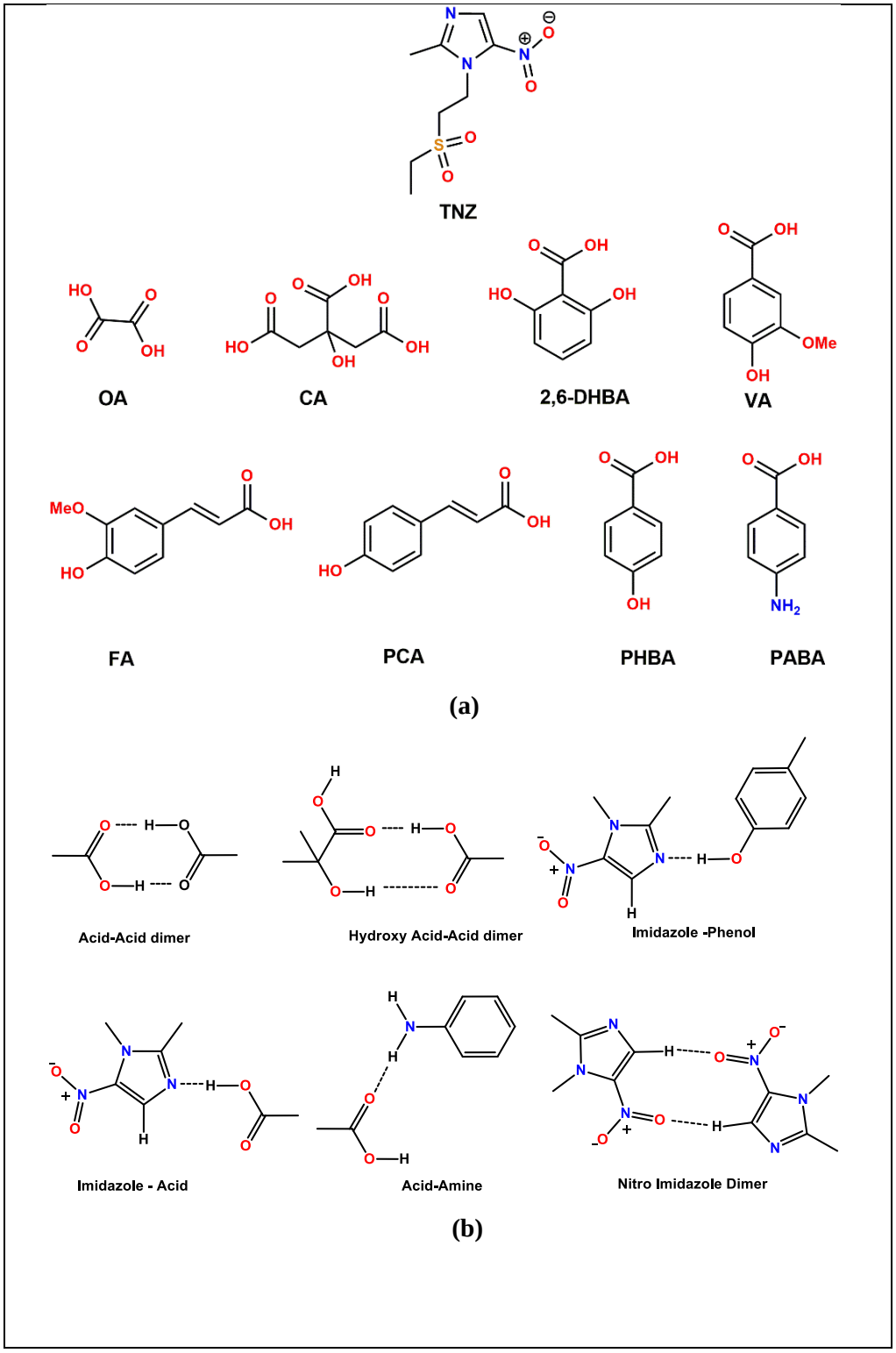


**Figure 6.1: (a)** Chemical structures of Tinidazole with coformers and (b) basic supramolecular synthons acid –imidazole and hydroxyl-imidazole, etc.

## 6.2.1 Crystal Structure Description

**Crystal structure description of tinidazole cocrystals**

pKa studies shows that all values ΔpKa are less than 3 hence it difficult to predict whether new solid form is salt or cocrystal. However, mostly we obtained cocrystals. TNZ crystallizes in the monoclinic space group $P2_1/n$ with one molecule of tinidazole in asymmetric unit and the crystal structure contains weak auxiliary C–H···O interactions, The packing diagram of TNZ is shown in Figure 6.2. Cocrystals of tinidazole were crystallized by using solvent-assist grinding, sonication, melting, rotary evaporation and neat grinding, etc.

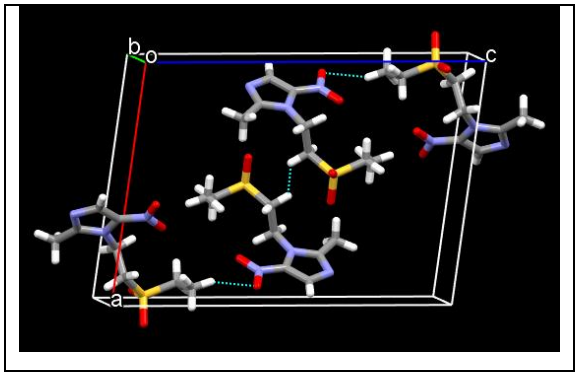


**Figure 6.2:** Molecular packing of TNZ molecules through b-axis.

**TNZ-OA (1:0.5):** The ground material of TNZ−OA (1:0.5) crystallize in the orthorhombic crystal system and exhibited space group *P*bca, one molecule of tinidazole and half molecule oxalic acid in the asymmetric unit. TNZ contains imidazole nitrogen interacted with carboxylic acid of oxalic acid (OA) *via* O−H···N (O5−H5A···N3, 1.92 Å, 162°) hydrogen bond (acid-imidazole synthon) and oxalic acid is sitting on inversion center. Ethyl sulfonyl forms auxiliary C−H···O dimer ring motif (C4−H4B···O1, 2.53 Å, 149°). The crystal packing extended *via* C−H···O dimer (Figure 6.3) Crystallographic data and hydrogen bond are listed in Table 6.2 and 6.3.

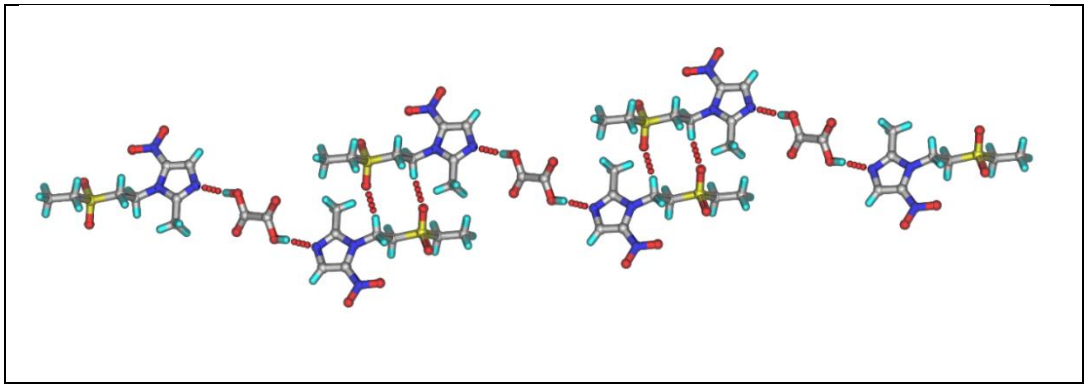

**Figure 6.3:** Two molecules of TNZ are connected to one molecule of oxalic acid by O–H···N synthon followed by chain extend via auxiliary C–H···O dimer interactions.

**TNZ-CA (1:1):** TNZ-CA (1:1) crystallize in the monoclinic crystal system with $P2_1/n$ space group and one molecule tinidazole and one molecule citric acid consistent in the asymmetric unit. It forms a 1:1 tinidazole citric acid cocrystal. The structure consists of tinidazole imidazole nitrogen interacted with secondary acid of citric acid *via* O−H···N (O5−H5A···N3, 1.94 Å, 154°) (Figure 6.4) to form acid-imidazole synthon. Hydrogen bond through citric acid molecular chains cross link through the acid ···tertiary alcohol hydrogen bond *via* (O6−H6A···O8 1.86 Å, 171°; O7−H7A···O5 2.00Å, 157°) followed by acid ···acid dimer ring motif *via* O−H···O (O11−H11A···O10, 1.84 Å, 166°) (Figure 6.4a). The coformer acid molecules arranged corrugated sheet and TNZ molecules hang on alternatively through O5−H5A···N3 bond. The crystal packing forms wave like pattern *via* acid-acid supramolecular synthons along *ac* direction. It is formed due to compensation of excess carboxylic acids.

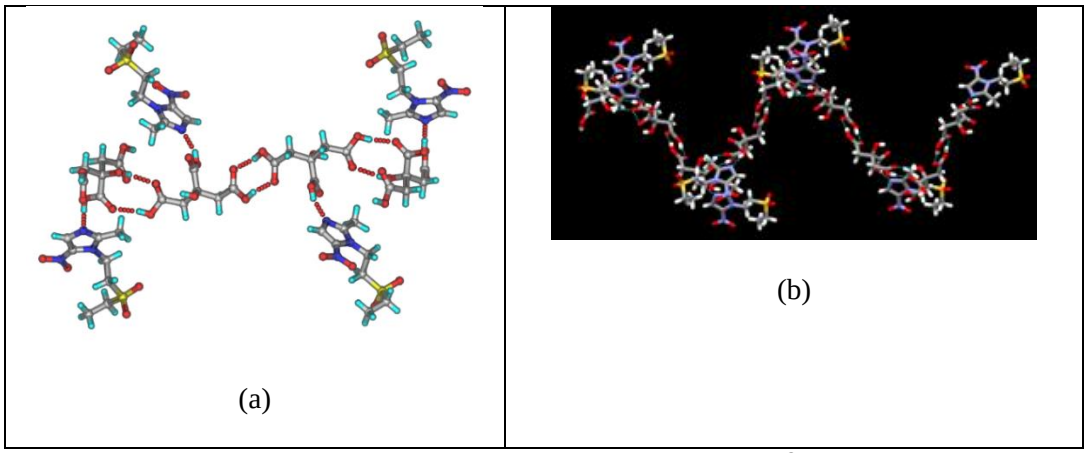

(a) (b)

**Figure 6.4:** (a) TNZ-CA(1:1) cocrystal forms acid dimer ring $R_2^2(8)$ motif *via* O−H···O hydrogen bonds followed by acid-hydroxyl dimer ring $R_2^2(9)$ via O−H···O hydrogen

bonds through inversion center followed by citric acid and imidazole nitrogen of TNZ. (b) TNZ-CA cocrystal wave like pattern via acid-acid supramolecular synthon.

**TNZ-2,6-DHBA (1:1):** TNZ-2,6-DHBA (1:1) crystallize in the monoclinic crystal system with $P2_1/c$ space group. The crystal structure contains one molecule of tinidazole and one molecule of 2,6-DHBA in the asymmetric unit. The structure contains TNZ imidazole nitrogen interacted with aromatic acid *via* O−H···N (O6−H6A···N3, 1.72 Å, 170°) (Figure 6.5) to form acid-imidazole synthon. The intramolecular hydrogen bonds (O7−H7A···O6 1.83 Å, 145°; O8−H8A···O5 1.82Å, 147°) and phenolic OH, nitro group forms weak C−H···O auxiliary interaction (C6−H6···O8 2.46 Å, 173°; C12−H12···O4 2.48Å, 166°) followed by ethyl sulfonyl weak C−H···O (C4−H4B···O1, 2.41 Å, 158°) dimer ring motif.

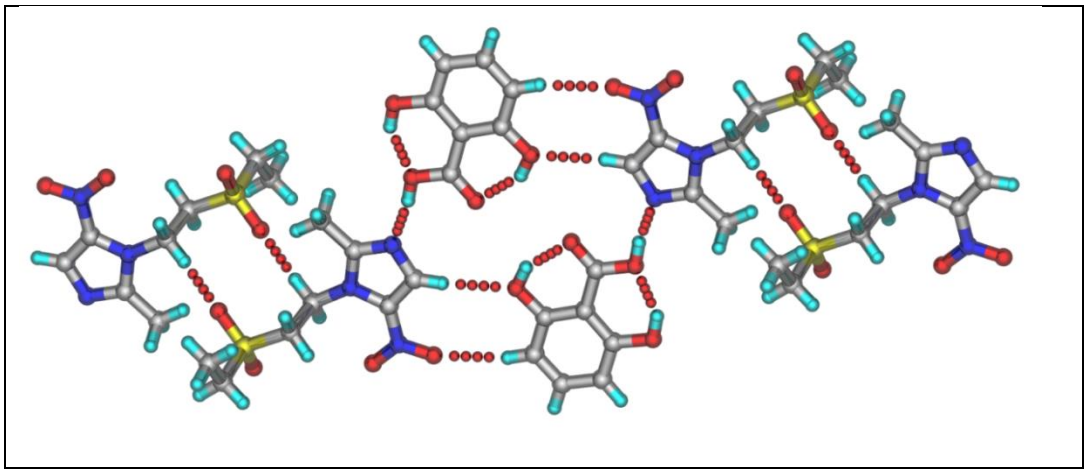

**Figure 6.5:** 2,6-DHBA acid and imidazole nitrogen of tinidazole via O−H···O hydrogen bond and nitroimidazole-phenol, ethylsulfonyl auxiliary C−H···O dimer ring $R_2^2(9)$, $R_2^2(10)$ motif interactions.

**TNZ-FA (1:1):** TNZ-FA (1:1) crystallize in the triclinic crystal system with *P*-1 space group and the asymmetric unit contains one molecule of TNZ and one molecule of FA. Though strong hydrogen bond functional group present in the system, surprisingly the stronger acid-imidazole hydrogen bond (acid-imidazole synthon) is not present in this crystal structure. Instead, the weaker phenol-imidazole hydrogen bond (hydroxy-imidazole synthon) between the phenol OH of FA and basic imidazole nitrogen N3 of TNZ via O−H···N synthon (O7−H7A···N3, 1.92 Å, 166°) followed by acid-acid dimer ring motif O−H···O (O6−H6A···O5, 1.79 Å, 174°). Inversion center related molecules

(nitro group) are connected by C−H···O (C6−H6···O4, 2.52 Å, 161°) auxiliary interactions (Figure 6.6).

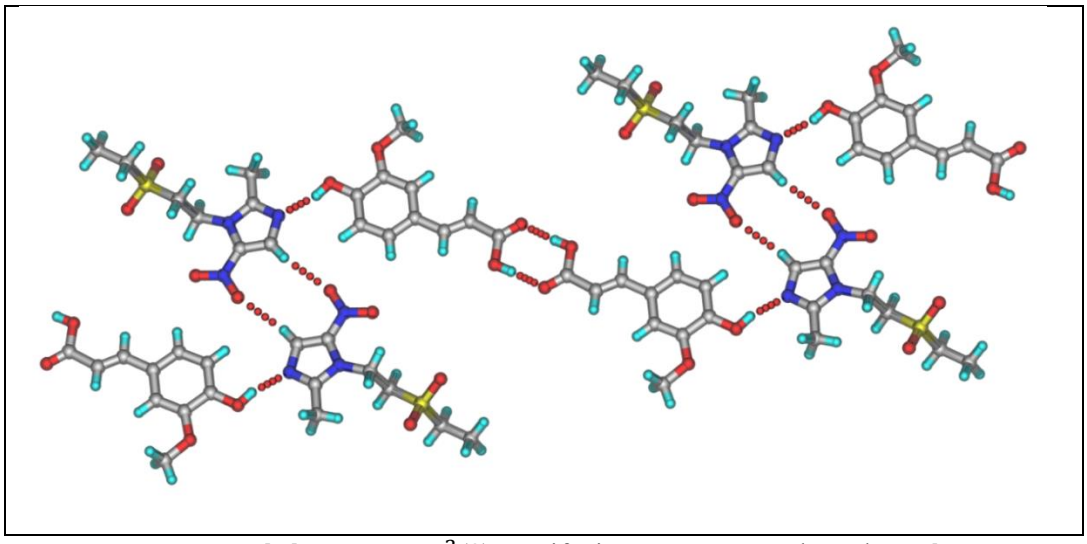

**Figure 6.6:** FA acid dimer ring $R_2^2(8)$ motif via O−H···O synthon through inversion center phenol-imidazole O−H···N synthon followed by auxiliary C−H···O dimers.

**TNZ-PCA (1:1):** TNZ-PCA (1:1) crystallize in the triclinic crystal system with *P*-1 space group. The asymmetric unit contains one molecule of TNZ and one molecule PCA. This crystal structure similar to above cocrystals same stoichiometry and crystal packing. The phenol-imidazole hydrogen bond (hydroxy-imidazole synthon) between the phenol OH of PCA and basic imidazole nitrogen N3 of TNZ via O−H···N synthon (O7−H7A···N3, 1.96 Å, 163°) followed by acid-acid dimer ring motif O−H···O (O6−H6A···O5, 1.83 Å, 172°). Inversion related molecules (nitro group) are connected by C−H···O (C6−H6···O3, 2.38 Å, 160°) auxiliary interactions (Figure 6.7).

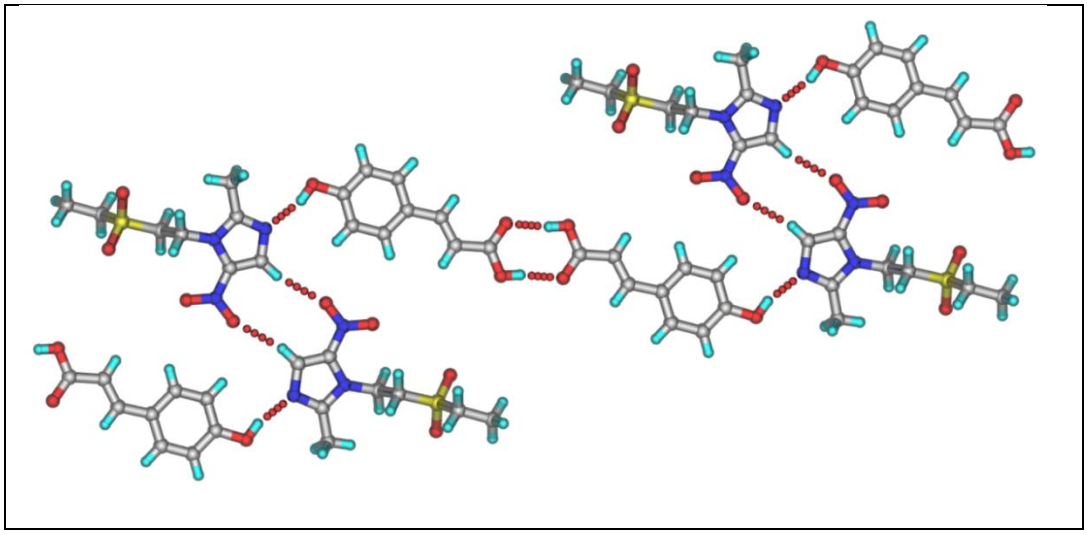

**Figure 6.7:** TNZ-PCA (1:1) cocrystal, like earlier cocrystal, PCA (aromatic acid) molecules are connected through dimeric O−H···O synthon ring motif $R_2^2(8)$ followed by phenol-imidazole O−H···O synthon through inversion center C−H···O dimer auxiliary interactions.

**TNZ-VA (2:2):** The title cocrystal was crystallized in the triclinic crystal system with *P*-1 space group. The crystal structure confirms two TNZ and two VA in the asymmetric unit. The two VA acid-acid dimer ring motif O−H···O (O9−H9A···O13 1.81 Å, 170°; O14−H14A···O10 1.79Å, 176°) followed by two phenol-imidazole hydrogen bond (hydroxy-imidazole synthon) between the phenol OH of VA and basic imidazole nitrogen N3 of TNZ via O−H···N synthon (O12−H12A···N6 1.95 Å, 168°; O15−H15A···N3 1.97Å, 163°) Inversion related molecules (nitro group) are connected by C−H···O (C6−H6···O8 2.56 Å, 164°; C14−H14···O3 2.38Å, 167°) auxiliary interactions (Figure 6.8).

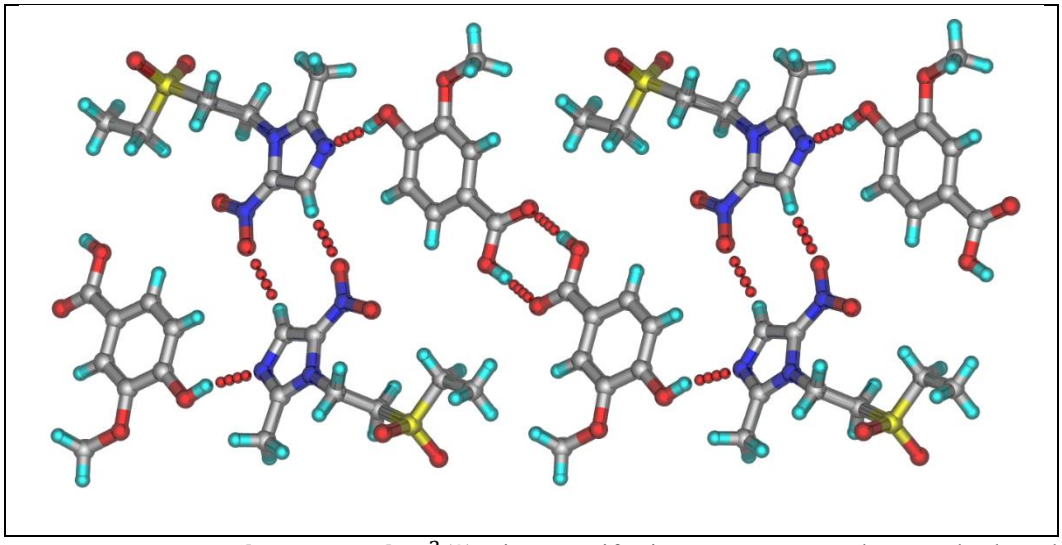

**Figure 6.8:** VA dimeric acid $R_2^2(8)$ ring motif via O−H···O synthon and phenol-imidazole O−H···N synthon through inversion center auxiliary C−H···O dimeric interactions.

**TNZ-PHBA (1:1):** TNZ and 4-hydroxy benzoic acid was crystallized in the monoclinic space group $P2_1/n$ with one TNZ and one PHBA in the asymmetric unit. The crystal structure contains acid-acid homodimer synthon $R_2^2(8)$ ring motif O−H···O (O6−H6A···O5 1.73 Å, 175°) followed by phenol-imidazole O−H···N (O7−H7A···N3 1.93 Å, 156°) (hydroxy-imidazole synthon) through 1-D tape inversion center nitro imidazole auxiliary C−H···O dimeric interactions through unit cell b-axis hydrogen bond packing are present in this system (Figure 6.9a,b).

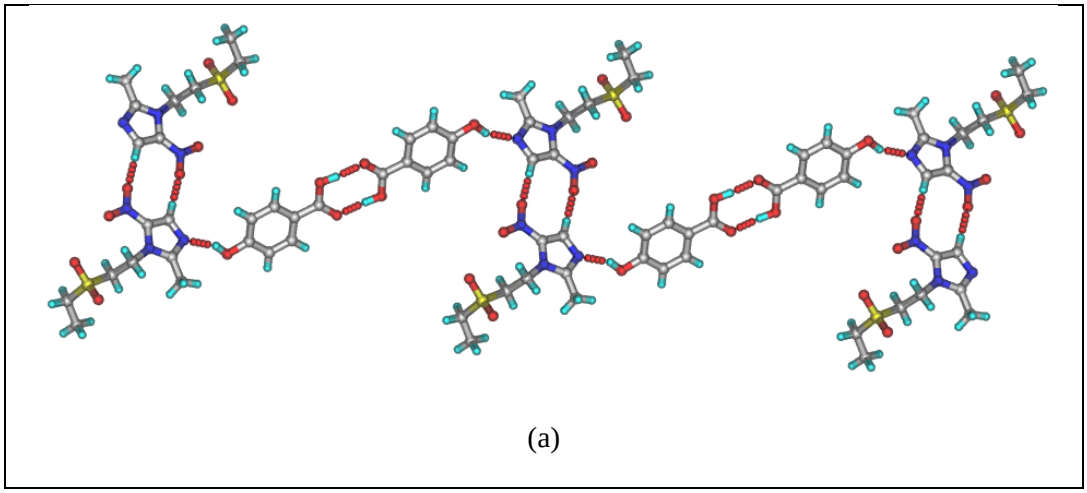

(a)

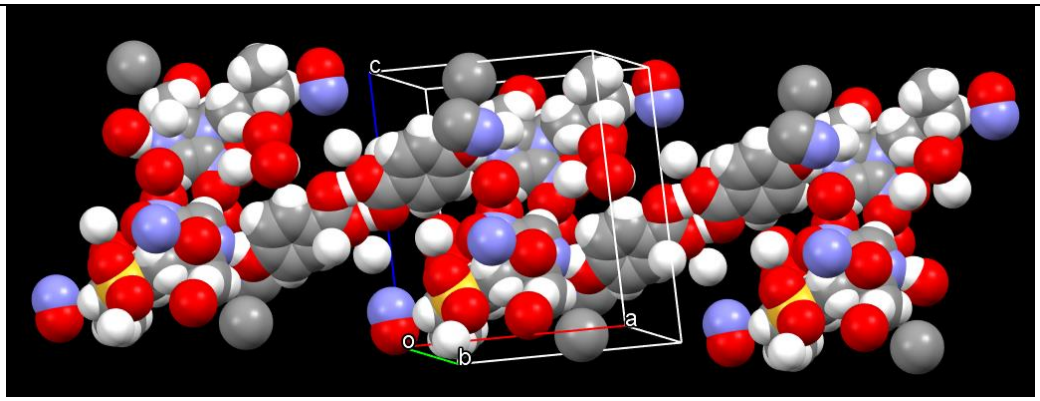


(b)

**Figure 6.9:** (a) TNZ-PHBA (1:1) cocrystals are connected through phenol-imidazole via O−H···N synthon followed by 1-D tape hydrogen packing diagram through unit cell b-axis (b) space fill hydrogen bond packing through unit cell b-axis.

**TNZ-PHBA (2:1):** TNZ and 4-hydroxy benzoic acid was crystallized in the monoclinic space group $P2_1/c$ with two TNZ and one PHBA in the asymmetric unit. Presence of two hydrogen bond acceptors tow donor system compromises to form both acid-imidazole and hydroxy-imidazole synthons to form O−H···N (O9−H9A···N3 2.00 Å, 155°; O11−H11A···N6 1.90Å, 161°). In addition, ethyl sulfoxy auxiliary C−H···O dimeric interactions are seen the unit cell. (Figure 6.10a,b)

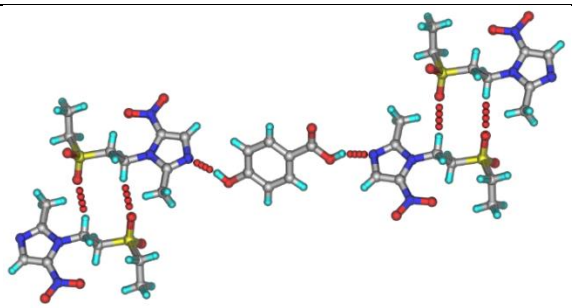

(a)

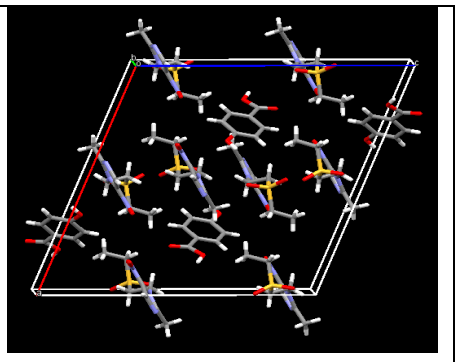

(b)

**Figure 6.10:** (a) TNZ-PHBA (2:1) cocrystal, coformer molecule connected through acid-imidazole and hydroxyl-imidazole O−H···N synthons with two molecules of TNZ further extended by C−H···O dimeric interactions. (b) Crystal packing in TNZ-PHBA (2:1)

**TNZ-PABA (1:1):** TNZ and 4-Amino benzoic acid was crystallized in the monoclinic space group $P2_1/n$ with one TNZ and one PABA in the asymmetric unit. The crystal structure contains acid-imidazole synthon O−H···N (O6−H6A···N31.93 Å, 152°) followed by amino group bifurcated hydrogen bond with amine-carbonyl N−H···O (N4−H4C···O5 2.00 Å, 171°) synthon through 2D tape via $R_4^4(20)$ ring motif are present in this system (Figure 6.11).

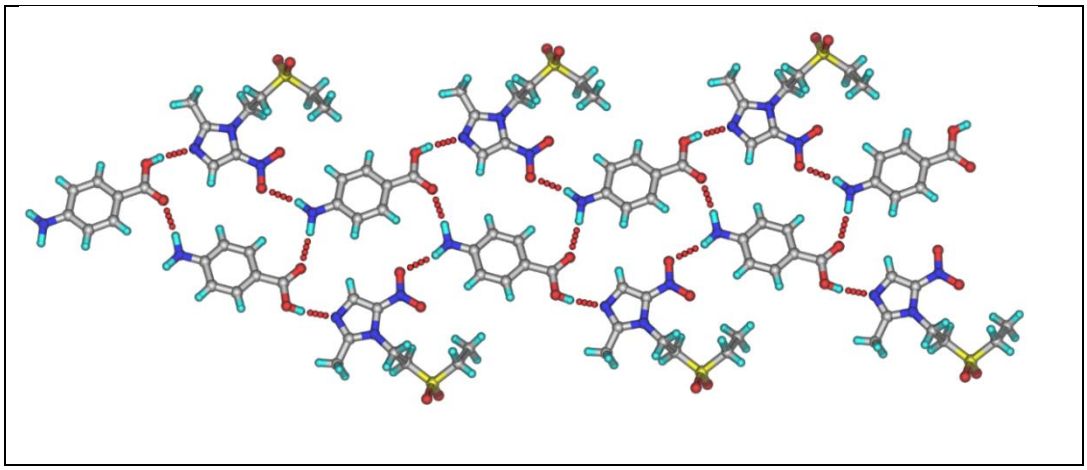

**Figure 6.11:** TNZ-PABA (1:1) cocrystal molecules are connected through acid-imidazole O−H···N synthon and amino group bifurcated hydrogen bond with nitro and carbonyl via N−H···O synthon and it shows layered 2-D tape $R_4^4(20)$ ring motif.

**Table 6.2:** Crystallographic parameters of tinidazole cocrystals.

| | **TNZ-OA (1:0.5)** | **TNZ-CA (1:1)** | **TNZ-26-DHBA (1:1)** | **TNZ-VA (1:1)** | **TNZ-PCA (1:1)** |
|---|---|---|---|---|---|
| **Empirical Formula** | $C_8H_{13}N_3O_4S$, $C_1H_1O_2$ | $C_8H_{13}N_3O_4S$, $C_6H_8O_7$ | $C_8H_{13}N_3O_4S$, $C_7H_6O_4$ | $C_8H_{13}N_3O_4S$, $C_8H_8O_4$ | $C_8H_{13}N_3O_4S$, $C_9H_8O_3$ |
| **Formula weight** | 292.29 | 439.40 | 401.39 | 830.83 | 411.43 |
| **Crystal System** | Orthorhombic | Monoclinic | Monoclinic | Triclinic | Triclinic |
| **Space Group** | *Pbca* | $P2_1/n$ | $P2_1/c$ | *P*-1 | *P*-1 |
| **T (K)** | 298(2) | 298(2) | 298(2) | 298(2) | 298(2) |
| ***a* (Å)** | 7.4044 (6) | 17.146 (4) | 6.0405 (9) | 11.2037 (11) | 5.7171 (2) |
| ***b* (Å)** | 17.2512 (17) | 5.7712 (14) | 16.181 (2) | 12.7620 (13) | 13.1440 (5) |
| ***c* (Å)** | 20.717 (2) | 19.510 (5) | 18.391 (3) | 13.7505 (14) | 13.2077 (5) |
| ***α* (°)** | 90 | 90 | 90 | 98.532 (5) | 89.098 (2) |
| ***β* (°)** | 90 | 99.977 (15) | 94.654 (10) | 98.491 (5) | 77.700 (2) |

| | | | | | |
|---|---|---|---|---|---|
| **$\gamma$(°)** | 90 | 90 | 90 | 98.904 (5) | 86.556 (2) |
| **$V$ (Å$^3$)** | 2646.3 (4) | 1901.4 (8) | 1791.6 (4) | 1891.4 (3) | 967.96 (6) |
| **$D_{calc}$ (g cm$^{-3}$)** | 1.467 | 1.535 | 1.488 | 1.459 | 1.412 |
| **Z** | 8 | 4 | 4 | 2 | 2 |
| ***F*(000)** | 1224 | 920 | 840 | 872 | 432 |
| **$\Delta\rho_{max}$, $\Delta\rho_{min}$ (e Å$^{-3}$)** | 0.29, −0.38 | 0.38, −0.41 | 0.39, −0.29 | 0.45, −0.39 | 0.38, −0.34 |
| **h range** | -9 → 8 | -21 → 21 | -7 → 7 | -13 → 14 | -7 → 7 |
| **k range** | -21 → 21 | -7 → 7 | -19 → 18 | -15 → 15 | -16 → 16 |
| **l range** | -25 → 25 | -24 → 24 | -21 → 21 | -17 → 17 | -16 → 16 |
| **measured reflections** | 26831 | 17361 | 16271 | 43557 | 45938 |
| **independent reflections** | 2689 | 3947 | 2875 | 7789 | 4276 |
| **Reflections with I> 2σ(I)** | 2244 | 2677 | 1868 | 6225 | 3241 |
| **$R_{int}$** | 0.050 | 0.059 | 0.097 | 0.032 | 0.058 |
| **$R_1[I > 2\sigma(I)]$** | 0.044 | 0.050 | 0.061 | 0.043 | 0.048 |
| **$wR_2$ (all)** | 0.122 | 0.148 | 0.166 | 0.133 | 0.139 |
| **Goodness of fit** | 1.07 | 1.07 | 1.10 | 1.04 | 1.01 |
| **X-ray diffractometer** | BRUKER APEX | BRUKER APEX | BRUKER APEX | BRUKER APEX | BRUKER APEX |

| | **TNZ-FA (1:1)** | **TNZ-PHBA (1:1)** | **TNZ-PHBA (2:1)** | **TNZ-PABA (1:1)** |
|---|---|---|---|---|
| **Empirical Formula** | $C_8H_{13}N_3O_4S$, $C_{10}H_{10}O_4$ | $C_8H_{13}N_3O_4S$, $C_7H_6O_3$ | $2(C_8H_{13}N_3O_4S)$, $C_7H_6O_3$ | $C_8H_{13}N_3O_4S$, $C_7H_7NO_2$ |
| **Formula Weight** | 441.45 | 385.39 | 632.66 | 384.41 |
| **Crystal system** | Triclinic | Monoclinic | Monoclinic | Monoclinic |
| **Space group** | *P*-1 | $P2_1/n$ | $P2_1/c$ | $P2_1/n$ |
| **T (K)** | 298(2) | 298(2) | 298(2) | 298(2) |
| **a (Å)** | 5.883 (13) | 18.2049 (9) | 18.1416 (10) | 5.8568 (2) |
| **b (Å)** | 12.38 (3) | 5.5059 (3) | 9.7498 (5) | 14.1441 (4) |
| **c (Å)** | 14.53 (4) | 18.3572 (10) | 17.9368 (9) | 24.7186 (8) |

| | | | | |
|---|---|---|---|---|
| **α (°)** | 89.66 (12) | 90 | 90 | 90 |
| **β (°)** | 80.82 (10) | 103.379 (3) | 110.635 (2) | 90.530 (2) |
| **γ (°)** | 87.02 (9) | 90 | 90 | 90 |
| **V (Å3)** | 1043 (5) | 1790.08 (17) | 2969.1 (3) | 2047.58 (11) |
| **Dcalc (gcm–3)** | 1.406 | 1.430 | 1.415 | 1.247 |
| **Z** | 2 | 4 | 4 | 4 |
| **F(000)** | 464 | 808 | 1328 | 808 |
| **Δρmax, Δρmin (e Å−3)** | 1.41, −0.50 | 0.33, −0.37 | 1.92, −0.37 | 1.69, −0.41 |
| **h range** | -7 → 7 | -23 → 23 | -21 → 21 | -7 → 7 |
| **k range** | -15 → 15 | -7 → 7 | -11 → 11 | -18 → 18 |
| **l range** | -18 → 18 | -23 → 23 | -21 → 21 | -32 → 32 |
| **measured reflections** | 23922 | 30044 | 61920 | 28532 |
| **independent reflections** | 4646 | 3958 | 5242 | 4717 |
| **Reflections with I> 2σ(I)** | 2685 | 2539 | 4154 | 3347 |
| **$R_{int}$** | 0.075 | 0.075 | 0.043 | 0.043 |
| **$R_1$[I >2σ(I)]** | 0.082 | 0.060 | 0.094 | 0.099 |
| **wR2 (all)** | 0.245 | 0.143 | 0.289 | 0.345 |
| **Goodness-of-fit** | 1.04 | 1.05 | 1.03 | 1.37 |
| **X–ray Diffractometer** | BRUKER APEX | BRUKER APEX | BRUKER APEX | BRUKER APEX |

**Table 6.3:** Hydrogen-bonds geometry in TNZ Cocrystals (neutron-normalized).

| D−H···A | D···A (Å) | H···A (Å) | D−H···A (°) | symmetry code |
|---|---|---|---|---|
| **TNZ(reported structure)** | | | | |
| C1–H1B···O4 | 3.427(3) | 2.58 | 147 | ½-x,-1/2+y,3/2-z |
| C3–H3A···O2 | 3.355(2) | 2.51 | 146 | x ,1+y,z |
| C3–H3B···O2 | 3.282(2) | 2.51 | 136 | 1-x,-y,1-z |
| C4–H4B···O3 | 2.827(3) | 2.35 | 109 | Intramolecular |
| C6–H6···O4 | 3.354(3) | 2.43 | 171 | -x,2-y,1-z |
| **TNZ–OA (1:0.5)** | | | | |
| O5–H5A···N3 | 2.711(2) | 1.92 | 162 | -1+x,y,z |
| C4–H4A···O3 | 2.865(3) | 2.35 | 113 | Intramolecular |
| C4–H4B···O1 | 3.403(3) | 2.53 | 150 | 2-x,1-y,-z |
| C6–H6···O2 | 3.050(3) | 2.26 | 143 | 5/2-x,-1/2+y,z |
| **TNZ–2,6-DHBA (1:1)** | | | | |
| O6–H6A···N3 | 2.537(4) | 1.73 | 170 | -1+x,1/2-y,1/2+z |

| | | | | |
|---|---|---|---|---|
| O7–H7A···O6 | 2.554(4) | 1.84 | 145 | Intramolecular |
| O8–H8A···O5 | 2.559(5) | 1.83 | 148 | Intramolecular |
| C2–H2A···O4 | 3.187(6) | 2.44 | 134 | 1-x,1/2+y,1/2-z |
| C4–H4A···O3 | 2.840(5) | 2.36 | 110 | Intramolecular |
| C4–H4B···O1 | 3.337(4) | 2.41 | 159 | 1-x,1-y,-z |
| C6–H6···O8 | 3.385(6) | 2.46 | 174 | 2-x,-1/2+y,1/2-z |
| C12–H12···O4 | 3.391(6) | 2.48 | 167 | 2-x,1/2+y,1/2-z |
| **TNZ–CA (1:1)** | | | | |
| O6–H6A···O8 | 2.680(3) | 1.87 | 171 | 1/2-x,1/2+y,1/2-z |
| O7–H7A···O5 | 2.780(3) | 2.00 | 158 | 1/2-x,-1/2+y,1/2-z |
| O9–H9A···N3 | 2.703(3) | 1.94 | 154 | 1/2-x,1/2+y,1/2-z |
| O11–H11A···O10 | 2.645(3) | 1.84 | 166 | -x,-y,-z |
| C2–H2A···O2 | 3.346(4) | 2.51 | 144 | 1-x,2-y,-z |
| C4–H4B···O3 | 2.861(4) | 2.34 | 113 | Intramolecular |
| C10–H10B···O1 | 3.355(4) | 2.42 | 163 | 1-x,1-y,-z |
| C12–H12B···O10 | 3.318(3) | 2.46 | 147 | -x,1-y,-z |
| **TNZ–VA (1:1)** | | | | |
| O9–H9A···O13 | 2.630(2) | 1.82 | 171 | 2-x,1-y,1-z |
| O12–H12A···N6 | 2.768(2) | 1.96 | 169 | Intramolecular |
| O14–H14A···O10 | 2.617(2) | 1.80 | 177 | 2-x,1-y,1-z |
| O15–H15A···N3 | 2.766(2) | 1.97 | 163 | -1+x,1+y,z |
| C1–H1A···O13 | 3.328(3) | 2.39 | 166 | Intramolecular |
| C3–H3A···O4 | 3.094(3) | 2.55 | 116 | Intramolecular |
| C3–H3B···O6 | 3.390(3) | 2.51 | 150 | 1-x,1-y,-z |
| C6–H6···O8 | 3.470(3) | 2.56 | 165 | 2-x,1-y,1-z |
| C8–H8A···O5 | 3.501(3) | 2.60 | 157 | 1-x,1-y,-z |
| C9–H9B···O10 | 3.414(4) | 2.46 | 174 | -1+x,1+y,z |
| C11–H11B···O1 | 3.248(3) | 2.28 | 177 | x,1+y,z |
| C12–H12B···O7 | 2.864(3) | 2.36 | 112 | Intramolecular |
| C14–H14···O3 | 3.301(3) | 2.39 | 167 | 2-x,1-y,1-z |
| C16–H16A···O2 | 3.201(3) | 2.31 | 155 | 1-x,1-y,-z |
| **TNZ–PCA (1:1)** | | | | |
| O6–H6A···O5 | 2.647(3) | 1.83 | 172 | 1-x,2-y,1-z |
| O7–H7A···N3 | 2.755(2) | 1.96 | 163 | -2+x,y,z |
| C2–H2A···O1 | 3.280(3) | 2.52 | 135 | 2-x,-y,-z |
| C2–H2B···O5 | 3.354(3) | 2.47 | 151 | x,-1+y,z |
| C3–H3A···O6 | 3.426(3) | 2.48 | 164 | 1-x,1-y,1-z |
| C3–H3B···O2 | 3.268(3) | 2.37 | 154 | 1+x,y,z |
| C4–H4B···O4 | 2.842(3) | 2.36 | 110 | Intramolecular |
| C6–H6···O3 | 3.278(3) | 2.39 | 160 | 2-x,1-y,1-z |
| **TNZ–FA (1:1)** | | | | |
| O6–H6A···O5 | 2.615(10) | 1.80 | 174 | 1-x,2-y,1-z |
| O7–H7A···N3 | 2.728(9) | 1.93 | 166 | -2+x,y,z |
| C4–H4A···O3 | 2.855(10) | 2.30 | 116 | Intramolecular |
| C4–H4B···O1 | 3.014(10) | 2.54 | 110 | Intramolecular |

| | | | | |
|---|---|---|---|---|
| C6–H6···O4 | 3.421(11) | 2.53 | 161 | 2-x,1-y,1-z |
| C11–H11···O6 | 2.814(11) | 2.42 | 106 | Intramolecular |
| C16–H16···O4 | 3.306(11) | 2.55 | 138 | -x,1-y,1-z |
| **TNZ–PABA (1:1)** | | | | |
| N4–H4C···O5 | 2.995(5) | 2.00 | 172 | 3/2-x,1/2+y,1/2-z |
| N4–H4D···O4 | 3.071(5) | 2.14 | 162 | -1+x,y,z |
| O6–H6A···N3 | 2.687(4) | 1.93 | 152 | -1+x,-1+y,z |
| C3–H3B···O2 | 3.354(5) | 2.57 | 138 | 1-x,1-y,-z |
| C4–H4A···O3 | 2.830(5) | 2.36 | 109 | Intramolecular |
| C15–H15···O6 | 2.725(5) | 2.40 | 100 | Intramolecular |
| **TNZ–PHBA (1:1)** | | | | |
| O6–H6A···O5 | 2.633(3) | 1.73 | 175 | -x,1-y,1-z |
| O7–H7A···N3 | 2.749(3) | 1.94 | 156 | 1/2+x,5/2-y,1/2+z |
| C2–H2A···O4 | 3.426(5) | 2.60 | 144 | 1/2-x,-1/2+y,1/2-z |
| C2–H2A···N2 | 3.417(4) | 2.61 | 141 | 1/2-x,-1/2+y,1/2-z |
| C4–H4A···O3 | 2.822(4) | 2.34 | 110 | Intramolecular |
| C6–H6···O4 | 3.303(4) | 2.40 | 164 | -x,2-y,-z |
| C8–H8A···O5 | 3.464(4) | 2.59 | 152 | -x,1-y,1-z |
| **TNZ–PHBA (2:1)** | | | | |
| O9–H9A···N3 | 2.762(6) | 2.00 | 155 | -x,1/2+y,1/2-z |
| O11–H11A···N6 | 2.686(5) | 1.90 | 161 | 1-x,-y,1-z |
| C3–H3B···O1 | 3.334(4) | 2.56 | 137 | -x,-1/2+y,1/2-z |
| C4–H4A···O10 | 3.356(7) | 2.42 | 161 | x,3/2-y,-1/2+z |
| C4–H4B···O2 | 3.424(5) | 2.50 | 160 | -x,2-y,-z |
| C6–H6···O2 | 3.329(5) | 2.50 | 149 | x,-1+y,z |
| C11–H11C···O6 | 3.249(5) | 2.49 | 134 | 1-x,-1/2+y,1/2-z |
| C12–H12A···O5 | 3.405(5) | 2.52 | 151 | 1-x,1-y,1-z |
| C14–H14···O5 | 3.307(5) | 2.48 | 148 | x,-1+y,z |
| C20–H20···O4 | 3.285(7) | 2.59 | 132 | Intramolecular |

## 6.2.2 Molecular electrostatic potential calculations

Whenever there is a competition to form hydrogen bond of carboxylic acid and hydroxy group with pyridine, hydroxy group, O–H, acts as better donor compare to compare to carboxylic acid. However, we have studied how carboxylic acid and hydroxy group interact with imidazole by experimentally and theoretically. Except 2,6-DHBA case, higher difference in the energy between imidazole and acid/hydroxy coformers act as best complementary hydrogen bonds. For instance, in CA case, it has three carboxylic acids which have -301.20, -301.20 -309.98 kcal/mole energies and one hydroxy group has -359.56 kcal/mole. The energy of imidazole has -296.81 kcal/mole. When energy difference between imidazole and acid/hydroxy are compared, hydroxy group and imidazole are observed more compare to acid and imidazole hence it is predicted that

hydroxy-imidazole preferred over acid-imidazole. This perception is true for other systems as well. In addition, the theory is proved experimentally by studying cocrystals of TNZ and coformers (Figure 6.12 and Table 6.4).

| | |
|---|---|
| 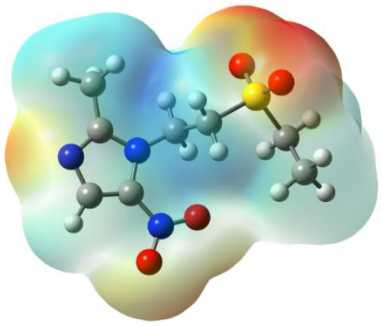 TNZ | 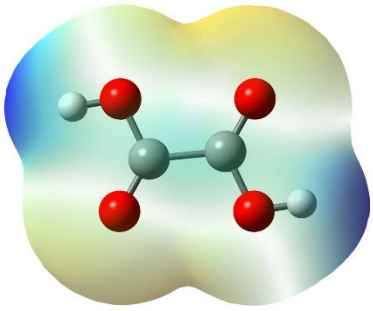 OA |
| 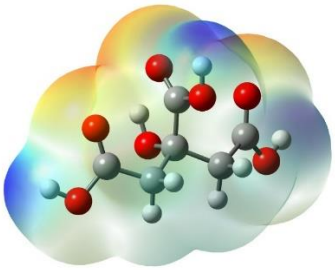 CA | 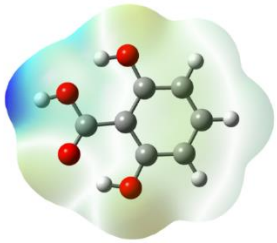 2,6-DHBA |
| 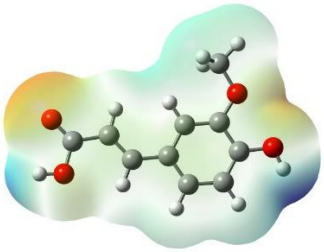 FA | 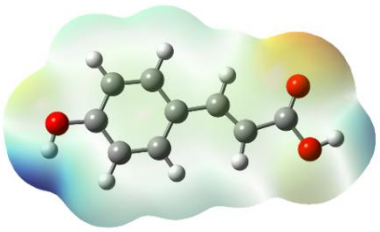 PCA |
| 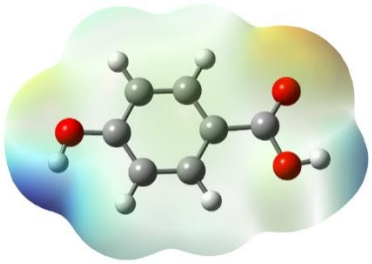 | 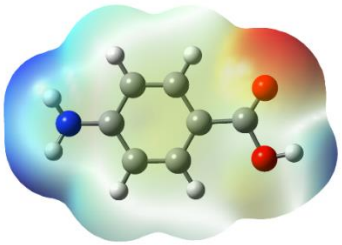 PABA |

| PHBA | |
|---|---|
| 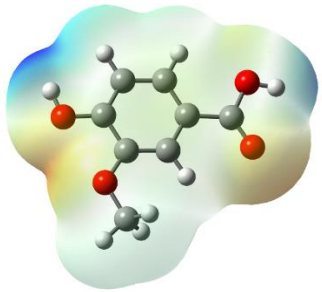 VA | |

**Figure 6.12:** Molecular electrostatic potential surface energy maps MEPSE (kcal $mol^{-1}$) of the different functional-group molecules of TNZ and all coformers.

**Table 6.4:** MEPSE (kcal $mol^{-1}$) of the different functional-groups of TNZ and all coformers.

| **Molecules** | **Imidazole/Amine Kcal/mole** | **Acid group Kcal/mole** | **Hydroxyl group Kcal/mole** |
|---|---|---|---|
| **TNZ** | -296.81 | | |
| **OA** | | -283.00 | |
| **CA** | | -301.20,-301.20,-309.98 | -359.56 |
| **2,6-DHBA** | | -339.48 | -351.40 |
| **PHBA** | | -317.52 | -343.87 |
| **PABA** | | -319.40 | |
| **PCA** | | -316.89 | -344.50 |
| **FA** | | -319.40 | -338.22 |
| **VA** | | -318.14 | -338.22 |

In general, hydroxy substituted benzoic acid forms either acid-imidazole and/or hydroxy-imidazole synthons depends on position hydroxy groups and the stoichiometry is used for crystallization. The 4-hydroxy substituted benzoic acids form acid-acid dimer along with hydroxy-imidazole and 2-hydroxy substituted benzoic acids form only acid-imidazole synthons. Formation of acid-imidazole and hydroxy imidazole synthons depends on position of hydroxy substitute in the molecule. In presence of acid and hydroxy substitution, If the hydroxy is present at less hindered position, it preference to form hydroxy-imidazole than acid-imidazole. When stoichiometry is taken into the account, excess imidazole will always leads to form both acid-imidazole and hydroxy imidazole.

In addition, we have attempted to synthesize ternary cocrystals where we would like see competition between hydroxy subtitled molecules and aliphatic acids with imidazole? In such scenario, smaller size aliphatic acids dominate to form acid-imidazole containing phase than hydroxy substituted acids. In ternary cocrystal synthesis, when aromatic 2,6-hydroxy substituted acids and 4-hydroxy substituted acids are taken together with imidazole containing molecules, 2,6-hydroxy substituted acids-imidazole containing phase dominates to form acid-imidazole. It could be due to intramolecular hydrogen bond further support the acid to involve in stronger hydrogen bond with imidazole (Figure 6.13-6.15 and Table 6.5).

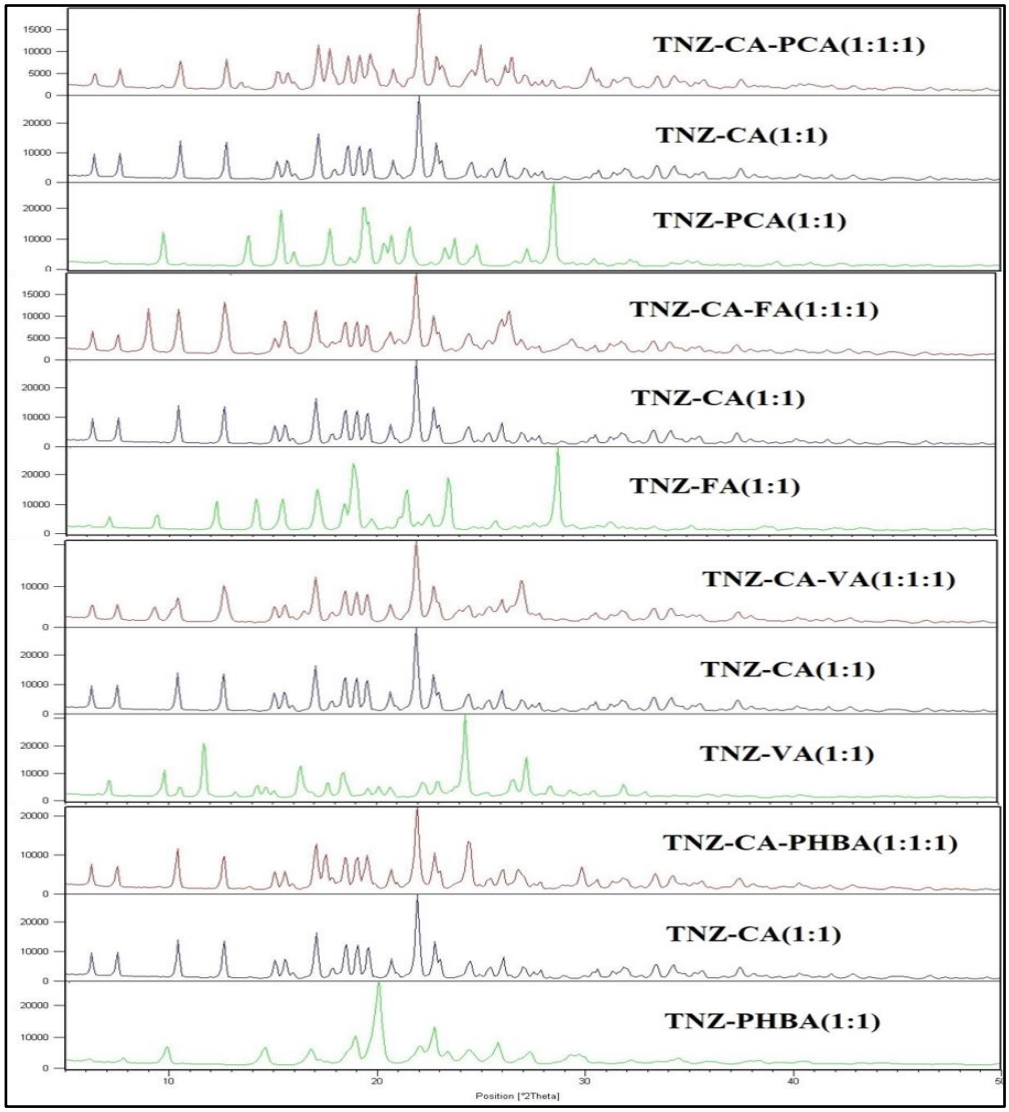


**Figure 6.13:** Cocrystals of hydroxyl and acid substituted molecules with Tinidazole molecule through PXRD study.

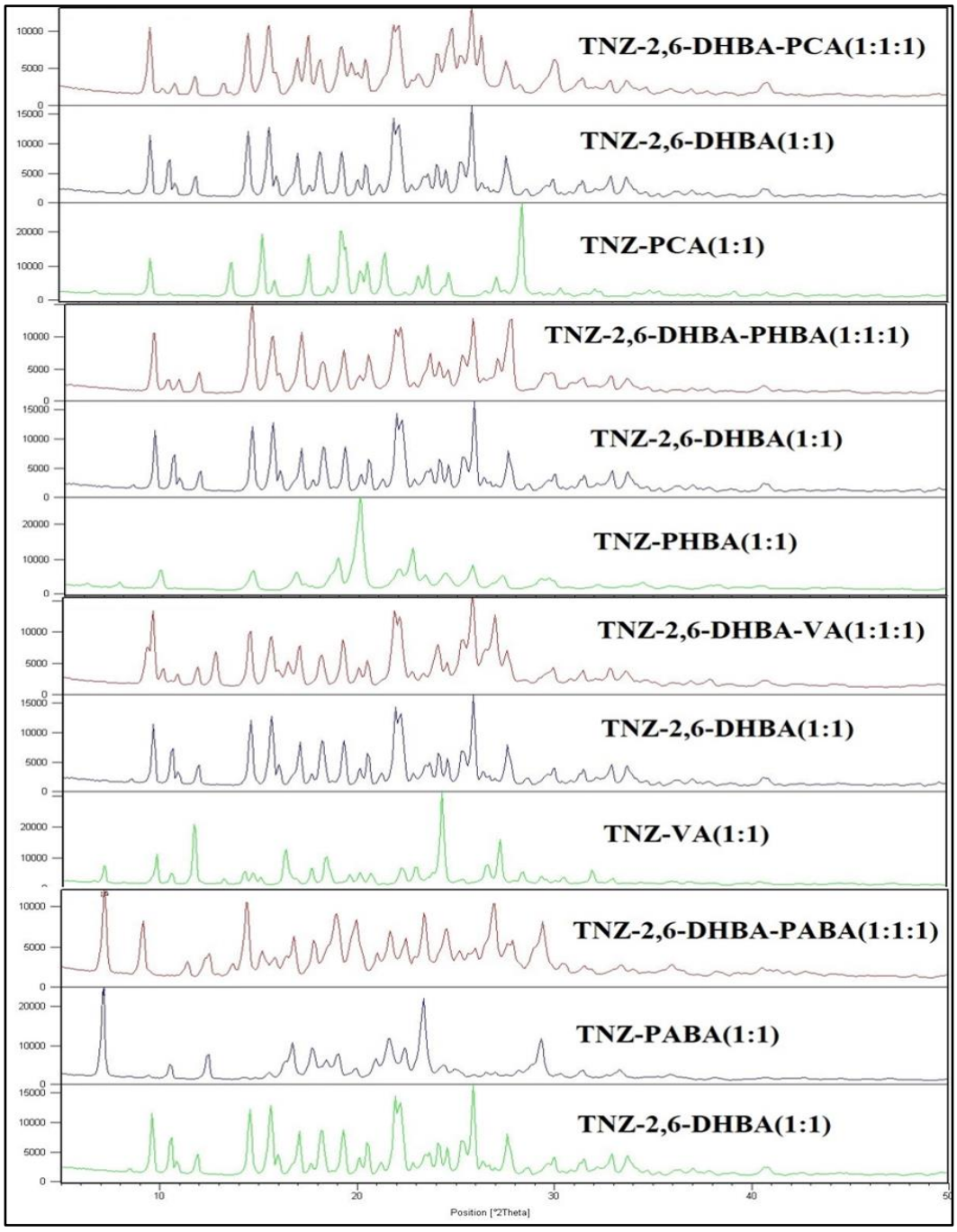


**Figure 6.14:** Cocrystals of hydroxyl and acid substituted molecules with Tinidazole molecule through PXRD study.

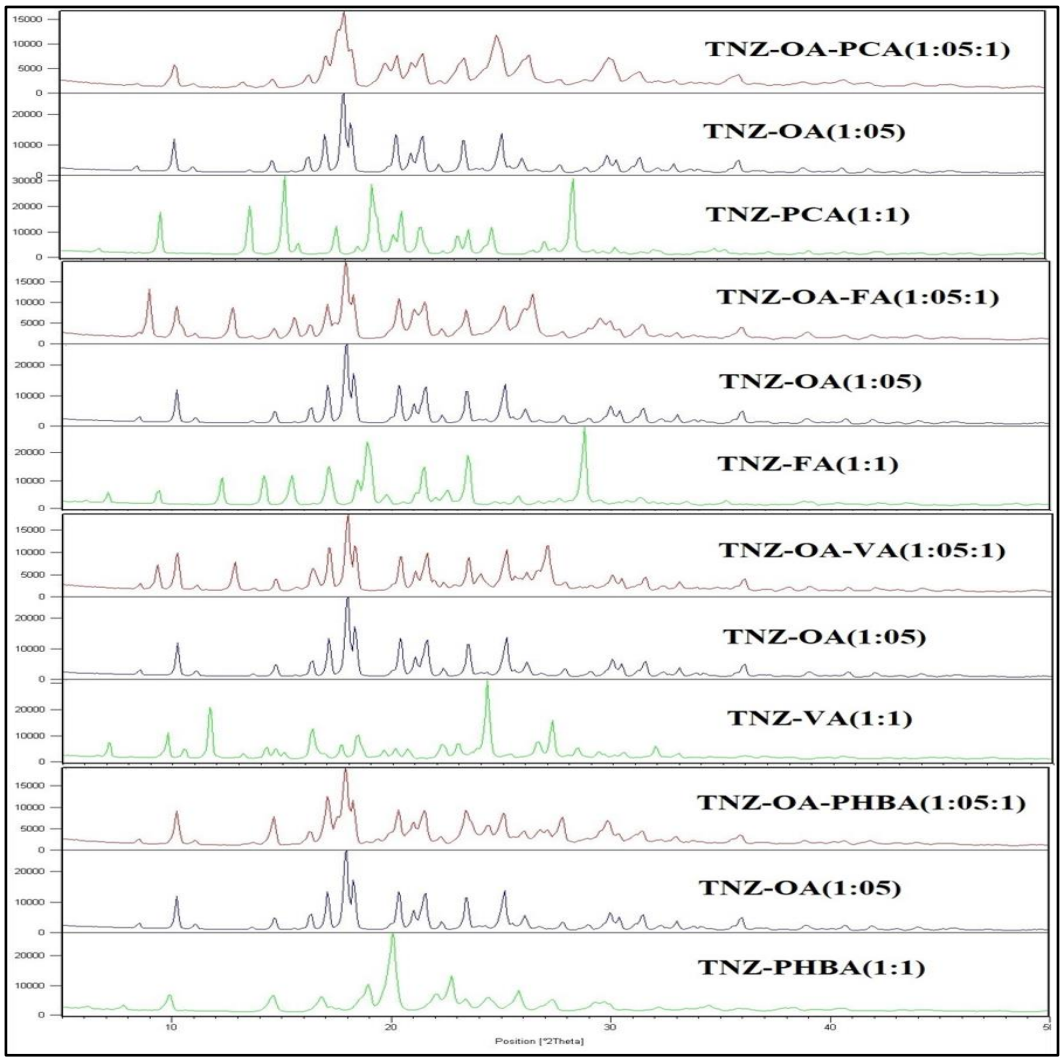


**Figure 6.15:** Cocrystals of hydroxyl and acid substituted molecules with Tinidazole molecule through PXRD study.

**Table 6.5:** Acid and phenols synthons competition with imidazole nitrogen it's showing mostly Acid-imidazole synthon favored comparative to phenol-imidazole through powder X-ray diffraction study.

| | TNZ-OA | TNZ-CA | TNZ-2,6-DHBA | TNZ-FA | TNZ-PCA | TNZ-PHBA | TNZ-PABA | TNZ-VA |
|---|---|---|---|---|---|---|---|---|
| **TNZ-OA-FA(1:0.5:1)** | √ | | | X | | | | |
| **TNZ-OA-PCA(1:0.5:1)** | √ | | | | X | | | |
| **TNZ-OA-PHBA(1:0.5:1)** | √ | | | | | X | | |
| **TNZ-OA-PABA(1:0.5:1)** | √ | | | | | | X | |

| | | | | | | | | |
|---|---|---|---|---|---|---|---|---|
| **TNZ-OA-VA(1:0.5:1)** | √ | | | | | | | X |
| **TNZ-CA-FA(1:1:1)** | | √ | | X | | | | |
| **TNZ-CA-PCA(1:1:1)** | | √ | | | X | | | |
| **TNZ-CA-PHBA(1:1:1)** | | √ | | | | X | | |
| **TNZ-CA-PABA(1:1:1)** | | √ | | | | | X | |
| **TNZ-CA-VA(1:1:1)** | | √ | | | | | | X |
| **TNZ-2,6-DHBA-FA(1:1:1)** | | | √ | X | | | | |
| **TNZ-2,6-DHBA-PCA(1:1:1)** | | | √ | | X | | | |
| **TNZ-2,6-DHBA-PHBA(1:1:1)** | | | √ | | | X | | |
| **TNZ-2,6-DHBA-PABA(1:1:1)** | | | √ | | | | X | |
| **TNZ-2,6-DHBA-VA(1:1:1)** | | | √ | | | | | X |

**Here √ means product formed, Here X means product not formed.**

## 6.2.3 Conformational Analysis

**Conformation:** Tinidazole contains nitroimidazole ring with freely rotatable alkylsufonyl chain though the conformation of the TNZ are different for instance TNZ(red), TNZ-CA(yellow), TNZ-PABA(blue), TNZ-VA1(purpule), TNZ-PCA(light-blue) (conformer 1) and TNZ-2,6-DHBA(light-green), TNZ-FA(green), TNZ-VA2(magenta), TNZ-PHBA(cyan), TNZ-OA(orange) (conformer 2). These observations suggest that the torsion angles are shown in Table 6.6 and Figure 6.16.

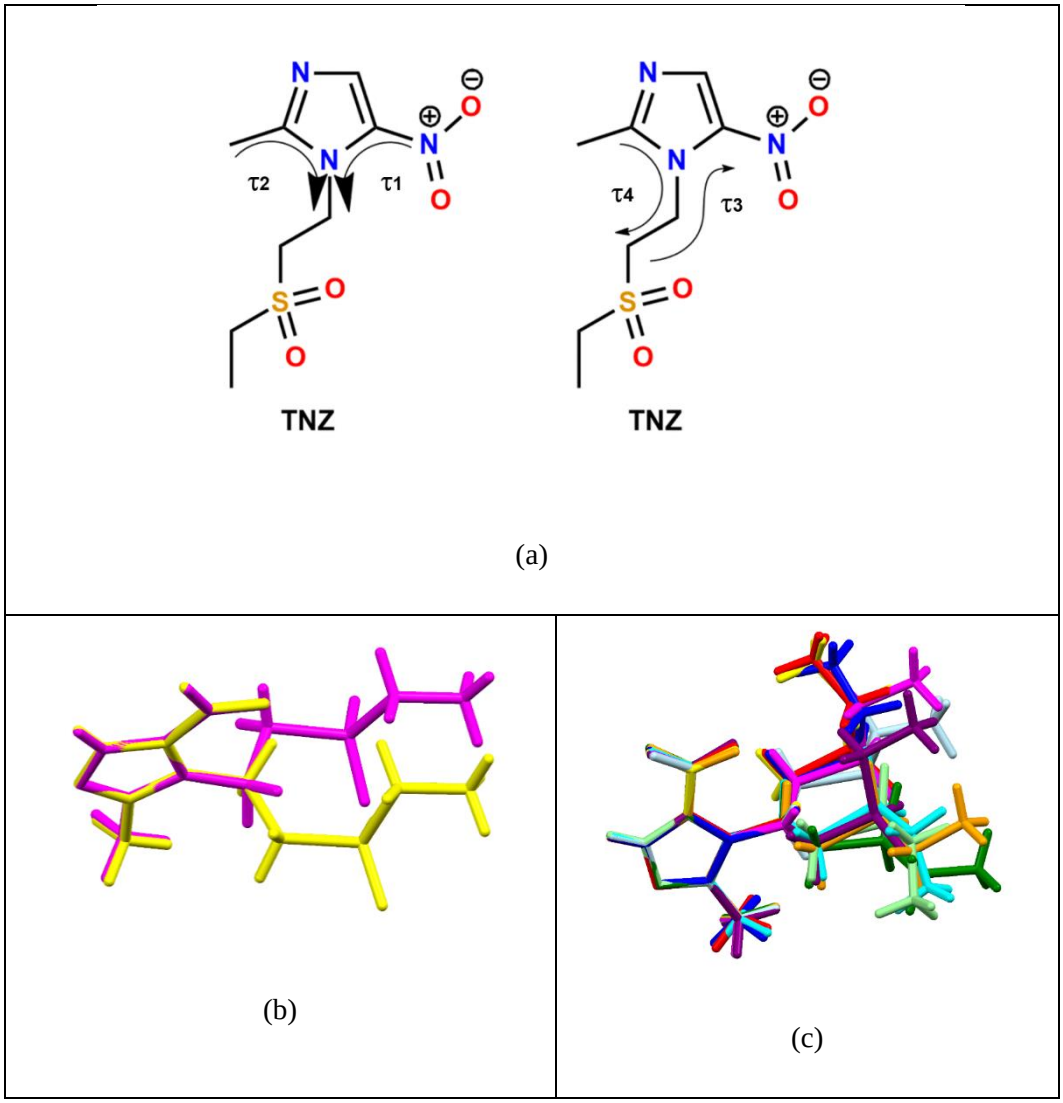


**Figure 6.16:** (a) Conformational flexibility of tinidazole with four torsions (b) Two types of the conformers in TNZ-VLA cocrystal. (c) Overlay of TNZ cocrystals to show the changes in molecular conformations of alkyl sulfonyl chain.

**Table 6.6:** Torsion angles of the TNZ in different adducts.

| | **Torsion 1(τ1) (°) N2C5N1C4** | **Torsion 2(τ2) (°) C8C7N1C4** | **Torsion 3(τ3) (°) C5N1C4C3** | **Torsion 4(τ4) (°) C7N1C4C3** |
|---|---|---|---|---|
| TNZ(Red) | -4.43 | 1.19 | -77.55 | 97.32 |
| TNZ-OA (Orange) | -3.95 | 0.63 | 93.83 | -88.59 |
| TNZ-CA(Yellow) | -11.05 | 6.45 | -77.48 | 93.11 |
| TNZ-2,6-DHBA(Light green) | 0.99 | 1.65 | 82.53 | -98.80 |

| | | | | |
|---|---|---|---|---|
| TNZ-FA(Green) | -0.34 | 2.13 | 94.18 | -89.96 |
| TNZ-PCA(Light blue) | 1.86 | -2.18 | -88.74 | 95.97 |
| TNZ-VA1(Purple) | 2.05 | 0.45 | 81.77 | -94.86 |
| TNZ-VA2(Magenta) | 1.95 | -3.64 | -83.53 | 99.87 |
| TNZ-PHBA(Cyan) | -5.75 | 4.22 | 86.74 | -99.08 |
| TNZ-PABA(Blue) | 0.92 | -3.09 | -82.20 | 97.69 |

## 6.2.4 Powder X-ray Diffraction

Novel solid forms identification and bulk phase purity using PXRD is a prime characterization technique for standard practice in pharmaceutics through their unique diffraction lines. Herein, Tinidazole(TNZ) multicomponent solid forms (cocrystals) prepared in this work confirm the exhibit unique diffraction pattern show excellent match of the experimental PXRD with the calculated pattern from the X-ray crystal structure (Figure 6.17). Tinidazole solid forms determined through their unique diffraction patterns which are different from that of the starting components demonstrating new solid forms.

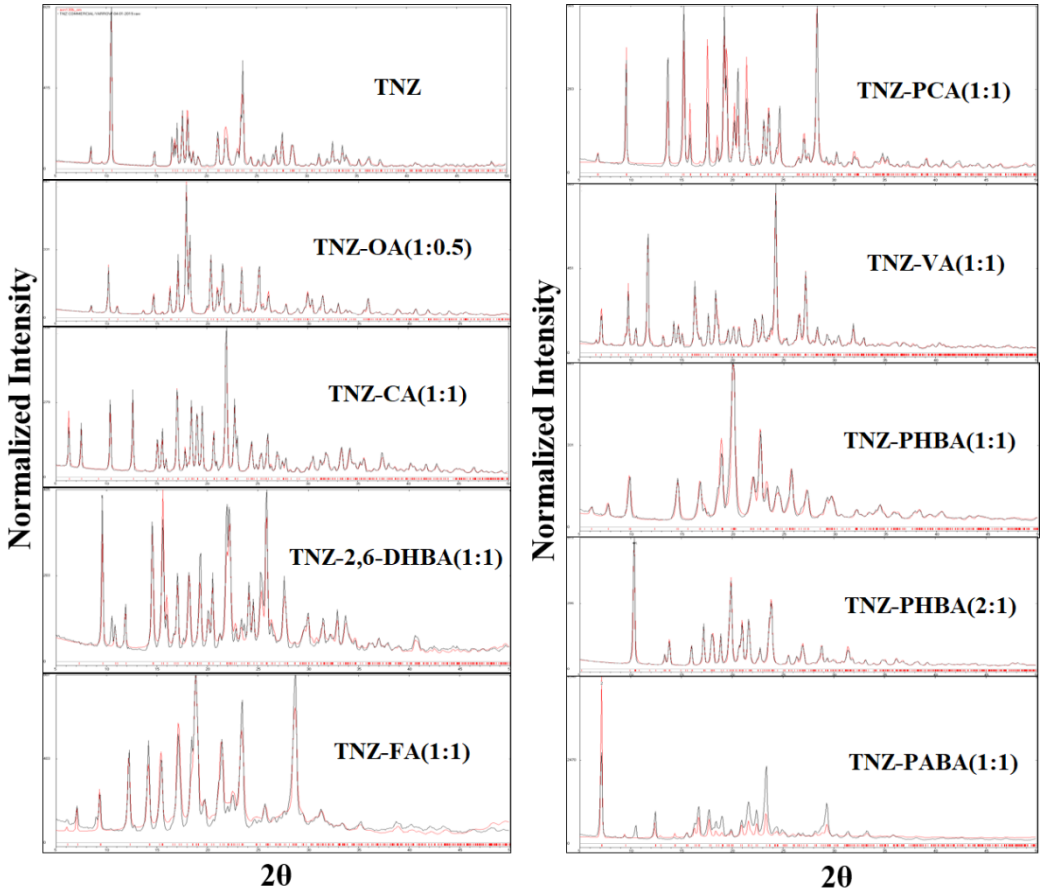


**Figure 6.17:** Overlay of experimental PXRD patterns (black) of novel crystal forms of TNZ on the calculated lines (red) from the X-ray crystal structure.

## 6.2.5 Thermal Analysis

Tinidazole showed sharp endotherm at 125 °C without any phase transformation. The grinding material of TNZ and OA cocrystal melts at 142 °C. The melting points of other TNZ cocrystals with CA,2,6-DHBA,FA,PCA,VA,PABA 122 °C, 145 °C, 102 °C, 130°C, 128 °C, and PHBA(1:1) & PHBA(2:1) 140 °C, 132 °C respectively . TNZ-2,6-DHBA exhibited the highest melting point (145 °C ) and TNZ-FA has the lowest melting point (102 °C ). Differential scanning calorimetry thermograms are displayed in Figure 6.18 and melting points are listed in Table 6.7.

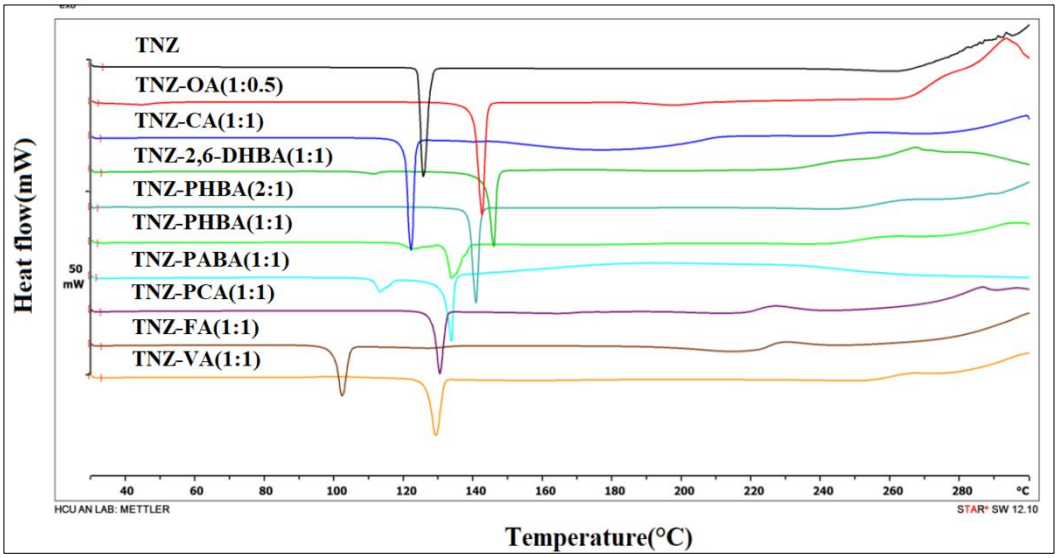


**Figure 6.18:** DSC thermograms of TNZ Cocrystals.

**Table 6.7:** Melting point table of Tinidazole Cocrystals

| Compound name | API/Coformers M.P (°C) | Cocrystals M.P (°C) |
|---|---|---|
| TNZ | 123-127 | ---- |
| TNZ-OA(1:05) | 189-191 | 140-144 |
| TNZ-CA(1:1) | 154-156 | 120-124 |
| TNZ-2,6-DHBA(1:1) | 163-165 | 143-147 |
| TNZ-FA(1:1) | 168-172 | 100-104 |
| TNZ-PCA(1:1) | 210-213 | 128-132 |
| TNZ-VA(1:1) | 210-213 | 126-131 |
| TNZ-PHBA(1:1) | 213-215 | 132-138 |
| TNZ-PHBA(2:1) | 213-215 | 138-142 |
| TNZ-PABA(1:1) | 187-189 | 130-134 |

## 6.2.6 Infrared Spectroscopy

FT-IR spectra were useful to analyse and differentiate the solid form nature of cocrystals/salts based on a vibrational stretching frequencies exhibited by TNZ and its cocrystals (Figure 6.19). FT-IR spectra of TNZ molecule at 3020-2913, 1762, 1522 and 1479, 1302 and 1264, 1191-1123 $cm^{-1}$ was assigned to C-H stretching, C=C (imidazole ring), C=N (imidazole ring), S=O, N=O ($NO_2$), symmetric/asymmetric stretching frequencies respectively. In case of the TNZ cocrystal shows (blue shift) carbonyl/ C=N (imidazole ring) stretching frequency at 1743-1669 $cm^{-1}$. The acid OH/amine NH groups are absent in TNZ but cocrystals of TNZ shows stretching frequency appeared in the range 3442-3126 cm-1 (Figure 6.19, Table 6.8). In other case FT-IR spectra of TNZ cocrystals shows significant changes in their vibrational frequencies pattern on cocrystal

formation, it is observed that the bands associated with S=O and N=O ($NO_2$) stretching frequencies appeared in the range 1285-1311 and 1456-1479 $cm^{-1}$ respectively indicating for the formation of TNZ cocrystals.

**Table 6.8:** Selected functional group stretching frequency in FT-IR spectra of TNZ cocrystals.

| | **C=O/C=C/C=N (carboxylic acid),imidazole ring) (cm−1)** | **Acid/Hydroxyl−OH/Amine NH($cm^{-1}$)** | **$SO_2$/$NO_2$ ($cm^{-1}$)** |
|---|---|---|---|
| **TNZ** | 1762,1522 | ––– | 1302,1479 |
| **TNZ−OA (1:1)** | 1715,1547,1499 | 3154 | 1311,1477 |
| **TNZ−CA (1:1)** | 1743,1715,1541,1488 | 3366 | 1306,1456 |
| **TNZ−2,6-DHBA (1:1)** | 1670,1635,1580,1546 | 3114 | 1309,1490 |
| **TNZ-FA (1:1)** | 1692,1666,1601,1520 | 3437 | 1302,1457 |
| **TNZ-PCA(1:1)** | 1683,1624,1537 | 3147 | 1308,1474 |
| **TNZ-VA(1:1)** | 1669,1592,1538 | 3126 | 1285,1472 |
| **TNZ−PHBA (1:1)** | 1698 | 3146 | 1305, 1478 |
| **TNZ−PABA (1:1)** | 1678,1650,1539 | 3442,3356,3247 | 1310,1459 |
| **OA** | 1701 | 3431 | ––– |
| **CA** | 1755,1711 | 3495 | ––– |
| **2,6-DHBA** | 1685 | 3475 | ––– |
| **FA** | 1691 | 3436 | ––– |
| **PCA** | 1672 | 3368 | ––– |
| **VA** | 1682 | 3484 | |
| **PHBA** | ––– | 3436 | ––– |
| **PABA** | 1667 | 3460,3381,3363 | ––– |

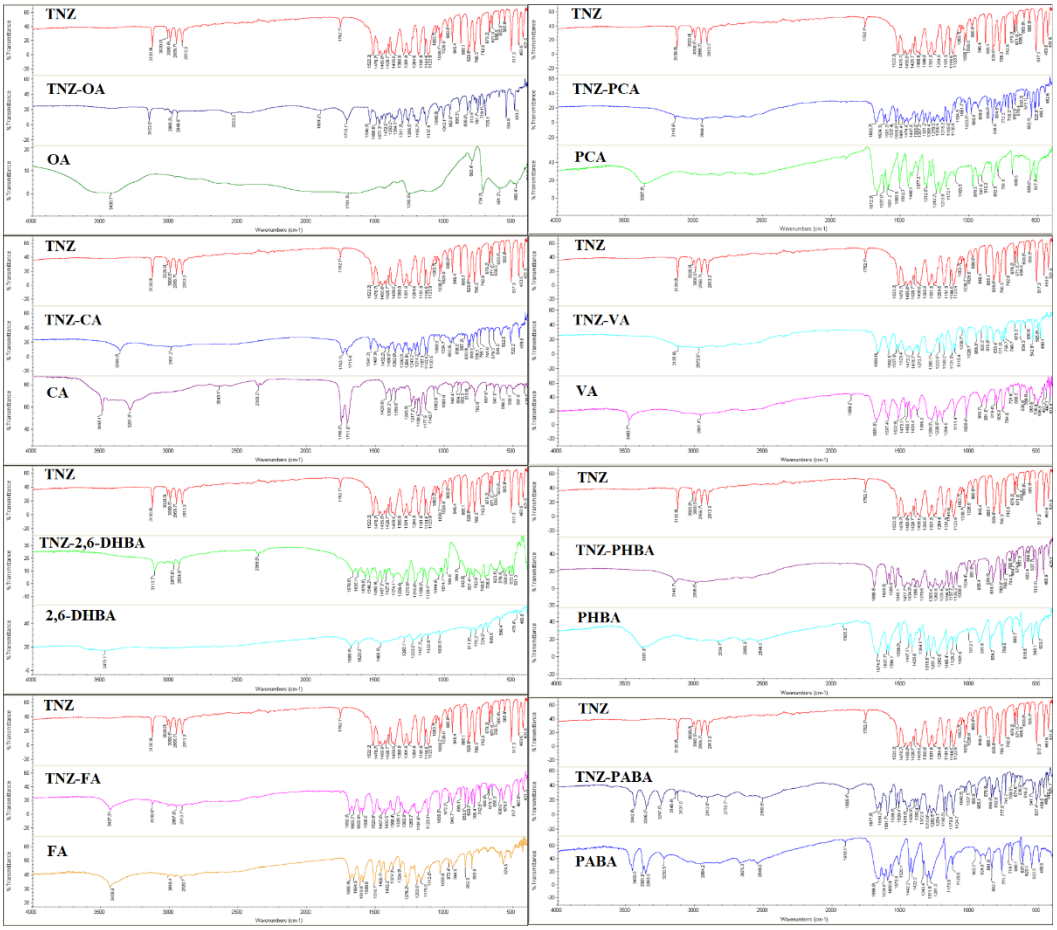


**Figure 6.19:** IR comparison of TNZ novel solid forms with its starting materials.

## 6.2.7 FE-SEM Analysis

The field emission scanning electron microscope (FESEM) technique is used to visualize the particles surface morphology, size and shape topographic features of crystalline solids. TNZ SEM micrographs and its cocrystals are shown in Figure 6.20(a-f). The morphology of TNZ particles shows irregular flattened shape with varying size (1-20 µm) in Figure 6.18a. TNZ-OA cocrystal particles showed stacking agglomerated rod shapes in Figure 6.18b. TNZ-CA cocrystal shows smooth surface with hexagonal rod shapes in Figure 6.18c. TNZ-2,6-DHBA shows irregular rectangular rod shapes particles(2 µm) in Figure 6.18d. TNZ-FA cocrystal showed flattened irregular rectangular shapes in Figure 6.18e. TNZ-PCA cocrystal showed smooth surface with rectangular shapes in Figure 6.18f.

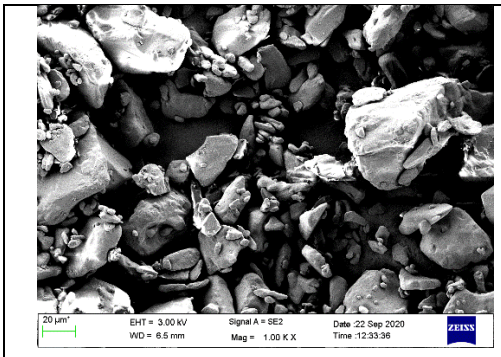


(a)TNZ

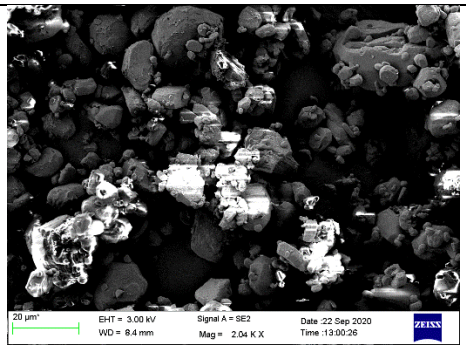


(b)TNZ-OA

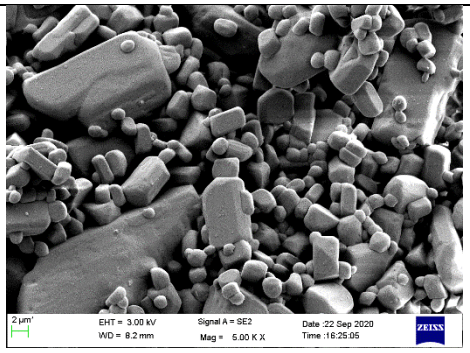


(c) TNZ-CA

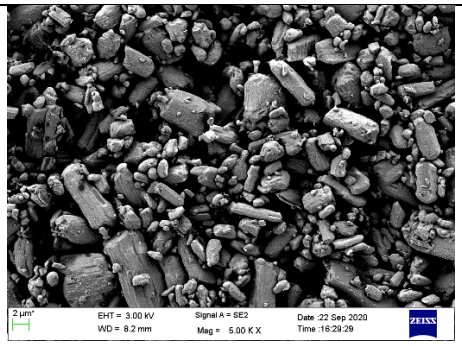


(d) TNZ-2,6-DHBA

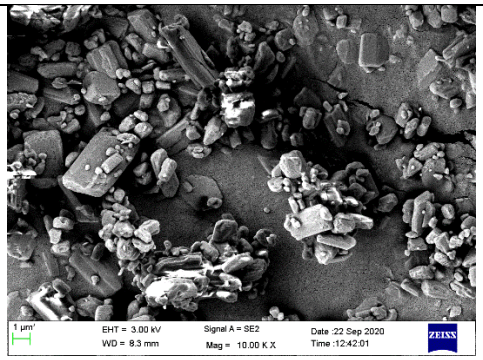


(e) TNZ-FA

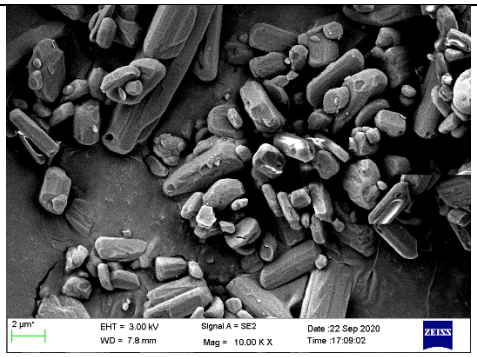


(f) TNZ-PCA

**Figure 6.20:** FE-SEM images at 1-20 µm resolution. (a) TNZ (b) TNZ-OA (c) TNZ-CA (d) TNZ-2,6-DHBA (e) TNZ-FA (f) TNZ-PCA.

## 6.2.8 Solubility and Dissolution Studies

Solubility studies on tinidazole cocrystal forms (solid systems with GRAS coformers) were conducted; dissolution studies in phosphate buffer (pH 7) media. The tinidazole cocrystal forms shows high dissolution rate compare to TNZ crystalline form (Figure 6.21, Table 6.9). TNZ-2,6DHBA, TNZ-FA, TNZ-OA, TNZ-CA, TNZ-PCA cocrystals exhibit higher dissolution rate compared to TNZ dissolution rate. It is due to fine tuning of supramolecular synthon structural modification of API through crystal engineering. More importantly, suitable cofomers are identified which can form complementary

hydrogen bonds for imidazole containing API molecules. In general, the solubility and dissolution experiments of TNZ and TNZ cocrystals were measured by plotting a calibration curve for the chromophore in the drug molecule using UV-vis spectroscopy. If the coformer and API chromophore absorptions are different, UV-vis spectroscopy can be used without any complication. However, cocrystals contains both aliphatic and aromatic acids and coformer absorption interferes with that of TNZ (at 278 nm). Hence, the solubility of the cocrystals was determined by analytical HPLC (Table 6.9) using pH 7 buffer 80% and acetonitrile 20% 0.05M orthophosporic acid as the mobile phase.

We have further performed intrinsic dissolution experiments of new solid forms and compared with TNZ dissolution rate, all the new adducts showed enhanced dissolute rate. TNZ-2,6-DHBA showed 1.6 fold IDR of the TNZ. However, the cocrystals TNZ which are formed with OA, CA was left over as TNZ after 24h slurry experiments, whereas aromatic acid adducts were stable in medium even after 24h. The stable cocrystals of the TNZ is introduced in present study. The cocrystals shows stability after 24hrs equilibrium solubility experiments. But two cocrystals such as TNZ-OA (1:05) and TNZ-CA(1:1) are unstable and its converted to pure form of TNZ at the end of 24 hrs equilibrium solubility(Figure 6.22) however these crystalline materials completely dissociates into corresponding starting material TNZ. We also performed intrinsic dissolution rate (IDR) measurements for cocrystal systems interestingly, till 8hrs the new solid phase of TNZ-OA and TNZ-CA are matches with calculated phase hence the system is stable till 8hrs (Figure 6.23). TNZ-2,6-DHBA, TNZ-FA and TNZ-OA, TNZ-CA, TNZ-PCA, TNZ follow the solubility order respectively.

**Table 6.9:** Solubility and intrinsic dissolution rate results of the TNZ and new solid phases in present study.

| Compound | Equilibrium solubility after 24 h slurry (mg $mL^{-1}$ ) | Residual ppt after 24 slurry confirmed by PXRD | Intrinsic dissolution rate, IDR ($mg/cm^2$)/min ($x10^{-3}$) (x)[a] | Residual pellet after IDR confirmed by PXRD |
|---|---|---|---|---|
| TNZ | 1.00 | TNZ(stable) | 0.72 | TNZ(stable) |
| TNZ-OA (1:0.5) | 1.66 | Converted to TNZ | 0.907(x1.26) | TNZ-OA |
| TNZ-CA (1:1) | 1.43 | Converted to TNZ | 0.896(x1.24) | TNZ-CA |
| TNZ-2,6-DHBA (1:1) | 1.54 | TNZ-2,6-DHBA | 1.033(x1.43) | TNZ-2,6-DHBA |
| TNZ-FA (1:1) | 1.35 | TNZ-FA | 0.913(x1.26) | TNZ-FA |
| TNZ-PCA (1:1) | 1.36 | TNZ-PCA | 0.897(x1.24) | TNZ-PCA |

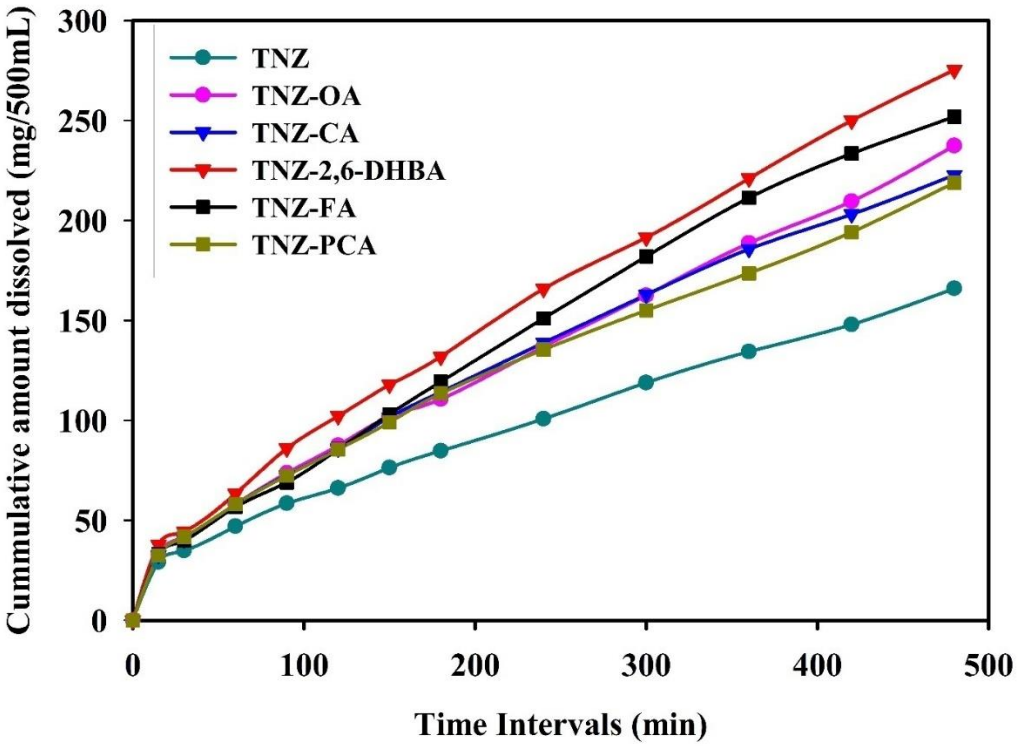


**Figure 6.21:** Intrinsic dissolution profile of TNZ cocrystals measured over a time period of 8 hours and at pH 7.0 in phosphate buffer

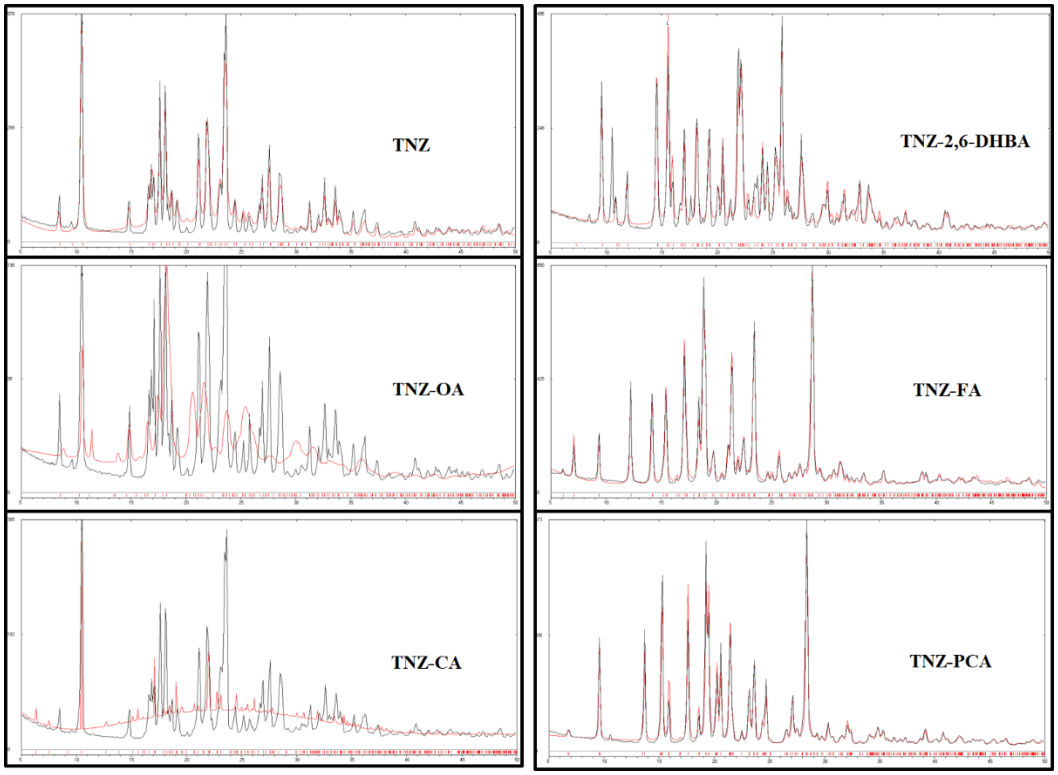


**Figure 6.22:** Comparison of powder XRD pattern of TNZ and cocrystals insoluble residue after 24 h in pH 7.0 buffer with the calculated line pattern from the X-ray crystal structure shows the stability of these adducts in the solubility medium for 24 h.

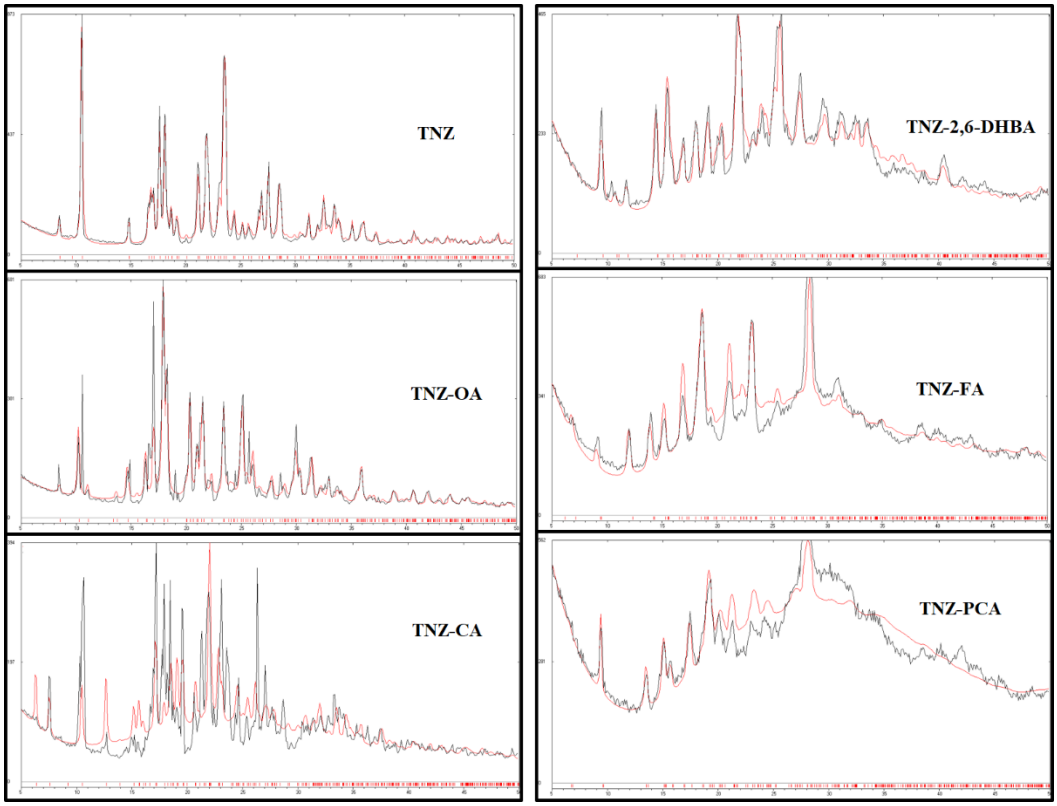


**Figure 6.23:** Comparison of powder XRD pattern of TNZ and cocrystals insoluble residue after 8 h in pH 7.0 buffer with the calculated line pattern from the X-ray crystal structure shows the stability of these adducts in the solubility medium for 8 h.

**Permeability**

The diffusion studies of the new solid forms of TNZ in the present study was performed using a diffusion cell membrane, which measures relative permeation. The diffusion behavior of all cocrystals was measured in pH 7.0 buffer at different intervals mention in Figure 6.24. In the current study, we have noticed the cumulative amount of the TNZ diffusing through the membrane increases slowly with time 8h whereas the flux increases rapidly in the first hour and reaches a steady state in 2h. The plots of cumulative drug diffused and flux against the per unit time indicate that all TNZ cocrystals showed a marginal increase near two-fold in the diffusion and in all cases, flux rate compared to the parent API TNZ.

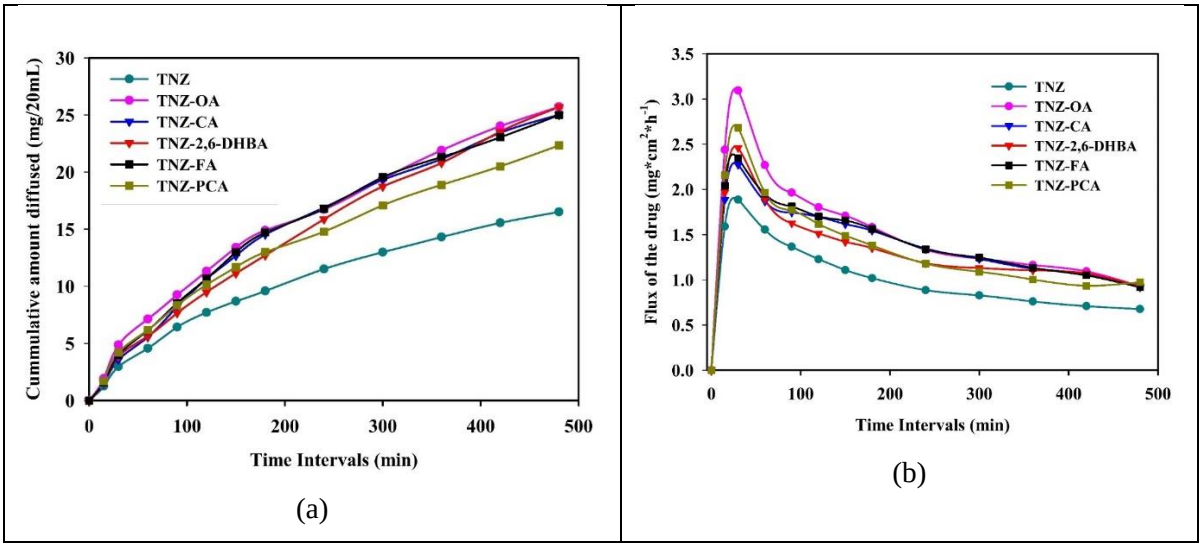


**Figure 6.24:** (a) Cumulative amount of the TNZ, cocrystals diffused with respective time. (b) Flux of the TNZ, cocrystals with respective time.

## 6.3 Conclusions

We systematically synthesized eight cocrystals and one salt cocrystal continuum of TNZ. We completely explored the acid-imidazole, hydroxy-imidazole and acid-acid dimer synthons. The formation of particular synthons depends on both stoichiometry and position of functional groups present in the molecules of API and cofomers. The acid-imidazole synthon prevail where system contains no 4-hydroxy benzoic acid cofomers. The hydroxy-imidazole predominate if the system contain 4-hydroxy benzoic acid cofomers in addition, it also forms acid-acid supramolecular synthon. If the 2:1 stoichiometry of API and coformer forms both acid-imidazole, hydroxy-imidazole. Finally we also studied the solubility, dissolution rate of permeability of new solid forms. Most of the new solid forms showed improved physicochemical properties of API. Currently working on pharmaceutical cocrystals stoichiometry rules.

## 6.4 Experimental Section

Active pharmaceutical ingredient tinidazole was purchased from Yarrow chemicals, Mumbai India. Its purity is confirmed by PXRD and DSC. All The coformers used in this study were purchased from Sigma-Aldrich, Hyderabad, India. All chemicals are of analytical or chromatographic grade was used in the experiments.

**TNZ−OA (1:0.5):** TNZ (100mg, 0.404 mmol) and OA (36.45 mg, 0.404 mmol) were ground in a mortar and pestle for 20-25 min in stoichiometric ratio by adding catalytic

amount (four or five drops) of $CH_3CN$ solvent.[64-68] The ground material was kept for crystallization from solvent mixture MeOH and $CHCl_3$ (5mL) solvents in 10 mL test tubes at room temperature. Later experiments were repeated in the same ratio for bulk material preparation and bulk powder purity conformed by PXRD. Colorless good quality single crystals were observed by slow evaporation and structure determination by single crystal X-ray diffraction confirmed as 1:0.5 ratios of TNZ and OA. M.P 140-144 °C

**TNZ−CA (1:1):** TNZ (100mg, 0.404 mmol) and CA (38.89mg, 0.404 mmol) were ground in a mortar and pestle for 20-25 min in stoichiometric ratio by adding catalytic amount (four or five drops) of $CH_3CN$ solvent. The ground material was kept for crystallization from solvent mixture MeOH and THF (5mL) in 10 mL test tubes at room temperature. Later experiments were repeated in the same ratio for bulk material preparation and bulk powder purity conformed by PXRD. Colorless good quality single crystals were observed by slow evaporation. M.P 120-123 °C

**TNZ−2,6-DHBA (1:1):** TNZ (100mg, 0.404 mmol) and 2,6-DHBA (62.39 mg, 0.404 mmol) were ground in a mortar and pestle for 20-25 min in stoichiometric ratio by adding catalytic amount (four or five drops) of $CH_3CN$ solvent. The ground material was kept for crystallization from solvent mixture MeOH and $CHCl_3$ (5mL) in 10 mL test tubes at room temperature. Good quality single crystals were observed by slow evaporation. Later experiments were repeated in the same ratio for bulk material preparation and bulk powder purity conformed by PXRD. M.P 143-147 °C

**TNZ−VA (1:1):** TNZ (100mg, 0.404 mmol) and VA (68.07mg, 0.404 mmol) were ground in a mortar and pestle for 20-25 min in stoichiometric ratio by adding catalytic amount (four or five drops) of $CH_3CN$ solvent. The ground material was kept for crystallization from solvent mixture EtOH and Anisole (5mL) in 10 mL test tubes at room temperature. Good quality single crystals were observed by slow evaporation. Later experiments were repeated in the same ratio for bulk material preparation and bulk powder purity conformed by PXRD. M.P 127-132 °C

**TNZ-PCA (1:1):** TNZ (100mg, 0.404 mmol) and PCA (66.46mg, 0.404 mmol) were ground in a mortar and pestle for 20-25 min in stoichiometric ratio by adding catalytic amount (four or five drops) of $CH_3CN$ solvent. The ground material was kept for crystallization from solvent mixture THF and $CH_3OH$ (5mL) as well as individual

solvents in 10 mL test tubes at room temperature. Good quality single crystals were observed by slow evaporation. Later experiments were repeated in the same ratio for bulk material preparation and bulk powder purity conformed by PXRD. M.P 128-132 °C

**TNZ-FA (1:1):** TNZ (100mg, 0.404 mmol) and FA (78.61mg, 0.404 mmol) were ground in a mortar and pestle for 20-25 min in stoichiometric ratio by adding catalytic amount (four or five drops) of $CH_3CN$ solvent. The ground material was kept for crystallization from solvent mixture THF and $CH_3OH$ (5mL) in 10 mL test tubes at room temperature. Later experiments were repeated in the same ratio for bulk material preparation and bulk powder purity conformed by PXRD. Colorless good quality single crystals were observed by slow evaporation. M.P 100-105 °C

**TNZ–PHBA (1:1):** TNZ (100mg, 0.404 mmol) and PHBA (55.91mg, 0.404 mmol) were ground in a mortar and pestle for 20-25 min in stoichiometric ratio by adding catalytic amount (four or five drops) of $CH_3CN$ solvent. The ground material was kept for crystallization from solvent mixture MeOH and $CH_3CN$ (5mL) in 10 mL test tubes at room temperature. Single crystals were observed by slow evaporation. Later experiments were repeated in the same ratio for bulk material preparation and bulk powder purity conformed by PXRD. M.P 132-138° C

**TNZ–PHBA (2:1):** TNZ (100mg, 0.404 mmol) and PHBA (27.95mg, 0.202 mmol) were ground in a mortar and pestle for 20-25 min in stoichiometric ratio by adding catalytic amount (four or five drops) of $CH_3CN$ solvent. The ground material was kept for crystallization from solvent mixture MeOH and $CHCl_3$ (5mL) in 10 mL test tubes at room temperature. Single crystals were observed by slow evaporation. Later experiments were repeated in the same ratio for bulk material preparation and bulk powder purity conformed by PXRD. M.P 138-142 °C

**TNZ–PABA (1:1):** TNZ (100mg, 0.404 mmol) and PABA (55.52mg, 0.404 mmol) were ground in a mortar and pestle for 20-25 min in stoichiometric ratio by adding catalytic amount (four or five drops) of $CH_3CN$ solvent. The ground material was kept for crystallization from solvent mixture EtOH and Anisole (5mL) in 10 mL test tubes at room temperature. Pale orange yellow color good quality Single crystals were observed by slow evaporation. Later experiments were repeated in the same ratio for bulk material preparation and bulk powder purity conformed by PXRD. M.P 131-135 °C

**Vibrational spectroscopy**

Thermo-Nicolet 6700 Fourier transform infrared spectrophotometer (Thermo Scientific, Waltham, Massachusetts) was used to record IR spectra. IR spectra were recorded on samples dispersed in KBr pellets. Data was analyzed using the Omnic software (Thermo Scientific, Waltham, Massachusetts).

**Differential Scanning Calorimetry**

DSC was performed on a Mettler Toledo DSC 822e module. Samples were placed in crimped but vented aluminum sample pans. The typical sample size is 3-4 mg, and the temperature range is 30-300 °C @ 10°C/min. Samples were purged by a stream of dry nitrogen flowing at 80 mL/min.

**X-ray crystallography**

X-ray reflections for the TNZ-OA,TNZ-CA,TNZ-2,6-DHBA, TNZ-FA, TNZ-PCA, TNZ-VA, TNZ-PHBA and TNZ-PABA solid forms were collected on Bruker SMART-APEX CCD diffractometer equipped with a graphite monochromator and Mo-Kα fine-focus sealed tube (λ=0.71073 Å). Data reduction was performed using Bruker SAINT Software.[69] Intensities were corrected for absorption using SADABS,[70] and the structure was solved and refined using SHELX-97.[71]All non-hydrogen atoms were refined as anisotropic. Hydrogen atoms on heteroatoms were located from difference electron density maps and all C−H hydrogens were fixed geometrically. Hydrogen bond geometries were determined in Platon.[72] X-Seed[73] and Mercury was used to prepare packing diagrams. Crystallographic cif files are available at www.ccdc.cam.ac.uk/data.

**Powder X-ray diffraction**

Powder X-ray diffraction of all the samples were recorded on Bruker D8 Advance diffractometer (Bruker-AXS, Karlsruhe, Germany) using Cu-Kα X-radiation (λ=1.5406 Å) at 40 kV and 30 mA power. X-ray diffraction patterns were collected over the 2θrange 5-50° at a scan rate of 1°/min. Powder Cell 2.4[74] was used for Rietveld refinement of experimental PXRD and calculated lines from the X-ray crystal structure.

**Dissolution and solubility measurements**

The solubility curves of TNZ cocrystals was measured using the pH 7.0 buffer medium at ambient conditions. First, the absorbance of a known concentration of the cocrystals was measured at the given $\lambda_{max}$ (TNZ at 278 nm) in pH 7.0 buffer medium on Thermo Scientific Evolution 300 UV-vis spectrometer (Thermo Scientific, Waltham, MA). These

absorbance values were plotted against several known concentrations to prepare the concentration vs. intensity calibration curve. From the slope of the calibration curves, molar extinction coefficients for all the TNZ solid forms were calculated. Intrinsic dissolution rate (IDR) measurements were carried out on a USP certified Electrolab TDT-08 L Dissolution Tester (Electrolab, Mumbai, MH, India). Dissolution experiments were performed for 480 min in PH 7.0 buffer at 37 °C. Prior to IDR estimation, standard curves for all the compounds were obtained spectrophotometrically at their respective $\lambda_{max}$. The slope of the plot from the standard curve gave the molar extinction coefficient (ε) by applying the Beer–Lambert's law, which was used to determine the IDR values. For IDR measurements, 400mg of the solid material of each solid form was taken in the intrinsic attachment and compressed to a 0.5 $cm^2$ pellet using a hydraulic press at a pressure of 2.5 ton/$inch^2$ about 4 min. The pellet was compressed to provide a flat surface on one side and the other side was sealed. Then the pellet was dipped into 500 mL of pH 7.0 buffer water medium at 37 °C with the paddle rotating at 100 rpm. At a specific time, interval, 5 mL of the dissolution medium was withdrawn and replaced by an equal volume of fresh medium to maintain a constant volume. The solid samples after solubility/dissolution measurements was verified by PXRD to know if there is any phase stability. The amount of drug dissolved in each time intervals was calculated using the calibration curve.

**Diffusion Study and Permeability Measurements**

The diffusion studies were performed using a diffusion apparatus (Model EMFDC-06, Orchid Scientific, Maharashtra, India). TNZ, TNZ cocrystals were carried out through a dialysismembrane-135 (dialysis membrane-135, average flat width 33.12 mm, average diameter 23.8 mm, capacity approximately 4.45 mL/cm) obtained from HiMedia, India. The treated dialysis membrane was placed in diffusion cells with an effective surface area of 3.14 $cm^2$. Suspensions of the TNZ and it adducts were prepared and placed on the dialysis membrane in donor compartment. The temperature of diffusion medium maintained at 37 °C ± 1 °C throughout the experiment and stir at 600 rpm and diffuse through the membrane toward the receptor compartment containing 20 mL of phosphate-buffered solution (PBS, pH = 7). The release of the compounds at predetermined intervals were withdrawn (0.5 mL for each intervals) and replaced by equal volume and The AUC was calculated using the linear trapezoidal rule of drug bioavailability.

**HPLC Analysis**

HPLC Separation was carried out on a Shimadzu LC-20AD liquid chromatography, Diode Array SPD-M20A detector, degasser DGU-20A3 with a RPHPLC column C18G (250 × 4.6 mm, 5 µm particle size) which was protected by a guard column of 33 mm × 4.6 mm. UV absorbance at 278 nm was used to quantify the TNZ. The calibration curve was obtained by spiking TNZ (linearity $R^2 > 0.999$) and TNZ cocrystals. The separation was carried out using a mobile phase consisting of 0.05M potassium dihydrogen phosphate buffer (pH 3.25, adjusted with orthophosphoric acid) and acetonitrile (80:20, v/v) which was filtered through a 0.45 µm membrane filter, degassed by ultrasonication, and delivered at a rate of 1mL/min. A 20 µL of each analyte was injected into an HPLC column with a run time of 12 min.

**DFT Computation**

Electrostatic potentials on the molecular surfaces of TNZ and coformer structures were optimized by using DFT based B3LYP1/6-31G(d,p) level of theory. The initial geometry parameters for the structural motifs were taken from crystal data. Software was used to extract local maxima and minima from the molecular electrostatic potential mapped on to the 0.002 Bohr $Å^{-3}$ electron density isosurface (gas phase or vacuum as probe). The negative and positive potentials are shown as red and blue surfaces, respectively, indicating the interaction energy value (kcal mol−1) of the molecule at that particular atom. All the calculations were carried out with GAUSSIAN09[75] suite of programme.

**CSD analysis**

There are about 355 crystal structures which contain imidazole ring can be seen in CSD.[76-78]Among all, only 13 structures form new solid forms such as salt/cocrystals/solvates with acid or hydroxy functional group. Very few structures are known with O–H···N (hydroxy –imidazole) synthon of imidazole and acids/hydroxy functional groups and those are not completely explored. Hence, the present study focused on acids and or hydroxy functional group containing molecules (coformer) in synthesis of solid forms of TNZ

## 6.5 References

1. Gamekkanda, J. C.; Sinha, A. S.; and Aakeroy, C. B. Cocrystals and Salts of Tetrazole-Based Energetic Materials. *Cryst. Growth Des*. **2020**, 20, 2432−2439

2. Koshima, H.; Miyamoto, H.; Yagi, I.; and Uosaki, K. Preparation of Cocrystals of 2-Amino-3-nitropyridine with Benzenesulfonic Acids for Second-Order Nonlinear Optical Materials. *Crystal Growth & Design* **2004**, 4, 807–811
3. Desiraju, G. R. Crystal Engineering: The Design of Organic Solids; Elesevier: Amsterdam, **1989**.
4. Desiraju, G. R.; Vittal, J. J.; and Ramanan, A. Crystal Engineering. A Textbook. *J. Appl. Cryst*. **2012**, 45, 374
5. Desiraju, G. R. Supramolecular Synthons in Crystal Engineering-A New Organic Synthesis. *Angew. Chem Int/ Ed. Engl.* **1995**, 34. 2311 -2327
6. Nangia, A.; Desiraju, G. R. Supramolecular Synthons and Pattern Recognition. *Design of Organic Solids*. **1998**, 57-95
7. Rivera, R. C.; Chavez, B.; Robles, A. G.; Tapia, A.; and Mulia, L.Y. In Vitro Effect of Nitazoxanide Against Entamoeba histolytica, Giardia intestinalis and Trichomonas vaginalis Trophozoites. *J. Eukaryat. Microbial.*, **2002**, 49, 201-208.
8. Chasseaud, L. F.; Henrick, K.; Matthews, R. W.; Scott, P. W.; and Wood, S. G. Metabolic Ring Hydroxylation of Tinidazolet involving a Novel Nitro-group Migration: X-Ray Structures of Tinidazole and the NH4+ Salt of its Ring Hydroxylated Metabolite. *J. Chem. Soc., Chem. Commun.*, **1984**, 491-492
9. Patnala, S. R. C. M.; Khagga, M.; Bhavani, R.; and Bhavani, V. Novel Salt of Tinidazole with Improved Solubility and Antibacterial Activity. Orient. J. Chem., **2017**, 33, 490-499
10. Patnala, R. C. M.; Khagga, M.; Bhavani, R.; and Bhavani, V. Synthesis, Characterization and Biological Activity of Novel Salt/Molecular Salts of Tinidazole. Orient. J. Chem., **2017**, 33, 859-872
11. Fung, H. B.; and Doan, T. L. Tinidazole: A Nitroimidazole Antiprotozoal Agent. *Clinical Therapeutics.*, **2005**, 27, 1859-1884
12. Zheng, K.; Li, A.; Wu, W.; Qian, S.; Liu, B.; Pang, Q. Preparation, characterization, in vitro and in vivo evaluation of metronidazole Gallic acid cocrystal: A combined experimental and theoretical investigation. *J. Mol. Struct.* ***2019****, 1197, 727-735*
13. Fandino, O. E.; Reviglio, L.; Linck, Y. G.; Monti, G. A.; Valdez, M. M. M.; Faudone, S. N.; Caira, M. R.; Sperandeo, N. R. Novel Cocrystals and Eutectics

of the Antiprotozoal Tinidazole: Mechanochemical Synthesis, Cocrystallization, and Characterization. *Cryst. Growth Des*. **2020**, 20, 2930−2942

14. Remenar, J. F.; Morissette, S. L.; Peterson, M. L.; Moulton, B.; Macphee, J. M.; Guzman, H. R.; Almarsson, O. Crystal Engineering of Novel Cocrystals of a Triazole Drug with 1,4-Dicarboxylic Acids. *J. Am. Chem. Soc.* **2003**, 125, 28, 8456-8457
15. Schultheiss, N.; Newman, A. Pharmaceutical Cocrystals and Their Physicochemical Properties. *Cryst. Growth Des.* **2009**, 9, 2950-2967
16. Aitipamula, S.; Vangala, V. R.; Chow, P. S.; and Tan, R. B. H. Cocrystal Hydrate of an Antifungal Drug, Griseofulvin, with Promising Physicochemical Properties. *Cryst. Growth Des.* **2012**, 12, 5858-5863
17. Duggirala, N. K.; Perry, M. L.; Almarsson, O.; Zaworotko, M. J. Pharmaceutical cocrystals: along the path to improved medicines. *Chem. Commun.*, **2016**, *52*, 640-655
18. Almarsson, O.; and Zaworotko, M. J. Crystal engineering of the composition of pharmaceutical phases. Do pharmaceutical co-crystals represent a new path to improved medicines? Chem Commun. **2004**, 1889-1896.
19. Dai, X. L.; Chen, J. M.; Lu, T. B. Pharmaceutical cocrystallization: an effective approach to modulate the physicochemical properties of solid-state drugs. CrystEngComm, **2018**, 20, 5292–5316
20. Good, D. J.; Rodriguez-Hornedo, N. Solubility Advantage of Pharmaceutical Cocrystals. *Cryst. Growth Des.* **2009**, 9, 2252-2264
21. Martin, F. A.; Pop, M. M.; Borodi, G.; Filip, X.; and Kacso, I. Ketoconazole Salt and Co-crystals with Enhanced Aqueous Solubility. *Cryst. Growth Des.* **2013**, *13*, 4295-4304
22. Chen, J. M.; Wang, Z. Z.; Wu, C. B.; Li, S.; and Lu, T. B. Crystal engineering approach to improve the solubility of mebendazole. CrystEngComm **2012**, 14, 6221−6229
23. Blagden, N.; de Matas, M.; Gavan, P.; York, P. Crystal engineering of active pharmaceutical ingredients to improve solubility and dissolution rates. Adv. Drug Delivery Rev. **2007**, 59, 617−630
24. Suresh, K.; Minkov, V. S.; Namila, K. K.; Derevyannikova, E.; Losev, E.; Nangia, A.; and Boldyreva, E.V. Novel Synthons in Sulfamethizole Cocrystals:

Structure−Property Relations and Solubility. *Cryst. Growth Des*. **2015**, 15, 3498−3510

25. Aakeroy, C. B.; Forbes, S.; and Desper, J. Using Cocrystals To Systematically Modulate Aqueous Solubility and Melting Behavior of an Anticancer Drug. *J. Am. Chem. Soc.* **2009**, 131, 17048-17049
26. Lipinski, C. Poor aqueous solubility-an industry wide problem in drug discovery. *Am. Pharm. Rev.* **2002**, 5, 82−85
27. Banik, M.; Gopi, S. P.; Ganguly, S.; Desiraju, G. R. Hydrogen Bond Synthons in the Interplay of Solubility and Membrane Permeability/Diffusion in Variable Stoichiometry Drug Cocrystals. Cryst. Growth Des. **2016,** 16, 5418−5428.
28. Dai, X.; Li, S.; Chen, J.; Lu, T. Improving the Membrane Permeability of 5-Fluorouracil via Cocrystallization. *Cryst. Growth Des*. **2016**, *16*, 4430−4438.
29. Guzman, H. R.; Tawa, M.; Zhang, Z.; Ratanabanangkoon, P.; Shaw, P.; Gardner, C. R.; Chen, H.; Moreau, J. P.; Almarsson, O.; Remenar, J. Combined Use of Crystalline Salt Forms and Precipitation Inhibitors to Improve Oral Absorption of Celecoxib from Solid Oral Formulations. *J. Pharm. Sci.* **2007**, 96, 2686−2702
30. Brouwers, J.; Brewster, M. E.; Augustijns, P. Supersaturating Drug Delivery Systems: The Answer to Solubility-Limited Oral Bioavailability? *J. Pharm. Sci.* **2009**, 98, 2549−2572.
31. Childs, S. L.; Kandi, P.; and Lingireddy, S. R. Formulation of a Danazol Cocrystal with Controlled Supersaturation Plays an Essential Role in Improving Bioavailability. Mol. Pharmaceutics 2013, 10, 3112−3127
32. Smith, A. J.; Kavuru, P.; Wojtas, L.; Zaworotko, M. J.; and Shytle, R. D. Cocrystals of Quercetin with Improved Solubility and Oral Bioavailability. *Mol. Pharmaceutics* **2011**, 8, 1867–1876
33. McNamara, D. P.; Childs, S. L.; Giordano, J.; Iarriccio, A.; Cassidy, J.; Shet, M. S.; Mannion, R.; O'Donnell, E.; and Park, A. Use of a glutaric acid cocrystal to improve oral bioavailability of a low solubility API. *Pharma Res.* **2006**, 23, 1888-1897.
34. Mutalik, S.; Anju, P.; Manoj, K.; Usha, A. N. Enhancement of dissolution rate and bioavailability of aceclofenac: A chitosan based solvent change approach. *Int. J. Pharm.* **2008**, 350, 279-90.
35. Bolla, G.; Nangia, A. Pharmaceutical cocrystals: walking the talk. *Chem. Commun.* **2016**, 52, 8342– 8360.

36. Yousef, M. A.; Vangala, V. R. Pharmaceutical Co-crystals: Molecules, Crystals, Formulations, Medicines. *Cryst. Growth Des.* **2019,** 19, 7420-7438.

37. Nangia, A. K.; Desiraju, G. R. Crystal Engineering. An Outlook for the Future. *Angew. Chem. Int. Ed.* 2019, 58, 4100 – 4107.

38. Liu, Y.; Zeng, Q.; Zou, B.; Liu, Y.; Xu, B.; and Tian, W. Piezochromic Luminescence of Donor–Acceptor Cocrystals: Distinct Responses to Anisotropic Grinding and Isotropic Compression. *Angew. Chem. Int. Ed.* ***2018****,57,15670–15674*

39. Tothadi, S.; and Desiraju, G. R. Synthon Modularity in 4-Hydroxybenzamide–Dicarboxylic Acid Cocrystals. *Cryst. Growth Des.* **2012**, 12, 6188-6198

40. Allu, S.; Bolla, G.; Tothadi, S.; Nangia, A. Supramolecular Synthons in Bumetanide Cocrystals and Ternary Products. *Cryst. Growth Des.* **2017**, *17*, 4225–4236.

41. Mittapalli, S.; Mannava, M. K. C.; Khandavilli, U. B. R.; Allu, S.; and Nangia, A. Soluble Salts and Cocrystals of Clotrimazole. *Cryst. Growth Des.* **2015**, *15*, 2493-2504

42. Sanphui, P.; Tothadi, S.; Ganguly, S.; and Desiraju, G. R. Salt and Cocrystals of Sildenafil with Dicarboxylic Acids: Solubility and Pharmacokinetic Advantage of the Glutarate Salt. *Mol. Pharmaceutics* **2013**, 10, 4687-4697

43. Kumar, S. S.; Thakuria, R.; and Nangia, A. Pharmaceutical cocrystals and a nitrate salt of voriconazole. *CrystEngComm*, **2014**, 16, 4722–4731

44. Goud, N. R.; Suresh, K.; and Nangia, A. Solubility and Stability Advantage of Aceclofenac Salts. Cryst. Growth Des. **2013**, 13, 1590−1601

45. Banerjee, R.; Bhatt, P. M.; Ravindra, N. V.; and Desiraju, G. R. Saccharin Salts of Active Pharmaceutical Ingredients, Their Crystal Structures, and Increased Water Solubilities. Crystal. Growth Des, **2005**, 5, 2299-2309

46. Banerjee, R.; Bhatt, P. M.; and Desiraju, G. R. Solvates of Sildenafil Saccharinate. A New Host Material. *Cryst. Growth Des.* **2006**, 6, 1468-1478

47. Grothe, E.; Meekes, H.; Vlieg, E.; ter Horst, J. H.; and de Gelder, R. Solvates, Salts, and Cocrystals: A Proposal for a Feasible Classification System. *Cryst. Growth Des.* **2016**, 16, 3237−3243

*48.* Thakuria, R.; Delori, A.; Jones, W.; Lipert, M. P.; Roy, L.; Rodriguez-Hornedo, N. Pharmaceutical cocrystals and poorly soluble drugs. *Int. J. Pharm.,* **2013**, 453, 101-125.

49. Shan, N.; Zaworotko, M. J. The role of cocrystals in pharmaceutical science. *Drug Discovery Today*. ***2008***, *13, 440-446.*

50. https://www.fda.gov/food/food-ingredients-packaging/generally-recognized-safe-gras, accessed 12/05/2019.

51. https://www.novartis.com/news/media-releases/novartis-new-heartfailuremedicine-lcz696-now-called-entrestotm-approved-fda. Accessed 23–03–2016.

52. Harrison, W. T. A.; Yathirajan, H. S.; Bindya, S.; Anilkumar, H. G.; and Devaraju. Escitalopram oxalate: co-existence of oxalate dianions and oxalic acid molecules in the same crystal. *Acta Cryst.* **2007**. C63, o129-o131

53. Aakeroy, C. B.; Epa, K.; Forbes, S.; Schultheiss, N.; and Desper, J. Ranking Relative Hydrogen-Bond Strengths in Hydroxybenzoic Acids for Crystal-Engineering Purposes. *Chem. Eur. J.* **2013**, 19, 14998 – 15003

54. Thalladi, V. R.; Goud, B. S.; Hoy, V. J.; Allen, F. H.; Howard, J. K.; and Desiraju, G. R. Supramolecular synthons in crystal engineering. Structure simplification, synthon robustness and supramolecular retrosynthesis. *Chem. Commun.*, **1996**, 401-402

55. Shattock, T. R.; Arora, K. K.; Vishweshwar, P.; Zaworotko, M. J. Hierarchy of Supramolecular Synthons: Persistent Carboxylic Acid···Pyridine Hydrogen Bonds in Cocrystals that also Contain a Hydroxyl Moiety. *Cryst. Growth Des.* **2008**, 8, 4533-4545.

56. Thakuria, R.; Sarma, B.; and Nangia, A. Supramolecular networks of a H-shaped aromatic phenol host. *New J. Chem.*, **2010**, 34, 623–636

*57.* Etter, M. C. A new role for hydrogen-bond acceptors in influencing packing patterns of carboxylic acids and amides. *J. Am. Chem. Soc.* **1982,** *104*, 1095–1096.

58. Macgillivray, L. R.; Reid, J. L.; Ripmeester, J. A. Supramolecular Control of Reactivity in the Solid State Using Linear Molecular Templates. *J. Am. Chem. Soc.* **2000**, 122, 7817-7818

59. Lehn, J. M. Supramolecular Chemistry-Scope and Perspectives Molecules, Supermolecules, and Molecular Devices (Nobel Lecture). *Angew Chem. Int. Ed. Engl.* **1988**, 27, 89-112

60. Babu, N. J.; Reddy, L. S.; Nangia, A. Amide−*N*-Oxide Heterosynthon and Amide Dimer Homosynthon in Cocrystals of Carboxamide Drugs and Pyridine *N*-Oxides. *Mol. Pharmaceutics.,* **2007**, 4, 417-434

61. Johnson, S. L.; Rumon, K. A. Infrared Spectra of Solid 1:1 Pyridine -Benzoic Acid Complexes; the Nature of the Hydrogen Bond as a Function of the Acid-Base Levels in the Complex. *J. Phys. Chem.* **1965**, 69, 74-86

62. Sarma, B.; Nath, N. K.; Bhogala, B. R.; and Nangia, A. Synthon Competition and Cooperation in Molecular Salts of Hydroxybenzoic Acids and Aminopyridines. *Cryst. Growth Des.* **2009**, 9, 1546-1557

63. Tao, Q.; Chen, J.-M.; Ma, L.; and Lu, T.-B. Phenazopyridine Cocrystal and Salts That Exhibit Enhanced Solubility and Stability. *Cryst. Growth Des*. **2012**, 12, 3144−3152

64. Friscic, T.; Jones, W. Recent Advances in Understanding the Mechanism of Cocrystal Formation via Grinding. *Cryst. Growth Des.* **2009**, *9*, 1621–1637.

65. Friscic, T.; Fabian, L.; Burley, J. C.; Jones, W.; Motherwell, W. D. S. Exploring cocrystal–cocrystal reactivity *via* liquid-assisted grinding: the assembling of racemic and dismantling of enantiomeric cocrystals. *Chem. Commun*. **2006**, 5009−5011.

66. Shan, N.; Toda, F.; and Jones, W.Mechanochemistry and co-crystal formation: effect of solvent on reaction kinetics. *Chem. Commun.*, **2002**, 2372-2373

*67.* Tan, D.; Loots, L.; Friscic, T. Towards medicinal mechanochemistry: evolution of milling from pharmaceutical solid form screening to the synthesis of active pharmaceutical ingredients (APIs). *Chem. Commun.*, **2016**, *52*, 7760-7781

*68.* Karki, S.; Friscic, T.; Fabian, L.; Laity, P. R.; Day, G. M.; and Jones, W. Improving Mechanical Properties of Crystalline Solids by Cocrystal Formation: New Compressible Forms of Paracetamol. *Adv. Mater*. **2009**, 21, 3905–3909

69. SAINT-Plus, Ver. 6.45; Bruker AXS: Madison, WI, **2003**.

70. Sheldrick, G. M. *SADABS, Program for Empirical Absorption Correction of Area Detector Data*; University of Göttingen: Göttingen, Germany, **1997**.

71. Sheldrick, G. M. *SHELX-97, Program for the Solution and Refinement of Crystal Structures*; University of Göttingen: Göttingen, Germany, **1997**.

72. PLATON, A Multipurpose Crystallographic Tool; Spek, A. L., Ed.;Utrecht University: Utrecht, The Netherlands, **2002**.

73. Barbour, L. J.X-Seed, Graphical Interface to SHELX-97 and POV-Ray; University of Missouri–Columbia: Columbus, MO, **1999**.

74. Powder Cell, a program for structure visualization, powder pattern calculation and profile fitting. http://www.ccp14.ac.uk/tutorial/powdcell/.

75. Frisch, M. J.; Trucks, G. W.; Schlegel, H. B.; Scuseria, G. E.; Robb, M. A.; Cheeseman, J. R.; Scalmani, G.; Barone, V.; Mennucci, B.; Petersson, G. A.; Nakatsuji, H.; Caricato, M.; Li, X.; Hratchian, H. P.; Izmaylov, A. F.; Bloino, J.; Zheng, G.; Sonnenberg, J. L.; Hada, M.; Ehara, M.; Toyota, K.; Fukuda, R.; Hasegawa, J.; Ishida, M.; Nakajima, T.; Honda, Y.; Kitao, O.; Nakai, H.; Vreven, T.; Montgomery, J. A.; Peralta, Jr., J. E.; Ogliaro, F.; Bearpark, M.; Heyd, J. J.; Brothers, E.; Kudin, K. N.; Staroverov, V. N.; Kobayashi, R.; Normand, J. ; Raghavachari, K.; Rendell, A.; Burant, J. C.; Iyengar, S. S.; Tomasi, J.; Cossi, M.; Rega, N.; Millam, J. M.; Klene, M.; Knox, J. E.; Cross, J. B.; Bakken, V.; Adamo, C.; Jaramillo, J.; Gomperts, R.; Stratmann, R. E.; Yazyev, O. ; Austin, A. J.; Cammi, R.; Pomelli, C.; Ochterski, J. W.; Martin, R. L.; Morokuma, K.; Zakrzewski, V. G.; Voth, G. A.; Salvador, P.; Dannenberg, J. J.; Dapprich, S.; Daniels, A. D. Farkas, J.; Foresman, B.; Ortiz, J. V.; Cioslowski, J.; Fox, D. J. *Gaussian 09*, Revision A.02; Gaussian, Inc.: Wallingford, CT, **2009**.

76. The Cambridge Structural Database version 5.40 November **2018** (update 3 Aug 2019). ConQuest 2.03; Cambridge Crystallographic Data Centre: Cambridge, U.K.

*77.* Fabian, L. Cambridge Structural Database Analysis of Molecular Complementarity in Cocrystals. *Cryst. Growth Des.* **2009**, *9*, 1436-1443

*78.* Oswald, I. D. H.; Allan, D. R.; Mcgregor, P. A.; Motherwell, W. D. S.; Parsons, S.; and Pulham, C. R. The formation of paracetamol (acetaminophen) adducts with hydrogen-bond acceptors. *Acta Cryst*. **2002**, B58, 1057-1066

# CHAPTER SEVEN

# Conclusions and Future Prospects

## 7.1 Conclusions

This thesis covers the design, identification, screening, characterization and applications towards pharmaceuticals based on supramolecular synthon approach the various novel solid forms such as polymorphs, cocrystlas, salts, amorphous/coamorphous multicomponent crystalline Active pharmaceutical Ingredients (APIs). Detailed studies on different APIs that includes polymorphs are presented in Chapter 2, 5, salts are discussed in Chapter 4, cocrystals are in Chapter 2, 3, 4, 5, and 6 and finally coamorphous solids in Chapter 3. These APIs were studied to understand their crystal structure and improving the problems of solubility and permeability.

Chapter 1 deals about an introduction of supramolecular chemistry, crystal engineering, various synthons, non-covalent interactions, and many probable solid forms of APIs and model organic compounds.

In chapter 2, bumetanide cocrystals, cocrystal-polymorphs, salts, salt-cocrystals and ternary products were prepared which have potential pharmaceutical applications.

Bumetanide (BUM) is the diuretic sulfonamide drug. Design strategy for cocrystals with carboxamides is carried out based on reliable supramolecular synthons. Binary cocrystals of BUM with with pyridine carboxamide, pyridine, lactams, amines and aromatic carboxylic acid coformers. All cocrystal structures exhibit hydrogen bonding of the coformer with the carboxylic acid group of BUM via heterosynthons which replace the acid homodimer in the drug crystal structure. Pyridones are inserted as N−H···O dimers which are in turn bonded to the acid group of bumetanide, while the pyridine amide coformers interact via the acid−amide heterosynthon. Cocrystal polymorphs were obtained for bumetanide-isonicotinamide Cocrystal structure with the sulphonamide-pyridine and sulphonamide-acid synthons. Careful crystal packing analysis of BUM structure and fourteen new binary adducts gave an idea for the design ternary cocrystals, and four new ternary crystalline products namely BUM–INA–PCA, BUM–INA–PASA, BUM–INA–VLA, and BUM–2HP–PCA were successfully crystallized and characterized by X-ray crystallography (PXRD, SXRD), thermal technique (DSC, TGA),

and spectroscopy techniques such as IR and NMR. In that ten binary cocrystals, two salt-cocrystal continuum and two salts. Urea and lactams such as valerolactam, caprolactam, and N-methylcaprolactam formed cocrystals with bumetanide, whereas 4-aminopyridine gave a salt. Piperazine afforded a salt hydrate, and 5-fluorocytosine gave a salt-cocrystal. The supramolecular synthons in bumetanide−lactam cocrystals are amide dimer between drug and coformer, and acid homo dimer between bumetanide molecules. In bumetanide salts, the acid proton is transferred from bumetanide to coformer amine, whereas in bumetanide salt-cocrystal proton transfer and free acid were observed in the crystal structure. Furthermore, solubility, dissolution, and diffusion membrane permeability experiments were performed on all solid forms. The piperazine salt shows high dissolution and permeability crossover when compared to other binary forms of bumetanide. Dissolution studies of the crystal forms showed that BUM–PIP has the highest dissolution rate which is attributed to the coformer being highly soluble in water and this release in turn drags the drug faster into solution. The cocrystals exhibit 2-fold improvement in solubility, while the increase for PIP salt is 4-fold compared to BUM. Permeability improved 5-fold with piperazine salt but only a marginal improvement with cocrystals. BUM-CPR cocrystal improved permeability and solubility nearly two-fold and this could be an alternative formulation for BUM.

In chapter 3, the effect of hydrogen bonding by forming cocrystals and coamorphous solids of IDP was investigated. The results showed that hydrogen bonding is considerably stronger in the cocrystals compared to coamorphous forms.

Indapamide (IDP), a sulfonamide diuretic drug utilized in the treatment of hypertension. we explored the structural landscape via cocrystallization using solvent assisted grinding, rota evaporation and isothermal crystallization techniques, where we screened IDP with various GRAS coformers of piperazine derivatives such as piperazine (PIP), methylpiperazine (MPIP), ethylpiperazine (EPIP), butyloxycarbonyl piperazine (BPIP) and amino acids like arginine (ARG), lysine (LYS) and non-grass coformers like pyridine derivatives (DIP, BIP, DPE, PHE, MeHP) which resulted in cocrystals. Cocrystals and coamorphus forms of IDP have been identified and characterized by X-ray powder diffraction (XRD), differential scanning calorimetry (DSC) and FT-IR. The apparent solubility, dissolution and permeability studies of coamorphous IDP samples were performed in aqueous media. A systematic gradation in supramolecular synthons resulting in a cocrystal or coamorphous product of IDP is observed as the hydrogen bonds between the drug and the coformer become weaker. The robust sulfonamide-

pyridine ($SO_2NH_2\cdots Py$) and sulfonamide-carboxamide ($SO_2NH_2\cdots CONRH$) hetero synthons with rigid/ aromatic coformers drive cocrystal products while the weaker sulfonamide-amine ($SO_2NH_2\cdots NR_2H$) synthon with flexible molecules gave coamorphous products of IDP. Furthermore, the higher aqueous solubility and better diffusion membrane permeability of IDP-ARG shows that amino acids can be used to enhance not only powder dissolution but also diffusion kinetics. Surprisingly, IDP-PIP coamorphous is stable for 3 months but the other forms of piperazine derivatives were unstable and transformed to the crystalline form post 24 h under the accelerated ICH conditions (40 °C, 75% RH). These results suggest that is the one among other methods to synthesize coamorphous forms and solid dispersions (amorphous) directed by crystal engineering for better solid-state pharmaceuticals.

Chapter 4 deals with improving pharmacological properties of ETD through various salts of ETD with amines containing different chain lengths. The salts showed higher solubility, dissolution rate and permeability along with phase stability.

This work deals with the salts and cocrystal screening of an anti-inflammatory drug Etodolac (ETD), which has poor aqueous solubility and high permeability. A series of salts and cocrystals of ETD were prepared to establish a relation for solubility and dissolution with respect to nature of the coformer. Salts of Etodolac with amines like isopropylamine (isoPA), n-hexylamine (nHA), cyclohexylamine (cycloHA), piperazine (PPZ), phenylethylamine (phEA). In case of cocrystals only one adduct with isonicotinamide (INT) ETD•INT were successfully crystallized and characterized by X-ray crystallography (PXRD, SXRD), thermal technique (DSC, TGA), and IR. Solubility and dissolution and permeability experiments were done for the salts in pH 7.0 phosphate buffer solution. The obtained equilibrium solubility order was $ETD^-\bullet isoPA^+$ > $ETD^-\bullet nHA^+$ > $ETD^-\bullet cycloHA^+$ > $2(ETD)^-\bullet PPZ^{2+}$ > $ETD^-\bullet phEA^+$ > ETD, and IDR order was $ETD^-\bullet isoPA^+$ > $ETD^-\bullet nHA^+$ > $2(ETD)^-\bullet PPZ^{2+}$ > ETD > $ETD^-\bullet cycloHA^+$ > $ETD^-\bullet phEA^+$. Analysis with respect to pH of saturated solubility media did not support any of these orders. Similarly, lipophilicity of counter ions was also not established in any direct relation with respect to the solubility and IDR. PXRD analysis showed solid phase stability of all salts under solubility and dissolution conditions. Yet another correlation with respect to melting point of salts was done but it was also without a pattern. Finally, analysis of intermolecular interactions showed that crystal lattice of all salts were stabilized by a network of strong N–H···O hydrogen bonds but patterns of hydrogen bonding were different in each of the salts. $ETD^-\bullet isoPA^+$ showed highest

solubility and dissolution rate due to lower lipophilicity of counter ion and high affinity towards hydration (since $2(ETD)^{-}$•$PPZ^{2+}$ is a 2:1 salt, it is difficult to compare its solubility with 1:1 salts of monoamines). Permeability and flux studies of ETD salts suggested that tight ion-pairs were intact during the membrane permeation process and thus directed the rate of permeability. Molecular mobility and dissolution rate were the key factors to determine the rate of permeability in the same series of salts. Consequently, $ETD^{-}$•$isoPA^{+}$ showed highest cumulative permeability and flux. Overall, short chain (low lipophilic) amines are preferred over long chain (high lipophilic) amines to improve the solubility, dissolution and permeability of new chemical entities or existing drugs like Etodolac.

Chapter 5 deals with a designed ternary cocrystals of acefylline with coformers is discussed. The ternary cosryatsl ACF-INA-GA (1:1:1) exhibits dimorphism with higher solubility, dissolution rate and permeability than ACF.

Acefylline (ACF), a stimulant xanthane derivative drug, in combination with piperazine, is used in the treatment of bronchial asthma. However, its poor rate of permeability limits the development of ACF drug in pharmaceutical formulation. In this chapter, ACF binary and ternary cocrystals/salt-cocrystals/polymorphs are designed and synthesized using solvent assisted grinding with various coformers. The remaining ternary complexes were formed in different stoichiometric ratios. Eight ternary salt-cocrystals and two polymorphs of acefylline are synthesized by design of multi-component cocrystal engineering using solvent-assisted grinding method. All salts and cocrystals were analysed by SCXRD diffraction analysis, PXRD diffraction analysis, and thermal analysis by differential scanning calorimetry (DSC). Single crystal X-ray data show hydrogen bonding synthons such as imidazole-acid and carboxylate-pyridinium in ternary systems. The intermolecular interactions in ternary cocrystal polymorphs of ACF are further substantiated by Hirshfeld surface analysis, 2D fingerprint plots and energy frameworks. An increase in the permeability and solubility of ACF salt cocrystals/ polymorphs is observed in the binary and ternary systems, which is related to the lower melting point and ionic hydrogen bonding interactions. The improvement in the solubility and permeability of ACF in ternary systems may find application in fixed dose combination of drugs for solubility permeability enhancement. The ability to modulate both solubility and permeability of difficult to formulate drugs is demonstrated by crystal

engineering. The need to confirm the stoichiometry and composition of ternary and higher composition cocrystals by 1H NMR spectroscopy is emphasized in this chapter.

In chapter 6, cocrystals of TNZ with different coformers showed better physicochemical properties. The acid-imidazole and/or hydroxy-imidazole synthons in this cocrystal were studied computationally and validated by experimental cocrystal synthesis. Tinidazole (TNZ) is a 5-nitroimidazole derivative used as an antiamoebic, antiprotozoal, antibacterial, antiparastic and also used to treat vaginal trichomoniasis including giardiasis. TNZ is BCS class II drug with low solubility and high permeability. Nine novel solid forms (cocrystals) of tinidazole (TNZ) were synthesized with both aliphatic acids like oxalic acid (OA), citric acid (CA) and aromatic acids like 2,6-dihydroxy benzoic acid (2,6-DHBA), 4-hydroxy benzoic acid (PHBA), 4-amino benzoic acid (PABA), ferulic acid (FA), p-coumaric acid (PCA), and vanillic acid (VA). The acid-imidazole and acid-acid supramolecular synthons are observed in TNZ-OA, TNZ-CA, TNZ-2,6-DHBA cocrystals. FA, PCA, VA, PHBA, PABA coformers form different synthons with tinidazole, such as phenol-imidazole, acid-acid dimer, amine-carbonyl and nitroimidazole dimer synthons in crystal structures. Preference of acid-imidazole and/or hydroxy-imidazole was studied computationally and validated via experimental cocrystal synthesis. Solubility, dissolution and permeability experiments were performed on TNZ and new solid forms show high dissolution rates: TNZ-2,6DHBA, TNZ-FA, TNZ-OA, TNZ-CA, and TNZ-PCA. All products were characterized by PXRD, SC-XRD, DSC and IR. Similarities and differences in the crystal packing thermal behavior of crystalline materials are also studied. These studies improve our understanding and knowledge about crystal engineering of novel organic solid forms of active pharmaceutical cocrystals, polymorphs, slats and coamorphous forms to improve physicochemical properties and pharmacological activity and their potential use in novel pharmaceutical formulations.

## 7.2 Future prospects

The studies of Chapter 2 encourage us to test the novel binary/ternary cocrystals, salt of BUM to cure diseases and also to explore anti-hypertension therapy in the future. Bumetanide (BUM) drug-drug formulations are getting huge attention in recent days as these systems have better medicinal, pharmaceutical, physiochemical properties and improved solubility and dissolution properties. Chapter 3 on Indapamide deals with the structural analysis of multi-component salts, cocrystals and coamorphous followed by

supramolecular design and synthon complementarity at molecular level in IDP with pyridine, piperzine, and amino acid derivatives as conformers resulted cocrystals and coamorphous with enhanced physicochemical properties such as better stability, improved solubility that result in increased permeation i.e molecular behavior. This case study can be applied in exploring more cocrystals using structurally related drugs like Bumetanide, furosemide, torsemide which comes under BCS class II to know their pharmacokinetics which results in better compliance to patients.

The Acefylline ternary salt-cocrystal hydrates with different stoichiometric ratios such as ACF-INA-3,5DHBA-H2O (1:1:1:4), ACF-PIP-GA-H2O (1:0.5:1:2), ACF-PIP-3,5-DHBA-H2O (1:0.5:1:2, and 1:1:2:2) opens a window for these multi-component salt-cocrystals hydrates to further get replaced by complimentary supramolecular synthon (chapter 5) providing further directions for the preparation of quaternary/quintinary/hexanary systems or solid solutions.

# ABOUT THE AUTHOR

Suryanarayana Allu, son of Mr. Polinaidu (Late) and Mrs. Roddamma, was born in Gobhyam, Vizianagaram District, Andhra Pradesh, India. He received primary education at MPPS Gobhyam and secondary education at Zilla Parishad High (ZPH) School, Dattirajeru. He completed Intermediate (B.I.E., 2004-06) in Maths, Physics and Chemistry at MSN Junior College, Vizianagaram. He pursued Bachelor of Science (B.Sc., Maths, Physics and Chemistry, 2006-09) at Gayatri Degree College, Gajapathinagaram and Master of Science (M. Sc., Chemical Science, 2010-12) from Pondicherry University, Pondicherry. He cleared GATE (2013) Examination (AIR-838) and later he was qualified for UGC BSR fellowship and obtained fellowship for a term of five years (2014-19). He then joined (in 2014) Prof. Ashwini Nangia's Research Group, School of Chemistry, University of Hyderabad, as a PhD Student and was upgraded as a 'Senior Research Fellow' (SRF) in 2016. During PhD, he qualified CSIR-JRF National Eligibility test and ranked 93$^{rd}$ for 'Junior Research Fellowship' (JRF) held in June 2016. He was actively involved in the research that deals with the improvement of physicochemical properties of Active Pharmaceutical Ingredients using crystal engineering principles and submitted his thesis work on "Crystal Engineering of Novel Solid Forms of Active Pharmaceutical Ingredients and their Physicochemical Properties" in November 2020.

## List of Publications

1. Soluble Salts and Cocrystals of Clotrimazole. Sudhir Mittapalli, M. K. Chaitanya Mannava, U. B. R. Khandavilli, **Suryanarayana Allu** and Ashwini Nangia *Cryst. Growth Design.* **2015**, 15, 2493–2504.
2. Supramolecular Synthons in Bumetanide Cocrystals and Ternary Products. **Suryanarayana Allu**, Geetha Bolla, Srinu Tothadi, and Ashwini Nangia. *Cryst. Growth Design.* **2017**, 17, 4225−4236.
3. Supramolecular synthon hierarchy in bumetanide cocrystals. **Suryanarayana Allu**, Geetha Bolla, Srinu Tothadi, and Ashwini K. Nangia. *Acta Cryst.* **2017**. A73, C721.
4. Role of hydrogen bonding in cocrystals and coamorphous solids: indapamide as a case study. **Suryanarayana Allu**, Kuthuru Suresh,Geetha Bolla,M.K. Chaitanya Mannava,and Ashwini Nangia. *CrystEngComm*, **2019**, 21, 2043–2048.
5. Crystal Forms of Acylhydrazone Photoswitches with Multiple Mechanical Responses. Poonam Gupta,Tamas Panda,**Suryanarayana Allu**, Silpisikha Borah, Anamika Baishya,Anilkumar Gunnam, Ashwini Nangia, Panče Naumov, and Naba K. Nath. *Cryst. Growth Design.* **2019,** 19, 3039−3044.
6. Novel Pharmaceutical Cocrystals and Salts of Bumetanide. **Suryanarayana Allu**, Geetha Bolla, Srinu Tothadi, and Ashwini K. Nangia. *Cryst. Growth Design*. **2020**, 20, 793−803.
7. Salts and Cocrystal of Etodolac: Advantage of Solubility, Dissolution and Permeability. Sunil K. Rai, **Suryanarayana Allu** and Ashwini K. Nangia. *Cryst. Growth Design.* **2020**, 20, 4512−4522.
8. Organic Molecular Crystals with Visible Regions of Elastic and Plastic Response. Poonam Gupta, **Suryanarayana Allu**, Durga Prasad Karothu, Tamas Panda, Ashwini Nangia, Naba K. Nath (Under Revision *Cryst. Growth Des*).
9. Enhancing the Permeability of Acefylline in Ternary Salt, Cocrystals and Polymorphs. **Suryanarayana Allu**, Vladimir V. Chernyshev and Ashwini K. Nangia. (to be communicated).
10. Synergistic Interactions in Tinidazole Cocrystals with Acid-hydroxyl Synthon and their Dissolution and Permeability. **Suryanarayana Allu**, Srinu Tothadi, Geetha Bolla and Ashwini K. Nangia. (to be communicated).

***Patents Filed:***

11. Soluble Salts and Cocrystals of Clotrimazole. Ashwini Nangia, Sudhir Mittapalli, M. K. Chaitanya Mannava, U. B. R. Khandavilli and **Suryanarayana Allu**.
Indian Patent, 2015, Provisional Patent Application No. 1747/CHE/2015.13.

## Conferences, Symposia and Workshops Attended

1. Presented a poster entitled "**Supramolecular synthon hierarchy in bumetanide cocrystals.**" at the 14th Annual In-house Symposium "**Chemfest-2017**" held at University of Hyderabad, Hyderabad, India, during March 3-4, 2017.
2. Presented a poster entitled "**Supramolecular synthon hierarchy in bumetanide cocrystals.**" at "**24th Congress and General Assembly of the International Union of Crystallography (IUCR-2017)**" held at HICC, Hyderabad, India, during August 21-28, 2017.
3. Presented a poster entitled "**Role of hydrogen bonding in cocrystals and coamorphous solids: indapamide as a case study.**" and awarded ChemComm poster prize at the "24th CRSI National Symposium in Chemistry and 13thCRSI-RSC Joint Symposium in Chemistry" jointly organized by CSIR-CLRI, Chennai and IIT Madras, Chennai, February 8-10, 2019.
4. Delivered an oral presentation entitled "**Acefylline ternary polymorphs, salt-cocrystals synthon hierarchy**" at the 16th Annual In-house Symposium "**Chemfest-2019**" at University of Hyderabad, Hyderabad, India, during Feb 22-23, 2019.
5. Participated the workshop on "**Cryo-electron microscopy: An indispensable solution for structural biology"** at the 24th congress and General Assembly of the International Union of Crystallography in Hyderabad, during August 24, 2017.
6. Participated the workshop on "**X-ray Absorption Spectroscopy for the Crystallographer"** at the 24th congress and General Assembly of the International Union of Crystallography in Hyderabad, during August 24, 2017.
7. Participated the workshop on "**Electron Diffraction for Pharmaceutical Applications**" held at IICT Hyderabad 10$^{th}$ July 2018.

# Crystal Engineering of Novel Solid Forms of Active Pharmaceutical Ingredients and their Physicochemical Properties

*by* Suryanarayana Allu

# Crystal Engineering of Novel Solid Forms of Active Pharmaceutical Ingredients and their Physicochemical Properties

ORIGINALITY REPORT

| 43% | 12% | 42% | 4% |
|---|---|---|---|
| SIMILARITY INDEX | INTERNET SOURCES | PUBLICATIONS | STUDENT PAPERS |

PRIMARY SOURCES

| | | |
|---|---|---|
| 1 | Sunil K. Rai, Suryanarayana Allu, Ashwini K. Nangia. "Salts and Cocrystal of Etodolac: Advantage of Solubility, Dissolution, and Permeability", Crystal Growth & Design, 2020<br>Publication | 9% |
| 2 | Suryanarayana Allu, Geetha Bolla, Srinu Tothadi, Ashwini Nangia. "Supramolecular Synthons in Bumetanide Cocrystals and Ternary Products", Crystal Growth & Design, 2017<br>Publication | 7% |
| 3 | Suryanarayana Allu, Geetha Bolla, Srinu Tothadi, Ashwini K. Nangia. "Novel Pharmaceutical Cocrystals and Salts of Bumetanide", Crystal Growth & Design, 2019<br>Publication | 7% |
| 4 | Sunil K. Rai, Suryanarayana Allu, Ashwini K. Nangia. "Salts and Cocrystal of Etodolac: Advantage of Solubility, Dissolution and Permeability", Crystal Growth & Design, 2020<br>Publication | 4% |

S K Das
13/11/2020
Prof. Samar K. Das
School of Chemistry
University of Hyderabad
Hyderabad-500 046., INDIA.

S K Das
13/11/2020
Prof. Samar K. Das
School of Chemistry
University of Hyderabad
Hyderabad-500 046., INDIA.

S K Das
13/11/2020
Prof. Samar K. Das
School of Chemistry
University of Hyderabad
Hyderabad-500 046., INDIA.

S K Das
13/11/2020
Prof. Samar K. Das
School of Chemistry
University of Hyderabad
Hyderabad-500 046., INDIA.

S K Das
Prof. Ashwini Nangia
School of Chemistry
University of Hyderabad
Hyderabad-500 046, INDIA.

| | | |
|---|---|---|
| 5 | Ashwini Nangia, Suryanarayana Allu, Kuthuru Suresh, Geetha Bolla, Chaitanya Mannava. "Role of hydrogen bonding in cocrystal and coamorphous solids: Indapamide as a case study", CrystEngComm, 2018<br>Publication | 4% |
| 6 | pubs.rsc.org<br>Internet Source | 3% |
| 7 | Submitted to University of Hyderabad, Hyderabad<br>Student Paper | 1% |
| 8 | Jacques Vicens. "Origins and emergences of supramolecular chemistry", Journal of Inclusion Phenomena and Macrocyclic Chemistry, 06/27/2009<br>Publication | <1% |
| 9 | Sudhir Mittapalli, M. K. Chaitanya Mannava, U. B. Rao Khandavilli, Suryanarayana Allu, Ashwini Nangia. "Soluble Salts and Cocrystals of Clotrimazole", Crystal Growth & Design, 2015<br>Publication | <1% |
| 10 | Z. Wojnarowska, K. Grzybowska, L. Hawelek, M. Dulski et al. "Molecular Dynamics, Physical Stability and Solubility Advantage from Amorphous Indapamide Drug", Molecular Pharmaceutics, 2013<br>Publication | <1% |

S.K.Das 13/11/2020

Prof. Samar K. Das
School of Chemistry
University of Hyderabad
Hyderabad-500 046., INDIA.

S.K.Das 13/11/2020

Prof. Samar K. Das
School of Chemistry
University of Hyderabad
Hyderabad-500 046., INDIA.

S.K.Das 13/11/2020

Prof. Samar K. Das
School of Chemistry
University of Hyderabad
Hyderabad-500 046., INDIA.

S.K.Das 13/11/2020

Prof. Samar K. Das
School of Chemistry
University of Hyderabad
Hyderabad-500 046., INDIA.

S.K.Das

Prof. Ashwini Nangia
School of Chemistry
University of Hyderabad
Hyderabad-500 046, INDIA.

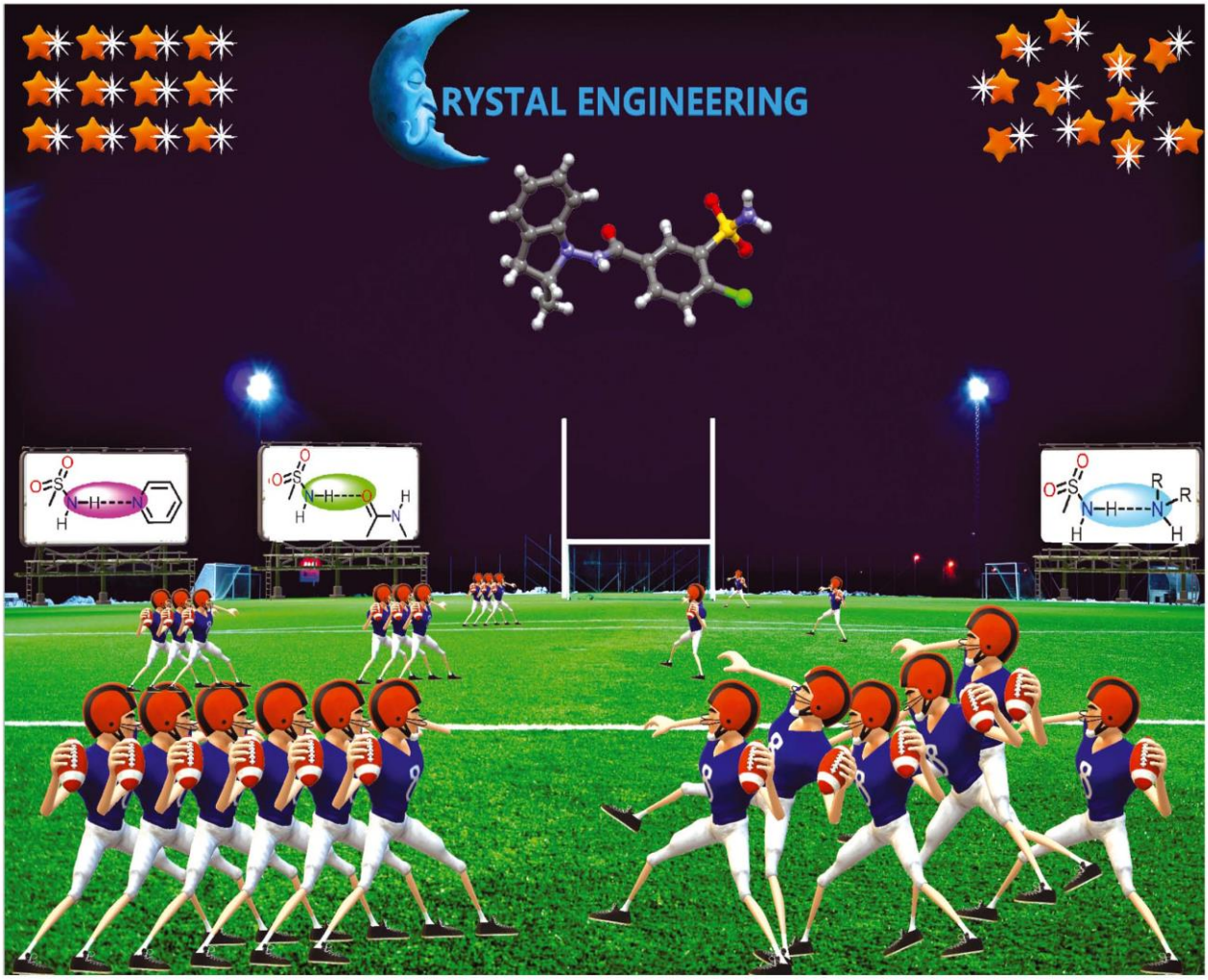


**Showcasing research work done by Suryanarayana Allu, Kuthuru Suresh, Geetha Bolla, M. K. Chaitanya Mannava, and Ashwini Nangia from School of Chemistry, University of Hyderabad and CSIR-National Chemical Laboratory, India.**

Role of hydrogen bonding in cocrystals and coamorphous solids: indapamide as a case study

The stronger sulfonamide–pyridine ($SO_2NH_2$···N–Py) and sulfonamide–carboxamide ($SO_2NH_2$···O=C–NH) hydrogen bonds direct the formation of cocrystals, whereas the weaker sulfonamide–amine ($SO_2NH_2$···N–H) hydrogen bond results in coamorphous products. IDP–PIP and IDP–ARG coamorphous solids exhibit remarkable stability under accelerated conditions.

## As featured in:

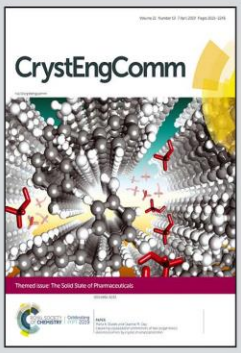


See Ashwini Nangia *et al.*, *CrystEngComm*, 2019, **21**, 2043.

ROYAL SOCIETY OF CHEMISTRY | Celebrating IYPT 2019

rsc.li/crystengcomm

Registered charity number: 207890